UNCLASSIFIED

AD NUMBER
ADB006948
LIMITATION CHANGES

TO:

Approved for public release; distribution is unlimited.

FROM:

Distribution authorized to U.S. Gov't. agencies only; Test and Evaluation; JUN 1975. Other requests shall be referred to Air Force Materials Lab., Wright-Patterson AFB, OH 45433.

AUTHORITY

AFAL ltr 8 Dec 1978

THIS PAGE IS UNCLASSIFIED

LEAD-TIN TELLURIDE SPUTTERED THIN FILMS FOR INFRARED SENSORS

GENERAL DYNAMICS
POMONA DIVISION
P.O. BOX 2507, POMONA, CALIFORNIA 91766
APPLIED RESEARCH LABORATORY

JUNE 1975

D D C
RECEIVED
OCT 14 1975
A

AIR FORCE MATERIALS LABORATORY
Air Force Systems Command
Wright-Patterson AFB, Ohio 45433

FOR THE COMMANDER

WILLIAM G. D. FREDERICK, Chief
Laser and Optical Materials Branch
Electromagnetic Materials Division
Air Force Materials Laboratory

SECURITY CLASSIFICATION OF THIS PAGE *(When Date Entered)*

REPORT DOCUMENTATION PAGE	READ INSTRUCTIONS BEFORE COMPLETING FORM

1. REPORT NUMBER	2. GOVT ACCESSION NO.	3. RECIPIENT'S CATALOG NUMBER
AFML-TR-75-63		

4. TITLE *(and Subtitle)*

LEAD-TIN TELLURIDE SPUTTERED THIN FILMS FOR INFRARED SENSORS

5. TYPE OF REPORT & PERIOD COVERED

Final Technical Report
15 Aug 71 - 15 Oct 74

6. PERFORMING ORG. REPORT NUMBER

TM-6-125PH-431

7. AUTHOR(s)

Esther Krikorian
M. J. Crisp
R. J. Sneed

8. CONTRACT OR GRANT NUMBER(s)

F33615-72-C-1042

9. PERFORMING ORGANIZATION NAME AND ADDRESS

General Dynamics
Pomona Division
P. O. Box 2507, Pomona, CA 91766

10. PROGRAM ELEMENT, PROJECT, TASK AREA & WORK UNIT NUMBERS

62102F
7371
73710819

11. CONTROLLING OFFICE NAME AND ADDRESS

Laser and Optical Materials Branch, AFML/LPO
Air Force Materials Laboratory
Wright-Patterson Air Force Base, OH 45433

12. REPORT DATE

June 1975

13. NUMBER OF PAGES

425

14. MONITORING AGENCY NAME & ADDRESS*(If different from Controlling Office)*

15. SECURITY CLASS. *(of this report)*

unclassified

15a. DECLASSIFICATION/DOWNGRADING SCHEDULE

16. DISTRIBUTION STATEMENT *(of this Report)*

Distribution limited to U.S. Government agencies only: Test and Evaluation Data included. Other requests for this document must be referred to AFML/LPO.   June 1975.

17. DISTRIBUTION STATEMENT *(of the abstract entered in Block 20, if different from Report)*

Unlimited

18. SUPPLEMENTARY NOTES

19. KEY WORDS *(Continue on reverse side if necessary and identify by block number)*

Lead Tin Telluride
Sputtered Thin Films
Electrical Properties

Photoconductive Response
Optical Properties

20. ABSTRACT *(Continue on reverse side if necessary and identify by block number)*

A study was carried out aimed at preparing thin ternary compound films suitable for infrared sensor application. In particular, an systematic experimental investigation was pursued to control or optimize the structural, compositional, electrical and electro-optical film properties by means of well defined deposition parameters and conditions. Techniques were first developed for sputtering single crystal thin films of lead tin telluride (PbSnTe) on barium fluoride and calcium fluoride substrates. Both supported discharge and ion beam sputtering were used. The sputtering gas was argon. Most data was obtained by supported

DD FORM 1 JAN 73 **1473**   EDITION OF 1 NOV 65 IS OBSOLETE

AIR FORCE - 22-9-75 - 150

SECURITY CLASSIFICATION OF THIS PAGE *(When Date Entered)*

- A -

from p. A

micrometers

discharge sputtering. Thirteen sputtering targets of PbSnTe were used with ratios of tin to total metal (lead plus tin) of x = 0.15 to x = 0.32. Some targets were prepared metal or tellurium rich but most were stoichiometric, i.e. having the same number of tellurium atoms as metal atoms. The upper substrate temperature for single crystal growth was about 350°C and the lower temperature ranged from about 225 to 300°C for growth rates from 0.5 to 2.5 μm/hr. Outside this temperature-growth rate regime the films were not single crystal.

The x-value of the deposited film, which defines the energy gap, was found to be controllable by the x-value of the target, the substrate temperature, and the deposition rate. Adjusting the latter two adjusts the x-value of the deposited films to x-values significantly different from the x-value of the target. For example, films with x as low as 0.15 or as high as 0.27 could be sputtered from a target with x = 0.20. Aside from film x-values, the stoichiometry of the film materials was found to be also controllable by adjustment of the substrate temperature and deposition rate. Complete stoichiometry, which is associated with the lowest achievable carrier concentrations, was found to occur at critical temperature-rate products - which differ with different target x-values. Adjustment of the same two deposition parameters was also established as a means for controlling the film carrier type. Typically, conditions yielding films with x-values lower than that of the target produce p-type film, those yielding x-values larger than that of the target produce n-type film. Biasing of the substrate in the range of ±30 volts was found to serve as an additional control parameter. Such a bias drives the films n- or p-type, depending on the polarity of the bias, without changing its x-value. A critical bias voltage exists for each film x-value at which the material is stoichiometric - as exhibited by a distinct minimum in film carrier concentration. Finally, it was found that the addition of controlled quantities of O_2 or N_2 to the sputtering gas tends to produce p- or n-type film, respectively.

Under optimized deposition conditions, as-deposited, i.e. unannealed, PbSnTe films were prepared with structural and electrical properties at least equivalent to bulk single crystals and with photoconductive responses as high or higher than observed in bulk crystals. In films deposited with gaseous additives (N_2 or O_2) the measured photoconductive responses were orders-of-magnitude higher than in films deposited with Ar only. For example, at LN_2 temperatures, carrier concentrations were below 10^{17}, carrier mobilities were over 10,000, and lifetimes were less than 100 nanoseconds in films grown in pure Ar under optimized conditions. Photoconductive responsivities were in the range of 1 to 10 volt/watt. Photoconductive D*'s exceeded 10^9 without antireflection. For films deposited with gaseous additives, effective carrier concentrations were in the 1×10^{16} cm^{-3} range or lower, carrier mobilities were still in the 10,000 cm^2/v-sec, range while photoconductive responsivities were typically in the 20 v/watt range but in isolated cases, photoconductive responsivities in the 10^3 v/w range were measured. Photoconductive D*'s approached 1×10^{10} for the latter cases. Although trapping behavior was not established it is thought that trap formation is the mechanism by which the additives produce enhanced photoresponse. These developments could result in worthwhile photoconductive PbSnTe sensors.

The results established also the material base for the fabrication of photovoltaic infrared sensors using sputtered thin film PbSnTe. First, it was determined that the adjustment of deposition rate, substrate temperature, composition of sputtering gas and substrate bias during film deposition permits the production of thin film homo- or heterojunctions, having desired levels of the carrier concentrations without requiring a post-growth anneal to adjust stoichiometry. Secondly, the feasibility of photoresponsive Schottky devices was shown using p-type films with platinum for the ohmic contacts and aluminum, lead, or indium for the barrier.

13

FOREWORD

TABLE OF CONTENTS

Page

iv

Table of Contents (Continued)

vi

Table of Contents (Continued)

LIST OF FIGURES

List of Figures (Continued)

List of Figures (Continued)

List of Figures (Continued)

List of Figures   (Continued)

List of Figures (Continued)

List of Figures   (Continued)

List of Figures (Continued)

List of Figures (Continued)

List of Figures   (Continued)

List of Figures   (Continued)

List of Figures (Continued)

List of Figures (Continued)

LIST OF TABLES

List of Tables (Continued)

List of Tables (Continued)

List of Tables (Continued)

Section 1

INTRODUCTION

1.1 PROGRAM OBJECTIVES AND GENERAL APPROACHES

Electro-optical systems for surface oriented, airborne and exo-atmospheric applications have increasing requirements for the utilization of the long wavelength portion of the infrared spectrum. Terrain surveillance, as well as the detection, acquisition and tracking of cold surface targets such as tanks, ships and surface weapon sites are examples of potential applications of this spectral band as are engagements of emission controlled or countermeasured aircraft and other vehicles lacking significant self emission. Unfortunately, sensor systems which operate at such long wavelengths will remain inherently costly unless new detector fabrication techniques are introduced. Considerable, but still insufficient progress has been made to overcome these problems with the introduction of intrinsic detectors such as HgCdTe which retain high sensitivity at operating temperatures of $77^{\circ}K$ or above - thus considerably reducing the cryogenic requirements of earlier sensors such as doped germanium detectors. The reason that even this progress was insufficient stems from the fact that aside from a tendency to operate at longer wavelengths, the sophistication required of modern electro-optical sensor systems is increasing at an extremely rapid rate. Spatial and spectral resolution requirements for target-background discrimination, precision terminal guidance and operation in severe IRCM environments call for rather complex sensor configurations. It is doubtful that the desired functional performances can be achieved with conventional approaches; it is certain that these approaches would not lead to cost effective device fabrication.

These are the considerations which led to the selection of the overall technical objectives and approaches for this program.

Based on various early feasibility studies in our laboratory, one of the general objectives was to develop techniques for the preparation of high sensitivity, thin film detector materials which are responsive

in the desired spectral band. The inherent advantages of thin film
sensors are manyfold. This will be demonstrated in the next section,
and will become even more evident in the remainder of this report. Suffice
it to say here, that all predictable advantages have been established as
fully achievable - in fact others were identified as the program progressed.
In most cases, the latter relate to the ease of fabrication and perfor-
mance control by thin film deposition techniques.

It should also be emphasized, that the study was exclusively oriented
toward materials preparation and processing. That is, the development
of full-up detection devices was not an objective. However, all materials
studies were designed to use photoresponse characteristics as the final
criterion for assessing the value of the various specific techniques
developed and for judging the quality of the results in general. As will
be elaborated on later, this led to an iterative experimental approach
whereby the film preparation techniques were in turn tailored to optimize
the structural, the electrical and finally the electro-optical properties.
An extremely systematic approach was taken, such that all preparation
parameters and conditions could be fully correlated with the ultimate
response characteristics - thus providing a solid basis for the eventual
manufacturing control of these parameters in the fabrication of optimized
detectors.

Based on early feasibility studies, the exclusive deposition techni-
que selected was sputtering. However, several variations of this
technique - such as triode sputtering, ion beam sputtering, bias sputtering
and sputtering in composition controlled background atmospheres were
explored. Ease of deposition condition control, potentially superior
thermo-mechanical stability, simple film composition control, coupled
with the demonstrated feasibility of depositing high quality, single
crystal compound semiconductor films are but a few of the inherent advant-
ages of sputtering. Again, not only were these and other predicted
advantages fully validated during the course of this work, but other un-
forseen advantages were identified - many of which either have not been
or cannot be demonstrated with other thin film deposition techniques.

The selection of $Pb_{1-x}Sn_xTe$ as the thin film sensor material, was the most logical at the initiation of this program. An intrinsic material was prerequisite, the basic desired electro-optical response characteristics were already demonstrated with bulk single crystal materials and the only other suitable intrinsic material that had been demonstrated to have the desired performance characteristics, $Hg_{1-x}Cd_xTe$, is extremely difficult to prepare in high quality thin film form. As the results of this effort will show and as the extensive activities that have been initiated by laboratories and detector suppliers throughout this country corroborate, the propriety of this material selection was also fully substantiated.

1.2 BACKGROUND

In recent years, considerable progress has been made in the development of small and/or variable energy gap IV-VI alloy systems - in particular $Pb_{1-x}Sn_xTe$, for detector applications. Photovoltaic diodes of these materials have become available with reasonably good properties. But, as stated, most of the device work was up to very recently, confined to the utilization of bulk single crystal materials. However, thin film detectors, although still in the state of development, are now receiving considerable emphasis.

Thin film devices are particularly appealing for application in infrared detector or photo-transistor arrays. Thus, the recent progress in the development of high quality thin film $Pb_{1-x}Sn_xTe$ materials as well as of other thin film binary and ternary IV-VI compounds has resulted in, and promises further, very significant advancements in the electro-optical device field in general. In particular, this technology should result in a new generation of economical, complex sensors and sensor arrays for critical portions of the infrared spectrum.

At present high quality infrared detectors with theoretically limited sensitivity are available for most all useful portions of the spectrum. The reason that detector research, and in particular thin film research, is still a very active, if not increasingly active field, is due to the fact that most detectors are still extremely expensive and/or have impractical cooling requirements for many military applications. In fact, if some of the more modern requirements such as detector arrays for guidance, surveillance and FLIR applications or, even more so, if multi-color elements are considered, the present prices are intolerable - at least for tactical systems. Thin films provide considerable hope for a solution of this problem. In addition to cost economy, uniformity, low thermal loads, inherently higher efficiency of thickness optimized detectors and other factors are first order advantages that should be achievable with thin film array configurations. Beyond these advantages, thin film photo-electric materials have other inherent advantages over

their bulk or thick film counterparts which should contribute to the feasibility of increased sophistication in electro-optical devices. Multi-color sensors, charge-coupled integrated elements and elements for sensor integrated optics systems are but a few examples of areas in which thin film technology should make rather complex devices practical.

Table 1-1 indicates some of the reasons why thin film detector technology has a definite place in the attempt to achieve cost-effective sensors. It may be worth noting that some of the apparent advantages (such as no annealing time required) were only identified after considerable work in our laboratory with sputtered $Pb_{1-x}Sn_xTe$. That is, the potential of thin film sensors increased rather than decreased as the work proceeded.

At the initiation of this program, it was recognized that before the utilization of thin film elements could be a realistic goal, the material properties had to be improved beyond the level of quality achieved with bulk single crystals of the pertinent compounds. Also we felt that the real pay-off of the thin film work would be realized if electro-optical devices which were more sophisticated than the diodes available at that time could be derived from the techniques developed under this program.

As extensively documented throughout this report, several investigators, including those of this laboratory, have advanced the thin film technology of $Pb_{1-x}Sn_xTe$ and other narrow and/or variable energy gap compounds in recent years to a very promising level. This becomes apparent if one reviews the various thin film detector programs presently underway. One finds an obvious emphasis, and corresponding progress, in the exploration of binary and ternary IV-VI compound materials. Table 1-2 shows the five most extensively investigated materials for thin film sensors, along with the response ranges defined by λ_c, the response cutoff wavelengths. A number of investigators have now succeeded in preparing excellent single crystal film of these compounds utilizing such deposition techniques as sputtering (References 1 & 2), evaporation (Reference 3, 4, 5, 6), vapor phase (Reference 7), and liquid phase

TABLE 1-1 THIN FILM E-O SENSORS: EXAMPLES OF REAL AND POTENTIAL ADVANTAGES

- REDUCED CRYSTAL GROWTH TIME
- LOW TEMPERATURE PREPARATION PROCESSES
- REDUCED OR NO ANNEALING TIME
- ELIMINATION OF SURFACE PREPARATION STEPS
- THICKNESS OPTIMIZATION
- SIMPLIFIED ACTIVE AREA DEFINITION
  (SINGLE DETECTORS, ARRAYS)
- COMPOSITION, STOICHIOMETRY AND CARRIER TYPE CONTROL
- APPLICABILITY TO MULTI – COLOR SANDWICH DETECTORS
- POSSIBLE INTEGRATION WITH CCD TECHNOLOGY

F123555-1 775

1-6

TABLE 1-2 THIN FILM E-O SENSOR MATERIALS: RECENT INVESTIGATION

MATERIAL	NOMINAL RESPONSE RANGE
Pb Se	λ_c (77°K) = 7 μm
Pb Te	λ_c (77°K) = 5.7 μm
Pb Sn Te	λ_c (77°K) = 4 μm TO 15 μm
Pb Sn Se	λ_c (77°K) = 5 μm TO 15 μm
Pb Se Te	λ_c (170°K) = 4.7 μm TO 5.9 μm
Pb Se Te	λ_c (77°K) = 5.7 μm TO 7 μm

F123552 7104

epitaxy (Reference 8). It is recognized that liquid phase epitaxy may
not be considered a thin film deposition process, since the deposition
takes place in the liquid phase, does not employ a vacuum, requires a
IV-VI compound - substrate such as, for example, PbTe or PbSnTe, and
is generally limited to a minimum thickness for sufficient uniformity.
However, we include it in this background introduction since comparison
of the properties of the LP-eptiaxial layer with properties of layers
deposited by vacuum deposition techniques is of interest; also the
types of devices which can and have been prepared by LPE can thus be
compared with those which can and have been prepared by vacuum deposition
techniques. Of particular interest are those devices prepared by LPE
which utilize only epitaxial layers to produce photo-sensitivity. This
includes, for example photovoltaic detectors consisting of devices with
n-epi-layers on p-epi-layers grown on p-bulk substrates.

Referring back to Table 1-2, we see that the compounds represented
here have response ranges from the mid-IR to the long wavelength IR.
For example PbTe and PbSe are intrinsic mid-IR detectors with a cut-off
between 5μm to 7μm. Ternary IV-VI materials, as we know, are responsive
from the mid-IR to long wavelength IR and their spectral responses are
very sensitive to composition. As is shown in Table 1-2, more recently
some ternary compounds (e.g., PbSeTe) are being explored for application
at mid-IR wavelengths. The hope is that they can be used at higher
operating temperatures than conventional mid-IR sensors - without loss
in sensitivity.

Significant is the fact that the emphasis is on materials whose
spectral characteristics and operating temperatures make them candidates
for those device application which are in direst need of more cost
effective preparation methods, i.e., on materials which are suitable
for long wavelength application, the spectral band which is most in need of
array sensors (since a spatial discrimination capability is a critical
requirement in the LWIR band which is plagued by severe background clutter
from natural environments). These materials are also spectrally tailor-
able for multi-color application in spectral discrimination systems

1-8

aimed at reducing false target information.

Significant also is the absence, in Table 1-2, of another ternary compound which, as a bulk material, has shown some very desirable behavior - namely HgCdTe. It too is an intrinsic, variable band gap material useful from the mid to long wavelength portions of the IR spectrum and has good sensitivity at reasonably high operating temperatures. Unfortunately, this material, by virtue of the vapor pressure of its mercury component, is not readily producible in the form of single crystal films. Even without this problem, its composition control would be extremely difficult by most thin film deposition techniques. This again is due to the large differences of vapor pressure of the alloy components in HgCdTe.

We do not pretend that the materials listed in Table 1-2 represent a complete and comprehensive list of all thin film sensor materials being prepared in this country. Scanning through the various journals which publish work in this area of research (e.g., JAP, APL, IRIS Proceedings), it is obvious that the list is extensive. It may suffice to list some of the more active groups in the field. They include: a) the Scientific Research Staff of the Ford Motor Co., the University of Pennsylvania, the Night Vision Laboratory (as an in-house activity), the Applied Research Laboratory of the General Dynamics Pomona Division - in the deposition of these materials by vacuum techniques including evaporation and sputtering; b) the North American Science Center, the Lincoln Laboratory, Aerojet General and the Santa Barbara Research Center-in the preparation of these materials by liquid phase epitaxy; and c) very recently Texas Instruments and others-in vapor phase deposition.

Work on vacuum deposition of IV-VI thin films is also being performed in Germany at Telefunken and in Italy at the C.N.R. Solid State Laboratories.

The number of techniques used in this field as well as the number of laboratories active in it illustrate the importance of exploring

various approaches to insure that the ideal materials will eventually come into being and the need for practical processes. Based on the potential pay-off, a certain amount of redundancy seems well advised until an optimum approach is clearly defined. Table 1-3 lists some of the more promising techniques---that is, only those techniques which are presently most likely to produce high quality epitaxial films of the various materials of interest. It has, of course, become quite apparent that any useful film material for sensor application must be single crystal in nature. This is the only structure which can avoid the imperfections which cause the scattering mechanisms that impede the carrier mobility and increase noise. But having high quality films is only a prerequisite for the fabrication of sensors.

Most of the film methods used to produce electro-optical devices of the IV-VI compounds as well as the mode of operation of the device (e.g., photo-voltaic, photoconductive) have to date, been borrowed from bulk crystal technology. Table 1-4 presents some of these various film processing methods being used at present. Of course, these film processing techniques apply also for hetero- or homojunction formation on appropriate substrates. As can be seen, most of the techniques listed in Table 1-4 are aimed at thin film junction formation as required for photo-voltaic elements. The exception is the last technique which also represents a means for the film property control required for achieving enhanced photoconductive sensor response, namely the use of gaseous additives.

All but two of the techniques listed have been used for the preparation of electrical or electro-optical devices prior to this work. The two new approaches are sputtering of junctions as well as the control of the carrier type by O_2 and N_2 additives during sputtering, referred to above, which were developed in this laboratory for $Pb_{1-x}Sn_xTe$. Both must be considered rather unique and easily controllable techniques for device preparation as will be thoroughly discussed later in this report.

TABLE 1-3 THIN FILM E-O SENSOR MATERIALS: MOST COMMON DEPOSITION TECHNIQUES

EVAPORATION — SINGLE BOAT SOURCE
MULTIPLE BOAT SOURCES
KNUDSEN CELL (2 AND 3 CELLS)

SPUTTERING — TRIODE SPUTTERING - SINGLE TARGET
WITH AND WITHOUT BIAS
WITH AND WITHOUT ADDITIVES —
RF SPUTTERING — MULTIPLE TARGETS

LIQUID PHASE EPITAXY — HOMO—AND HETERO—EPITAXY
($t_f \geqslant 10 \ \mu M$)

F123553 7104

1-11

TABLE 1-4 THIN FILM E-O SENSOR MATERIALS:FILM PROCESSING TECHNIQUES FOR DEVICE APPLICATION

ANNEALING	STOICHIOMETRY, TYPE CONTROL
PROTON BOMBARDMENT	p – n JUNCTION FORMATION
ION IMPLANTATION	p – n JUNCTION FORMATION
BIAS SPUTTERING	p – n JUNCTION FORMATION
SCHOTTKY BARRIERS	SCHOTTKY DIODE
GASEOUS ADDITIVES	pc RESPONSE ENHANCEMENT (p – n JUNCTION FORMATION)

F123554 7104

The present status of the various thin film techniques and materials for the preparation of sensor device, can be better assessed by those material and device properties which are critical for high performance. In Table 1-5 some first order criteria for device worthy films and film structures are presented in terms of some minimum material and device property values one should strive for. For comparison, Tables 1-6A and 1-6B review some actual results on the as-deposited and annealed film properties of the various IV-VI compounds prepared to date by various techniques and by a number of investigators. In Table 1-6A PbTe, PbSe, PbSnSe and PbSeTe are reviewed while in Table 1-6B, PbSnTe is reviewed. As is apparent from these results, PbSnTe has been much more extensively investigated by more techniques than any of the other IV-VI compounds.

The progress made in preparing high quality films of these materials is readily apparent from the two tables. The results show that in most cases it has not only been possible to deposit structurally high quality epitaxial films but that the electrical properties of these films are quite good and approach those of good single crystal bulk materials. In fact, the carrier concentrations and carrier mobility range achieved by most of the techniques are adequate for at least state-of-the-art device application. In all cases the films are single crystals and were deposited on suitable substrates.

In assessing the values in Tables 1-6A and 1-6B, some rather large ranges in carrier concentration and mobility are indicated. In all but one case these represent actual experimental scatter, reflecting a certain lack of repeatibility. By contrast, the values for triode sputtered PbSnTe in Table 1-6B reflect a range which can be fully correlated with specific deposition conditions. This will become obvious in the Result section. It is likely, that a similar correlation could be established for the values of n and μ achieved by the other techniques if an equally systematic dependence on the deposition conditions had been defined as has been for triode sputtered

TABLE 1-5 FIRST ORDER CRITERIA: HIGH SENSITIVITY, PRACTICAL IV-VI COMPOUND SENSORS

MATERIAL PROPERTIES (77°K)

n, p $\leq$ 10^{17} cm^{-3}

μ $\geq$ 10^4 cm^2/VOLT–SEC

DEVICE PROPERTIES (77°K)

η $\geq$ 80%

R·A $\sim$ 10 ohm–cm^2

D* (300°K, 2π, 1000 Hz) $\sim$ 3×10^{10} WATT^{-1} cm Hz$^{1/2}$

τ_R $\leq$ 1 μsec

F123581 7104

TABLE 1-6(A) STATUS SURVEY: EPITAXIAL FILM PREPARATION

FILM MATERIAL	TECHNIQUE	AS–DEPOSITED		ANNEALED	
		n (10^{17} cm^{-3})	μ (10^4 cm^2/V-sec)	n (10^{17} cm^{-3})	μ (10^4 cm^2/V-sec)
PbTe	EVAPORATION (KNUDSEN CELL)	0.1 – 0.5	0.5 – 2.0	0.6 – 40.0	2.0
	LPE	1.0 – 2.0	–	–	–
PbSe	EVAPORATION PbSe & Se (2 CELLS)	0.5 – 10.0	1.0 – 3.0	4.5 – 250.0	1.0 – 4.0
PbSnSe	EVAPORATION PbSe, SnSe, Se (3 CELLS)	1.0 – 5.0	1.0 – 3.0	2.0	2.0 – 3.0
PbSe$_\chi$ Te$_{1-\chi}$ χ = 0.8 ONLY	EVAPORATION PbSe, PbTe, Se (3 CELLS)	2.0 – 10.0	0.6 – 1.0	–	–

F123579 7104

TABLE 1-6(B) STATUS SURVEY (CONTINUED): EPITAXIAL FILM PREPARATION

FILM MATERIAL	TECHNIQUE	AS DEPOSITED		ANNEALED		COMMENT
		n (10^{17} cm^{-3})	μ' (10^4 cm^2/V–sec)	n (10^{17} cm^{-3})	μ (10^4 cm^2/V–Sec)	
PbSnTe	TRIODE SPUTTERING PbSnTe (1 TARGET)	0.6 – 1.0	0.6 – 2.0	0.09 – 2.0	1.0 – 3.0	GD
	RF SPUTTERING PbSnTe & Te (2 TARGETS)	1.0 – 5.0	0.1 – 1.0	–	–	CNR
	EVAPORATION PbTe & SnTe (2 CELLS)	1.0 – 10.0	0.3 – 2.0	0.5 – 3.0	1.0 – 3.0	FORD
	PbSnTe (1 BOAT)	1.0 – 10.0	–	–	–	NVL
	LPE	0.05	1.0 – 3.0	–	–	NA
	LPE	1.0 – 3.0		–	–	LINCOLN

F123580 7104

1–16

PbSnTe film in this laboratory. As will be shown, the listed film properties are functions of interdependent parameters which include the film composition in ternary compounds and the deposition temperatures and the deposition rates in all compounds. Composition is selected to control spectral response, deposition conditions to control the sensitivity and carrier type. None can be independently optimized for best results. Fortunately all have very systematic effects on the critical film properties and are thus readily controllable. The fact that the properties are extremely sensitive to the deposition conditions explains easily why large experimental scatter is observed in work that does not carefully define their effects. It may be added also that the sensitivity of film properties to deposition conditions is the reason that better film properties have not been achieved as of the time of preparation of these tables. The values listed do definitely not represent an inherent limit in IV-VI compound films. As will be seen later, with more extensive, careful control of deposition conditions, order of magnitude lower carrier concentrations and corresponding increases in mobility are quite likely. For example, the critical substrate temperature or the critical annealing temperature should be uniformly controlled to better than 0.2^oC throughout the film area for optimized condition. While this is difficult, it can be achieved. In the case of PbSnTe at least, this can also be circumvented with a substrate bias, which is much easier and more precisely controllable.

Since device worthy materials are the final objective of all this work, it is of interest to review the thin film devices explored to date using the various IV-VI materials and techniques. We attempt to do this in Table 1-7 which summarizes some results on thin film devices prepared from some of the IV-VI compounds--PbTe, PbSe, $PbSe_{.8}Te_{.2}$ and PbSnSe. In the first two columns of Table 1-7, we list the active film material used in the device (not the substrate or contact films) and the film deposition technique employed in making the device. For these film materials, evaporation was obviously the most commonly used technique. In the following columns we define the basic device related

1-17

TABLE 1-7   STATUS SURVEY: THIN FILM DEVICE CONFIGURATIONS

FILM MATERIAL	DEPOSITION TECHNIQUE	JUNCTION PREPARATION	D^* (cm Hz$^{1/2}$W^{-1})	$R \cdot A$ (ohm-cm^2)
PbTe	EVAPORATION	SCHOTTKY – Pb	1×10^{11} (77°K) 2×10^{10} (170°K)	50 – 1650 (77°K) 4.0 – 5.0 (170°K)
PbTe	EVAPORATION	p–n–PROTON BOMBM'T	$2 – 6 \times 10^{11}$ (77°K) f/20	500 (77°K)
PbTe	EVAPORATION	p–n–ION IMPL. (Sb)	4×10^{11} (77°K Backg.)	1.4×10^3 (77°K) η = 55%
PbTe	SPUTTERING	pc[O_2 ENHANCED]	8×10^{10} PHOTOCONDUCTOR	
PbTe	LPE	n–PbTe/PbTe (homo)	LASER SOURCE	
PbSe$_{.8}$ Te$_{.2}$	EVAPORATION	SCHOTTKY	6×10^{10} (170°K) 1×10^{11} (77°K)	4.5 (170°K) ~400 (77°K)
PbSe	EVAPORATION	SCHOTTKY	B.B. f/0.6 2×10^{10} (77°K)	12 – 80 (77°K)

F123577–1 775

1–18

film processing technique. That is, we show the technique that changes the film, once deposited, from a material to a device component. In most cases, the E-O sensor (or laser) prepared with the IV-VI compound film is a junction device. Therefore, detectors prepared in this manner will be photovoltaic devices. The reason for this is inherent in these materials. As already mentioned, we have recently found ways to overcome this one limiting factor and it appears now that photoconductive sensors may be realizable after all. This will be discussed later in the report.

The D* values are presented in as comparable a form as possible. As the reader is well aware, this detectivity indicator is very sensitive to conditions and extreme care must be taken when comparing vendor or research information of this nature. On comparison of these D* values with the first order criterion for a high performance device listed in Table 1-5, it may be cautiously concluded that the listed devices and corresponding materials are certainly approaching the desired values. Caution is required since in some cases the FOV and background conditions are not indicated. However, in those cases where the conditions are given, the values are comparable with desired values. Similar comments can be made in connection with the RA product.

Table 1-8 relates some additional device research results which can be quantitatively defined (within reason). As noted, most of these devices were prepared by liquid phase epitaxy. The diode functions are, in all cases, performed by heterojunctions. The order of the materials in these junctions affects the direction of illumination that can be used in the device. As can be seen from this table, the epitaxial layers which are active in the devices reported have included n-PbTe, p-PbSnTe and n-PbTe/p-PbSnTe. In the first three entries in Table 1-8, a bulk crystal of p-$Pb_{1-x}Sn_xTe$ or n-PbTe constitute, the substrate on to which the n-PbTe or p-$Pb_{1-x}Sn_xTe$ (respectively) is deposited by liquid-phase epitaxy to form the junction. The D* values reported for these devices are some of the highest reported for any photovoltaic long wavelength detector. In the last entry in Table 1-8,

TABLE 1-8   STATUS SURVEY: E-O DEVICE CONFIGURATIONS WITH LPE

FILM MATERIALS	DEPOSITION TECHNIQUES	JUNCTION PREPARATION	D^* (cm Hz$^{1/2}$W^{-1})	R·A ohm·cm^2	COMMENTS
PbTe	LPE	n–PbTe/p–PbSnTe$_{ss}$ (HETERO)	5×10^{10}	— (η = 85%)	NA (73)
PbTe	LPE	n–PbTe/p–PbSnTe$_{ss}$ (HETERO)	8×10^{10} (80°K) 34° f.o.v.	4.5 (η = 51%)	SBR
PbSnTe	LPE	p–PbSnTe/n–PbTe$_{ss}$ (INVERTED HETERO)	2×10^{10} (77°K) 70° f.o.v.	14.0	NA (74)
PbTe/PbSnTe	LPE	n–PbTe/p–PbSnTe/ PbSnTe$_{ss}$ (HETERO)	2×10^{10}	3.0 (η = 23%)	AEROJET (74)

F123576-1 775

both the p- and n-type materials which are active in the device are epitaxial layers. As also noted the D* value reported for this device can be considered quite adequate for most applications--this result would indicate that if layers of comparable properties are deposited by any technique, devices of comparable performance can be expected.

As a final input we list in Table 1-9 the device studies presently underway, utilizing thin film PbSnTe exclusively--this in contrast with the liquid epitaxial work in which bulk crystals are required as a substrate or as one or the other portion of a heterojunction. As noted, the work represented includes the formation of p-n junctions (homo- and hetero-), Schottky barrier junctions, p-n junctions produced by proton bombardment, and in one case the preparation of enhanced photoconductive device. In most cases the work, to date, on these PbSnTe devices is still in the feasibility stage, thus the presentation of quantitative data is premature. However, the investigations in this laboratory as well as elsewhere are very promising. Some initial results of our work are presented later. It shows that in a very short time, orders of magnitude improvements were achieved, implying that a thorough effort should rapidly lead to high sensitivity or Blip elements. All devices listed in Table 1-9 have been feasibility demonstrated. As can be noted also, all devices prepared in this laboratory utilize the sputtering technique--however, of all the work done in our laboratory, the last two techniques, i.e., p-n diode preparation by bias sputtering and the photoconductor preparation by oxygen enhancement are, by far, the most promising. They have all the potential cost effectiveness ingredients one would desire. Detailed discussions of these techniques and further results are presented later in this report.

TABLE 1-9   STATUS SURVEY: DEMONSTRATED FEASIBILITY CONFIGURATION (PbSnTe)

$Pb_{1-x}Sn_x Te$ COMPOSITION	DEPOSITION TECHNIQUE	JUNCTION PREPARATION	COMMENTS
$\chi = 0.017$	EVAPORATION	SCHOTTKY – Pb	FORD
—	EVAPORATION	SCHOTTKY – In, Pb	NVL
$0.1 < X < 0.2$	SPUTTERING	SCHOTTKY – In, Pb	GD
$0.1 < X < 0.2$	SPUTTERING	p–n–Proton	GD
$0.1 < X < 0.2$	SPUTTERING	p–n–Bias	GD
$0.0 < X < 0.2$	SPUTTERING	pc (O_2 ENHANCED)	GD (Photo-Cond)

F123578-1 775

1-22

1.3 SUMMARY OF GENERAL RESULTS

The following will provide a very limited summary of the results achieved during the course of this program. Only a few highlights of general nature will be alluded to, with the more specific data being deferred to Section 3.0 for discussion. As will be obvious from even these few examples, observations which should be of considerable interest to the materials researcher as well as findings which are of importance to the manufacture of detector devices have resulted from this work. It should also be apparent that the systematic experimental approach employed throughout this work led to results which show an equally systematic interdependence between film preparation parameters and all film properties of interest to sensor applications.

The most important, first result, which established sputtering as a viable technique for the preparation of thin film $Pb_{1-x}Sn_xTe$ detectors, is the feasibility to deposit structurally high quality single crystal films with any specified composition or x-value in the range $0 < x < 0.30$. That this can be done with a single sputtering target having a composition anywhere within this range and by simple control of two readily measurable deposition parameters - the substrate temperature, T, and the film growth-rate, R - makes this result even more valuable. If the as-deposited films are annealed, excellent transport and electrical properties can be produced, by stoichiometry control, over the entire range of compositions.

It was however found, that a target of any composition will, in conjunction with a critical set of deposition conditions $(R \cdot T)_0$, yield stoichiometrically optimized, as-deposited films with a reasonable range of compositions up to an x-value equal to that of the particular target. That is, as-deposited films can be produced with low carrier concentrations and high mobilities equivalent to those which can be produced by annealing. Thus, we have a second method to produce sensor quality films which avoids the need for the annealing process. Moreover, as with suitable annealing conditions, the $(R \cdot T)$ product can be used in this method to produce, in a predictable manner, either p- or n-type films of low carrier concentration.

1-23

Introducing substrate bias as a third deposition parameter increased both the versatility and the control simplicity of the sputtering process. This bias, which only requires nominal values on the order of ± 30 volts, can be adjusted to yield a critical value, V_o, which by itself has the effect of stoichiometry optimization for any desired film composition. That is, with a single target of convenient composition and with any convenient set of deposition conditions (R,T), simple control of the bias voltage can yield films of lowest carrier concentration, of correspondingly high mobilities and of the desired carrier type for a large range of compositions. As an added advantage over films sputtered without bias, n- and p-type films can have identical compositions if desired. By contrast, without bias the film must be deposited under conditions with a finite $\pm$ deviation from the critical $(R \cdot T)_o$ product to produce p- or n-type film which consequently have small composition differences. The latter aspect is important in the preparation of p-n junction diodes in a single sputtering run.

It is thus apparent that three basic approaches have been sequentially defined to prepare device worthy $Pb_{1-x}Sn_xTe$ films by sputtering: One, by which sputtering conditions yield structural quality and composition control while annealing optimizes the electrical and transport properties as well as defines the carrier type; Two others, by which the sputtering conditions alone, i.e. without annealing, control structure, composition, carrier type and optimized electrical and transport properties.

While none of the three techniques was optimized to the degree possible, the primary quality indicators yielded in all three cases values which are equal to and better than those in bulk materials presently used in commercial PbSnTe detectors. Aside from excellent film structures, carrier concentrations in the low 10^{16} cm^{-3} range and mobilities exceeding 10^4 cm^2/volt-sec are readily achieved at 77°K - with even lower carrier concentrations observed in selected instances. In particular, bias sputtering showed a phonon limited mobility dependence on temperature ($T^{-5/2}$ relation) to temperatures as low as 30°K.

1-24

The possibility of further property improvements by all three techniques will be quite obvious from the restuls. For example, near intrinsic $77^{\circ}K$ carrier concentrations seem to be feasible. However, considering the control requirements to achieve such improvements, bias sputtering stands out as the most promising technique. Both annealing and the use of the critical $(R \cdot T)_0$ product without annealing, require uniform temperature control over the entire film area with an accuracy on the order of $0.1^{\circ}C$ for reaching ultimate properties - not easily achieved in production. By contrast, with bias sputtering the required equivalently accurate voltage control to a fraction of a volt is quite readily achieved and only reasonable tolerances in deposition temperatures must be accommodated.

As a final trade-off consideration, aside from avoiding a lengthy high temperature annealing cycle, the latter two sputtering techniques permit the sequential deposition of p-n junction layers in one pumpdown. The value of this is obvious. Coupled with the fact that each layer can be precisely thickness controlled for highest quantum efficiency and minimal noise contributions from diode material not contributing to carrier conversion, both techniques show considerable promise for high sensitivity photo-diode fabrication. Again, bias sputtering is superior, since the basic deposition conditions (R,T) can be kept constant during the entire deposition process, while the easiest to control parameter - the bias voltage - is changed to change carrier type at the desired thickness. The feasibility of diode formation by both techniques has been demonstrated and is reported.

The electro-optical characteristics achieved in films deposited by all three techniques - as reflected by photoconductive response and noise values - correspond entirely to the quality of the structural and electrical properties they yielded. Peak responsivities of up to 4 v/w - depending, of course, to some degree on composition - were observed as were noise values approaching Johnson noise to relatively high bias currents. These values, measured at $77^{\circ}K$ compare well with those observed in the best single crystal bulk materials of PbSnTe - parti-

cularly since no antireflection coatings were applied and no effort was made to optimize the film thickness. Noteworthy is also that the highest values reported pertain to as-deposited films. All measured response cut-off wavelengths are directly correlatable to film composition - which, as indicated, can be readily controlled. Another quality indicator is the fact that the photoconductive response of the films increases by about two orders of magnitude if the sensor temperature is reduced from $77^{\circ}K$ to $30^{\circ}K$.

The three, increasingly advantageous sputtering techniques leading to the results discussed above have their principal potential in the preparation of photo-voltaic sensors employing p-n homo- or hetero-junctions as well as Schottky barriers. A fourth sputtering method was also explored with encouraging results which promises, in addition, to lead to high responsivity photoconductive sensors. This technique, by employing controlled partial pressures of gaseous additives in the inert (Ar) sputtering environment - in particular O_2 and N_2 - introduces impurities in the as-deposited $Pb_{1-x}Sn_xTe$ films which considerably enhance their photoconductive response. The apparent mechanism is carrier compensation and trap formation. ppO_2 values below 10^{-5} torr and ppN_2 values on the order of 10^{-4} torr cause reductions in the effective carrier concentration of some two orders of magnitude relative to films sputtered under identical conditions but without additives.

Those reductions are systematic functions of the partial pressures and can be readily controlled. The addition of O_2 leads to p-type and the addition of N_2 to n-type films. More important though is the fact that for equivalent carrier concentrations, such compensated films yield photoconductive responses of over an order of magnitude higher than "undoped" films. With carefully controlled experiments relative to additive pressures - values in excess of 20 v/watt were achieved. However, what is even more encouraging is the fact that in some relatively uncontrolled experiments - which led to this investigation - PbSnTe film with photoconductive responses as high as 1000 v/watt were observed. These $77^{\circ}K$ values we e again measured without the benefit

of antireflection coatings or film thicknesses optimization. While
trap enhancement appears to take place, there is, from the standpoint
of typical sensor applications, no significant effect on the transport
properties. The temperature dependence of the carrier mobility is still
phonon limited to near 30°K ($\mu \sim T^{-5/2}$) and the responsivity values
are unaffected to chopping frequencies as high as 100 Mhz - the limit
of evaluation. Dark noise values, which have a 1/f component below
1 Khz, remain also low - being on the order of 5 nV/$\sqrt{hz}$ above 1 KHz.

Having initially anticipated the need for annealing of as-deposited
film to produce sensor worthy materials, an extensive annealing study
was also executed. Optimized annealing and quenching cycles were explored
as were various annealing charge compositions. While this work led
to various interesting results, one of these stands out as potentially
significant particularly from a scientific point of view. The equili-
brium phase diagram of $Pb_{1-x}Sn_xTe$, as established by others, defines
a critical temperature T_x at which the solidus crosses over from a
tellurium saturated to a metal saturated state. T_x, a function of the
composition, defines a stoichiometric mixture - above and below which
the compound becomes p- and n-type respectively. Of course, T_x, is
used as the critical annealing temperature and is typically above
500°C in $Pb_{1-x}Sn_xTe$. A series of annealing experiments at lower and
lower temperatures led, in the course of this program, to the
discovery of a second crossover temperature, T_x' in the equilibrium
phase diagram - which, as its high temperature counterpart, produces
apparent stoichiometry and type switching. T_x' is on the order of 350°C
depending on the $Pb_{1-x}Sn_xTe$ composition. Its existence will provide
for a completion of the equilibrium phase diagram of PbSnTe - which
to date was only cursorily extrapolated to low temperatures. Its
discovery in bulk crystal studies was hampered by the fact that at
such low temperatures, annealing times on the order of months would
be required to achieve stoichiometric conditions. In thin films the
annealing times are less than one day. From a practical standpoint,

this low temperature crossover seems to explain why it is possible to obtain stoichiometric, as-deposited films by sputtering. Typically, film substrates are held at temperatures in excess of 300°C during deposition - as governed by the requirements for epitaxial film formation. Apparently, during the deposition process the films are effectively annealed at or near the temperature T_x'. This is also compatible with the existence of the critical deposition conditions $(R \cdot T)_o$ discussed above.

Finally, of particular interest should also be the results of a feasibility study relative to the exploitation of the techniques developed under this program in the fabrication of sensors. Sample results of this feasibility study, although it was carried as a parallel effort under corporate sponsorship, are reported here since they clearly show that the sputtering approaches have the anticipated device potential. While only very simple configurations were employed without, for example, surface passivation and optimized geometry, it was demonstrated that photovoltaic response can be obtained both with sequentially (bias) sputtered p-n (homo) junction diodes and with thin film $Pb_{1-x}Sn_xTe$ Schottky barrier diodes using either transparent Pb or In barrier metals. At this early stage, the absolute responsivities, though rapidly increasing, are still below the level desired for device application. But, since no full-up device development effort had as yet been initiated as these results were obtained, the confidence level is very high that Blip limited devices of this nature can be produced by sputtering in both single detector and array configurations.

In the remainder of the report the results of several other approaches for the preparation of detector materials - specifically ion implantation, and ion beam sputtering techniques - will also be presented. However, these approaches were only investigated to a very limited degree and the results are correspondingly limited at this time.

2.0

EXPERIMENTAL TECHNIQUES

2.1 INTRODUCTION.

A large number of experimental tasks, ranging from the preparation of starting materials to the measurement of functional performance (e.g. photo-response) of thin film $Pb_{1-x}Sn_xTe$, were involved in this program. In fact, the success of accomplishing the objectives of this program depended, to a major degree, on the experimental procedures and techniques utilized. In this section, these experimental techniques and the description of the equipment used, will be presented in some detail.

As will become apparent from the discussion in this section as well as in the section covering the results, many changes and improvements, both in techniques and equipment, were implemented during the course of this program. These have included improvements in material preparation, target preparation, modifications in sputtering equipment and others. Also, during the course of this program, a new facility for performing electrical and electro-optical measurements from room temperature down to $4^{o}K$ was installed to supplement a liquid N_2 facility which was initially employed.

As will be seen, great emphasis was placed on the utilization of high purity material, on ultra-clean environments and handling techniques used in the preparation of targets and annealing charges, on clean deposition environments and on a complete and thorough analysis of the deposited $Pb_{1-x}Sn_xTe$ films.

Furthermore, each of the data points presented generally represents the result of a large number of experiments in order to establish reproducibility. Finally, as will also be seen, an abundance of consistent information obtained from this study, is indicative, not only of a very systematic approach adopted for this study, but also of the care taken in pursuing the experimental phases of the work.

2.2 MATERIAL PREPARATION.

2.2.1 AS-RECEIVED MATERIALS. All $Pb_{1-x}Sn_xTe$ sputtering targets and annealing charges, utilized for this program, were prepared in this laboratory directly from the elements, or, in some cases, from the compounds PbTe and SnTe. The standard procedures used for preparing the elements and/or compounds before utilizing them for target and/or annealing charge preparation is as follows:

The elements are zone refined 6N Pb, Sn and Te purchased from two suppliers, Cominco American Inc., Spokane, Washington, and Atomergic Chemicals, New York, New York. Typical lot analyses are made available for each material from both suppliers as are actual lot analyses when available. Table 2-1 shows one typical lot analysis for each material and two actual analyses. The method used to determine impurities was carbon arc emission spectrometry, with an approximate limit of detectibility of 0.1 parts per million (ppm) by weight.

The compounds PbTe and SnTe are purchased from Semi-elements, Inc., Allendale, New Jersey. Both are 5N sevac grade material. A typical analysis of the starting materials used for the preparation of the compounds is given in Table 2-2.

These as-received starting materials are subject to subsequent treatment in our laboratory, before use in the preparation of sputtering targets and annealing charges. In the case of the as-received Pb and Sn this consists of etching before reaction. An etch found to be useful for Pb consists of 40% $HC_2H_3O_2$, 40% H_2O_2, and 20% H_2O. After a five minute etch with vigorous stirring, the acid is successively diluted and flushed with distilled water. Sn is etched in 4% reagent grade HCl for one minute and then a few drops of dilute reagent grade HNO_3 are added followed by vigorous stirring for another minute. The etch is then quenched by successive dilution and flushing with distilled water.

2-2

Table 2-1

TYPICAL LOT ANALYSIS
6-9 GRADE
COMINCO AMERICAN INC.

Pb		Sn		Te	
ppm		ppm		ppm	
Bi	.2	In	.2	Se < 1	
Sb	.1	Pb	.2	S	.3
Ca	.1	Bi	.1	Al	.1
Fe	.1	Ca	.1	Bi	.1
Si	.1	Cu	.1	Ca	.1
Cu<	.1	Fe	.1	Fe	.1
Mg<	.1	Mg	.1	Mg	.1
Ag<	.1	Si	.1	Pb	.1
				Si	.1
				Cu <	.1

TYPICAL LOT ANALYSIS
6-9 GRADE
ATOMERGIC CHEMICALS

Bi .2	Pb < .3	S < .5
Sb .2	Bi < .1	Cu < .1
Ag .1	Cu < .1	Fe < .1
Cu .1	Fe < .1	Mg < .1
Fe .1	Sb < .1	Pb < .1
Other metals < .2		Si < .1
		Other metals nil

ACTUAL LOT ANALYSIS
COMINCO AMERICAN INC.

Pb		Sn	
log HPM 3776		lot HPM 2725	
Si	.2	Al	.1
Ag <	.1	Bi	.1
Cu <	.1	Ca	.1
Mg <	.1	Si	.1
		Ag <	.1
		Mg <	.1

Table 2-2

TYPICAL ANALYSIS OF STARTING MATERIALS

FOR PbTe and SnTe REACTION

SEMI-ELEMENTS, INC.

Pb	Tin	Te
Sb 0.5 ppm	Sb 1.0	Cu 0.1
Bi 2.0	Bi 0.3	Fe 0.1
Cu 0.5	Cu 0.5	Pb 0.1
Fe 0.3	In 0.5	Mg 0.1
Ag 0.2	Fe 0.3	Si 0.2
Th 1.0	Pb 2.0	S 0.5
		Se<2.0

Te is purchased in ingot form and when the material is needed, suitable chunks are broken off and only material with freshly cleaved surfaces is used for the reaction mixture. However, for Te with an oxide layer, melting in a reducing atmosphere has been found to remove the oxides.

Freshly etched Pb and Sn is kept under distilled water until ready to be weighed, along with Te, and immediately placed in a quartz reaction vessel, evacuated, and sealed under vacuum ($< 10^{-6}$ torr).

As discussed in Section 2.1, a continuous effort to improve all experimental aspects of this program for producing $Pb_{1-x}Sn_xTe$ films with superior properties, has been in progress throughout the course of this program. This has included the preparation and handling techniques utilized with our starting materials. Such improvements have involved the following additional purification steps and/or modifications in handling procedures.

1. Much of the earlier work utilized singly zone refined 6N Te; later we introduced the use of doubly zone refined Te. During the course of the study, as a further purification step,, the Te in most cases was melted in a reducing atmosphere to remove any oxygen inclusions.

2. As stated, the as-received Pb and Sn are etched immediately before use to remove surface oxides; an additional sublimation purification step was added to the preparation procedures for both Pb and Sn. To this end, the metal is sealed in a cleaned, evacuated quartz tube which is constricted at one end. The tube is then placed in a furnace and a temperature gradient is established such that the hot end of the tube which contains the metal is held slightly above the melting point while the cold end is held some $50^{\circ}C$ below this value. After about 80% to 90% of the metal is sublimed to the cold end, the tube is removed from the furnace and quenched. The unsublimed residue, assumedly containing the bulk of the impurities, is discarded.

A similar sublimation step is now also being used in a final purification of the reacted PbSnTe, prior to the preparation of targets and annealing charges.

3. In the preparation of PbSnTe from the elements, a large number of steps such as weighing, etching and transfer into reaction tubes occurs during which contamination from the environment is possible; to minimize such contamination, the handling of all starting materials as well as the sealing into the reaction tubes takes place in an oxygen and water free environmental chamber. Thus from the preparation of the starting materials to the completion of the sputtering target, all exposure to the ambient air environment is prevented.

The effects of these improvements, as will be seen later in this report, are reflected in the results from the various targets and annealing charges which utilized the improved starting materials.

2.2.2 PREPARATION OF ANNEALING CHARGES. The preparation of such charges involves first the reaction of the elements to form the desired $Pb_{1-x}Sn_xTe$ compound. As discussed above, after the starting materials have been properly treated they are immediately placed in a quartz reaction vessel for sealing under a vacuum. After the quartz vessel is sealed, the materials are pre-reacted by passing a torch flame over the outside of the quartz container. As the material heats up, reaction is indicated by an orange glow of the mixture. The quartz container is then placed in a $1000^{\circ}C$ vacuum furnace for at least 3 hours, where final reaction takes place. During this time the tube is occasionally rotated to insure a homogeneous alloy. The tube is then removed and immediately water quenched. The material is kept under vacuum in the tube until it is ready to be used.

Metal rich and tellurium rich annealing charges are prepared in the same manner as the stoichiometric charges described above. After etching, the desired percentage of excess metal $Pb_{1-x}Sn_x$ or excess Te, is carefully weighed out and added to the stoichiometric $Pb_{1-x}Sn_xTe$ mixture before the initial reaction.

As already mentioned in the last section, an additional purification step was added to the preparation of annealing charges as well as sputtering targets - the sublimation of the reacted $Pb_{1-x}Sn_xTe$ and the disposal of that unsublimed residue. However, as also stated, in some cases this sublimation purification is performed on the starting elements which are then reacted to produce the annealing charge or target material.

In addition to the utilization of high purity starting materials discussed above, and the use of techniques which prevent contamination before and during reaction, the most essential consideration is to insure complete mixing and reaction. That is, the homogeneity of the charge material in terms of composition and alloy phase is extremely important. To this end, an improved mixing technique during reaction was implemented during the course of this program. An automatically controlled furnace shaker which is capable of supporting any of our reaction furnaces is used to thoroughly mix, for the duration of the entire reaction time, any size reaction tube or flask.

Finally, an additional annealing step, to further control material stoichiometry and homogeneity, was introduced in the preparation of annealing charges. For this purpose the mixing and sublimation purifi-cation steps if used, are followed by annealing in sealed quartz tubes for over a week. X-ray analysis showed that this procedure not only produced a single phase and a more uniform composition throughout the sample, but it resulted also in material which could be more accurately analyzed by x-ray techniques due to the improved structural character-istics resulting from the annealing.

2.2.3 SPUTTERING TARGET PREPARATION. Materials used for the $Pb_{1-x}Sn_xTe$ sputtering targets are also prepared from either the elements Pb, Sn and Te or, in some cases, from the constituent compounds PbTe and SnTe. In general, the initial procedure used for preparation of our early targets was the same as that used for the preparation of annealing charges except that special sealing flasks were used to form the desired target shape. The heating and cooling cycles require careful

2-7

control to insure the formation of a mechanically stable target after the reaction is completed.

After prereaction of the elements by using a blow torch on the outer walls of the sealed flask, the reaction is carried out at $1000^{\circ}C$ for six hours in a vacuum furnace, followed by a three hour programmed cooling period at the rate of $200^{\circ}C/hour$. After the target is removed from the flask it is lapped to its final dimensions and finally electrochemically etched to obtain a clean shiny surface. The target is then attached to a high purity copper backplate using a conductive silver epoxy. The epoxy is carefully located such that it provides a good electrical and thermal contact but is not exposed to the sputtering plasma. Otherwise it contributes to film contamination.

Again, as in the case of starting materials and annealing charges, new experimental procedures, including improved handling and target preparation techniques were implemented during the course of this program. These, of course, included all the modifications and improvements discussed above in connection with the preparation of as-received starting materials and the preparation of annealing charges. Some of these modifications are of even greater importance for sputtering targets since, for their preparation, large amounts of materials are reacted and uniformity and stoichiometry control is quite difficult. Thus the automatic, thorough mixing during the reaction and the additional annealing step after the reacting cycle have proven to be quite essential. Since their introduction, x-ray analysis of various samples from any one batch has shown excellent uniformity within each batch. Of course, the procedure to avoid exposure to the ambient air environment or other sources of impurity contamination from the initial preparation of the starting materials to the completion of the sputtering target, has also been utilized for preparation of some of the later targets.

In mounting the PbSnTe target to the copper backplate, a conductive silver epoxy, as discussed, had been used in preparing the targets utilized

early in the program. However, for later targets an improved technique which utilizes a specially prepared high purity $Pb_{1-x}Sn_x$ solder alloy was and is still being used. The target is heated and soldered to the backplate in a high vacuum environment. Sufficient electrical and thermal contact has been obtained with the added benefit of a significant reduction in potential target and film contamination from the bonding agent.

Again, not all these changes have taken place at the same time or simultaneously for annealing charges and targets, and many of the results to be presented in the present study were obtained without the benefit of some of these modifications.

A second type of sputtering target was prepared using as-purchased PbTe and SnTe, which were weighed into proportions corresponding to the desired composition, e.g. $(PbTe)_{.80}(SnTe)_{.20}$, and sealed in the fused quartz flask as described above. After a six hour reaction at $1000^{\circ}C$ the target was cooled at the rate of $400^{\circ}C$/hour, removed from the reaction flask and mounted on a sputtering probe as discussed.

2.2.4 QUARTZWARE PREPARATION. All quartzware used in this work is prepared in the same manner. For the preparation of sputtering targets, a vitreous silica Erlenmeyer shaped flask with a specially constructed neck is used. For preparation of annealing charges and for the annealing experiments themselves nominally 13 mm bore vitreous silica quartz tubing is used. All quartz is purchased from Thermal American Fused Quartz Co., Montville, New Jersey, or Quartz General Co., El Monte, California.

The quartz is first thoroughly washed in a soapy solution, rinsed and etched inside and out by filling the tube or flask with concentrated HF to one-fourth of the volume and with concentrated HNO_3 up to one-half the volume. A splash of glacial acetic acid and distilled H_2O to overflowing is then added. After mixing, the etch is allowed to stand for one minute, is poured out and the quartz is rinsed five times with distilled H_2O. Upon air-drying the tubes are vacuum-baked for 2 or 3 hours at $1100^{\circ}C$ using a diffusion pump, Liq. N_2 trapped vacuum system.

2.2.5 SUBSTRATE PREPARATION. Substrate materials were primarily limited to single crystal CaF_2 and BaF_2. Both substrate materials were obtained from two sources, Semielements Inc., and Harshaw Chemical Corp. Both CaF_2 and BaF_2 are received in half inch diameter rod with the [111] direction parallel to the axis of the rod. In addition, CaF_2 is also received with its [100] direction parallel to the rod axis.

The [111] materials are cleaved into substrate wafers about .050 inches thick (as the last step in setting up the sputtering systems).

The CaF_2 [100] is cut, with a diamond saw into .050 inch wafers. The [100] wafers are checked for orientation by cleaving them in two different directions and measuring the angle between the cleavage plane and the cutting plane. The wafers are then lapped, on a mechanical lapping wheel, with successively finer grinding compounds ranging from 5μ to 0.5μ. Finally they are polished on a silk covered polishing wheel.

2.3 DEPOSITION APPARATUS AND PROCEDURES

2.3.1 SUPPORTED DISCHARGE SPUTTERING. The supported discharge sputtering system used in this work is diagramed in Figure 2-1. Ultra high purity Argon passes through a gas purifier for additional purifi- cation and is introduced into the top plate of the system. A diffuse plasma is produced, between a tunsten thermionic emitter and a low voltage anode, in the horizontal arms of the 6" x 6" hard Pyrex cross.

The material to be sputtered (target) is attached to the water- cooled target probe which is inserted through the top arm of the pyrex pipe cross. The system can operate in both a DC and RF mode. Since $Pb_{1-x}Sn_xTe$ is electrically conductive, the direct current mode is employed. The target voltage is maintained by a d.c. supply with a maximum 10 kilovolt, 50 ma capacity. All substrate holders are fabri- cated from tantalum. The sputtered material is collected on substrates in a tantalum holder on the horizontal receiving surface. Each subst- rate holder can accommodate up to nine substrates and a shutter allows for carrying out three experiments with three different deposition con- ditions each with a set of 3 substrates - all in one pump down. A
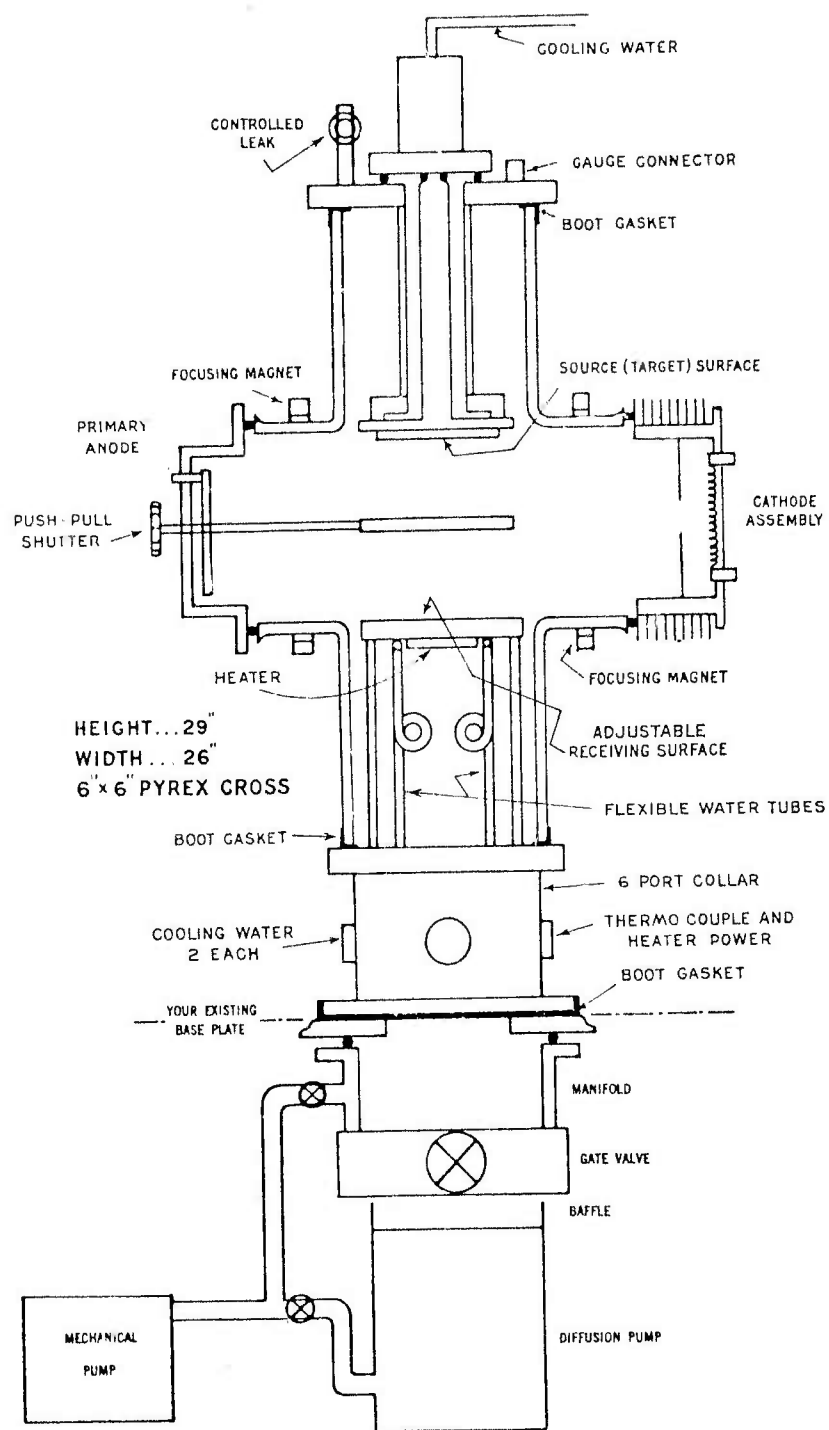
Figure 2-1 Triode Sputtering System for $Pb_{1-x}Sn_xTe$ Thin Film Deposition

heater allows substrate heating up to 450°C. Substrate temperatures are measured with a chromel alumel thermocouple in intimate contact with both the substrate holder and the substrate (next to the film being deposited). The sputtering module was used with two types of vacuum stations - both providing for a background pressure in the low to mid 10^{-7} torr range. Initially the system consisted of a carefully cold trapped (LN_2) 4" diffusion pump station (CVC). Early in the program, these pumps were replaced by turbomolecular pumping stations (Welch). The sputtering gas, exclusively ultra high purity, argon, was controlled by means of needle valves and monitored by appropriate vacuum gauges. Generally the argon pressure was in the range from 1 to 10 microns, depending on specifically desired conditions. During the course of this program, a continuous effort has been and is being made to improve the equipment used in our supported discharge sputtering experiments. Several improvements were introduced during the earlier phases to minimize the probability of introducing impurities in the film during deposition and to improve the substrate temperature control and uniformity, etc. These, as discussed in the Interim Reports for this program (Reference 1), utilized radiative substrate heaters with all tantalum shielding designed to improve temperature uniformity and eliminate any outgassing from the heaters, themselves.

In addition to these early modifications, three important modifications, in the effort to further improve our films, were introduced. First, the sputtering modules were provided with first order mass analysis capability to evaluate the relative purity of the sputtering environment. Secondly, all-metal seals and feedthroughs were introduced into the modules. Finally, both supported discharge systems were provided with substrate bias control.

The mass spectrometer was found to be instrumental in optimizing sputtering procedures relative to bake-out periods, system and target conditioning and other environmental controls - and gave direction to the second modification. This involved the replacement, of the non-metal gaskets at all-metal to glass contacts of the triode cross and

the feedthrough collar by high purity, crushed indium gaskets. It included also the redesign of the original shutter feedthrough system and its replacement by a new all-metal bellows systems. The latter, aside from its environmental advantages provides the system also with a shutter position indexing system which is intended to permit multi-condition deposits during any one pumpdown. It is apparent that the changeover resulted in a reduced background pressure, and a lowering of background species as measured with the mass spectrometer. In addition, the changeover rendered the supported discharge sputtering system to be bakeable to a far larger degree than was previously possible.

The introduction of substrate bias control turned out to be the most valuable of the modifications from the standpoint of impact on the results. The original reason for applying substrate bias was simply the experience gained during earlier work in this laboratory with metal sputtering. Substrate bias had the definite effect, in metals such as tantalum, to substantially decrease or increase the impurity content as exhibited by a conductivity variations. It was hoped, therefore, that a bias would aid in reducing the impurity concentration in as-deposited PbSnTe also. As will be discussed later, this was indeed feasible but in addition bias sputtering had a significant effect on the film stoichiometry and in turn on carrier type as well as concentration. To achieve bias control, the entire tantalum substrate holder-which accommodates nine substrates - was electrically isolated from the substrate heater with ceramic stand-offs. The shutter and system components other than the cathode were positively grounded to avoid the presence of any "floating" metal parts. The DC bias voltage ($\pm$) is applied to the substrate holder. The construction of this holder is such that the substrates are pressed, by means of individual threaded plugs against a multiple-mask Ta plate. On application of a bias voltage, there are essentially no voltage drops across or within the substrate holder. Also the exposed surface of the substrate, even if the latter is dielectric, will become quite conductive soon after the deposition starts.

The reason is that the ternary PbSnTe has a fairly good conductivity particularly at the temperatures above $300^{o}C$ at which the substrates are typically held during deposition. The end result of all this is that the bias does not, within the deposited material, establish any significant field gradients normal or parallel to the substrate that could be credited with producing the rather large effects of biasing on the material properties.

2.3.2 ION BEAM SPUTTERING. The Ion beam system is schematically shown in Figure 2-2. High purity Argon gas is injected into the Duoplasmatron acceleration section, where it is ionized, accelerated (through a voltage ranging from 0 to 30 Kv), electrostatically focused and collimated. The argon ion beam passes into the ultra high vacuum chamber through a small orifice and impinges on the sputtering target. The ion beam current is measured before and after sputtering by introducing a Faraday cup into the beam below the orifice.

The ion beam system described above was equipped with a new ion beam gun in 1973 primarily to improve the deposition rates and to provide independent beam current and energy control. Unfortunately the gun system did have extensive problems on receipt from the vendor. On-site acceptance checks revealed numerous shortcomings and eventually an insulator crack forced rework of the gun. As a consequence, long delays were experienced in implementing ion beam sputtering. However, using an old gun with the new controls made it possible to initiate a sequence of experiments which revealed many basic phenomena to be dealt with in ion beam sputtering of ternary compounds such as PbSnTe - i.e. materials with components having relatively high vapor pressures.

In the present operational model deposition takes place with a typical background pressure of $\leq 1 \times 10^{-8}$ torr and a working pressure (argon beam on, target cooled and substrate heated) of 1.5×10^{-7} torr. Substrate temperatures are readily controlled to considerably above the present range of interest which does not exceed $400^{o}C$. After considerable optimization, film growth rates of up to .5 micron/hr were finally achieved with argon ion beam energies of up to 10 kV. Such rates

2-14
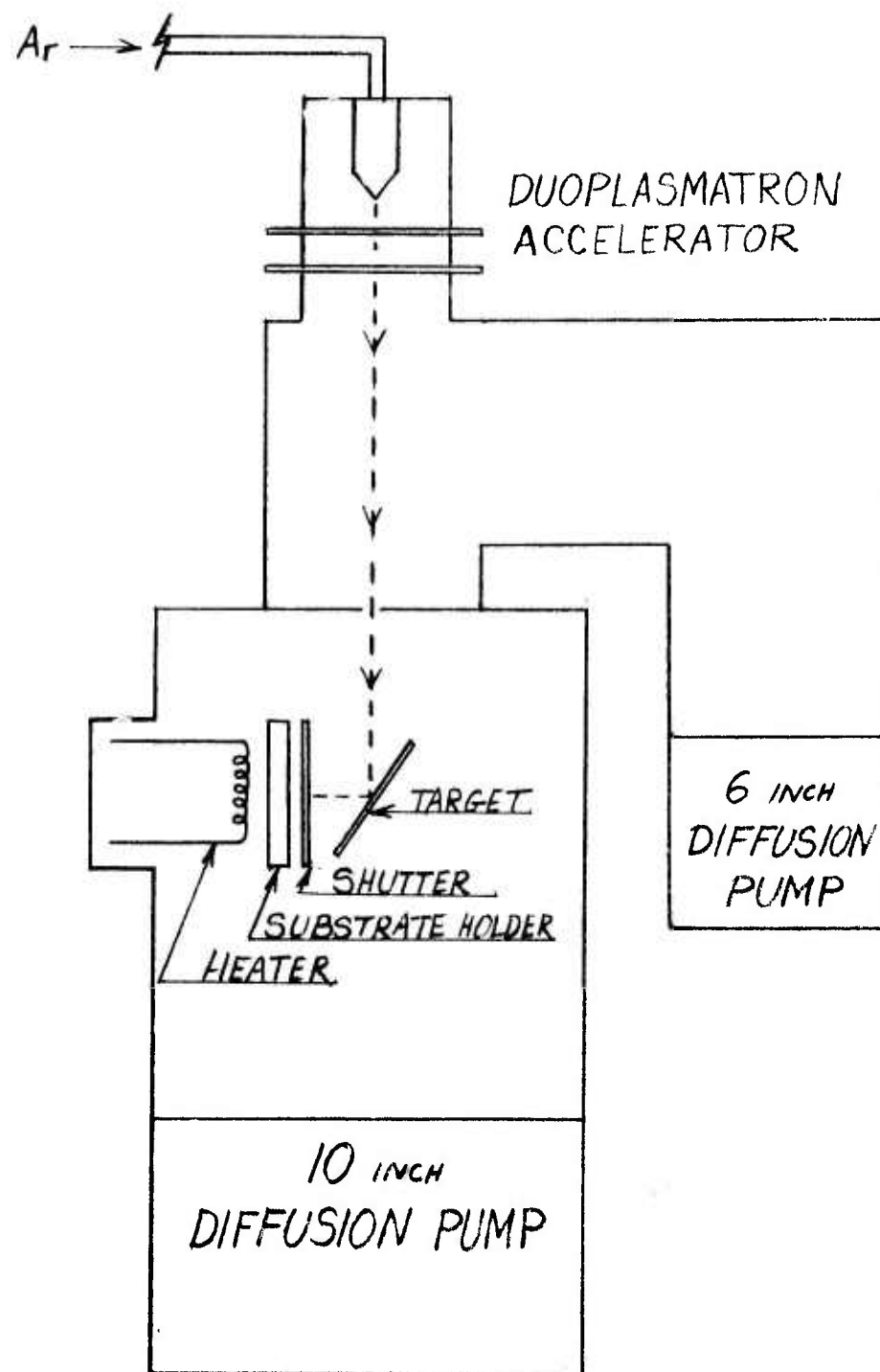
Figure 2-2   Schematic of Ion Beam Sputtering System

represent a considerable improvement over attempts in previous years with the old gun. This is very encouraging since it implies that the new gun provides very acceptable deposition rates for the fabrication of thin film detectors which will generally be considerably thicker than 1 micrometer. Other features are that up to nine substrates can be deposited, in sets of three, during anyone pumpdown and that the beam current can now be varied without changing the beam energy, by controlling the argon pressure in the source chamber. Interestingly, the current change occurs from a maximum value - which is achieved for all accelerating voltages at the lowest argon pressure at which an arc is sustained - to lower values with increasing argon pressures.

During earlier work, special targets had to be prepared for ion beam sputtering which were generally larger than those used in supported discharge sputtering and required different support mounts than the latter.

Due to suitable modifications, it is now possible to use the same sputtering targets in the ion beam sputtering system as in the supported discharge sputtering system. This is a desirable cost saving factor since target materials as well as purification and preparation processes are still relatively expensive. More importantly, though, it is now possible to achieve direct correlation of the effects of the two deposition techniques with the same target. We have found target composition is a critical parameter in sputtering depositions and even small differences could mask the effects relatable to the deposition techniques.

2.4 ANNEALING TECHNIQUES

2.4.1 ANNEALING TUBES. Samples to be annealed are sealed, three or less at a time, in a normally 13 mm bore quartz tube which has been prepared as discussed in Section 2.1.4. The annealing charge is placed at the end of the quartz annealing tube, and separated from the samples by about 2 cm. The annealing charge is first prepared as discussed in Section 2.1.2, then powdered in a pre-etched mortar and pestle, just before placing it in the annealing tube. The loaded tube is then pumped to the low to mid 10^{-7} torr range with a liquid nitrogen trapped

diffusion pump. The tubes are then normally backfilled with high
purity argon to a pressure that will bring it to 1 atm at the annealing
temperature. The tubes are then sealed and placed in the furnace for
the desired period of time.

2.4.2 ANNEALING FURNACE. Isothermal annealing of the $Pb_{1-x}Sn_xTe$
films is performed in a Marshall High Temperature testing furnace,
Norton Vacuum Equipment, Columbus, Ohio. A large block of Beryllium
Copper, with holes to accommodate the annealing sample tubes, is used
in the furnace to minimize spatial and temporal variations in tempera-
ture. The furnace door is kept closed during the entire annealing run
to reduce convection currents as much as possible.

Temperature control of the furnace is maintained by an SCR proporti-
onal power controller coupled with a chromel alumel thermocouple, placed
in the furnace bore region and connected to a Barber Colman Capitrol
millivoltmeter-type controller, which in turn, is connected to the
power controller.

2.4.3 ANNEALING PROCEDURES AND TECHNIQUES. The thin film samples
to be annealed and the annealing charges are vacuum sealed in a 13 mm
bore quartz tube. The annealing charges, prepared by the techniques pre-
viously described, are reduced to a powder and placed about 2 cm from the
sample. The selection of charge composition is either based on the
sample composition, i.e. equal x-values are normally used, or it is
tailored for the desired systematic evaluation of the effects of non-
stoichiometric charge composition by using charges with various degrees
of metal richness or metal deficiency. The basic annealing technique
is iso-thermal annealing with the temperatures and charge compositions
(x-values) selected to be compatible with the film composition of each
sample to be annealed. This selection is based on the equilibrium
phase diagram for $Pb_{1-x}Sn_xTe$ as will be discussed in a later section.
During the latter phase of this program, the emphasis was on generating
comparable data. That is, instead of exploring new charge compositions
and conditions previously used, "standard" 4% and 6% metal rich charges
and "standard" conditions were employed. This allowed for the comparison

of the film properties achieved with the newly introduced deposition procedure and conditions (including, for example the application of various bias voltages) with the results of earlier procedures - without having the comparison negated by effects due to new annealing conditions.

During early work it has been observed that relative fast quenching produced improved and more systematic results. This, in turn, revealed problems with BaF_2 substrates which, although they have a good thermal coefficient match with $Pb_{1-x}Sn_xTe$ film, are more susceptible to thermal shock failure than CaF_2. To overcome this problem, a flat quartz sample shelf was introduced into the annealing tube to provide for a more uniform heat distribution in the sample substrates. This modification was not fully satisfactory since, it did not significantly improve the BaF_2 breakage problem. However, the shelf does implement the faster quenching procedures now used which consist of immediate submersion of annealing tubes into ambient temperature water, after completion of the annealing cycle followed rapidly by immersion into liquid nitrogen.

2.5 CONTROLLED INTRODUCTION OF IMPURITIES

2.5.1 DOPING WITH GASEOUS ADDITIVES DURING SPUTTERING. The controlled introduction of gaseous additives, specifically oxygen and nitrogen, was performed during the sputtering depositions in order to study trap-enhanced photoconductivity. Introduction of the high purity dopant gases was allowed through a needle valved entrance port in a manner similar to the introduction of the argon support gas. It was found that premixing of the argon and the dopant gas prior to introduction to the sputtering chamber was unnecessary, and the gases could be introduced separately. The partial pressure of the dopant gas was maintained at the desired preset level above the background pressure, by adjusting the dopant gas leak rate prior to the introduction of argon and the actual deposition.

2.5.2 DOPING BY DIFFUSION OF IMPURITIES. Metallic impurities with a high vapor pressure, such as cadmium, were introduced by a closed tube vapor transport method similar to that used during annealing cycles. The selected epitaxial sputtered films were masked and coated with a

2-18

3000-5000A layer of RF sputtered SiO_2. The specific areas of the films
to be doped were left uncoated and the SiO_2 masked film was sealed in
the center of the quartz tube under vacuum with a weighed charge of the
metallic dopant placed at one end of the tube. The impurity was then
allowed to vapor transport and deposit onto the unmasked portion of the
films by placing the tubes in a tube furnace at a controlled temperature
with a selected temperature gradient. After the deposition process
occurred, the tube was removed from the furnace, air quenched, and the
sample removed for SiO_2 mask stripping. The SiO_2 was stripped using a
buffered HF acid etch consisting of the following: 1 part (vol) 49% HF,
9 parts sat'd NH_4F solution (approximately 40 gm NH_4F dissolved in 60 ml
H_2O, at $25^{\circ}C$).

Diffusion of the metallic impurity into the PbSnTe host lattice
was performed on a temperature-controlled high purity graphite block in
a vacuum chamber. After the initial thermal calibration using this
set-up, the temperature could be monitored and kept to within $\pm 2^{\circ}C$ of
the desired diffusion temperature. Warm-up and cooling cycles of about
15 minutes were used for many of these experiments, with the actual
diffusion time varying from 15 minutes to several hours.

2.6 FILM STRUCTURAL AND COMPOSITIONAL EVALUATION TECHNIQUES

In this section, the discussion is held to a minimum since standard
techniques are used whose capability and limitations are generally
known. Moreover, specific evaluation conditions or deviations from
standard practice are discussed as they apply in later sections.

2.6.1 STRUCTURAL DETERMINATION. The crystalline structure of
the $Pb_{1-x}Sn_xTe$ films are first evaluated with HS-6 and HU-11A Hitachi
Electron Microscopes. To date only reflection electron diffraction with
the HS-6 unit has been used in this program since the film thicknesses
do not allow for electron transmission analysis. The depth of penetra-
tion of the reflection diffraction electrons (~ 50Å normal to the film
surface) permits rapid evaluation of the structure of the deposited
film without interference from the substrate diffraction maxima.

X-ray diffraction techniques have been used on a number of control samples to verify that the structure of the entire film is adequately described by the structure of the surface. The pattern seen with reflection electron diffraction have been broadly classified into five types for purposes of this report. Given in decending degree of crystallinity they are: single crystal (SC), fibrous (F), broad fiber (BF), polycrystalline preferred (PP), and polycrystalline (PC). Films of each type have been observed with the fibrous films generally occurring far above the epitaxial temperatures and the polycrystalline types below the epitaxial temperatures.

2.6.2 FILM COMPOSITION

2.6.2.1 <u>X-Ray Analysis</u>. X-ray analysis is used to determine the composition (or x-value) of the films. The x-value is obtained from a measurement of the lattice parameter and application of Vegards' law, which is generally considered valid for $Pb_{1-x}Sn_xTe$ with carrier concentrations of less than about 10^{20} cm^{-3}.

A Siemens x-ray diffractometer with a Cu target is used in this work. The characteristic wavelengths are:

$$K\alpha_1 = 1.54051 \overset{o}{A}$$

$$K\alpha_2 = 1.54433 \overset{o}{A}$$

$$K\beta = 1.31217 \overset{o}{A}$$

Only the $K\alpha$ lines are of interest. The $K\beta$ line is (almost) completely filtered with an Ni filter.

2θ scans are also carried out to determine film orientation. Figures 2-3 and 2-4 show examples of (111) epitaxial film on (111) CaF_2 and BaF_2 substrates. Figure 2-3a represents a typical, cleaved CaF_2 substrate, while Figure 2-3b shows the scan of an epitaxial (111) $Pb_{.84}Sn_{.16}Te$ film on cleaved CaF_2. It must be pointed out, that although the major portion of this film has an epitaxial (111) orientation there

2-20

RELATIVE INTENSITY

Cleaved CaF$_2$ Substrate

35 KVP/20 mA

Kα_2(444)

Kα_1(444)

Kβ(444)

Kα_2(333)

Kα_1(333)

Kβ(333)

2θ

150   140   130   120   110   100   90
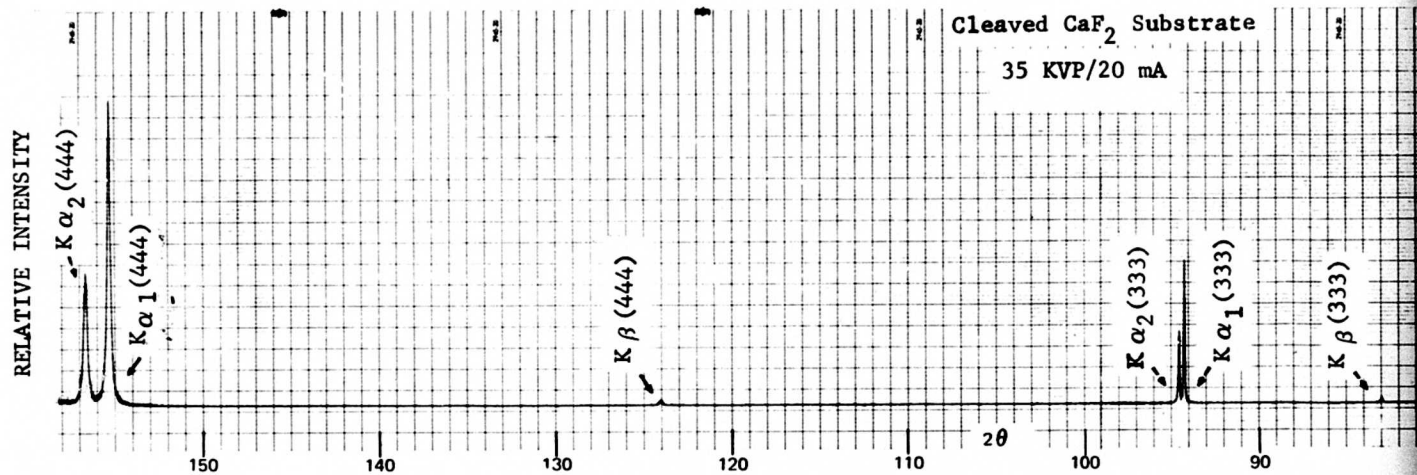
Figure 2-3a Two Theta Scan of Cleaved CaF$_2$ Substrate

RELATIVE INTENSITY

35 KVP/20 mA

CaF$_2$ Kα_2(444)

CaF$_2$ Kα_1(444)

CaF$_2$ Kβ(444)

Kα_2(444)

Kα_1(444)

Kβ(444)

CaF$_2$ Kα_2(333)

CaF$_2$ Kα_1(333)

CaF$_2$ Kβ(333)

2θ

150   140   130   120   110   100   90
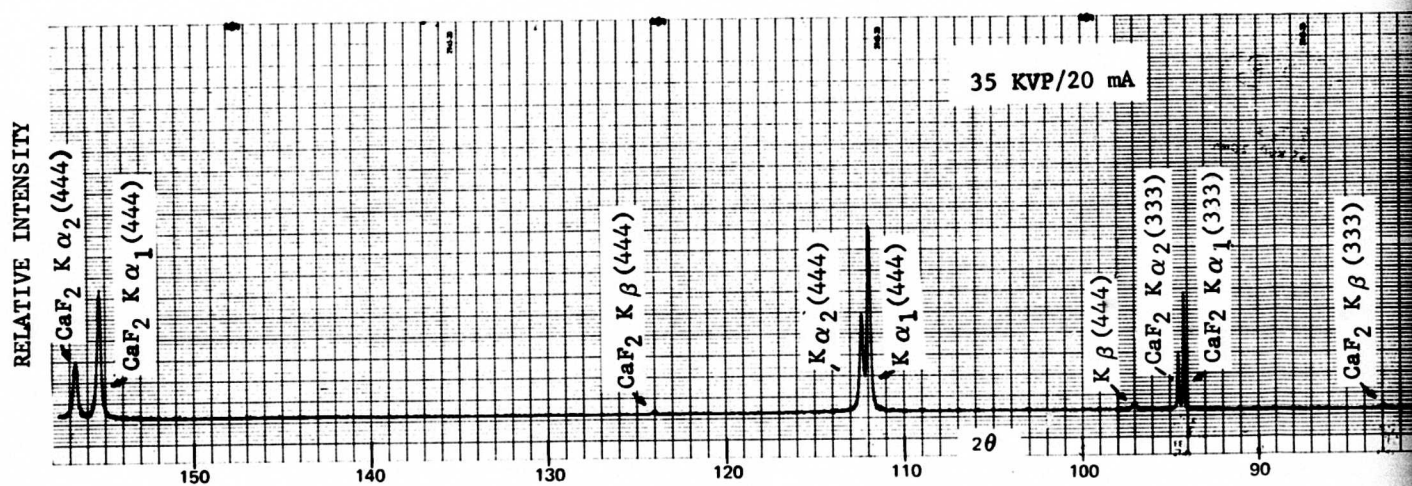
Figure 2-3b Two Theta Scan of Pb$_{.84}$Sn$_{.16}$T   Film on

Figure 2-3 Typical 2θ Scan of CaF$_2$ Substrate With and Wit

CaF$_2$ Substrate

KVP/20 mA

Kα_2(333) Kα_1(333) Kβ(333) Kα_2(222) Kα_1(222) Kα(111) Kβ(111)

100   90   80   70   60   50   40   30

of Cleaved CaF$_2$ Substrate

KVP/20 mA

20 KVP/8 mA

Kβ(444) CaF$_2$ Kα_2(333) CaF$_2$ Kα_1(333) CaF$_2$ Kβ(333) Kα_2(333) Kα_1(333) CaF$_2$ Kα_2(222) CaF$_2$ Kα_1(222) Kα(222) Kβ(222) Kα(200) CaF$_2$ Kα(111) CaF$_2$ Kβ(111) Kα(111)

100   90   80   70   60   50   40   30
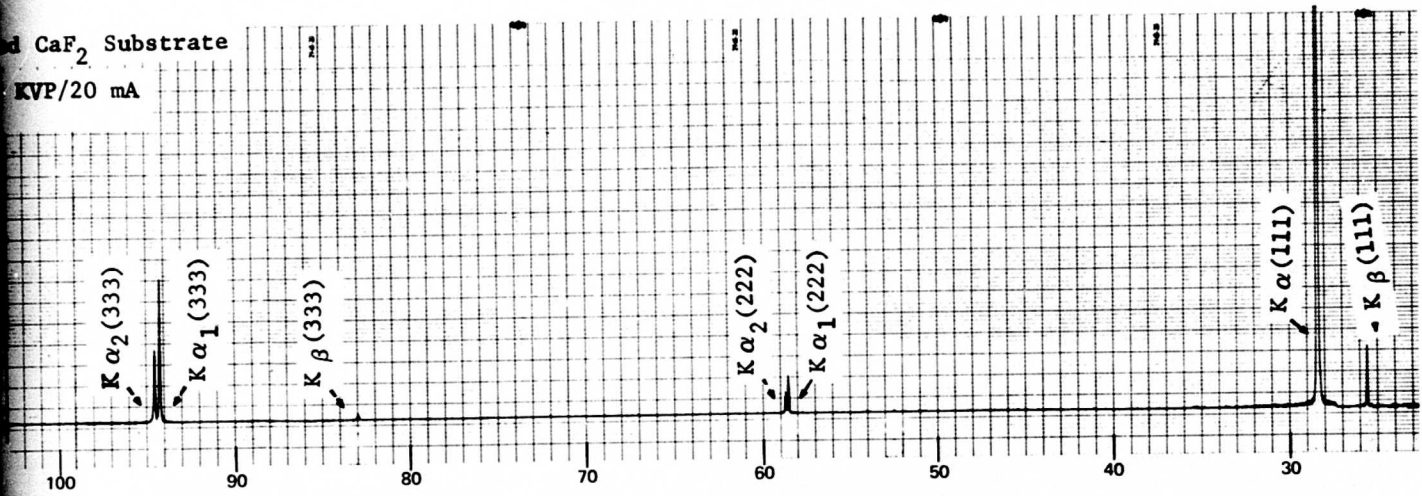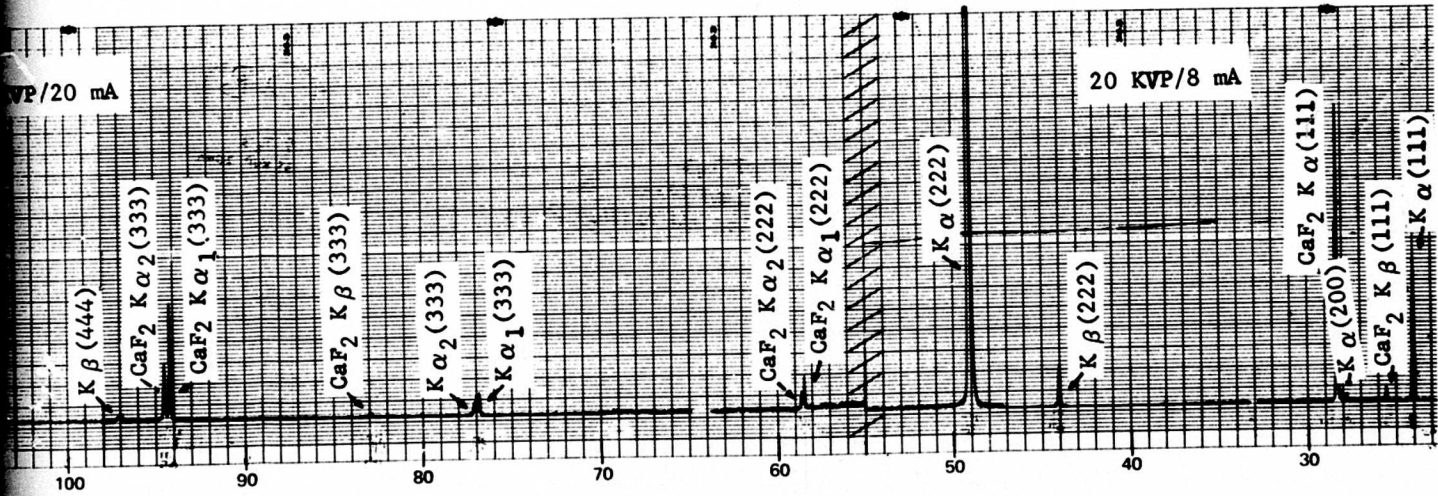
an of Pb$_{.84}$Sn$_{.16}$T Film on CaF$_2$ Substrate

f CaF$_2$ Substrate With and Without Film

2-21/22
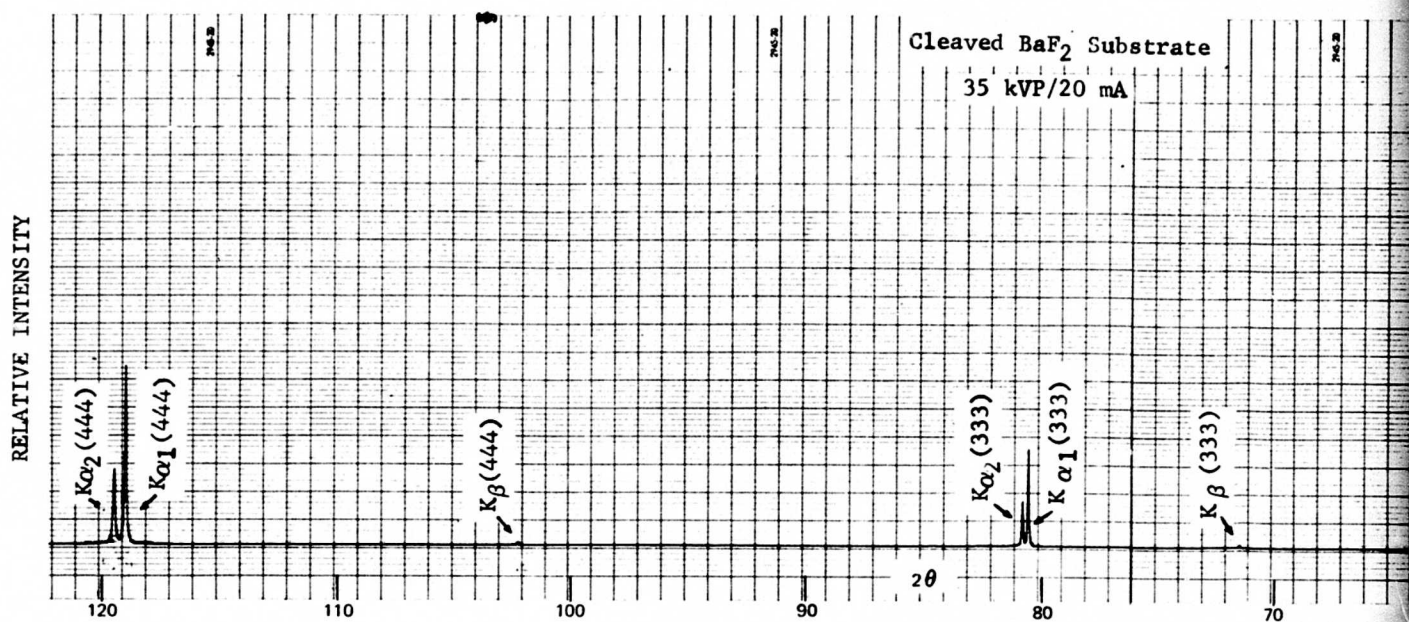
Figure 2-4a   Two Theta Scan of Cleaved BaF$_2$ Substrate
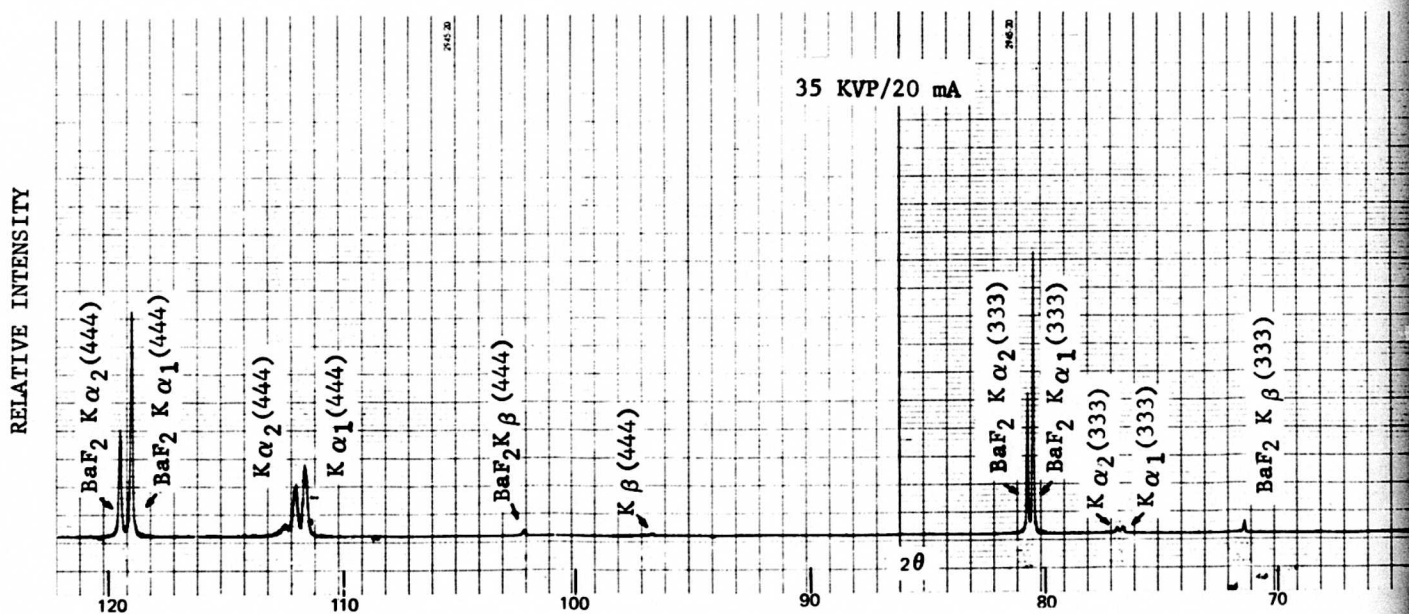
Figure 2-4b Two Theta Scan of Pb$_{.86}$Sn$_{.14}$Te Film on BaF$_2$

Figure 2-4   Typical 2θ Scan of BaF$_2$ S

Substrate

0 mA

$K_\beta (333)$

$K_\alpha (222)$

$K_\beta (222)$

$K_\alpha (111)$

$K_\beta (111)$

70   60   50   40   30

of Cleaved BaF$_2$ Substrate

$K_\alpha_2 (333)$

$K_\alpha_1 (333)$

BaF$_2$ K$_\beta$ (333)

BaF$_2$ K$_\alpha$ (222)

$K_\alpha (222)$

BaF$_2$ K$_\beta$ (222)

$K_\beta (222)$

BaF$_2$ K$_\alpha$ (111)

$K_\alpha (111)$

BaF$_2$ K$_\beta$ (111)

70   60   50   40   30

.86^{Sn}.14 Film on BaF$_2$ Substrate

Typical 20 Scan of BaF$_2$ Substrate With and Without Film

2-23/24

is some occurrence of (100) film. Figure 2-4a and 2-4b show similar 2θ scans for a BaF_2 substrate and for an epitaxial $Pb_{.86}Sn_{.14}Te$ film on this substrate.

2.6.2.2 <u>Infrared Transmission and Reflection Measurement</u>. To characterize the optical properties of $Pb_{1-x}Sn_xTe$ films (i.e. index of refraction and absorption coefficient), infrared transmission and reflection measurements are used. The instrument used for such measurements is a Beckman IR4 Infrared Spectrophotometer which operates in the double beam mode for both transmission and reflection. This instrument has a 17 meter path length, in air, and has interchangeable prisms to cover the 1 micrometer to over 20 micrometer range.

Typical transmission and reflection data of a PbSnTe film are shown in Figure 2-5. The absorption coefficients are a function of wavelength, and are calculated by using a Chi square fitting program in conjunction with the Baldini and Rigaldi (Reference 9) equations, which takes into account multiple reflections in both the film and substrate, but assumes no absorption in the substrate. In those cases where the films are highly absorptive it is not necessary to use the multiple reflection calculation. The simplified expression for the absorption coefficient

$$\alpha = \frac{1}{d} \ln \left(\frac{T}{1-R} \right)$$

compares quite satisfactorily with the more elaborate calculation. Here, d is the film thickness, T and R are transmission and reflection respectively.

While more elaborate tools are available, the index of refraction (n) is generally determined from the transmission and reflection maxima by the simple relation.

$$2n (\lambda)d = m\lambda$$

where d is the physical thickness, m the order of the maxima and λ the measurement wavelength.
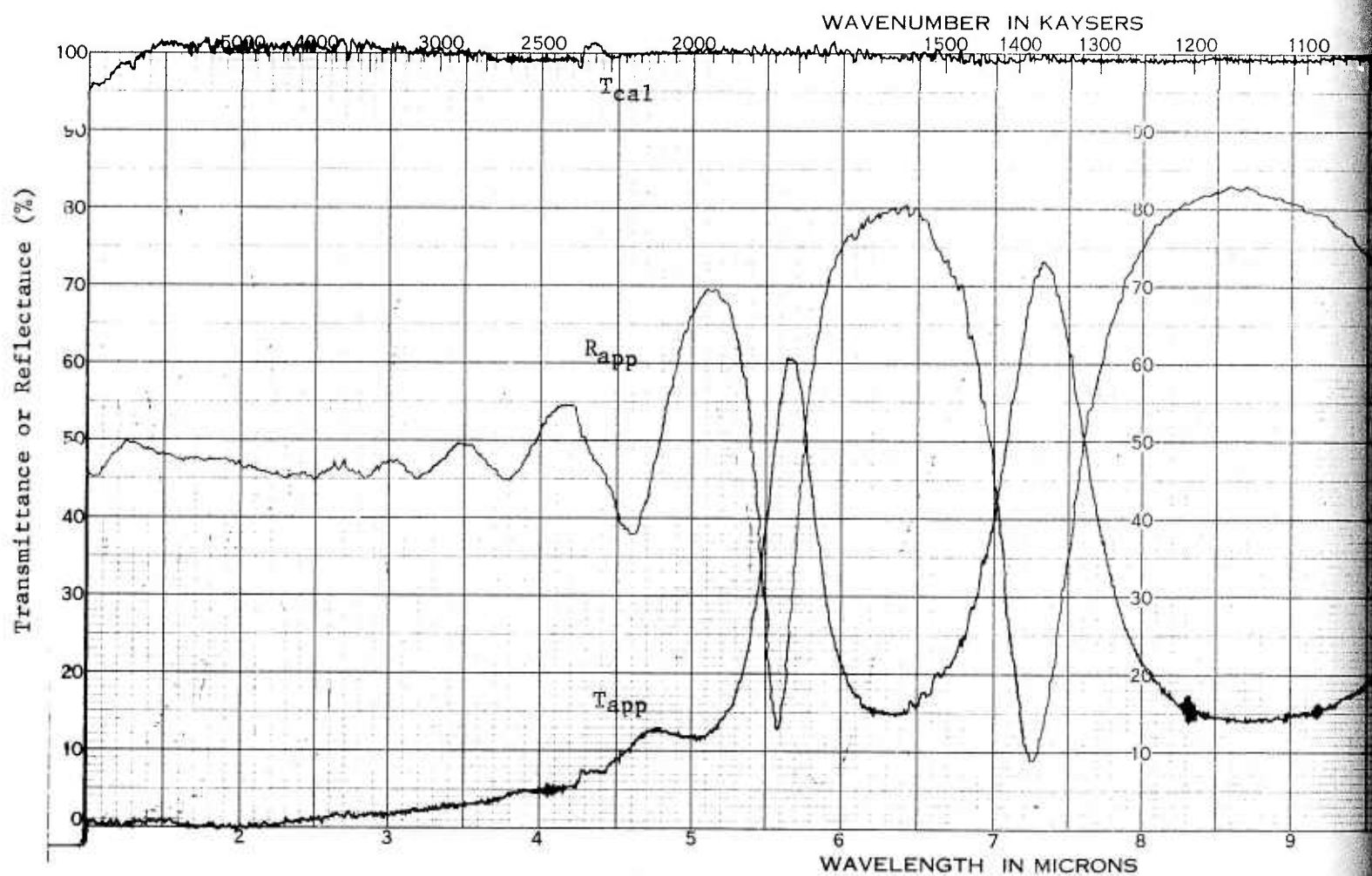
Figure 2-5 Transmission and Reflection Spectra of Pb$_{.82}$S
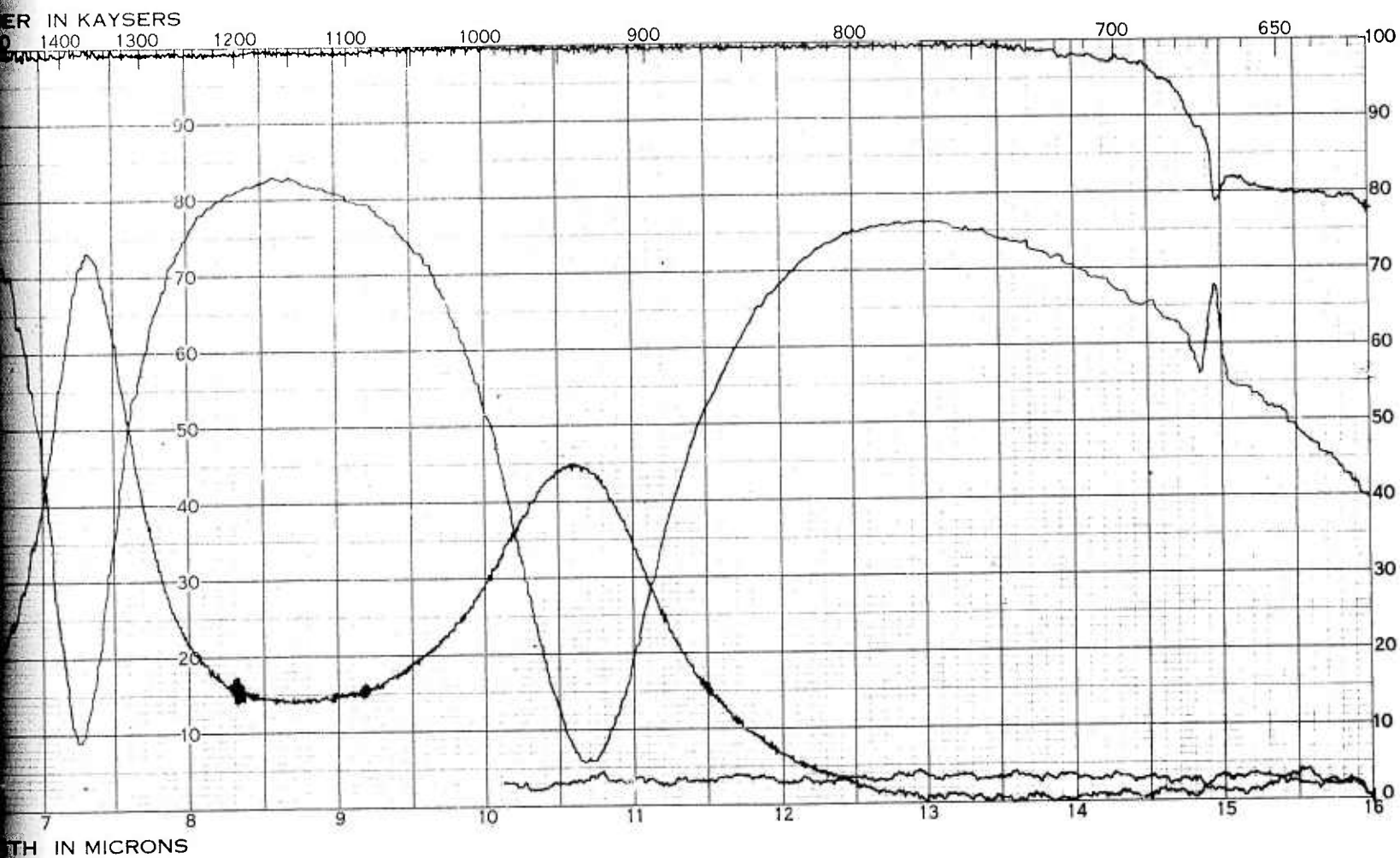
Reflection Spectra of Pb$_{.82}$Sn$_{.18}$Te Film on a CaF$_2$(111) Substrate

TH IN MICRONS

2-26/27

2.6.3 FILM THICKNESS MEASUREMENTS. Film thickness measurements
are needed for the definition of the optical and electrical properties
as well as for the calibration runs to determine exact deposition rates.
These measurements are performed with a Talystep I thickness gauge, which
measures films as thin as 50Å, and with an accuracy of better than 15Å if
sharp film edges and relatively smooth substrate surfaces are available.

2.7 FILM ELECTRICAL EVALUATION TECHNIQUE

Resistivity, carrier mobility, carrier concentration and carrier
type, are measured by Van der Pauw techniques. This technique was
decided upon because of its flexibility and simplicity. Furthermore,
a four probe point contact method is used in lieu of the typical method
employing evaporated metallic contacts. The point contact method is
"non destructive". For example, it permits films to be further processed
by annealing after a measurement or used for other types of measurements,
all of which is difficult once contacts have been evaporated on the
samples.

Temperature dependent measurements, from 300°K to 77°K, before
and after any annealing step, are performed on each useful sample. The
considerable time involved in making these temperature dependent measure-
ments has, for the most part, been overcome by the use of a specially
designed multiple sample Hall probe. An exploded view of the probe is
shown in Figure 2-6. The probe can hold, front and back, two sets of
three samples. Each sample is sensed by a square array of four contacts.
The contacts are small phosphor bronze spring loaded balls as shown in
the insert of Figure 2-6. The electronic switching circuit for the
Van der Pauw probe is shown in Figure 2-7. Switch S2 indicates a sample,
selector switch, so that anyone of the six samples can be selected and
measured individually, without any crosstalk problems.

A Keithley 150B electrometer is used to measure the voltage drop
and a Keithley 602 electrometer is used to measure the current. The
magnet, with the particular pole pieces and gap configuration used in
this work, provides a 4.5 kilogauss maximum field.

2-28

Ball and spring contact
(see insert)

Inserts

Leads

Phenolic block

Sample

C_u sample holder

Insert *
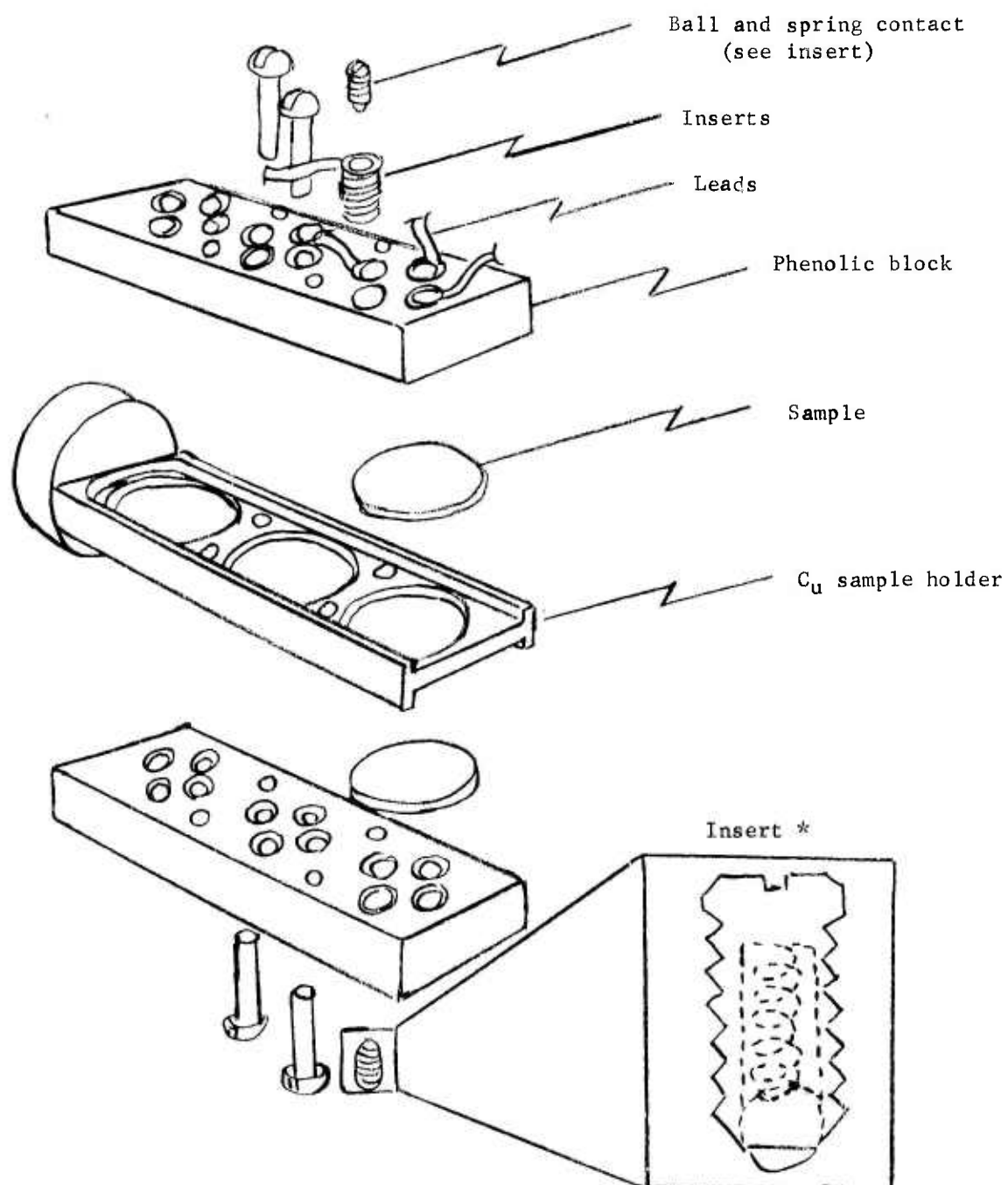
Figure 2-6 Exploded View of Multisample Hall Probe

*   (Brass contacts with phospher bronze spring)

2-29
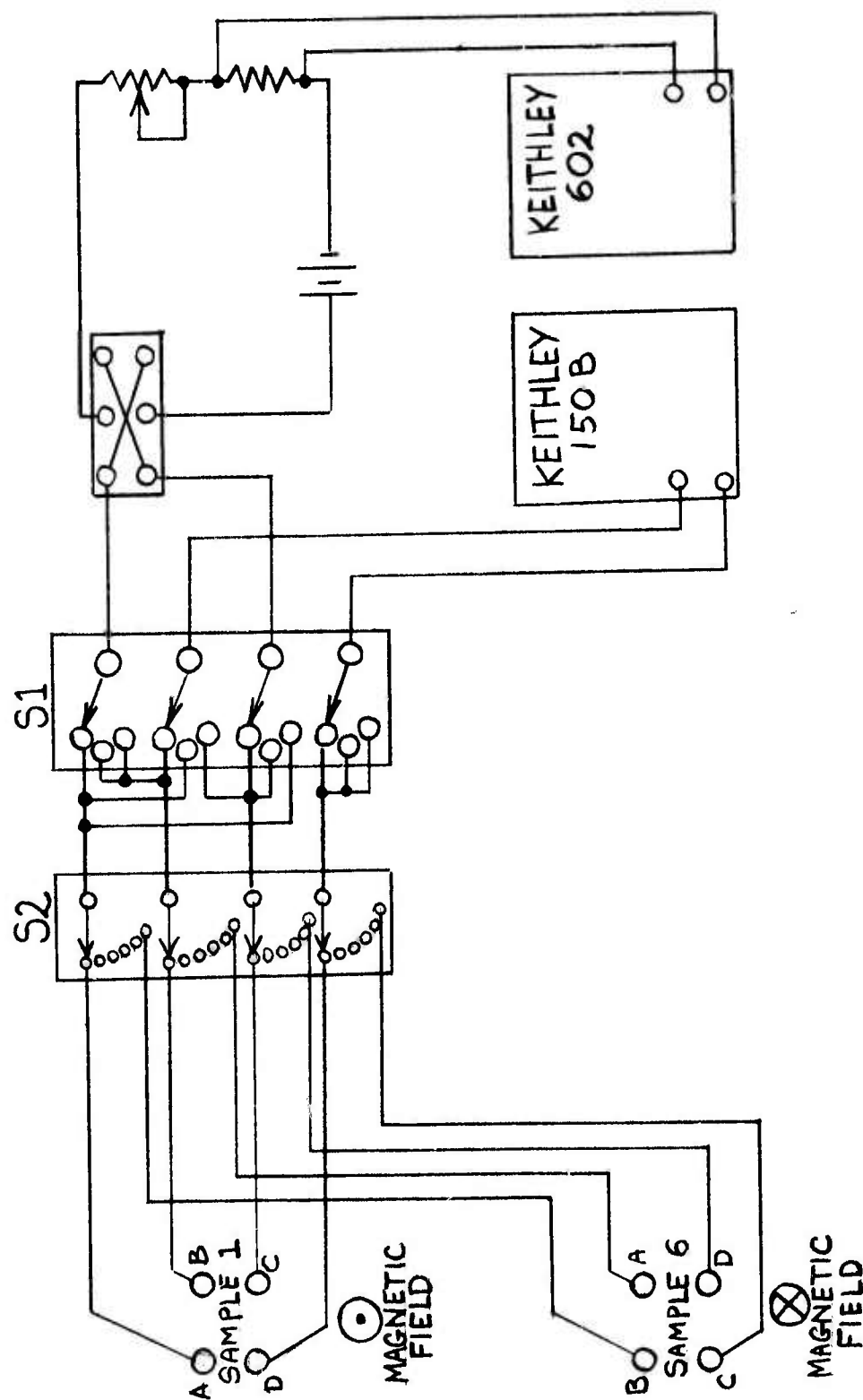
Figure 2-7 Switching Circuit for Van der Pauw Probe

2-30

For the temperature-dependent measurements the probe described above is mounted in a Sulfurian variable temperature dewar. The dewar is capable of a temperature range from room temperature to liquid helium temperature ($4.2^{\circ}K$). An internal heater is used to stabilize the temperature at any point desired. Data points are generally obtained during the cooling cycle. The slow drift downward in temperature is stopped with the heater during the actual measurements. The temperature is measured with a Chromel-constantan thermocouple, which is mounted to the brass base of the probe. The validity of the thermocouple readings was established from measurements with the samples submerged and equilibrated in liquid nitrogen.

The measurement procedure follows that prescribed by Van der Pauw (Reference 10). With S1 in position 2 (see Figure 2-7) the current flows through a sample from point B to point C (all measurements are checked with forward and reverse currents and magnetic fields). The voltage drop is measured from A to D and the resistance is defined as

$$R_{BC,\ AD} = \frac{V_A - V_D}{I_{BC}}$$

A second measurement is made with switch S1 in position 3 so that the current flows from A to B. The voltage drop is then measured from C to D. This defines

$$R_{AB,\ CD} = \frac{V_D - V_C}{I_{AB}}$$

The resistivity is then obtained from

$$\rho = 2.266\ fd\ (R_{AB,\ CD} + R_{BC,\ AD})$$

where d is the thickness of the film and f is a correction factor which is a function of $R_{AB,\ CD} / R_{BC,\ DA}$ (see Reference 10).

The Hall mobility μ_H is measured with switch S1 in position 1. The current enters A and leaves C. The change in voltage due to the magnetic field is measured from B to D. The change in resistance of

2-31

the sample is defined as

$$R_{AC, BD} = R_{AC, BD}(B) - R_{AC, BD}(0)$$

The Hall mobility is then calculated from

$$\mu_H = \frac{d}{B} \frac{\Delta R_{AC, BC}}{\rho}$$

From these two measurements the carrier concentration (n) can be obtained, as long as a one carrier model applies, by

$$n = \frac{1}{\rho \mu_H e}$$

The electrical properties measured by this method do not directly give the exact values. The reason is that it is assumed by Van der Pauw that the point contacts are infinitely small and exactly on the boundary of the sample; in practice this is not possible. As a consequence, a geometric correction factor must be defined by careful calibration for each probe and substrate configuration to take into account the deviation from the exact case. Such a calibration was performed for our system and correlation experiments were performed using conventional Hall samples (evaporated contacts) and identical samples measured with the Van der Pauw point probe to establish the validity of the calibration.

The following outlines the calibration procedure.

Van der Pauw showed that, to a first order, the corrections are

$$\frac{\Delta \rho}{\rho} = \frac{1}{2 \ln 2} \left(\frac{d}{D}\right)^2$$

and

$$\frac{\Delta \mu}{\mu} = \frac{2}{\pi} \left(\frac{d}{D}\right)$$

and

$$\frac{\Delta n}{n} = \frac{\Delta P}{P} - \frac{\Delta \mu}{\mu} = \frac{1}{2 \ln 2} \left(\frac{d}{D}\right)^2 + \frac{2}{\pi} \left(\frac{d}{D}\right)$$

where d is distance from the probe point to the nearest boundary of the sample and D is the diameter of the sample. He suggested that this effect could be reduced by the use of a "clover leaf" bridge. Figure 2-8 shows the results of an experiment which experimently determines the geometric correction factors for the mobility. Similar results are obtained for p/p and n/n. Each successive point was obtained by cutting the "clover leaf" bridge deeper and deeper into the sample. After the last cut (S = .06 inch), a normal bridge was cut into the sample which is shown by the dotted lines in the insert in Figure 2-8. Indium pads were then evaporated on each arm, and gold wires were applied with a InGa alloy, and a standard Hall measurement was made. The measurements obtained with the four point probe were then normalized to the measurements obtained with the standard bridge geometry. The solid curve in Figure 2-8 is a fit of Van der Pauw's first order correction.

Experimentally it was established, for our probe configuration, that the following corrections apply:

$$\text{(corrected)} \quad \mu_H = \frac{\text{(measured)} \, \mu_H}{0.75}$$

$$\text{(corrected)} \quad \rho = 1.035 \, \text{(measured)} \, \rho$$

and

$$n \text{ (or p) corrected} = \frac{n \text{ (or p) measured}}{1.38}$$

A further important point considered was the possibility of rectification at the point contacts of our probe. This would produce a nonlinear current-voltage relationship across the sample. To explore this possibility, typical samples were measured as a function of current and magnetic field. The results showed a linear current voltage relationship over 3 decades and no magnetic field dependence between 500g and 4000g. Experimental samples were only spot checked as a function of current and magnetic field except for high resistivity samples. These were routinely evaluated. Nonohmic contact effects have never been observed
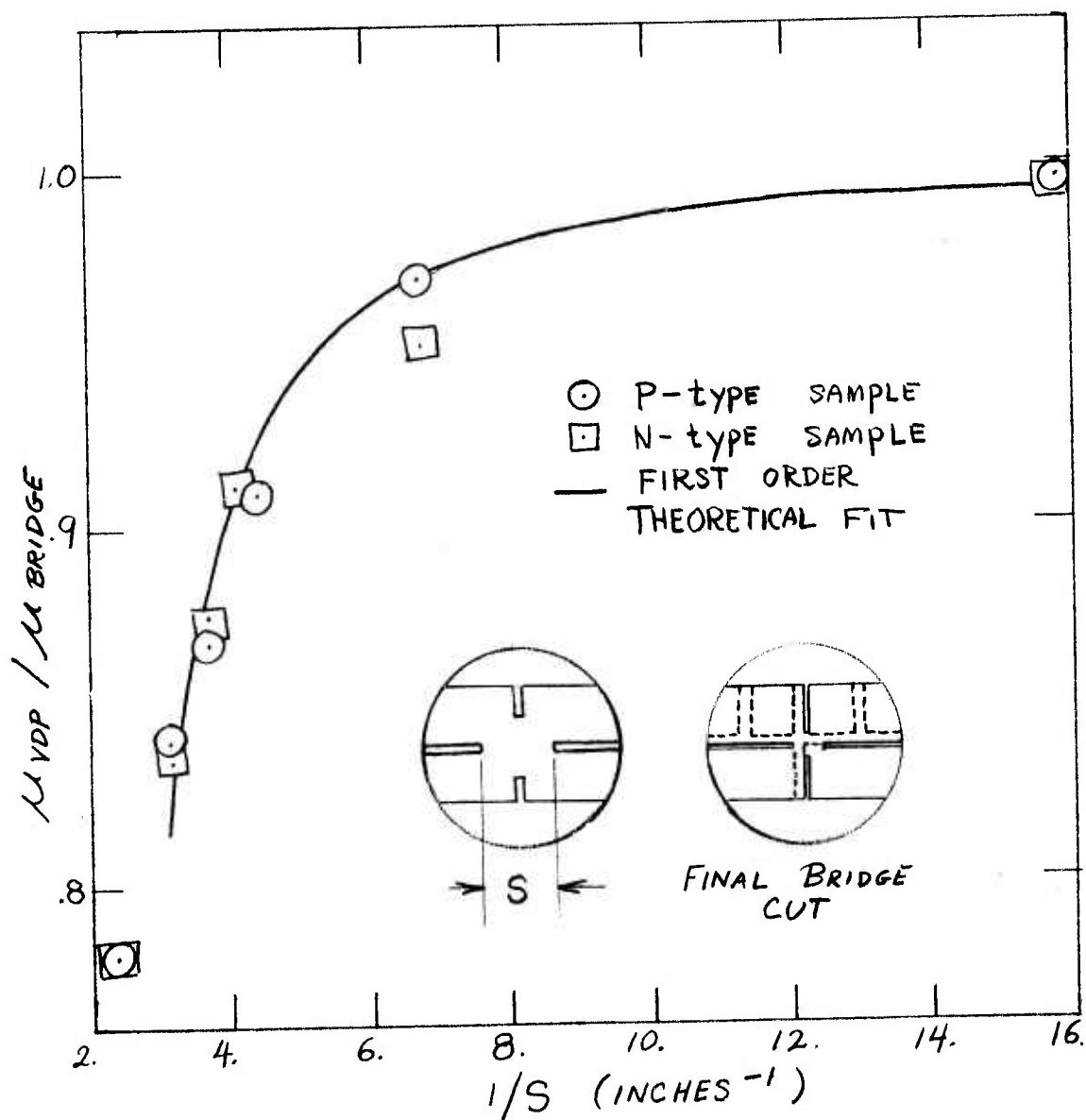
Figure 2-8   Experimentally Determined Geometric Correction
Factors

2.8 FILM ELECTRO-OPTICAL EVALUATION TECHNIQUES

2.8.1 PHOTORESPONSE MEASUREMENT

2.8.1.1 Instrumentation. The apparatus used is shown in Figure 2-9.
The source of radiation is a Globar, operated at about 35 volts, 4
amperes, 140 watts. Radiation from the Globar is focused, by means of
mirrors, onto the entrance slit of a Perkin-Elmer Model 99 Monochromator.
Before entering the slit, the radiation is modulated by a Brower 312C
variable - speed chopper. After leaving the exit slit of the mono-
chromator, the radiation is focused, again by mirrors, onto the sample.

The sample is mounted and cooled to about 80°K in a Janis Research
Corporation liquid-nitrogen dewar, whose windows are KRS-5 or to very
low temperature of less than 2°K in a Janis Model 8DT Dewar (those very
low temperature measurements will be discussed in later section). Both
before and after cooling down, the sample resistance is measured with
a Keithley 602 electrometer. In the case of the Liq-N_2 Dewar some
thermocouples built into the system provide a method for actually
obtaining the temperature of the sample. The sample can be measured
in either a photoconductive or photovoltaic mode. For photoconductive
measurements, a variety of bias settings, from 3 to 22.5 volts, are
available from a multiple-terminal battery. A variety of load resistors
are also available, ranging from 10 ohms to 10 megohms. A 22 μ-farad
capacitor across the sample is used to draw off the AC signal without
disturbing the bias current.

From the sample, the signal is fed into either a Type A or Type B
(depending on the sample resistance) preamplifier of a Princeton
Applied Research HR-8 lock-in amplifier. A reference signal for the
lock-in is provided by the chopper. The signal, then, is read, as a
function of wavelength, from the lock-in amplifier. The noise is
measured by using the HR-8 as a tuned a.c. voltmeter.

While there is room for only one substrate in the cold-finger at
the bottom of the dewar, it is possible to have several samples
deposited on the same substrate. In this case, one can hook up more
than one sample at a time with the multiple connectors in the dewar,
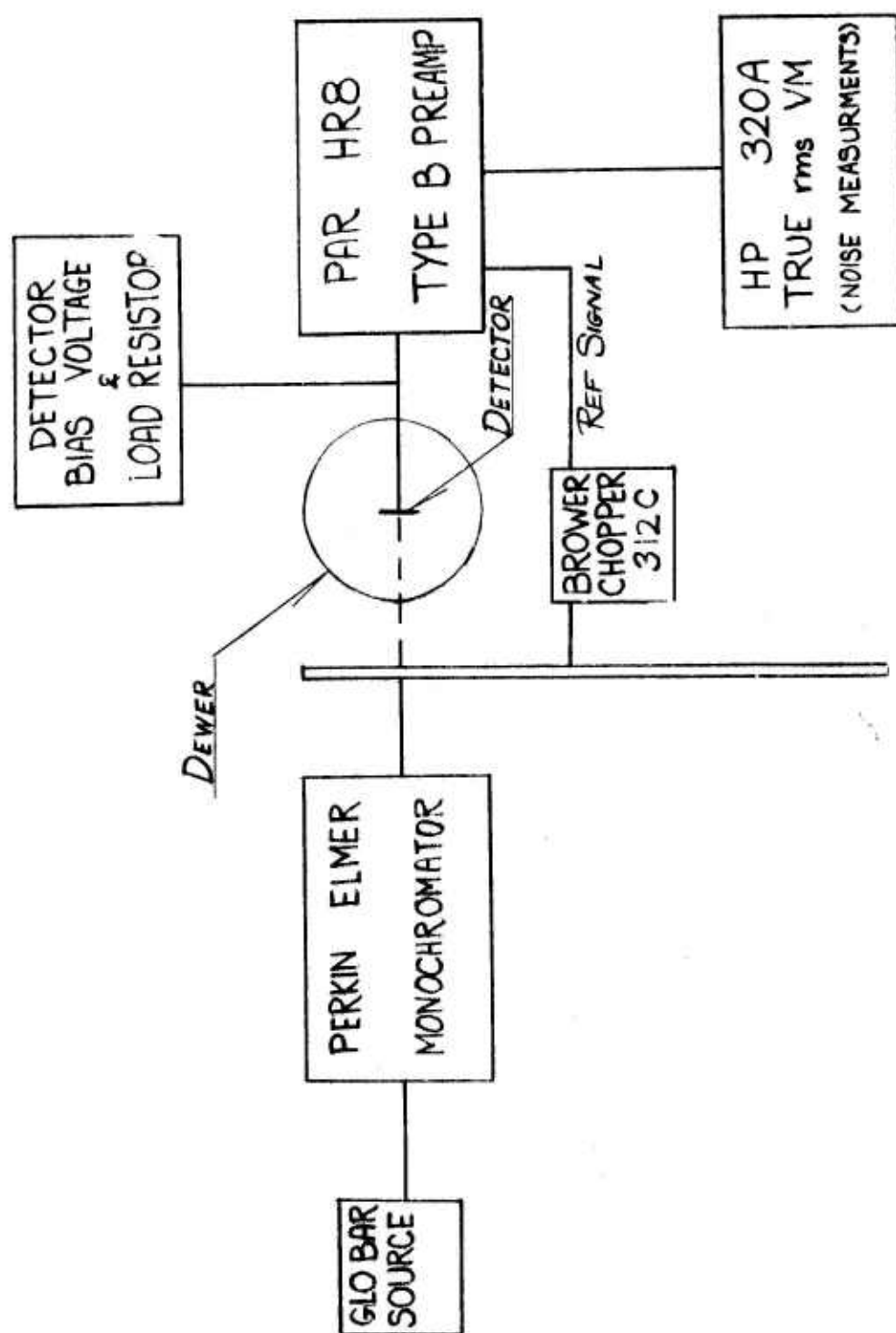
Figure 2-9 Electro-Optical Measurement Set-up

thus eliminating the need for cooling down and warming up for each individual sample. After measurement, samples can be checked for diode characteristic curves, while still cold utilizing a Tektronix 575 Transistor-curve Tracer.

As well as the spectral response measurements referred to, blackbody measurements can be made by using a standard blackbody source.

2.8.1.2 <u>Electrode Deposition and Sample Preparation</u>. Since photoconductive cells are of considerable concern in this study, the development of good ohmic contacts is critical. Since some ambiguities the ohmic or non-ohmic behavior of some metals on PbSnTe have been reported, one is forced to experimentally establish such behavior for each material. For example although it has been reported that gold electrodes have been used to make ohmic contacts onto both n- and p-type PbSnTe (References 11 & 12) recent experiments (Reference 13) have shown that gold forms a barrier to both n- and p-type material, but the barrier height is small. A proposed model for metal to PbSnTe contacts (Reference 12) which states that the surface states do not control the position of the Fermi level indicates indium and lead should be ohmic on n-type surfaces, and should form barriers on p-type surfaces.

Our own work, which has involved a rather comprehensive study of ohmic and barrier contacts on thin film PbSnTe, has shown that as in the case of Reference 11 and 12, gold does form ohmic contacts on both n- and p-type thin film PbSnTe. Furthermore, consistent with the model proposed in Reference 12, indium does form ohmic contacts on n-type thin film PbSnTe while Pb and In form barriers on p-type thin film PbSnTe (we have not used Pb for a contact on n-type PbSnTe). Thus our own work seems to support the simple model in which the barrier height is governed by the metal work function.

Based on our results to date, the following procedure was adopted for preparing ohmic contacts to n-type photoconductive samples. First, indium is vacuum deposited on the film ($\sim 1500 \overset{o}{A}$ thick). Indium/Gallium solder (In/Ga = 27/75) or indium solder by itself is next applied to the

indium layer and 5 to 10 mil Au wires are placed into the solder. For p-type photoconductive samples, either gold or sputtered platinum has been used for the ohmic contact and the same procedure as in the case of n-type samples is used for attaching the leads.

The electrode geometry and design have been kept as simple as possible. For the photoconductive samples, the electrodes are simultaneously evaporated (or sputtered in the case of platinum) at opposite ends of the PbSnTe films. The indium or InGa solder is applied to both of these contacts. While this simple arrangement is satisfactory (i.e. very low noise levels have been measured in our photoconductive samples with this arrangement) the contact geometry could be improved to further reduce the contact noise voltage as is presently being pursued.

Due to possible effects of surface states, it is extremely important to prepare the semiconductor surfaces properly and to keep them as clean as possible prior to and during the metal deposition. Thus background pressures for the evaporation of contacts have been kept to less than 10^{-7} torr. Special care (i.e. cooling sample) was also taken, in some cases (in particular with samples having carrier concentrations in the high 10^{15} cm^{-3} to low 10^{-16} cm^{-3} range) to avoid the diffusion, during evaporation, of the evaporated contact metal into the PbSnTe thus possibly altering both the electrical properties and carrier lifetimes in the films.

2.8.1.3 <u>Response Time Measurements</u>. High quality, single crystal PbSnTe films of sufficient thickness do exhibit bulk electrical and optical properties, have response times of less than 50 nanoseconds, comparable to those found in the bulk material. In order to measure these response times by the photoconductive decay method, a pulsed radiation source is required with pulse rise and fall times much shorter than the response times to be observed and with sufficient intensity to excite appreciable photoconductivity. Ideally, the wavelengths of the emitter should be in the operational response band of the photoconductor being evaluated. Practically, one finds that pulsed IR lasers with wavelengths greater than $5\,\mu$m are not very economical for test purposes.

Consequently we have used a GaAs laser source ($\sim 8900\overset{o}{A}$) pulsed with Savant Engineering Pulser Model LDP-3. The laser diode is mounted on the pulser unit and its output is checked with an ITT high speed phototube model F4000S-1 with response time of 10^{-9} second. The laser diode output had response times of 50-70 nanoseconds depending on the amplitude, width and repetition rate of the driving current pulse.

The above mentioned setup has two disadvantages: the response of the PbSnTe samples is relatively low at $8900\overset{o}{A}$, calling for a higher intensity laser source and the laser output pulses are rather long. We have procured a laser diode array to increase the radiant power output and have designed a different pulse generating circuit to generate fast pulses. This setup is shown in Figure 2-10.

The pulse generating circuit is composed of a Tektronix Pulse Generator, a delay line cable and a high voltage power supply. It is necessary to terminate the pulse generator output into a 50 ohm load in order to avoid reflections and to preserve the pulse shape. If properly terminated, it is possible to generate pulses with rise and fall times of 1-5 nanoseconds. For room temperature operation the laser diode array threshold current is 25 amperes. Since the pulse generator is not capable of supplying 1250 volt (50 x 25 amps) peak pulse, it is necessary to cool the laser diode array in order to reduce the lasing threshold current. At 77°K, a peak current of .6 amps is required which can be easily supplied by the setup of Figure 2-10. The laser diode array will be mounted in the dewar in close proximity to the PbSnTe sample. The photoconductive decay of the sample if observed on a Tektronix sample scope type 661.

For large and wavelength dependent response time evaluation, chopper controlled irradiation from monochromatically filtered blackbody sources is utilized as discussed in the result section.

2.8.2 NOISE MEASUREMENTS. For noise measurements, the same setup shown in Figure 2-9 for electro-optical measurements is still being utilized, except that the chopper is turned off and all radiation is blocked from being incident on the sample other than that due the internal background. The detector field-of-view is 2π steradians. For high performance detectors, interchangeable cold shields can easily
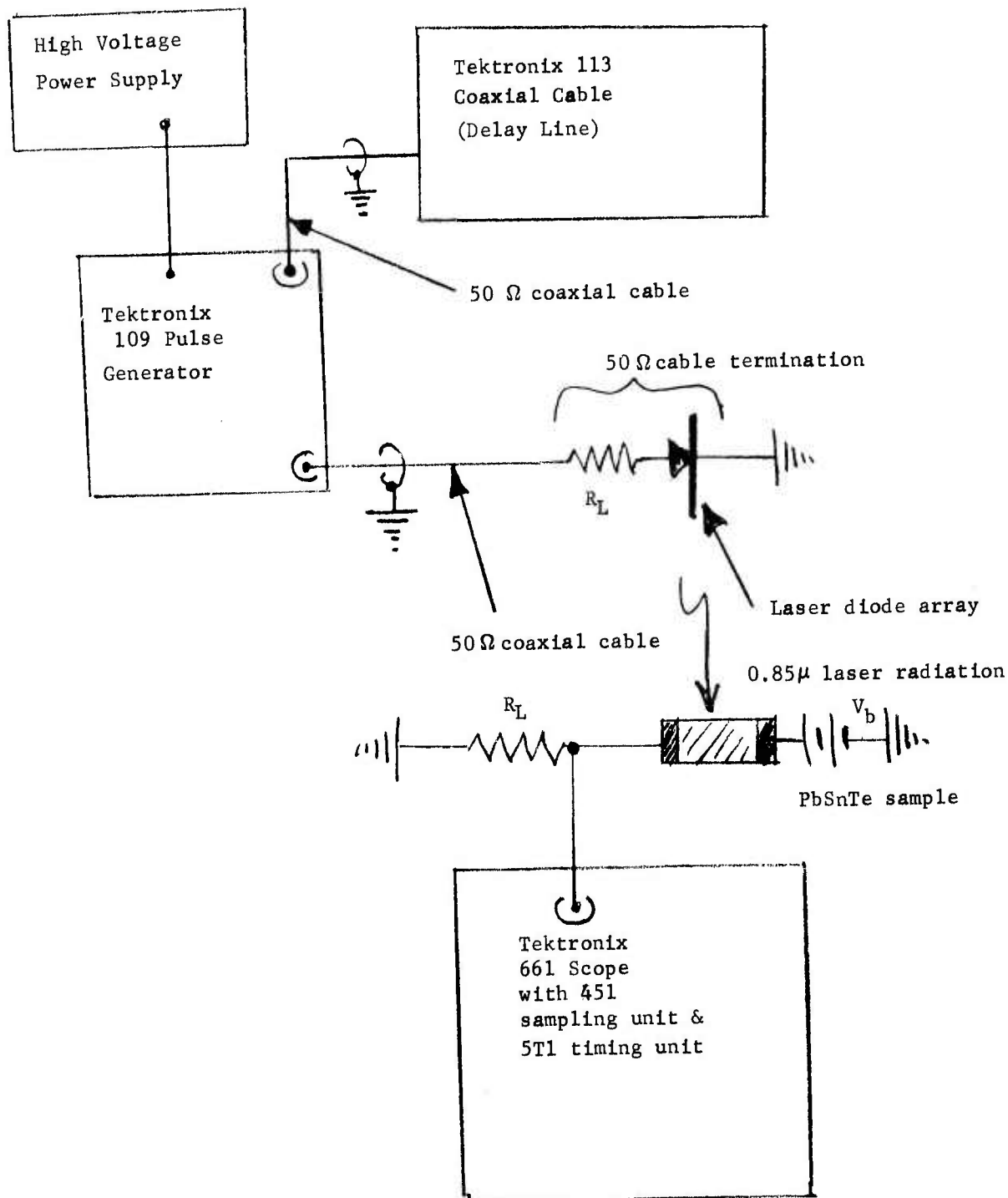
Figure 2-10 Equipment for Measurement of Photoconductive Decay Time

2-40

be inserted into the present system to reduce the internal background
radiation incident on the detector. This type of test is performed in
a liquid He dewar. The sample can be either a photoconductor or a photo-
voltaic detector. In the latter case, the biasing network is disconnected
from the detector. The detector output is directly coupled to a PAR
preamplifier-either type B with 100:1 transformer ratio or type A,
depending upon the detector impedance level. The preamplifier is an
integral part of the phase locked amplifier type HR-8. The a.c. output
of the amplifier is fed into a true RMS reading voltmeter such as HP 320A.
The noise bandwidth is determined by the ratio of the measurement frequency
to the Q of the tuned circuit of the HR-8 amplifier. This arrangement
has the advantage that excess noise or current noise (which is proportional
to $\Delta f/f$, where f is the measurement frequency and Δf is the noise
bandwidth) remains constant as a function of frequency. Noise frequency
spectra can be recorded over a wide range of frequencies limited only
by the frequency response of the transformer in the type B preamplifier.
For type A, the frequency limit is in excess of 100 KHz. With adequate
shielding and elimination of ground loops, it is possible to measure
noise with an RMS amplitude in the subnanovolt range.

2.8.3 PHOTOVOLTAIC RESPONSE MEASUREMENTS. The experimental setup
for photovoltaic response measurement is identical to that used for
photoconductive measurements with the exception that the detector bias
circuit is disconnected. Signal and noise voltages are measured in the
same manner as for photoconductive response. In addition, for the
Schottky barrier photovoltaic detectors, it is possible to have both
front wall and back wall excitation. This is accomplished by mounting
the sample on a Cu finger containing a hole large enough to expose the
sample to radiation incident through the BaF_2/CaF_2 substrate. Back wall
radiation is required when the metal is not transparent to the incident
radiation on the front side.

2.8.3.1 _Electrode Deposition and Sample Preparation_. The photo-voltaic detectors investigated in this study include both Schottky barrier diodes and p-n junction photodiodes. For the Schottky barrier devices, both the barrier and ohmic contacts are deposited on top of the sputtered PbSnTe film. First the ohmic contact, which is either platinum or gold for p-type film (platinum in most cases) is deposited on one end of the film extending onto the substrate for subsequent lead attach-ment. The Schottky barrier metal (In, Pb or Al for P-type film) is then evaporated onto the PbSnTe film through a metal mask giving, in some cases, several islands consisting of approximately 2 mm x 10 mm strips, which again extend onto the substrate. The lead attachment to these contacts is the same as discussed above. As also discussed previously, the contact deposition conditions (i.e. temperature, back-ground pressures, etc.) for Schottky barrier devices are also very critical for device performance. Surfaces are extremely important; therefore, background pressures are kept in the 10^{-8} torr range.

Contacts on the p-n junction devices consist of sputtered or evaporated platinum (or evaporated Au) for the p-type layer and evaporated indium for the n-type layer. The contacts are deposited as tabs on the p- and n-type films and extend onto the substrate. Lead attachment to the contacts is performed in the same way as discussed previously for photoconductive devices. Various configurations for the p-n junction devices were used and are discussed in the result section.

2.8.4 LOW TEMPERATURE AND REDUCED BACKGROUND MEASUREMENTS. For low temperature measurements, a Janis model 8 DT research dewar was setup, checked out, and put into operation. The dewar is designed for electro-optical measurements on samples cooled down to $2^{\circ}K$ or less (liquid helium cryofluid). The samples can be immersed in the cryofluid by operation of a valve which causes the cryofluid in the inner "helium" reservoir to flow through a small tube into the sample chamber. Figure 2-11 is a cross-section schematic sketch of the dewar configuration.

Heaters in the dewar permit prolonged operation at any temperature from $4^{\circ}K$ to room temperature and an electronic controller, Antronix,

2-42

Shaft to Sample Mount

LN$_2$ & He Filler
Tubes, Sample
  Orienter,
Vacuum Fixtures
etc. not shown.

Liquid-nitrogen
Reservoir

Vacuum Space

Control Rod
for He Valve

Sample Chamber

Liquid Helium
Reservoir

He Valve

Vacuum Space

Radiation Shield

Capillary Tube
to Transport He
to Sample Chamber

Sample Mount with Heater &
Temperature Sensors

KRS-5 Window

Ge Window

Vaporizer Assy. with
Heater

Figure 2-11 Janis 80T He Dewar - not to scale

2-43

automatically maintains the temperature. The temperature can be measured from 4° to 300°K by means of platinum and germanium sensors. The sample position can also be varied during operation, by rotation or by varying the height over a span of two inches.

There are two sets of windows on the dewar which permit optical transmission measurements on cooled samples. These windows, of KRS-5 and germanium, allow measurements at any wavelengths from 2 to 40 microns.

The photoresponse measurements at low temperatures can also be made under reduced background conditions. We have developed, for this purpose, some interchangeable cold shields which can be rapidly introduced into the liquid He dewar. The shields are cooled to 77°K and are provided with field-of-view limiting orifices. Presently, the shield with the smallest orifice has an f stop of f/20. The f number can easily be increased if desired.

The cold background measurements help not only in determining the ultimate performance of the detector but also are necessary for material characterization such as detection of trapping centers.

3.0

RESULTS AND DISCUSSION

3.1 GENERAL COMMENTS AND SUMMARY OF APPROACHES

Throughout all phases of this program, one common objective has been the preparation of improved high quality $Pb_{1-x}Sn_xTe$ film materials using sputtering as the primary deposition technique. In line with this general objective, a materials development study of sputtered thin film PbSnTe has been continuously in progress. However, the ultimate purpose of this program, as stated earlier, has been that all results of this material study would be of utility in the fabrication of high quality infrared sensors and ultimately in the fabrication of cost effective, high density detector arrays. Therefore, the criterion for material quality was in the end defined by the performance character- istics of each type of deposited $Pb_{1-x}Sn_xTe$ film relative to photon response or detectivity. Based on this, an iterative approach was taken throughout the program. This approach has been to first system- atically establish the various preparation parameters which lead to high quality $Pb_{1-x}Sn_xTe$ film materials. Then the parametric relation- ships were established between the preparation conditions and the resulting, device related properties including electrical and photo- electric properties. Finally, the functional, i.e. photo responsive performance of PbSnTe films was optimized by iteratively optimizing the preparation conditions.

For this iterative approach, photoconductive responsivity as well as all properties contributing to photoconductive detectivity were used as the ultimate film quality indicators. It is recognized that, as of this date, PbSnTe is still exclusively used in a photovoltaic mode due to the limited photoconductive sensitivity in conventionally prepared materials. Still, it was felt that photoconductive performance is more directly relatable to material properties and, therefore, a more desirable quality indicator. Photovoltaic response, unless evaluated with perfectly fabricated cells, is more strongly influenced by factors such as junction geometry, thickness, surface leakage and others. But, to prepare sufficiently

large numbers of perfect cells as test samples, is obviously a time consuming task and requires considerable device research by itself.

A second reason for using photoconductivity as the evaluation criterion was that we undertook this program in the firm belief that PbSnTe film, suitably prepared and processed, should yield photoconductive detectivities comparable to those of other infrared sensors responsive in the LWIR spectral bands - in particular to $Hg_{1-x}Cd_xTe$. Methods such as trap enhancement were foreseen as approaches to make this feasible.

Some of the relevant material properties requiring optimization can be deduced by considering the parameters defining the photoconductive sensitivity. Among these are the photoconductive responsivity (R), specific detectivity (D*) and gain (g). These are related to the material properties by expressions such as:

$$R_i = g \cdot \frac{e\eta}{E_p} \quad amps/watt .$$

$$D^*_J = g \cdot \frac{e\eta}{2E_p} \cdot \left(\frac{L^2}{t \, e \, k \, T \, (n \, \mu_n + p \, \mu_p)} \right)^{\frac{1}{2}} \quad cm\text{-}Hz^{\frac{1}{2}}/watt,$$

for Johnson noise limited conditions.

$$g = I \frac{\tau}{neU} \quad or \quad g = I \frac{\tau}{peU} \quad ,$$

for n- and p-type materials, respectively.

Here, τ is the lifetime of photo-excited carriers; n, p the respective carrier concentrations; $U = WLt$ the sensor volume; η the quantum efficiency of incident photon conversion; μ_n, μ_p the respective carrier mobilities, E_p the photoelectric energy gap; T the material temperature and I the bias current.

3-2

If one can make the realistic assumption that sweep-out limited gain is not approached, it is apparent from even these few simple but basic expressions which material properties have to be optimized for maximizing the photoconductive responsivity and detectivity.

The effective carrier concentration should be minimized, preferably approaching the intrinsic value n_i which at a temperature of $77^{\circ}K$ is below but approaching 10^{14} cm^{-3} in PbSnTe. Material purity, or carefully controlled compensation, is the key to this. The lifetime calls for maximization, requiring material perfection to reduce recombination rates, or careful control over trapping centers. Since $\tau = 1/B \cdot (n+p)$, reduction in carrier concentration also increases the lifetime. The lifetime must, of course, be limited to a value compatible with the sensor response speeds required in typical applications. Generally this calls for response times of no more than microseconds. Mobilities, though not explicit in the expressions given above, require maximization as long as conditions above the sweep-out limit are maintained. The reason is that sensor response times and in turn sensitivites are critically affected by mobilities also. Material perfection is again the limiting parameter here. In PbSnTe, values in excess of 10^4 cm^2/v-sec are mandatory for high sensitivity. Film thickness is material unrelated, but indicative of the value of thin film sensor fabrication. All three relations given above reveal that the thickness should be minimized. But, the minimal thickness desirable is defined by its effect on the quantum efficiency. The latter calls for a minimum thickness on the order of an absorption length for radiation at the cutoff wavelength of the desired sensor. In PbSnTe this entails a magnitude of about 1 micrometer.

To achieve the stated objective, the work was pursued through the following stages of development:

1) The initial phase of the work was concerned with an investigation of the material properties of sputtered $Pb_{1-x}Sn_xTe$ films which included: the definition of epitaxial deposition conditions on various substrates including single crystal $CaF_2(111)$, $CaF_2(100)$, and $BaF_2(111)$; the characterization of film composition as a

function of deposition conditions; the correlation of as-deposited electrical and electro-optical properties with deposition conditions, and, in turn, with film structure; the correlation of electrical properties of annealed films with the various annealing conditions and with the initial electrical properties of as-deposited films.

As the results in the following sections will show in detail, it was soon demonstrated (i.e. early in the program) that single crystal films with excellent structural, electrical and electro-optical properties can be deposited, on various substrates, by the sputtering process. The properties of these films compared very favorably with those achieved in bulk single crystal PbSnTe. In addition, the sputtering process yielded a considerable number of results which were not only interesting and rather unique but appeared to be of major significance for the fabrication of high quality or sophisticated sensor devices for LWIR application.

A significant finding, for example, was the result that compositional, optical, structural, electrical, and electro-optical properties of sputtered $Pb_{1-x}Sn_xTe$ films could all be controlled, over relatively wide ranges, by simple control of two basic deposition parameters. That is, films of desired composition or x-value (which, in turn, controls the energy gap or spectral response) of either n- or p-type, can be produced by suitable selection of deposition rate and substrate temperature combinations. Furthermore, films with a controlled range of such properties can be deposited with a single PbSnTe target.

Guided by the original work with bulk PbSnTe in other laboratories, annealing was employed in the early stages of this program in order to improve film properties (i.e. by improving stoichiometry) over those found in as-deposited films. However, it soon became apparent that $Pb_{1-x}Sn_xTe$ films with electrical properties suitable for detector application could be prepared without the necessity of annealing. This very encouraging result is related to the observation that accurate control of the two basic deposition conditions alone is sufficient for optimizing the film stoichiometry. Such a result is, of course, quite important for device preparation. Not only does the use of as-deposited PbSnTe

3-4

film imply considerable cost and time-savings, but it should also improve performance and reliability characteristics since, e.g., fewer processing steps reduce the chance for contamination and handling failures.

Although these results were showing that the necessity for annealing may be eliminated, we continued this work until a sufficient amount of data was collected on the effects of annealing on sputtered $Pb_{1-x}Sn_xTe$ films to validate this. As will be shown in later sections, all of these data demonstrated that annealing effects in $Pb_{1-x}Sn_xTe$ films are consistent with those observed in good quality, bulk single crystal. A very significant outcome, however, of the annealing studies was the demonstration of a critical low temperature annealing condition at which a significant reduction in carrier concentration is obtained. This critical temperature seems quite analogous to the critical high temperature annealing condition usually employed to achieve stoichiometry in bulk crystals of $Pb_{1-x}Sn_xTe$. In effect, it defines a second crossover (in the equilbrium phase diagram for $Pb_{1-x}Sn_xTe$) from the metal saturated solidus field with the stoichiometric composition. This result is not only of interest from a scientific standpoint, but also from a practical standpoint, since the availability of a low temperature annealing condition is obviously of significance for reducing thin film device fabrication difficulties. Also, as will be seen later, the existence of the low temperature annealing conditions may be relatable to the fact that stoichiometry control is possible in as-deposited film, i.e. without post-deposition anneal.

2) The next phase of the program included a continuous effort to improve the properties of our sputtered $Pb_{1-x}Sn_xTe$ films beyond the "state-of-the-art" they had already achieved in the first phase, as well as an effort to exploit the encouraging results of the initial phases for defining and optimizing fabrication techniques which showed a real potential for generating new and more economical detector devices. The basic means selected for further film material improvement were, for example, extensive improvements and modification in deposition techniques, handling techniques, starting material preparation techniques and others

as discussed in Section 2.0. The new approaches for fabricating films with significantly improved electrical properties and enhanced photo-response included technique for effecting a more critical control over film stoichiometry and for doping or trap formation. Specifically, this phase of the work included:

a) The use of discharge sputtering with <u>substrate bias</u>. Originally this was proposed as a technique to improve PbSnTe purity, but as we shall see, it yielded some unexpected, extremely interesting results which are particularly useful for device fabrication.

b) The utilization of <u>ion-beam sputtering</u>. This was to permit sputtering in a significantly improved environment as well as control over the kinetic energies of the depositing particles.

c) The introduction of sputtering from <u>non-stoichiometric targets</u>. This was to be a possible means of carrier type control or control of as-deposited film stoichiometry.

d) The controlled <u>doping</u> of $Pb_{1-x}Sn_xTe$ films during deposition by sputtering in controlled environments <u>with specified gaseous components</u>. Again in-situ carrier type control was the objective. Carrier compensation was an apparent additional result.

e) The initial investigation of <u>proton bombardment</u> of sputtered PbSnTe films. Carrier control and trap enhancement were the desired objectives.

f) The extension of electrical, optical and electro-optical <u>measurements to temperatures of less than $15^\circ K$</u>. This was to facilitate the study of scattering mechanisms as well as the search and identification of trapping centers.

Parallel with the final phases of this program, work was also carried out, under IRAD projects sponsored by General Dynamics, to exploit the results of this contract for demonstrating the feasibility of preparing infrared sensor devices with the most promising film preparation techniques that had evolved. This work consisted of the following:

a) the preparation of photosensitive p-n junctions utilizing the bias sputtering technique, b) the preparation of photosensitive p-n junctions utilizing doping techniques, c) the preparation of response enhanced photoconductors, and d) the preparation of photosensitive Schottky barrier diodes. For purposes of completeness and continuity, the relevant results of these IRAD studies are also included in the following sections. Their value is that they demonstrate the sputtering technique to be not only capable of producing high quality films with controlled properties but also viable as a fabrication technique for thin film infrared detectors operating in the socalled LWIR band.

3.2 MATERIAL PROPERTIES OF AS-DEPOSITED SPUTTERED PbSnTe FILMS

3.2.1 SUMMARY OF TARGETS INVESTIGATED AND THEIR CHARACTERISTICS. As the reader is well aware by this point, major emphasis in this program has been on a thorough investigation of the material properties of sputtered $Pb_{1-x}Sn_xTe$ films as well as on a continuous effort to improve the sputtered film properties. One basic task along these lines was a study of the effect of target composition on film properties. For this purpose a considerable number of sputtering targets were prepared with selected differences in composition or x-values.

In general, great care was taken to achieve a stoichiometric target composition but a number of targets were prepared to be either Te or metal-rich by specified percentages. The purpose was to explore stoichiometry as an additional parameter with regard to film carrier type and concentration control.

The bulk of the targets were prepared by a "standard" technique, adopted early in this study, which did meet first order film quality criteria relative to crystal structure, composition and electrical properties. During later phases, when it was desired to significantly improve the electrical properties of as-deposited films, a modified preparation method was adopted which improved the quality of the target materials themselves. All techniques were described in Section 2.2.3. Table 1[*] summarizes all targets prepared and investigated in this program. As can be seen Target #1 through Target #9 were prepared utilizing the standard procedure. The makeup of these targets differed in composition from $x = 0.15$ to $x = 0.32$.

[*] All tables applying to Section 3.0 are compiled in Appendix A.

The more recent targets (i.e. Targets #10 through #13) utilized the above mentioned improved preparation techniques.

In order to investigate the effects of controlled doping or deviation from stoichiometry on film properties, non-stoichiometric targets were prepared and utilized. Examples are Targets #5, #9. As noted in all cases, the composition of the non-stoichiometric targets is such that the results can be compared with a stoichiometric target of equal composition. E.g. Target #9 with $x = .20$ is 1% Te rich and can be compared to Target #2 with $x = 0.20$ which is stoichiometric.

As is further noted in Table 1, in some cases more than one target was prepared with the same composition and preparation procedure. Examples are Targets #4 and #8. In such cases, the older of the two targets had broken or become mechanically degraded through extensive use and needed to be replaced. As we shall see later, in such cases the results from both targets were found to be completely correlatable.

Targets #10 through #13 were prepared utilizing some of the modified preparation and handling techniques, suggested by the results achieved with previous targets. In particular these results indicated that device quality PbSnTe films could be prepared without the annealing requirements typical in bulk material. However, all of these results pointed out that this was only feasible if the film stoichiometry was critically controlled during the deposition. It became quite apparent that control of stoichiometry in the film depends among other factors, strongly on the stoichiometry and homogeneity of the target. While all targets fabricated prior to Target #10, had been prepared with the utmost care to insure complete mixing and reaction, it was found that even better control of target stoichiometry and homogeneity could be expected with a newer mixing technique discussed in Section 2.0. This technique was used in preparation of Target #10. The additional target annealing step discussed in Section 2.0 was also introduced in the preparation of Target #10. As the results with this target will show, these modifications seem to have had a definite effect on thin film properties.

Aside from improved target stoichiometry, higher purity in starting materials are expected to also result in as-deposited films with better properties. An attempt along these lines was made in the preparation of Target #11. In particular, the sublimation process described in Section 2.0 was utilized for further purification of the starting materials. Also the handling and the sealing of all starting materials into the reaction tubes, as well as all other steps through target preparations were, for the first time, carried out entirely in a oxygen and water free controlled chamber environment. This should have minimized any possible oxidation or other contamination during the target preparation process. Again, as we shall see, further improvement in film properties was realized with Target #11.

While purification procedures implemented in the preparation of Target #11, as discussed above, involved only the starting materials, we discussed in Section 2.2.3 a procedure involving the purification of the reacted $Pb_{1-x}Sn_xTe$ by sublimation. This was also utilized in this study, in particular in the preparation of Target #12. Comparison of results from Target #12 with those from Target #11 showed additional improvement in film properties.

All targets referred to above (i.e. Targets #1 - #12) were prepared having essentially the same dimensions (i.e. approximately 2 1/4" by 3/8"). The particular dimensions were selected based on the following considerations: costliness of materials; size of available quartz flasks for target molding; reasonable target size without too much risk of breakage during preparation, etc. However, as discussed in the introductory sections, one objective in the later stages of the program was to utilize the result of our materials study to prepare initial detector devices. Since a larger diameter target results in a uniform deposition over a larger area than a smaller diameter target, and since uniformity over large areas is highly desirable in the preparation of high performance devices, a larger diameter target was prepared (Target #13) for our device studies. The preparatory procedures for this target, as indicated in Table 1 were the same as those used in the preparation of Target #12.

3-9

The effect on the properties of films sputtered from the various targets discussed above are presented in the following sections.

3.2.2 AS-DEPOSITED FILM CHARACTERISTICS - ZERO SUBSTRATE BIAS

3.2.2.1 Film Structure, Composition and Carrier Type - Dependence on Target Characteristics and Deposition Conditions.

3.2.2.1.1 Epitaxial Thin Film Growth - General Experimental Parameters. The prerequisite for rendering $Pb_{1-x}Sn_xTe$ thin films suitable for photodetector application, is that the films have high quality single crystal structures. Polycrystallinity will seriously degrade the transport properties via grain boundary scattering and other mechanisms induced by the high concentration of imperfections in other than good single crystal films. Therefore, the formation of high quality single-crystal films with controlled composition and with the thicknesses required for efficient infrared detectors had to be the first objective of this work. As will be shown in the following discussion, in the course of this work deposition conditions have been well established for producing excellent, sputtered single crystal $Pb_{1-x}Sn_xTe$ film up to several microns thick having controllable composition over a rather wide range of x-values. This result could be achieved on various substrates including $CaF_2(111)$, $CaF_2(100)$, $BaF_2(111)$, i.e. all substrates selected for the various phases of this work.

The sputtering results reported below were achieved with the triode, supported discharge sputtering module discussed in Section 2.0, using both the diffusion pumped and turbo-molecularly pumped systems. The working, background pressures was in all cases held in the 10^{-7} torr region. Deposition rates were controlled over the range from $0.1\ \mu m/hr$ to about $0.3\ \mu m/hr$. Substrate temperatures were explored over the range from room temperature to $500^\circ C$, but were confined to a range between $200^\circ C$ and $400^\circ C$ once the initial results provided guidelines on the epitaxial temperature range. The deposition rate was varied by the sputtering voltage and current control to the target.

The targets utilized for the study were already discussed in the section above. The designation of these targets, as used throughout the text, and their composition has been given in Table 1.

3.2.2.1.2 The Structural and Compositional "PHASE DIAGRAM" of Sputtered $Pb_{1-x}Sn_xTe$. All of our earlier work on epitaxy (Reference 14) has shown that the structural order of thin films of any monatomic or compound system is a systematic function of a few basic deposition parameters which are independent of the deposition technique used. The primary deposition parameters are the film growth rate and the substrate temperature if, as is the case here, the system background pressure remains constant. For any system investigated to date, the dependence of structural order of these two deposition parameters can be represented by a so called structural "phase diagram" which defines the regions of growth rate and substrate temperature in which the deposited film is either single crystal, polycrystalline or amorphous.

As was expected, this generalized behavior applies also to sputtered $Pb_{1-x}Sn_xTe$ and typical phase diagrams are presented in Figures 3-1 to 3-6 for this system.

An observation which was unexpected and new is that not only the film structural quality but also the film composition can be related to the two basic deposition parameters - at least under conditions yielding epitaxy - in a very systematic fashion. This is also illustrated in Figures 3-1 to 3-6.

Finally, as is also indicated in these figures, the carrier type of epitaxial films shows well behaved trends relatable to the same deposition parameters.

Figure 3-1 illustrates these various observations for $Pb_{1-x}Sn_xTe$ film sputtered with Target #2 which has the composition $x = 0.20$ and was prepared from the Pb, Sn and Te elements. Significant is that the diagrams in Figure 3-1 apply, within the experimental limit, to all three substrates used which, as may be recalled, include cleaved $CaF_2(111)$, cleaved $BaF_2(111)$ and polished $CaF_2(100)$.

Figure 3-1 Characterization of Epitaxy, Carrier Type and Composition
of $Pb_{1-x}Sn_xTe$ Sputtered Thin Films as a Function of
Deposition Conditions. - Sputtering Target #2 $(Pb_{.80}Sn_{.20}Te)$

The upper Figure (3-1a) is representative of a structural phase diagram - limited to the polycrystal and single crystal film formation conditions. The amorphous region, not being of interest, was not explored. A typical epitaxial transition temperature curve is observed which shows the normal growth rate sensitivity. This satisfies the basic requirements for accommodating the ordering process. The higher the substrate temperature (or the resulting mobility of the adsorbed sputtered particles) the higher can be the particle incidence rate (or resulting adsorption rate) without interfering with the epitaxial ordering process on a given substrate. Thus, for any given growth rate between the values indicated in Figure 3-1a, epitaxial film is formed if the corresponding substrate temperature lies above the epitaxial transition temperature curve.

Now Figure 3-1 also shows the existence of an additional transition temperature which appears to be relatively independent of rate. Above this temperature the formation of a single-crystal films is no longer possible. Films grown at such high temperatures are generally polycrystalline or show broad fibered growth. These films are also considerably off-stoichiometry or, in some cases, consist of more than one phase. In fact, the reason for not achieving epitaxy is the compositional nonuniformity or lack of stoichiometry. This can occur for several reasons. One is the vapor pressure difference of the individual components in the $Pb_{1-x}Sn_xTe$ compound which will cause, at the higher temperatures low adsorption probability due to a short mean time of stay (or re-evaporation) of the higher vapor pressure components. Te for one has a vapor pressure of about 10^{-3} torr at $300^{\circ}C$ and will thus rapidly evaporate unless chemically adsorbed in the compound structure. Another mechanism which can account, in addition, for the high temperature limit to epitaxial growth is the potential, temperature enhanced precipitation of a second phase (e.g. Te) during the deposition.

Figure 3-1a gives also the first indication that the film composition or x-values within the epitaxial region vary systematically with substrate temperature and growth rate. Although all films represented in the figure were obtained with the same target, the annotated data in this figure shows that; (a) x-values increase with increasing growth rate for a constant temperature, (b) x-values increase with increasing temperature for a constant growth rate, and (c) that the x-values are not limited in magnitude to the x-value of that target which was 0.20 in this case. Also apparent in this figure is the observation that for each growth rate there is a maximum x-value for which epitaxy is feasible (e.g. maximum x-value for epitaxial film formation at growth rate of 2.0 μm/hr is x = 0.23). A similar boundary exists for each substrate temperature. It becomes thus quite clear that it is possible to control composition over a wide range (.15 $\leq$ x $\leq$ .275 in Figure 3-1a) by varying the sputtering conditions and still produce epitaxial films.

In fact, it was found that the x-values shown in Figure 3-1a can be represented by iso-compositional curves. As shown in Figure 3-1b, constant x-values can be achieved for a whole set of substrate temperature and rate conditions. In Figure 3-2, the same information is presented in an experimentally very useful form. This figure shows, for three fixed substrate temperatures, the deposition rate required to produce single crystal film with a desired x-value - again for a target x-value of 0.20 and any of the three substrates investigated.

Of considerable experimental interest is the fact that single crystal films having the same x-value but having been deposited under different deposition conditions show some differences in the quality of their structural and electrical properties. In general, single crystal films along any one of the iso-compositional lines in Figure 3-1a, (i.e. film having identical x-values) show the highest structural perfection and best as-deposited electrical properties if they are deposited at the highest temperature and lowest rate associated with each line. For example, referring to Figure 3-1b, films with an x-value = 0.17, have the best characteristics if deposited at about 345°C with a rate of 0.35 μm/hr.
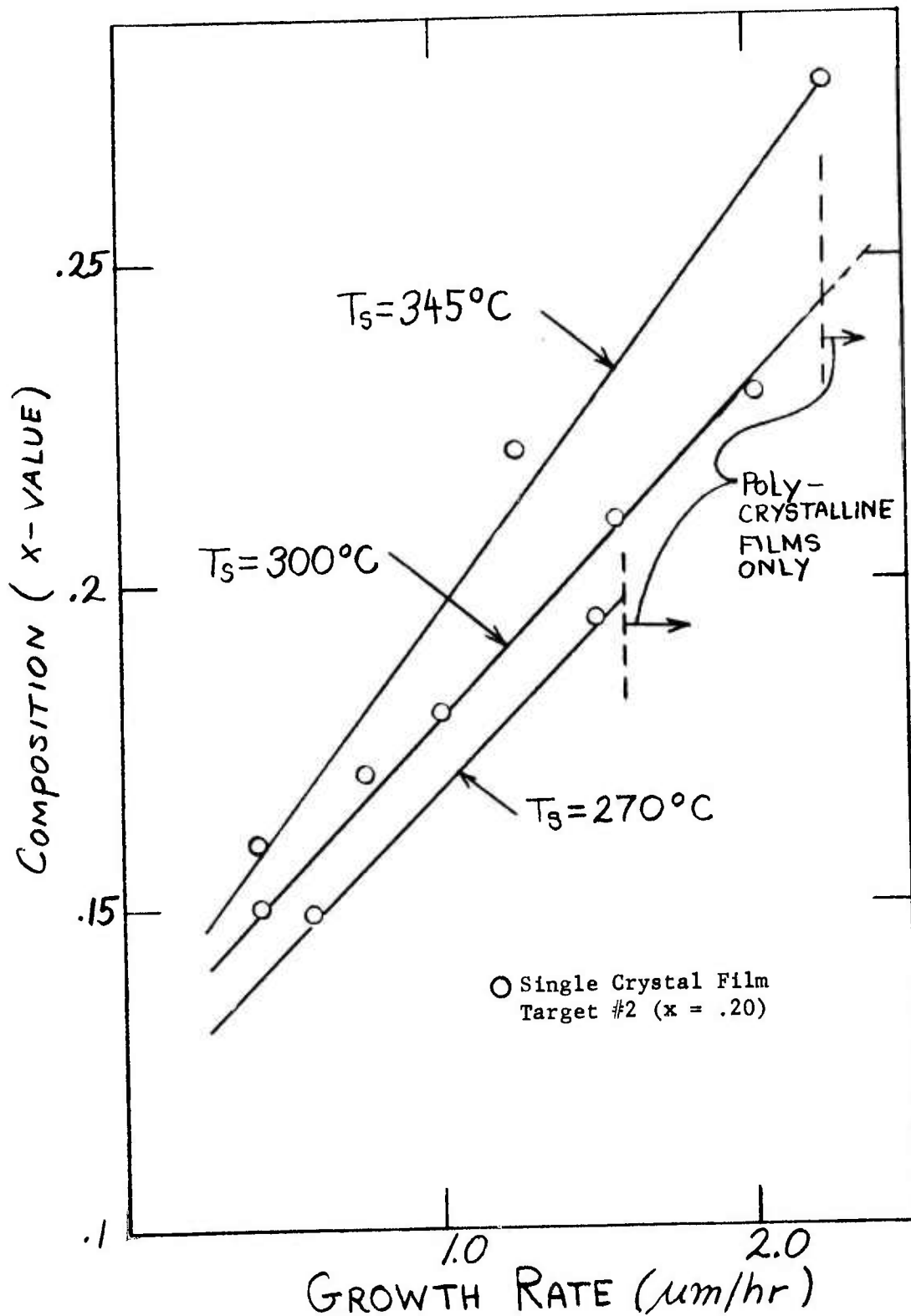
Figure 3-2 Growth Rate Dependence of Sputtered $Pb_{1-x}Sn_xTe$ Film
Composition

3-15

In summary, while it has been established that single crystal films having a large range of x-values can be produced with a single composition target, the formation of really high quality film is limited to a somewhat smaller range of x-values and conditions. This becomes more apparent when we discuss electrical properties and conditions under which as-deposited stoichiometric films can be deposited. A more limited range of deposition conditions and, thus, x-values exists for stoichiometric films. However, as we shall further show, with the use of bias sputtering these limitations are eliminated so that as-deposited stoichiometric films of all compositions (as specified by the phase diagram for each particular target) can be produced from a single target

This brings us to the third and also very interesting rate and temperature dependent behavior observed in this program which is shown in Figure 3-1c - the systematic dependence of film carrier type on these deposition parameters. The sputtered single crystal films plotted in this figure exhibited p-type or n-type characteristics in apparently well defined regions of conditions. High substrate temperatures and high rates tend to produce n-type film and, conversely, low temperatures and rates yield p-type material. The "transition" temperature is again very rate dependent. The boundary between the p- and n-type regions is later identified as a transition curve since it defines the sets of conditions (T_s, R) at which films switch from n- to p-type. This transition curve, as we shall show in the following, is different for each different target and changes with target composition in a consistent fashion.

The generality of the trends observed with Target #2 as well as the differences in specific values derived from different targets is illustrated in Figures 3-3 through 3-6. Here, the three types of "phase" diagrams (as shown in Figure 3-1) are given for the results achieved utilizing some of the targets investigated in the program. In most cases the targets differ in composition and in one case in stoichiometry (the preparation and some characteristics of each of these

3-16
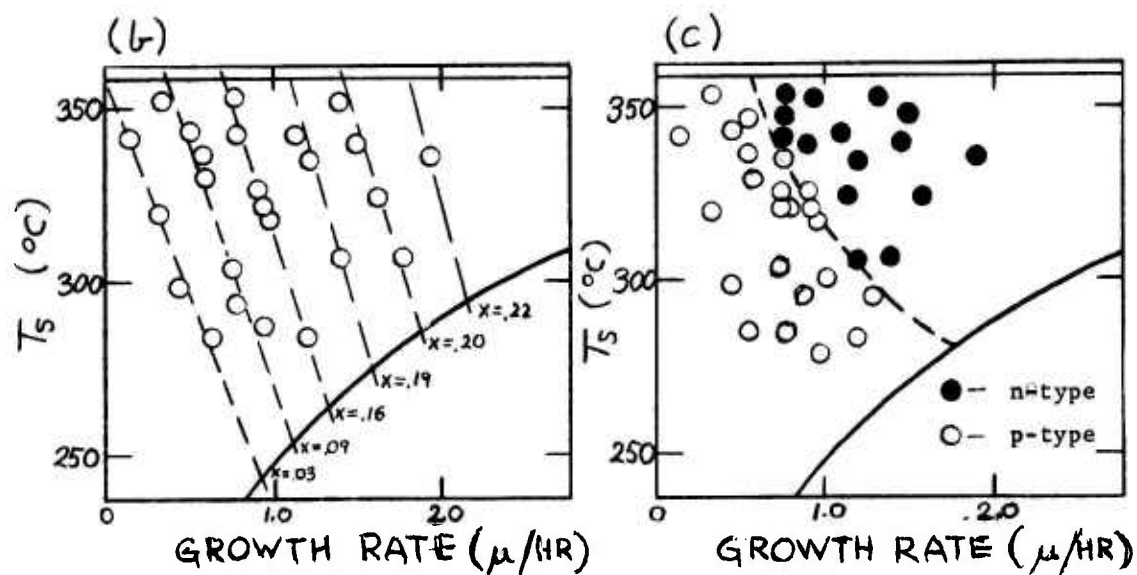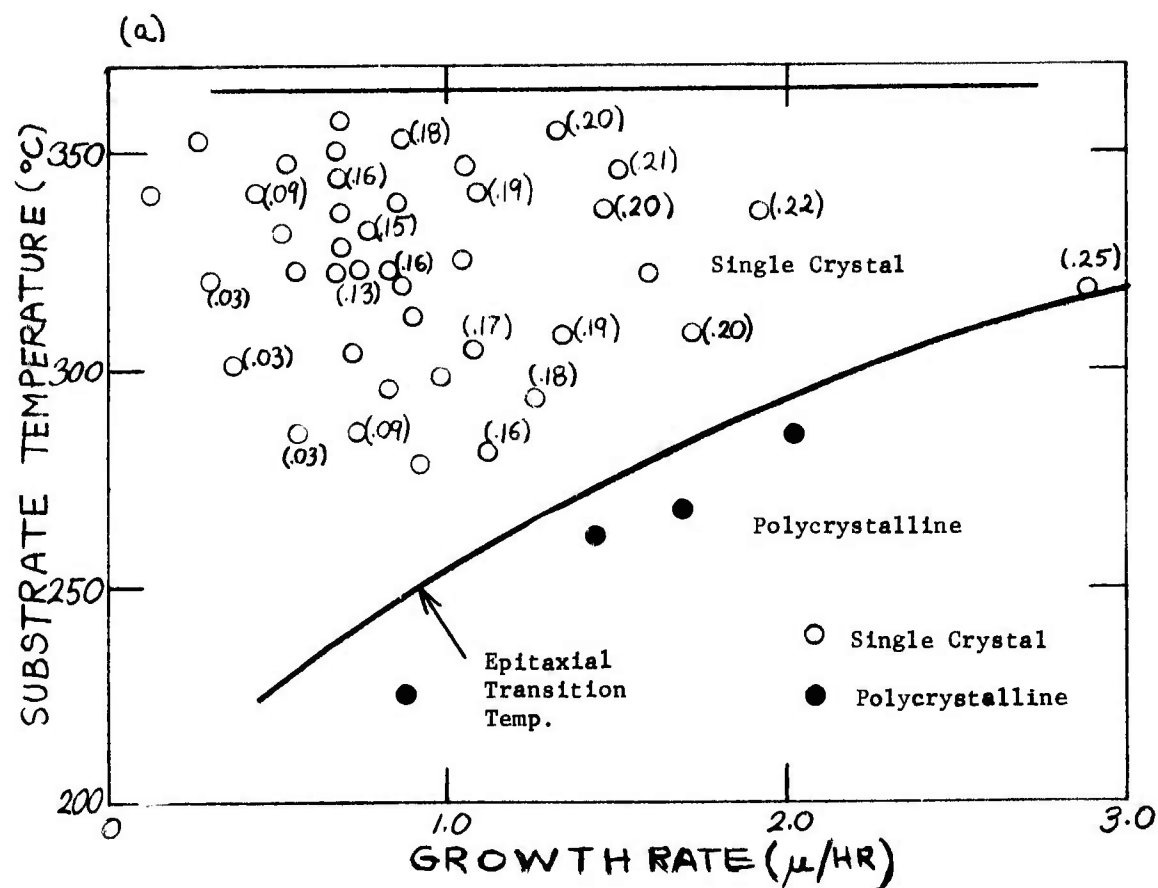
Figure 3-3 Characterization of Epitaxy, Carrier Type and Composition
of $Pb_{1-x}Sn_xTe$ Sputtered Thin Films as a Function of
Deposition Conditions - Sputtering Target #3 ($Pb_{.85}Sn_{.15}Te$)
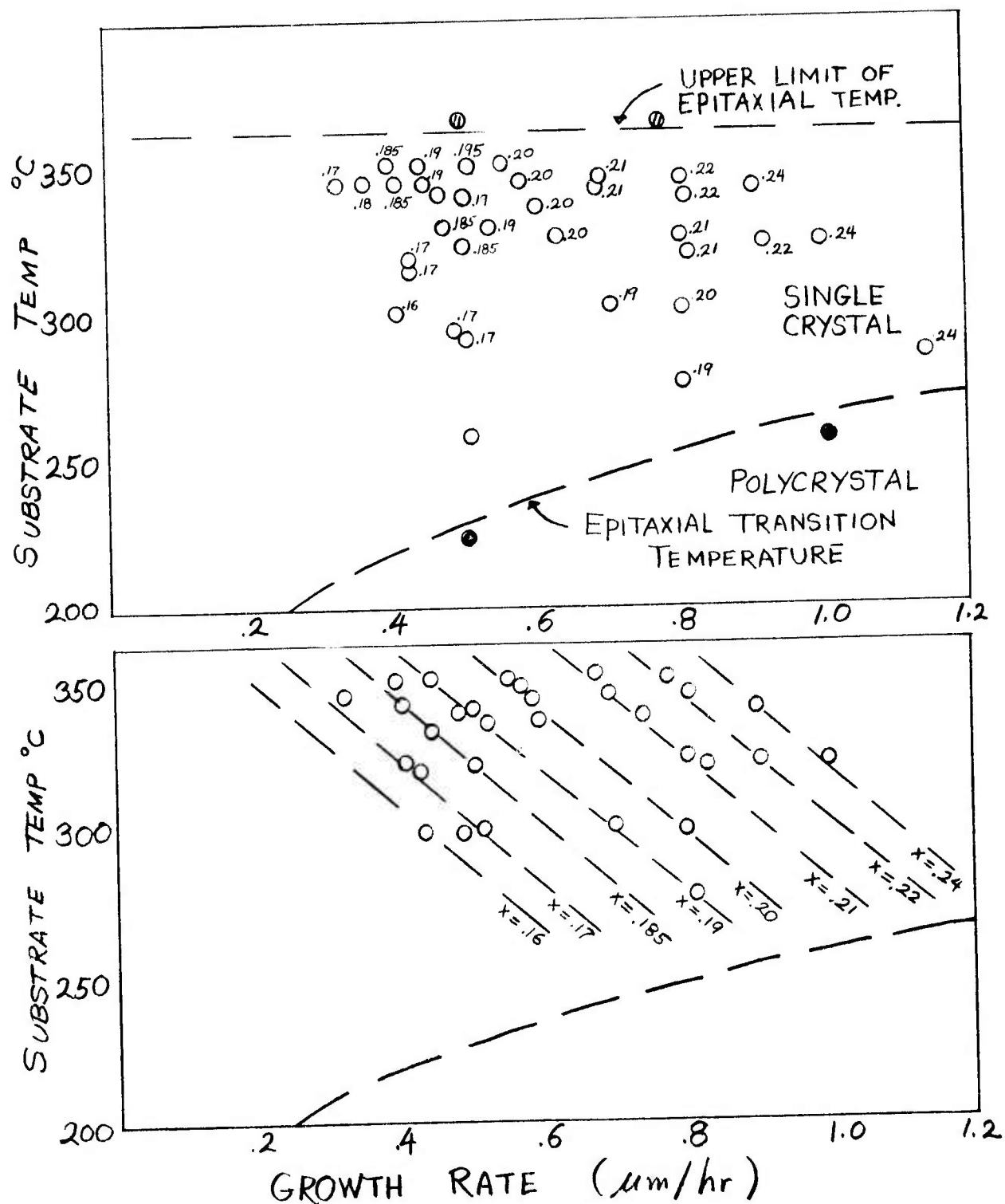
Figure 3-4   Characterization of Epitaxy and Composition of $Pb_{1-x}Sn_xTe$
Sputtered Thin Films as a Function of Deposition Conditions
Sputtering Target #4 ($Pb_{.75}Sn_{.25}Te$)

SUBSTRATE TEMPERATURE (°C)

350

300

250

O .20
O .19
O .21
.20 .20   O .21
O .19
    .22
O .22

Single Crystal

O .22   O .24   O .25   O .26
O .24   O .255
    .23   O .25   O .255   O .26   O .27
.22   O .26   O .27
.23 .24

O

O   O

Polycrystal

GROWTH RATE (μm/hr)

0.5   1.0   1.5

SUBSTRATE TEMPERATURE (°C)

350

300

250

X= .19 .20 .22 .23 .25 .26 .27

GROWTH RATE (μm/hr)
.5   1.0   1.5

350

300

250

● n-type
○ p-type

GROWTH RATE (μm/hr)
.5   1.0   1.5
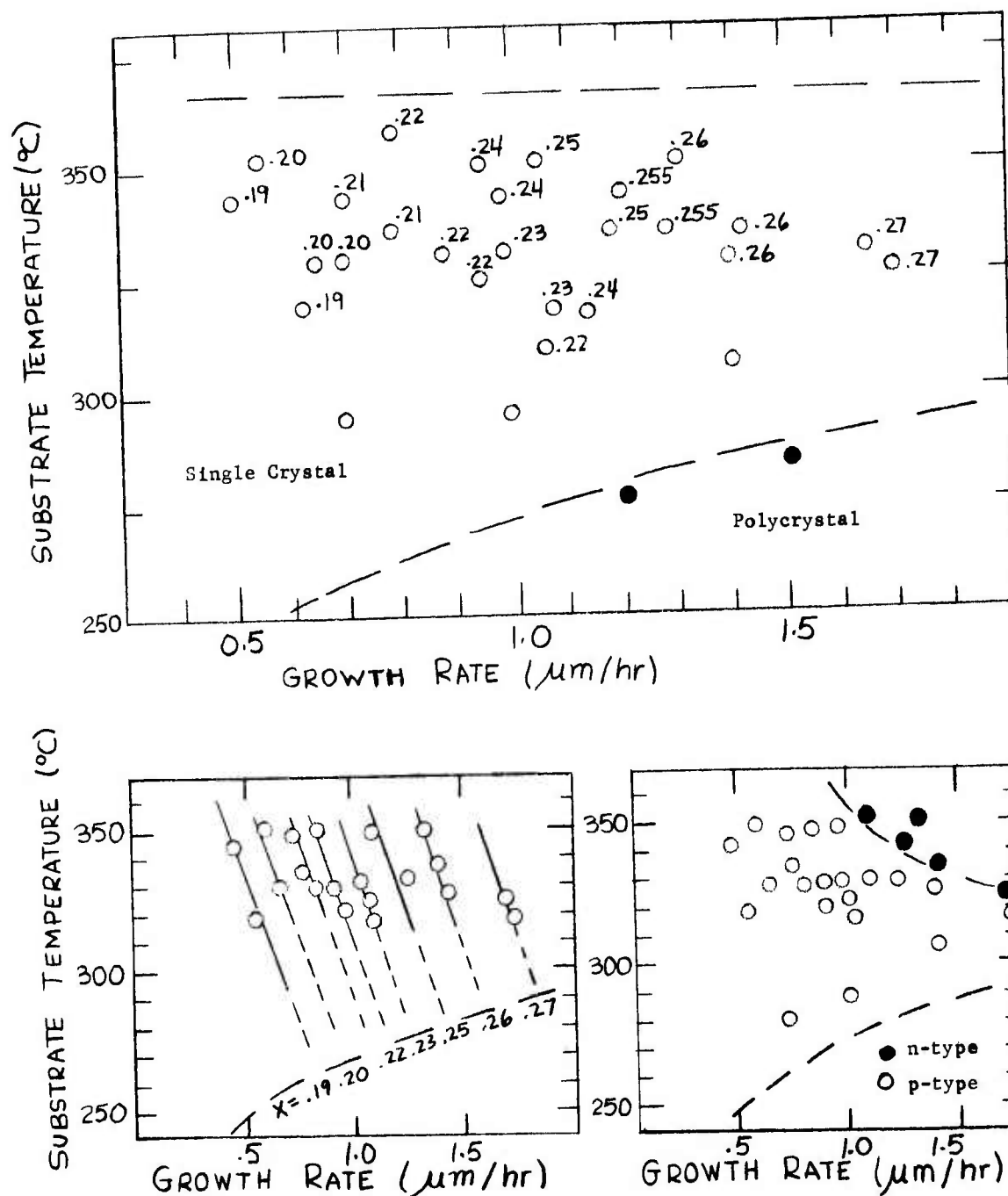
Figure 3-5 Characterization of Epitaxy, Carrier Type, and Composition of
$Pb_{1-x}Sn_xTe$ Sputtered Films as a Function of Deposition
Conditions - (Sputtering Target #8)

3-19

targets were discussed in the preceding section and listed in Table 1). A very significant observation from these figures is that for all targets investigated to date, the general observations made in connection with Target #2 are again apparent in these figures: - i.e. 1) the epitaxial film growth region is again defined by two structural transition temperatures, the epitaxial transition temperatures and the epitaxial temperature limit; 2) the systematic variation of film composition within the epitaxial region is again observed and defined by substrate temperature and growth rate; 3) finally, we again observe the existence of transition curves bounding the p- and n-type regions also defined by deposition rate and substrate temperature.

Effects of the target characteristics on these general trends are present. As can be noted from Figures 3-3 through 3-6, the two structural transition temperatures, the epitaxial transition temperature and the epitaxial temperature limit, where shown, may be slightly but not significantly different for the various targets. However, comparison of Figures 3-3 to 3-6 with 3-1a demonstrates that, as expected, the range of single crystal film x-values that can be achieved differs considerably for the various targets as do the conditions at which a particular x-value is observed. Furthermore, the same comparison also demonstrates that the critical "boundary" at which a change in the film characteristics from p- to n-type occurs, is shifted in rate and temperature depending on the x-value of the target.

Let us consider more specifically the results from the various targets as shown in Figures 3-1 through 3-6 in order to see how the target characteristics (i.e. composition, stoichiometry, etc.) effect the film compositions as well as the p- to n-type transition.* Inspection of the results shown in Figures 3-1 for Target #2 (x = .20), Figure 3-3 for Target #3 (x = 0.15), and Figure 3-4 for Target #4 (x = 0.25) show that the higher the target x-value, the higher are the single crystal film x-values that can be achieved within the range of epitaxial

---

* Actual values associated with the data shown in Figures 3-1 through 3-6 are documented in Tables 3 through 8 along with the film electrical properties.

deposition conditions. For example, for a nearly identical range of deposition conditions, Target #3 (x = 0.15) yielded single crystal film with x-values as low as 0.03, while the lower limit of x-values was about 0.15 for Target #2 (x = 0.20) and 0.17 for Target #4 (x = 0.25). This type of dependence is consistently observed for all deposition conditions. The results shown in Figure 3-5 and 3-6 for Targets #8 and #9 are also consistent with these observations. As already discussed in the Section 3.2.1, Target #8 (x = 0.25) was prepared to replace Target #4 which had become mechanically degraded. The experiments with Target #8 were concerned, therefore, with the reproducibility of results (e.g. composition, carrier type, etc.) and it was found that, for the same range of deposition conditions, all film properties from the two targets were consistent. However, as noted in Figure 3-5 for Target #8, a transition from p- to n-type films has been identified, whereas for the deposition conditions utilized with Target #4, this boundary was not identified (all films investigated from Target #4 showed p-type conductivity). The reason is simply that the deposition conditions used with Target #4 were limited to values below those for which a transition could be expected while, as shown in Figure 3-5, the range of deposition conditions used with Target #8 was expanded so that a transition should be observed—as indeed it was.

As in the case of Targets #8 and #4, Target #7 (see Table 1) was prepared to have the same composition as Target #2 (x = .20). Target #7 was investigated in some detail for comparison with Target #2. The structure, composition and carrier type of the films prepared from Target #7 are entirely consistent with those prepared from Target #2. In fact, as we shall show later, it is possible to utilize the combined results from Target #7 and Target #2 to demonstrate a relation between the p-n transition and as-deposited carrier concentrations.

For reasons discussed in Section 3.2.1, Target #9 was purposely prepared to be non-stoichiometric $((Pb_{.80}Sn_{.20})Te_{1.01})$. The evaluation of effects, if any, of target non-stoichiometry on the structural quality, the composition and the carrier types in the deposited films is done by comparing data from Target #9 with those previously collected utilizing Target #2 and #7. The latter are stoichiometric and have the same composition as Target #9. Figure 3-6 illustrates such a comparison between Targets #9 and #2. In this figure we focus our attention on the region of epitaxy only. That is, all data shown are derived from films which were single crystal. Figure 3-6(a) shows the now typical systematic variation of composition (i.e., x-value) with substrate temperature and growth rate. Of interest, however, is the fact that the compositions measured in films prepared with this Te rich target are, for equivalent conditions, the same as those derived from the corresponding stoichiometric targets (i.e. Targets #2 and #7 both with x = 0.20). It appears, therefore, that the compositions are not affected by the non-stoichiometry of the target. However, we do note in Figure 3-6(b) that the carrier type is measurably affected by the non-stoichiometry of the target. For this we focus our attention on the p- to n-type transition boundary established with Target #9 and the dashed line transition curve for Target #2 which is reproduced from Figure 3-1. We note that the transition from p-type to n-type behavior occurs at higher substrate temperatures for a given deposition rate (or at higher deposition rates for a given substrate temperature) with Target #9 than with the stoichiometric Target #2. This shift is qualitatively not inconsistent with the fact that Target #9 is Te rich-provided the transition conditions are associated with conditions at which the films approach good stoichiometry. Such a conclusion is consistent with all of the results presented and, as we shall see later, the electrical properties of the films deposited with all targets investigated support this hypothesis.

The variation of the transition conditions with target composition is further illustrated in Figure 3-7 for several other targets investigated to date. In all cases the as-deposited films prepared under condi-
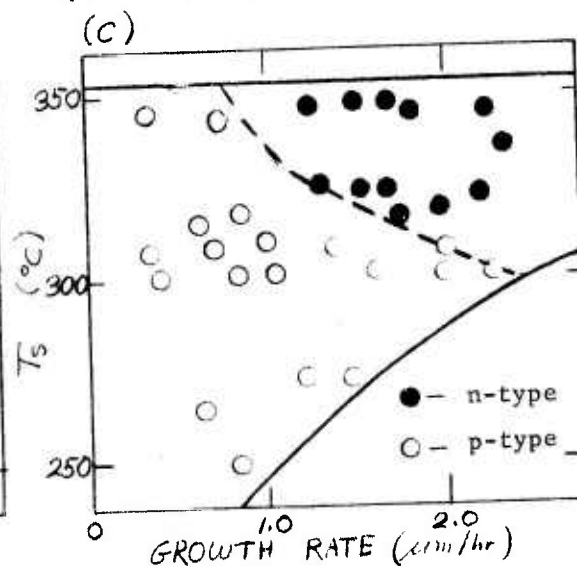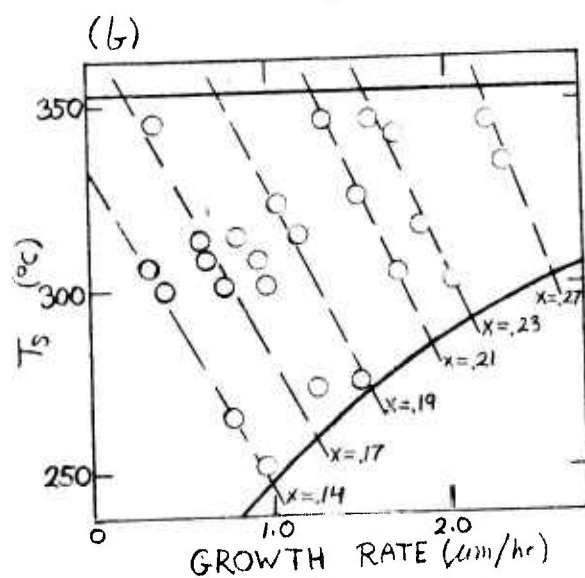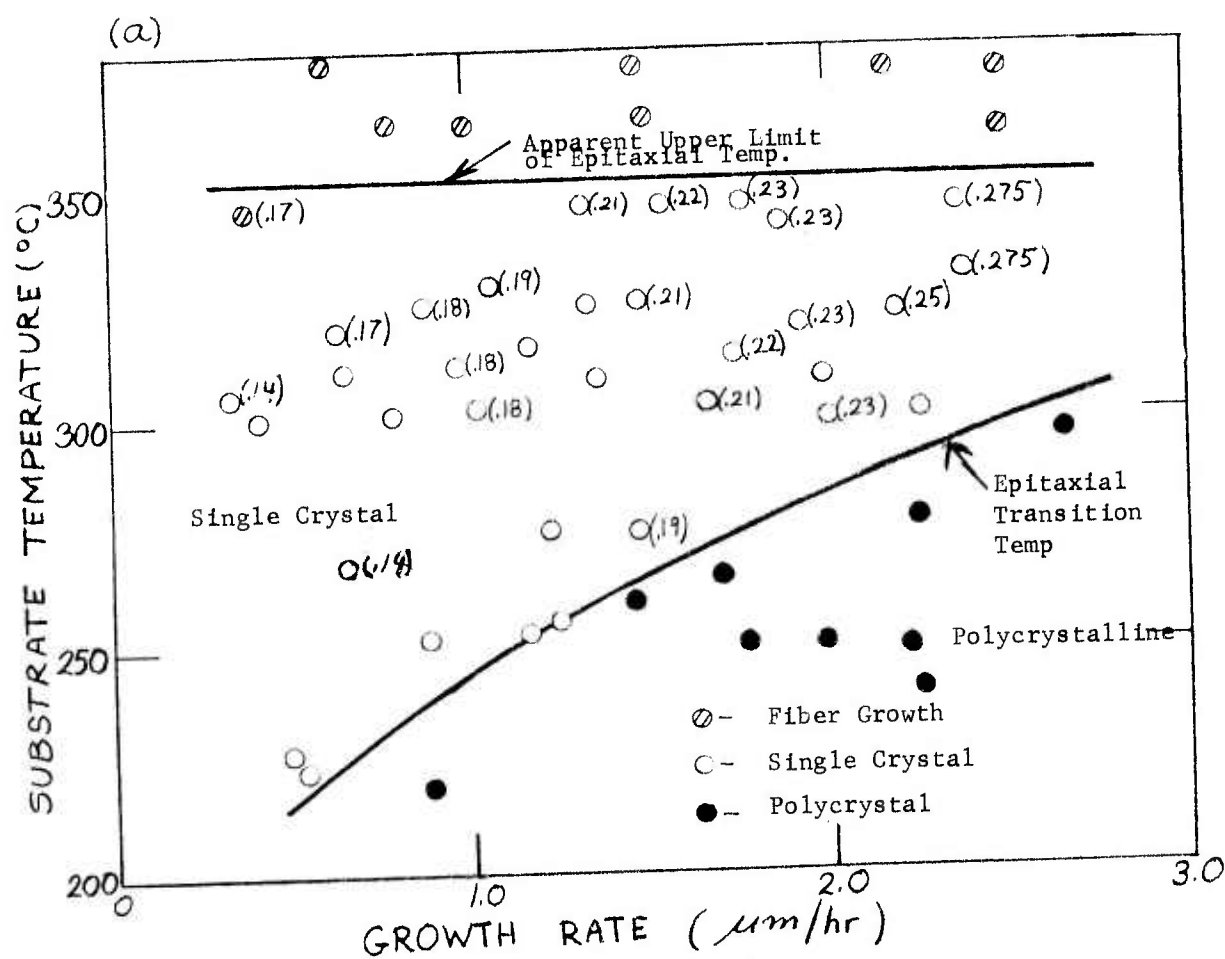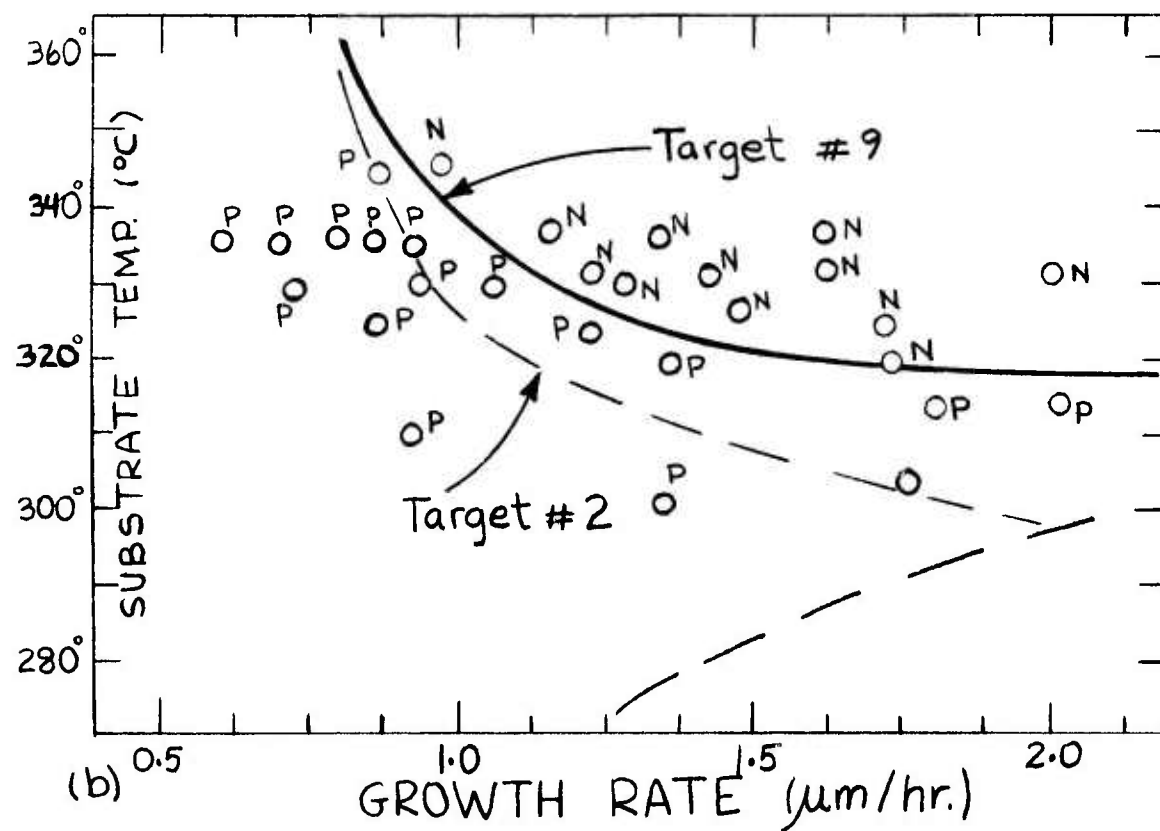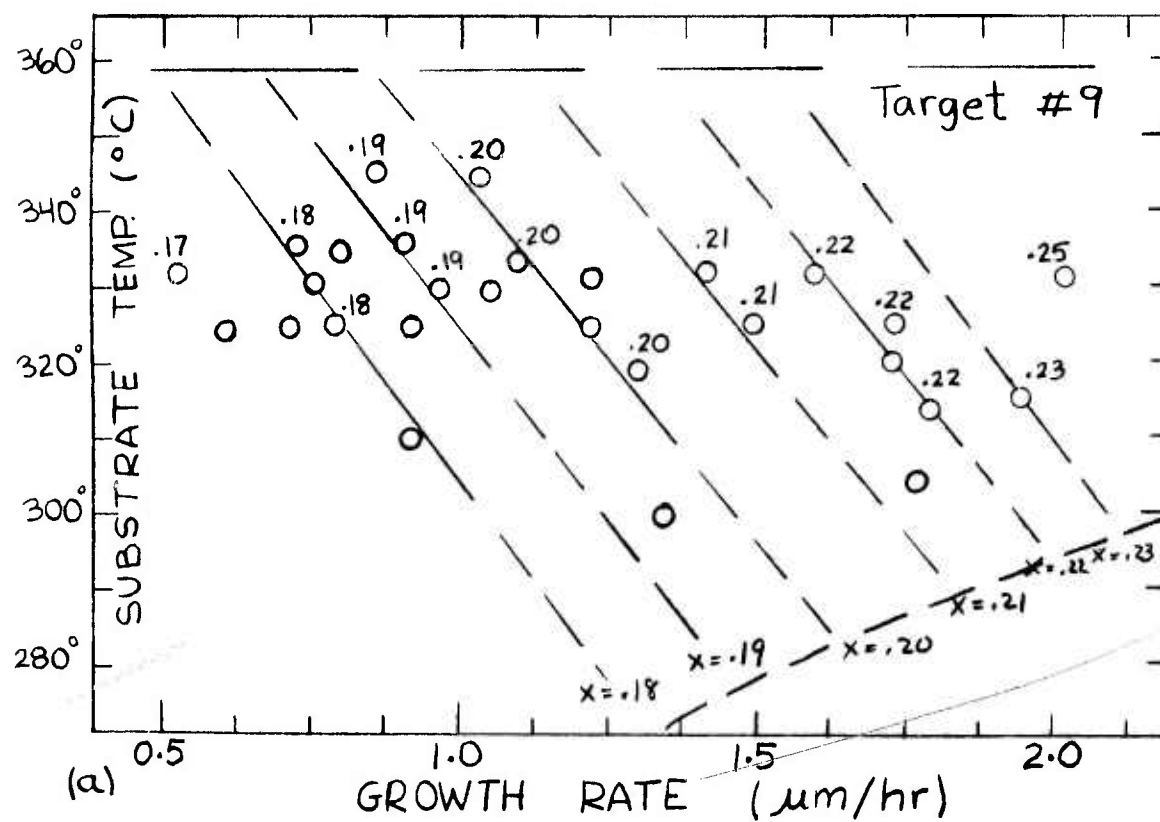
Figure 3-6 Characterization of Epitaxy, Carrier Type, and Composition of $Pb_{1-x}Sn_xTe$ Sputtered Films as a Function of Deposition Conditions - (Sputtering Target #9)
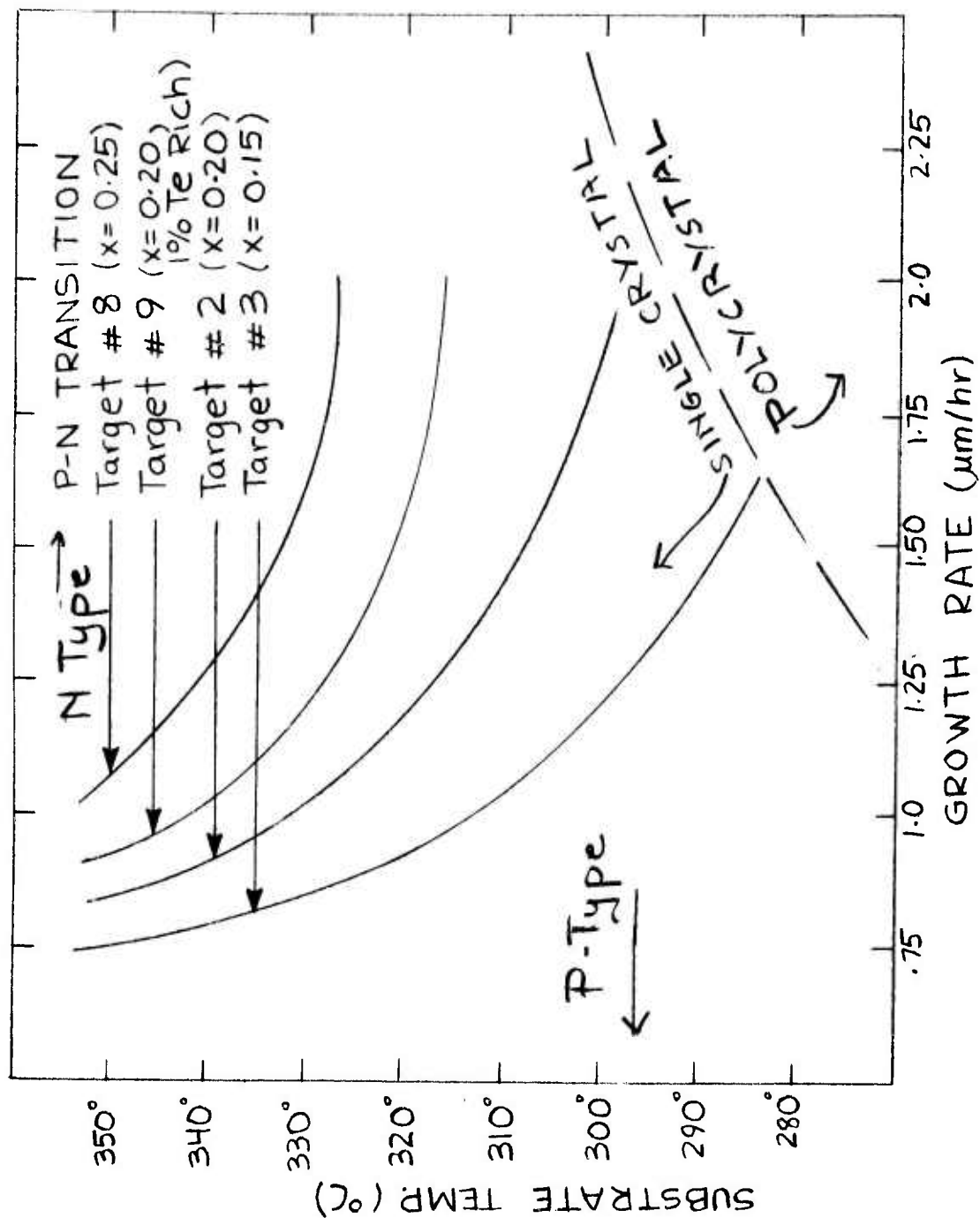
Figure 3-7 p-n Transition Conditions for Targets of Different Compositions

tions to the right of the transition curves are n-type and those to the left are p-type. As clearly shown, the transition conditions move to higher rates and temperatures with increasing target x-values. The trend for the non-stoichiometric targets (on the Te-rich side) is interesting. It shows that small deviations from stoichiometry are as effective in changing the transition conditions as are much larger composition differences.

Table 2 summarizes some of the information for the targets investigated to date and brings out an important point. While most of the trends are typical of what has been discussed above, i.e. the range of x-values of p- and n-type films from each target is a function of the target composition, the results shown in the last column show a different observation which is important in the target selection. Here we give, for each target, compositions of films deposited under conditions close to the p-n transition curve. Of interest is the fact that the range of such compositions, shift also to higher x-values with increasing target x-value. In fact the actual x-values of films prepared with conditions on the p-n transition curves are very closely bunched around a value which is the same as the target x-value. The consistency is as good as can be expected, considering the experimental tolerance limit of the measurements involved. This observation may be considered an additional indication that the p-n transition curve defines conditions under which the most stoichiometric films are produced. As already mentioned and as will be presented in a later section, electrical properties of films deposited near this transition curve for all targets investigated also suggest this.

The results discussed here certainly reconfirm that it is possible to sputter single crystal thin films of desired composition and carrier type with good reliability. Furthermore the feasibility of preparing single crystal film with controlled composition over a reasonably wide range with a target of a single composition is also verified. In this regard, a few additional observations should be made. First, if indeed, as discussed above, the transition curve is

3-25

related to film stoichiometry, then high quality p-type films which are nearly stoichiometric can be deposited under one set of conditions close to but to the left of the transition condition. This could be followed immediately by deposition of n-type films if either substrate temperature or rate is changed to yield a set of conditions slightly to the right of the transition curve. This should result in the deposition of a p-n junction in a single, simple deposition run. However, since the compositions of films deposited under conditions to the left and right of the transition curve are not exactly the same, this would present some difficulty in the deposition of a true homo-junction. One can, however, deposit a hetero-junction in this fashion. Also, if a post-deposition anneal is required, the difference in composition calls for a property degrading compromise since no single annealing temperature exists which produces the ultimate stoichiometry control in both film layers.

A second consideration involves the useful range of x-values from a single target i.e. the range in which the highest quality p- and n-type films can be produced. As is apparent from Table 2 and if indeed we restrict ourselves to the p-n transition region for high quality as-deposited films, this useful range of x-values is somewhat more restricted. As we shall see in a later section, a solution to these problems seems to have been found with the introduction of bias-sputtering.

The phenomena responsible for some of the observed results can be understood by referring to some of our earlier work with sputtered compounds. Although there has been no attempt to quantitatively define the observation presented thus far, certain deductions based on this previous work are consistent with the results. The existence of a growth-rate dependent epitaxial temperature is entirely in keeping with the epitaxial growth rate behavior of any system and the existence of an upper epitaxial temperature limit has already been related to the differences in the vapor pressure of the compound elements. Both of these phenomena could be observed if the deposition occurred by so called direct compound deposition or if reactive deposition takes place. This means, a rate

dependent epitaxial temperature is observed, a) if the target material does not dissociate during the sputtering process and stoichiometric $Pb_{1-x}Sn_xTe$ molecules are adsorbed on the substrate or, b) if dissociation takes places and the adsorbates consist of the elemental atoms, the compounds PbTe and SnTe, or a combination thereof. Between a) and b) should be a difference in the absolute epitaxial temperatures as controlled by the activation energy of the process, which, in turn, strongly depends on the relative surface mobilities of the adsorbates. The fact that the composition can be varied with substrate temperature and deposition rate provides strong indication that the target material dissociates. The formation of epitaxially ordered compounds becomes rather complex theoretically if three or more adsorbates are involved, particularly since here a simultaneous epitaxial ordering and composition adjustment takes place. In brief, the behavior may be related to the formation energy of the compounds PbTe and SnTe. With increasing substrate temperature, the relative formation rate of the compound with the lower formation energy should tend to increase far more rapidly than the one with the higher formation energy. Available data show that SnTe has a formation energy of only 14 Kcal while PbTe requires 52 Kcal. It is thus quite plausible that x-values, determined by the SnTe concentration tend to increase with temperature. Excess metal elements of either type, that come about by the readjustment of the composition of the adsorbed source particles (defined by the target), will be preferentially re-evaporated (relative to the compounds formed) if the substrate temperature is high enough for a given incidence rate. Thus, the magnitude of the so called epitaxial temperature is not only controlled by the requirements of the ordering process but also by re-evaporation rate requirements of the excess elements adsorbed on the substrate. It should also be clear that the epitaxial temperature will, in addition, vary with composition in this process since it is likely that the surface mobility of PbTe differs from that of SnTe. Unfortunately, data to this effect are not available.

As a final word relative to the structural and compositional phase diagrams, the fact that the observed behavior is similar on all three substrates is reasonable also, considering previous experience. It is apparent that once the initial continuous film is formed on a substrate, during the remaining growth and epitaxial process single crystal $Pb_{1-x}Sn_xTe$ represents the actual substrate. Earlier work has shown that the substrate controls epitaxial temperatures primarily by its heat dissipation characteristics. For example, large differences were observed between semiconductor substrates such as Ge and dielectric substrates such as CaF_2. In this respect, the substrates used here are fairly similar and since we are dealing with relatively thick films any differences are minimized. The reason is that the critical heat dissipation is that near the very surface where it affects the residual kinetic energy of the incident particles.

The above discussion shows that the observed rate and temperature dependencies of composition appear consistent with a rate-controlled mechanism. The observed rate and temperature dependence of carrier type, as already implied in earlier discussions and as results to be presented certainly indicate, is most likely associated with deviations from stoichiometry. In this case the mechanisms may involve the rate and temperature dependence of adsorption and/or re-evaporation of Te versus Pb and Sn species. Such a mechanism is consistent with the expected behavior based on the vapor pressures of the various species. At a constant rate, the lower the temperature the more Te is expected to remain in the film and thus the more p-type the film. Conversely, at higher temperatures, Te-deficient (i.e. n-type) films may be expected as observed. Thus, if indeed this qualitative description prevails, then, referring back again to Figures 3-1 to 3-6, it is not difficult to see that film stoichiometry control, by careful control of substrate temperature and deposition rate at deposition conditions as close as possible to the p-n transition curves shown in these figures, is comparable to the kind of stoichiometry adjustment one achieves by controlling; a) annealing temperatures as close to the metal-rich solidus and stoichio-

3-28

metric composition crossover in the $Pb_{1-x}Sn_xTe$ phase diagram, and b) by controlling the annealing charge composition. We shall show in a later section, several kinds of evidence that confirm this kind of comparison. One, of course, is the electrical properties near the p- to n-transition and another, along with annealing results, is the establishment of a low-temperature crossover in the phase diagram for sputtered thin film $Pb_{1-x}Sn_xTe$ which occurs in the same temperature range as our deposition temperatures (i.e. $\approx 300 - 350^{\circ}C$).

3.2.2.2 <u>Crystal Structure and Orientation of Epitaxial Films</u>. As determined by reflection electron diffraction and x-ray diffraction techniques (see Section 2), to date all single crystal films sputtered on CaF_2(111) and BaF_2(111) have shown a (111) orientation and all single crystal films deposited on CaF_2(100) have shown the (100) orientation. To illustrate, typical epitaxial film structures of sputtered $Pb_{1-x}Sn_xTe$ are shown in Figures 3-8 through 3-11. Figure 3-8 shows the $(1\bar{1}0)$ and $(1\bar{2}1)$ electron diffraction patterns on a cleaved CaF_2(111) substrate and of a $Pb_{.84}Sn_{.16}Te$ film deposited on the same substrate. The <111> direction in the film is normal to the surface and, therefore, parallel to the substrate <111> axis. The $(1\bar{1}0)$ and $(1\bar{2}1)$ patterns are obtained by proper positioning of the sample and rotation about its normal. A rotation angle of 30 degrees separates the $(1\bar{1}0)$ orientation from the $(1\bar{2}1)$ orientation, as expected for the cubic lattice. Figure 3-9 shows similar patterns for both a cleaved BaF_2(111) substrate and an epitaxial film of $Pb_{.83}Sn_{.17}Te$ deposited on this substrate. As expected the same two orientations are obtained. Figure 3-10 shows the reflection electron diffraction patterns for a (111) film with a higher x-value, i.e. (111) $Pb_{.75}Sn_{.25}Te$ film on CaF_2(111). Finally, Figure 3-11 illustrates the electron diffraction patterns of a polished CaF_2(100) substrate and the corresponding pattern of an epitaxial $Pb_{.77}Sn_{.23}Te$ film on this polished substrate. Here, the <100> film direction is normal to the surface and parallel to the substrate <100> axis. Shown in the figure are the (001) and (011) patterns of the film. In this case a rotation of 45 degrees separates the (001) and (011) orientations.

$444 - Pb_{.84}Sn_{.16}Te$

on

CaF_2 Cl(111)
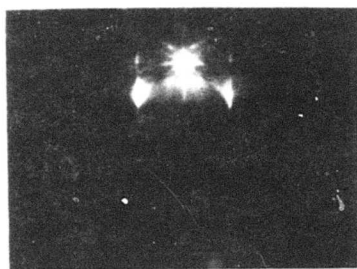
(1$\bar{2}$1)
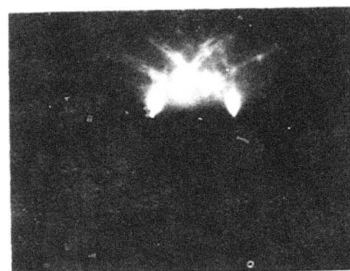
(1$\bar{1}$0)

CaF_2 Cl(111)

(1$\bar{2}$1)
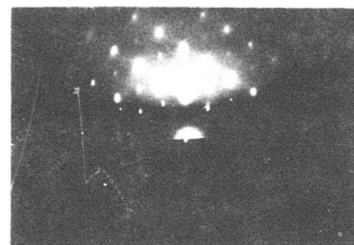
(1$\bar{1}$0)

(111) $Pb_{.84}Sn_{.16}Te$ Film

Figure 3-8 Reflection Electron Diffraction Patterns for
Sputtered Single Crystal $Pb_{.84}Sn_{.16}Te$ Film on CaF_2(111)

3-30

425 - $Pb_{.83}Sn_{.17}Te$
on
BaF_2 Cl(111)
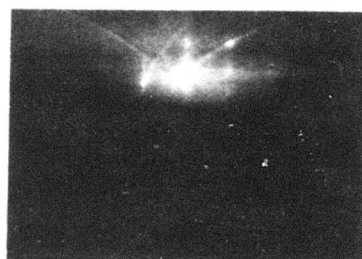
(1$\bar{2}$1)
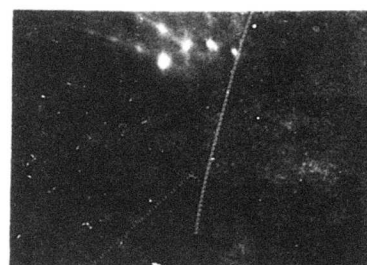
(1$\bar{1}$0)

BaF_2 Cl(111)
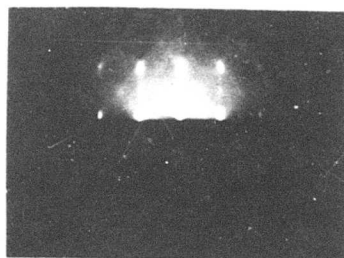
(1$\bar{2}$1)
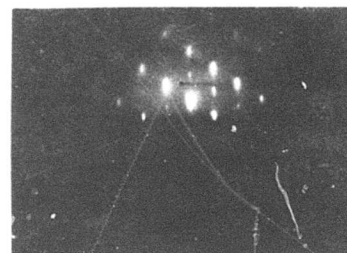
(1$\bar{1}$0)

(111) $Pb_{.83}Sn_{.17}Te$ Film

Figure 3-9 Reflection Electron Diffraction Patterns for
Sputtered Single Crystal $Pb_{.83}Sn_{.17}Te$ Film on BaF_2(111)
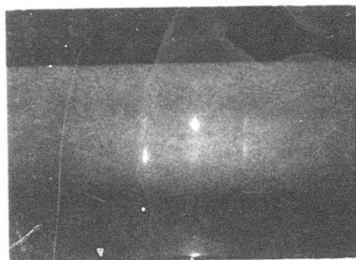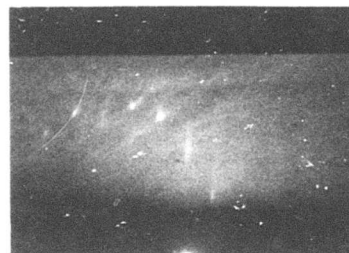
$(1\bar{2}1)$ $(0\bar{1}1)$

$CaF_2(111)$ Substrate
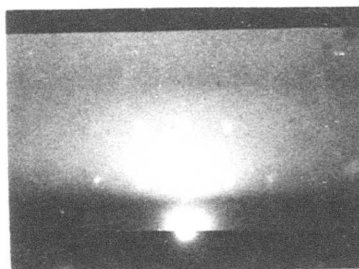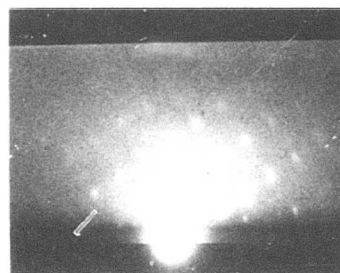
$(1\bar{2}1)$ $(0\bar{1}1)$

(111) $Pb_{.75}Sn_{.25}Te$ Film

Figure 3-10 Reflection Electron Diffraction Patterns for Sputtered Single Crystal $Pb_{.75}Sn_{.25}Te$ Film on $CaF_2(111)$

423 - Pb$_{.77}$Sn$_{.22}$Te
on
CaF$_2$ P(100)
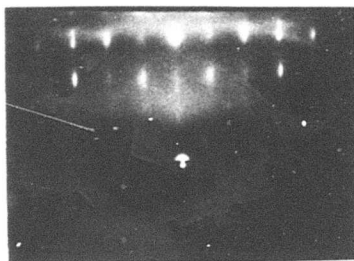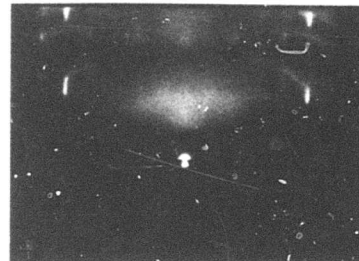
(001)   (011)

CaF$_2$ P(100)
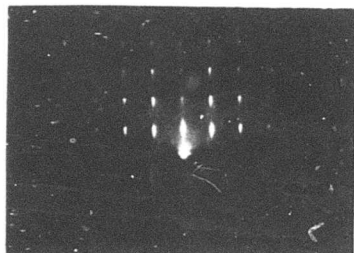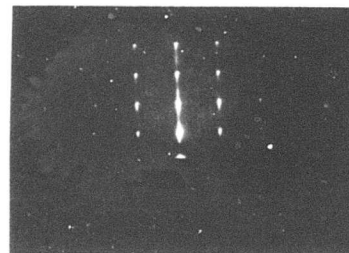
(001)   (011)

(100) Pb$_{.77}$Sn$_{.23}$Te Film

Figure 3-11 Reflection Electron Diffraction Patterns for
Sputtered Single Crystal Pb$_{.77}$Sn$_{.23}$Te Film on CaF$_2$(100)

3-33
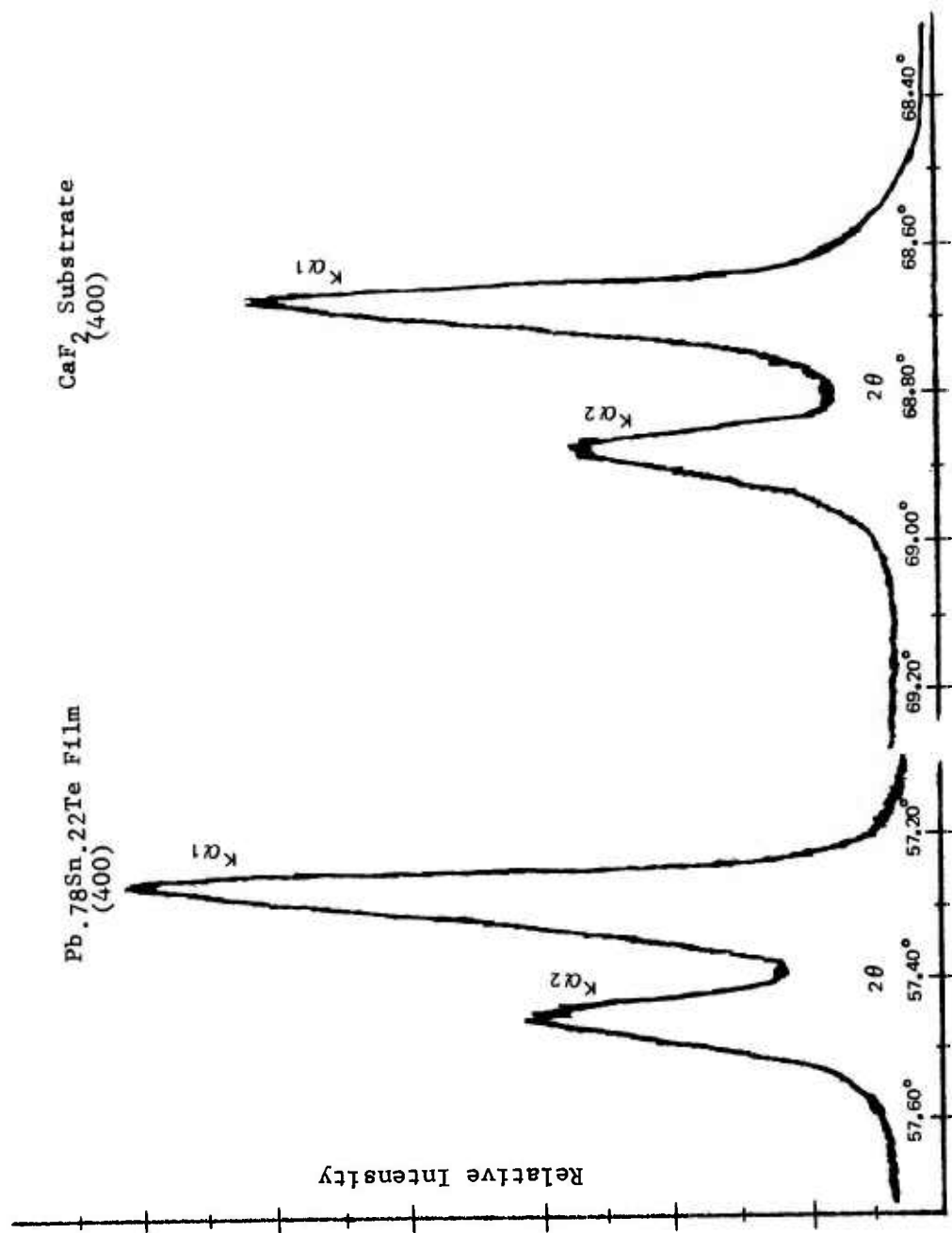
Figure 3-12 (400) Scans of Single Crystal Pb.78Sn.22Te Film and CaF2(100) Substrate

In all cases, the film patterns indicate a crystal quality which is comparable to that of the substrate. In the case of films deposited on the cleaved $CaF_2(111)$ and $BaF_2(111)$ substrate, Kikuchi lines are observed both in the film and substrate, which is evidence of excellent structural quality.

The (111) film orientation on (111) substrates and (100) orientation on (100) substrates was also clearly demonstrated by $2-\theta$ x-ray scans. Typical scans for films on $CaF_2(111)$, $BaF_2(111)$ were already shown in Figures 2-3 and 2-4, Section 2.0, along with the scans of each substrate. Referring to these figures, it can be stated that the presence of (111), (222), (444) lines for both the substrates and the films confirms the (111) orientation of the films on the $CaF_2(111)$ and $BaF_2(111)$ substrate. Similarly, scans of the polished $CaF_2(100)$ substrate and the deposited film show the presence of the (200), (400), (600) and (800) lines which indicate a (100) oriented film on the (100) substrate.

In addition to comparing the reflection electron diffraction patterns to assess, qualitatively, the crystal quality of our films, we have used comparison of the widths of x-ray diffraction lines of the deposited film and their substrate in selected cases. As an example, Figure 3-12 shows the $400K\alpha_1$ and $K\alpha_2$ lines of a $CaF_2(100)$ substrate as well as the 400 $K\alpha_1$ and $K\alpha_2$ lines of the single crystal $Pb_{.78}Sn_{.22}Te$ film deposited on the same substrate. In this case, the 400 diffraction lines of the film and of the substrate have nearly the same diffraction angle range so that a comparison of the line widths is meaningful. It can be noted that the $2-\theta$ half-width of the 400 $K\alpha_1$ line of the $CaF_2(100)$ is 0.075^O and that of the film is 0.08^O. This would indicate film quality close to that of the substrate.

3.2.2.3 <u>Carrier Concentrations of As-Deposited Films - Dependence on Target Characteristics and Deposition Conditions</u>. This section covers one of the interesting findings of this program, since it discloses a new avenue for the preparation of thin film PbSnTe with significantly improved electrical properties resulting possibly in the complete elimination of the need for lengthy annealing procedures.

3-35

We have seen, in the preceding sections, that the structural and compositional properties, as well as the carrier type of $Pb_{1-x}Sn_xTe$ films have shown rather systematic dependencies on deposition conditions The structural characteristics of $Pb_{1-x}Sn_xTe$ films are good first order indications of material quality; however, the more critical indicators for device applications are the electrical properties such as carrier concentration and mobility, and the electro-optical properties such as photoconductive response. While we shall show in a later section on transport properties of $Pb_{1-x}Sn_xTe$ films that the as-deposited electrical properties, in particular the mobility, of PbSnTe films are, in general, correlatable with deposition parameters and the resulting structural film quality, the importance of this correlation is generally minimized if annealing is required to further improve the electrical properties. One of the primary functions of annealing is to compensate for deviations from stoichiometry. Therefore, if direct deposition of films close to stoichio-metry were feasible, annealing would no longer be required. As already alluded to above and in earlier sections, results on sputtered $Pb_{1-x}Sn_xTe$ films show that appropriate deposition conditions for achieving stoichiometry on as-deposited films do, in fact, exist and are well enough definable to use as fabrication control parameters.

To illustrate these interesting results, we have utilized the data of films prepared from Targets #2, #3, #7, #8 and #9, (see Table 3 through 8). As discussed in Section 3.2.3.1, a set of deposition conditions can be defined which generates a transition curve for n- and p-type film formation. This was also schematically shown in Figure 3-7. Restating this observation in general terms, it was observed that (for a given composition) substrate temperatures and/or deposition rates which were higher than the critical values defined by the transition curves produced n-type films, lower values produced p-type film. It was then suggested that these transition conditions may be analogous to the critical annealing temperatures (switching temperatures) above which (for any given composition) films are p-type and below which they are

n-type (see for example Figure 3-77 of this report). This switching temperature, not unique to sputtered films, is assumed to correspond to a condition yielding near perfect stoichiometry. In all cases, films annealed near this switching temperature yield the lowest carrier concentrations. Thus, if there is any analogy between the p-n transition conditions and the critical annealing temperature, films sputtered with or near the p-n transition conditions should have the lowest carrier concentration also. Figures 3-13 through 3-20 illustrate that this is in fact observed.

Figure 3-13 shows applicable Target #3 data (Table 4). The solid line represents the transition curve (above which all films are found to be n-type). The data points are annotated with the measured carrier concentrations in units of 10^{18} cm^{-3}. Inspection shows that the lowest values for both p- and n-type films are located near the transition curve. Quite apparently the concentrations increase as the deposition conditions differ, increasingly, from those located on the transition curve. It is also apparent that p-type films are more sensitive to differences in deposition conditions than n-type film. Figure 3-14 provides a somewhat clearer representation of this behavior for the same set of data. Here the percentage deviation of the actual rate-temperature product (R·T) from the critical or transition product (R·T)$_0$ is used as the reference parameter and related to the as-deposited film carrier concentration. The trend is quite self evident.

That this trend is not unique for this set of experiments or this target is demonstrated by the evaluation of data from a number of targets investigated for this study, all of which show the same trends. This is illustrated in Figures 3-15 through 3-20. As noted in Figure 3-15, by comparison with Figure 3-13 (and shown schematically in Figure 3-7), the transition conditions of Targets #2 and #7 (x = 0.20) are shifted to higher temperatures and higher rates than those for Target #3 (x = 0.15). But, we again note the lowest carrier concentrations for both p- and n-type films nearest to the p-n transition conditions. Figure 3-16

3-37
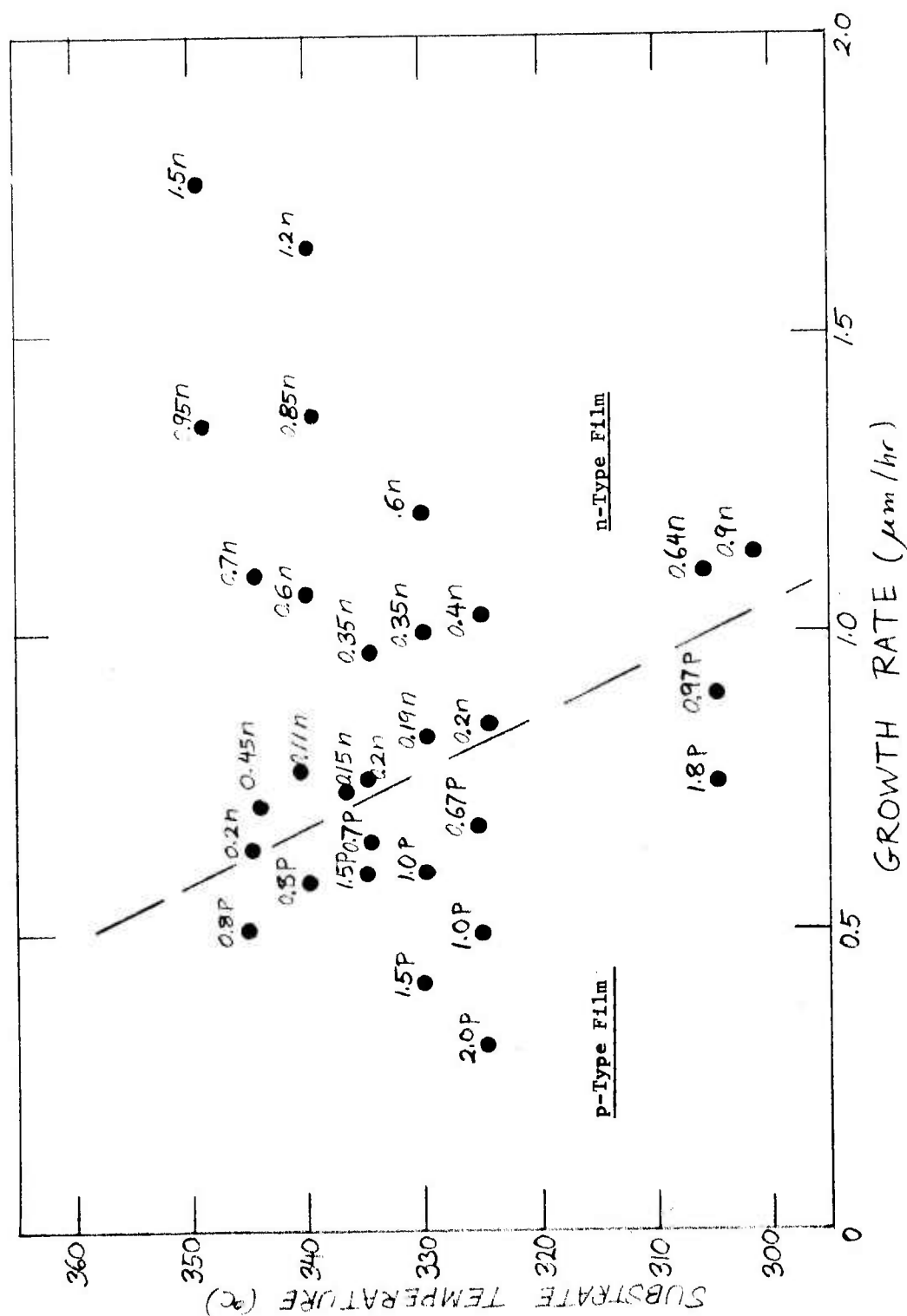
Figure 3-13   Characterization of Carrier Concentration of p- and n-Type Films Near
p-n Transition of As-Deposited Films - Sputtering Target #3
$(Pb_{.85}Sn_{.15}Te)$
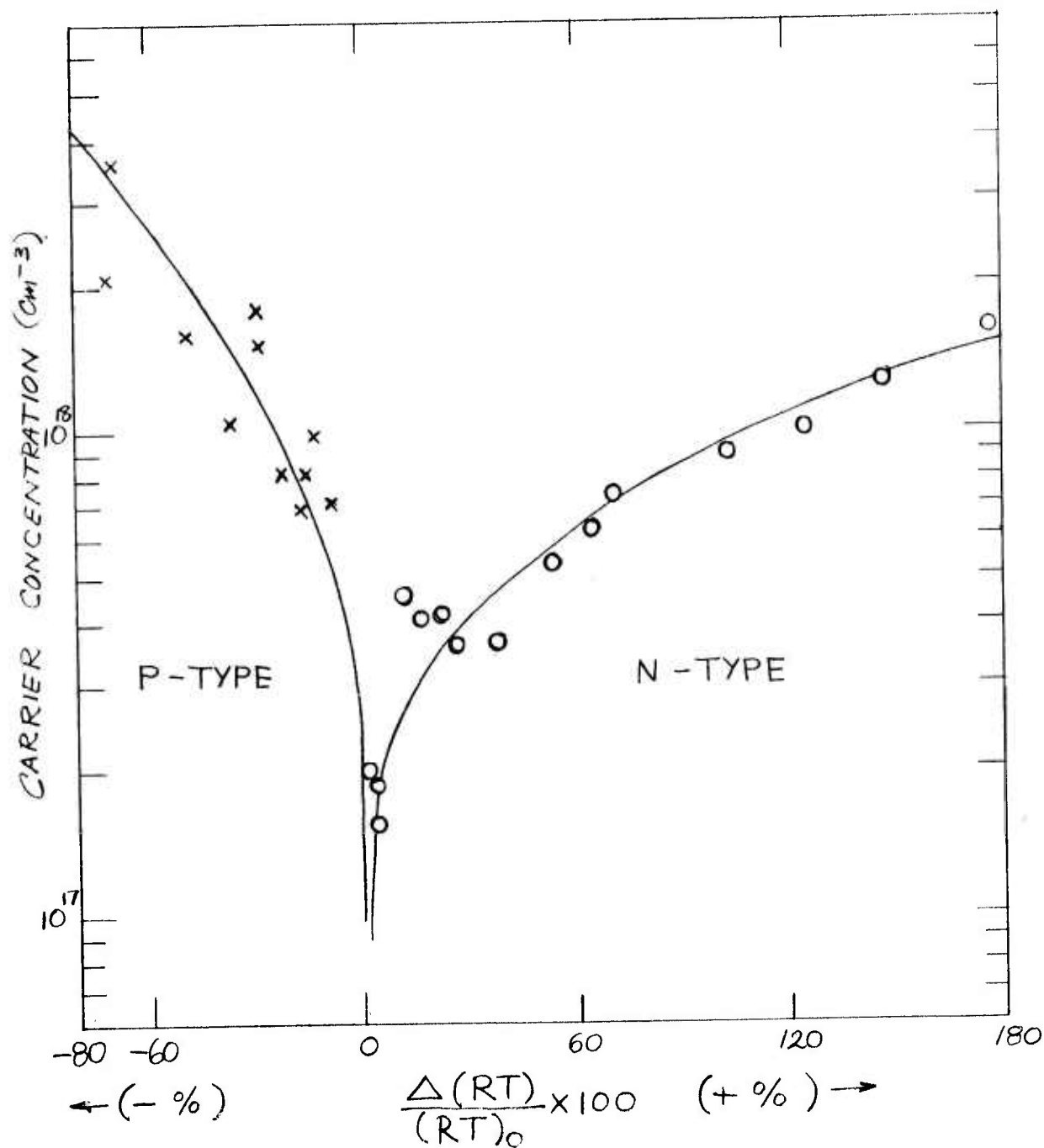
Figure **3-14** Effect of Deviation from Critical Deposition
Conditions on Carrier Concentration
(Target #3)
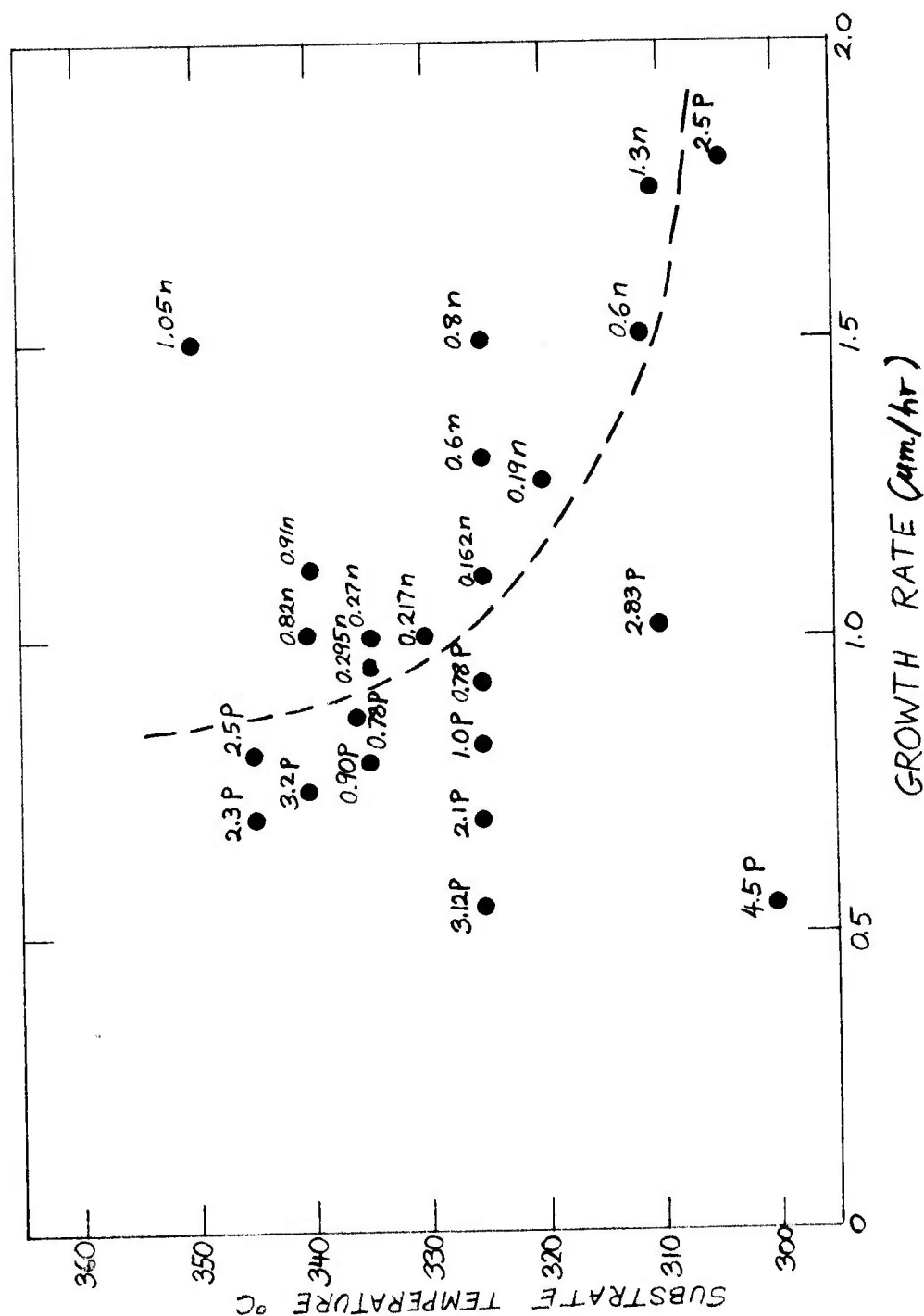
Figure 3-15 Characterization of Carrier Concentration of p- and n-Type Films Near p-n Transition of As-Deposited Films - Sputtering Targets #2 and #7 (Pb.80 Sn.20Te)

3-40
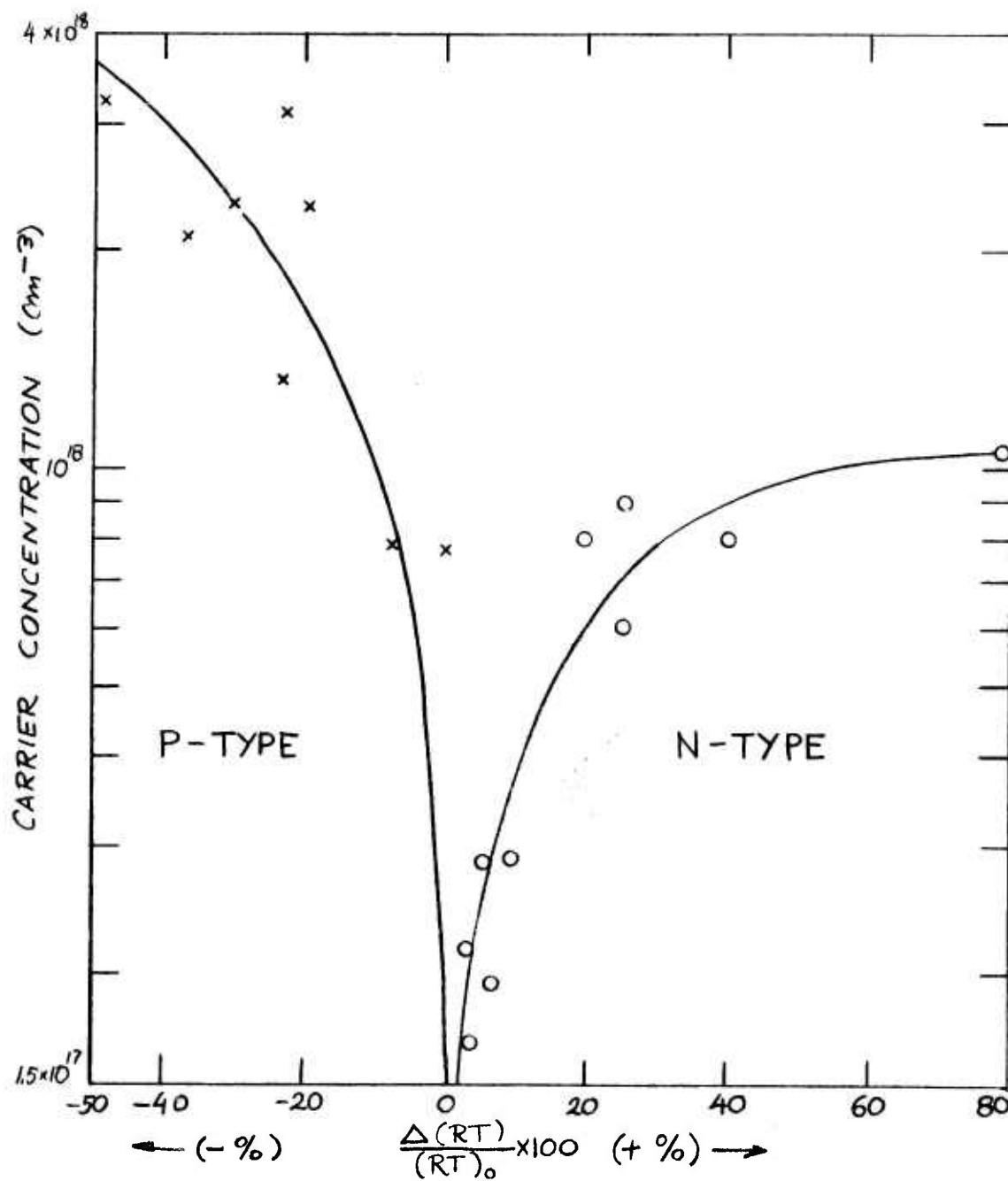
Figure 3-16   Effect of Deviation from Critical Deposition
Conditions on Carrier Concentration
(Targets #2, #7)
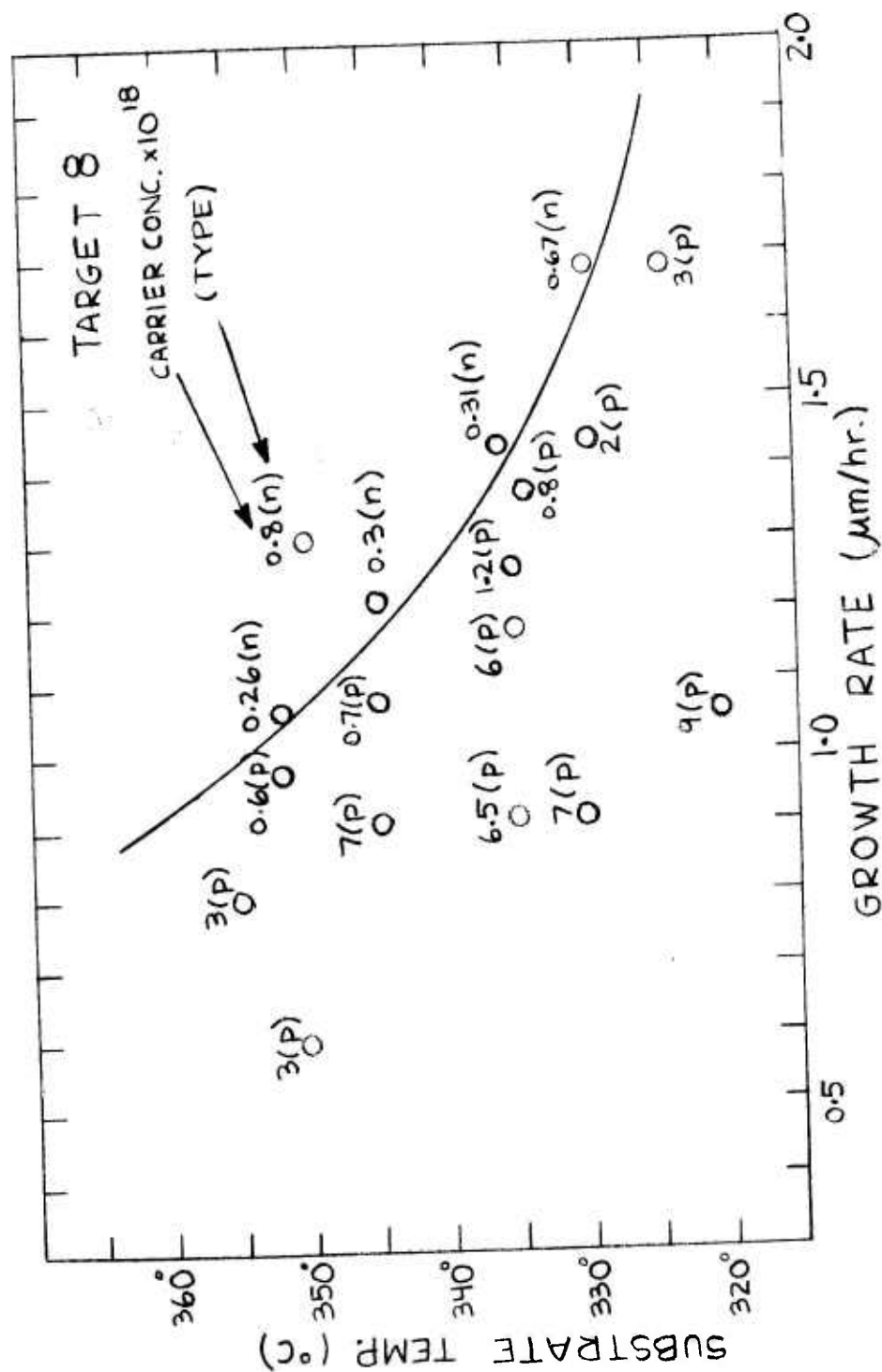
Figure 3-17 Characterization of As-Deposited Carrier Concentration of p- and n-Type Films near p-n Transition - Sputtering (Target #8)
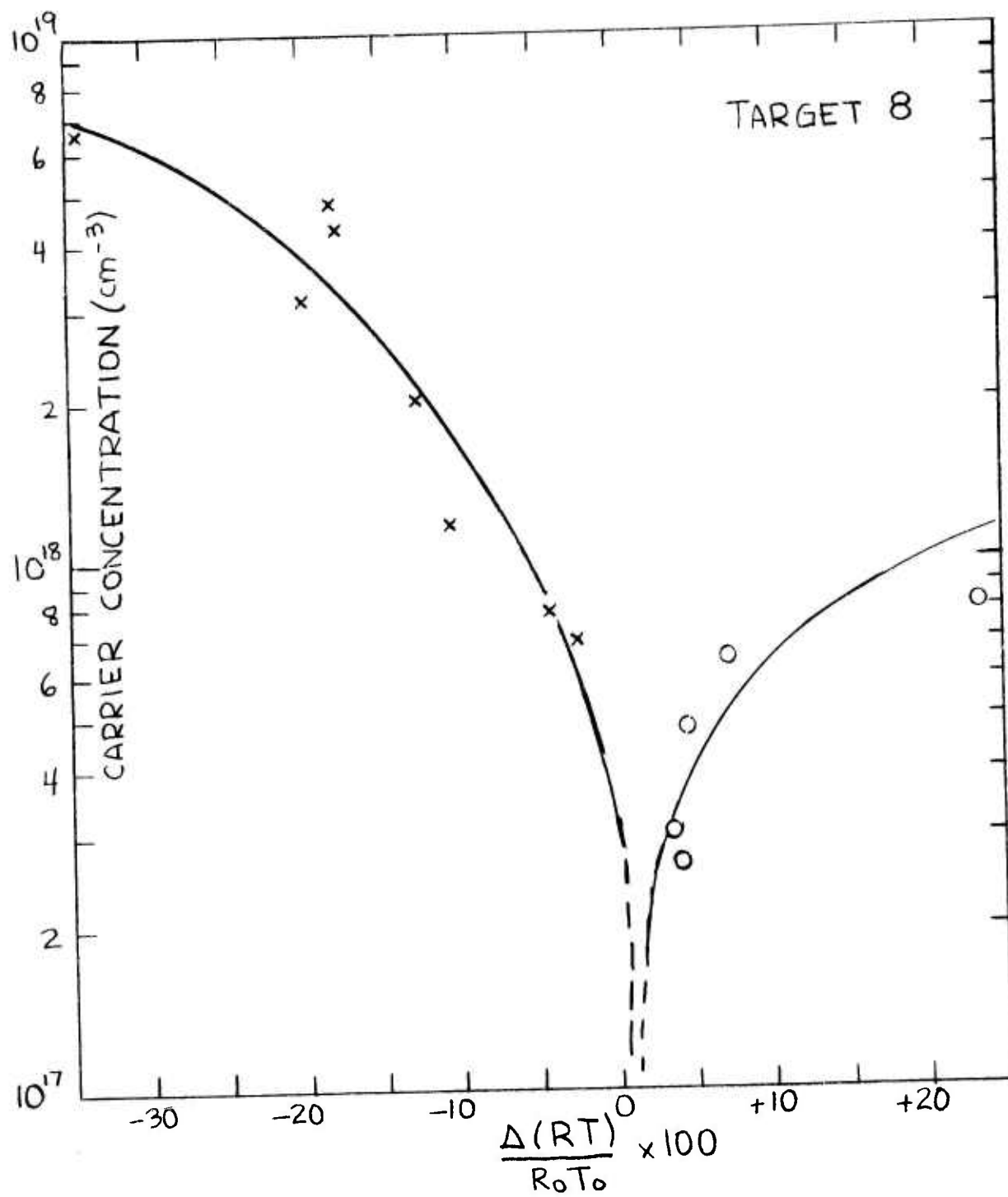
Figure 3-18 Effect of Deviation from Critical Deposition Conditions
on Carrier Concentration (Target #8)
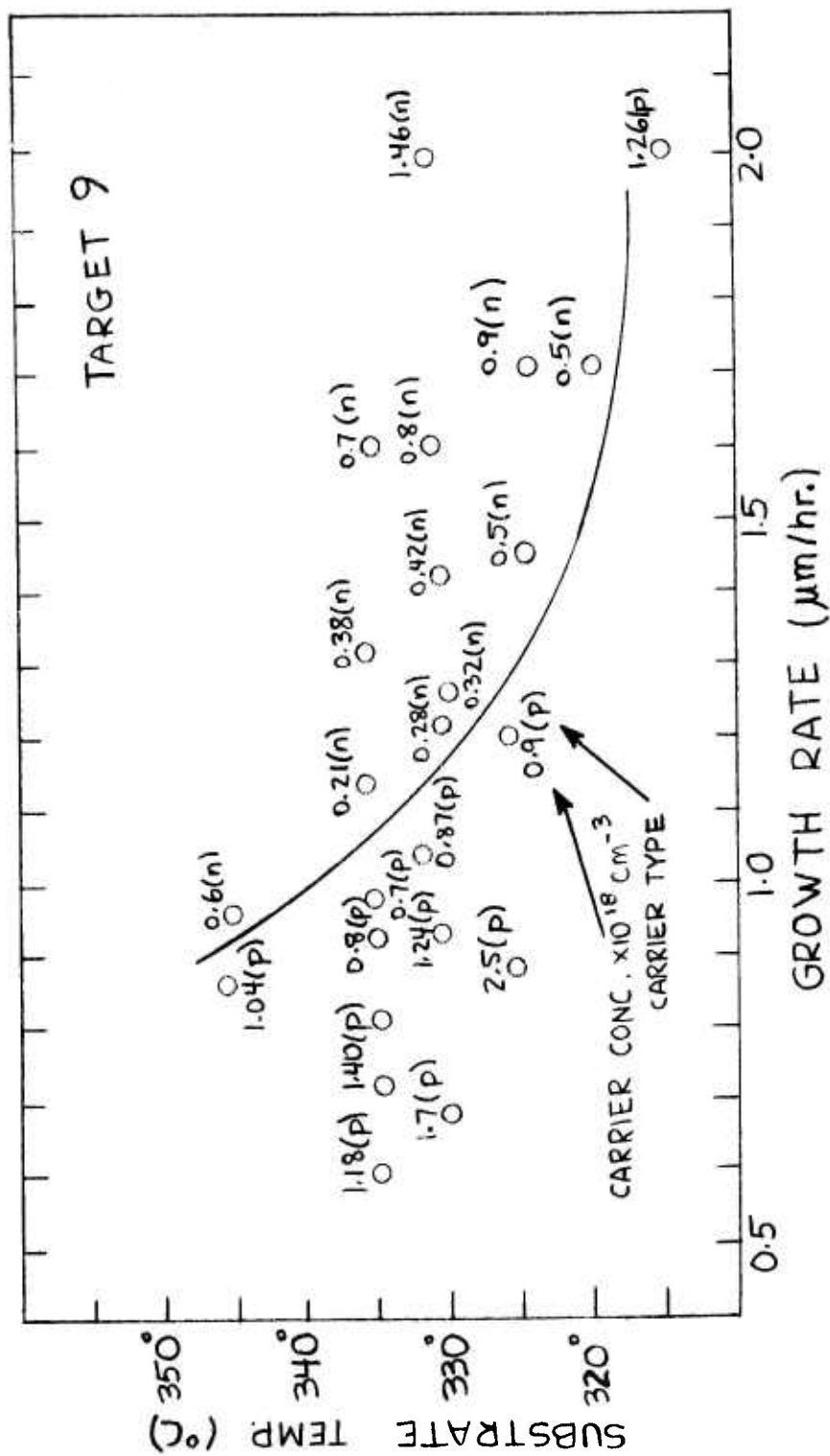
Figure 3-19 Characterization of As-Deposited Carrier Concentration of p-
and n-type Films near p-n Transition - Sputtering (Target #9)
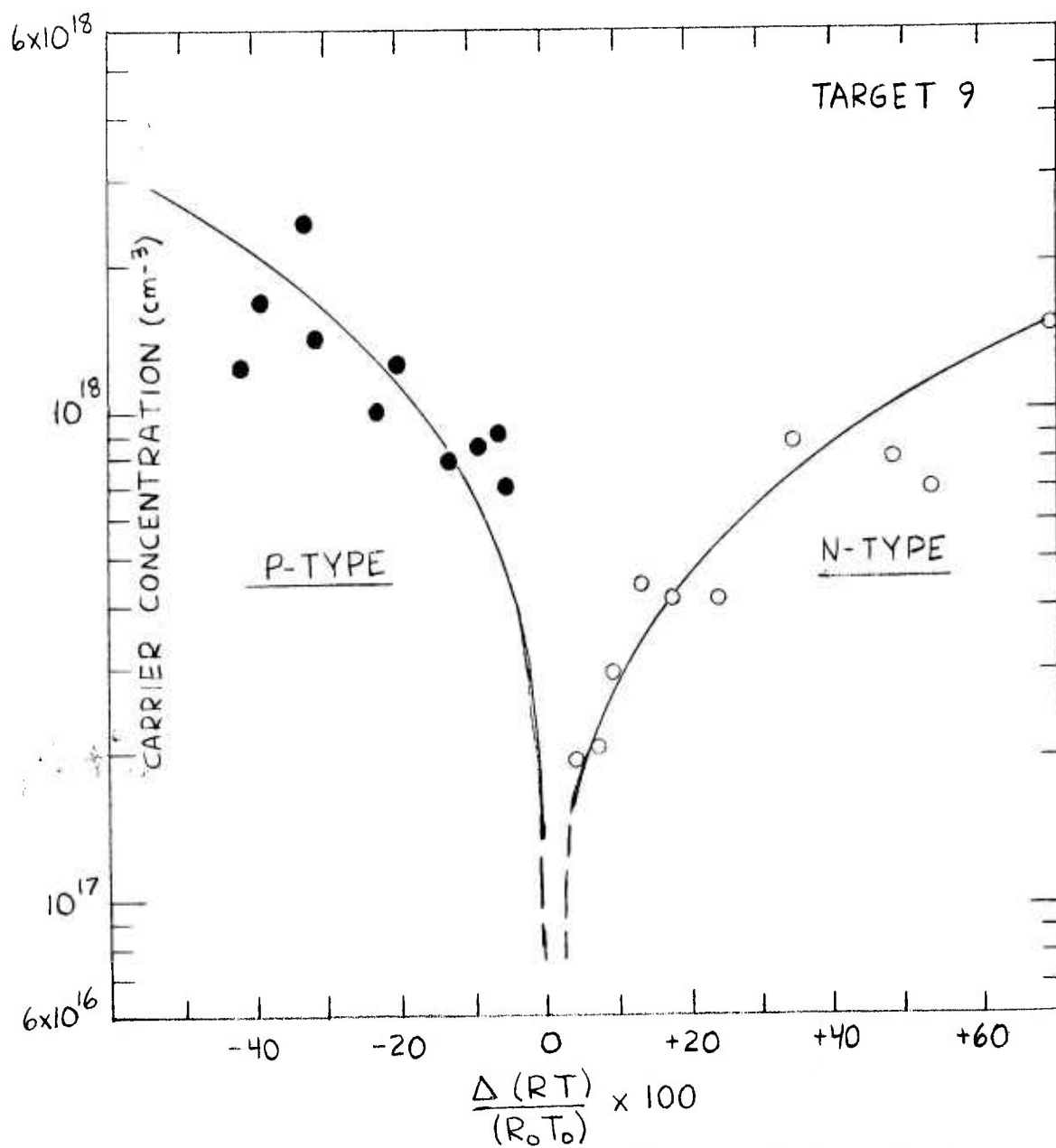
Figure 3-20 Effect of Deviation from Critical Deposition Conditions on Carrier Concentration (Target #9)

shows the corresponding relation between carrier concentration and the deviation from the critical transition conditions $(R \cdot T)_o$. Here we can see again the rapid increase in carrier concentration for both p- and n-type films as deposition conditions deviate (positively or negatively) from these conditions.

Finally, Figures 3-17 through 3-20 show corresponding results for Targets #8 and #9. The results in Figures 3-17 and 3-18 for Target #8 are entirely consistent with these described above for Target #2, #3 and #7. As has already been shown, a p-n transition curve has also been determined for Target #9 (x = .20, Te rich). The corresponding results on carrier concentration near the p-n transition are illustrated in Figures 3-19 and 3-20. From the similarity of the trends shown in these figures to those just shown for Target #8, it can be concluded that a similar mechanism is operative in both targets, even though Target #9 was purposely prepared to be non-stoichiometric or Te rich. It should be noted that a particular effort was made to determine, by x-ray diffraction, whether the single crystal films, particularly those deposited under conditions near the p-n transition curve, showed any species other than $Pb_{1-x}Sn_xTe$ which may be related to the target non-stoichiometry. None were found within the limits of this technique. In other words, it appears that films deposited at conditions defining the p-n transition for the non-stoichiometric Target #9 are as stoichiometric as those deposited under corresponding conditions from other targets investigated in this study. If one further compares the results from Target #9 with similar results from Target #2, which has the same composition as Target #9 but is stoichiometric (Figures 3-15 and 3-16), it becomes clear that the major effect of target non-stoichiometry (Te richness) is a change in deposition conditions at which the more stoichiometric films are formed; i.e., the p-n transition curve is shifted to different substrate temperatures and deposition rates as was shown in Figure 3-7. However, the mobilities in these films seem to be somewhat affected by target stoichiometry as we shall discuss in a later section.

3-46

It would be of interest to obtain similar data for Targets #10 through #12 for comparison. As may be recalled (see Table 1), Targets #10 through #12 were prepared utilizing modified techniques aimed at improved target stoichiometry and purity. However, experiments with biased substrates had been initiated when these targets were prepared. The results with biased substrates were so interesting that we decided to emphasize this aspect with all targets, including Targets #10 through #12. As a result, systematic experiments at zero bias conditions have not been performed with these later targets.

In any case, the results presented above continue to demonstrate and confirm the fact that deposition control can, if exercised properly, provide a substitute for the post-deposition anneal of PbSnTe. In both cases the carrier concentration is apparently controlled primarily by excess metal or Te and not by foreign impurities. It is apparent from data presented in Tables 3 through 8 and illustrated in the various figures just discussed that, without a specific effort to locate the transition conditions exactly, fairly respectable carrier concentrations were achieved without annealing ($\sim 1 \times 10^{17}$ cm^{-3}). This is compatible with carrier concentrations in (annealed) material now used commercially to produce acceptable photovoltaic cells.

And to repeat, the results also obviously indicate the possibility for depositing p-n diode junctions in one deposition process by simply changing rate or temperature slightly at a controlled film thickness. The technique has, as stated, one limitation. As could be readily seen from examples such as shown in Figures 3-1 through 3-6, critical p-n transition conditions do not exist for all potentially desired film compositions (x-values). Thus, different targets would have to be used to prepare p-n junctions of lowest carrier concentration films with widely different, desired spectral responses. This would be particularly undesirable for multi-color sensor fabrication. Again, as seen in the following sections, bias sputtering can be used to overcome this limitation.

3.2.3 AS-DEPOSITED FILM CHARACTERISTICS WITH SUBSTRATE BIAS.

3.2.3.1 <u>Structure, Composition and Carrier Type Dependence on Target Characteristics and Deposition Conditions</u>. In Section 3.2.2.1 we showed how two deposition parameters, substrate temperature and deposition rate affect the structure, composition and carrier types in films deposited from various $Pb_{1-x}Sn_xTe$ targets. In this section we introduce an additional parameter - that of substrate bias.

Bias sputtering is a relatively well established technique which has many variations. In our case, it consists simply of the application of a positive or negative DC potential to the substrate holder - relative to a common ground for the sputtering cathode (target), the shutters, substrate heaters, etc. As discussed in Section 2, the bias voltage is applied in such a fashion that it does not generate any large field gradients in the film being deposited - either parallel to or normal to the substrate surface.

While there were a number of interpretations as to what bias sputtering does to the deposited film by different investigators, the observed effects were generally the same. Our own work with tantalum showed decreases or increases in film resistivities, depending on the polarity and magnitude of the bias. We were able to correlate this to an apparent rejection (or attraction) of impurity ions, such as oxygen ions, in the argon plasma. This was, of course, the basis for applying bias sputtering to PbSnTe deposition. It was hoped that any impurity inclusion in the PbSnTe films could be substantially reduced during deposition - independent of any remaining impurities included in the target or contributed by the sputtering environment.

Thus it was expected that carrier concentrations in our films would show a systematic and continuous dependence on bias voltage. The actual results were initially somewhat surprising and unexpected, but nevertheless, very useful. We present in this section, the very substantial and dramatic effects of bias voltage on the structure, composition and carrier type utilizing the same targets investigated without, (i.e., zero) bias conditions. We will present similar effects on carrier concentration in a later section covering electrical properties.

In order to investigate the effects of bias voltage, it is treated as a completely independent deposition parameter. That is, during any one set of experiments, the other deposition parameters, in particular substrate temperatures and growth rate were kept constant while the bias voltage was changed over the range of interest. This was repeated, systematically for various sets of rate and temperature conditions. Selected, typical results of bias voltage effects on composition and carrier type are illustrated in Figures 3-21 through 3-27 for the various targets investigated. We consider first the results utilizing Target #9 ($x = 0.20$, 1% Te rich) shown in Figures 3-21 and 3-22. It immediately is apparent from Figure 3-21 that bias voltage provides a new method for controlling film carrier type. Referring to Figure 3-6 for the compositional and structural phase diagram for Target #9, we observe that for a substrate temperature of $345^{o}C$ and growth rate of .95 μm/hr, for example, the films deposited at zero bias conditions are single crystal, are n-type and have a composition of $x = 0.20$. Figure 3-21 illustrates that bias voltages over the range from +30V to -30V coupled with the same depositions conditions (i.e. $345^{o}C$ and .95 μm/hr) can yield both p- and n-type, single crystal $Pb_{1-x}Sn_xTe$ films. From this figure we can define a critical, temperature dependent bias voltage at which the films switch from n- to p-type. For example, Figure 3-21(a) shows that for a PbSnTe film on a BaF_2 substrate, the critical bias voltage is about +5V for the reference conditions of $345^{o}C$ and .95 μm/hr, respectively.

Important to note is that the film composition (indicated by the x-values in the parenthesis) shows no significant differences for the entire range of bias voltages for any one set of rate and temperature conditions - this in spite of the changes in carrier type and, as we shall see later, the rather large changes in the other electrical properties such as carrier concentration that are experienced. Also, if zero bias conditions produced single crystal films, the same rate-temperature conditions produced single crystal films over the entire range of bias voltage investigated.

Several other observations on the effect of substrate bias are apparent from Figures 3-21 and 3-22. In particular, they illustrate the dependence of the critical switching voltage on substrate temperature and deposition rate as well as the interdependence of all three parameters.

By comparing Figures 3-21(a) and 3-21(b) it is noted that the switching from p- to n-type film occurs at slightly different critical bias voltages for the two substrates (CaF_2 and BaF_2) used. Using the same conditions as above as an example ($345^{\circ}C/0.95 \mu/hr$), the critical bias voltage is seen to be +10 volts for films on CaF_2 as compared to about +5 volts for films on BaF_2.

Figure 3-21 also shows results for two substrate temperatures, namely $335^{\circ}C$ and $345^{\circ}C$, at one film growth rate, namely $0.95 \mu hr$. Reference to the zero-bias structural phase diagram for Target #9 in Figure 3-6 shows that at $335^{\circ}C$ and $345^{\circ}C$ the films are p-type and n-type, respectively, for a deposition rate of $.95 \mu m/hr$. As noted in Figure 3-21(a) the critical switching voltage changes from about -5 volts to +5 volts as the substrate temperature of BaF_2 is changed from $335^{\circ}C$ to $345^{\circ}C$. An effect of similar magnitude is observed for CaF_2 in Figure 3-21(b). The apparent reason for this behavior will be discussed later.

Figure 3-22, perhaps most clearly, illustrates the observations which by now must be considered typical. The bias voltage required to switch films from n- to p-type becomes more positive as either the substrate temperature or deposition rate (or both) are increased. The reverse holds, of course, for the voltage required to change a film from p- to n-type. These observations raised the suspicion that this bias influenced behavior is related to that previously established with zero bias, namely, that unbiased films are always more n-type if they are deposited at higher substrate temperatures and/or at higher deposition rates.

3-50

(a) BaF$_2$ Substrate

(b) CaF$_2$ Substrate
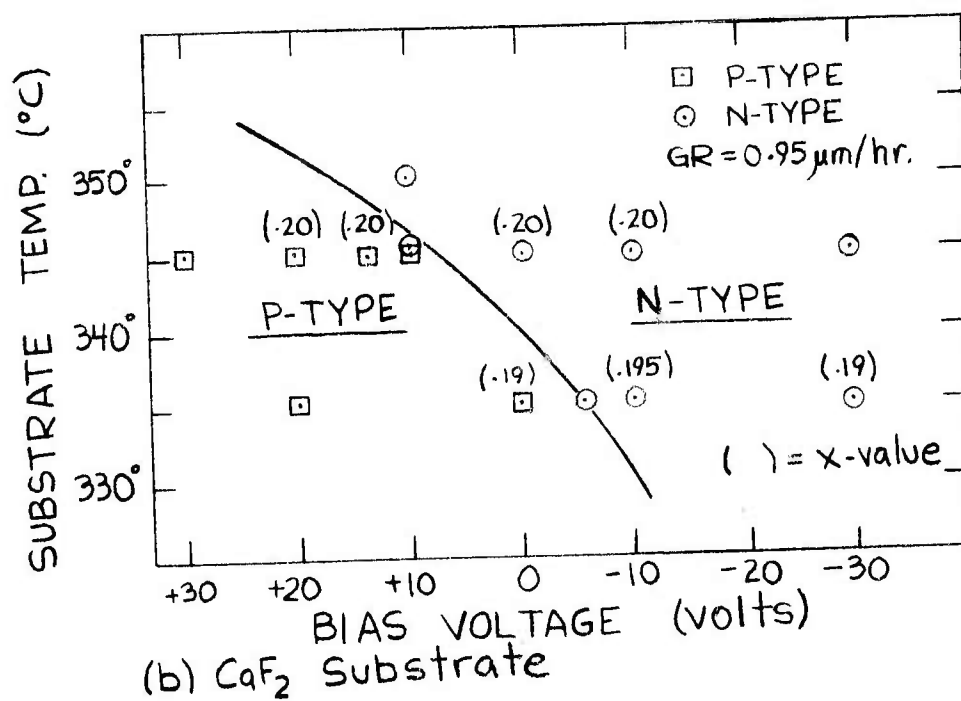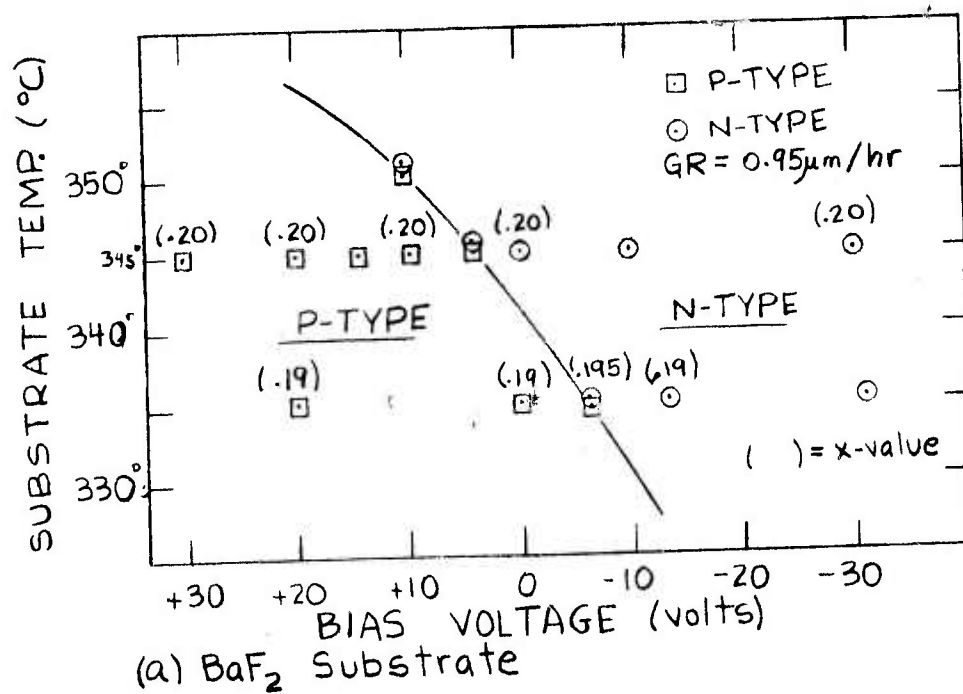
Figure 3-21 Substrate Bias Effects on Composition and Carrier Type (Target #9)

3-51
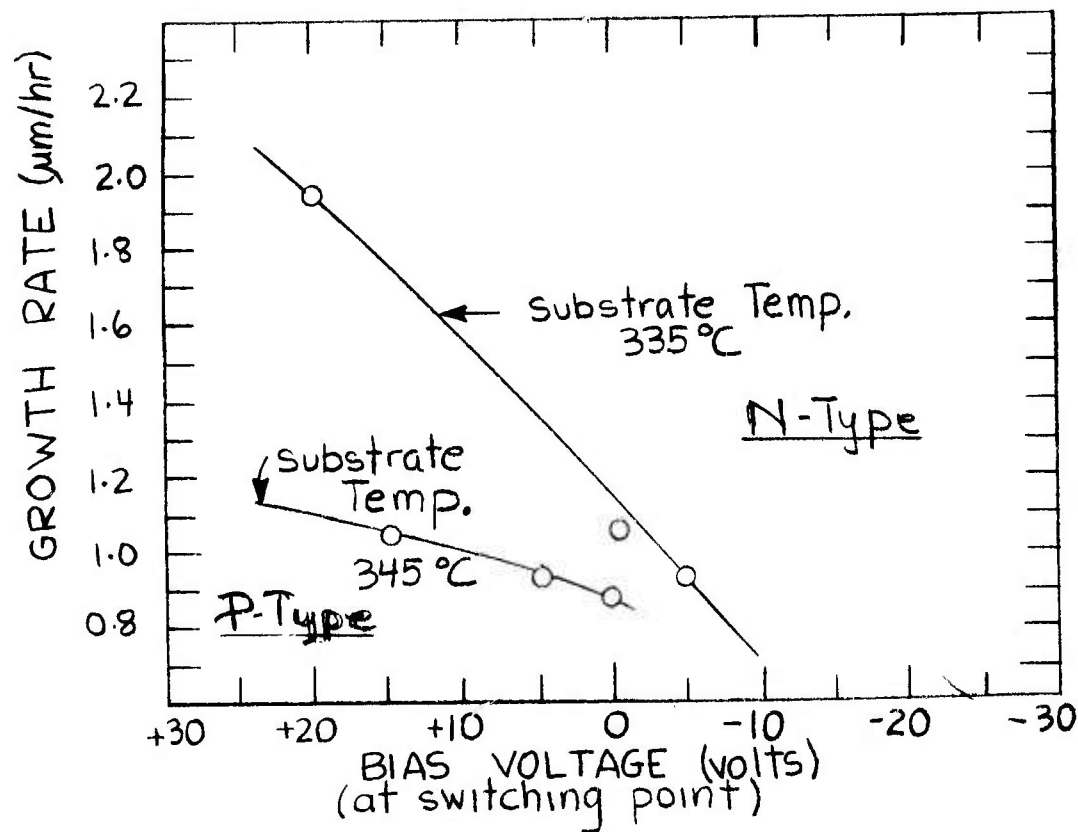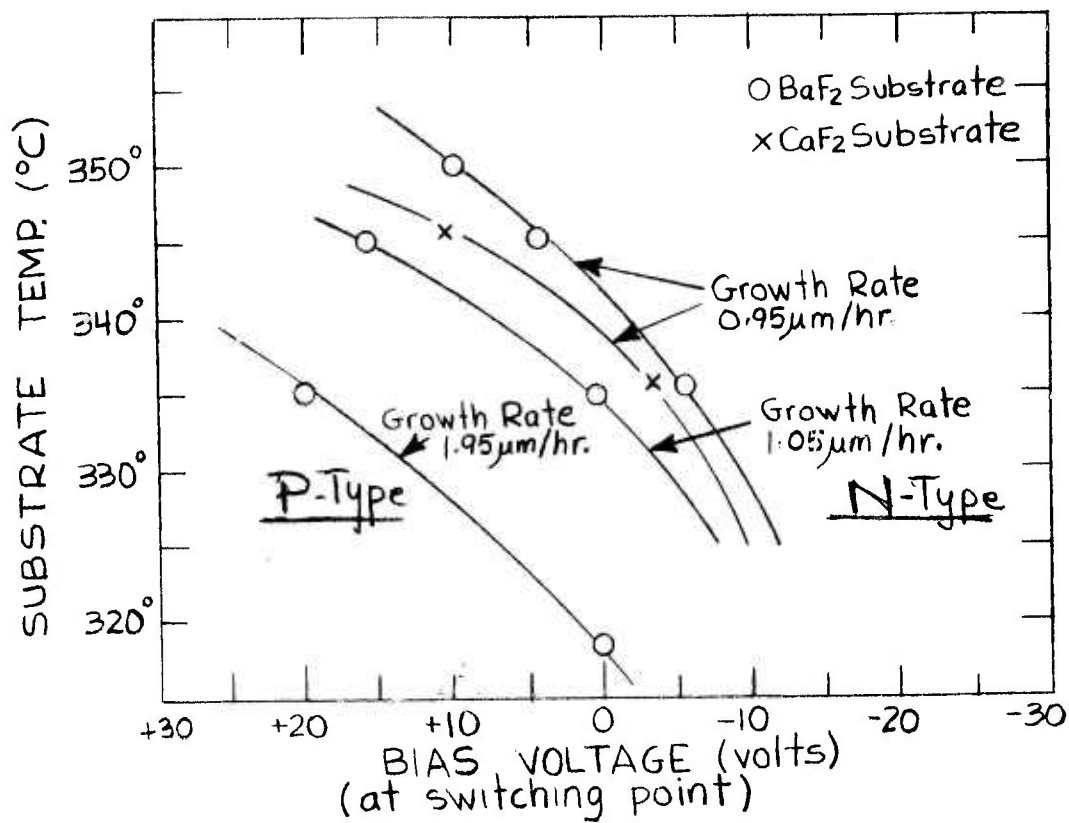
Figure 3-22 Effect of Deposition Parameters on Critical Bias Voltage
for Single Crystal Sputtered $Pb_{1-x}Sn_xTe$ Films (Target #9)
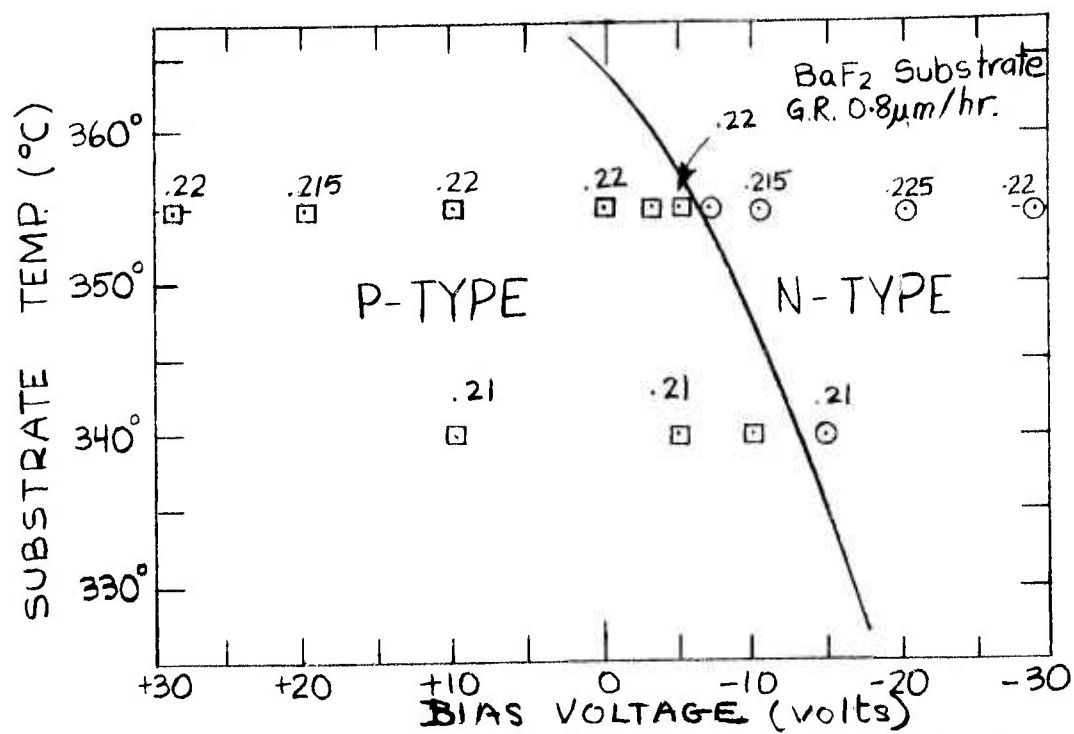
3-52

a) Characterization of Film Composition and Carrier Type vs.
    Deposition Conditions and Bias Voltage
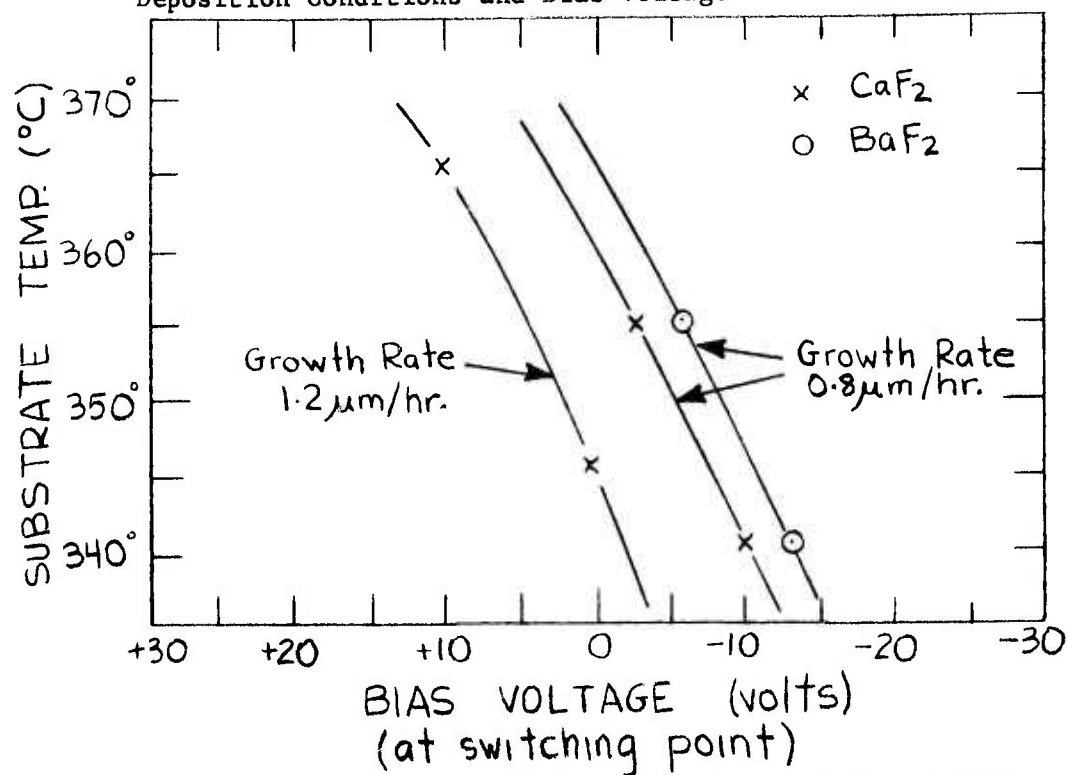
b) Effect of Deposition Parameters on Critical Bias Voltage

Figure 3-23 Substrate Bias Effects on Composition and
Carrier Type (Target #8)

3-53
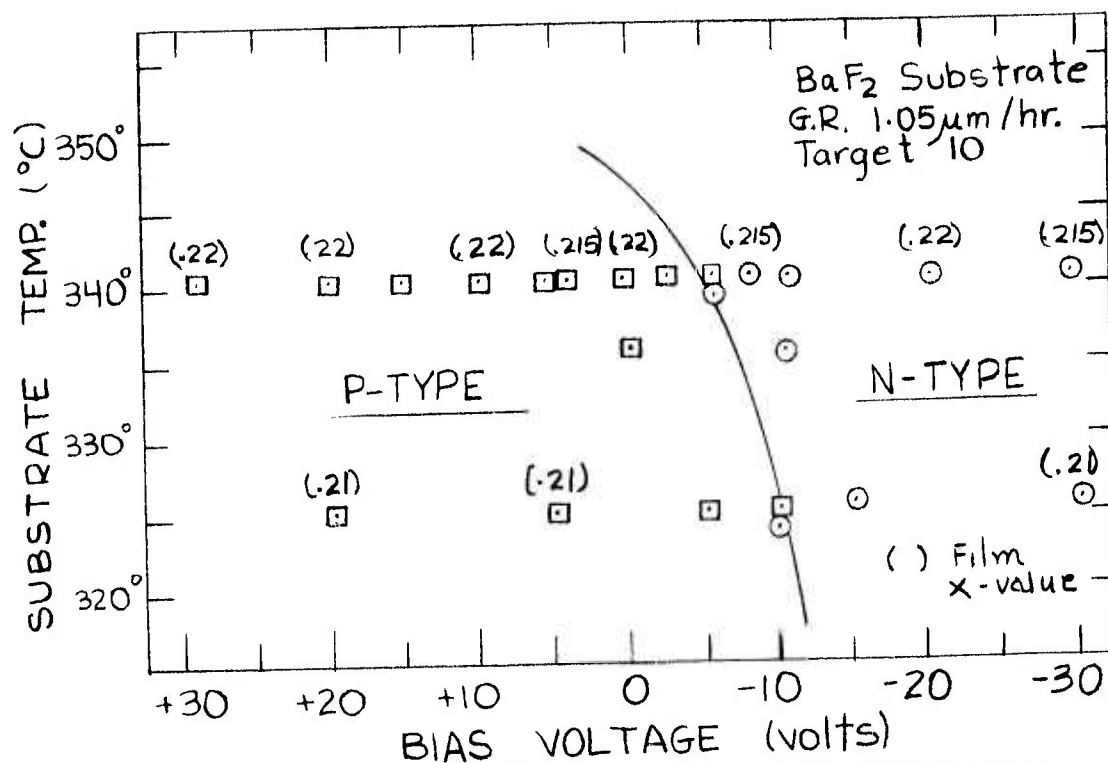
a) Characterization of Film Composition and Carrier Type vs. Deposition Condition and Bias Voltage
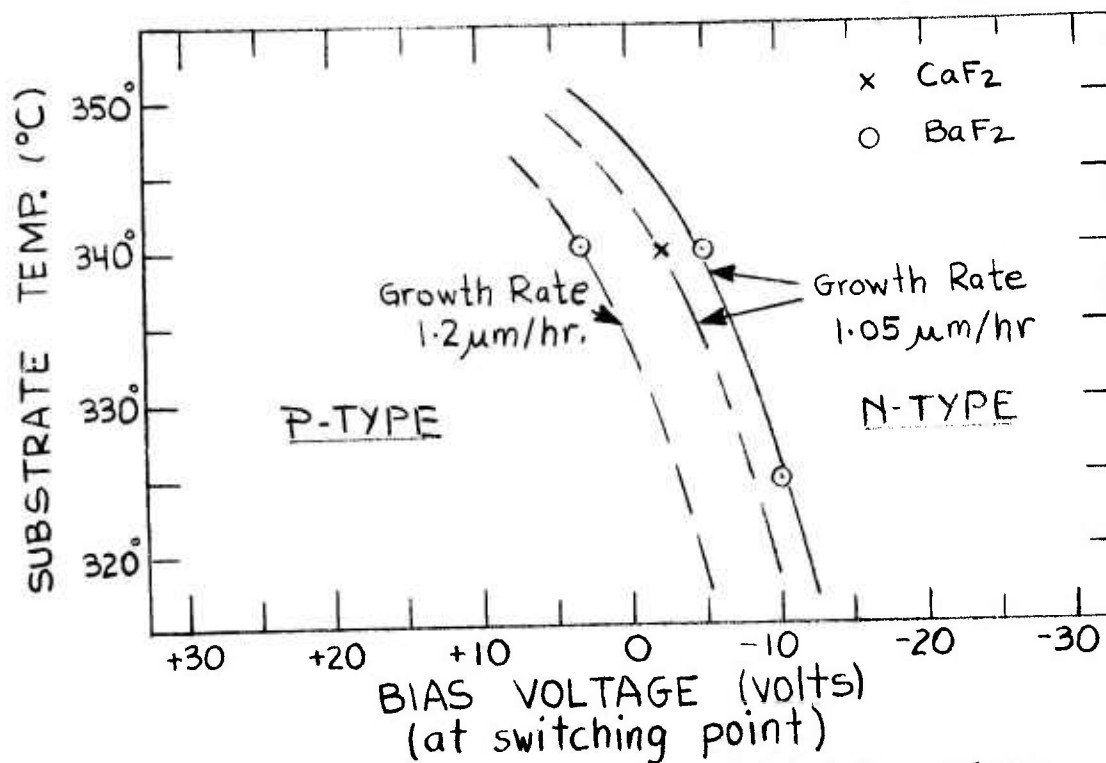
b) Effect of Deposition Parameters on Critical Bias Voltage

Figure 3-24 Substrate Bias Effects on Composition and Carrier Type (Target #10)

3-54
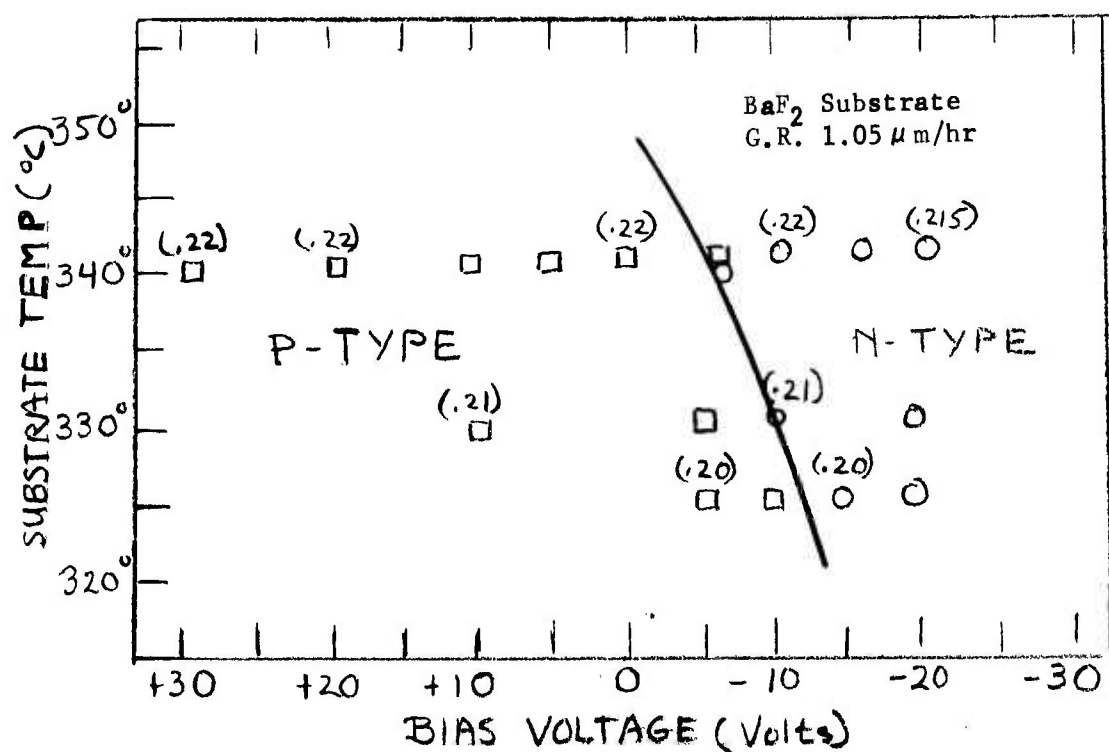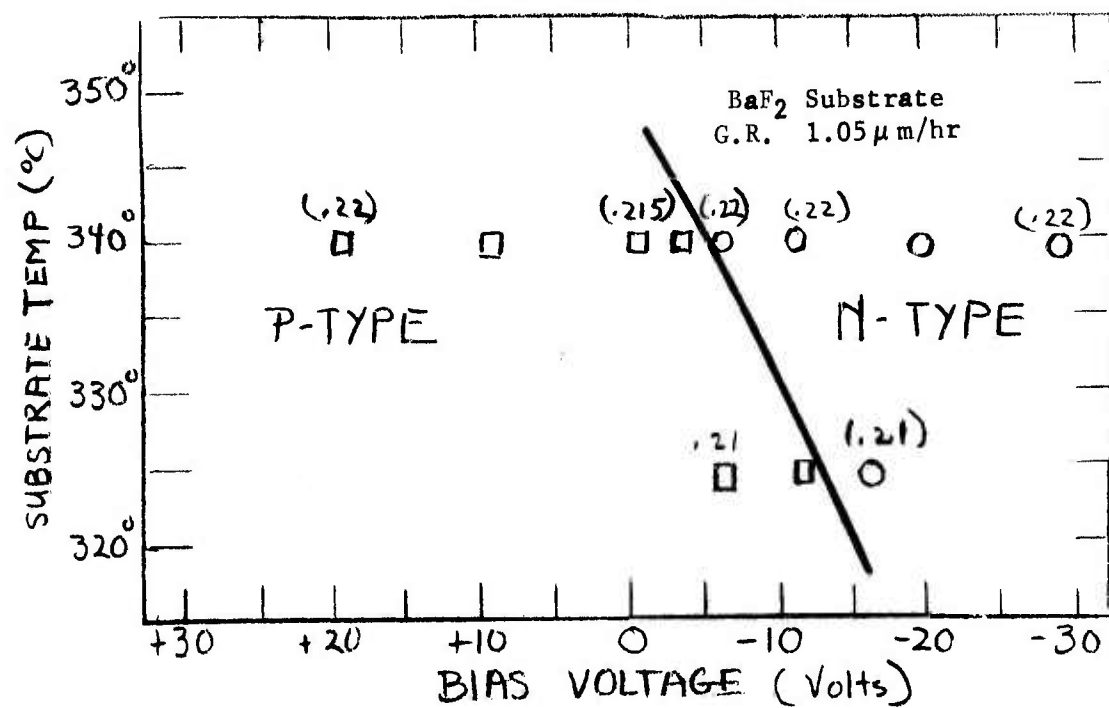
a) Target #11

b) Target #12

Figure 3-25 Substrate Bias Effect on Composition and Carrier Type

3-55
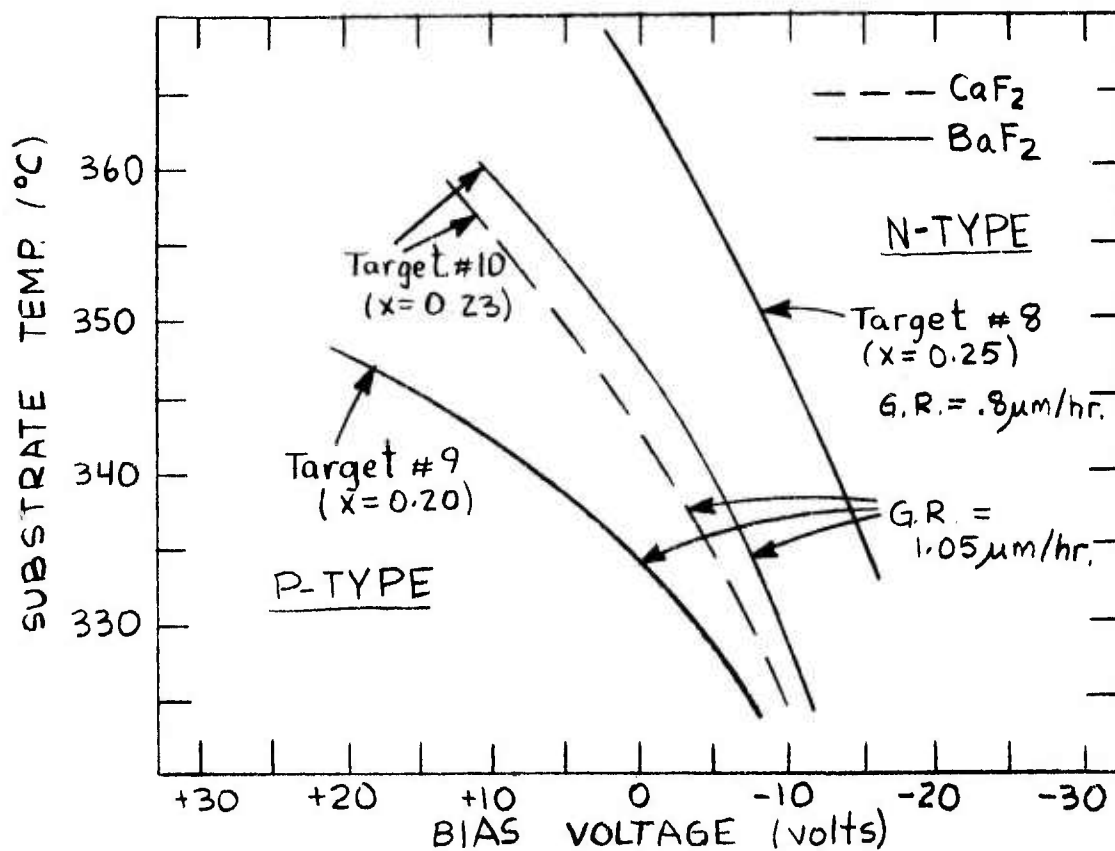
a) Effect of Target Composition
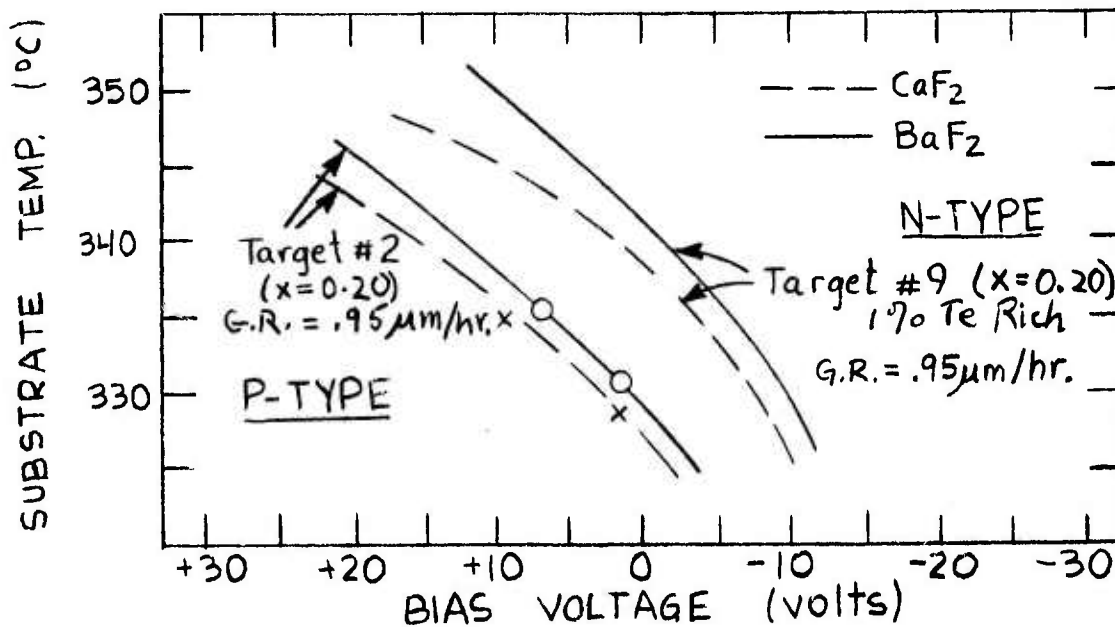
b) Effect of Target Stoichiometry

Figure 3-26 Effect of Target Characteristics on Substrate Bias
Effects (Film Carrier Type)
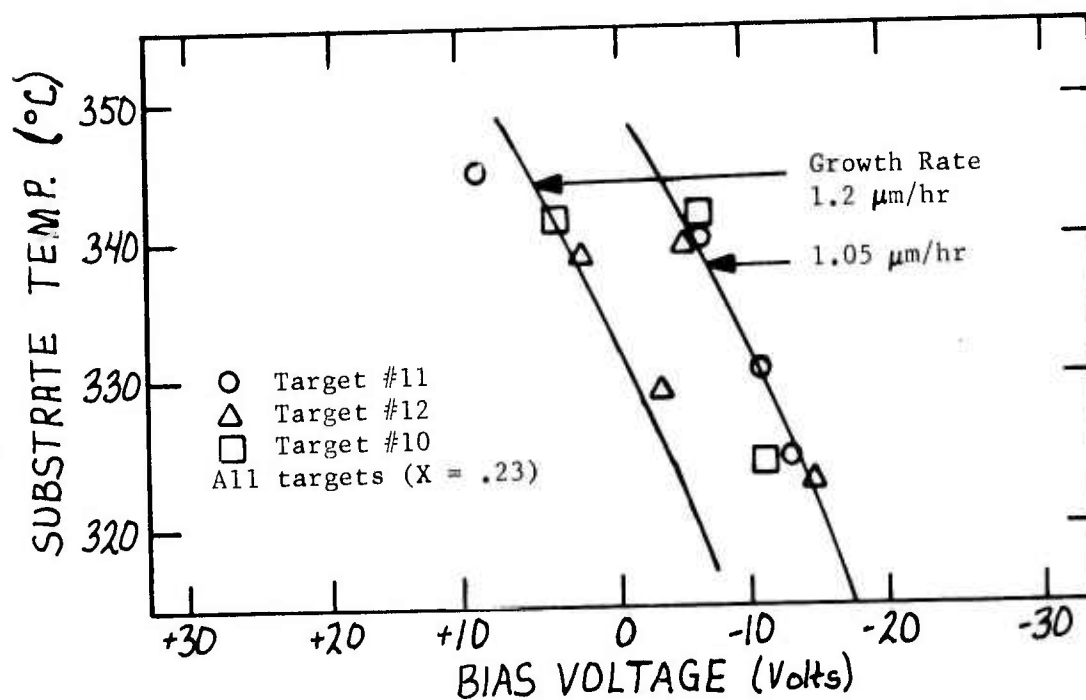
b) Bias Effects for Three Targets with the Same Composition.
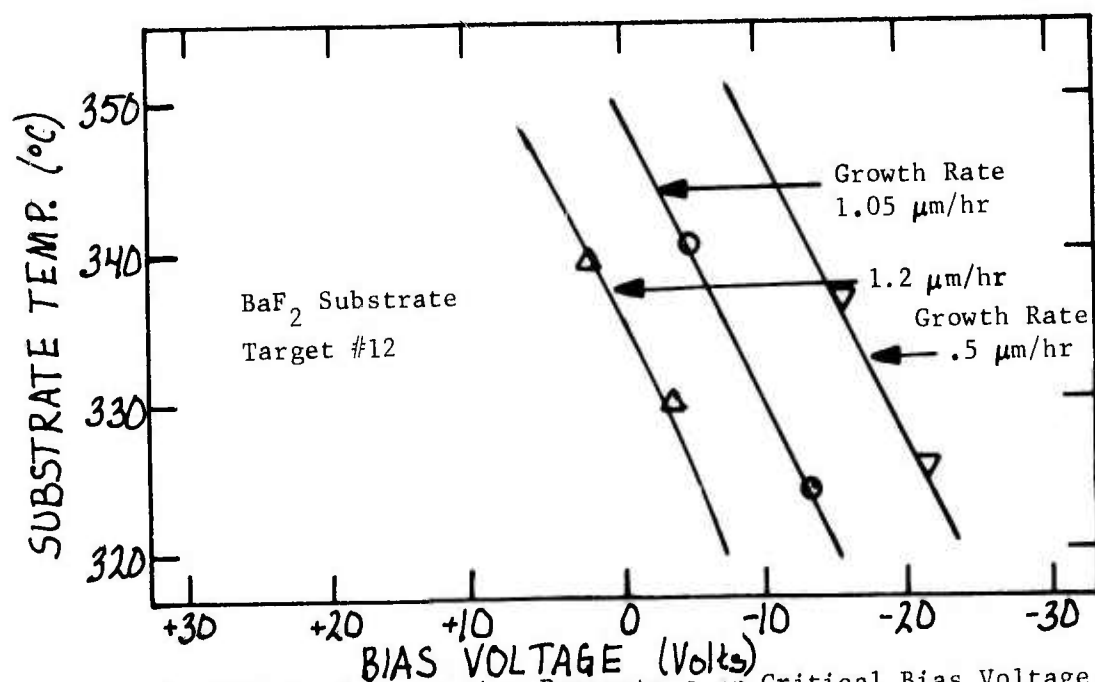
a) Effect of Deposition Parameters on Critical Bias Voltage.

Figure 3-27 Effect of Target Characteristics and Deposition
Conditions on Critical Bias Voltages.

3-57

Figures 3-23 through 3-25 present additional results of similar nature for Targets #8 (x = 0.25) and Targets #10, #11 and #12 (x = 0.23). As noted the trends are identical to those presented for Target #9 and indicate how general the observed bias effects are.

Figures 3-26 and 3-27 provide a direct comparison of the critical voltages observed with the various targets investigated. Apparently, target composition and stoichiometry have an effect on the critical bias or switching voltages. But, it remains to be determined whether this effect is direct or indirect. In other words, it is quite likely that the film properties which are the result of the target composition at any given set of deposition conditions, control the switching bias requirements rather than the target composition itself. To explain one might refer back to the trend curves in Figure 3-7. The general behavior revealed in this figure is that, if identical deposition conditions are used, targets with higher x-values yield, without bias, a) films which are more p-type (or less n-type) and b) films which have higher x-values. Thus, from Figure 3-26(a) it can be deduced: If a set of conditions, A, is chosen such that the film, deposited without bias, would be more p-type than for another set of conditions, B, then the negative bias required to deposit an n-type film must be larger for Set A than for Set B. The reverse holds true for n- to p-type conversion.

Figure 3-26(b) compares the results achieved with two targets - Target #9 and Target #2 - which have effectively the same composition (or x-value) but differ by the fact that Target #9 is Te rich. Again, without bias, films deposited with Target #2 would be more n-type, at any set of conditions, than those deposited with Target #9 - as trend curves in Figure 3-7 indicate. Consequently, the critical voltage is now expected, and in fact is, more positive for Target #2 at any set of deposition condition also.

Targets #10, #11, and #12, all prepared to have identical compositions but with modified preparation techniques, are compared relative to any effects on the switching bias voltage, in Figure 3-27. As can be seen and as may be expected the results from all three targets are

identical within experimental error.

All of these results have indicated; a) strong effect of substrate bias on carrier type, and b) the lack of a bias effect on the basic film composition. Coupled with an effect of substrate bias on carrier concentration, which will be presented later, these observations are consistent with a mechanism involving stoichiometric adjustment. That is, just as we hypothesized in the preceding section that the p-n transitions (at zero bias) may be defining conditions at which the most stoichiometric films are formed, the bias effect results suggest that the socalled critical bias voltage represents also a condition at which the most stoichiometric films are produced.

The ability to produce stoichiometric p- or n-type film by bias sputtering is of considerable practical significance. Here is a process which is extremely easy to control and, most importantly, maintains constant film composition. Consequently, control of carrier type will not affect the spectral response of individual layers deposited under conditions selected to produce a certain composition or x-value. This is obviously superior to the control of substrate temperature and deposition rate alone - which at zero bias conditions can also be used to produce p- or n-type films but not without changing composition.

3.2.3.2 <u>Crystal Structures and Orientation of Epitaxial Bias Sputtered Films</u>. As stated in earlier sections, only single crystal films are deposited for this work. As we have shown in Section 3.2.2.2, for films deposited without substrate bias, single crystal films sputtered on CaF_2(111) and BaF_2(111) have shown the (111) orientation only, while those on CaF_2(100) have shown the (100) orientation. As also noted, in the case of x-ray evaluation this simply means that in the 2-θ scans, films on CaF_2 and BaF_2(111) showed only lines for the (111) oriented films, while those of CaF_2(100) showed only lines expected for the (100) orientation. The single crystal films deposited with bias sputtering also exhibited the same characteristics. That is, the films were all single crystal in nature over the entire range of bias voltage investigated and showed the same orientation that is experienced in films

deposited at conditions, which at zero bias, yield single crystal
structures. Typical reflection electron diffraction patterns and
x-ray 2-θ scan were already presented in earlier sections of this
report for typical single crystal films deposited at zero substrate
bias conditions. The films deposited with substrate bias exhibit
completely similar patterns and scans. Therefore, we found no parti-
cular merit in including additional samples here.

     3.2.3.3 <u>Carrier Concentration of Bias Sputtered Films - Dependence</u>
<u>on Target Characteristics, Deposition Conditions and Bias Voltage</u>. It
was earlier revealed that, initially, the basis for utilizing bias
sputtering was past work in our laboratory which indicated that bias
sputtering can significantly reduce the impurity content in deposited
metal films. Thus, relative to the carrier concentration in $Pb_{1-x}Sn_xTe$,
it was hoped that the bias sputtered films would show a monotonic
decrease in concentration with decreasing bias voltages (from positive
to negative). This trend materialized, but there also occurred a
relatively large reduction in carrier concentration at a critical bias
voltage. Moreover, this critical voltage was the same as that defined
in Section 3.2.3.1, i.e., the voltage above which the film had p-type
carriers and below which the film had n-type. The expected, monotonic
drop in effective carrier concentration with decreasing substrate bias
did, at first, appeared to be only a secondary effect in PbSnTe film.
But it became apparent, as the range of applied bias voltages investigated
was increased, that this initially sought after effect is significant
also.

     Figures 3-28 through 3-31 illustrate the essential features of the
bias effect on carrier concentration. Two substrates, BaF_2 and CaF_2
and five different targets are investigated. In Tables 9 through 14
the data on composition, structure, carrier concentration and mobilities
are documented as are their dependence on bias voltage. It should be
noted that the carrier concentrations and mobility values given in these
tables, in many cases, represent average values for several samples with
deviations ranging anywhere from ±2% to ±15%.
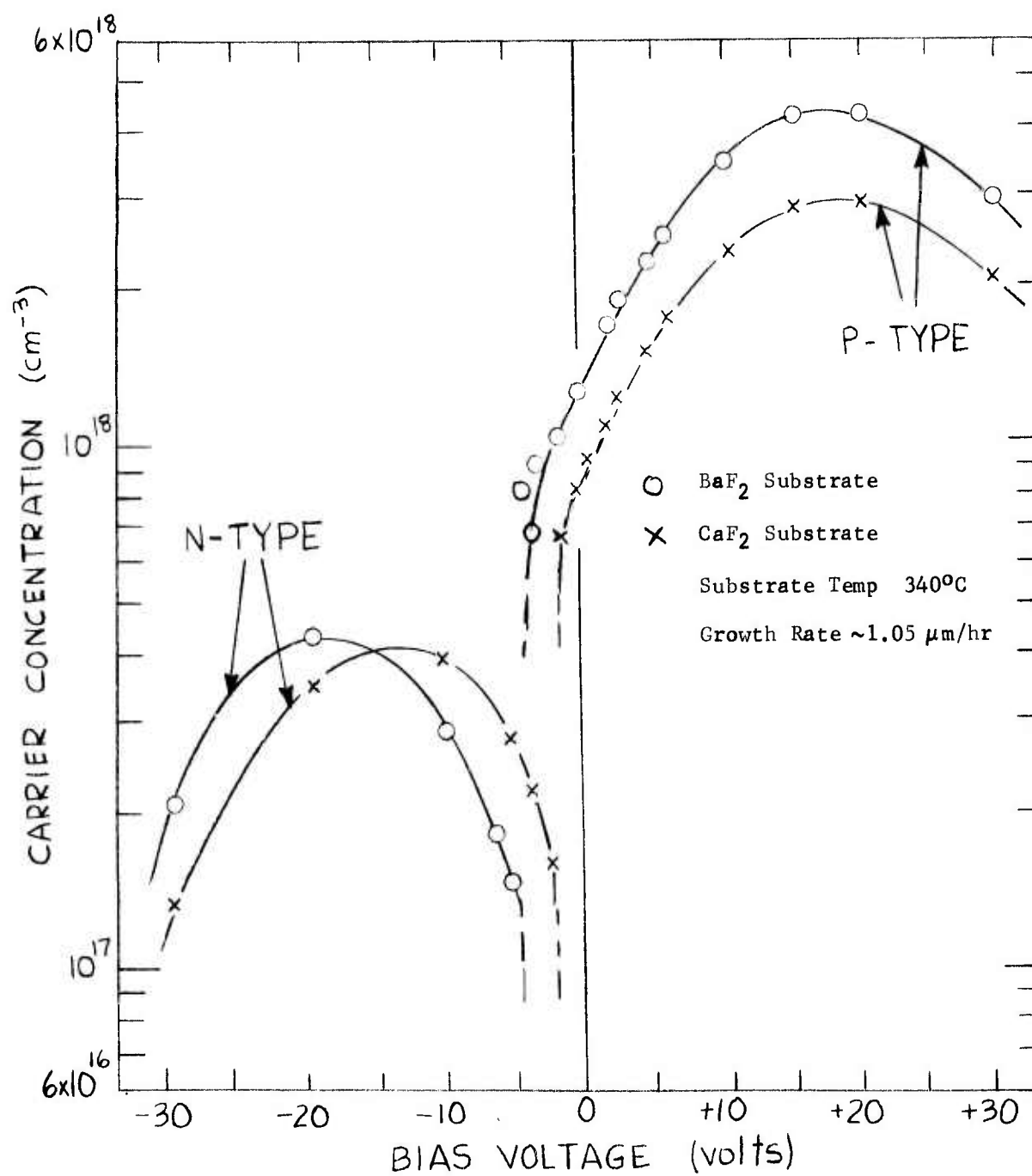
Figure 3-28 Effect of Substrate Bias Voltage on As-Deposited Carrier
Concentrations in Pb$_{.78}$Sn$_{.22}$Te Films (Target #10)
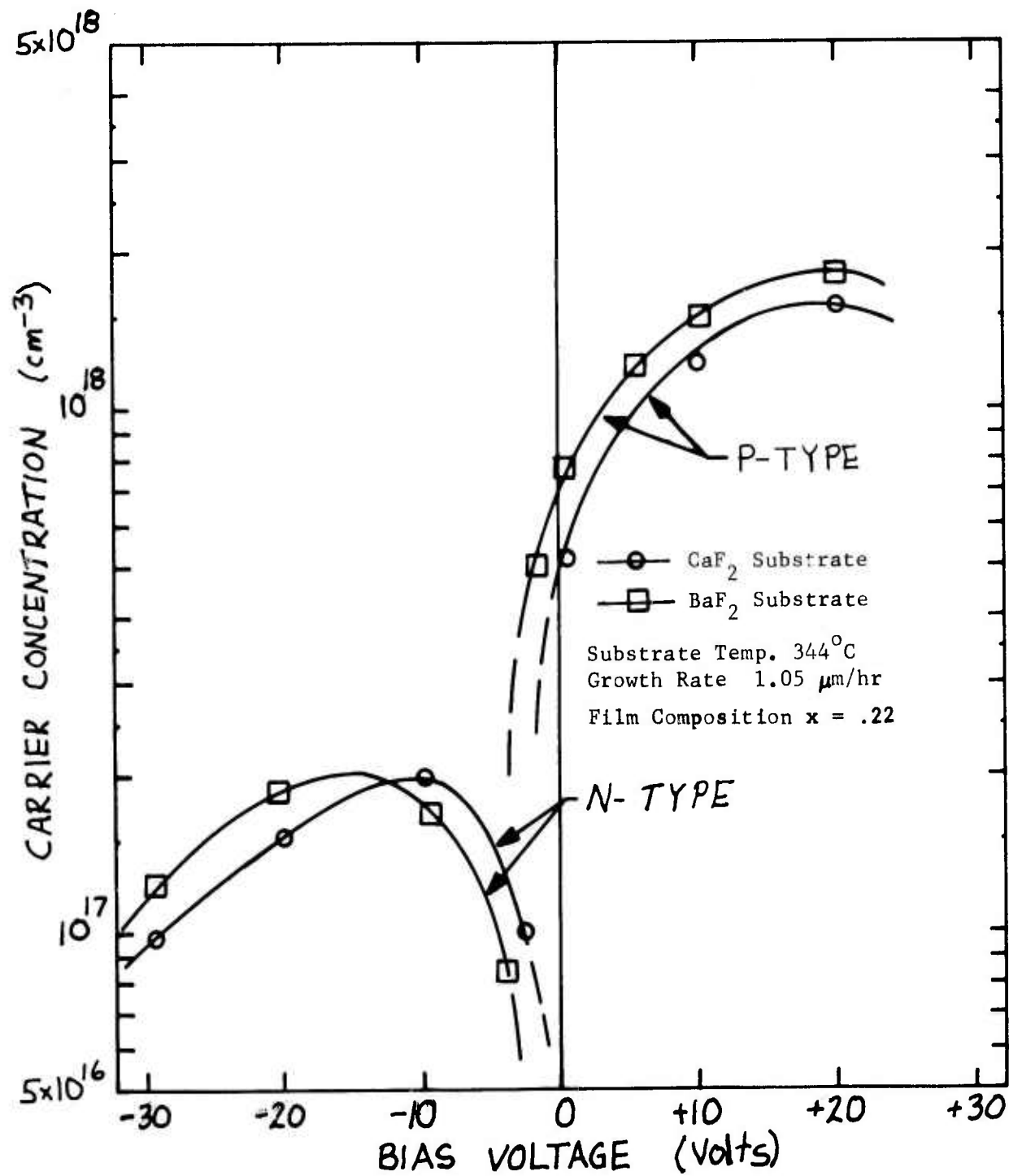
Figure 3-29   Effect of Substrate Bias Voltage on As-Deposited
Carrier Concentration (Target #12)
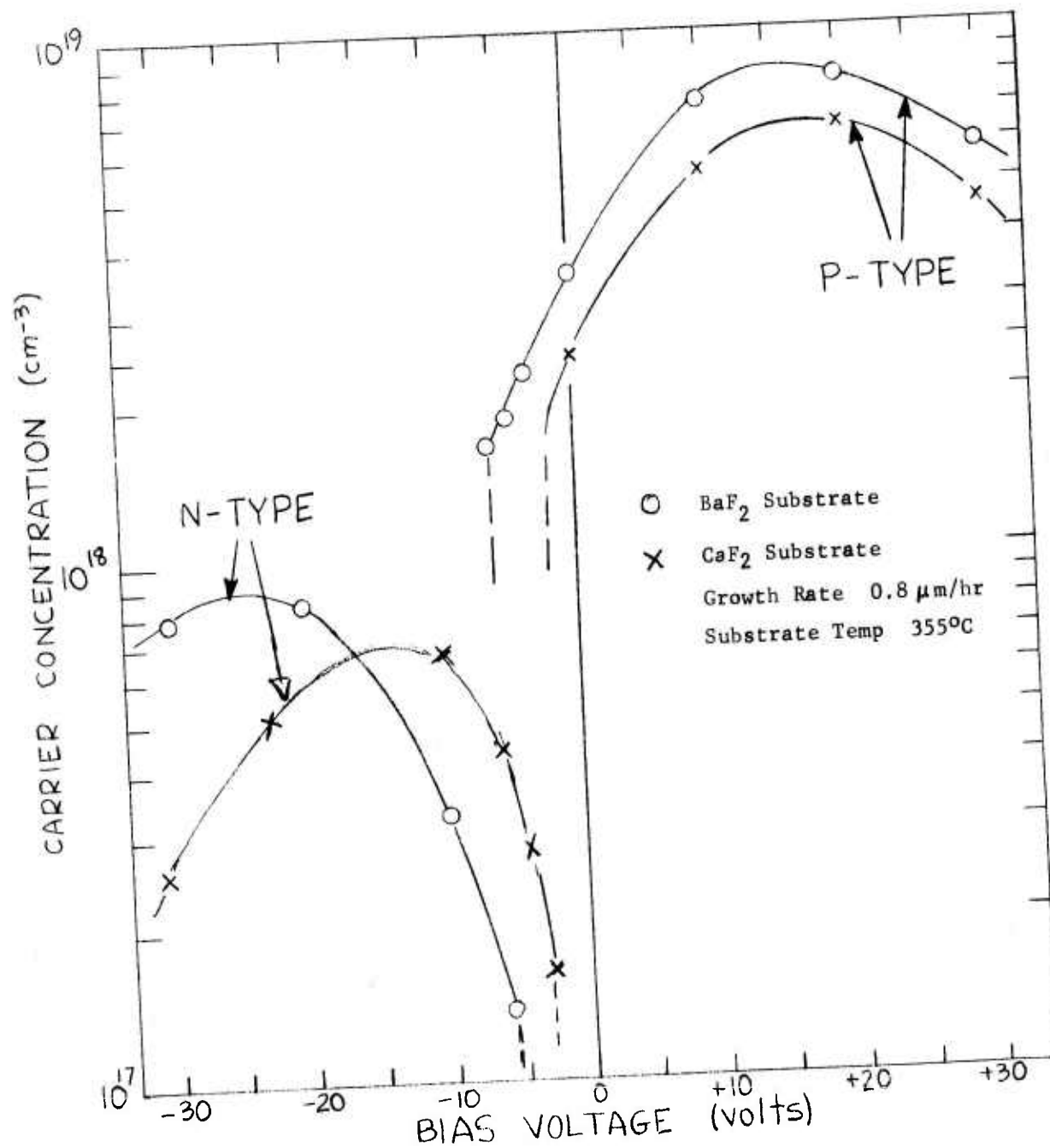
Figure 3-30 Effect of Substrate Bias Voltage on the As-Deposited Carrier Concentrations in $Pb_{.78}Sn_{.22}Te$ Films (Target #8)
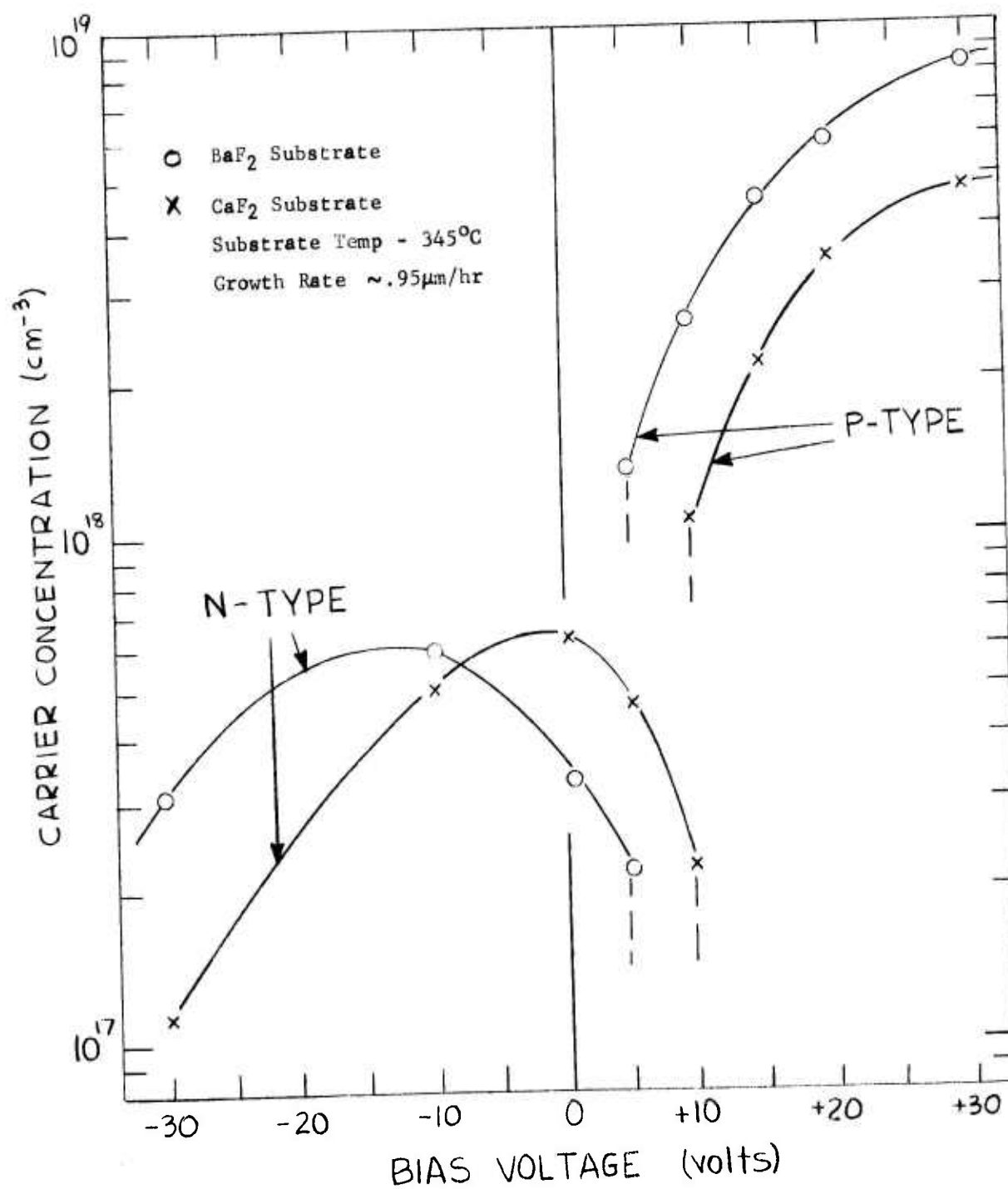
Figure 3-31 Effect of Substrate Bias Voltage on As-Deposited Carrier Concentrations in Pb$_{.80}$Sn$_{.20}$Te Films (Target #9)

The results shown in Figures 3-28 through 3-31 are representative of different sets of deposition conditions. However, in each case, the results are compared for both substrates, BaF_2 and CaF_2. For example, Figure 3-28 shows the carrier concentration as a function of bias voltage for films of composition $x = .22$. As previously noted, film composition remains the same over the whole range of bias voltages investigated. All films were deposited at a substrate temperature of 340^oC and $1.05\mu m/hr$ using Target #10. First, we note that all films deposited on the CaF_2 substrate are p-type with bias voltages above about -2V while those deposited with a lower bias voltage are n-type. It is also apparent that films deposited on CaF_2 have about an order-of-magnitude lower carrier concentration if deposited with an apparently critical bias of about -2V rather than without or zero bias. A similar reduction in carrier concentration is observed with BaF_2 substrates, but the minimum occurs at about -5V.

If we look at the overall trend in Figure 3-28, we can also observe the general monotonic decrease in carrier concentration alluded to earlier as the bias becomes increasingly negative. For example, on CaF_2, a carrier concentration (holes) of about 3×10^{18} cm^{-3} is observed at +17V, a value which changes to about 1.5×10^{17} cm^{-3} (electrons) at -30V.

Figure 3-29 shows similar trends for films deposited from Target #12. As may be recalled Targets #10 and #12 were prepared to have identical compositions, the only difference being the preparation techniques utilized. Furthermore, as noted in Figures 3-28 and 3-29, the deposition conditions used to generate the data shown for the two targets were the same within experimental error. This resulted in film compositions which are also the same. Finally, we note in Figure 3-29 that the bias voltage at which the films switch from p- to n-type and exhibits a minimum in carrier concentration is identical, within experimental error to that shown for Target #10 in Figure 3-28. The major difference between Figures 3-28 and 3-29 are the actual magnitudes in the carrier concentration. They are clearly lower with Target #12. This as we will

show, must be related to the improved target preparation techniques used for Target #12.

Figures 3-30 and 3-31 show results on bias effects for other targets with different compositions and/or stoichiometry. In Figure 3-30 for Target #8 we again note: (1) the small but real differences in carrier concentrations in films deposited on the two different substrates; (2) a minimum in carrier concentration associated with the critical bias voltage at which films switch from p- to n-type; (3) a general reduction in carrier concentration as the bias voltage becomes more negative. In this case, the deposition conditions used ($355^{o}C$, $0.8 \mu m/hr$) were such as to result in films with a composition of $x = 0.22$. This is the same composition as that of the films discussed in Figure 3-29 and 3-30. The negative, critical bias voltages are -3V for CaF_2 and -6V for BaF_2, respectively. Obviously, the deposition conditions utilized to generate the data in Figures 3-28, 3-29 and 3-30, though not exactly the same, yield quite similar results as regards composition and critical bias voltage. However, further observation reveals even greater differences in the actual magnitude of the carrier concentration between those shown in Figure 3-30 and those observed in Figures 3-28 and 3-29. These must, again be related to the differences in the preparation techniques used for Target #8 and Targets #10 through #12. We will discuss this point somewhat later.

The effect of substrate bias on the carrier concentration of films deposited with Target #9 are presented in Table 13 and Figure 3-31. In this case the critical bias voltages are positive for both substrates. As expected (see Figures 3-6 and 3-19) for the deposition condition used to obtain these data, i.e. $345^{o}C$ substrate temperature and $.95 \mu m/hr$ growth rate, the films deposited at zero bias are n-type. Thus, based on our earlier hypothesis, a positive bias potential should in fact be required to produce p-type films at the same deposition conditions. As can be seen, the critical bias potential is, on CaF_2, about +10V and, on BaF_2, about +5V. The composition of the film is specified as

x = 0.20. Reference to Table 13 shows that this composition, again, remains constant for all bias voltages investigated.

The results in Figures 3-28 through 3-31 and Tables 9 through 14 definitely show that the trends observed for the various films are quite general. However, the critical bias voltage changes for the different samples, and is affected by differences in the deposition conditions, target composition, target stoichiometry, etc. The interdependence of the bias voltage effect on the electrical film properties and of the target and deposition parameters is further explored by means of the results illustrated in Figures 3-32 through 3-39.

Results for three different sets of deposition conditions are shown in Figure 3-32 for films sputtered on BaF_2 with Target #10. As noted, all three sets of films have a different composition reflecting the three different conditions used. First, we note that a change in the substrate temperature alone (deposition rate constant) results in a shift of the critical bias voltage. In the given case, the critical bias became more negative, i.e. changed from -5V to -10V, as the substrate temperature was reduced from 340°C to 325°C. A similar shift to more negative values is observed if the deposition rate alone is decreased (substrate temperature constant). Finally, we note that these decreases in the critical bias voltage are associated with decreasing film x-values. The latter relation is, of course, a direct result of the differences in the deposition conditions.

For CaF_2 substrates, shown in Figure 3-33, only the deposition rate effect is illustrated. Still the relation between the rate or corresponding x-value and the critical bias voltage holds as for BaF_2.

Figures 3-34 and 3-35 (also Tables 10 and 11) show the same effects for Target #11 and #12, respectively. Results are presented for films deposited on BaF_2 substrate only.. As may be recalled, Targets #11 and #12 have the same composition as Target #10. It is satisfying to again find fairly good consistency in terms of critical bias voltages, film compositions, etc., between the results with Target #10 and those shown in Figures 3-34 and 3-35 for Targets #11 and #12. However, there

3-67

CARRIER CONCENTRATION (cm^{-3})

BIAS VOLTAGE (volts)

9×10^{18}

10^{18}

10^{17}

7×10^{16}

P-TYPE

N-TYPE

-30   -20   -10   0   +10   +20   +30

BaF$_2$ Substrate

	Subst. Temp. ^{o}C	G.R. μm/hr	Comp. (x)
X	340	1.2	.23
O	340	1.05	.22
□	325	1.05	.21
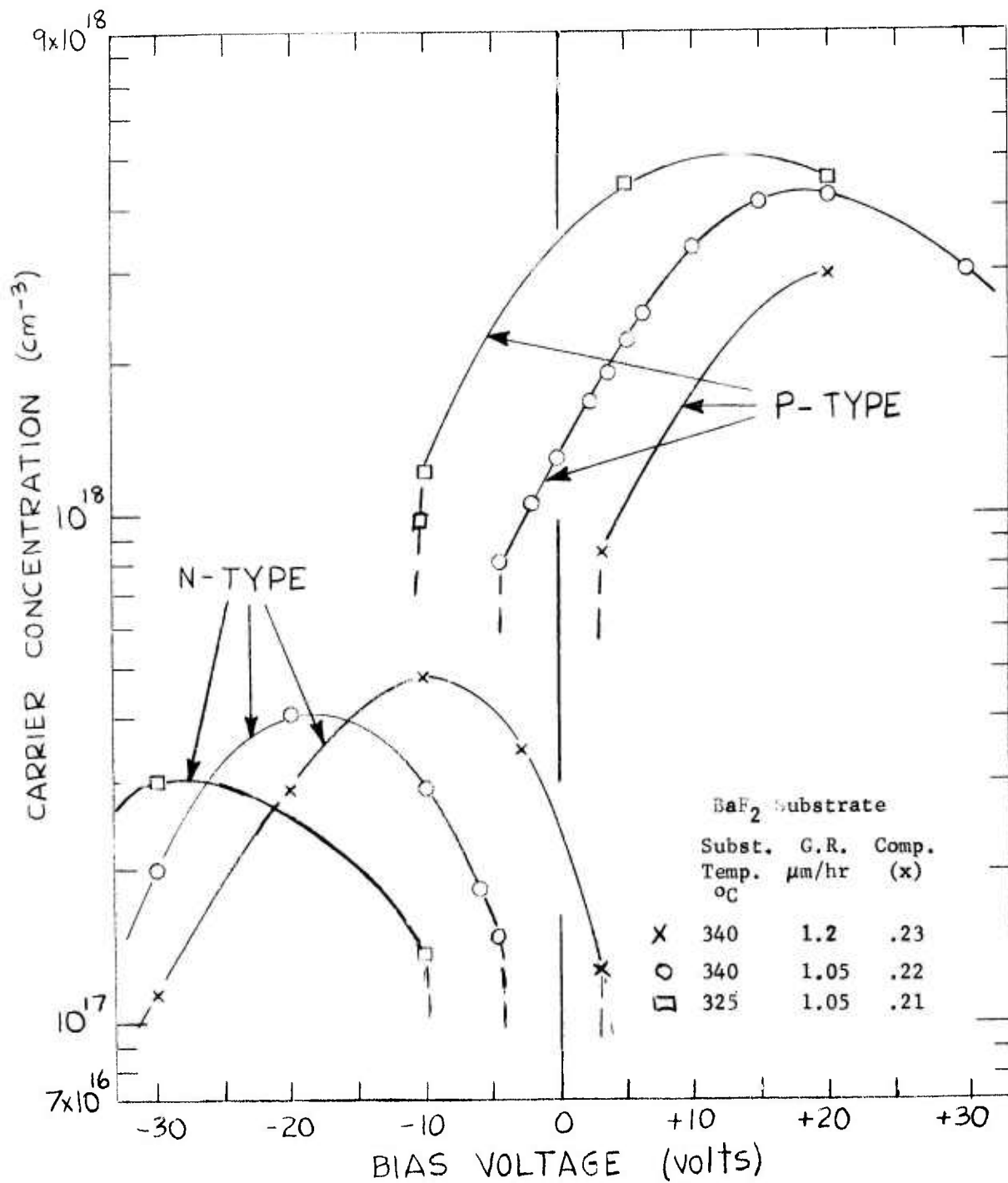
Figure 3-32   Effect of Substrate Bias and Deposition Conditions
on Carrier Concentration Substrate: BaF$_2$ - Target #10
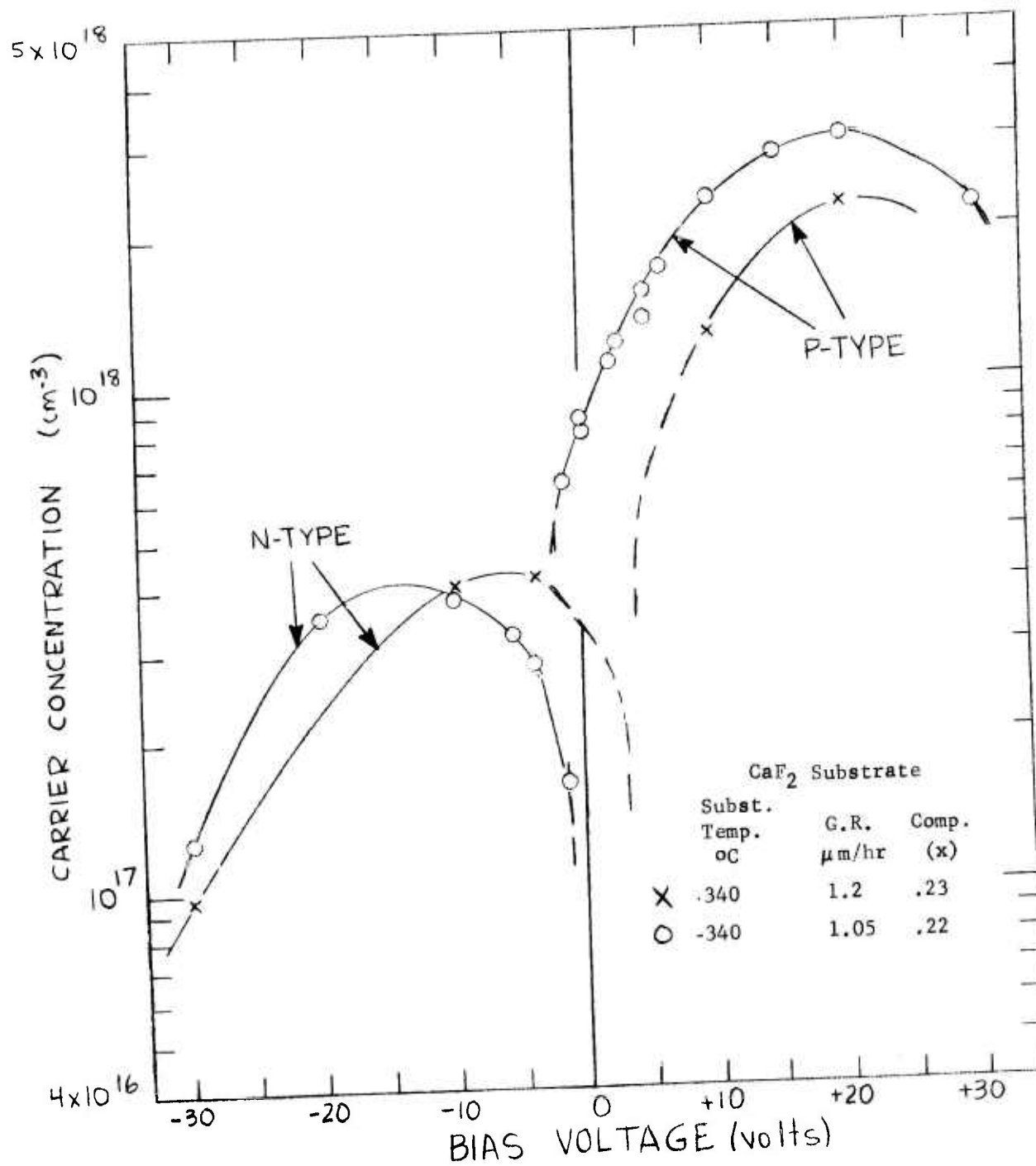
Figure 3-33 Effect of Substrate Bias and Deposition Conditions on Carrier Concentration Substrate: CaF_2 - Target #10
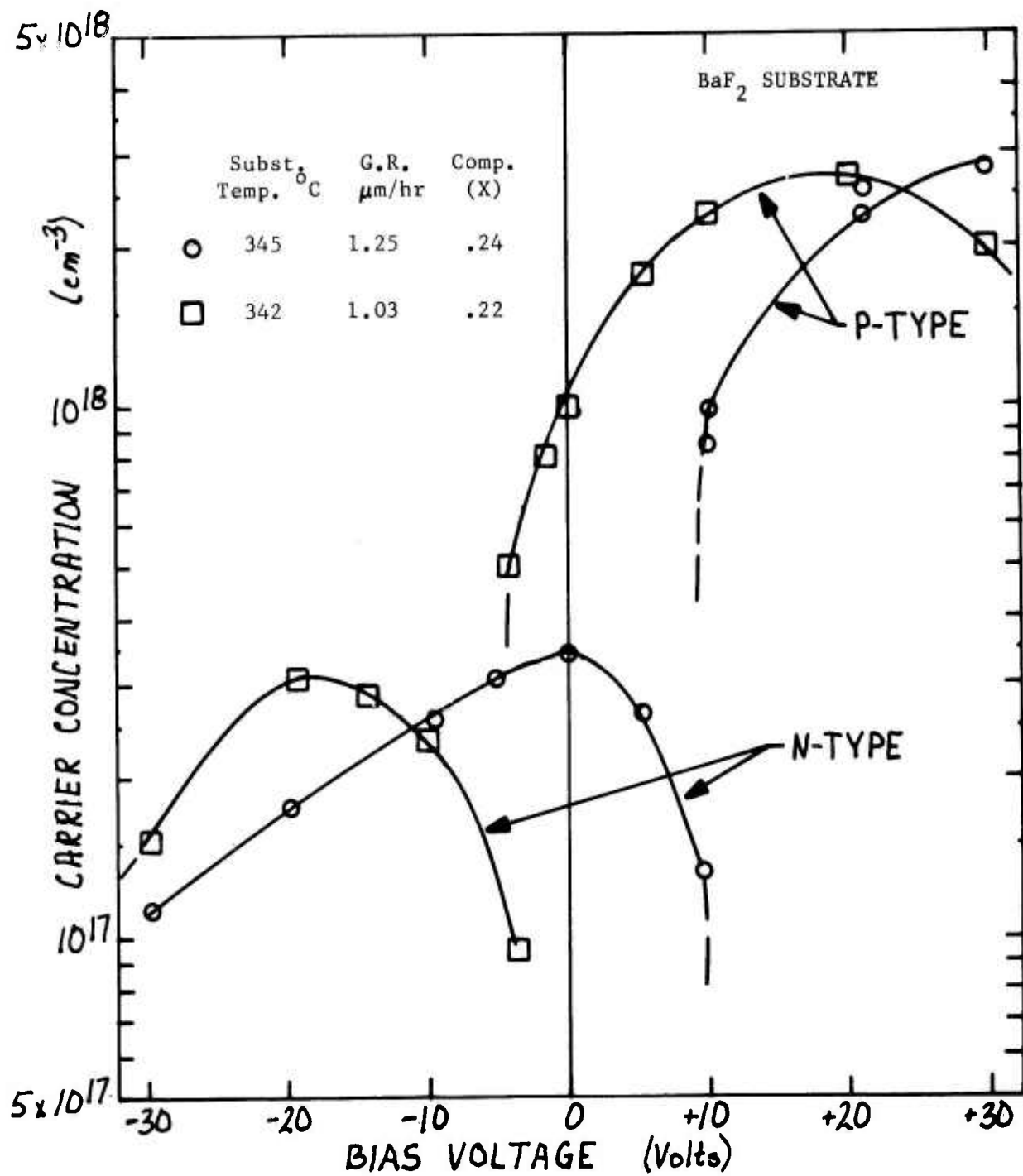
Figure 3-34   Effect of Substrate Bias and Deposition Condition on
Carrier Concentration - Substrate: BaF$_2$ - Target #11
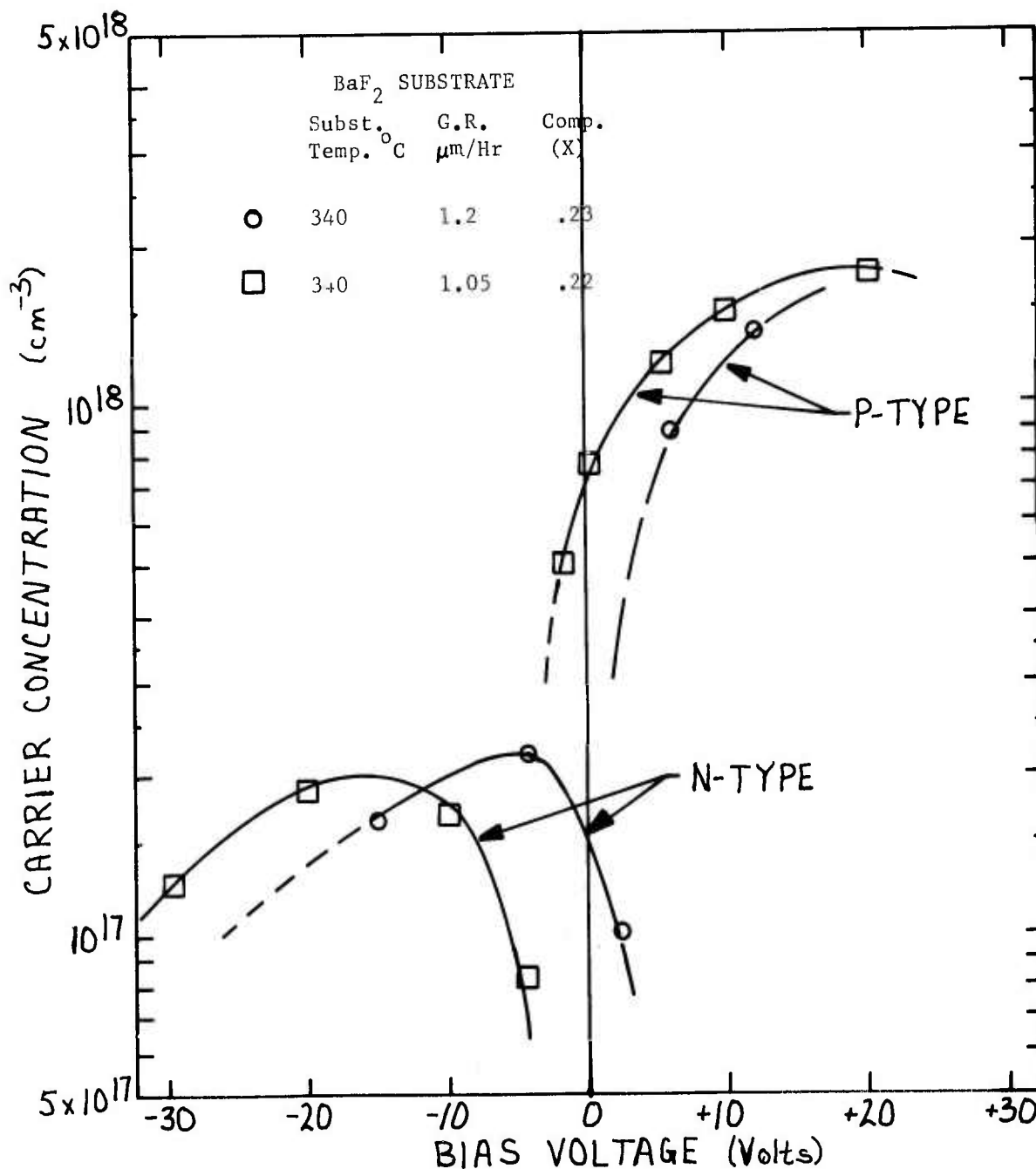
Figure 3-35 Effect of Substrate Bias and Deposition Conditions
on Carrier Concentration - Substrate BaF$_2$ - Target #12
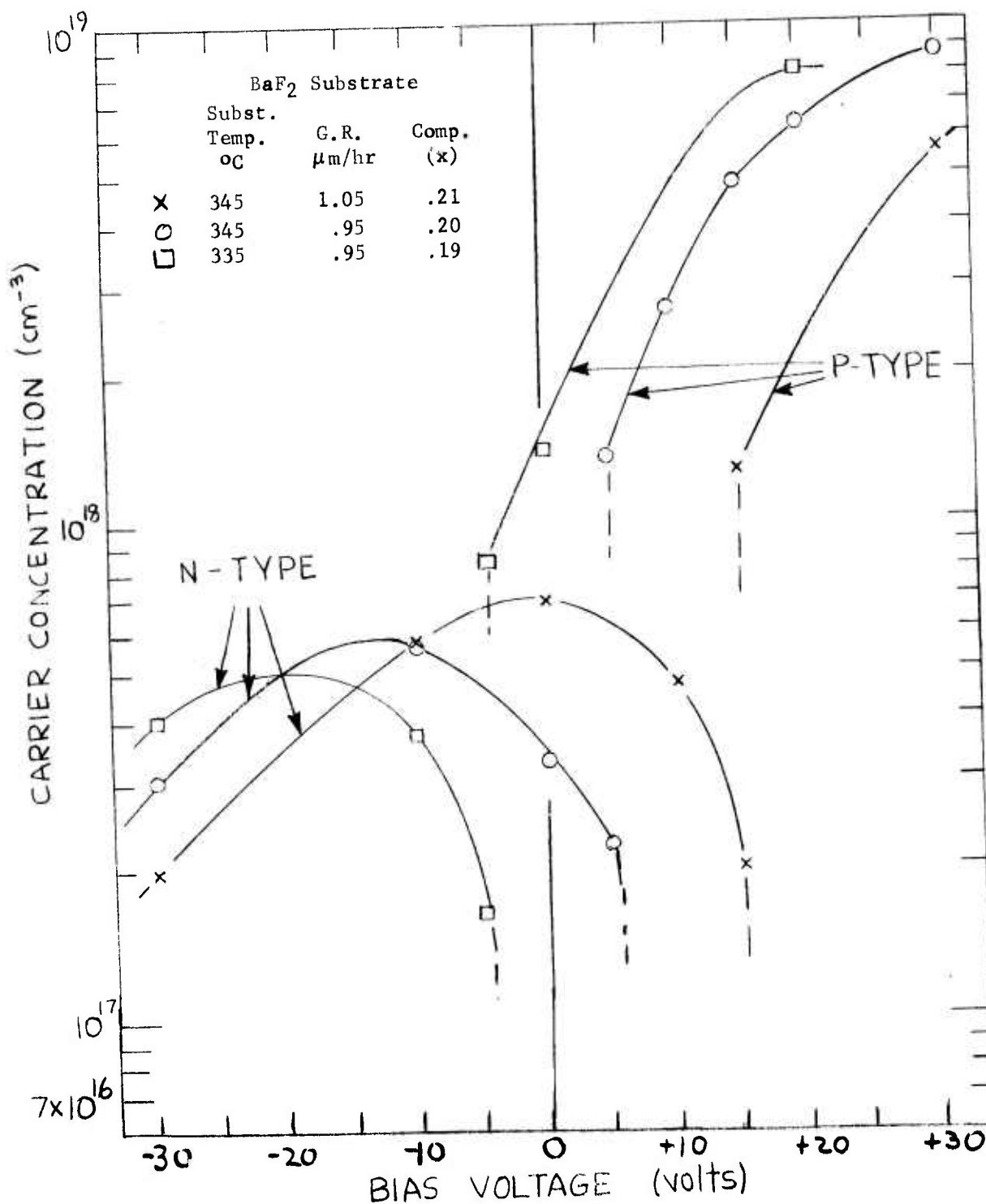
Figure 3-36   Effect of Substrate Bias and Deposition Conditions
on Carrier Concentration - Substrate: BaF_2 - Target #9

3-72
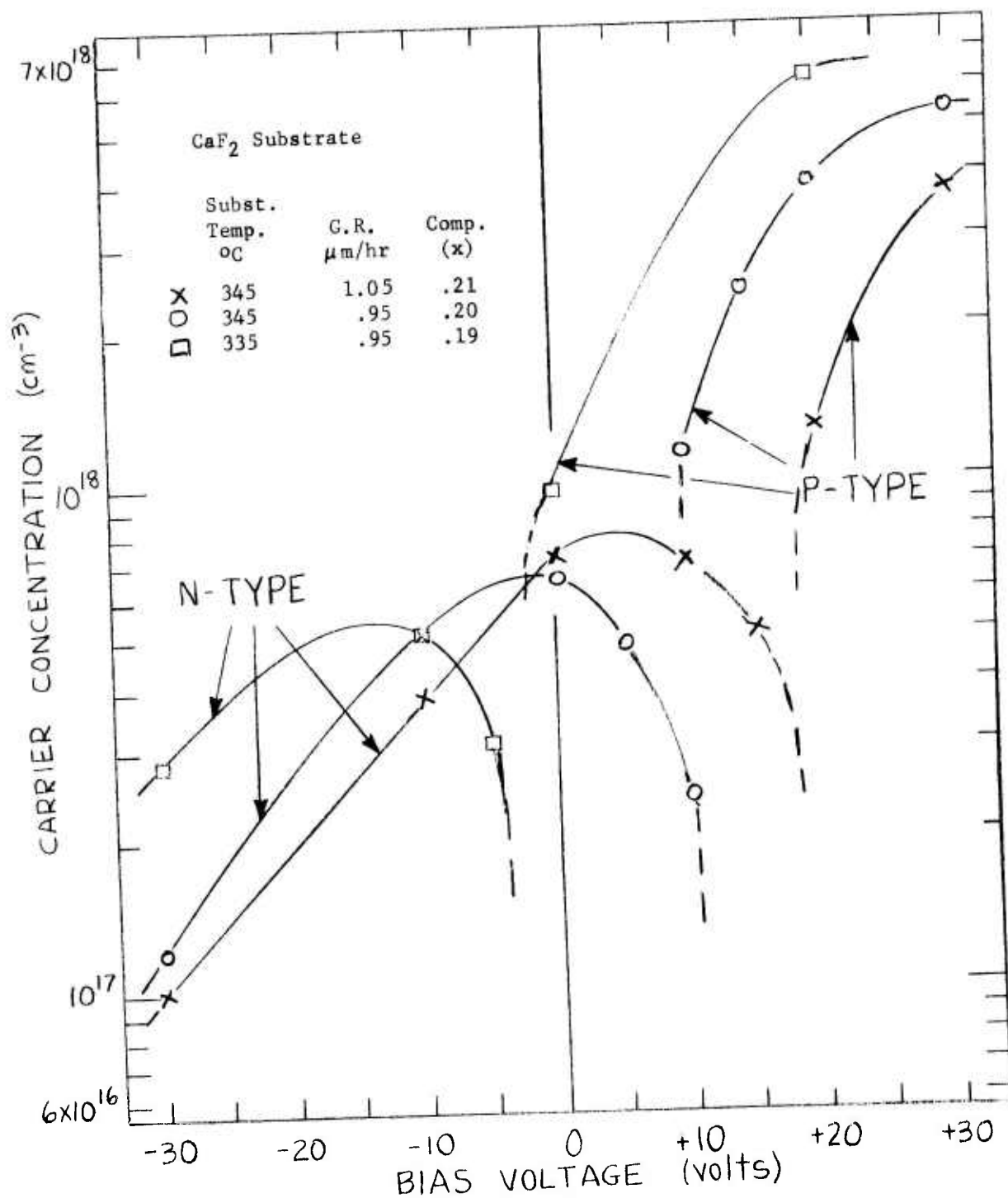
Figure 3-37   Effect of Substrate Bias and Deposition Conditions on Carrier Concentration - Substrate: CaF_2 Target #9

are again differences in the absolute magnitudes of the carrier concentrations relatable to differences in target preparation techniques.

Finally, Figures 3-36 and 3-37 show results for the dependence of carrier concentration on bias voltage for different deposition conditions for films sputtered with Target #9, on BaF_2 and CaF_2 respectively. The trends are again similar to those observed for the other targets investigated. Naturally, there are differences in the magnitude of the carrier concentrations and in the value of the critical bias voltages, which are due to differences in deposition conditions, target composition and stoichiometry (i.e. Target #9 was prepared to be Te-rich).and target preparation.

At this point it may be enlightening to amplify on the effect of improved target preparation techniques repeatedly alluded to above. For example, a point by point comparison of results shown in Figures 3-29 through 3-37 shows that carrier concentrations for films sputtered from Target #12 are lower, over the complete range of bias voltages investigated, than for films sputtered from Targets #8 through #11. Furthermore carrier concentrations for films sputtered from Targets #10 and #11 are lower than for films sputtered from Targets #8 and #9. This can be easily seen in Figure 3-38 which summarizes the effect of bias voltages on carrier concentration for films deposited from five targets on BaF_2 substrates. The deposition conditions, target compositions and film compositions are specified. In this figure, it is possible to directly compare the effect of the target preparation techniques on carrier concentrations and critical bias voltages for Targets #10, #11 and #12. All three targets have the same composition and essentially the same deposition conditions were used to generate the data. The results shown definitely demonstrate: 1) the critical bias voltages are nearly identical for all three targets; 2) the carrier concentrations are consistently lowest in films sputtered from Target #12, with the carrier concentrations in films sputtered from Target #11 being the next lowest followed by the carrier concentrations in films sputtered from Target #10. As discussed

3-74

in Section 2, (see also Table 1), increasingly improved preparation techniques were utilized for Targets #10 through #12. First, we aimed to produce a more homogeneous and stoichiometric composition in Target #10; secondly, we introduced methods for the preparation in an oxygen and water-free environment of Target #11, and finally, we added purification of reacted $Pb_{1-x}Sn_xTe$ target material by sublimation for Target #12. Apparently, all improvements had the desired effects as reflected by the reduced carrier concentrations. In Figure 3-38, these impressive effects can be seen by comparing the results for all five targets. We see a substantial reduction in carrier concentration in films sputtered from Target #12 as compared to those sputtered from Target #8 (prepared in the early standard way). Similarly impressive differences are seen by comparing results for Target #9 and #12. Since Target #9 was prepared to be non-stoichiometric and Target #8 has a higher x-value than Target #12, it might be argued that these are the factors which are influencing the relative carrier concentration between Targets #8 and #9; however, the effects of improved target preparation techniques resulting from Targets #10 through #12 cannot be mistaken.

The added results shown in Figures 3-39 and 3-40 are even more revealing in this respect. Figure 3-39 presents the dependence of carrier concentration on bias voltage for films deposited from the stoichiometric Targets #12 (with x = 0.23) and #2 (x = 0.20, stoichiometric). The deposition conditions although not the same seem close enough for comparison. As noted, even though the target and film x-values are both higher, the carrier concentration in films from Target #12 are the lower ones. This is contrary to typical trends based on x-value effects only.

In Figure 3-40 we concentrate on the relative effect of target stoichiometry using films deposited under identical deposition conditions from Target #2 (x = 0.20, stoichiometric) and Target #9 (x = 0.20, non-stoichiometric). As noted, the film compositions (x = 0.19) are the same for both sets of films. However, the important observation is that the carrier concentrations are comparable in both sets of films. Therefore, it is evident that the non-stoichiometry of Target #9 cannot

3-75
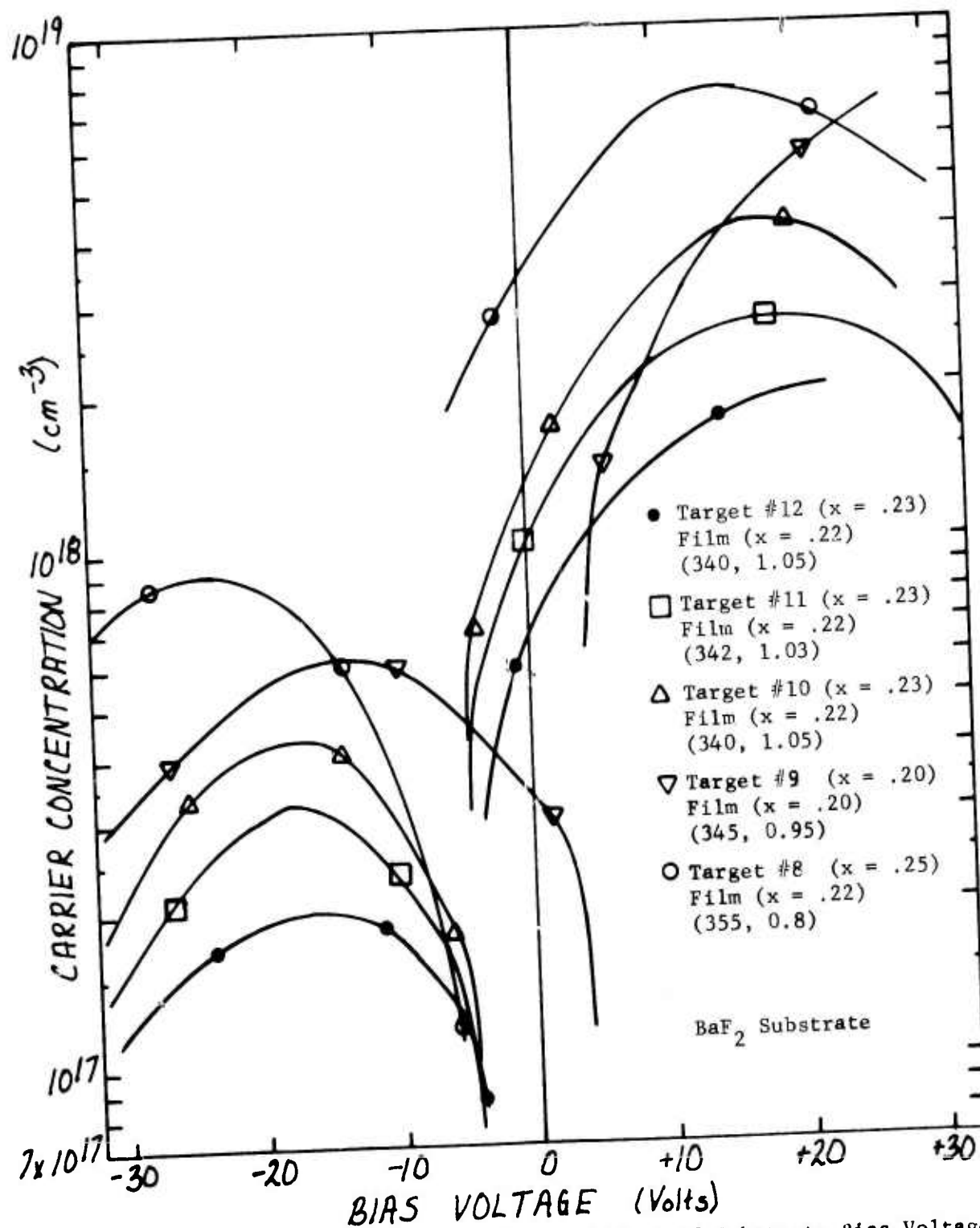
Figure 3-38. Comparison of Results on Effect of Substrate Bias Voltage on As-Deposited Carrier Concentrations in PbSnTe Films from Various Targets

3-76
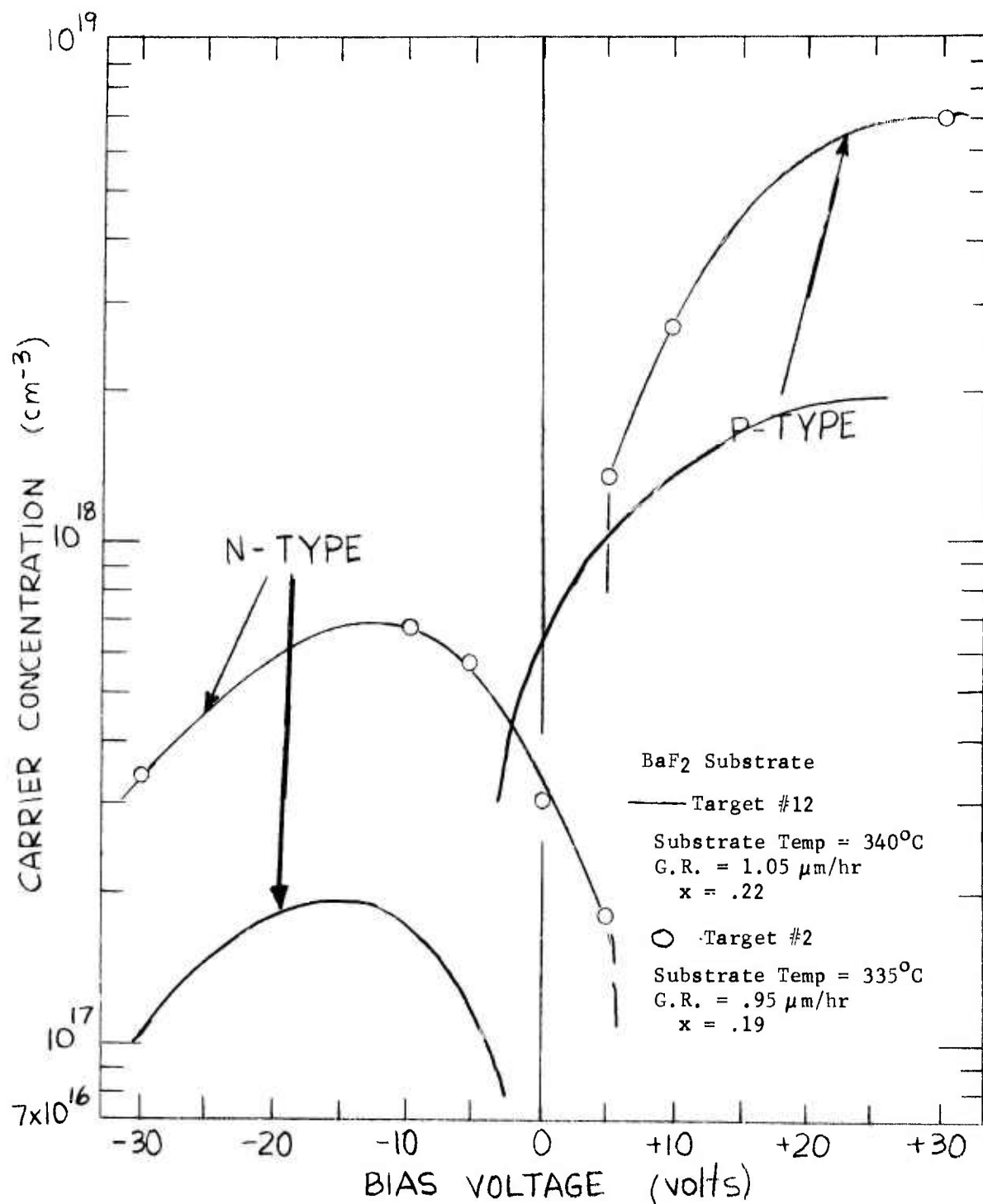
Figure 3-39 Dependence of the Effect of Substrate Bias Voltage on
Target Characteristics - BaF₂ Substrate
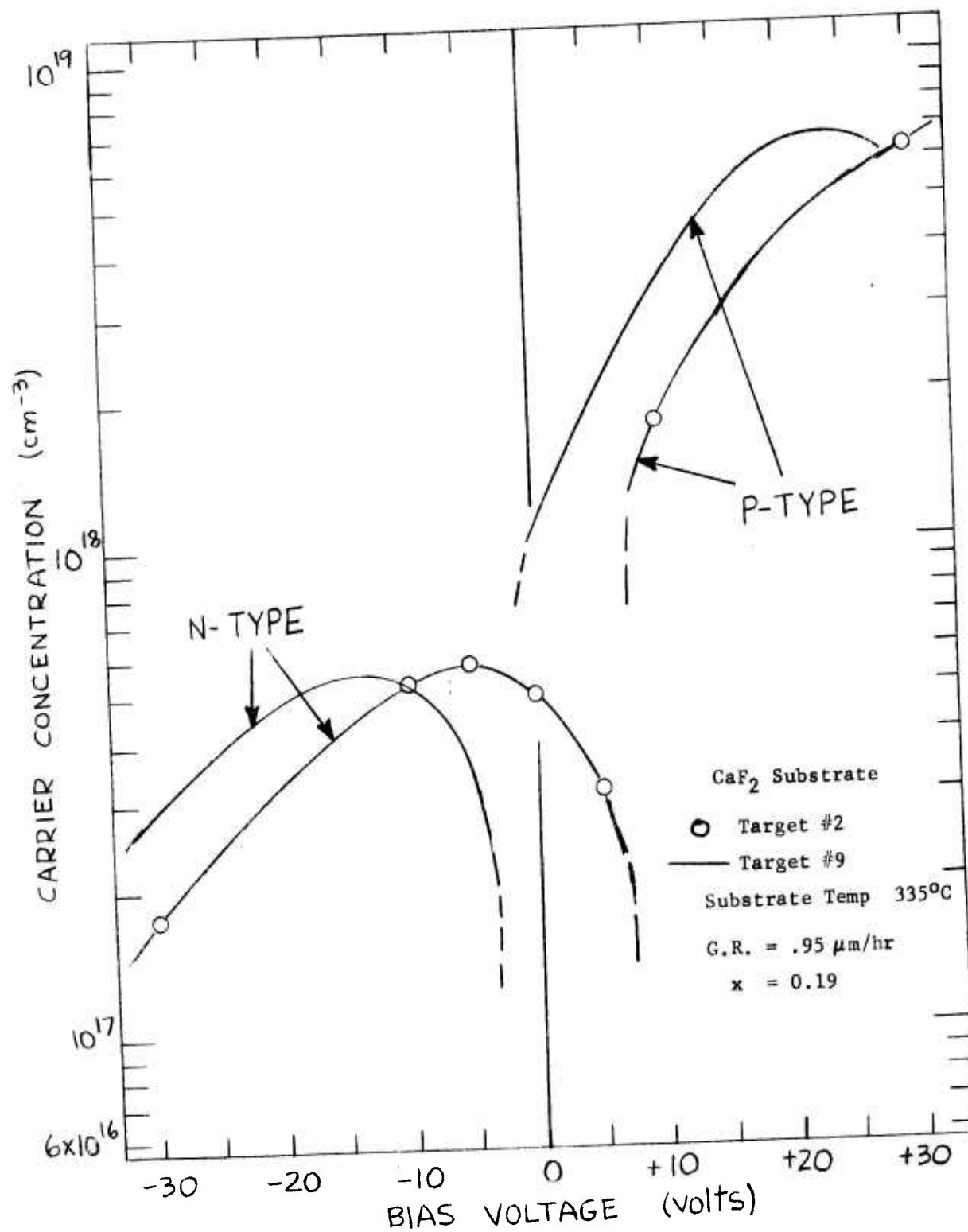
Figure 3-40 Dependence of the Effect of Substrate Bias Voltage on Target Stoichiometry (CaF2 Substrate)

explain its higher carrier concentration relative to films prepared from Target #12 - as indicated in Figure 3-38. Thus, there appears to be no other significant reason for the significantly lower carrier concentration of films deposited from Targets #10, #11 and #12, than the improved target preparation techniques.

While these effects of preparation technique are obviously real, it should not be overlooked that the most significant carrier reduction occurs at the critical bias voltage. For example, at the critical voltage the films have the lowest carrier concentrations namely in the 8×10^{16} cm^{-3} to 1×10^{17} (cm^{-3}) range in all three cases where the modified preparation technique is employed. This emphasizes the fact that in spite of all other parameters having an effect on the carrier concentration, the critical bias voltage has a very strong influence. Full advantage has not, as yet, been taken of this phenomenon since, to date, our emphasis has been on establishing the trends so as to understand the mechanisms and, further, on defining film characteristics as a function of deposition conditions.

We are now fully convinced that the reduction in carrier concentration near the critical bias is the result of a bias induced, <u>stoichiometric adjustment</u>. There is such an abundance of consistent data to this effect that it leaves little doubt as to what is occurring. The simplest and clearest indication of this comes from a comparison of the observed behavior of carrier concentration as a function of substrate bias voltages with other, similar behavior induced by other techniques, such as annealing, which have been identified as controlling the stoichiometry. Reference to various figures in Section 3.4 shows the striking similarity between the critical bias voltage and the critical annealing temperature. Both cause large reductions in carrier concentration - both represent critical values above and below which the carrier type changes.

As further evidence we chose to compare the apparent relation between film property behavior near the critical bias voltages to the film property behavior near the critical $(RT)_0$ product discussed in Section 3.2.2.3 (see Figures 3-16, 3-18 and 3-20). The similarity between the

trends in these figures and data such as shown in Figure 3-29 through 3-40 cannot be mistaken and implies that the responsible mechanisms coincide. A critical point for carrier type switching from n- to p-type and for a corresponding carrier concentration minimum is common to both and can in both cases only be assumed to be the result of stoichiometrical adjustment. If this is so, a real correlation should exist between the critical bias voltage, V_o, and the critical product, $(RT)_o$. This has if fact, been demonstrated and is illustrated in Figure 3-41. Here we plot the deviation $\Delta(RT)/R_oT_o \times 100$ from Figures 3-18 and 3-20 against corresponding critical switching bias voltages observed for the corresponding targets. That is, we selected the critical bias (V_o) for selected deposition conditions (RT) which yielded carrier concentration minima in experiments using substrate bias. We then defined, for the same target and film compositions, the critical conditions $(RT)_o$ which produce carrier concentration minima if no bias is applied to the substrate. This latter data was derived from earlier results such as those shown in Figure 3-7. The differences between the two sets of conditions (RT) with bias and $(RT)_o$ without bias, provided the input for the deviations plotted on the abcissa in Figure 3-41.

Quite obviously, the larger the deviation of the conditions (RT) under which a particular film has been deposited from $(RT)_o$, the larger is the positive or negative critical bias voltage required to minimize the carrier concentration (or switch the carrier type). More generally, if the deposition conditions are such that $\Delta RT/(RT)_o$ is negative and thus produces p-type film without bias (see Figure 3-20 for example), V_o has to be negative. The reverse holds true for film deposited under conditions which render the film n-type without bias. Therefore, it appears that at deposition conditions which are removed from the p-n transition conditions at zero bias, i.e., at conditions resulting in the formation of non-stoichiometric film and with high carrier concentration, the application of a bias voltage can adjust for stoichiometric deviations and correspondingly minimize the carrier concentration. An interesting consequence of this is that for a film being deposited exactly at a set of critical conditions $(RT)_o$ the critical bias condition is $V_o = 0$.
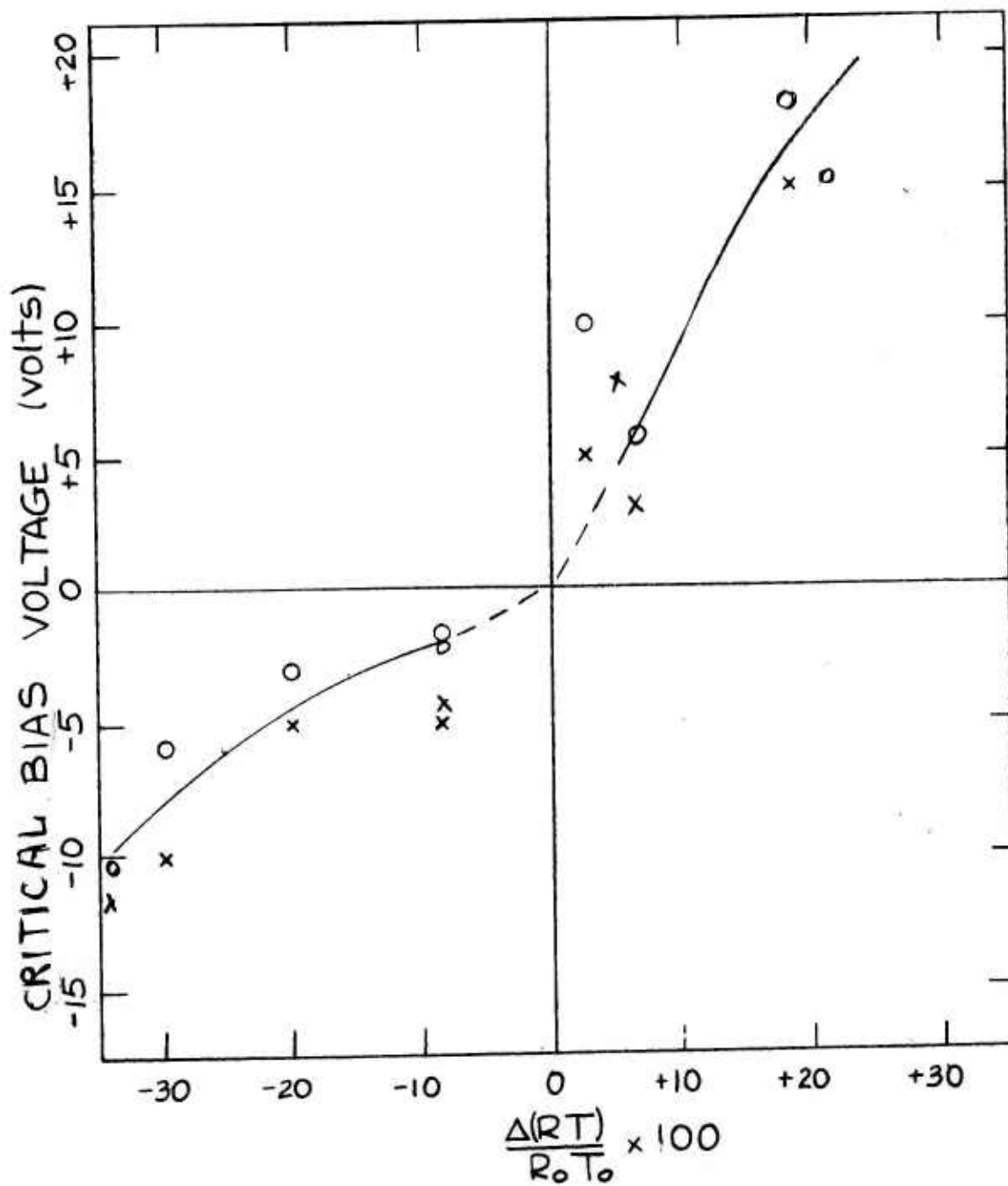
Figure 3-41 Effect of Deviation from Critical Deposition Conditions on Critical Bias Voltage (Targets #8, #9, & #10)

3-81

We have seen in Figures 3-32 through 3-37 that the critical bias voltage varies with film composition. This is reflected, in summary form, in Figure 3-42 and 3-43. Figure 3-42 is a replot of Figure 3-41 but identifies the various targets and the various film compositions applicable to each data point. Figure 3-43 actually plots the critical bias voltage for all film compositions produced by the various targets investigated. We note in both figures that, for any particular target, the variations of the critical bias voltage with film composition are quite systematic. Of particular interest are the compositions near the zero bias conditions. Here the film x-values approach the x-values of the targets themselves. This is indeed consistent with our earlier observation at zero bias. In that case, the compositions of films deposited at conditions near the p-n transition curve were limited to values not too far removed from the composition of the target (see Table 2). This clearly shows one of the advantages of bias sputtering. Films of a far larger range of x-values can be sputtered, stoichiometrically, from a given target with bias than without bias. This is amplified in Figure 3-44 in which the p-n transition at zero bias conditions for Target #9 (solid line) is reproduced from Figure 3-6, in addition to p-n transitions for different substrate bias voltages. This figure thus reflects that with this particular target p- and n-type films can be deposited which are very close to stoichiometry and have a large range of x-values. All other targets yielded the same observation.

It has not as yet been theoretically established why small biases can cause a stoichiometric adjustment. But it can be conjectured that deviations from stoichiometry in single crystal films are generally small for any set of conditions, in spite of large effects on carrier concentration. The latter is due to the fact that fractional percents in metal or tellurium richness are sufficient to produce order-of-magnitude changes in carrier density. Consequently, if only a small fraction of the impinging $Pb_{1-x}Sn_xTe$ beam is ionized or, for that matter, if only a small fraction of one component is ionized, a bias can cause preferential adsorption or desorption of the impinging material and consequently a

3-82
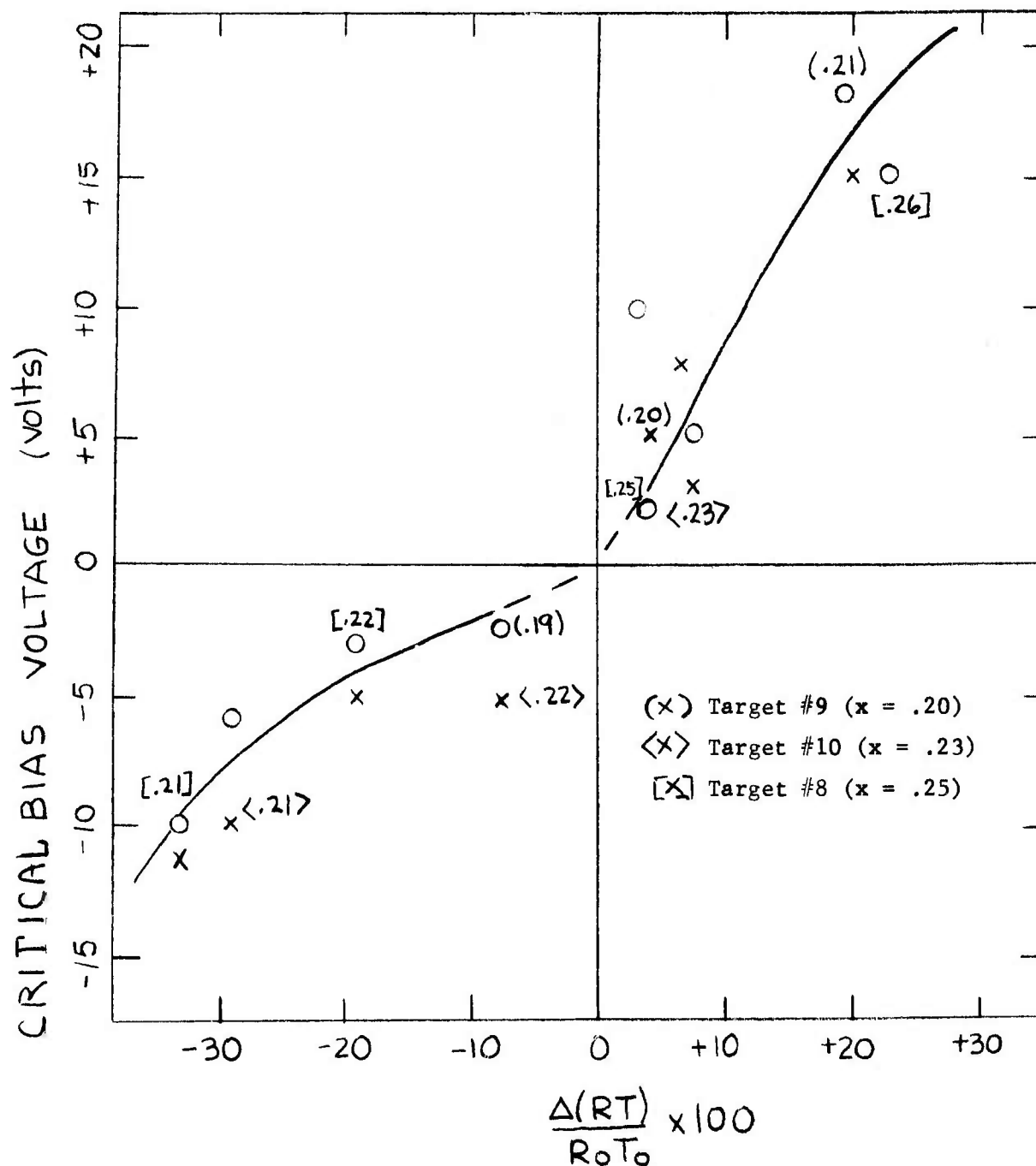
Figure 3-42 Film Composition as Related to the Effect of
Deviation from Critical Deposition Conditions
on Critical Bias Voltages (Targets #8, #9, & #10)

3-83
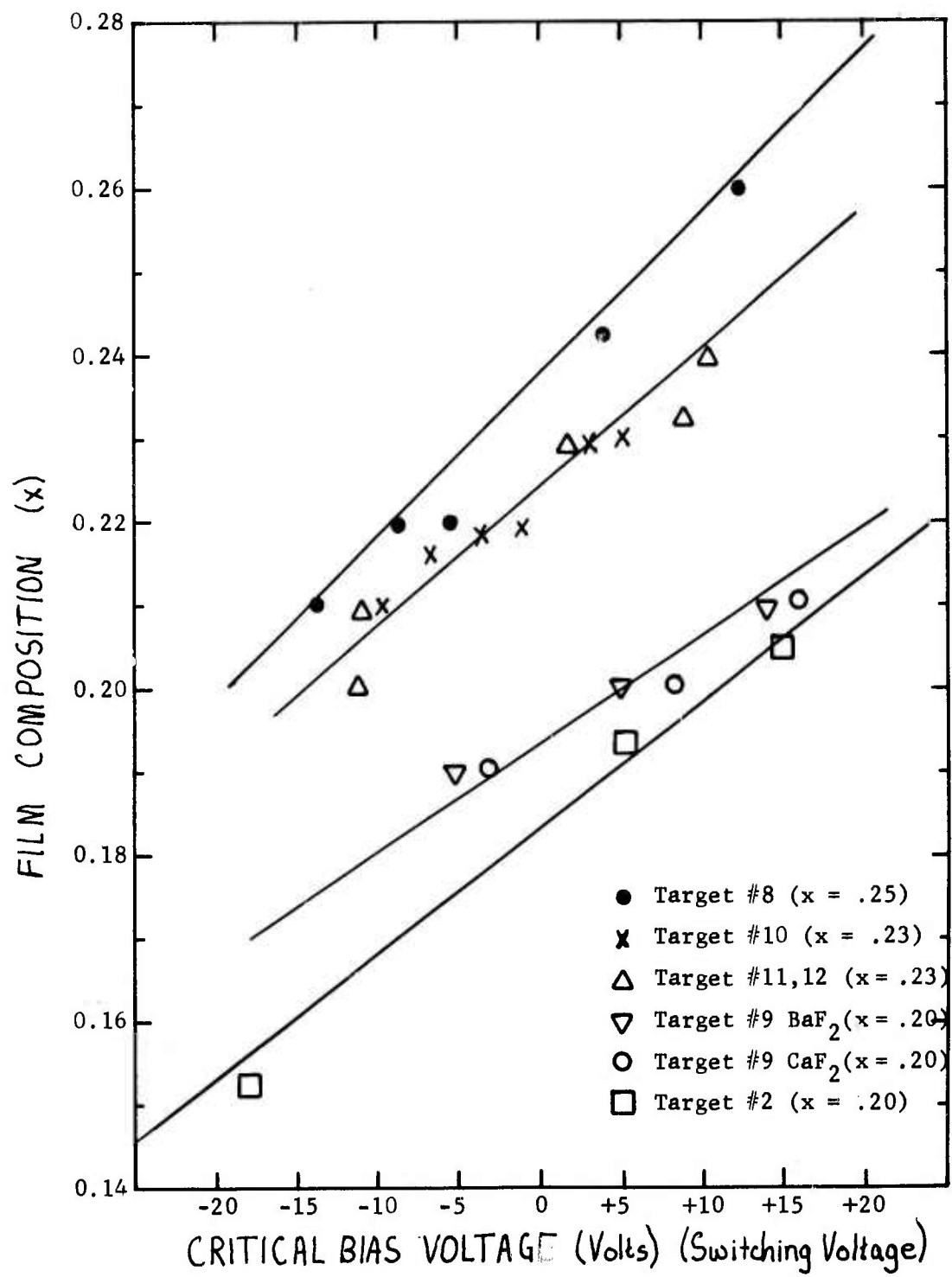
Figure 3-43. Critical Bias Voltage vs Film Composition
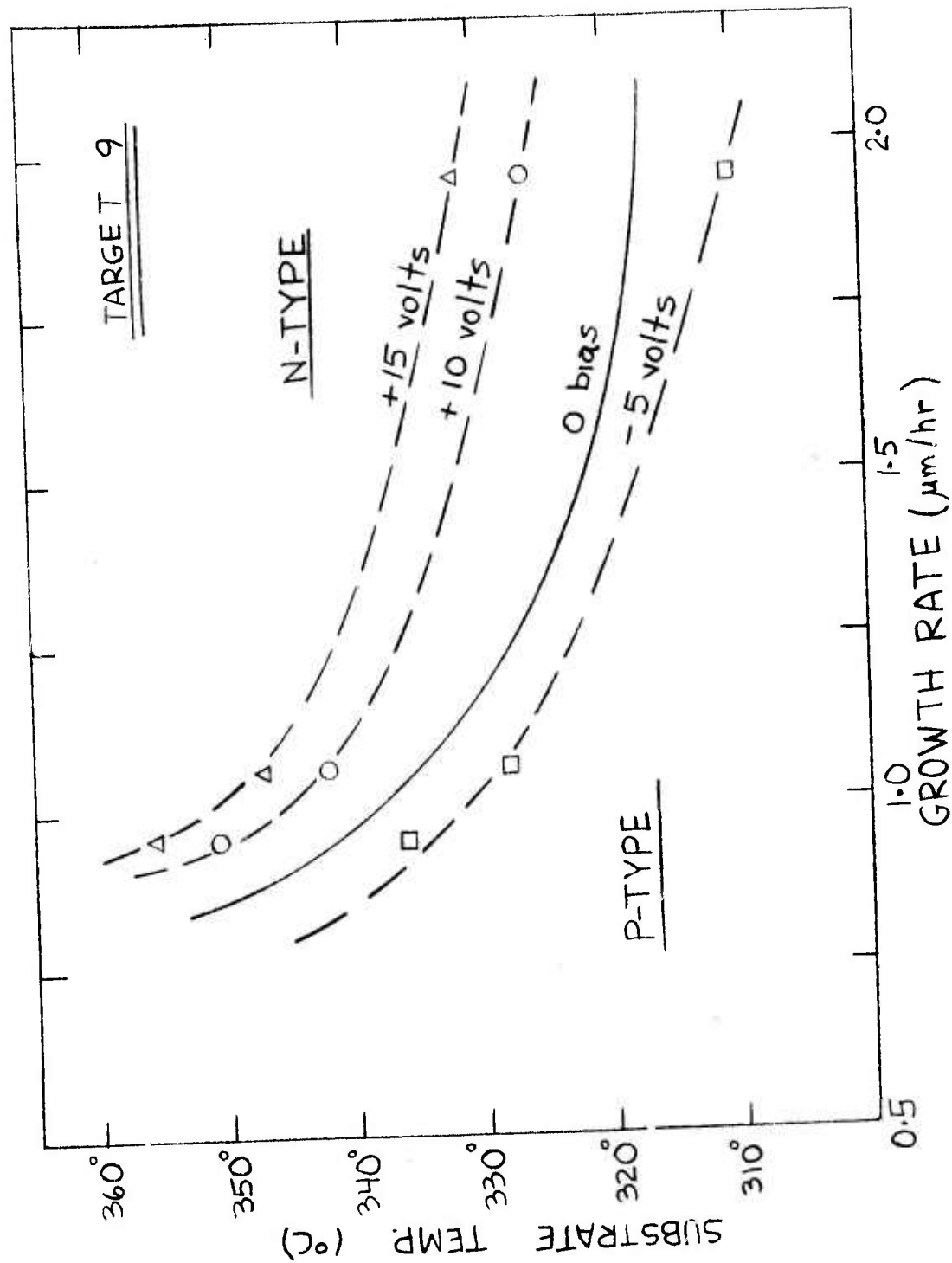
Figure 3-44 p-n Transition Conditions for Various Substrate Bias Voltages - Target #9

stoichiometric adjustment coupled with large changes in carrier con-
centration. Some attempts to identify what species may be present in
our sputtering system before, during and after sputtering have already
been made by the use of a mass spectrometer. Although the spectrometer
system can be and is being used to identify species before and after
the sputtering process, some difficulties have been encountered in
utilizing the system, as it stands, during sputtering. Some modifications
are necessary before this can be done.

One factor should not be overlooked. As noted earlier, large
reductions in carrier concentration are observed at the larger negative bias
voltage. This is reminiscent of results from our earlier work with thin
film metals, indicating an apparent impurity adsorption control. That
is to say, the mechanisms which are operative at the larger negative
biases are probably: (1) a bias-controlled retardation of the surface
adsorption of foreign impurity species which were ionized in the plasma,
(2) substrate cleaning by ion and/or electron bombardment. Both mechani-
sms would result in a monotonic variation in carrier concentration be-
tween positive and negative bias conditions.

Independent of the cause, these results represent a potential
breakthrough in photo-voltaic p-n diode fabrication. To summarize,
sputtering at a critical bias voltage is a process which is extremely
easy to control - in fact even easier and more precise than the control
of the $(RT)_0$ product which can also be used to form p-n junctions. Most
importantly, bias control maintains constant film composition (except
for stoichiometric adjustments) and consequently will not affect the
spectral response of individual layers deposited. It does produce
detector materials with relatively low as-deposited carrier concentrations.
Should annealing still be desired, the fact that the composition is the
same in all layers, makes it possible to use only one critical annealing
condition to improve all layers and insures that no concentration gradient
will induce interdiffusion of components across the p-n junctions - thus
degrading or destroying the junction characteristics.

3.2.4 TRANSPORT PROPERTIES OF AS-DEPOSITED FILMS-EFFECTS OF
SUBSTRATE BIAS, TARGET PROPERTIES AND TEMPERATURE.

3.2.4.1 Introductory Remarks. Further insight into the phenomena
associated with the observed results already presented can be obtained
from measured carrier mobilities and their dependence on deposition
conditions, carrier concentration and measurement temperature. For
example, we may expect that the Hall mobilities of our films show similar
dependences on sputtering conditions as the carrier concentrations - if
the observed carrier concentrations are not simply the results of
impurity compensation or similar causes. In the previous sections we
assumed that the reduction in carrier concentration at $(RT)_c$, i.e. at
the p-n transitions observed in films deposited at zero bias and in
films deposited at the critical bias voltage V_0 were associated with
conditions approaching stoichiometry. Furthermore the reduction in
carrier concentration at the larger negative biases was associated with
a purification process. If these mechanisms are correct, the mobilities
in the film may be expected to approach optimum behavior and values near
these critical conditions also. Results to be presented demonstrate
this to be the case.

Temperature dependencies of Hall mobilities and Hall coefficients
can also be used to aid in the definition of mechanisms which affect
the transport properties. In particular such data can be used to
determine types of scattering centers active in the films which in turn
aid in defining the mechanisms responsible for the observed phenomena
(e.g. non-stoichiometry or impurity compensation).

In the following sections we present data showing the dependence
of mobility on carrier concentrations for unannealed films deposited with
and without substrate bias, utilizing the various targets investigated,
and data showing the temperature dependencies from 300°K to 4°K of Hall
mobilities and Hall coefficients in films sputtered under a variety of
conditions also.

3.2.4.2 General Effects of Deposition Conditions, Target Character-
istics, Substrate Bias, Etc. on Transport Properties. Figures 3-45 through

3-87

3-54 (see Tables 3 through 14 for actual data points) illustrate results on the dependence of measured Hall mobilities on the carrier concentrations measured in the same films. In all of these figures there results for single crystal $Pb_{1-x}Sn_xTe$ films, deposited under a variety of conditions, follow the generally accepted trends. Any decrease in carrier concentration is associated with a corresponding increase in carrier mobility. As noted, the results shown contain data from films on both $CaF_2(111)$ and $BaF_2(111)$ substrates. The illustrated trends, are in full concurrence with and only explainable by suggested mechanisms involving stoichiometric adjustments or possible purification. If other mechanisms, such as impurity compensation, were responsible for the observed decreases in carrier concentration, it would be expected that, in some cases at least, the mobilities would experience a reduction rather than an increase with decreasing carrier concentrations. A typical cause would be impurity scattering if carrier compensation had occurred.

Figures 3-45 through 3-54 reveal, in addition, information on the effects of target stoichiometry, substrate bias, and general target characteristics on the mobility of p-type and n-type carriers in $Pb_{1-x}Sn_xTe$ films. We will cover the results on films prepared _without_ substrate bias first, followed by results on films prepared _with_ substrate bias. These results (with and without substrate bias) will then be compared. As may be recalled the work without substrate bias was performed with targets prepared early in this program (i.e. Target #2 through #7). Targets prepared last (i.e. Targets #10 through #13), were almost exclusively used for work with substrate bias. However, Targets #8 and #9 were utilized for deposition _with and without_ bias. Figures 3-45 and 3-46 present samples of results obtained with the early targets. In Figure 3-45, mobility versus carrier concentration relations are illustrated for single crystal p-type films sputtered with Targets #2 and #3 on $CaF_2(111)$ $BaF_2(111)$ substrates. The data utilized are given in Tables 3 and 4. The trends observed may be summarized as follows:

a) Both the low temperature (88°K) and high temperature (300°K) data show the nearly linear relation between mobility and carrier concentration that is typically observed in bulk and evaporated $Pb_{1-x}Sn_xTe$.

b) Films with the same range of x-values ($0.09 \leq x \leq 0.20$) fit on the same linear trend curve, independent of the target used or the substrate on which they are deposited.

c) The mobility increase,with decrease in carrier concentration is considerably higher at 88°K than at room temperature - a trend that is typical for bulk $Pb_{1-x}Sn_xTe$ also (Reference 15).

d) The few data points included to show the characteristics of polycrystalline films show the marked effect of film structure. Carrier concentrations are limited to rather high values and mobilities are considerably below those of the epitaxial films.

Figure 3-46 presents the relation between mobility and carrier concentration for as-deposited n-type films sputtered also from Targets #2 and #3 (data also listed in Tables 3 and 4). In general, the trends are quite similar to those observed with p-type film (Figure 3-45). Mobilities tend to increase with decreasing carrier concentration in a near linear fashion. Again, such decreases in mobility are more pronounced at the lower temperature. The mobilities in the n-type films are significantly higher, for equivalent carrier concentrations, than in p-type films. Comparison with Figure 3-45 shows also that lower carrier concentrations were achieved in the as-deposited n-type film than in the p-type films. Both of these behavioral differences are consistent with observations in bulk PbSnTe.

Distinctly different from the observations in p-type films is that the substrate affects the mobility of n-type carriers. The BaF_2 substrates, at both temperatures, are associated with higher mobilities than the CaF_2 substrate, over the entire range of carrier concentrations. No such distinction could reasonably be made in Figure 3-45. In fact no such distinction has been found in either n- or p-type films when any of the other targets were utilized, as we shall see. Also, the mobilities

3-89
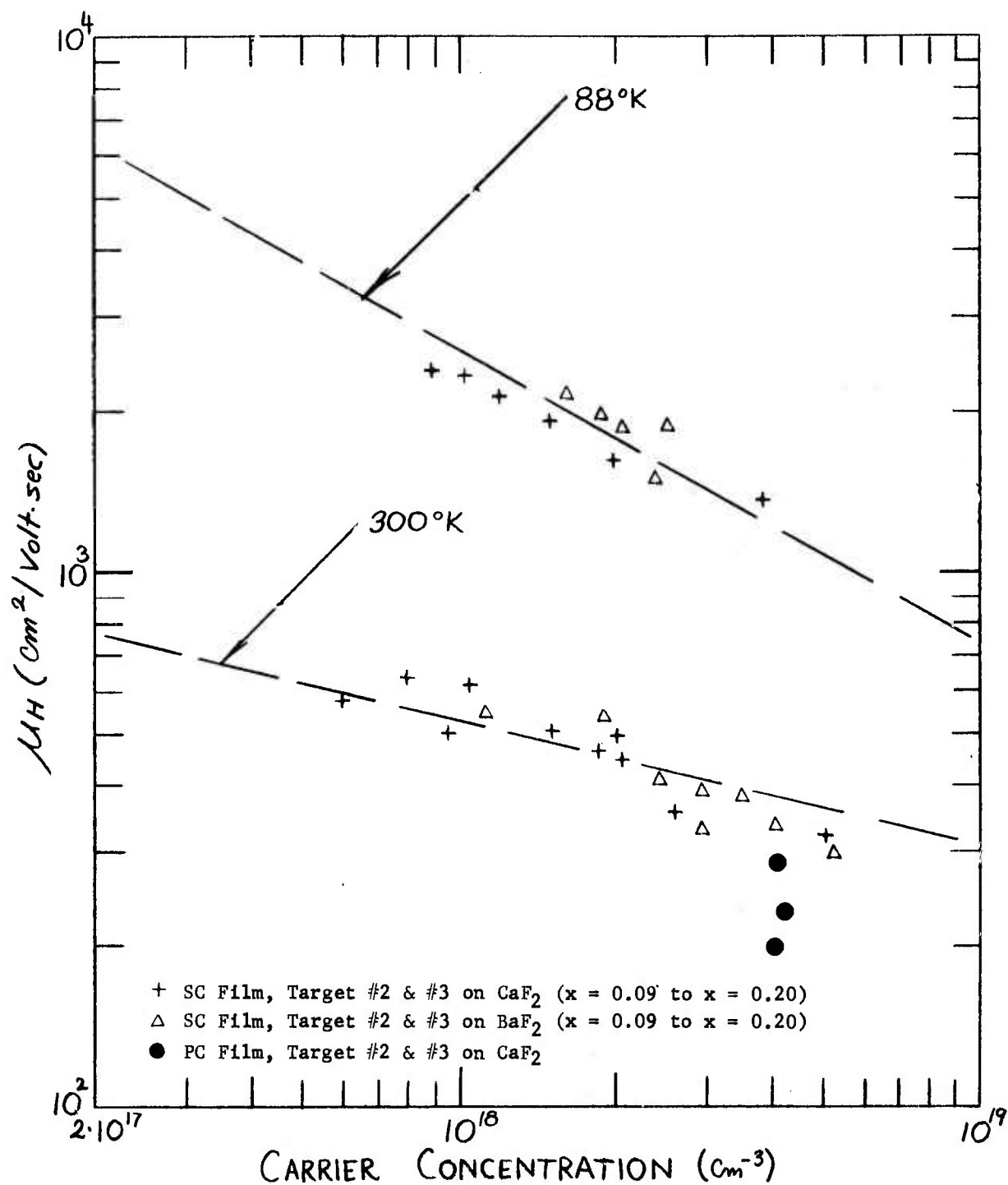
Figure 3-45 Electrical Properties of As-Deposited p-type $Pb_{1-x}Sn_xTe$
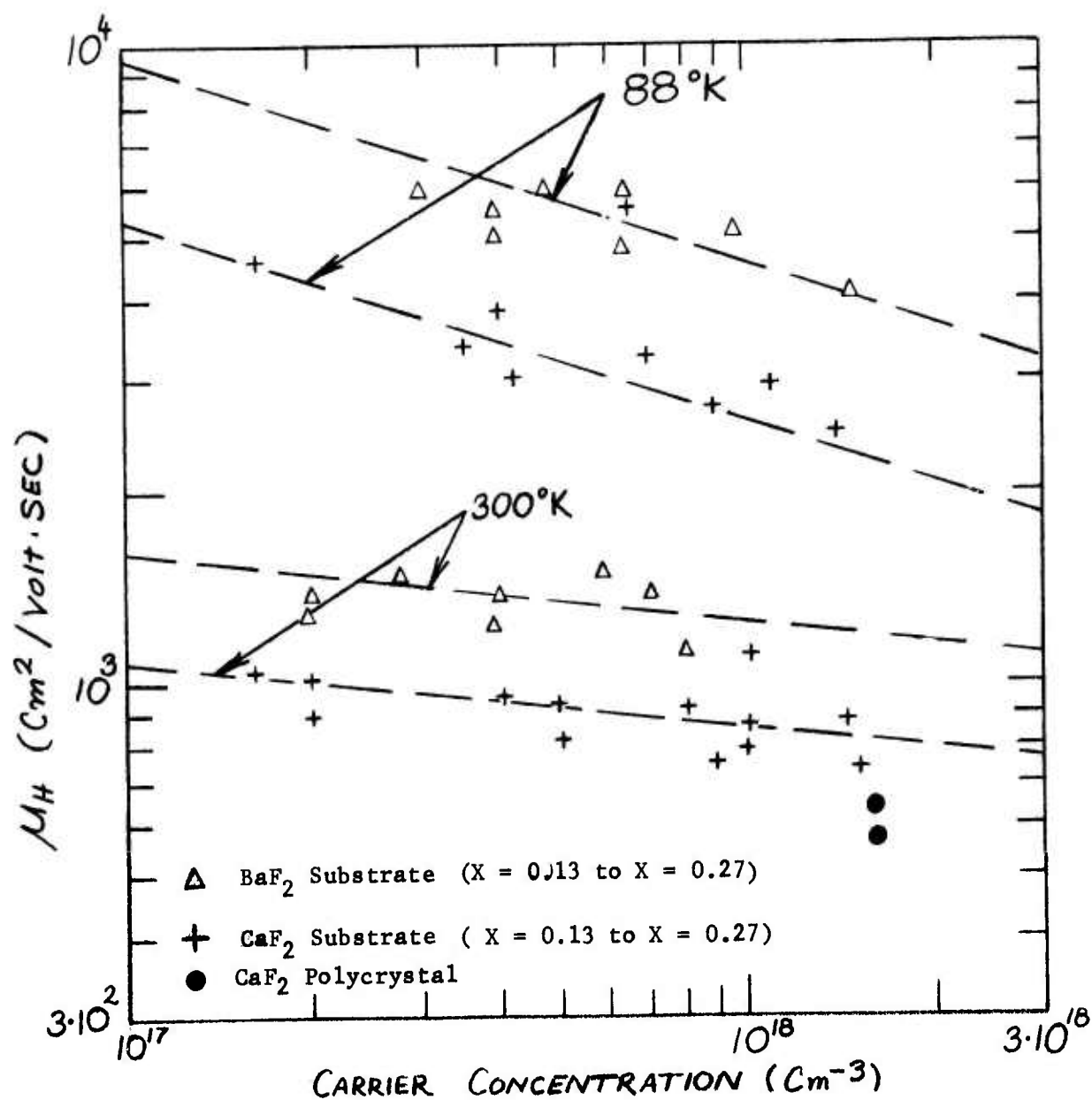
Figure 3-46 Electrical Properties of As-Deposited n-type $Pb_{1-x}Sn_xTe$
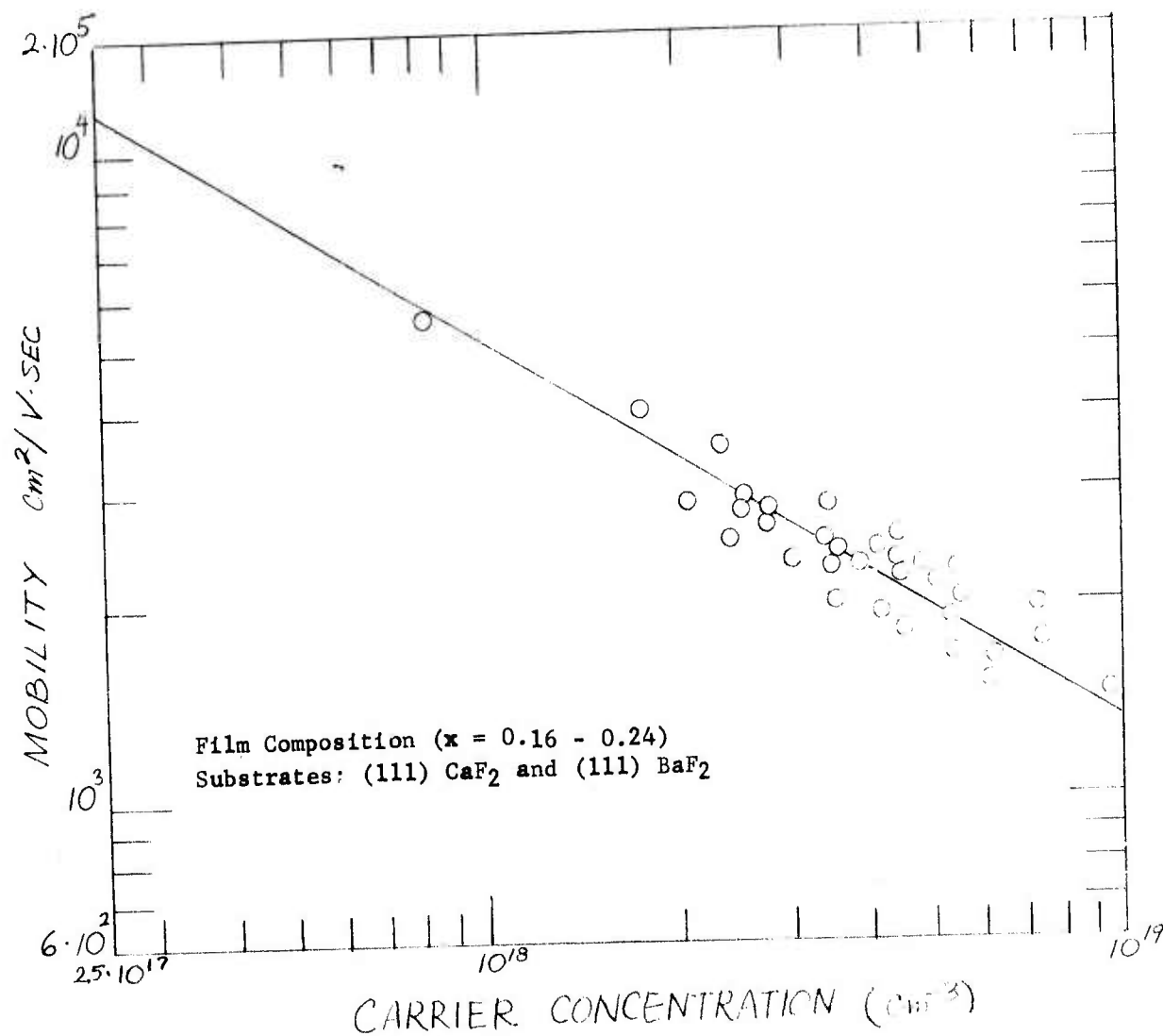
Figure 3-47 Electrical Properties of As-Deposited $Pb_{1-x}Sn_xTe$, p-Type Films-Target #4 (Measured at 77°K)
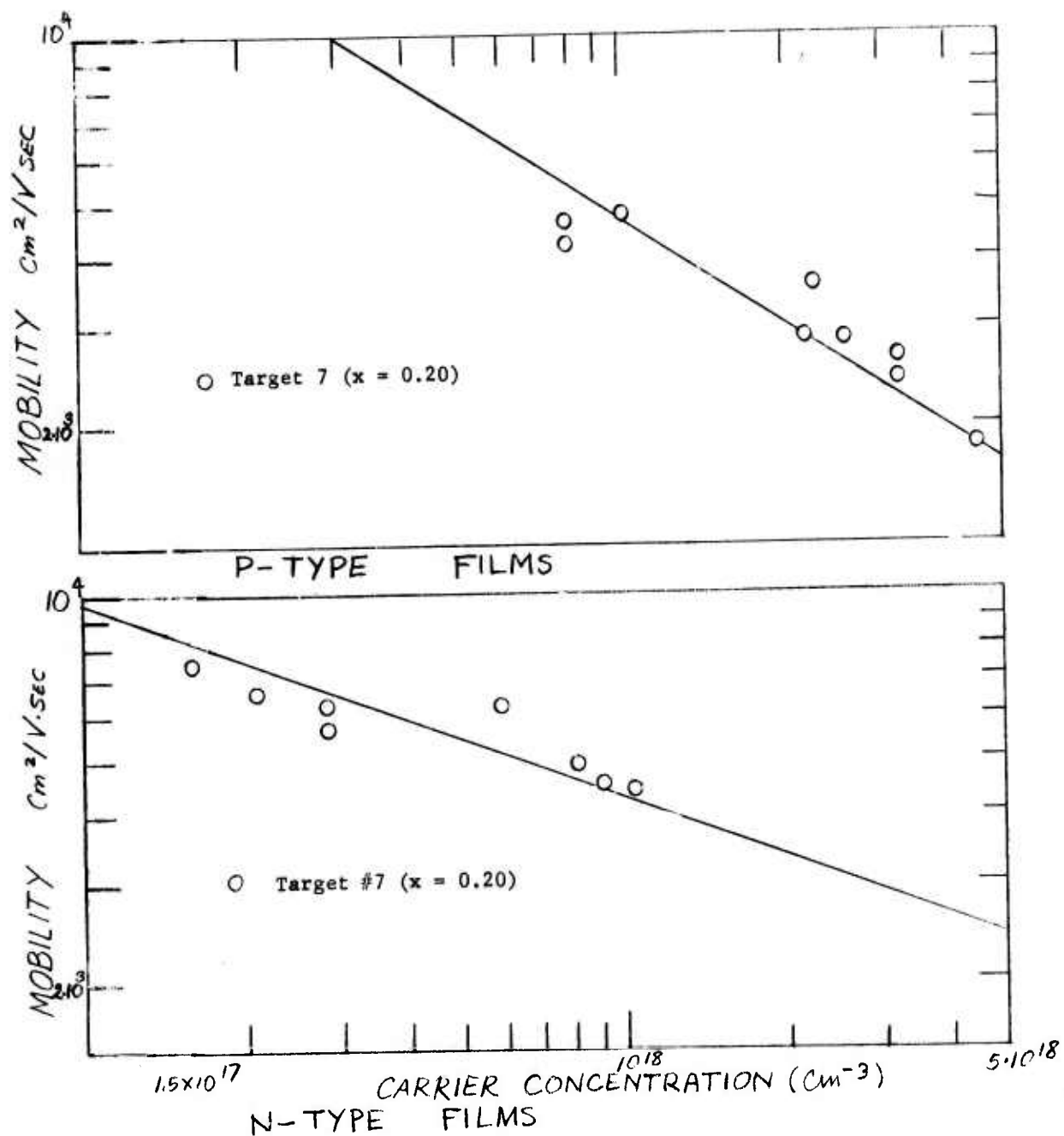
Figure 3-48 Electrical Properties of As-Deposited $Pb_{1-x}Sn_xTe$
Films - Target #7 (Measured at 77°K)
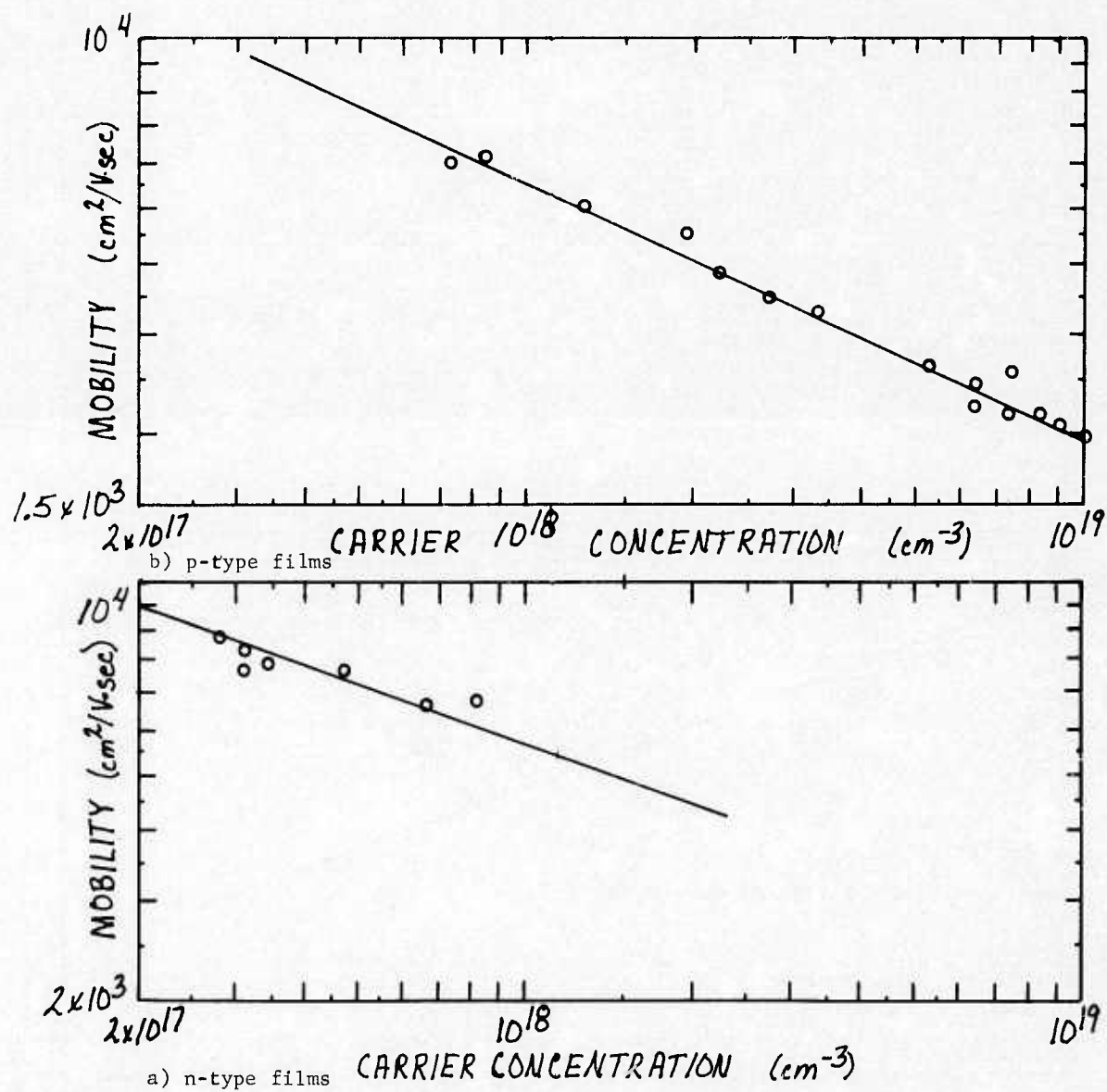
Figure 3-49   Electrical Properties of **As**-Deposited $Pb_{1-x}Sn_xTe$ Films - Target #8, -77°K, (Zero Substrate Bias)

b) P-type films
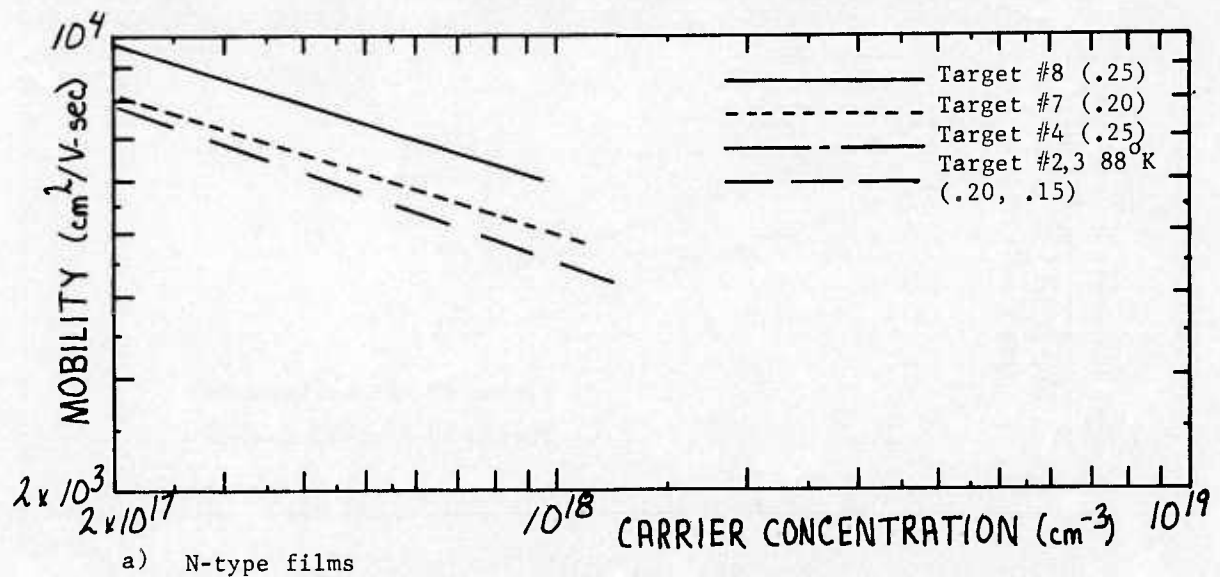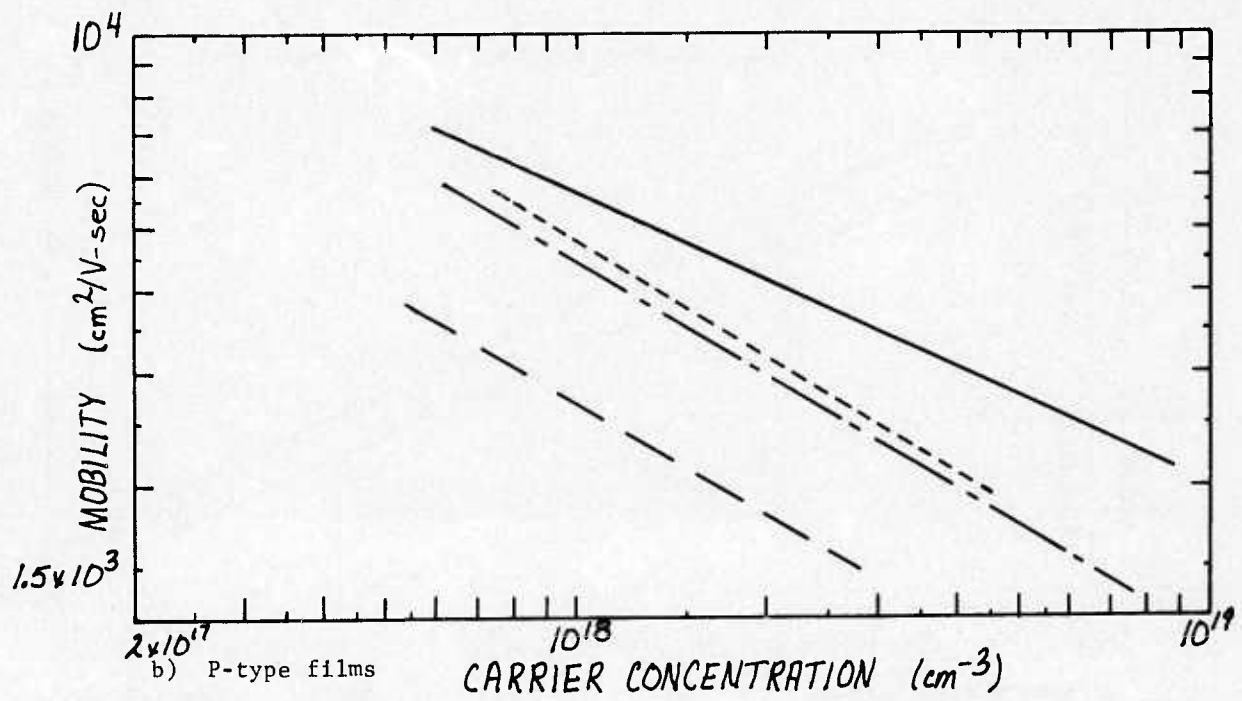
a) N-type films

Figure 3-50 Comparison of Trend Curves for Mobility vs. Carrier
Concentration for Various Targets (Zero Substrate Bias)

MOBILITY (cm²/volt-sec)

1x10⁴
8
6
4
2
1.5x10³

(a) p-Type Film

1x10⁴
8
6
4
2.5x10³

MOBILITY (cm²/volt-sec)

○ Target #8 (Stoichiometric)
△ Target #9 (Non-Stoichiometric)

2x10¹⁷   10¹⁸   10¹⁹
CARRIER CONCENTRATION (cm⁻³)
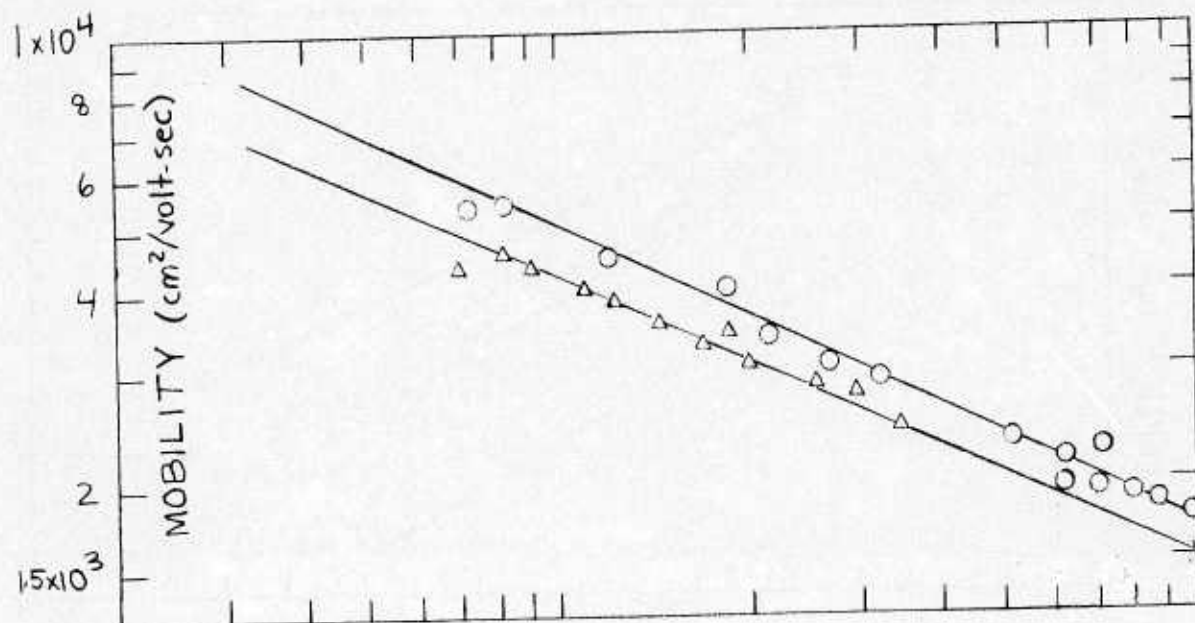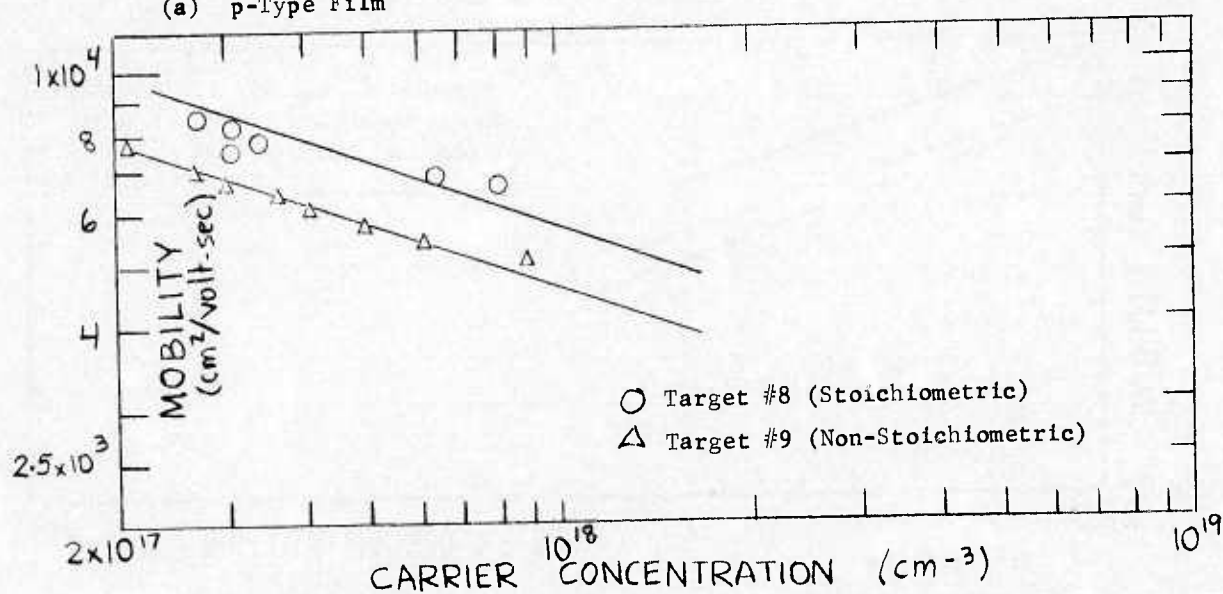
(b) n-Type Film

Figure 3-51 Effect of Target Stoichiometry on Electrical Properties
of As-Deposited Single Crystal $Pb_{1-x}Sn_xTe$ Films (Zero
Substrate Bias)

3-96
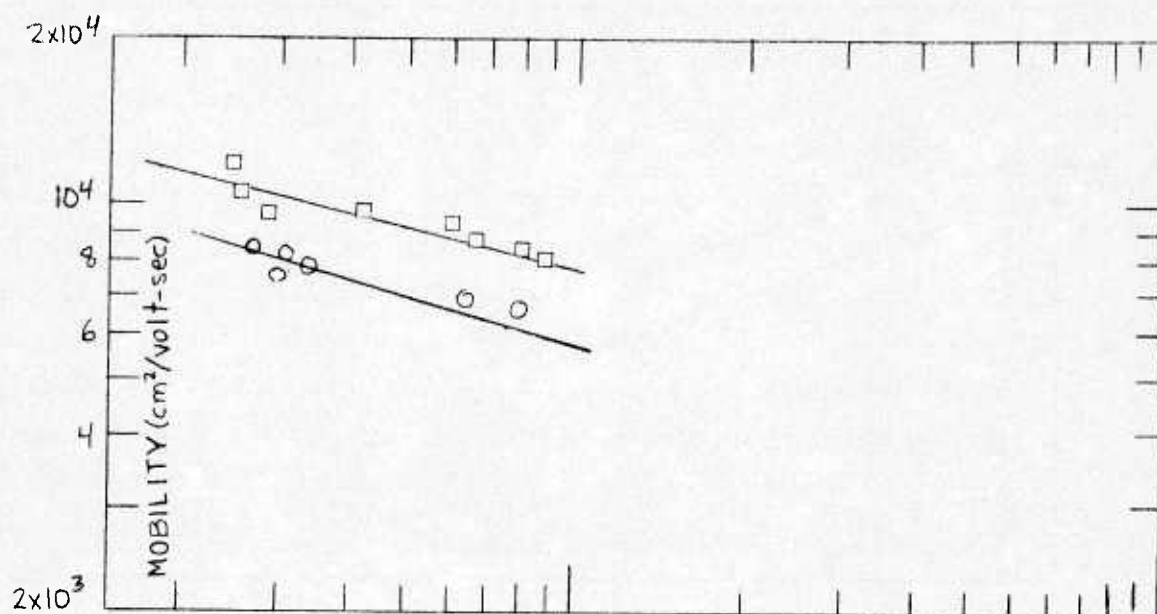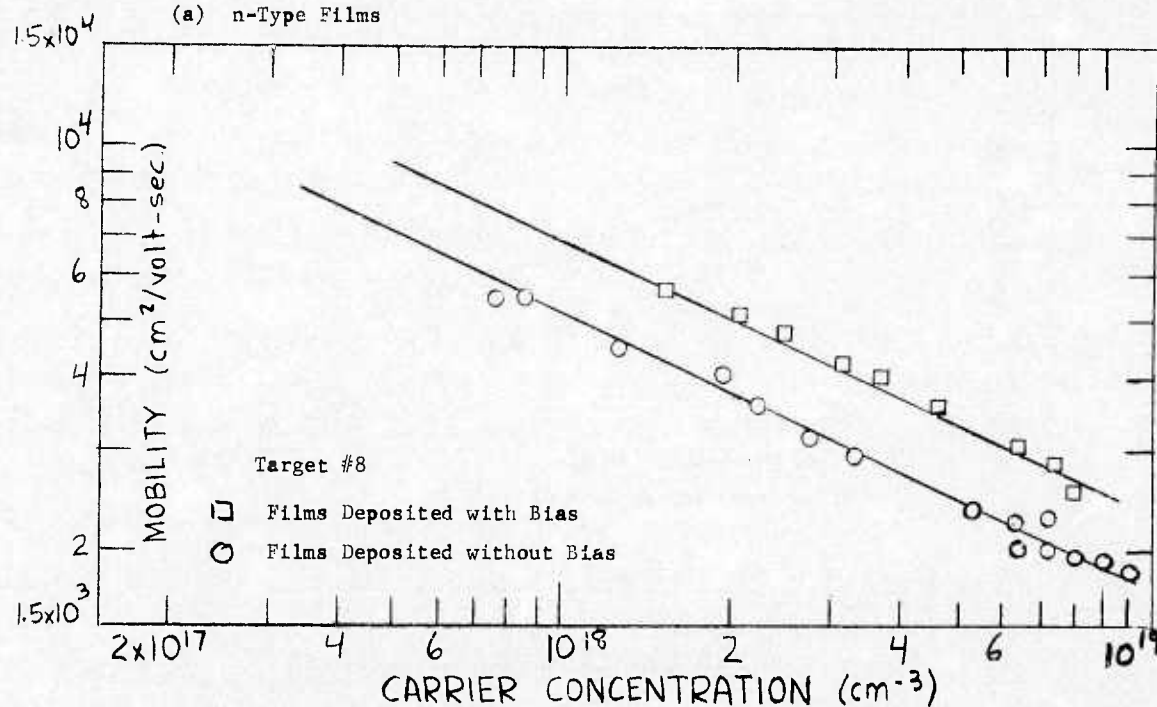
(a) n-Type Films

(b) p-Type Films

Figure 3-52 Effect of Substrate Bias on Electrical Properties of As-
Deposited Sputtered Single Crystal $Pb_{1-x}Sn_xTe$ Films (Target #8)

3-97
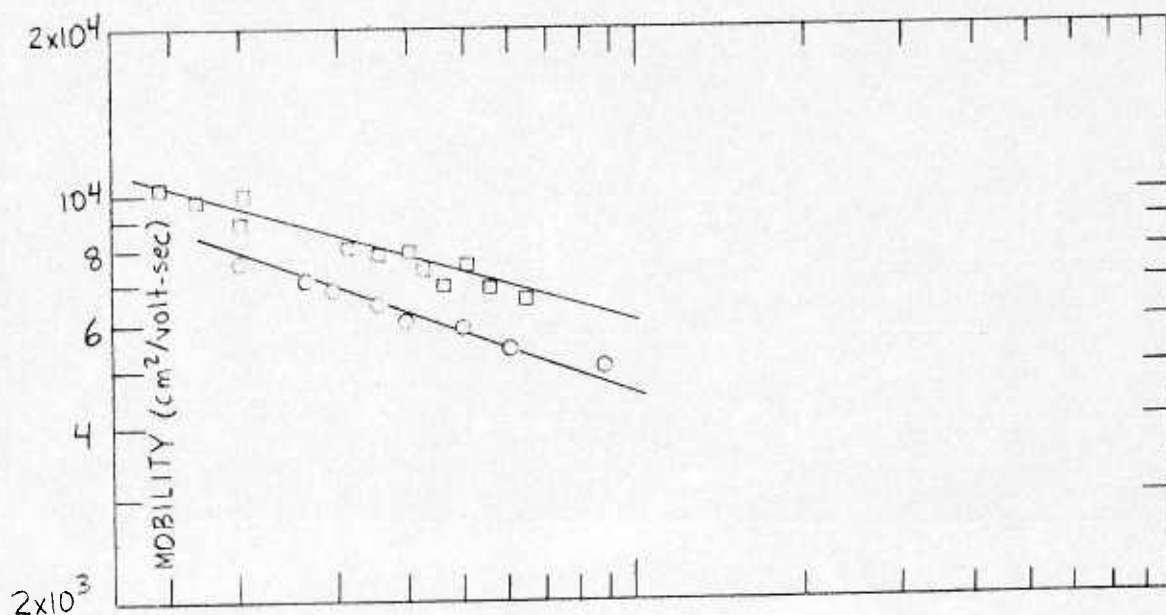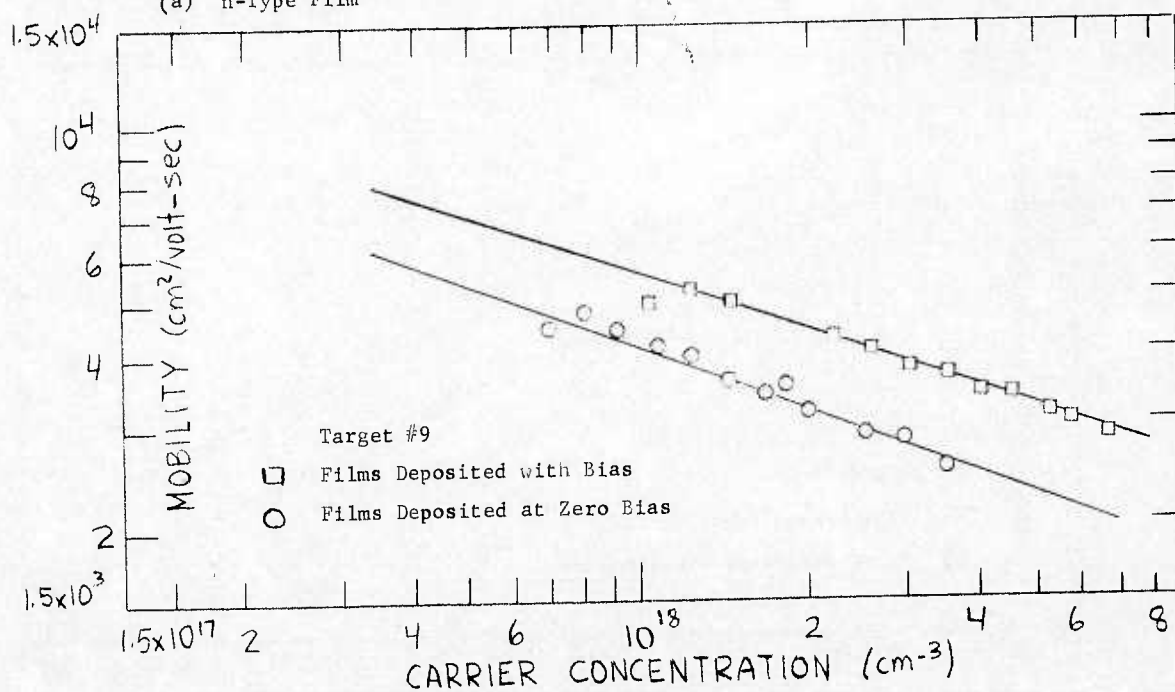
(a) n-Type Film

(b) p-Type Films

Figure 3-53 Effect of Substrate Bias on Electrical Properties of As-
Deposited Sputtered Single Crystal $Pb_{1-x}Sn_xTe$ Films (Target #9)

3-98

MOBILITY (cm^2/volt·sec)

2×10^4

10^4

8

6

4

2×10^3

(a) n-Type Film

MOBILITY (cm^2/volt·sec)

1.5×10^4

10^4

8

6

4

2

1.5×10^3

● Target #11

□ Target #10

○ Target #8 } With Substrate Bias

△ Target #9

▽ Target #12

1.5×10^{17} 2   4   6 10^{18} 2   4   6

CARRIER CONCENTRATION (cm^{-3})
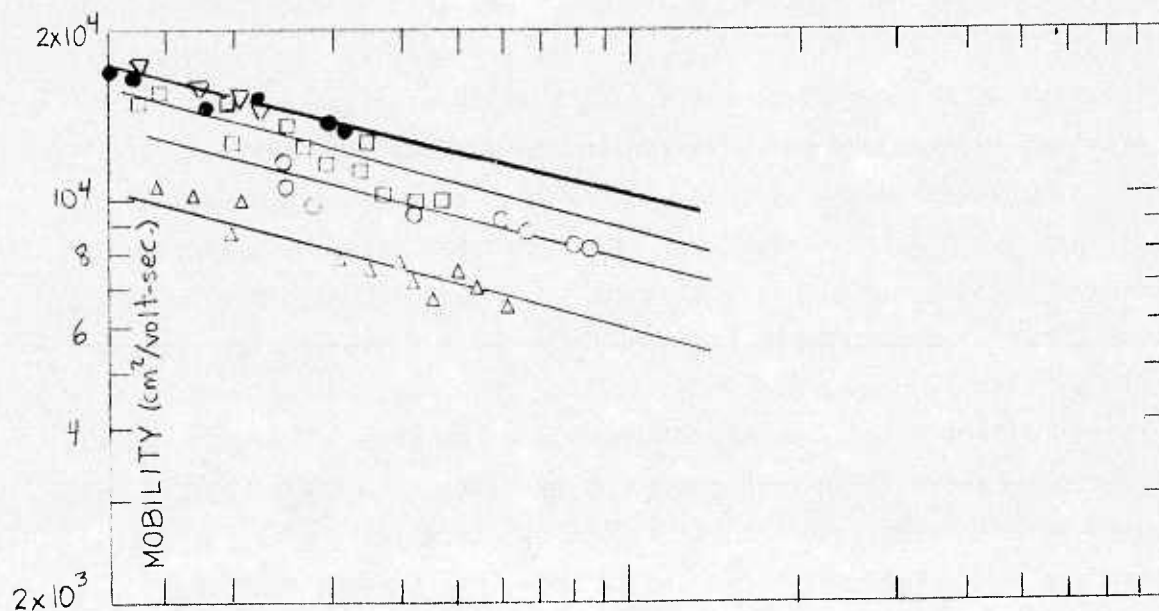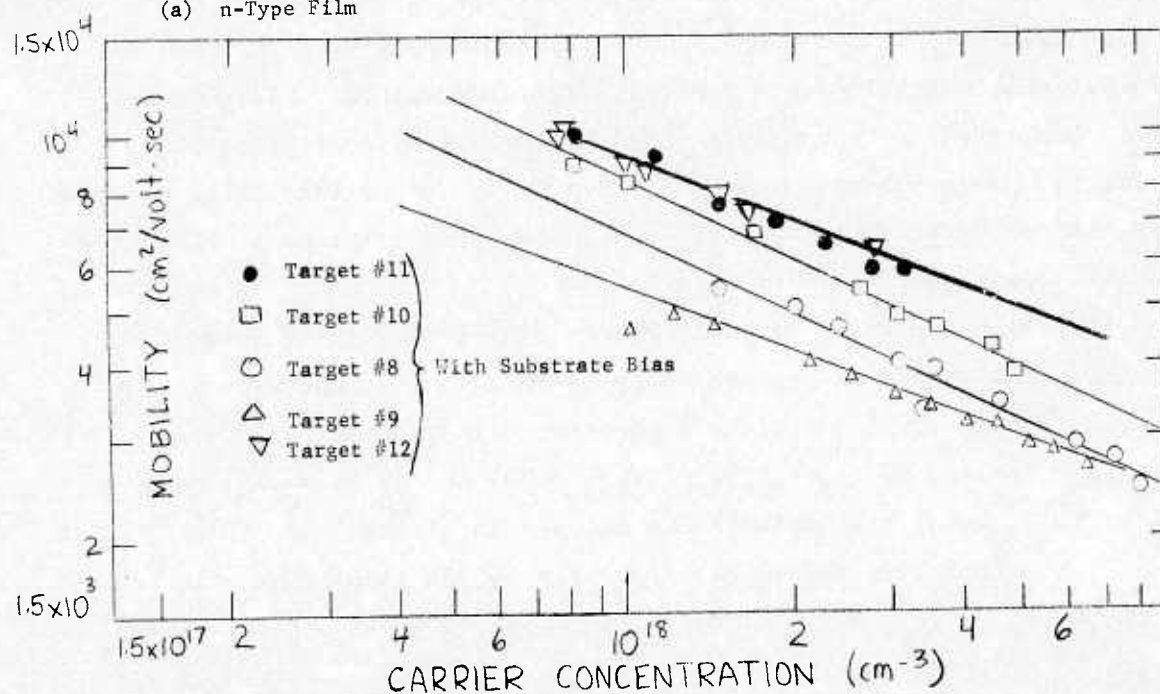
(b) p-Type Film

Figure 3-54 Comparison of Electrical Properties of As-Deposited Single
Crystal Pb$_{1-x}$Sn$_x$Te Films Sputtered with Various Targets
(with Substrate Bias)

3-99

measured in films sputtered from Targets #2 and #3 were somewhat lower, for the same carrier concentrations, than those sputtered from subsequently prepared targets. In fact, we will note a small improvement in mobilities with each target roughly in order of their preparation and apparently independent of the target composition. This type of improvement can only be related to improved preparation, handling and general experimental techniques as the program progressed. We have already seen, in Section 3.2.3.3, the reductions of carrier concentrations in films sputtered from the latest targets which were purposely prepared with improved modified techniques. We shall see also corresponding effects in the mobilities with these same targets. However, coming back to the substrate effect noted for n-type films sputtered from Targets #2 and #3, but not observed with later targets, it is difficult to see why general improvements in mobilities should result in the absence of a substrate effect for the n-type carriers. In essence this implies that the factors which are improving our film mobilities are apparently more effective on CaF_2 than BaF2. This could, of course, be simply due, in turn, to the fact that mobilities are better in films deposited on BaF_2 to begin with. Empirically, it has been observed that electrical properties of PbSnTe films deposited on BaF_2 are typically better than those of films deposited on CaF_2. This has been attributed in some cases to the better thermal expansion match of PbSnTe and BaF_2.

The following three figures, Figure 3-47 through 3-49 demonstrate the same consistency as seen above in the behavior of mobility versus carrier concentration for films deposited, without substrate bias, utilizing Targets #4 (x = .25), #7 (x = 0.20) and #8 (x = .25) (see Tables 5, 6, and 7 respectively for data). In Figure 3-47, data is shown for p-type single crystal films only, since as discussed in Section 3.2.2.1, the range of deposition conditions investigated with Target #4 included only the p-type region. Figures 3-48 and 3-49 for Targets #7 and #8, respectively, show results for both p- and n-type films and for both $CaF_2(111)$ and $BaF_2(111)$ substrates. As indicated

above and unlike the results from Targets #2 and #3, there appears to be no distinction between results obtained with the two substrates for either n- or p-type film.

Although the basic trends are much the same for all targets discussed so far, there are consistent differences from target-to-target in the mobilities at the same carrier concentrations. Figure 3-50 summarizes, for comparison, the trend curves of mobility versus carrier concentrations for all targets discussed in the preceding paragraphs. The consistent increase in mobility, for the same carrier concentration, from Targets #2 and #3 to Target #4 to Target #7 and finally to Target #8 are obvious. The difference appears slightly larger for the p-type films than for the n-type films. Since Targets #2 and #7 and Targets #4 and #8 have the same composition whereas Targets #2 and #3 do not, this indicates quite strongly that the differences are due to factors other than composition. However, one factor which could certainly affect these results is the measurement temperature. As noted the mobilities in films sputtered from Targets #2 and #3 were measured at $88^{o}K$, while in all other cases, the measurement temperature was $77^{o}K$. This was due to limitations of dewar used at the time of the earlier measurements. Since mobilities in PbSnTe increase with decreasing temperature, the mobilities in films from Targets #2 and #3 would be higher than shown in Figure 3-50 if the measurement temperatures had been $77^{o}K$. Estimates of the mobility difference between $88^{o}K$ and $77^{o}K$ indicate that for the n-type films, the trend curve in Figure 3-50 for Targets #2 and #3 might approach that shown for Target #7. However, for the p-type films, a relatively large difference in mobilities would still exist. Therefore, although the measurement temperature accounts for some of the differences, it cannot account for all of it. A more reasonable explanation is that alluded to earlier - namely that our general experimental procedures have continuously improved during the course of this program. Still, the improvements up to Target #9 did not involve the systematic target preparation modifications utilized for Targets #10 through #13 (see Table 1). Also, the effect of target stoichiometry on mobility has

not been represented. Finally, we have as yet not introduced the effect of substrate bias which, based on the decrease in carrier concentration it produces, should result in increases in mobility also. To illustrate these factors the next set of figures i.e. Figures 3-51 through 3-54 presents, in order, the dependence of mobility on carrier concentration as affected by target stoichiometry deviations, substrate bias and improved target preparation techniques.

Figure 3-51 shows, for example, some small effects which may be attributable to target stoichiometry. The mobilities of films deposited, at zero substrate bias, with Target #8 (x = 0.25) are higher in both p-type and n-type films for the same carrier concentration than of films deposited with Target #9 (x = 0.20, 1% Te rich). Although the effects are relatively small, the consistency throughout the range of carrier concentrations suggests that the effects are real.

The effect of substrate bias on as-deposited mobilities, again in both p- and n-type films deposited with Targets #8 and #9, is suggested in Figures 3-52 and 3-53 respectively. In both cases the mobilities versus carrier concentration data are plotted for films deposited with and without substrate bias. The substrate biases selected were near the value V_o for the specific compositions. A significant increase in the mobilities is apparently caused by the bias for all carrier concentrations. This result would certainly indicate that substrate bias could only be "improving" film properties. Mechanisms by which such film properties can primarily be improved by bias application are: (a) improved stoichiometry, (b) improved purity, (c) improved structure. Substrate bias is unlikely to improve film structure. However, other independent evidence has already been presented in support of ascribing improvement via film stoichiometry and purity to substrate bias.

Figure 3-54 plots as-deposited mobility data of bias sputtered films from the five targets most extensively investigated with substrate bias. Bias values were reasonably near V_o but far from optimized at that value. We see that the mobilities measured in films deposited from Targets #11, #12 are highest both for p- and n-type films. Mobilities,

in turn, are higher for films deposited from Target #10 than for films deposited from Target #8. Finally Target #9 shows the lowest mobilities for bias sputtered films. The improved mobilities measured in films from Target #10 through #12 verify the effects of the improved target preparation techniques. The difference in mobilities in films deposited from Targets #8 and #9 indicate that the effect of stoichiometry, already seen in Figure 3-51, is maintained under bias conditions.

The consistency of the overall behavior of mobilities just presented lends further support to the hypothesis that the observed behavior of carrier concentrations as a function of deposition conditions, (e.g. the p-n transition conditions $(RT)_0$) and bias voltage (e.g. the p-n transition at the critical bias voltage (V_0)), is associated with stoichiometric adjustment. Additional information in this regard may be obtained from results on Hall mobilities and Hall coefficients measured as a function of temperature as presented in the next section.

3.2.4.3 <u>Temperature Dependencies of Hall Mobility and Hall Coefficient in Sputtered $Pb_{1-x}Sn_xTe$ Films</u>. Temperature dependencies of Hall mobilities and Hall coefficients have always been valuable aids in defining mechanisms which effect the all important transport properties. Therefore, temperature dependencies of Hall mobilities and Hall coefficients should reflect some of the systematic trends presented in the preceding sections.

One of the more obvious trends was the continuous improvement in properties with improved experimental procedures and target preparation techniques. That this trend is also apparent in the data for temperature dependencies of Hall mobilities and coefficients is illustrated in Figures 3-55 through 3-57. Figures 3-55 and 3-56 show results for three n-type films sputtered from three different targets. We note a continuous change in the behavior starting from the film sputtered from Target #2, to Target #7 and Target #12. We consider first Figure 3-55, and define the deposition conditions and target characteristics associated with the three films for which data are shown. The temperature dependence of the Hall mobility for the films sputtered from Target #2 is typical of our

3-103
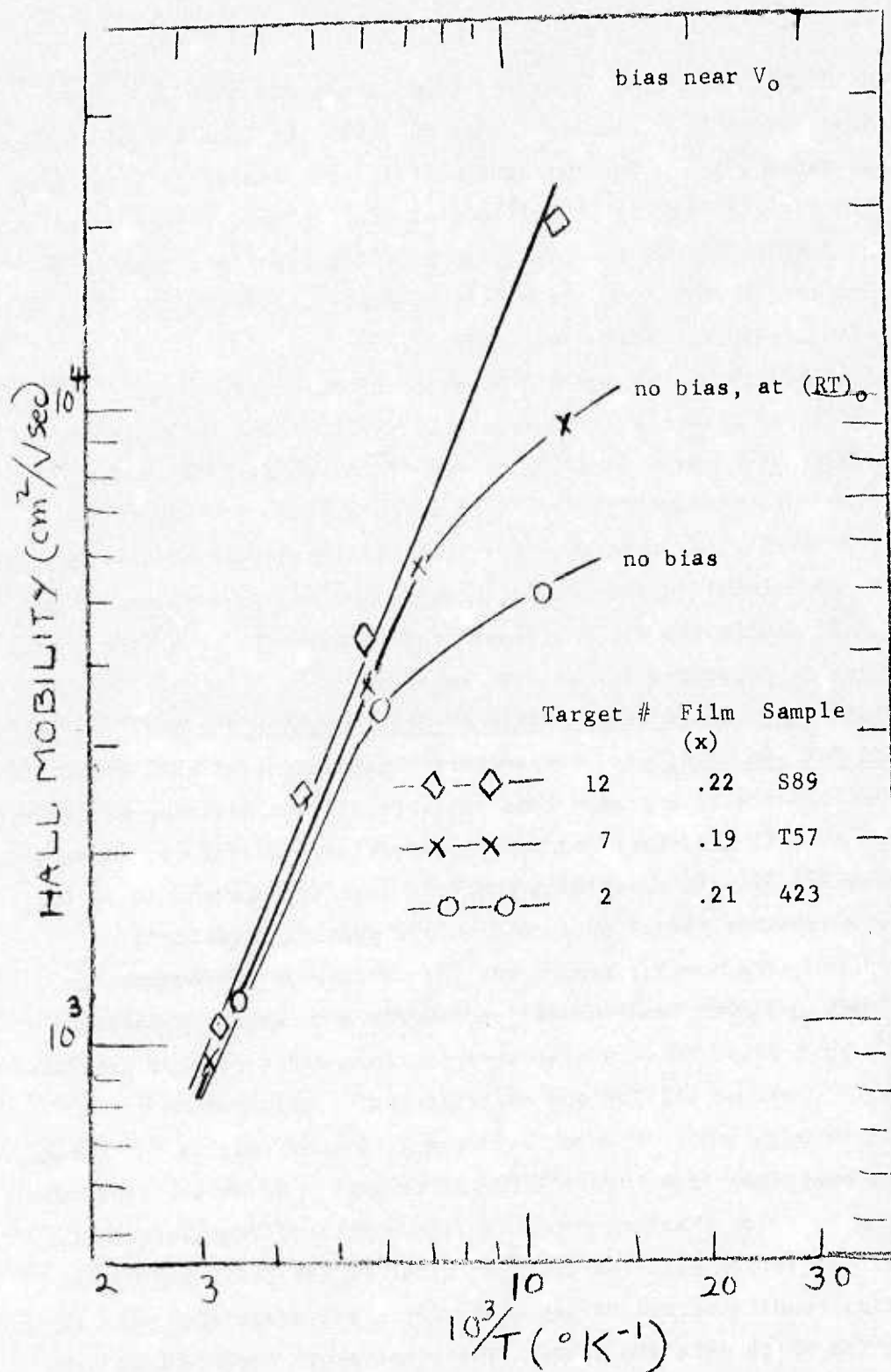
Figure 3-55   Comparison of As-Deposited Hall Mobility vs. 1000/T
for n-type Single Crystal $Pb_{1-x}Sn_xTe$ Films Sputtered
with Various Targets

3-104
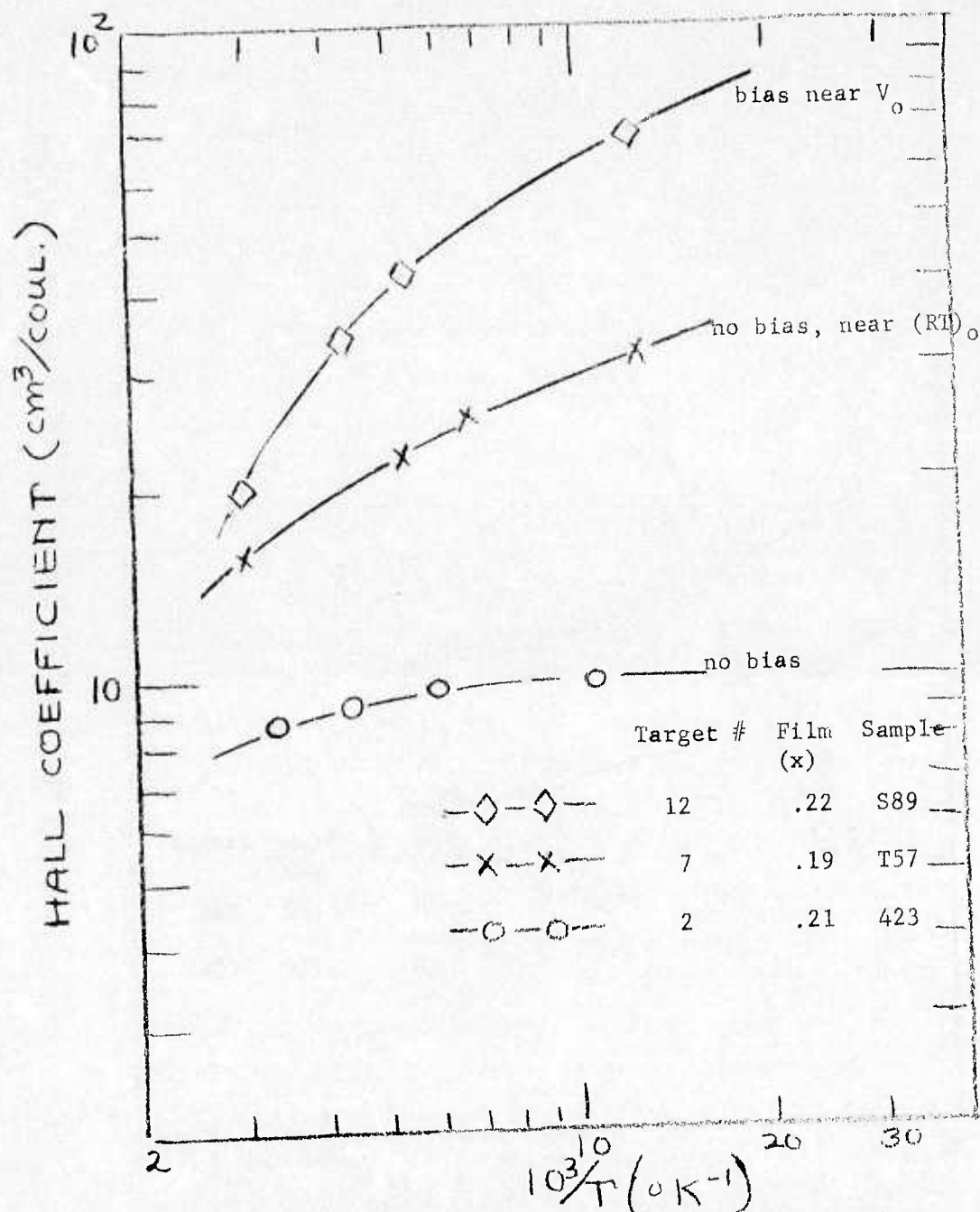
Figure 3-56 Comparison of As-Deposited Hall Coefficients
vs. 1000/T for n-type Single Crystal $Pb_{1-x}Sn_xTe$
Films Sputtered with Various Targets.

3-105
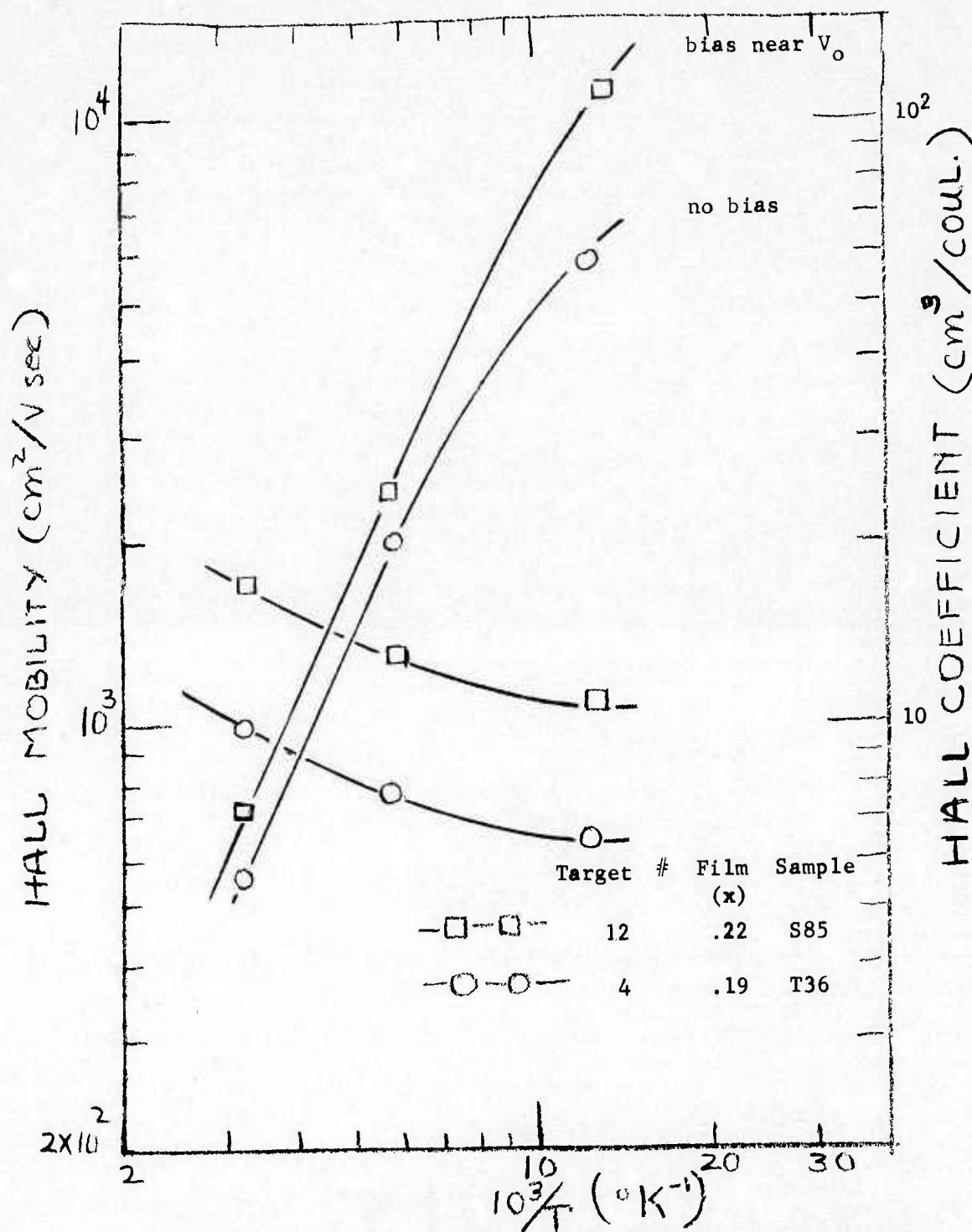
Figure 3-57   Comparison of As-Deposited Hall Mobility and R_H vs. 1000/T for p-type Single Crystal $Pb_{1-x}Sn_xTe$ Films Sputtered with Different Targets.

earliest n-type as-deposited films prepared under conditions disregarding the critical values $(RT)_o$ defined later. In contrast the mobilities of the film sputtered from Target #7 is representative of a film sputtered at deposition conditions closer to the socalled p-n transition conditions $(RT)_o$ but still at zero bias (see Figure 3-15). Finally, the film sputtered from Target #12 is typical of films sputtered with substrate bias near the critical bias voltage V_o. Furthermore, as repeatedly noted, improved preparation techniques were utilized in the preparation of Target #12. For the film sputtered from Target #12 we find that the Hall mobility follows closely the purely phonon scattering controlled relation $(\mu_H \sim (1/T)^{5/2}$ to the lowest temperature of measurement. For the films sputtered from Targets #7 and #2, respectively, we find the Hall mobility deviating from the $(1/T)^{5/2}$ dependence at progressively higher temperatures. In addition the trend is such that the films sputtered from Target #7 show lower mobilities than the films sputtered from Target #12 and those sputtered from Target #2 show the lowest mobilities at all temperatures. Figure 3-56 shows the Hall coefficients as a function of 1/T for the same three films shown in Figure 3-55. These data are consistent with the Hall mobility data with the film sputtered from Target #12 showing the highest Hall coefficient (or lowest carrier concentrations).

Figure 3-57 shows similar data for two p-type films, again deposited from two different targets and at different deposition conditions. The trends are consistent with those presented for n-type films discussed above.

Thus not only are the general improvements in film properties observed with improved deposition conditions and target preparation techniques improvements, but the temperatures dependences of μ_H and R_H show also that the film property improvements are not likely the result of carrier compensation or similar phenomena. Otherwise we should not see the tendency toward the ideal phonon scatter limit described by the $(1/T)^{5/2}$ behavior of mobility.

In order to show, more clearly, the generality of the effects related to the observed p-n transitions at zero bias as well as to the p-n transitions at the critical bias voltages on the temperature dependence of Hall mobility and Hall coefficient, we present the additional results shown in Figures 3-58 through 3-63.

Figure 3-58 shows the dependencies of the Hall mobility on $1000/T^{\circ}K$ for three as-deposited $Pb_{1-x}Sn_xTe$ films from Target #8 with zero bias. All three films were deposited at different deposition conditions (RT) which varied from conditions near to conditions reasonably removed from the p-n transition conditions $(RT)_0$ (see Figure 3-5). For the film deposited relatively close to the p-n transition condition (i.e., $350^{\circ}C$ $1.05 \mu m/hr$), we find that the Hall mobility follows most closely the phonon scattering controlled relation $[\mu_H \sim (1/T)^{5/2}]$ to the lowest temperature of measurement, i.e., to $77^{\circ}K$ in this case. However, for the two films deposited at conditions deviating from the p-n transition, the results show that the Hall mobility begins to deviate from the $(1/T)^{5/2}$ dependence at considerably higher temperatures. Furthermore, the latter two films also exhibit lower mobilities at all temperatures and particularly at $77^{\circ}K$. The film deposited under conditions deviating in the p- direction reflects the lowest mobilities as expected for hole mobilities.

Figure 3-59 shows the Hall coefficient as a function of $1/T$ for the same three films shown in Figure 3-58. These data are consistent with the Hall mobility data. The film closest to the p-n transition exhibits the highest Hall coefficient (or lowest carrier concentrations). Furthermore, the dependence of Hall coefficient on $(1/T)$ shows an increase in R_H with decreasing temperature for the two n-type films while the p-type film shows a decrease in R_H with decreasing temperature. This behavior is consistent with earlier observations in thin $Pb_{1-x}Sn_xTe$ films as well as with observations in single crystal bulk $Pb_{1-x}Sn_xTe$.

3-108
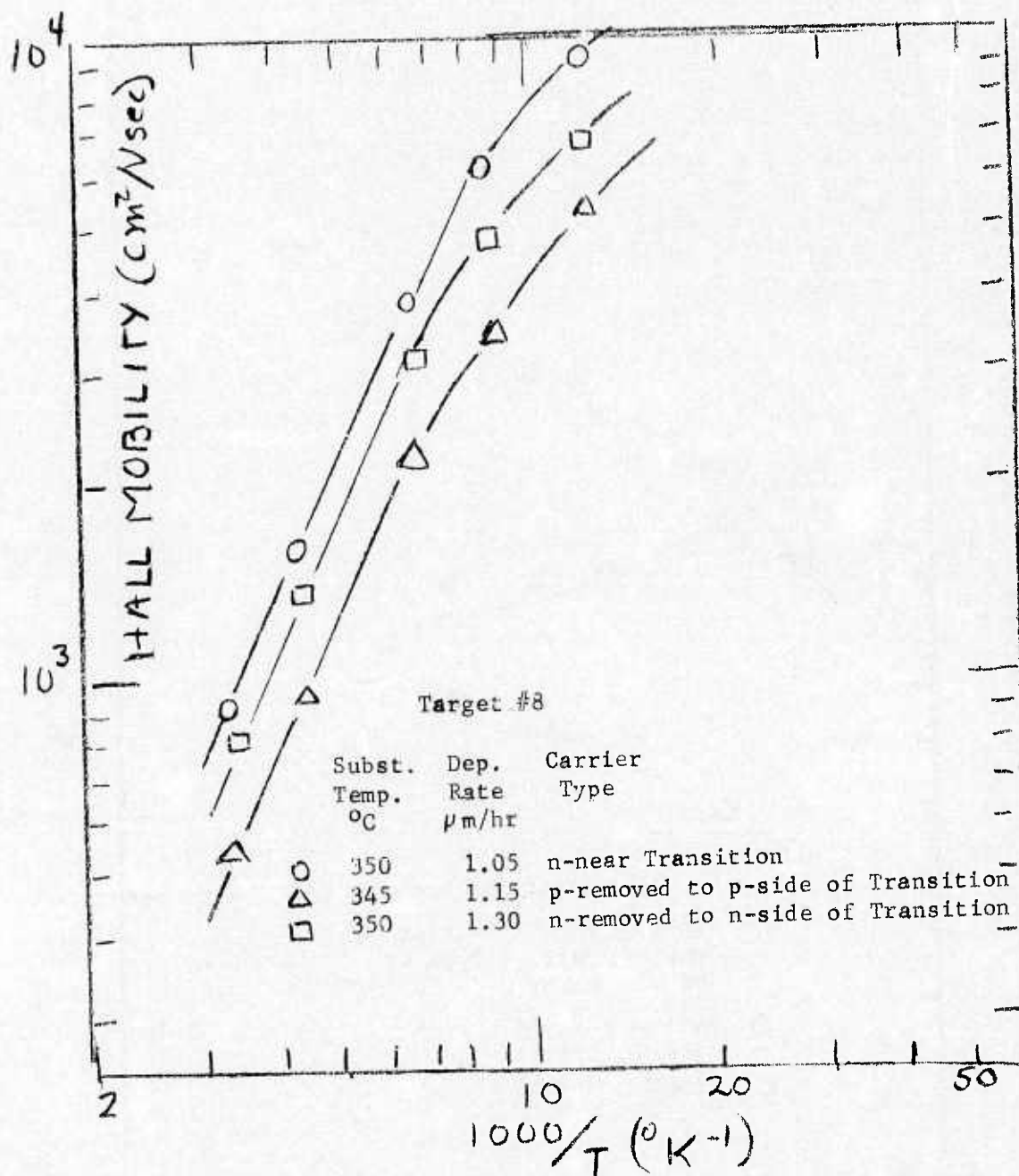
Figure 3-58 As-Deposited Hall Mobility vs $\frac{1000}{T}$ - Films Deposited at Conditions near and away from p-n Transition - Zero Bias Voltage
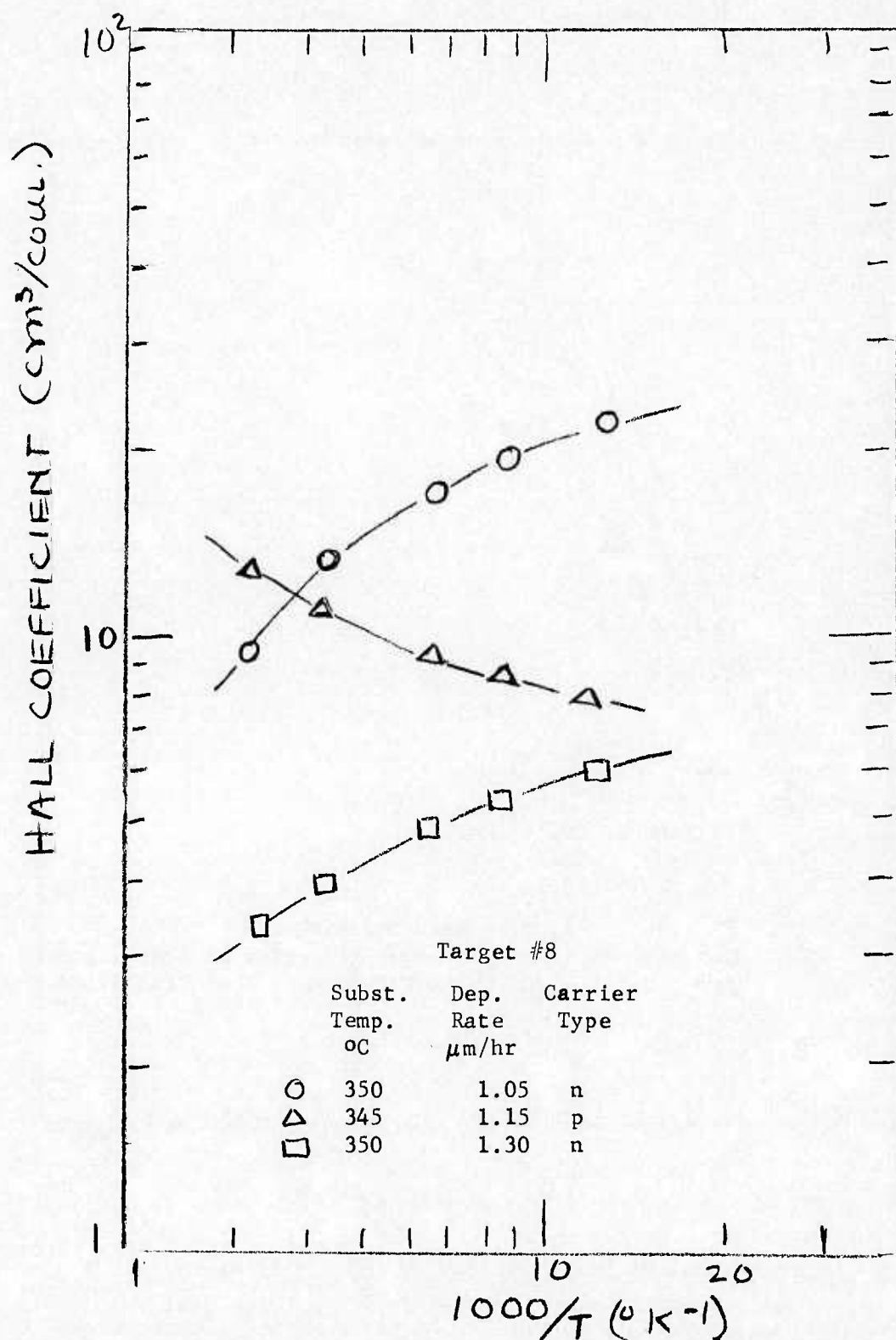
Figure 3-59 As-Deposited Hall Coefficient vs $\frac{1000}{T}$ - Films Deposited at Conditions near and away from p-n Transition - Zero Bias Voltage

3-110

The results shown in Figures 3-58 and 3-59 lend further support to the hypothesis that the $(RT)_0$ or p-n transitions are related to conditions of stoichiometric perfection. The higher carrier concentrations and lower mobilities as well as the temperature dependence of mobility of films deposited at conditions removed from the p-n transition are all indicative of effects caused by deviations from stoichiometry.

Figure 3-60 shows the temperature dependence of Hall mobility for three $Pb_{.81}Sn_{.19}Te$ films deposited with different substrate bias voltages. In each case, Target #2 was utilized and all films were deposited at identical deposition conditions (RT). As noted from the inset in Figure 3-60, the bias voltages were selected such that one was close to the critical bias voltage (i.e., +5V) and the other two were on either side of the critical bias voltage (i.e., at +10V and -10V). As typical, the high positive bias yielded a p-type film, the high negative bias an n-type film, while values near the critical bias voltage can produce either type but are typically associated with an n-type film. As apparent in Figure 3-60, the film deposited at a bias voltage close to the critical voltage showed the ideal temperature dependence of mobility or $\mu \sim T^{-5/2}$ behavior over almost the entire temperature range from 300°K to 77°K. By contrast, the temperature dependences of the other two films exhibited strong deviations from the $T^{-5/2}$ dependences at temperatures below 100°K. We note further that the Hall mobilities are highest for the film deposited with a bias closest to the critical voltage at all temperatures.

Consistent with the temperature dependencies of the Hall mobility are the temperature dependencies of the Hall coefficients for the same films as shown in Figure 3-61. We note a significantly higher Hall coefficient (i.e., lower carrier concentration) over the entire range of temperatures for the films deposited close to the critical bias voltage than for the other two. The generally observed direction of the temperature dependence for Hall coefficient is again observed in these three films: an increase with decreasing temperatures for n-type films and a decrease with decreasing temperatures for p-type films.
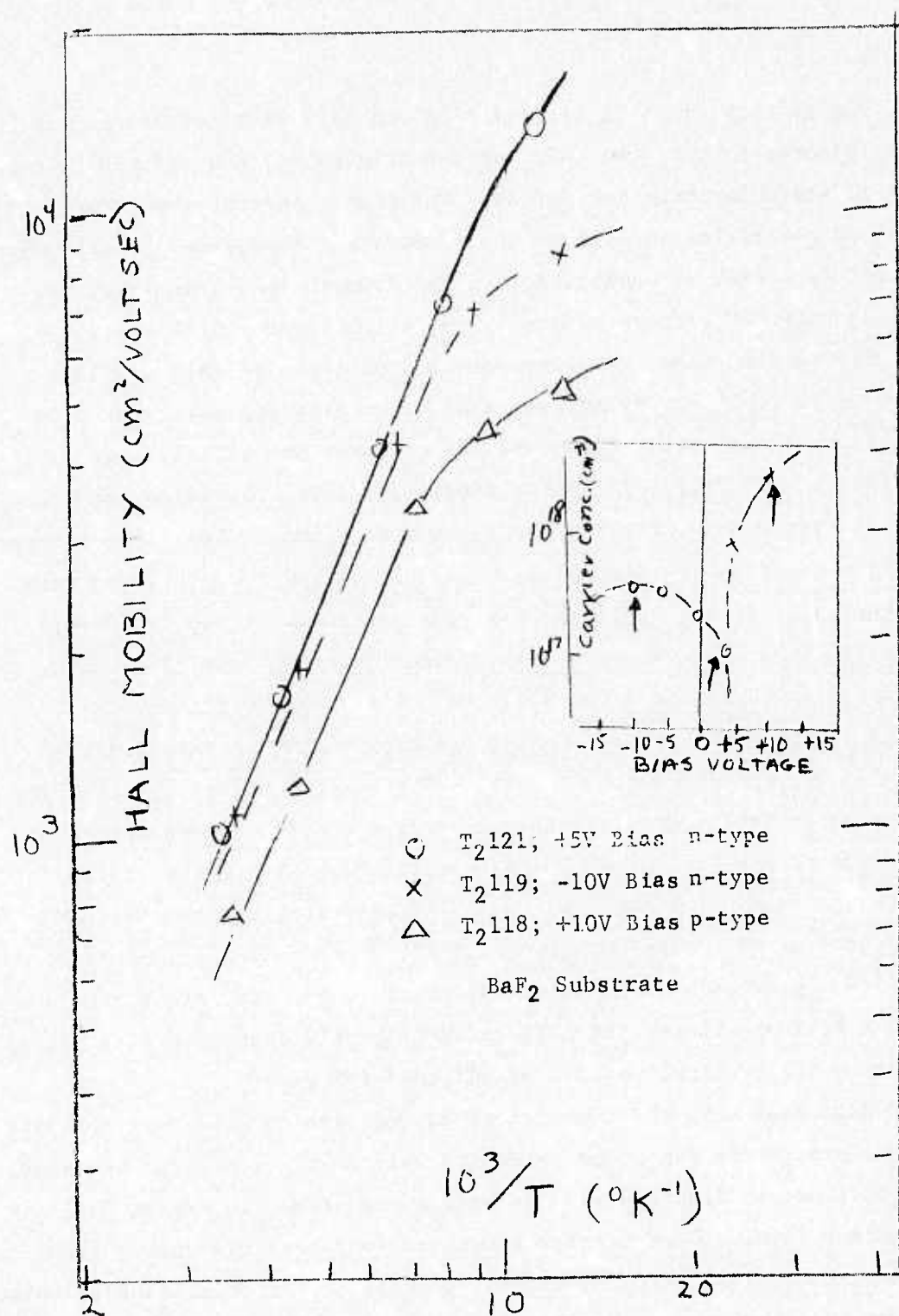
Figure 3-60 As-Deposited Hall Mobility vs $\frac{1000}{T}$ for Single Crystal $Pb_{.81}Sn_{.19}Te$ Films Deposited at Various Bias Voltages (Target #2)
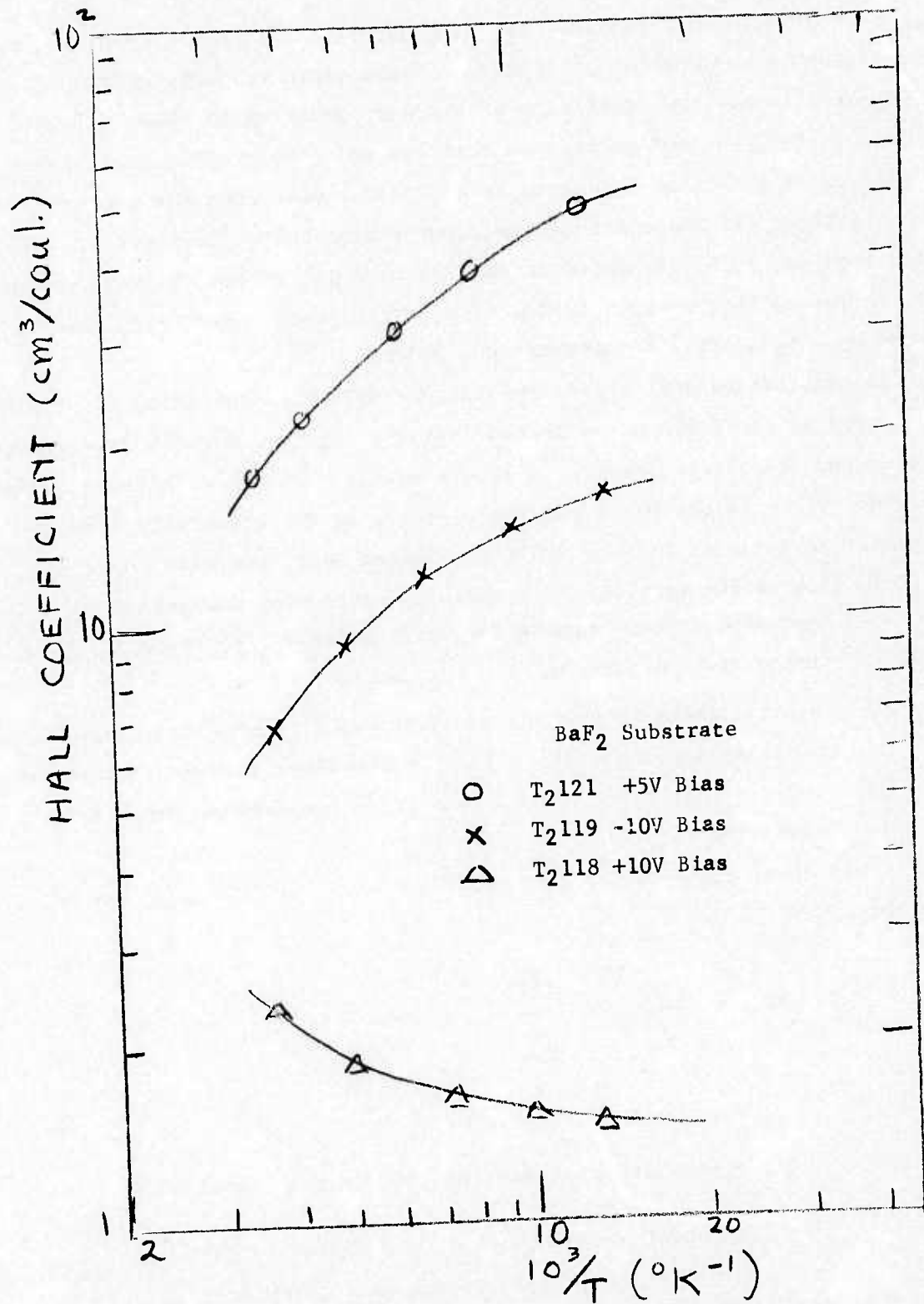
Figure 3-61　As Deposited Hall Coefficients vs. $\frac{1000}{T}$ for Single Crystal $Pb_{.81}Sn_{.19}Te$ Films Deposited at Various Bias Voltages (Target #2)

3-113

We have implied earlier that the differences in mobilities and temperature dependence of mobilities for the various samples are representative of the scattering mechanisms operating in these films. In particular, we tend to believe that the major scattering mechanisms operating in the films deposited at conditions away from the p-n transitions $(RT)_o$ or (V_o) are related to imperfections in stoichiometry. The fact that the films deposited at conditions close to the critical values result in mobilities which follow closely the phonon-scattering controlled relation, $\mu_H \sim (1/T)^{5/2}$ supports this belief.

A qualitative analysis of the various possible scattering mechanisms operating in the films shown in the last few figures, reveals some interesting and consistent results in this respect. Without detailed elaboration, we start with the realistic assumption that, in the relatively high temperature range of 77^oK to 300^oK considered here, the most important contribution to the mobility and resulting scattering mechanisms are:

1. Acoustic lattice scattering which cause a $T^{-5/2}$ mobility temperature dependence for $Pb_{1-x}Sn_xTe$

2. Neutral impurity scattering which has a temperature independent mobility component and a $T^{-1/2}$ temperature dependent component.

3. Surface scattering which has a $T^{-1/2}$ temperature dependent mobility.

From these contributors the effective Hall mobility, μ_H, can be expressed as:

$$\frac{1}{\mu_H} = \frac{T^{5/2}}{\bar{\mu}_L} + \frac{T^{1/2}}{\bar{\mu}_N} + \frac{1}{\bar{\mu}_{N^o}}$$

where

$\bar{\mu}_L$ = mobility contribution from lattice scattering

$\bar{\mu}_N$ = mobility contribution from either surface scattering or temperature dependent neutral scattering

$\bar{\mu}_{N^o}$ = mobility contribution from neutral scattering (temperature independent)

3-114

This can also be written as:

$$\left(\frac{1}{\mu_H} - \frac{1}{\bar{\mu}_{N^o}} \right) T^{-1/2} = \frac{1}{\bar{\mu}_L} T^2 + \frac{1}{\bar{\mu}_N}$$

Plotting $\left(\frac{1}{\mu_H} - \frac{1}{\bar{\mu}_{N^o}} \right) T^{-1/2}$ v.s. T^2 with $\bar{\mu}_{N^o}$ as the only

adjustable parameter, a linear relation should result (if assumptions
are valid) from which qualitative values of $\bar{\mu}_L$ and $\bar{\mu}_N$ are obtainable.

Utilizing this expression and the measured mobility trend in various
temperature ranges we were able to obtain a fit to this expression for a
number of our samples. In particular, such an analysis may be realistic
if used for comparison purposes. For example, one interesting observa-
tion which can be made from such an analysis concerns the differences
found between two of the films shown in Figure 3-60. We consider the
films labeled $T_2 121$ (n-type - deposited near V_o at +5V bias) and $T_2 118$
(p-type deposited removed from V_o at +10V bias). A preliminary analysis
has shown that, above 77°K, both surface scattering and neutral scattering
affect the mobility of the film $T_2 118$ deposited at a position ΔV relative
to V_o while, in the case of the film $T_2 121$ deposited near V_o, the only
scattering effects observed are, in addition to phonon scattering,
apparently due to neutral scattering modes in the same temperature range;
surface scattering and/or temperature dependent neutral scattering
appears to be negligible in the latter case. Furthermore, the lattice
mobilities for both films obtained from the analysis conform quite well
to experimental values found in high quality $Pb_{1-x}Sn_xTe$ bulk crystals
for both p- and n-type crystals where lattice scattering is assumed to
be the dominating mode. Similar results were obtained from such an
analysis for other films.

It is quite apparent that such an analysis over such a limited
temperature range cannot in itself reveal the nature or sources of
all scattering mechanisms which control the transport properties in these

films. A better indication of the scattering mechanisms which affect the transport properties can be obtained from Hall measurements over a temperature range which extends below $77^{\circ}K$. As has been discussed in Section 2.0, during the course of this program our electro-optical measurement facility was modified to permit both Hall and photoconductivity measurements to be made to below $4^{\circ}K$. Hall measurements performed on a few typical as-deposited films utilizing this facility are shown in Figures 3-62 and 3-63. Figure 3-62 shows both the Hall mobility and Hall coefficient for a $Pb_{.79}Sn_{.21}Te$ film deposited from Target #8 at the conditions specified. Reference to Table 12 will show that this film (SN 21) was deposited at a bias voltage (-10V) very close to the critical bias voltage. As can be seen, this as-deposited film shows a Hall mobility which varies as $T^{-5/2}$ over the range from $300^{\circ}K$ to about $30^{\circ}K$. Below about $30^{\circ}K$, the Hall mobility appears to "saturate". The Hall coefficient increases up to about $80^{\circ}K$, remains relatively constant to about $30^{\circ}K$, then decreases below $30^{\circ}K$.

The behavior of the mobility as a function of temperature at the very low temperatures, particularly the saturation, is again related to the types of scattering centers active at these low temperatures which may be due to non-stoichiometry or foreign impurities. In order to evaluate the scattering mechanisms operating in these films below $30^{\circ}K$ it is necessary to consider additional scattering modes not considered in the temperature range between $300^{\circ}K$ and $77^{\circ}K$ discussed above. For example, scattering from ionized impurity centers may become important at those low temperatures. Ionized impurity scattering is expected to have a T^{+C} temperature dependence as compared to the $T^{-C'}$ for lattice scattering as well as neutral impurity scattering. Therefore, at present, and as will be discussed somewhat later, from the observed dependence of mobility v.s. $1/T$ below $30^{\circ}K$ it is surmised that ionized scattering centers are responsible in part for the observed mobility saturation. The behavior of the Hall coefficient with temperature can be related to the concentration of imperfections such as lattice point defects
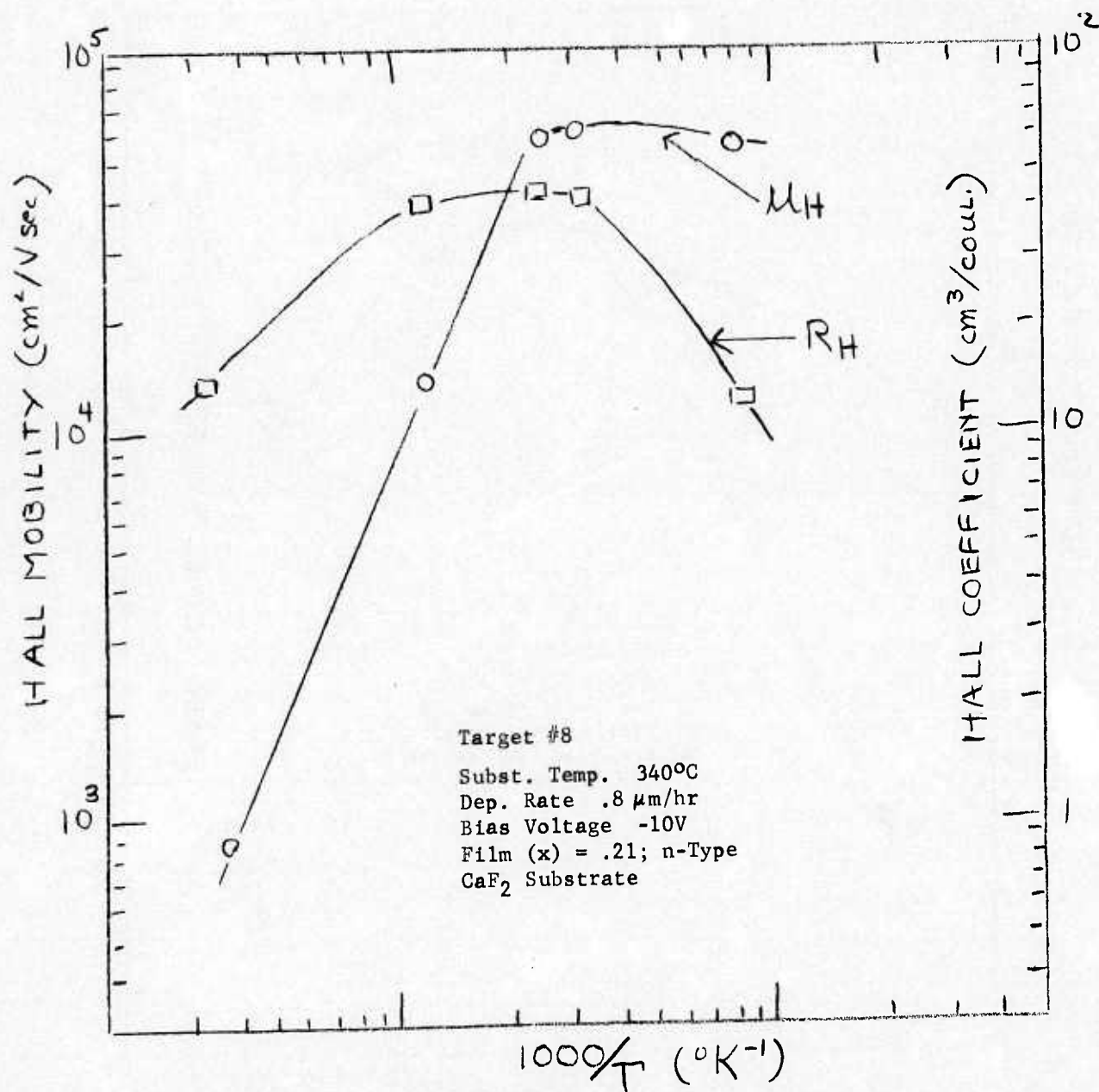
Figure 3-62 Temperature Dependence of Hall Mobility and Hall
Coefficient for As-Deposited Sputtered $Pb_{.79}Sn_{.21}Te$
Films - Liquid He Measurement Facility
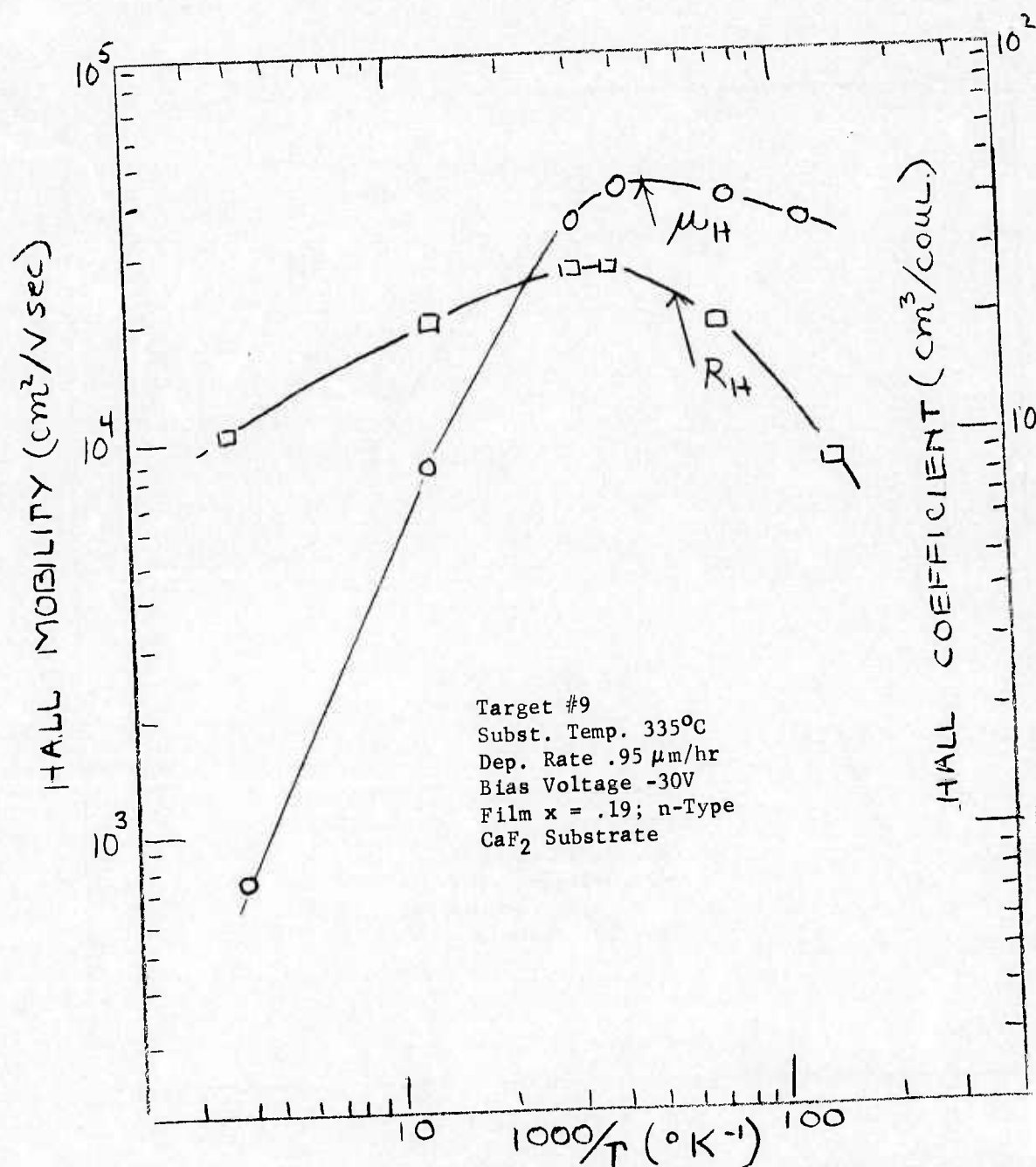
Figure 3-63 Temperature Dependence of Hall Mobility and Hall Coefficient for an As-Deposited Sputtered $Pb_{.81}Sn_{.19}Te$ Film - Liquid He Measurement Facility

(vacancies or interstitials), traces of foreign impurities, inclusions, precipitates, low angle grain boundaries, etc. As mentioned above and from results shown in Figures 3-60 and 3-61 which cover measurements down to 77°K only and from Figure 3-62 which includes results to temperature close to 4°K, it is quite evident that at least the very low temperature measurements are required in order to determine with any reliability and particularly completeness the nature of all scattering mechanisms and of the sources thereof. Measurements to only 77°K could obviously be misleading in a complete analysis. Expecially if this analysis is used to define the experimental approaches required for producing "ideal" films for highest quality sensors or sensors operating below 77°K for increased D* values in reduced (photon) background systems. However, measurements to 77°K only, used for a comparative analysis as discussed earlier to compare the dominant scattering modes in two films, appears to be valid if the same assumptions are used. The validity of the analysis, of course, depends on the validity of the assumptions.

Analyses utilizing these and other Hall data obtained down to liquid He temperatures are still in progress and additional low temperature measurements are being carried out to aid in this analysis.

Figure 3-63 shows an additional result of Hall measurements to temperatures close to the liquid He temperature. The film measured was deposited from Target #9 on a CaF_2 substrate. Reference to Figure 3-37 shows that at the specified conditions (335°C, 0.95 μm/hr and a large negative bias voltage of -30V) a relatively low carrier concentration is observed which should be primarily due to (ionized) impurity rejection. Obviously, the bias condition is far removed from the critical value which is $V_o \sim$ -3V and stoichiometry may be far from perfect also. However, the results in Figure 3-63 show considerable similarity to those shown in Figure 3-62. As noted the Hall mobility for this film varies as $T^{-5/2}$ between the range of 300°K and 77°K and the slope is only slightly less than 5/2 between 77°K and 30°K. Below about 30°K, the Hall mobility appears to again "saturate". However, the saturation level corresponds to a slightly lower mobility value and saturation occurs at a slightly lower temperature than for the film in Figure 3-63.

3-119

The Hall coefficient varies with temperature similarly to that shown in Figure 3-62 also. The Hall coefficient increases between the temperatures of $300^{\circ}K$ and $30^{\circ}K$ and then decreases at lower temperatures.

From the similarity of the behavior in Figures 3-62 and 3-63, it appears that similar scattering mechanisms are operative at the lowest temperatures even though the films were deposited from two different targets and at different deposition conditions. However, the differences in behavior above $30^{\circ}K$ are probably related to differences in film characteristics as related to the deposition conditions employed - particularly as related to deviations from conditions of stoichiometry.

The results shown in Figures 3-62 and 3-63 illustrate that reliable measurements from $300^{\circ}K$ (or higher) down to liquid hellium temperatures are now possible on a relatively routine basis in our laboratory although they are, of course quite time consuming. They also demonstrate that, in as-deposited films, mobilities approaching 10^5 cm^2/v-second can be attained with sputtered films. Since the data shown in Figures 3-62 and 3-63 are not representative of films with the best properties, further optimization of bias voltage control, for example, should further improve the film properties. Similarly, the properties of as-deposited films, without further optimization, seem to have reached at $77^{\circ}K$ typical carrier concentrations in the high 10^{16} or low 10^{17} cm^{-3} range with corresponding mobilities in the 1 to 2 x 10^4 cm^2/v-sec ranges. Further optimization of deposition conditions (e.g., bias voltage) and/or further implementation of new preparation techniques are certain to improve these values.

3.2.5 OPTICAL PROPERTIES OF AS-DEPOSITED FILMS - WITH AND WITHOUT SUBSTRATE BIAS.

3.2.5.1 Index of Refraction. As discussed in Section 2.0, utilizing infrared transmission and reflection measurements, the index of refraction is determined from the interference maxima or minima and the commonly used Bragg relation. Such calculations were performed to date on a number of films which were deposited with and without substrate bias. For films deposited without substrate bias, numerous data were collected

for various film compositions and for various temperatures of measurement. Typical results of these measurements are illustrated in Figure 3-64 in which a) room temperature indices of refraction are plotted as a function of photon energy for films of three different compositions, and b) indices of refraction for one film (x = .20) are plotted as a function of photon energy at three measurement temperatures. As noted, each film has a maximum in index (n_{max}) at a fairly well defined photon energy or wavelength. As further noted, n_{max} shifts to lower photon energies or longer wavelengths as the x-values of the films increase and as the film temperature is lowered. The presence of such a peak has been observed by other investigators for $Pb_{1-x}Sn_xTe$ as well as for other materials (References 16, 17, 18), and has been associated with the photon energy at which the maximum slope occurs in the absorption curve. From the absorption data, to be shown later, this concept is quite compatible with the observed shift of the peak to lower photon energies with increasing x-values and lower measurement temperatures. It should also be noted, from Figure 3-64 that, as the x-value in the films increases or as the measurement temperature is lowered, higher absolute index values are obtained at all wavelengths or photon energies. We have been unable to find in the literature any reported index of refraction values for bulk or thin film $Pb_{1-x}Sn_xTe$, as a function of composition, which allows us to evaluate or compare our data. However, the index of $Pb_{.80}Sn_{.20}Te$ film has been reported as a function of photon energy and temperature by Tao and Wang (Reference 17). The index values of these investigators fall within the range of those reported in Figure 3-64. Additionally, reported values for PbTe (Reference 19) and SnTe (Reference 20) show SnTe to have the considerably higher indices at $300^{\circ}K$. For example, SnTe was given an index of 6.5 at .62 e.v. and PbTe an index of 5.76 at .22 e.v. This is at least implicitly consistent with the increase in index (as the x-value of our films increases) shown in Figure 3-64.
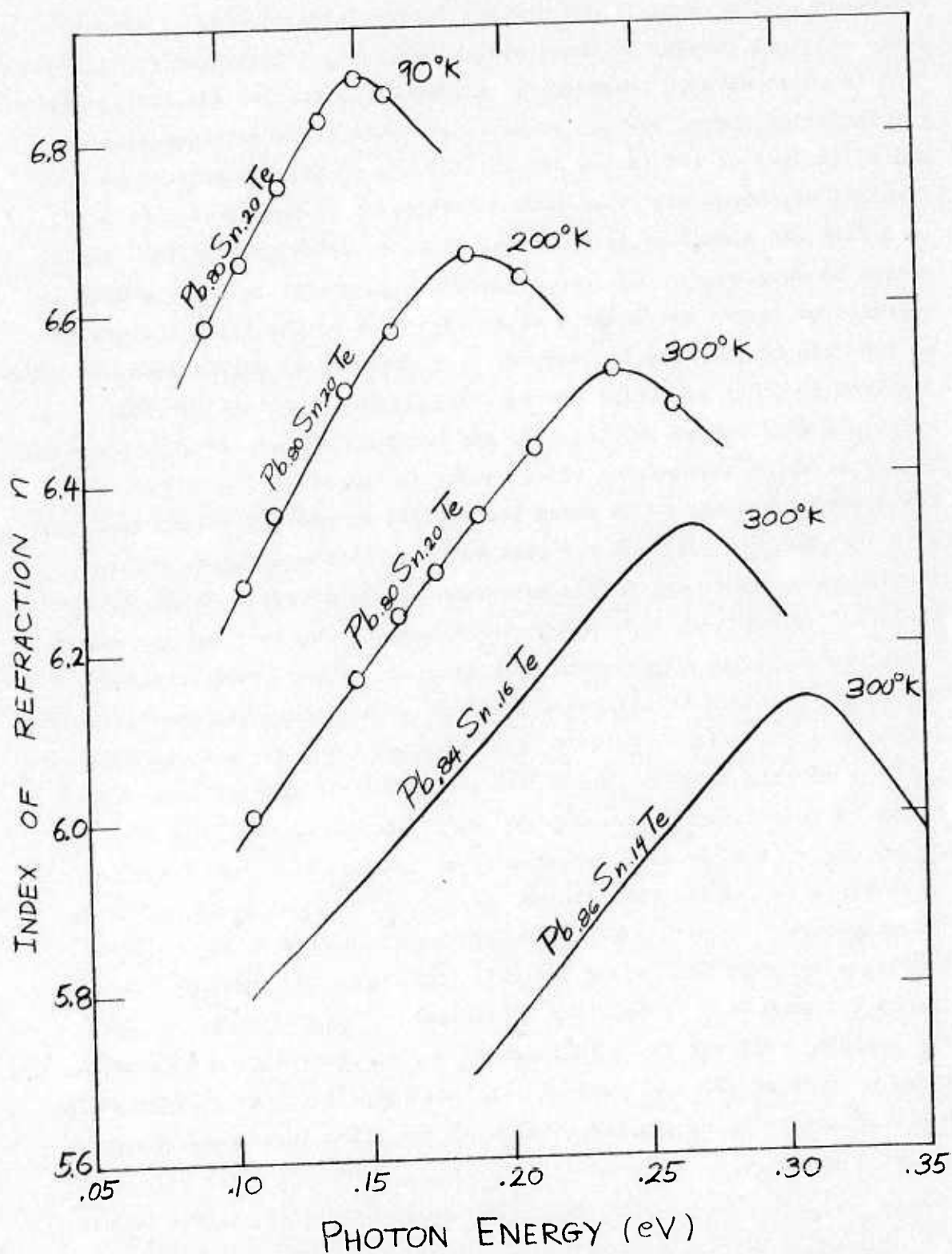
Figure   3-64 Index of Refraction vs Photon Energy for Sputtered
Pb$_{1-x}$Sn$_x$Te Films

3-122

As already mentioned, the results on indices of refraction presented above involved films deposited _without substrate bias_. Results on indices of refraction measured in films deposited _with substrate bias_ showed some rather significant differences as a function of substrate bias. Figures 3-65 and 3-66 illustrate such differences.

Figure 3-65 shows the indices of refraction for three $Pb_{.78}Sn_{.22}Te$ films which, though having the same composition, were deposited at three different bias conditions. We note again the presence of index maxima at a fairly well-defined photon energy. The maxima for all three films occur at approximately the same photon energy. This is, of course, consistent with the fact that all three films have about the same composition.

A schematic of the carrier concentration behavior versus substrate bias voltage, also shown as an inset in Figure 3-65, illustrates more clearly the significance of the bias voltages used in the preparation of these films. It appears that the index of refraction increases as the deposition conditions deviate from the p-n transition conditions, i.e. as the voltage deviates from the critical bias voltage. This implies that deviations from stoichiometry cause increases in indices of refraction also.

In Figure 3-65, the data shown were for films deposited with negative substrate biases only at values near and below V_0 and, therefore, all three films were n-type. Figure 3-66 includes some results on films deposited at positive biases greater than V_0 also, i.e., for p-type films. As can be seen in this figure the index of refraction increases as the bias voltage deviates either positively or negatively from the critical bias voltage. As may be noted, not all of the films shown in Figure 3-66 were deposited from the same target and under the same deposition conditions. However, the accompanying schematic inset, showing the general trend of carrier concentration vs. bias voltage, illustrates approximately the relative conditions with respect to bias voltage and resulting properties of the films shown. Included in Figure 3-66 are data on the index of refraction for a $Pb_{.80}Sn_{.20}Te$
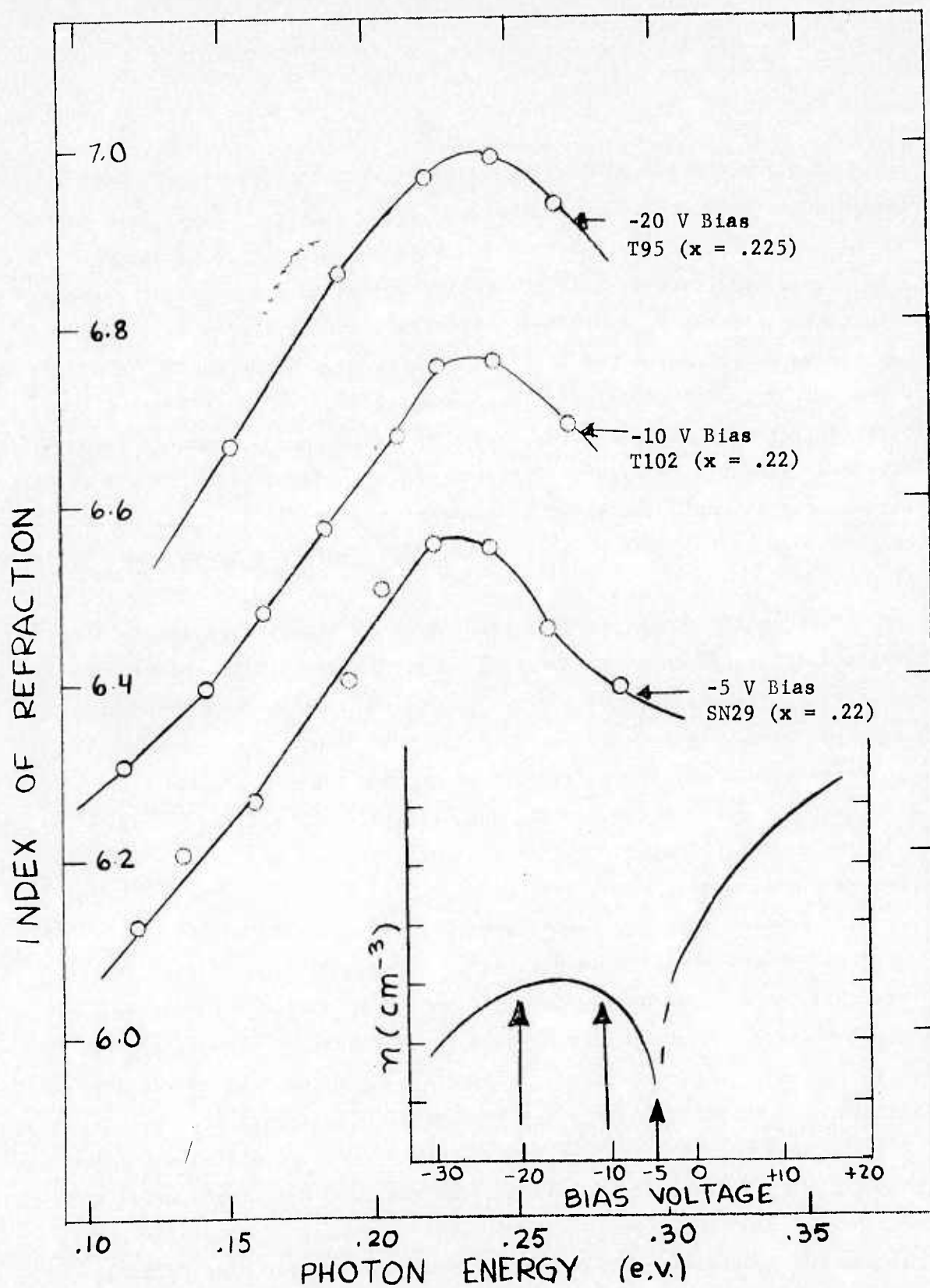
Figure 3-65 Index of Refraction vs. Photon Energy for Bias Sputtered $Pb_{1-x}Sn_xTe$ Films
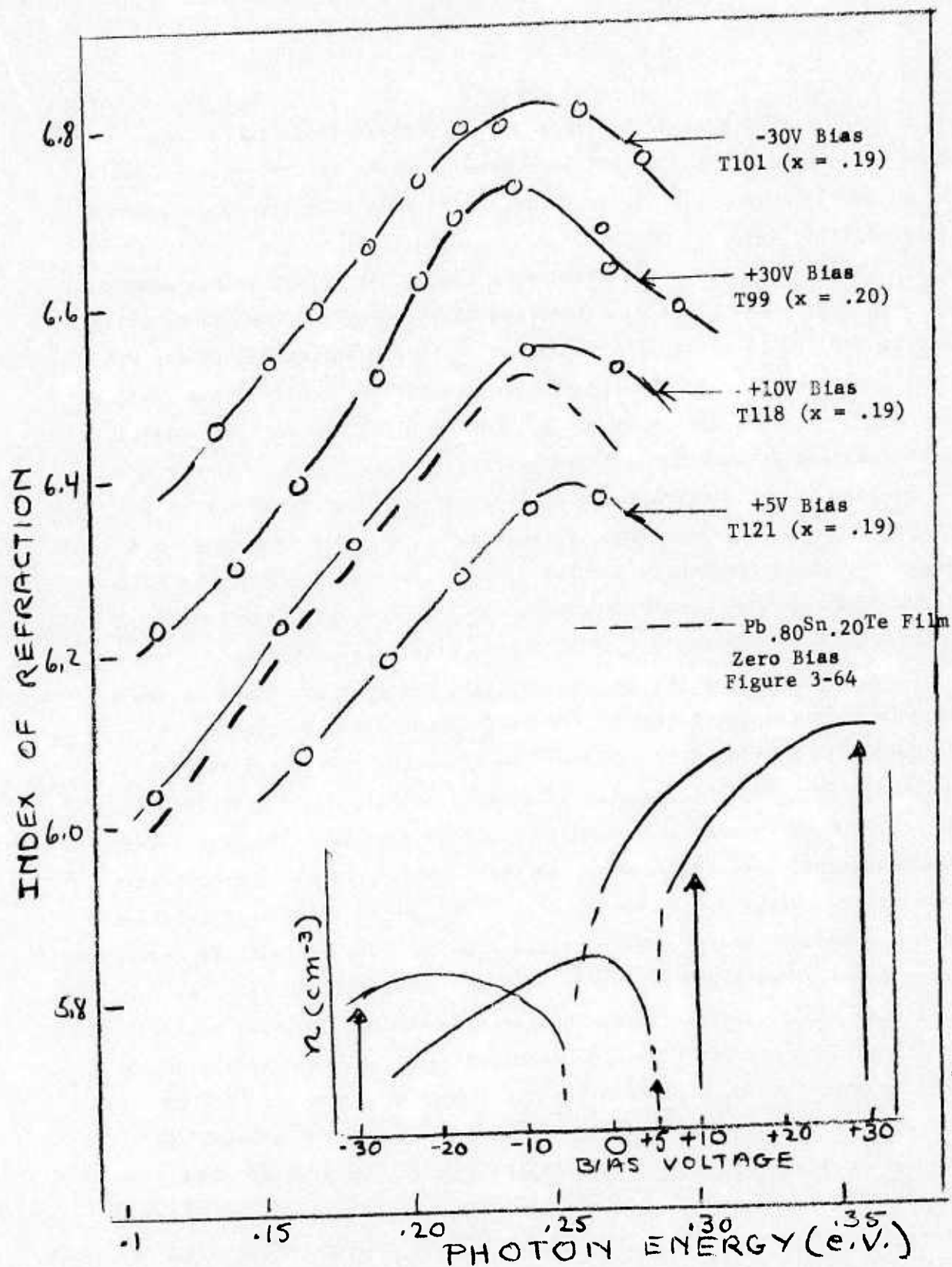
Figure 3-66 Index of Refraction vs. Photon Energy for $Pb_{1-x}Sn_xTe$ Films
Positively and Negatively Biased During Sputtering

3-125

film deposited at zero bias conditions reproduced from Figure 3-64. From the schematic we see that zero bias is about as far removed from V_o as is +10V bias. The index variation of this film with photon energy substantiates this.

The results presented above show that at any given photon energy or wavelength, the index of refraction of $Pb_{1-x}Sn_xTe$ films can be varied and controlled to a significant degree by simple variations in deposition conditions and by the use of bias sputtering. While these results are of interest in that they may provide some insight into the basic understanding of some material properties of $Pb_{1-x}Sn_xTe$, they appear to be very useful for practical application such as in the design and preparation of interferometric filters and other optical devices for the mid-to-long-wavelength portion of the infrared spectrum. Variable index films or films with differing indices can be laid down in one deposition run with one target by simple bias voltage control.

3.2.5.2 <u>Absorption Coefficients and Energy Gaps</u>. Typical plots of room temperature absorption coefficients obtained by the method discussed in Section 2.0 as a function of photon energy for several epitaxial $Pb_{1-x}Sn_xTe$ films with different compositions and sputtered without substrate bias are shown in Figure 3-67. As noted, relatively sharp absorption edges are obtained which readily permit the determination of the energy gap of our sputtered $Pb_{1-x}Sn_xTe$ films as a function of composition. Energy gaps obtained from the room temperature absorption edge data such as shown in Figure 3-67 are summarized in Table 15 for an assortment of films with compositions determined by x-ray analysis. In Figure 3-68 the 300°K optical energy gaps are plotted as a function of film composition. Included in this figure are data for bulk single crystal $Pb_{1-x}Sn_xTe$ (Reference 21,22) for purposes of comparison. As noted, the sputtered thin film data agree fairly well with values determined from bulk measurements, certainly within the experimental error of our measurements. It was, therefore, considered valid to utilize absorption edge data to determine the energy gaps and, consequently,
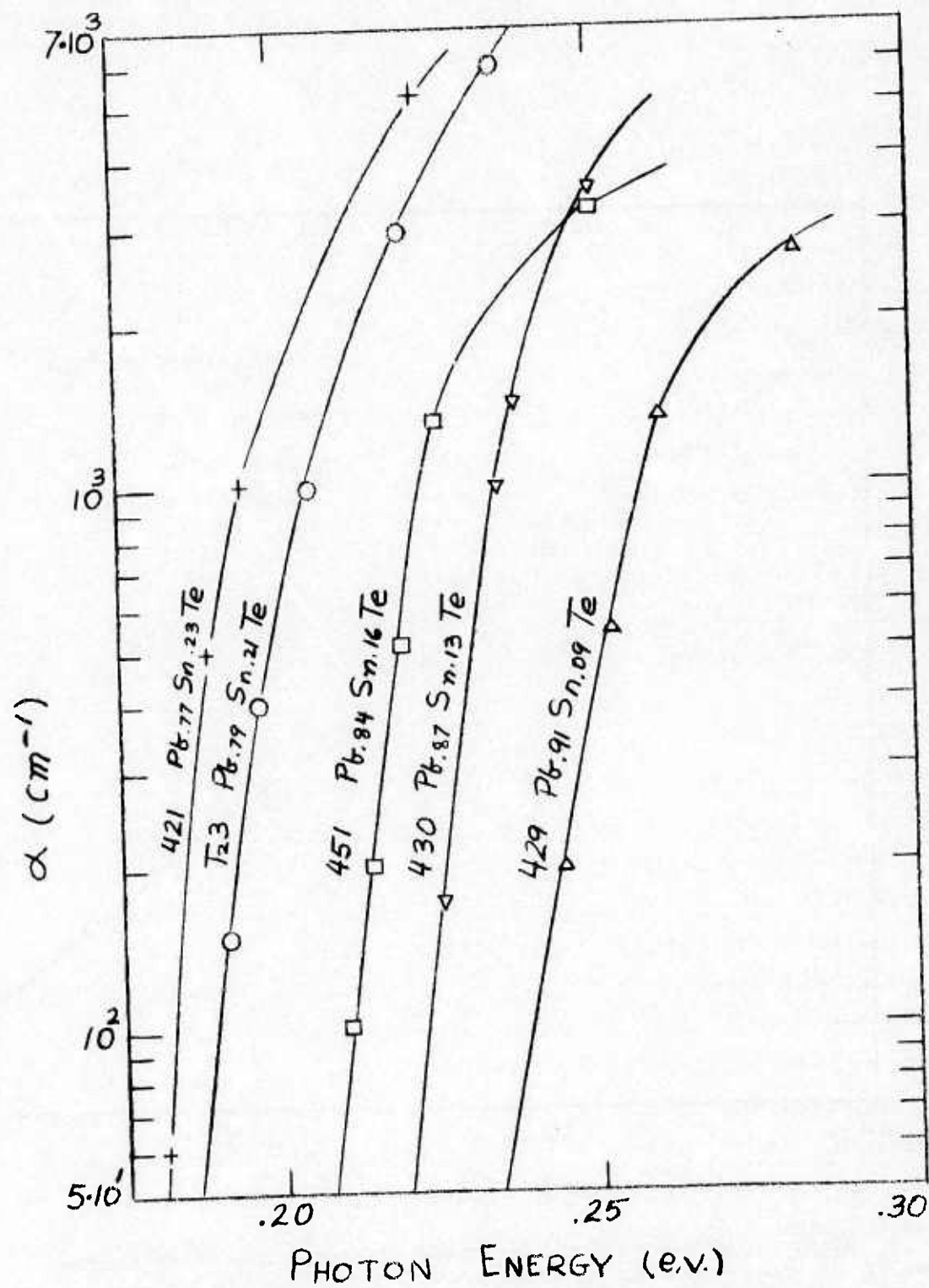
Figure 3-67   Absorption Coefficient for Sputtered $Pb_{1-x}Sn_xTe$ Films
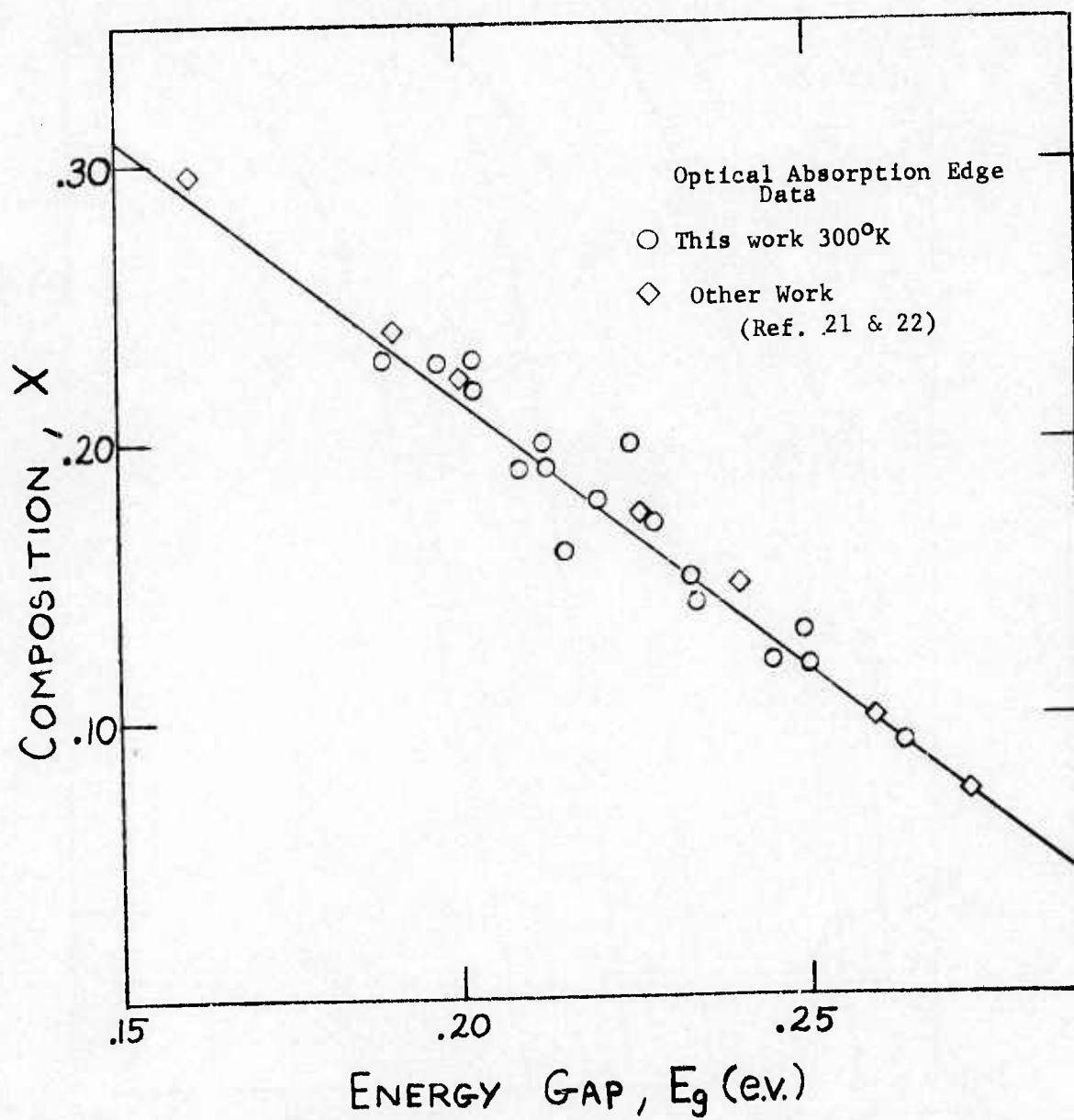
Figure 3-68 Composition Dependence of Energy Gap of Sputtered $Pb_{1-x}Sn_xTe$ Films
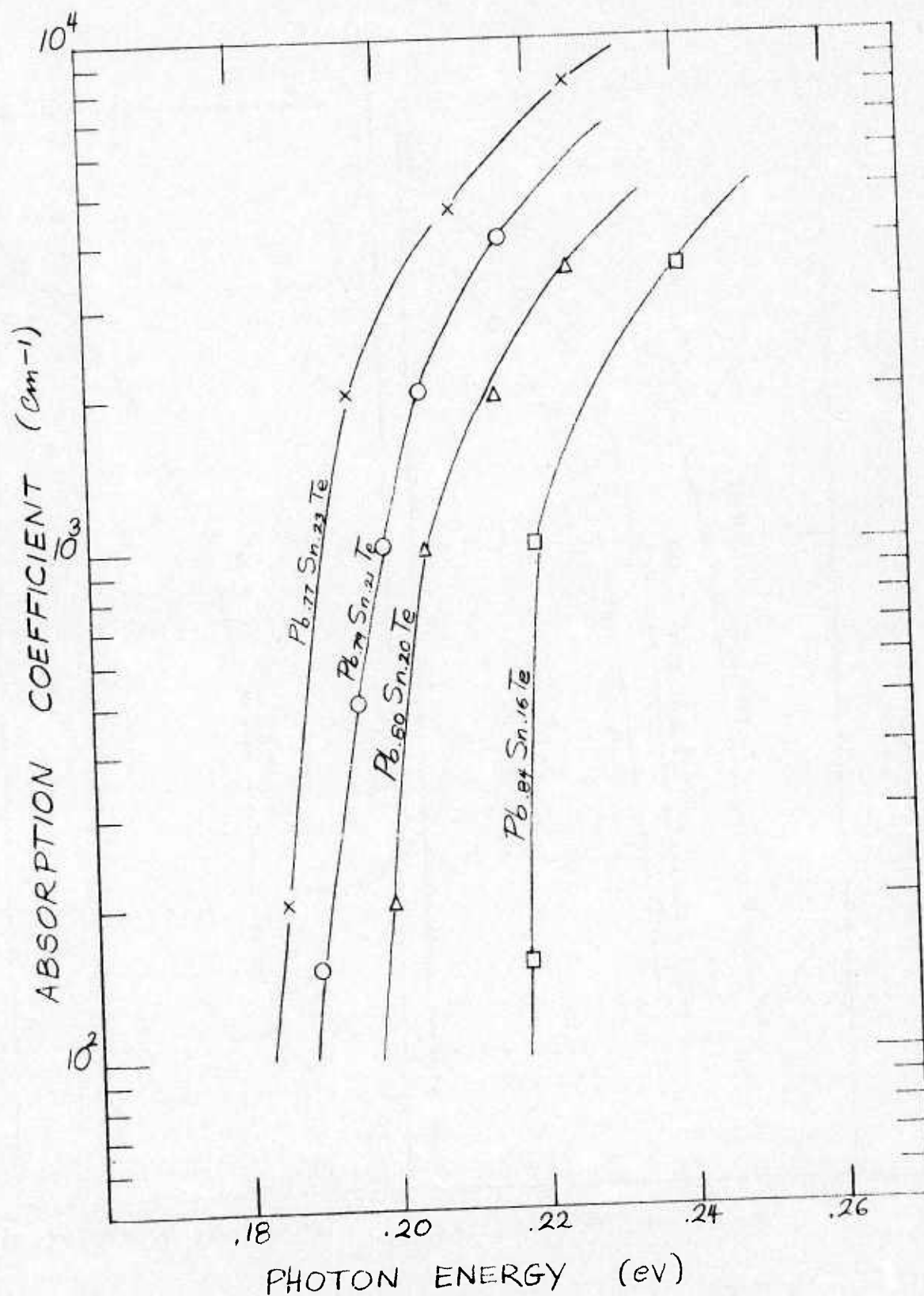
Figure 3-69 Absorption Coefficients for Sputtered
$Pb_{1-x}Sn_xTe$ Films
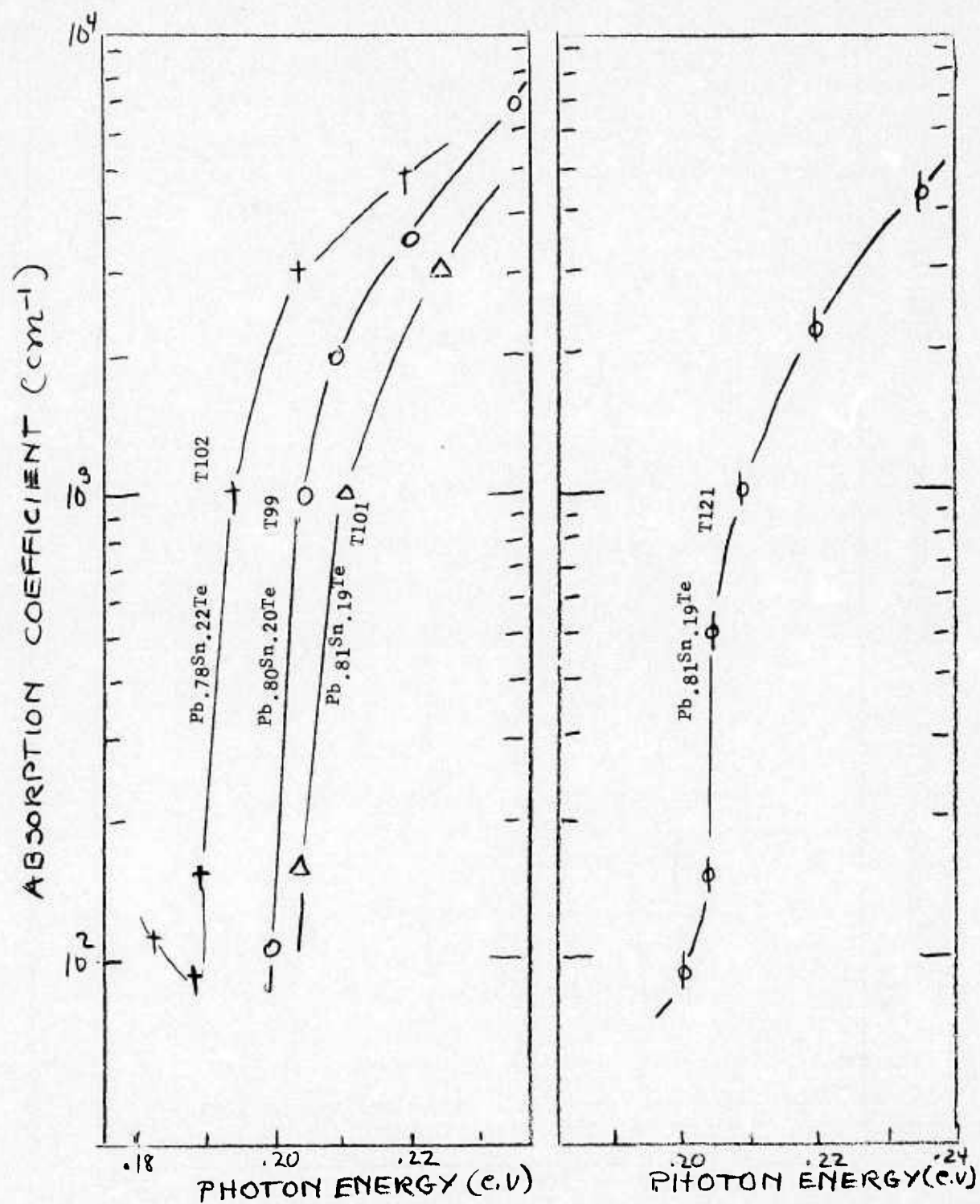
Figure 3-70 Absorption Coefficients for Bias Sputtered $Pb_{1-x}Sn_xTe$ Films

x-values of our thin films as a routine first order method. The final x-value determination, however, is checked and compared with x-ray data. As will be shown later similar consistency was obtained for energy gaps determined from photoconductive threshold data.

Finally, some additional typical plots of absorption coefficients versus photon energy are shown in Figures 3-69 and 3-70, which represent films sputtered without and with bias, respectively. The films yielding some of the data in Figure 3-69 are the same as those for which index values were represented in Figure 3-64 while those shown in Figure 3-70 are the same as those used for illustration of index behavior in Figures 3-65 and 3-66. While results, relative to indicated energy gaps, are consistent with the compositions measured by x-ray analysis in the films, there appears to be no particular effect of bias voltage on the behavior of absorption coefficients.

3.3 CONTROLLED INTRODUCTION OF IMPURITIES - "DOPING WITH GASEOUS ADDITIVES DURING SPUTTER DEPOSITION.

In line with the general objectives of this program, the results presented to this point were associated with the experiments utilizing improved techniques and modifications for the preparation of $Pb_{1-x}Sn_xTe$ films with highest electrical, structural and stoichiometric quality. However, we stated that the ultimate objective is to achieve film properties resulting in the highest possible photo-response. One approach we selected for achieving improvements in photo-response was to generate trap-enhanced photo-response by means of controlled doping of the $Pb_{1-x}Sn_xTe$ films. As an initial attempt to do this, experiments were performed in which $Pb_{1-x}Sn_xTe$ films were sputtered in controlled gaseous environments. This means of doping was selected initially based on some early results, presented in Reference 1, which showed significantly enhanced photoconductivity in films which were exposed to oxygen in an uncontrolled manner. With the feasibility of the approach thus established, sputtering experiments were systematically performed as a function of the partial pressure of the doping species in the

sputtering gas. To date, such experiments were confined to sputtering environments (Ar) containing pure oxygen or nitrogen as additives. As in the case of films deposited with substrate bias, very interesting and encouraging results have now been obtained on the properties of films which were sputtered with these two additives.

Representative data on the effect of such "doping" on the electrical, structural and compositional film properties are presented in Table 16 and Figures 3-71 through 3-76. As noted in Table 16 and the figures, sputterings with partial oxygen and nitrogen pressures were performed with and without substrate biasing.

We consider first the results of experiments performed with zero substrate bias.

In the example shown in Figure 3-71, the deposition conditions used, ($T = 330^{\circ}C$, $R \sim .8 \mu$/hr) resulted in p-type films if deposited without additives in the sputtering gas. The background pressure was in all cases in the low 10^{-7} torr range. As can be seen from either the table or Figure 3-71 the films remain p-type (but the p-type carrier concentration decreases) as the partial pressure of O_2 is increased above the background to approximately 5×10^{-6} torr. A further increase in the pp O_2 results in an increased p-type carrier concentration. As shown in Table 16, the film structures and compositions remain essentially the same as those of films deposited without the addition of O_2, at least up to pp O_2 close to 5×10^{-6} torr. Above that pressure, a) the structure deteriorates, b) regions with polycrystalline structure are observed, c) the film composition is significantly changed (i.e. from $x = .21$ to $x = .13$), and d) in some samples, x-ray data indicate the presence of more than one phase.

The addition of nitrogen during sputtering has somewhat different effects. First we note that for all partial nitrogen pressures used, the films are deposited with n-type properties. Since a film deposited
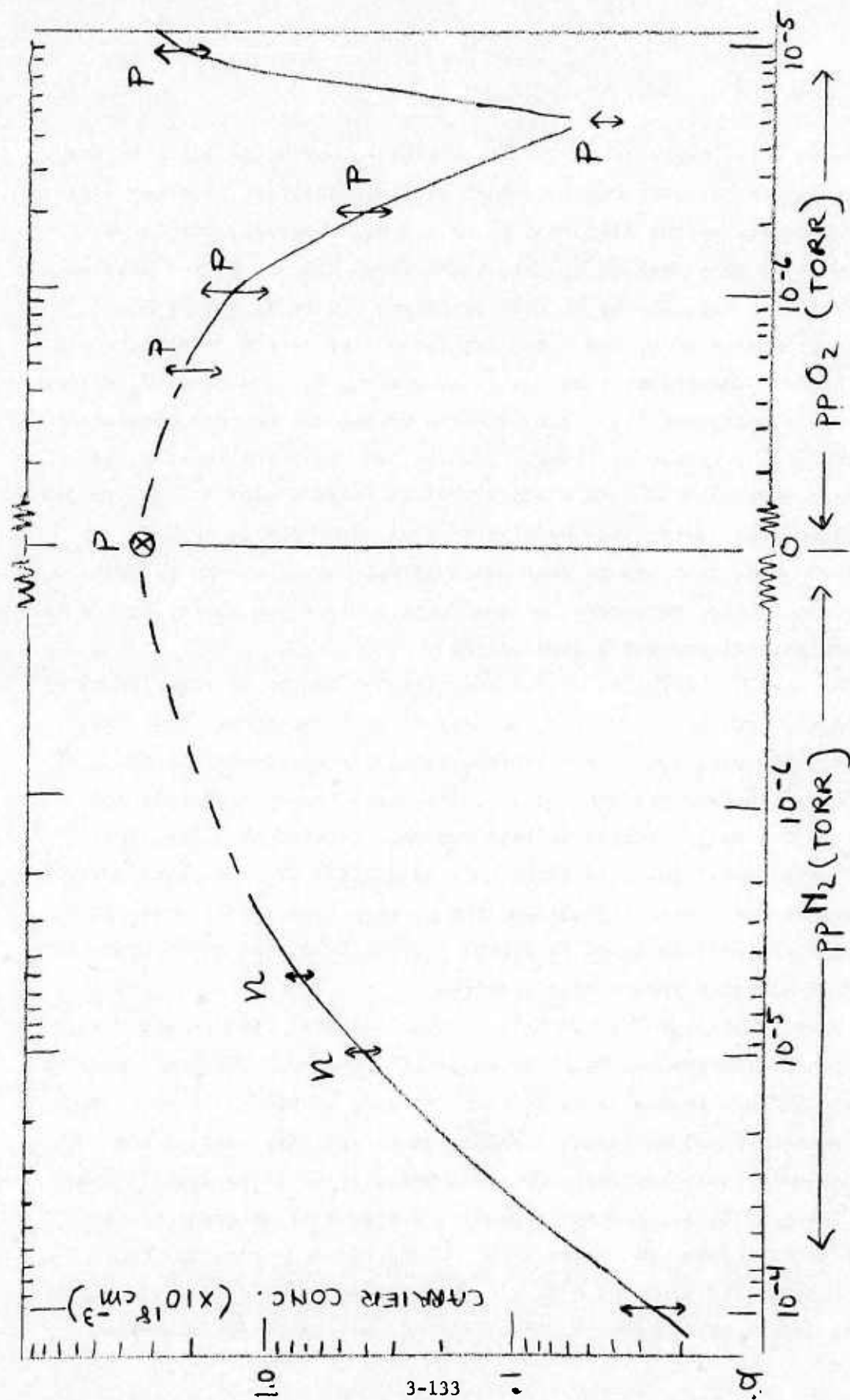
Figure 3-71 Effect of O_2 and N_2 Partial Pressures in Sputtering Gas on Carrier Concentration of $Pb_{1-x}Sn_xTe$ Films

at the same conditions is p-type if neither N_2 nor O_2 is added to the sputtering gas, we must conclude that even the smallest nitrogen addition used switches the film from p- to n-type. However, results with lower partial pressures of N_2 than those shown are not as yet available (see dotted line). It may be that switching occurs at very small partial pressures of N_2 and also that the n-type carrier concentration is critically reduced at some small value of pp N_2. Up to pp N_2 values of 1×10^{-5} torr, the film structures and compositions are consistent with those of the undoped films. However, as the pressure of N_2 is increased above 1×10^{-5} torr the structure deteriorates and the composition changes as in the case of high partial pressures of oxygen. On the other hand, contrary to what was observed with the oxygen addition, the n-type carrier concentration continues to decrease up to the highest nitrogen partial pressures used to date.

As seen in Table 16, only a very limited number of experiments of this nature have been performed to date in which substrate bias was applied. However, even these limited results are interesting and, therefore, the data are presented at this time in both Table 16 and Figure 3-72. Only one bias voltage was investigated thus far (i.e. +30V). The deposition conditions were maintained as closely as possible to those utilized with films deposited at zero bias conditions. In this figure, the data shown in Figure 3-71 at zero bias are reproduced (solid line) for purposes of comparison.

Most striking in Figure 3-72 is the fact that both p- and n-type films could be deposited with the application of +30V substrate bias at the same partial pressures of N_2 at which only n-type films were deposited at zero bias conditions. While the n-type film carrier concentrations were consistently below those measured in films deposited at zero bias conditions, the corresponding p-type carrier concentrations were somewhat higher with bias.

The application of a +30V substrate bias during deposition in a partial oxygen environment resulted in p-type films only, with the
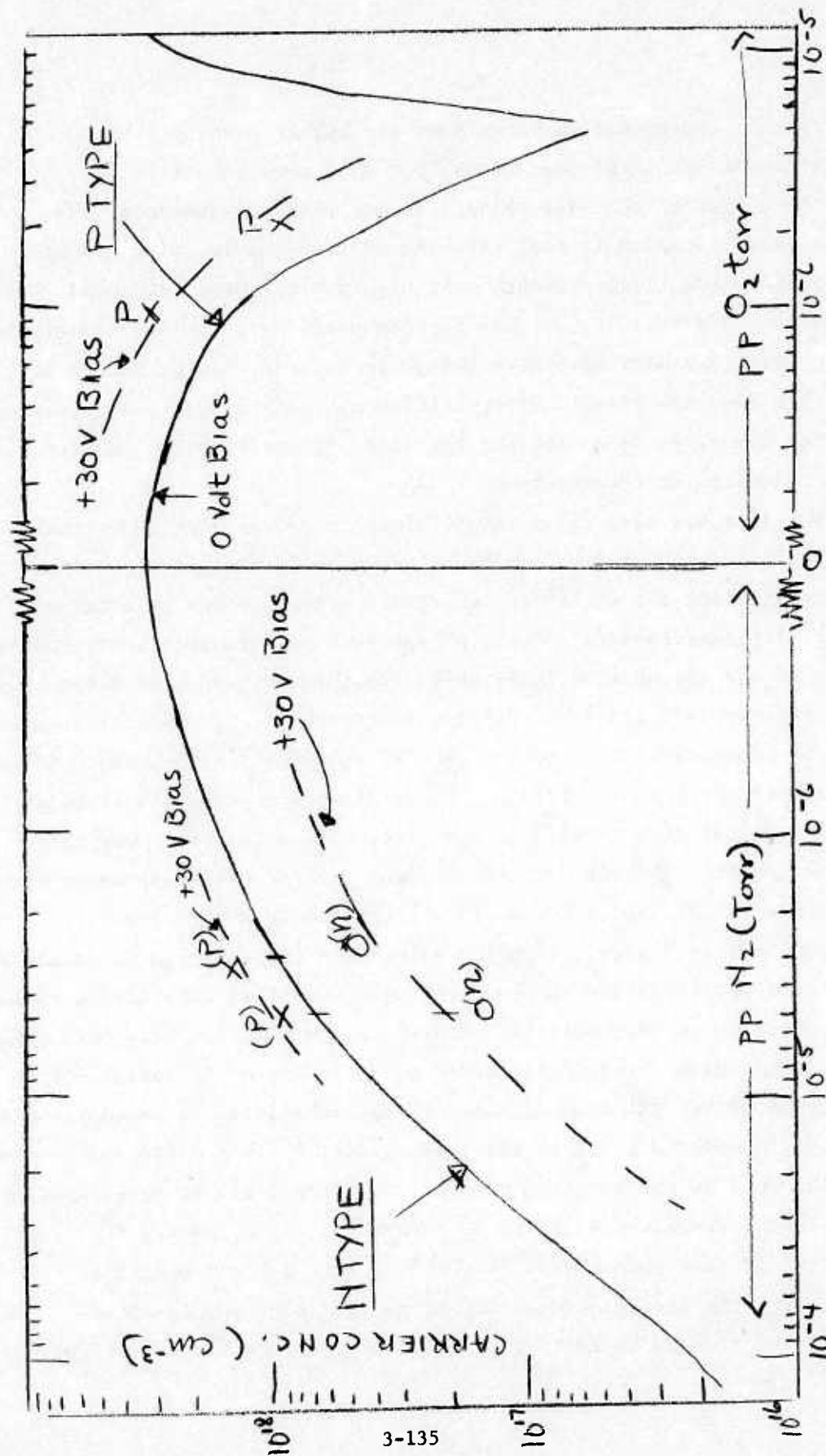
Figure 3-72 Effect of O_2 and N_2 Partial Pressure in Sputtering Gas on Carrier Concentration PbSnTe Films - (Target #8 - +30V Bias)

p-type carrier concentration being somewhat higher than in films
deposited under identical conditions, but with zero substrate bias.

The effect of the bias voltage is not easily understood; one
possible interpretation is that the bias affects any impurity content
in the gaseous additives - though only high purity gases were used.
In nitrogen, in particular, it may repulse positively ionized impurities
when the effective carrier concentration is lowered. In oxygen it may
in addition have the effect of repulsing some ionized O_2, thus requiring
a somewhat higher pp O_2 to achieve the same effects relative to effective
carrier reduction or compensation.

The data are also still insufficient to define with any certainty
the mechanisms which cause the effects of N_2 or O_2 themselves. Some
first insight into the mechanisms which are operative may be obtained
from mobility measurements. Results from such measurements are summarized
in Table 16 and illustrated in Figures 3-73 through 3-76. We first
note in Figures 3-73 and 3-74 that the linearity of the mobility dependence
on carrier concentration in these films is consistent with undoped films
over the entire range of partial nitrogen or oxygen pressures at which
the films are not structurally or compositionally changed. Over this
range the mobility increases in the typical fashion with decreasing carrier
concentrations. However, at the highest partial O_2 and N_2 pressures
(not shown in this figure), at which we noted a large change in composition
as well as a deterioration in the structure, the films exhibited a rather
drastic decrease in the mobility. Therefore, we consider here only films
which have not been structurally affected by the N_2 or O_2 addition. In
both figures we see the same effects: a) the mobilities in doped films are
lower than in undoped films of the same nature; b) this difference becomes
more pronounced as the measured carrier concentrations decrease (that is,
as the partial pressures of N_2 or O_2 increase). By comparing the two figures
it can be seen that the general "doping" effects are quite similar for biased
and unbiased film depositions or for oxygen and nitrogen additives.
These results seem to indicate the presence of an additional scattering

3-136
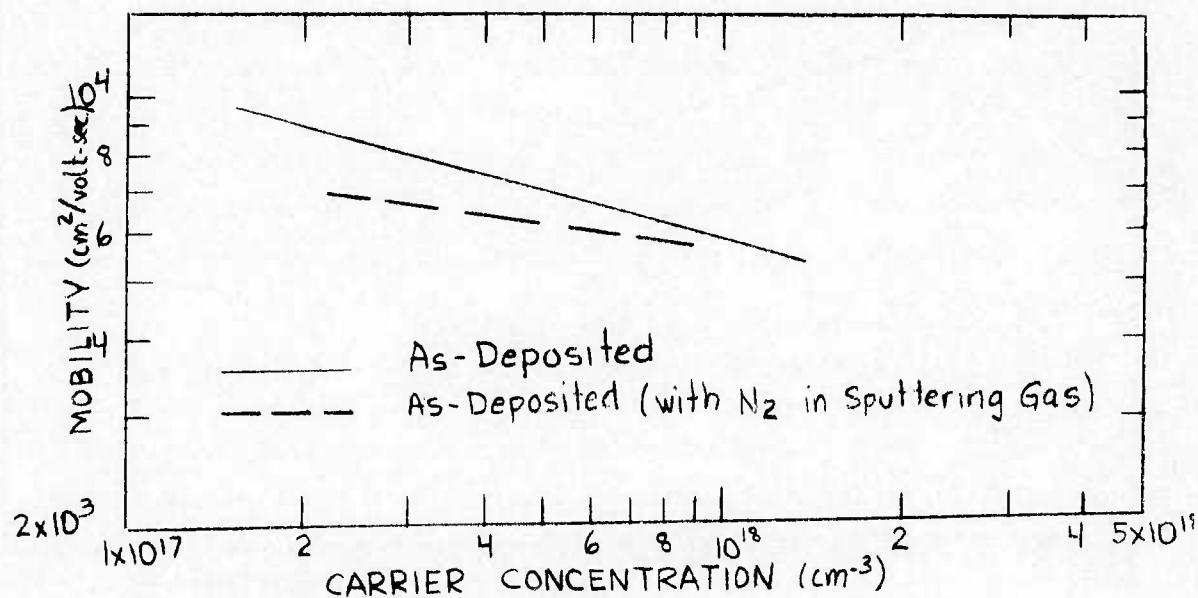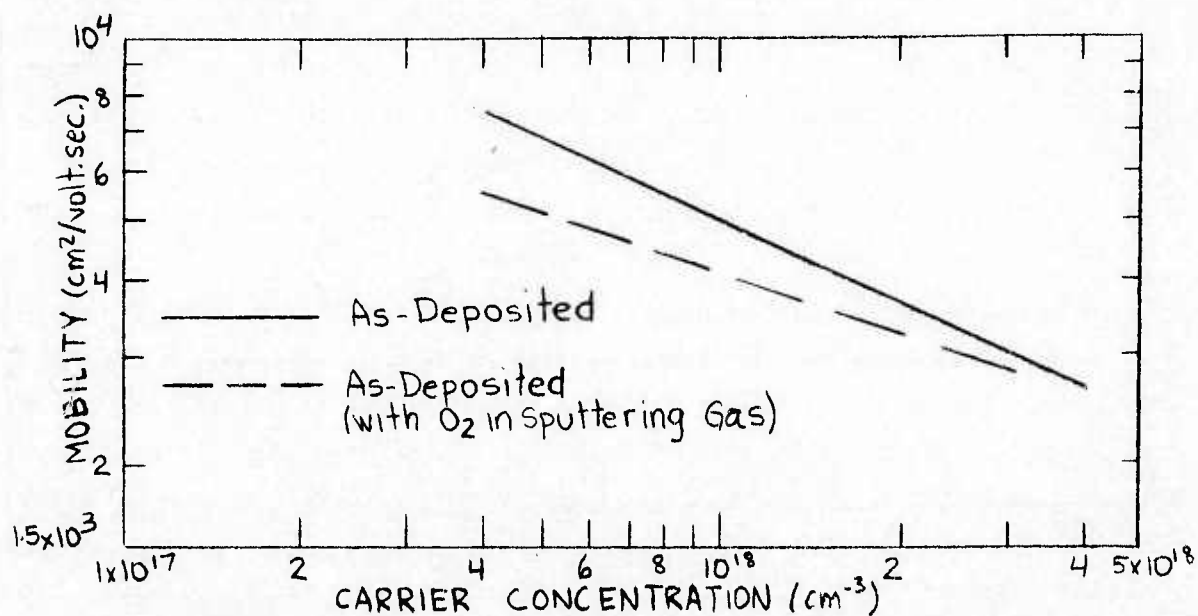
a) n-Type

b) p-Type

Figure   3-73   Effect of Doping (O_2 or N_2) on Electrical Properties of
As-Deposited $Pb_{1-x}Sn_xTe$ Films (Target #8 - Zero
Substrate Bias)
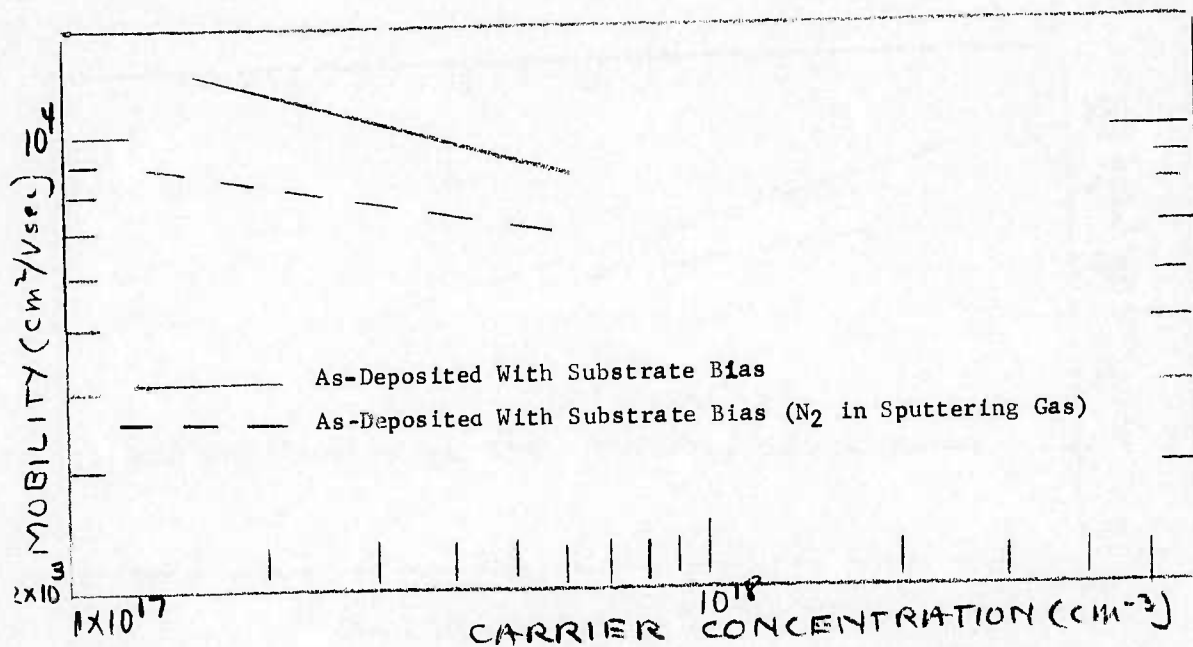
a) n-Type Film
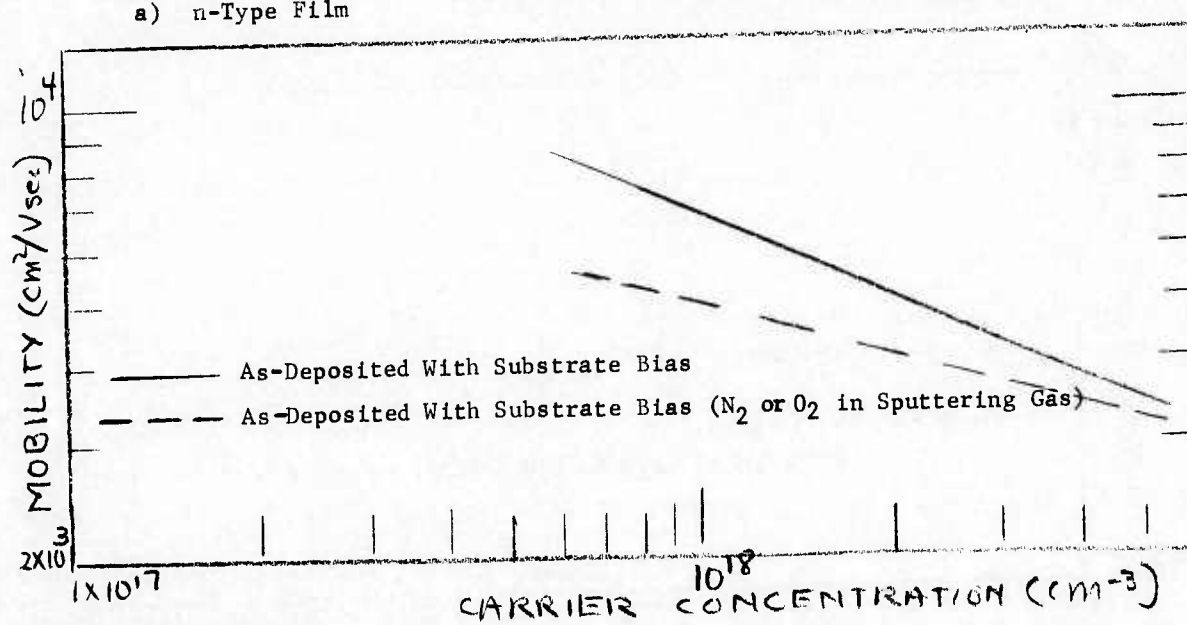
b) p-Type

Figure 3-74   Effect of Doping (O_2 and N_2) on Electrical Properties of As-Deposited $Pb_{1-x}Sn_xTe$ Films (Target #8 - with Substrate Bias)

3-138

mode which becomes increasingly operative in films deposited with increasing pp of O_2 or N_2 gas.

Figure 3-75 shows the mobility and Hall coefficient as a function of temperature between 300°K and less than 10°K for a film deposited in the presence of N_2 gas and at a positive substrate bias. We see that the major scattering mode remains due to lattice or phonon scattering as indicated by the $T^{-5/2}$ dependence to temperatures lower than 77°K. At temperatures below about 30°K the mobility seems to saturate as in undoped films and becomes nearly temperature independent. This behavior is probably the result of scattering due to imperfections related to the same active carriers that we have seen in undoped films. In order to see the effect of the N_2 addition more clearly we compare in Figure 3-76 the mobility and carrier concentration for the film shown in Figure 3-75 (deposited with N_2 gas) with those for a film deposited without the N_2 addition (Figure 3-62). Both films exhibit about the same temperature dependence of both the Hall mobility and the Hall coefficient down to about 77°K. Below 77°K, the mobilities in the N_2 doped film begin to deviate slightly from the $T^{-5/2}$ dependence. Although both films show a mobility saturation at temperatures below about 30°K, the mobility of the doped film saturates at a lower value.

Perhaps most revealing is the fact that the Hall coefficients in the N_2 doped film does not exhibit the anomolous drop at temperatures below 30°K which is very pronounced in the undoped films. This means that higher Hall coefficients-corresponding to lower carrier concentrations-are measured below 30°K in the doped films along with the lower mobilities. Although it is not possible to draw any firm conclusions as to scattering mechanisms from these few results, it is apparent that an additional scattering mode which appears to be carrier independent is operative in the doped films. This additional scattering mode may very well arise from neutral type scattering centers, attributable to neutrals resulting from trapped or compensated carriers. While more detailed information collection and analysis are planned to
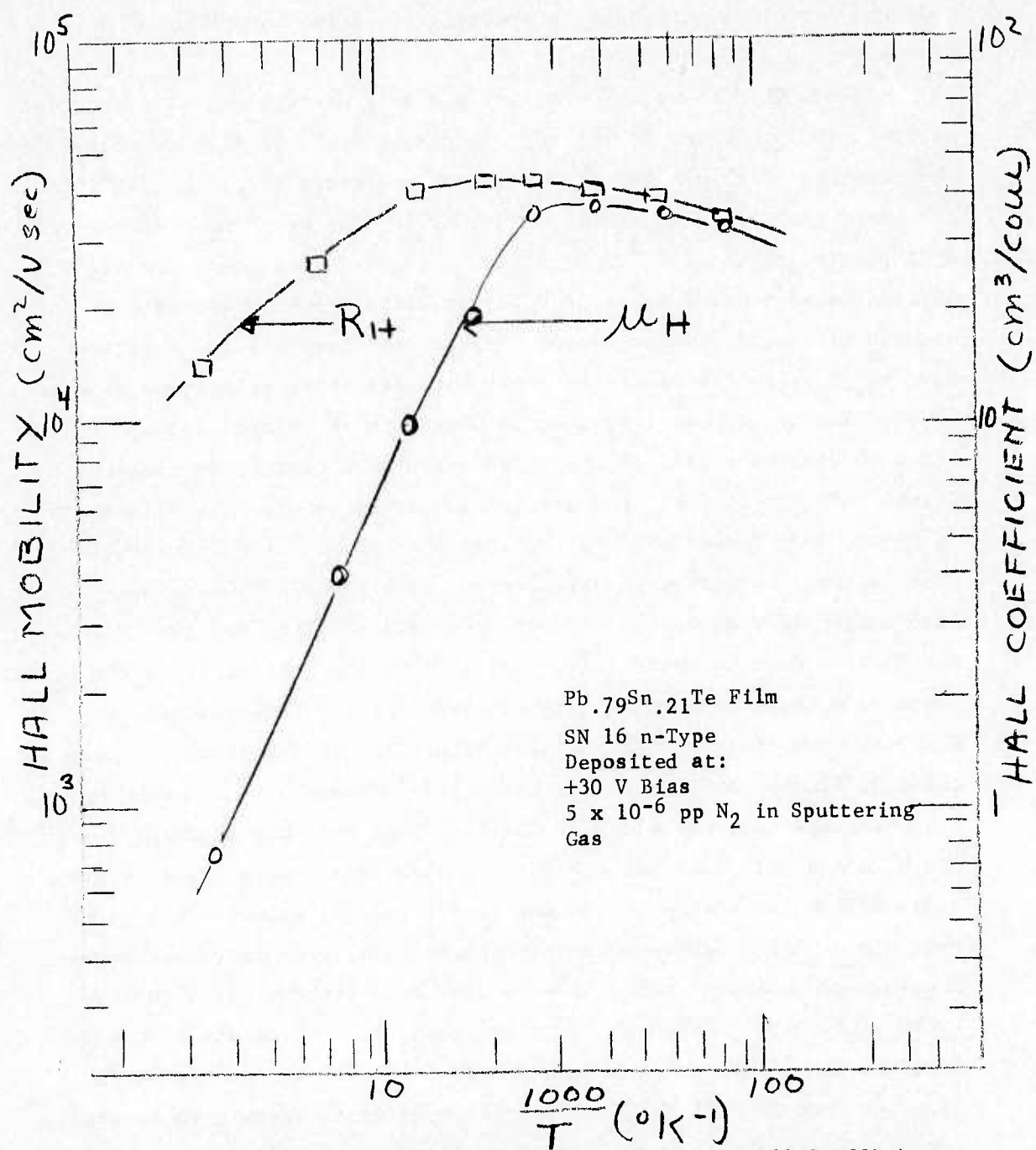
Figure 3-75 Temperature Dependence of Hall Mobility and Hall Coefficient
Film Sputtered in pp N_2 - Liquid He Measurement Facility
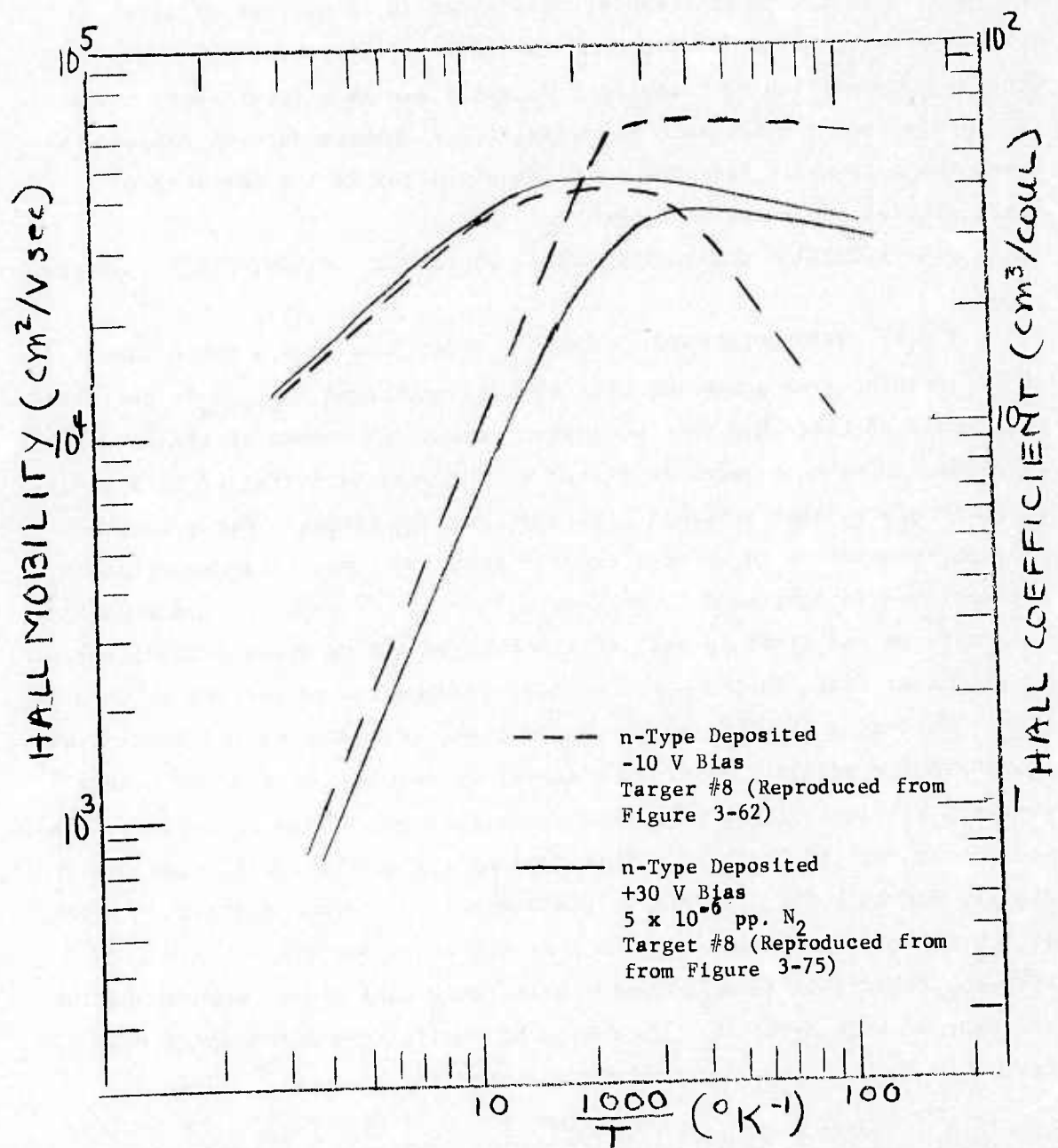
Figure 3-76 Comparison of As-Deposited Temperature Dependence of Hall
Mobility and Hall Coefficients for Two $Pb_{.79}Sn_{.21}Te$ Films
Deposited with and without the Addition of N_2 to Sputtering
Gas

3-141

identify conclusively the scattering mechanisms as well as the responsible carriers operating in these films, we have, to date, concentrated on the main objective of these studies which is to explore if electro-optical properties can be improved in these films by some means of carrier compensation or trapping. We shall see in a later section that it appears that a systematic and significant photoconductive response enhancement is quite feasible in films deposited in the presence of small partial pressures of O_2 and N_2.

3.4 ANNEALING CHARACTERISTICS - PROPERTIES OF ANNEALED $Pb_{1-x}Sn_xTe$ FILMS

3.4.1 INTRODUCTION AND GENERAL APPROACH. A considerable amount of information from annealing studies with sputtered $Pb_{1-x}Sn_xTe$ performed under this contract has been collected during the course of this contract. Annealing experiments were initiated at the very beginning of this program and, therefore, have progressed through various stages. Early in the program, procedures to be utilized for isothermal annealing experiments, as described in Section 2.0, were established. In general, the annealing temperatures and times as well as the type of charge was selected, for a particular film, on the basis of the as-deposited properties of this film - including its structure, composition, carrier type and concentration, carrier mobility, etc. The annealing results obtained by others for PbSnTe bulk crystals were used as initial guidelines to define annealing procedures for PbSnTe films. This included, e.g. the equilibrium phase diagram for bulk $Pb_{1-x}Sn_xTe$ near the stoichiometric composition. As the work progressed it became obvious that the annealing results obtained with sputtered thin films showed considerable consistency with annealing behavior of bulk crystals. This type of consistency aided considerably in the implementation of a systematic annealing program.

With the objective of optimizing the annealing conditions for the purpose of achieving the best electrical properties, that is, the lowest carrier concentrations and the highest mobilities, various systematic

3-142

investigations involving charge composition, degree of metal richness
etc. were performed. For example, 3%, 4%, 6% and 10% metal-rich charges
were investigated in some detail and are reported in the following
sections. In addition to the studies on the effects of various degrees
of metal richness, the effect of annealing charge composition on x-value
was also investigated. Specifically of interest was the effect of de-
viations of the x-values of the annealing charge from the x-value of the
film being annealed. As the following sections will show, small
deviations of this kind can result in significant changes in the
electrical properties particularly near the optimum annealing conditions.
Or, in other words, this portion of the study shows the necessity for
utilizing charge compositions identical to those of the films being
annealed in order to achieve the best electrical properties.

Another approach for metal-rich annealing was investigated which
utilizes small traces of the $Pb_{1-x}Sn_x$ alloy only, instead of metal-rich
charges $[(Pb_{1-x}Sn_x)_{1+y}Te]$. It was found that annealing with $Pb_{1-x}Sn_x$
only does not require the critical matching of film and charge composition
and, as will also be shown, films annealed in such charges exhibit film
properties which are as good as those annealed in the metal-rich $Pb_{1-x}Sn_xTe$
charges. However, the annealing procedure is very much simplified.

As repeatedly mentioned, the annealing results with the sputtered
$Pb_{1-x}Sn_xTe$ films are consistent with the bulk crystal equilibrium phase
diagram near the stoichiometric crossover. However, we found some
interesting results at annealing temperatures considerably different from
and below those near the stoichiometric crossover temperature. At the
initiation of this study, no investigation has been systematically pursued
by anyone for either bulk single crystals or epitaxial films at such low
temperatures. Such an investigation was initiated during the course of
this program with some interesting results to be reported in the following
sections.

The reason that all our early annealing studies utilized only
metal-rich $Pb_{1-x}Sn_xTe$ charges or traces of $Pb_{1-x}Sn_x$ alloy itself
was initially based on the equilibrium phase diagram coupled with
the fact that early starting, i.e. as-deposited films, were p-type in

nature. However, both p- and n-type as-deposited films, as we have seen, can now be deposited by sputtering. For as-deposited n-type films, isothermal annealing experiments utilizing Te rich $Pb_{1-x}Sn_xTe$ charges as well as "charges" consisting of small traces of Te only (no $Pb_{1-x}Sn_xTe$ charge) were therefore introduced and also systematically performed.

The availability of the bulk annealing data made it possible to immediately select near optimum annealing conditions and charges for the annealing of any particular sputtered $Pb_{1-x}Sn_xTe$ film and to achieve desired carrier types or desired carrier concentrations equal to or below and carrier mobilities equal to or above the limits achieved to date. Furthermore, it was possible to utilize the results of the annealing studies performed during the first phase of this program to readily initiate some annealing studies with bias sputtered films, as well as with some films sputtered in environments of nitrogen and oxygen partial pressures.

To investigate the substrate bias effects, standard annealing charges were selected in most cases (e.g. 6% metal-rich $Pb_{1-x}Sn_xTe$ charges with x-values equal to the film x-values) and annealing temperatures for each composition were selected based on the equilibrium phase diagram near the stoichiometric composition. Thus, a set of films deposited at the same deposition conditions but with different substrate biases was subjected to the identical annealing conditions and identical annealing charges for comparison. Since such films generally have very nearly the same as-deposited composition, the comparison is meaningful. For several films, annealings were performed at a number of temperatures to determine whether the critical annealing temperature (i.e., the temperature at which the metal-rich solidus crosses the stoichiometric composition in the equilibrium phase diagram) was affected by substrate bias. As the following results will show, if identical annealing conditions are used the lowest carrier concentrations are typically achieved in films which were deposited with relatively high bias voltages.

3.4.2 ANNEALING OF FILMS DEPOSITED WITHOUT (OR ZERO) SUBSTRATE BIAS.

3.4.2.1 Isothermal Annealing with 3%, 4%, 6%, and 10% Metal-Rich $Pb_{1-x}Sn_xTe$ Charges. As discussed above, one of our early annealing studies involved the systematic investigation of the effects due to the degree of metal richness of the annealing charge. The objective, of course, was the optimization of annealing conditions for achieving the best electrical properties. The experiments performed initially utilized 3% and 10% metal rich $Pb_{1-x}Sn_xTe$ charges; however, those initial studies revealed some differences in results between the 3% and 10% metal-rich charges. In order to evaluate these differences and provide a more reliable interpretation, charges with intermediate levels of metal-richness were also introduced. These included 6% and 4% metal-rich charges.

Typical results from some isothermal annealings in 3%, 4%, 6% and 10% metal-rich charges, performed in the course of this program, are presented in Tables 17 - 19 and Figures 3-77 thru 3-83. Tables 17 thru 19 present the data on structure, composition, annealing conditions as well as the unannealed and annealed electrical properties. As noted in these tables, all as-deposited films used in these experiments were initially p-type with similar as-deposited properties. We consider first Figure 3-77 which presents the $88^{\circ}K$ carrier concentrations of films with three different compositions as a function of annealing temperature (Table 17). As noted, these films were all annealed utilizing the 3% metal rich charges. As also noted the electrical measurements on these earlier samples were made to $88^{\circ}K$ only, due to limitations of the dewar at the time. Subsequent samples were all routinely measured to $77^{\circ}K$. As can be seen in Figure 3-77, the behaviour of carrier concentration as a function of temperature is quite consistent with bulk crystal behavior. For each composition, we find that the films remain p-type at the highest annealing temperatures. As the annealing temperature is decreased the p-type carrier concentration also decreases. At a critical annealing temperature, which

3-145
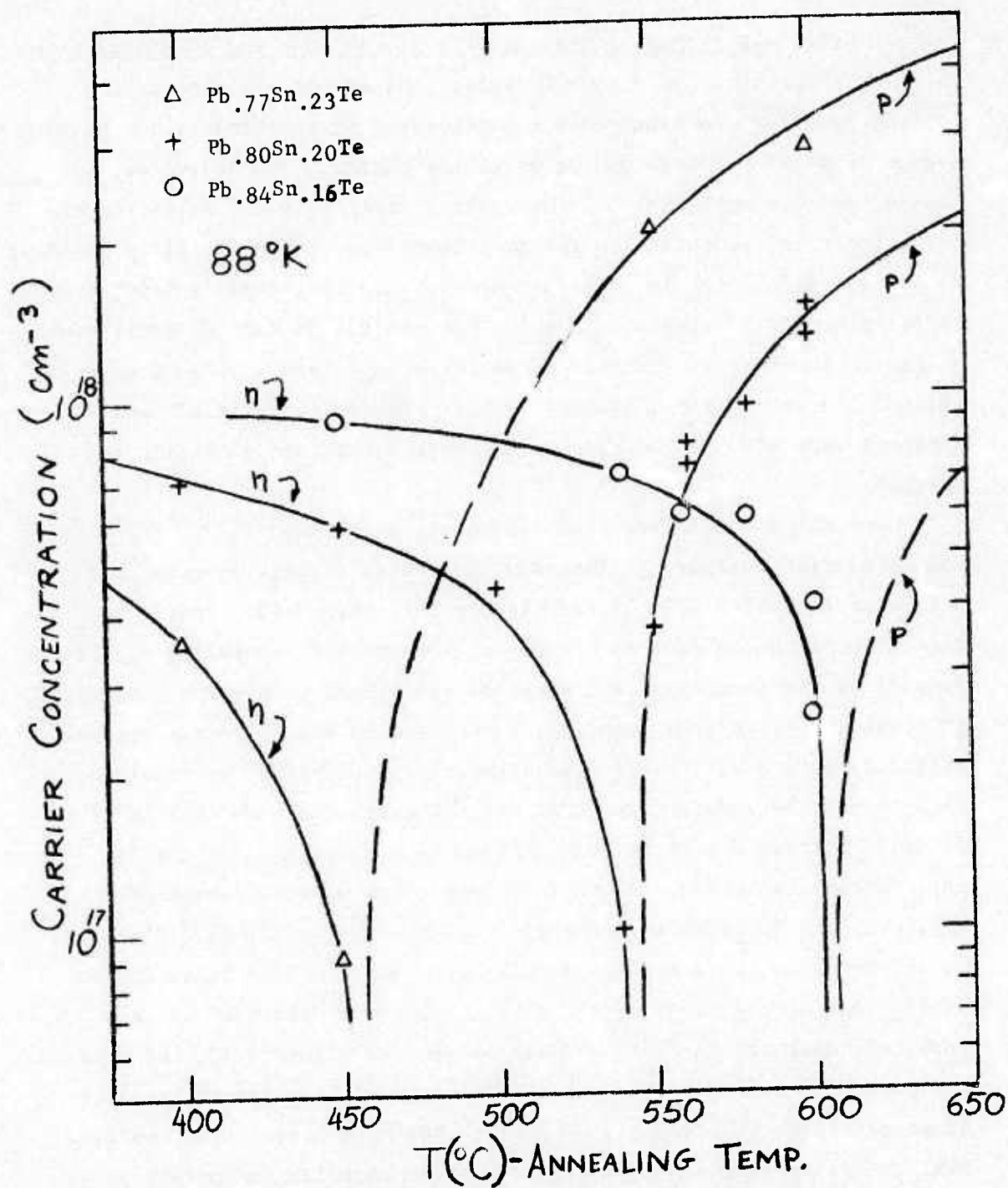
Figure 3-77 Isothermal Annealing Results in 3% Metal Rich Charge
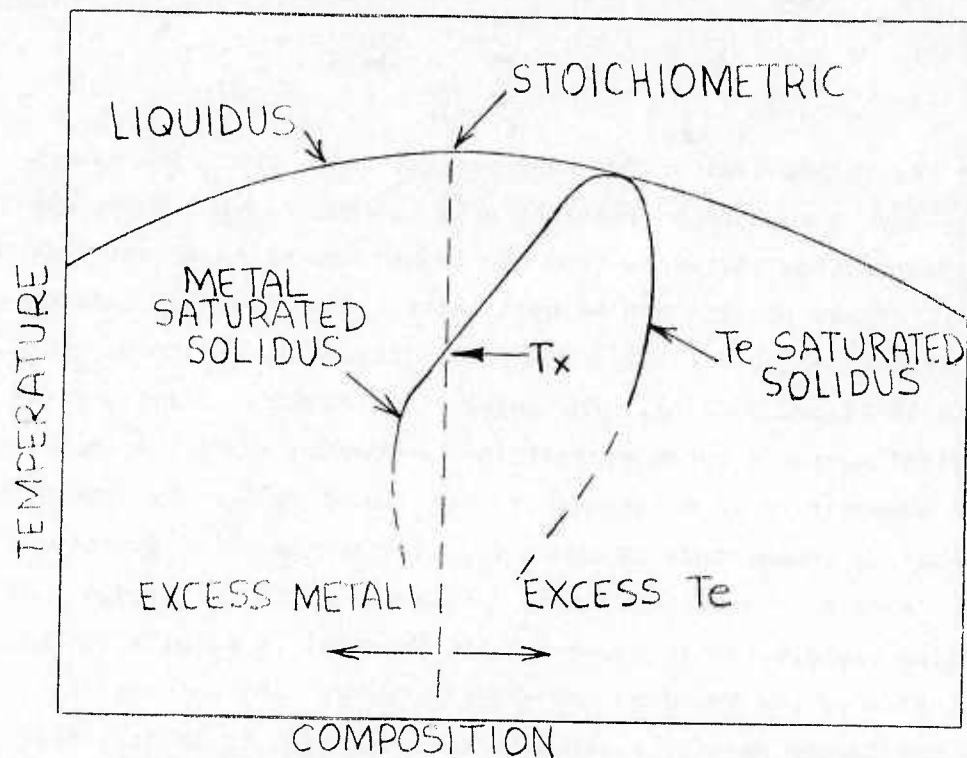
Figure 3-78(a) Schematic of the Equilibrium Phase Diagram of $Pb_{1-x}Sn_xTe$ Alloy Near the Stoichiometric Composition
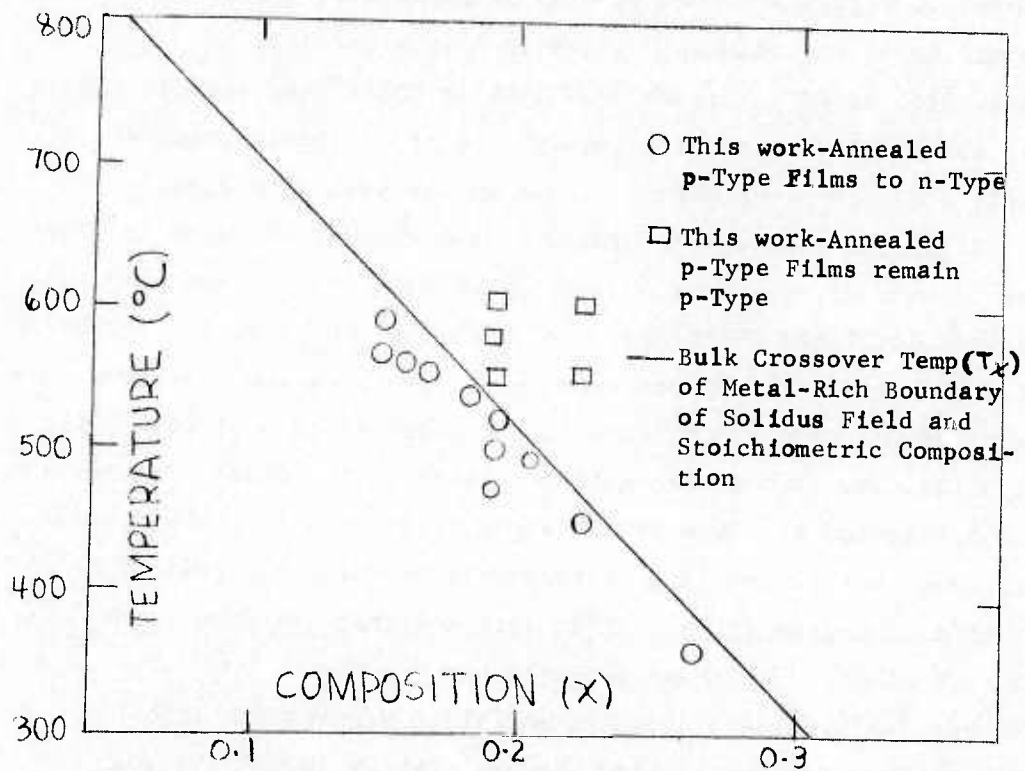
Figure 3-78(b) Annealing Temperature vs. Composition for the Characterization of Carrier Type in $Pb_{1-x}Sn_xTe$ Annealed in Metal-Rich Charge

depends on the composition of the as-deposited film, the films switch
to n-type. As the annealing temperature is further reduced the n-type
carrier concentration increases from the rather low value at the switching
temperature. These results can be qualitatively explained by reference
to the generally accepted equilibrium phase diagram for bulk $Pb_{1-x}Sn_xTe$
illustrated in Figure 3-78(a). The metal rich boundary of solidus field
for a material having a given composition is seen to cross the stoi-
chiometric composition at a temperature designated as T_x. We note that
if the annealing temperature is above T_x, the material will anneal on
the Te rich side of the boundary and, consequently, remain p-type. If
the annealing temperature is below T_x, the material is annealed to the
metal rich side of the boundary and exhibits n-type characteristics.
To obtain the lowest carrier concentrations possible, it is desirable
to anneal as close to T_x as possible. Thus, the switching or crossover
temperatures in Figure 3-77 can readily be assumed to correspond to the
T_x temperatures in the schematic given in Figure 3-78(a).

As we also noted in Figure 3-77 (but is not illustrated in Figure
3-78(a)), the critical switching temperature or crossover temperature
is a function of film composition. This can be seen more clearly in
Figures 3-78(b) which plots the crossover temperature observed in films
by us and in bulk by others as a function of film composition. This
plot has been developed on the basis of bulk $Pb_{1-x}Sn_xTe$ data. The solid
line for bulk annealing data was obtained by plotting the crossover tem-
peratures from Reference 23 (Figure 13 and Table IV in Reference 23)
shown as a function of the composition. Based on the phase diagram, any
composition annealed at temperatures above the solid line should result
in p-type films while annealing at temperatures below the solid line
should result in n-type films. It is apparent that the data points from
our film work concur with these predictions.

Figures 3-79 and 3-80 show the annealing effects for films
annealed with 4% and 6% metal-rich charges (Tables 18 and 19) and
deposited from Target #2 to #7. Here the 77^OK carrier concentrations
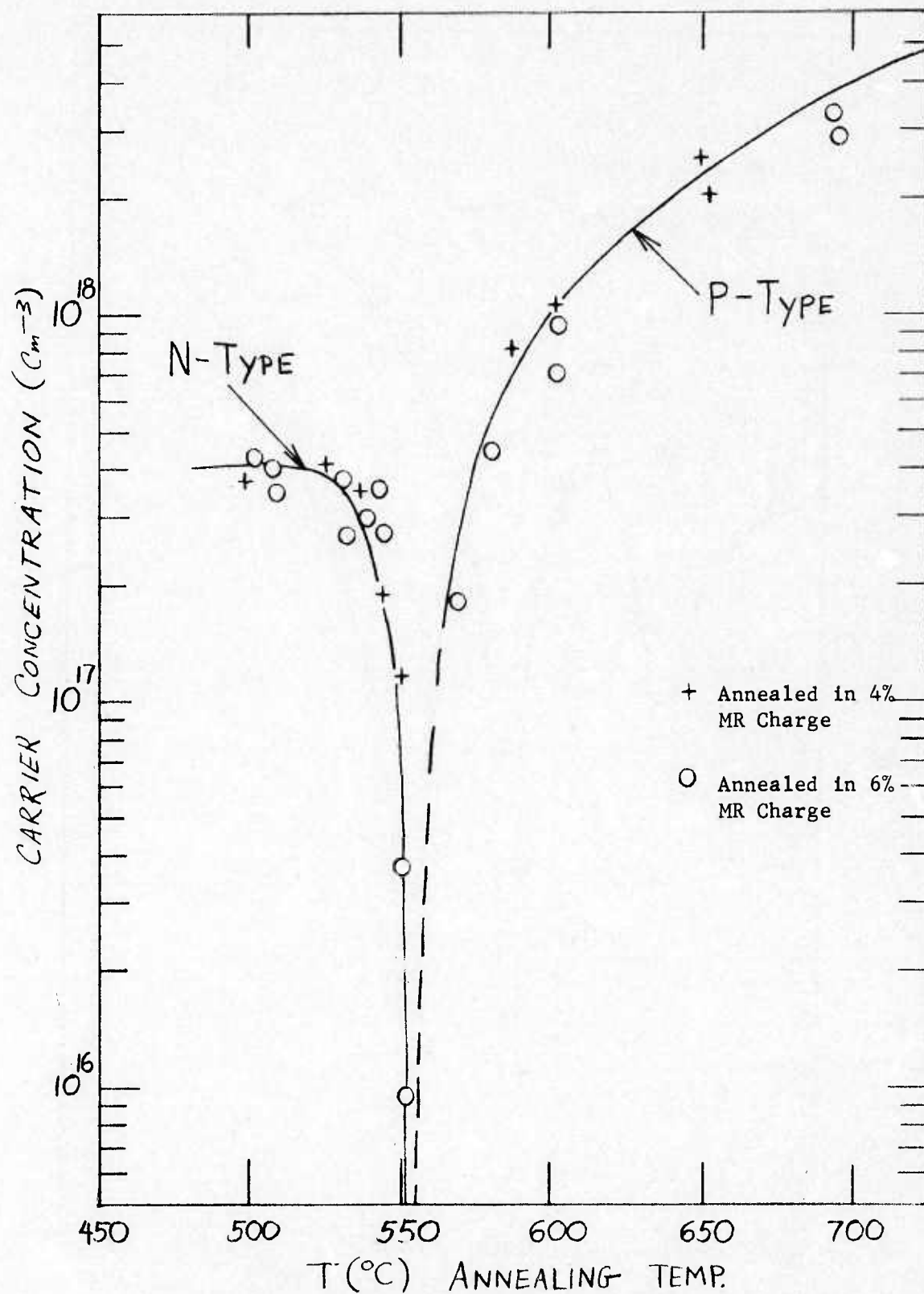
Figure 3-79 Isothermal Annealing Results in 4% and 6% Metal Rich Charge - Pb$_{.81}$Sn$_{.19}$Te Film

3-149
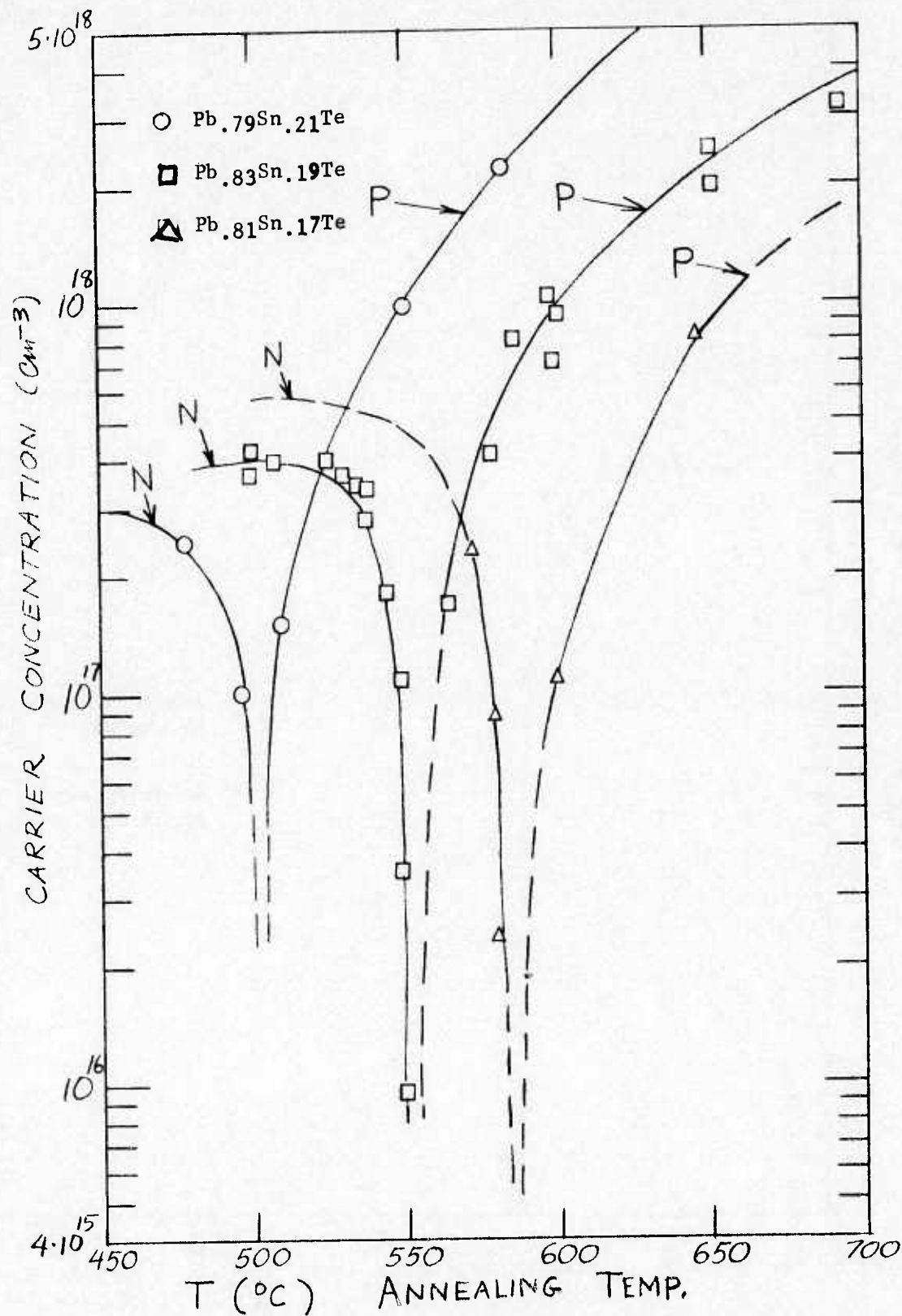
Figure 3-80 Isothermal Annealing Results in Metal Rich
Pb$_{1-x}$Sn$_x$Te Charges (4% and 6%)
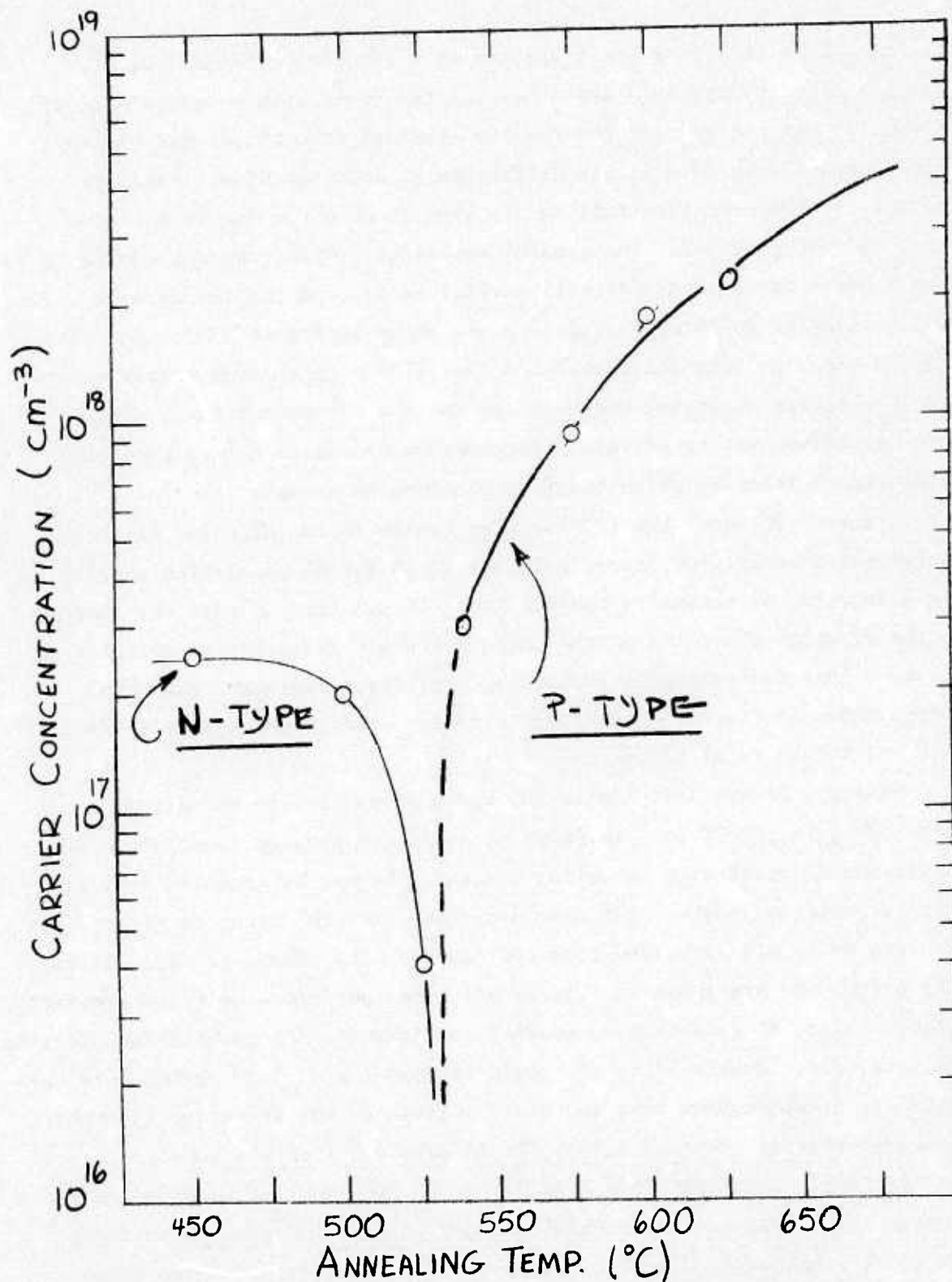
Figure 3-81 Isothermal Annealing Results for Single Crystal
Pb$_{.80}$Sn$_{.20}$Te Film Deposited at Zero Bias (Target
#8) 6% Metal Rich Annealing Charge

3-151

of $Pb_{1-x}Sn_xTe$ films are again plotted as a function of annealing temperature. Figure 3-79 shows results for films with a composition of x = 0.19. As can be seen the results obtained with the 4% and 6% metal-rich charges show very little difference in behavior, i.e., the data points for the two cases fall on the same trend curve for both the p-type and n-type films. The general annealing temperature dependence is again quite consistent with bulk crystal behavior as in the case of films annealed in 3% metal-rich charges shown in Figure 3-77. For this composition, we note again that the initially p-type films remain p-type at the highest annealing temperatures but the p-type carrier concentration decreases as the annealing temperature decreases toward a critical temperature value at which the film switches to n-type.

Figure 3-80 shows the 77°K carrier concentration of films of three different compositions, annealed again in 4% and 6% metal-rich charges, as a function of annealing temperature. It is observed that the temperatures at which the films of the three different compositions switch from p- to n-type decrease with increasing x-values, consistent with the trend shown in Figures 3-78(b) and are also independent of the difference (4% and 6%) in metal richness.

Finally, Figure 3-81 (Table 20) again shows similar annealing data for a $Pb_{.80}Sn_{.20}Te$ film, deposited later in the program from Target #8, utilizing 6% metal-rich annealing charges. As may be recalled from an earlier section, most of the work performed with the later targets (i.e. Targets #8 to #13) involved bias sputtering. Therefore, the annealings, for which data are shown in Figure 3-81, were performed on films deposited without bias, a) to determine whether consistency with results from earlier targets (i.e. Targets #2 to #7) could be found, and b) to establish a baseline for disseminating bias and other effects on the annealing behavior of more recently prepared films. As is apparent from the results in Figure 3-81, films sputtered from Target #8 (and for Target #9 to be presented later) are equally consistent with bulk PbSnTe crystal behavior as those prepared from earlier targets. The critical annealing temperature of about 530°C (i.e. the temperature at which the p-type film switches

to n-type) agrees, for the given composition, with the bulk crossover
temperature obtained from the equilibrium phase diagram and shown in
Figure 3-78(b).

Whenever annealing of $Pb_{1-x}Sn_xTe$ films is required to achieve
the desired properties, the type of data presented in this section
provides an excellent tool for selecting metal-rich annealing condi-
tions, for any film composition, which result in a reduction of
carrier concentration with or without changing the carrier type.
Reference to Figures 3-77 to 3-81 and Tables 17 to 20 shows that
utilizing 3%, 4%, and 6% metal-rich charges yields annealed sputtered
n-type films with significantly reduced carrier concentrations (e.g.
2×10^{16} to 9×10^{15} cm^{-3}). Such results are, of course, only possible
by using the systematic experimental approach which defined the cri-
tical switching temperatures with considerable degree of accuracy for
each film composition explored. It should be noted, however, that
improvement in annealed carrier concentrations was realized also as we
progressed into the program (i.e. with time). These lowered carrier
concentrations should, in addition, be the result of some of the opti-
mized annealing procedures which were gradually introduced. For example,
quenching speed after annealing as well as annealing times were inves-
tigated. Results of these investigations will be discussed in more
detail below. However, they are reflected to some degree in Tables 17,
18, and 19, with the data in the latter indicating the use of longer
annealing times and faster quenching conditions.

As discussed at the beginning of this section, early annealing
studies revealed some differences in results between the 3% and 10%
metal-rich charges. First, it had been observed that films annealed
in 10% metal-rich charges had consistently higher mobilities for the
same carrier concentrations than films annealed in 3% metal-rich charges.
Secondly, the observed crossover temperature (i.e. T_x in Figure 3-78(a))
for films annealed in the 10% metal-rich charges was different from
that expected from the equilibrium phase diagram and from other films

annealed with 3% metal-rich charges. Reference to Table 21 which presents some annealing results obtained with the 10% metal-rich charges shows qualitatively the effects discussed above. Although, as Table 21 shows, the 10% metal-rich annealing results are by no means as extensive as may be desired, they are adequate to demonstrate the effects. We note that annealing temperatures investigated were for the most part restricted to $600^{o}C$. One reason for this is that for all film compositions utilized ($0.16 \leq x \leq 0.22$), annealed with a 10% metal-rich charge produced exclusively n-type films, although the starting as-deposited films were p-type to begin with. Reference to Figure 3-78(b) shows that for a film with $x = 0.16$, a metal-rich anneal at $600^{o}C$ could change the film from p- to n-type since $600^{o}C$ is very close to the crossover temperature. However, for a film with $x = 0.20$, a change from p- to n-type would not be expected.

The reasons why a 10% metal-rich charge would change the crossover temperatures for a given film composition are not apparent. However, we considered the possibility that the speed of sample quenching on completion of the annealing run may be a factor since if the film is quenched too slow, it may remain sufficiently long below the crossover temperature for n-diffusion to take place. Thus it has become apparent that one should avoid the slow cooling process. To do this, as well as to try to resolve the unexplained results with the 10% metal-rich charges, various quenching procedures were compared. For example, Entry #1 in Table 21 corresponds to an annealed $Pb_{.84}Sn_{.16}Te$ film on BaF_2 which was air quenched after annealing while Entry #6 corresponds to a similar film on CaF_2, which was exposed to a more rapid water quench. As noted both films were annealed under the same conditions. However, the air-quenched films yielded a higher carrier concentration than those exposed to the more rapid water quench. Comparison of Entries #3 and #10 illustrates the same phenomenon. Still, even with the faster water quench, the change from p- to n-type persists.

Most of the examples in Table 21 which are denoted as "air quenched" correspond to films on BaF_2 substrates. The reason is that BaF_2 substrates cracked readily on fast quenching in our original set-up. CaF_2, on the other hand, could be quenched very rapidly without exhibiting thermal shock failure. Some redesign of our annealing ampoules to allow for a more uniform and faster heat dissipation from the substrate overcame this problem. Indeed it was possible to utilize an even faster quenching procedure: a combination of LN_2/water quench. Results with this faster quenching procedure are included in Table 21 and, as noted, the switching from p- to n-type at higher temperatures than expected still persisted. This behavior which appears to be related to charge composition rather than annealing conditions can also be seen on comparing some of the results in Table 21 for 10% metal-rich charges with those shown in Table 19 for 6% metal-rich charges. For example, films of composition x = 0.19 annealed with the 6% metal-rich charge at temperature of 700, 600 and 570°C followed by H_2O quenching remain p-type while those with the same x-value, annealed under the same conditions, with the 10% metal-rich charge change to n-type. This type of result has been observed repeatedly; the observation, therefore, appears valid. Explanations of these observations are not apparent at this time.

We refer to the results presented in Table 21 for 10% metal-rich anneals along with results for the 3%, 4% and 6% metal-rich anneals presented in Tables 17 to 20 to answer still another question in connection with the 10% metal-rich anneals. The question concerns the initially observed higher mobilities measured in films annealed with 10% metal-rich annealing charges as compared to the mobilities measured in films annealed with the 3% metal-rich charges. That is, are the mobilities measured in films annealed with the 4% and 6% metal-rich annealing charges consistent with these measured in the 10% metal-rich annealed film or 3% metal-rich annealed films? The results illustrated in Figures 3-82 and 3-83 show that the differences between the electrical
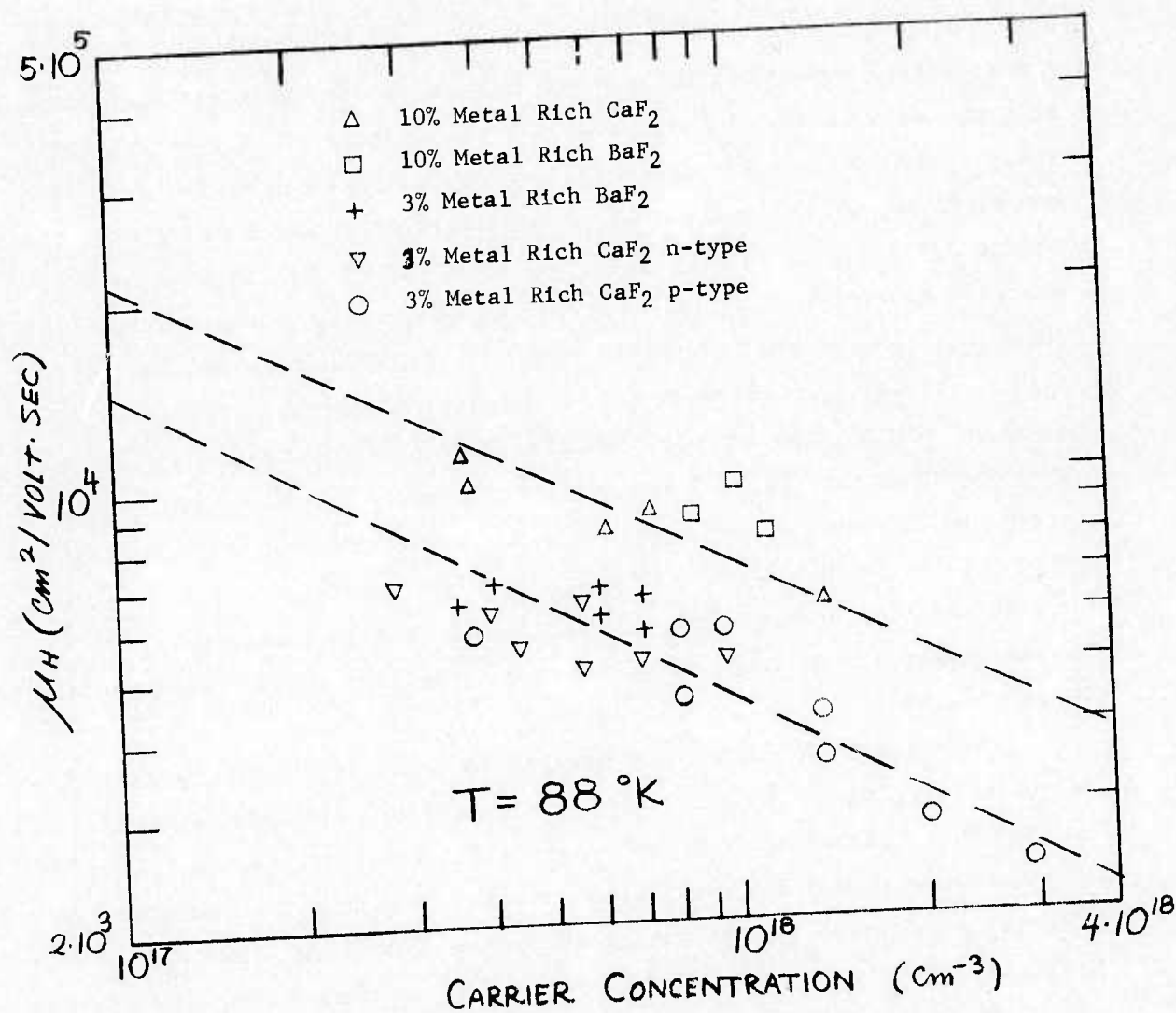
Figure 3-82 Isothermal Annealing Results - Electrical Properties of $Pb_{1-x}Sn_xTe$ Films Annealed in 3% and 10% Metal Rich Charges
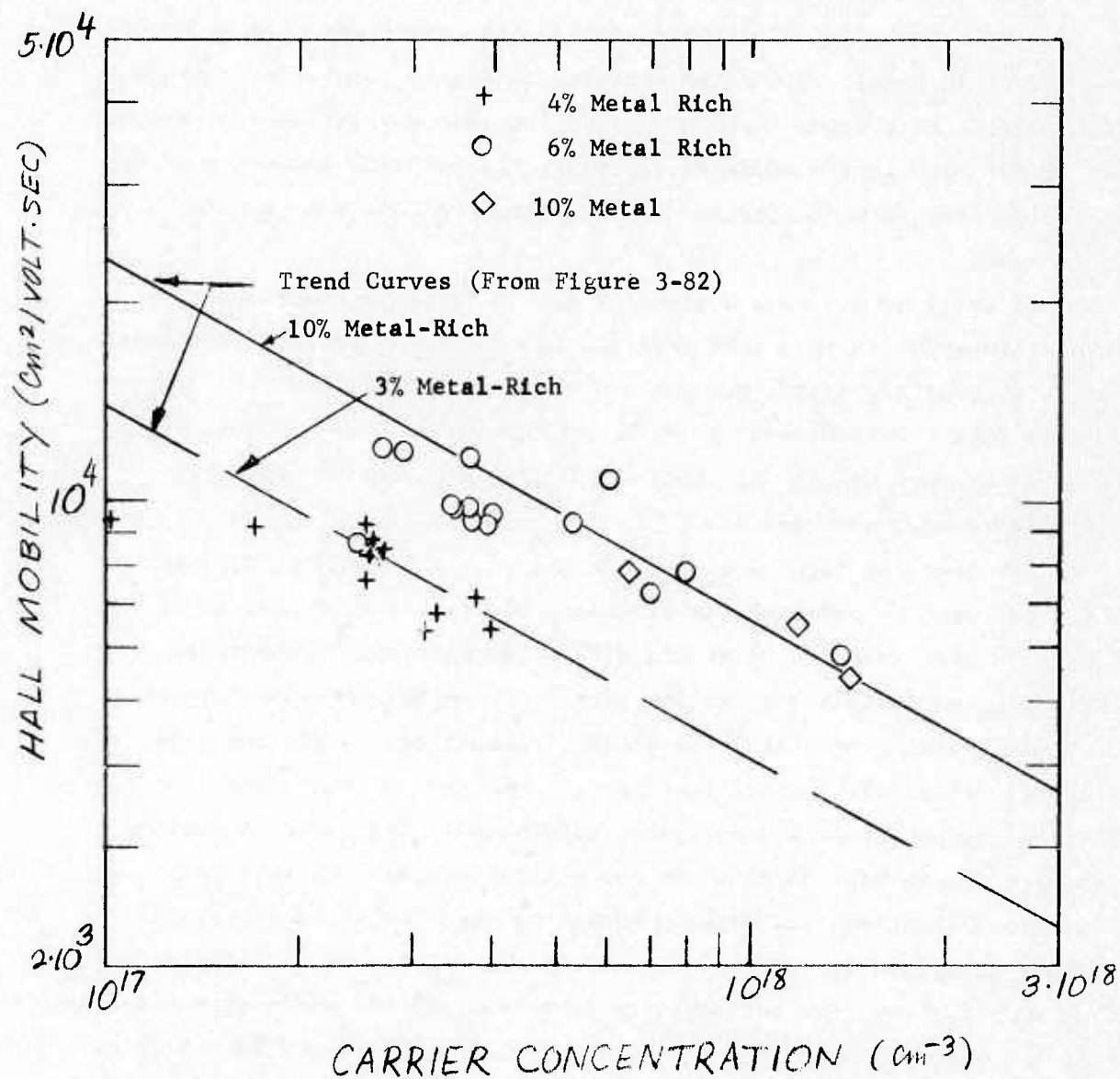
Figure 3-83 Electrical Properties of $Pb_{1-x}Sn_xTe$ Films Isothermally Annealed in 4%, 6%, and 10% Metal Rich Charges

properties of films annealed in low (to 4%) and in high (6% and 10%)
metal-rich charges persist. Figure 3-82 shows some of the earlier
results obtained with 3% and 10% metal-rich charges while Figure 3-83
shows similar data for the 4%, 6% and additional 10% metal-rich charges
investigated. All annealing conditions utilized for the data in Figure
3-83 were identical. The films annealed in highly metal-rich charges
show considerably higher mobilities for the same carrier concentration.
Still, for both levels of metal-richness, the mobility shows the syste-
matic increase with decreasing carrier concentrations expected for
$Pb_{1-x}Sn_xTe$.

We still do not have a specific answer for this behavior but it
is also apparent in this case that the degree of charge metal-richness
is the controlling factor and not the annealing conditions. In spite
of this lack of understanding, this empirical information should be of
value in the preparation of films for device application where high
mobility is always of value.

The next two figures illustrate one of the systematic approaches
which was used to optimize the annealing cycle. As discussed above we
had found that annealing time did affect the electrical properties.
Therefore, an optimized annealing time (i.e. optimized to achieve the
best electrical properties) was sought. Specifically, Figures 3-84
and 3-85 illustrate typical results on the effect of annealing time on
carrier concentration and mobility, respectively (all other annealing
parameters were kept constant in these experiments). We note from
Figure 3-84 that the increase in annealing time (or added annealing
cycles) continuously reduced the carrier concentration. Similarly
Figure 3-85 shows that the mobility increases significantly with annealing
time but seems to reach a limiting value of about 15 hours beyond which
the mobility decreases. Since further investigations of the effects of
annealing times on electrical properties with other annealing charges
showed similar results, an annealing time between 15 hours and 20 hours
was adopted as optimum for most later work. In addition, annealing times

Annealing Temp. 600°C

CARRIER CONCENTRATION (Cm^{-3})

$4 \cdot 10^{18}$

10^{18}

10^{17}

$5 \cdot 10^{16}$

0   10   20   30   40

ANNEALING TIME (HOURS)
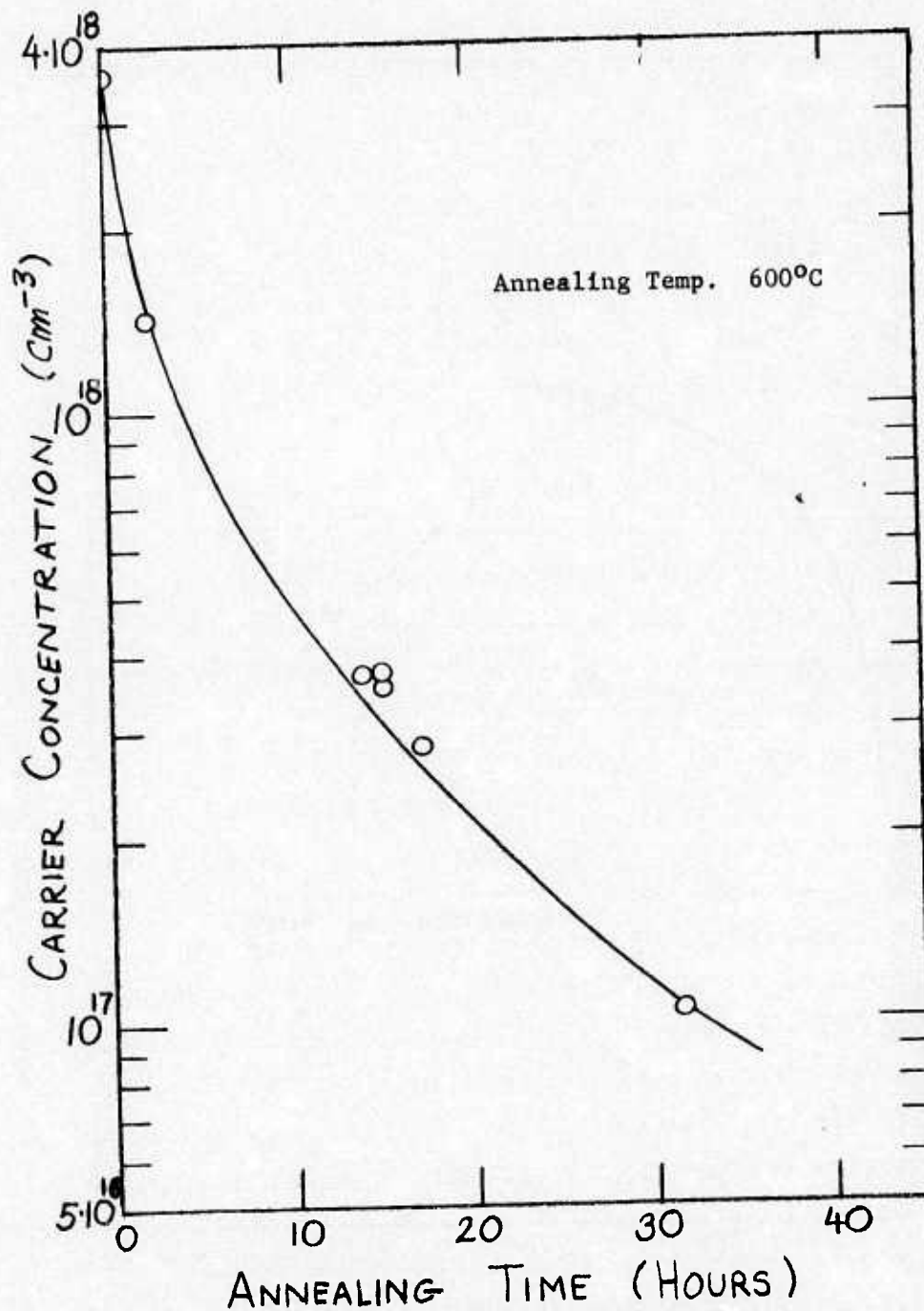
Figure 3-84 Some Results on Isothermal Annealing of (111) $Pb_{1-x}Sn_xTe$ Films in a 10% Metal Rich Charge - Carrier Concentration vs. Annealing Time
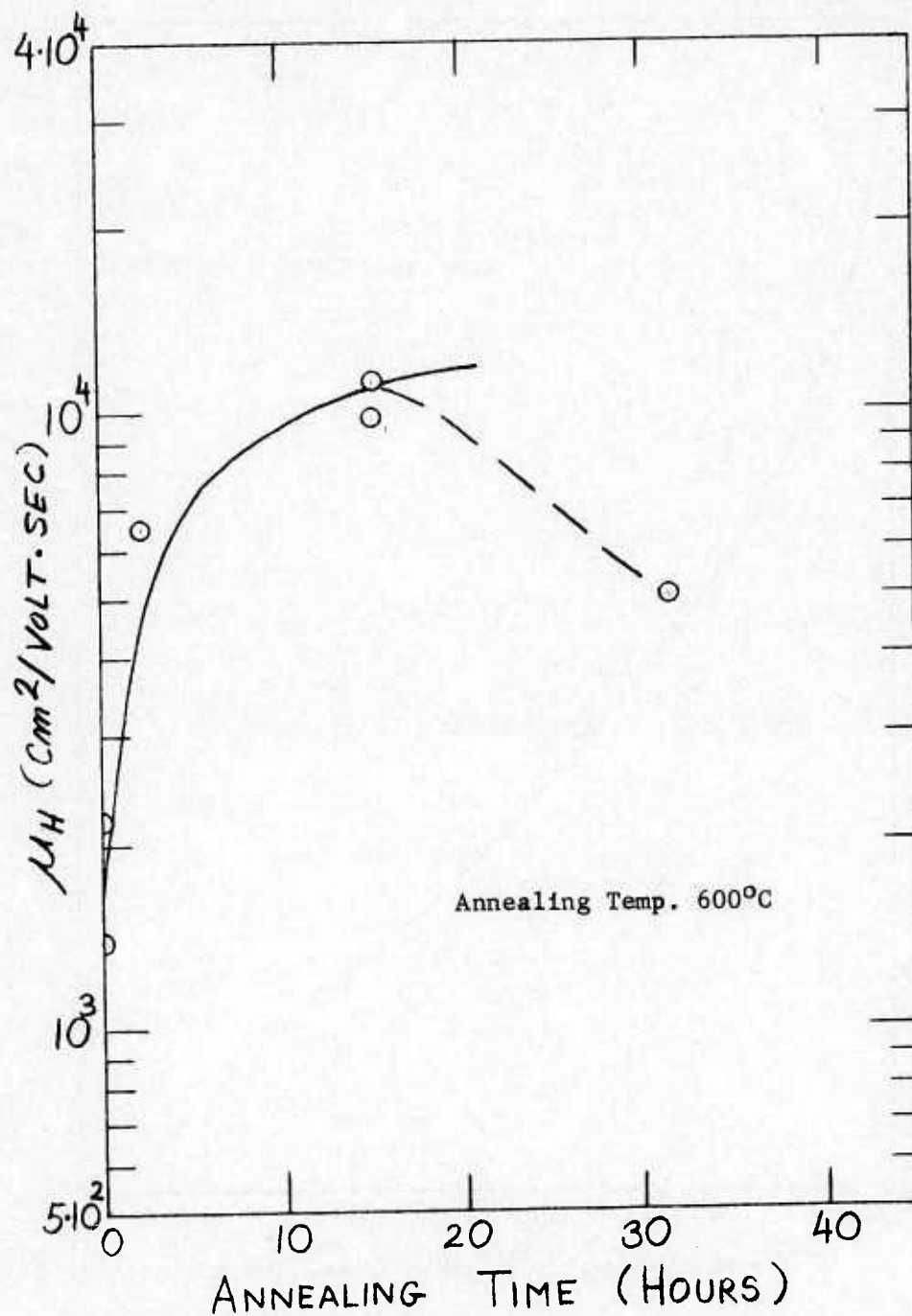
Figure 3-85: Some Results on Isothermal Annealing of $Pb_{1-x}Sn_xTe$ Films in a 10% Metal Rich Charge - Mobility vs. Annealing Time

were optimized for the more complex annealing cycles such as the final low temperature annealing cycles for carrier type control.

The improvement in film quality on annealing is also apparent in the results on the temperature dependence of electrical properties in annealed films. Figures 3-86 through 3-95 illustrate data on temperature dependence of electrical properties of typical films annealed with the metal-rich $Pb_{1-x}Sn_xTe$ charges just discussed. For example, Figure 3-86 shows the temperature dependence of mobility and Hall coefficient for an as-deposited p-type $(Pb_{.84}Sn_{.16}Te)$ film before and after annealing in a 3% metal-rich charge (see Table 17 for actual data points). Reference to Figure 3-78(b) shows that for a film with $x = 0.16$, the annealing temperature of $580^{o}C$ is below the crossover temperature so that the carrier type of the annealed film should be n-type. This is, of course, confirmed by the data (note also from Figure 3-78(a) as well as Figure 3-77 that annealing of this film at $600^{o}C$ should have produced a considerably lower carrier concentration than that obtained at $580^{o}C$ with a corresponding potential increase in mobility).

The results in Figure 3-86 demonstrate again the typical annealing effects in sputtered films. Aside from the mobility increase, a substantial increase in R_H or reduction in carrier concentration (since $R_H = -(ne)^{-1}$) occurs. The temperature dependence of mobility for the 3% metal-rich annealed films still shows some deviation from the $(1/T)^{5/2}$ relation at low temperature, i.e., some kind of low temperature scattering still persists after this particular annealing process. However, we have already seen that improvements in mobility in annealed films was possible by changing the concentration of the excess metal in the annealing charge (e.g. using 10% and 6% metal-rich annealing sources) and by increasing the annealing time.

Figures 3-87 and 3-88 give a few more examples of annealing results with the 3% metal-rich charges in terms of the temperature dependence of μ_H and R_H which show the criticalness of the annealing temperatures. In
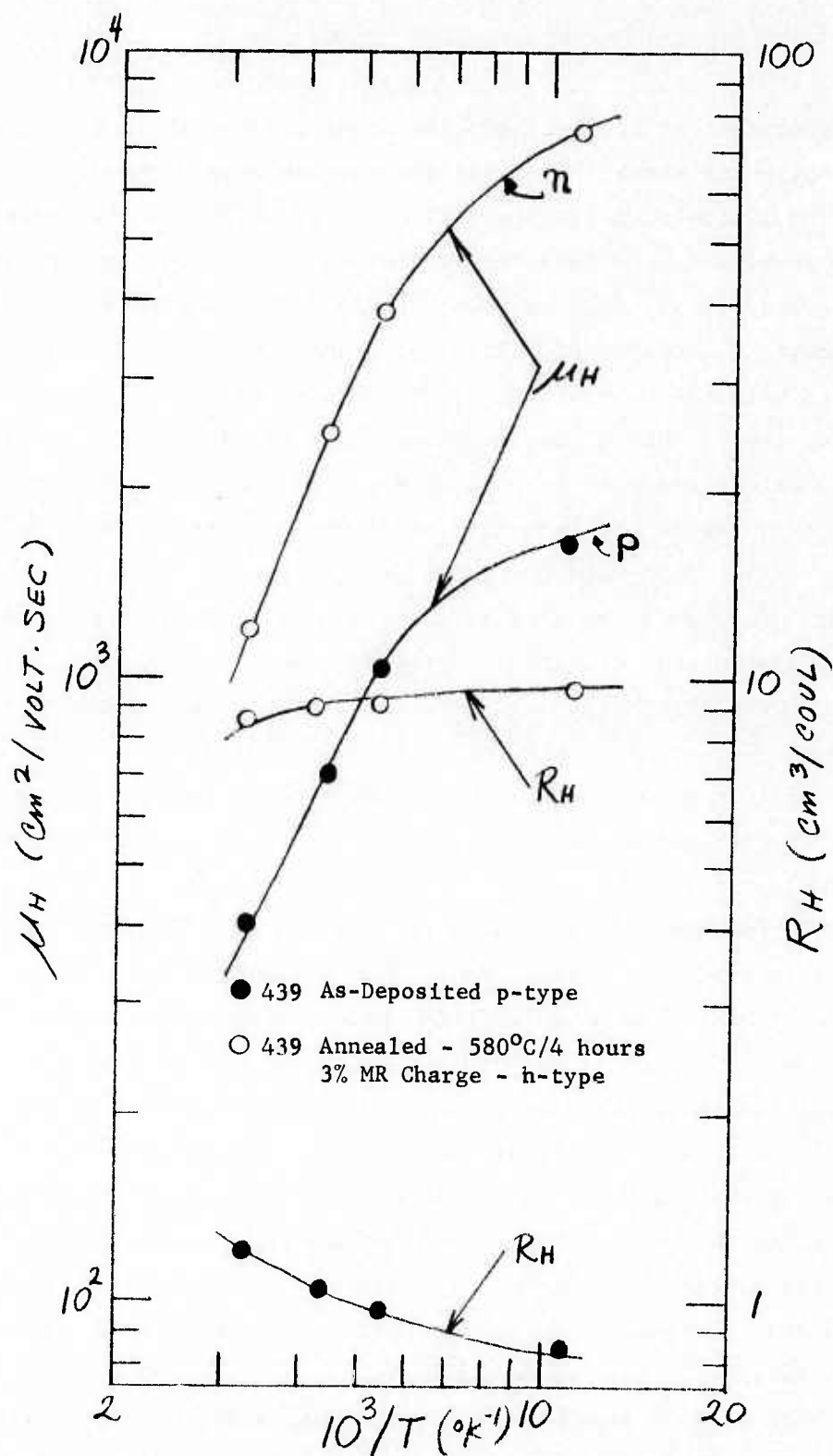
Figure 3-86 Improvement in Electrical Properties of $Pb_{.84}Sn_{.16}Te$ Film Annealed in 3% Metal Rich Charge

3-162
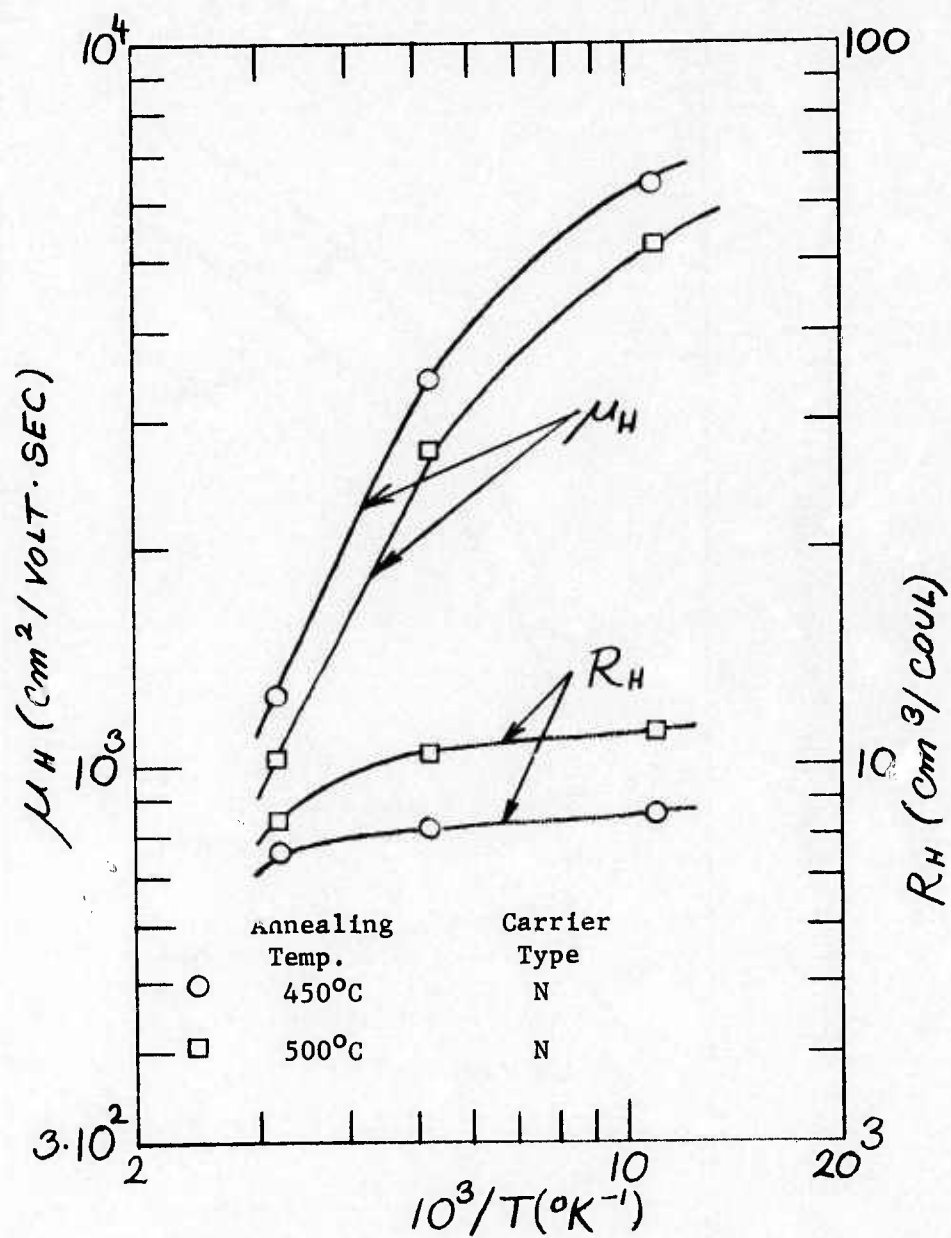
Figure 3-87 Electrical Properties of (111) Pb$_{.80}$Sn$_{.20}$Te Films on CaF$_2$(111) Annealed in 3% Metal Rich Charge
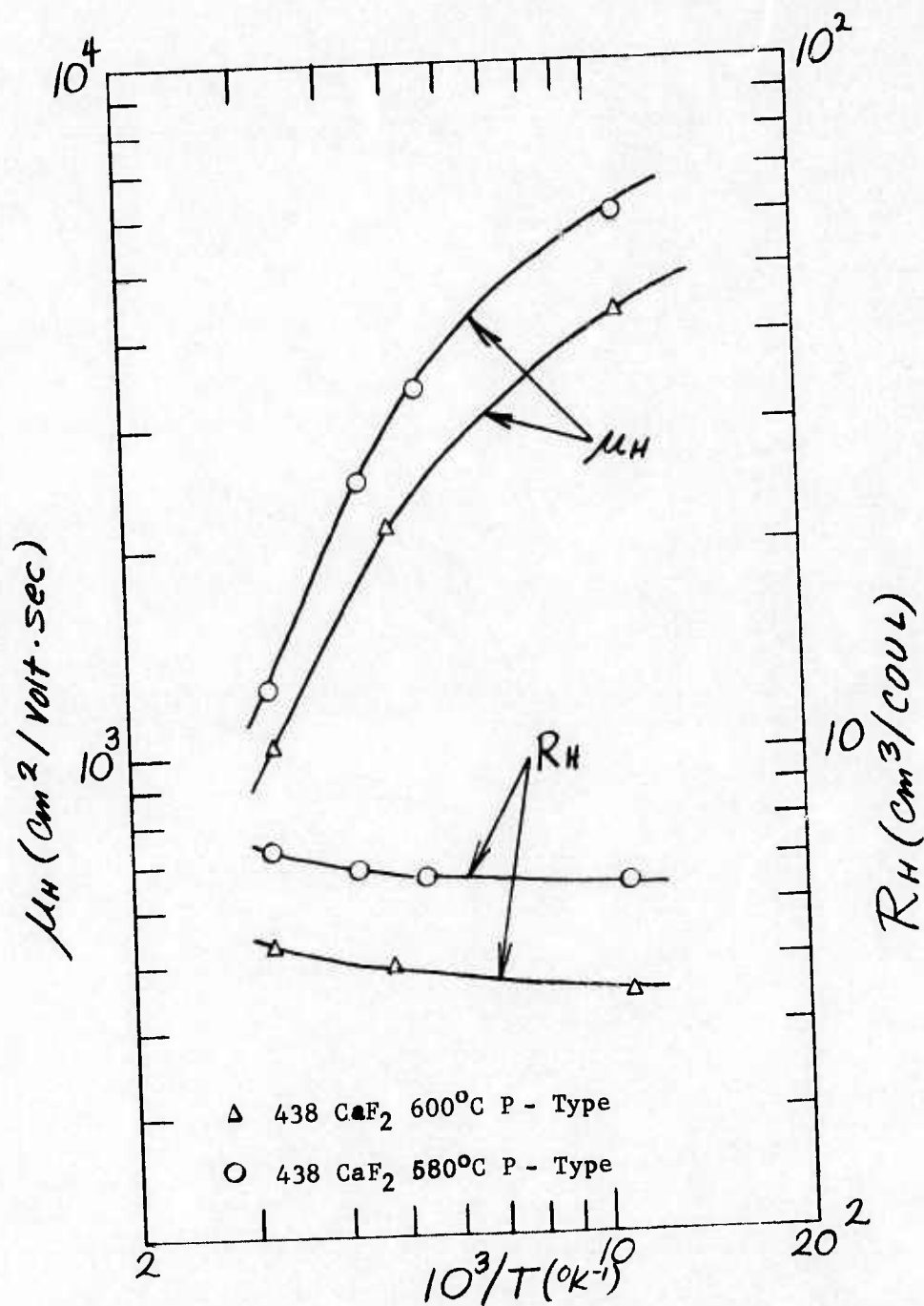
Figure 3-88 Electrical Properties of $Pb_{.79}Sn_{.21}Te$ Films Annealed in 3% Metal Rich Charge

both cases, the as-deposited films were p-type before annealing. In reviewing these figures it is again interesting to evaluate the results in terms of annealing temperature and composition as compared to the various crossover temperatures. This allows for a comparison of the expected with the actual carrier type as well as for an indication of the relative carrier concentration that one can expect at the chosen annealing temperature. For example, Figure 3-87 shows the properties of a film (x = 0.20) annealed at $450^{o}C$ and $500^{o}C$ which as expected (see Figure 3-77) has n-type characteristics and an increase in R_H (or reduction in carrier concentration) as the temperature is increased to $500^{o}C$. Figure 3-88 shows a relatively high temperature annealing result for x = 0.21 films. For both temperatures ($580^{o}C$ and $600^{o}C$) the film remains p-type and, as expected, the lower temperature produces lower carrier concentrations and higher mobilities. These examples, as well as all the other data already shown, demonstrate that the 3% metal-rich annealing results, while not representing the best mobility results that we have seen, do exhibit some rather systematic behavior.

Examples of the significant improvements achieved with the 10% and 6% metal-rich charges are presented in Figures 3-89 and 3-90. In either case, the as-deposited film properties (see Tables 19, 20) were far from the best values achieved (note that the sample designations - e.g. 451 - refer to a set of films prepared under identical deposition conditions rather than to one particular film). Figures 3-89 represents the change due to a 10% metal-rich annealing experiment with a duration of 15 hours at $600^{o}C$, i.e. considerably longer than was used for most 3% experiments.

The more significant change is that observed in Figure 3-90 from a 6% metal-rich annealing experiment. The $88^{o}K$ mobility changed from a value of about 1000 cm^2/V-sec to 12,000 cm^2/V-sec and the carrier concentration from a very high value of 8 x 10^{18} cm^{-3} to the low 10^{-16} range. This is, of course, also an example that includes the improved quenching technique and a more complex annealing cycle. We note also
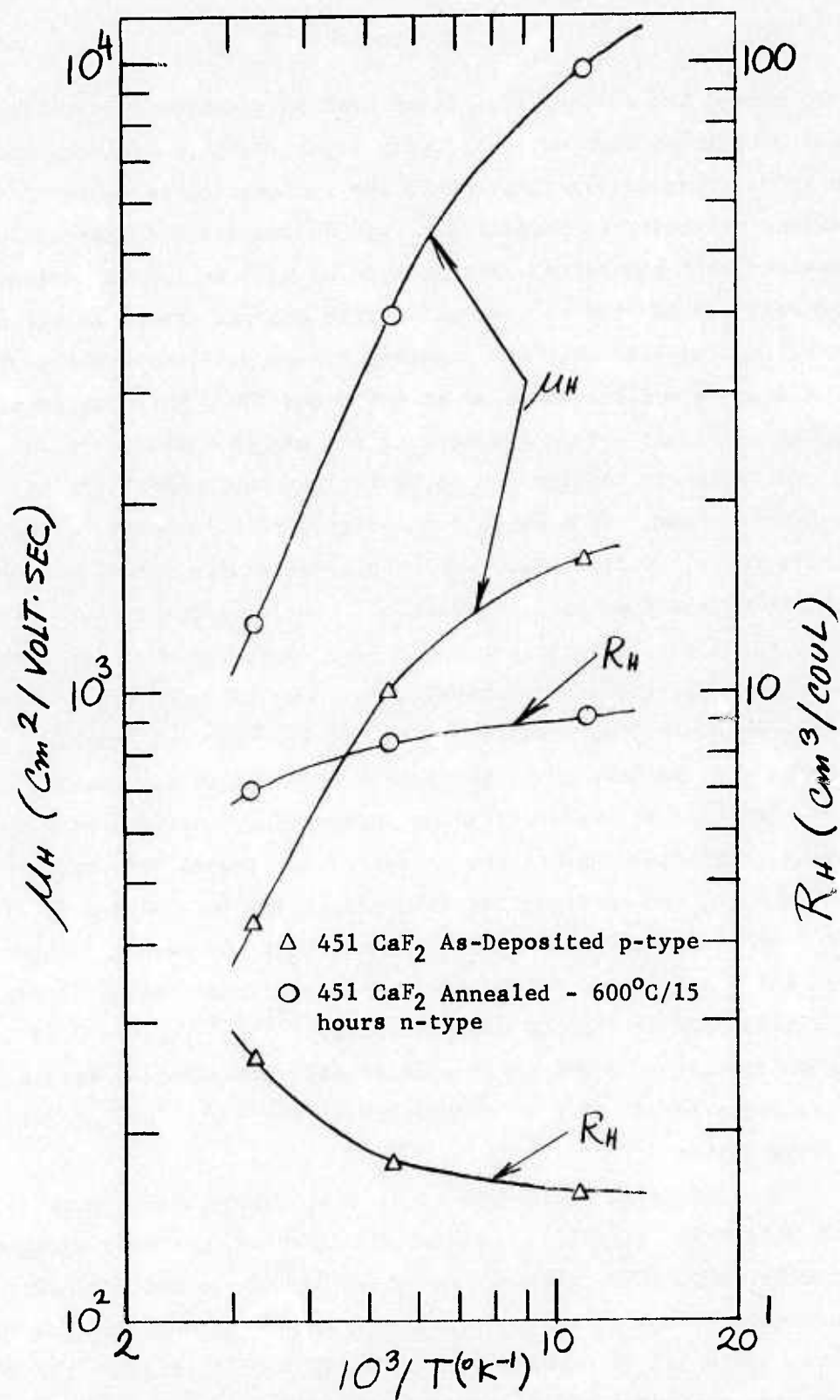
Figure 3-89 Improvement in Electrical Properties of Sputtered
Pb$_{.84}$Sn$_{.16}$Te Film on Annealing in 10% Metal Rich
Charge

3-166
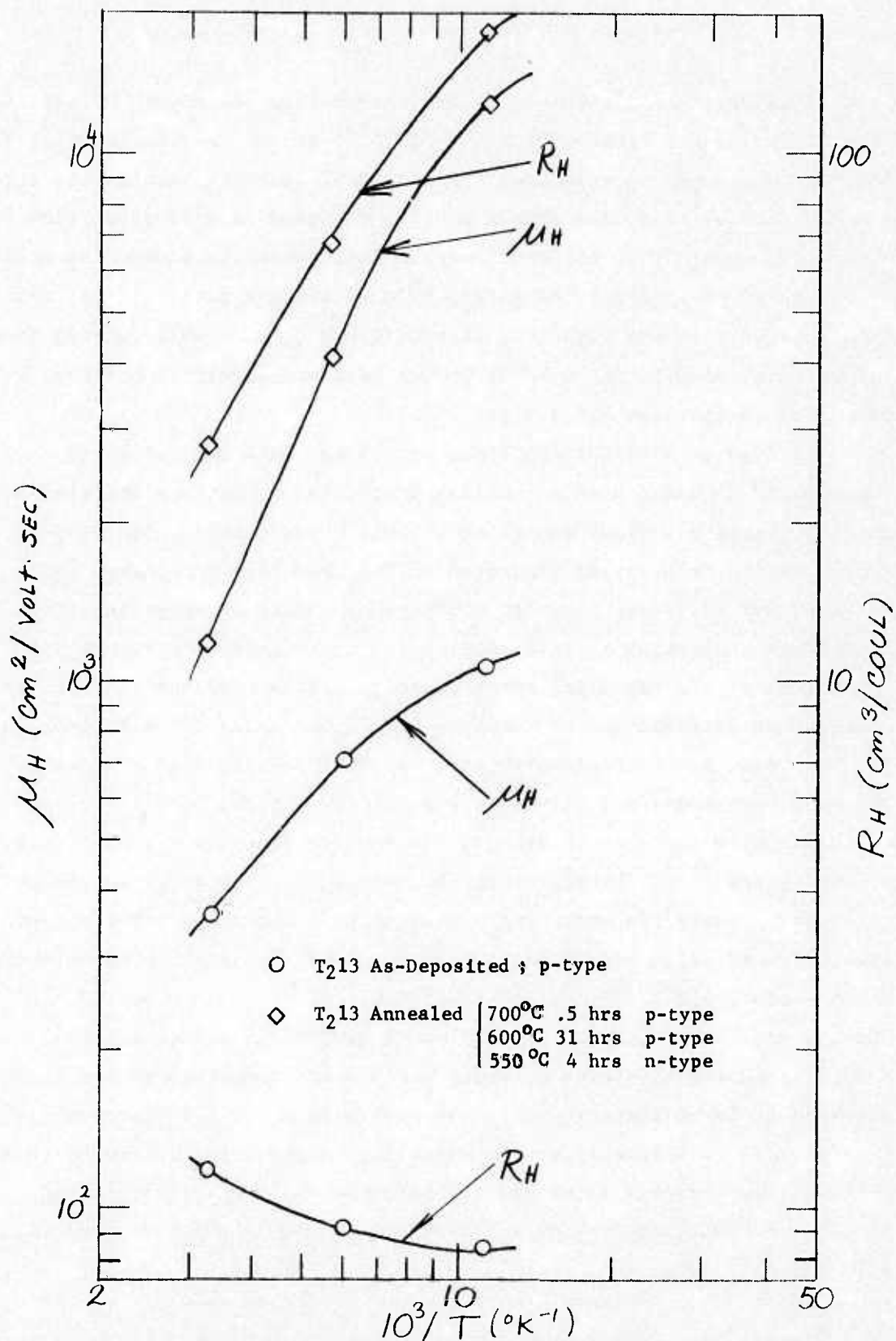
Figure 3-90 Improvement in Electrical Properties of $Pb_{.82}Sn_{.18}Te$
Sputtered Film on Annealing in 6% Metal Rich Charge

in this figure the improvement in the temperature dependence of mobility (i.e., less of a deviation from the $(1/T)^{5/2}$ dependence of the mobility down to the lowest temperature). Figure 3-91 presents results for still another sample, this time with $x = 0.20$, annealed in a 6% metal-rich charge. We again note the considerable improvement in properties achieved by annealing an as-deposited p-type film of average quality (i.e. the as-deposited film was deposited at conditions considerably removed from the critical conditions yielding lowest carrier concentrations that were discussed in Sections 3.2.3.3 and 3.2.4.3).

In Figures 3-92 through 3-95, additional data are presented on temperature dependence of electrical properties of various annealed films which illustrate various annealing effects. For example, Figure 3-92 shows results for samples deposited on CaF_2 and BaF_2 substrates and annealed for different times at 600°C. The effect of annealing times on electrical properties is self-evident in this figure. In Figure 3-93 the effect of the annealing temperature is further explored. Here the temperature dependencies of mobility and R_H are shown for a $Pb_{.81}Sn_{.19}Te$ film annealed at three temperatures, two at which the film remains p-type (as expected for a film of $x = 0.19$) and a third temperature at which the film switches to n-type. As the results show the mobilities of the p-type films increase consistently as the annealing temperature is lowered toward the crossover or switching temperature. The n-type film, also annealed near the switching temperature which apparently lies between 550°C and 570°C, has a higher mobility yet - as expected. Simultaneously the non-phonon scattering mechanisms (deviation from $\mu \sim T^{5/2}$) become effective at lower measurement temperatures for films annealed at lower temperatures. The change in R_H is also interesting. It increases considerably as the annealing temperature is lowered from 600°C to 570°C - that is within the range in which the films remain p-type. However, an even more dramatic increase is observed when the film switches to n-type.
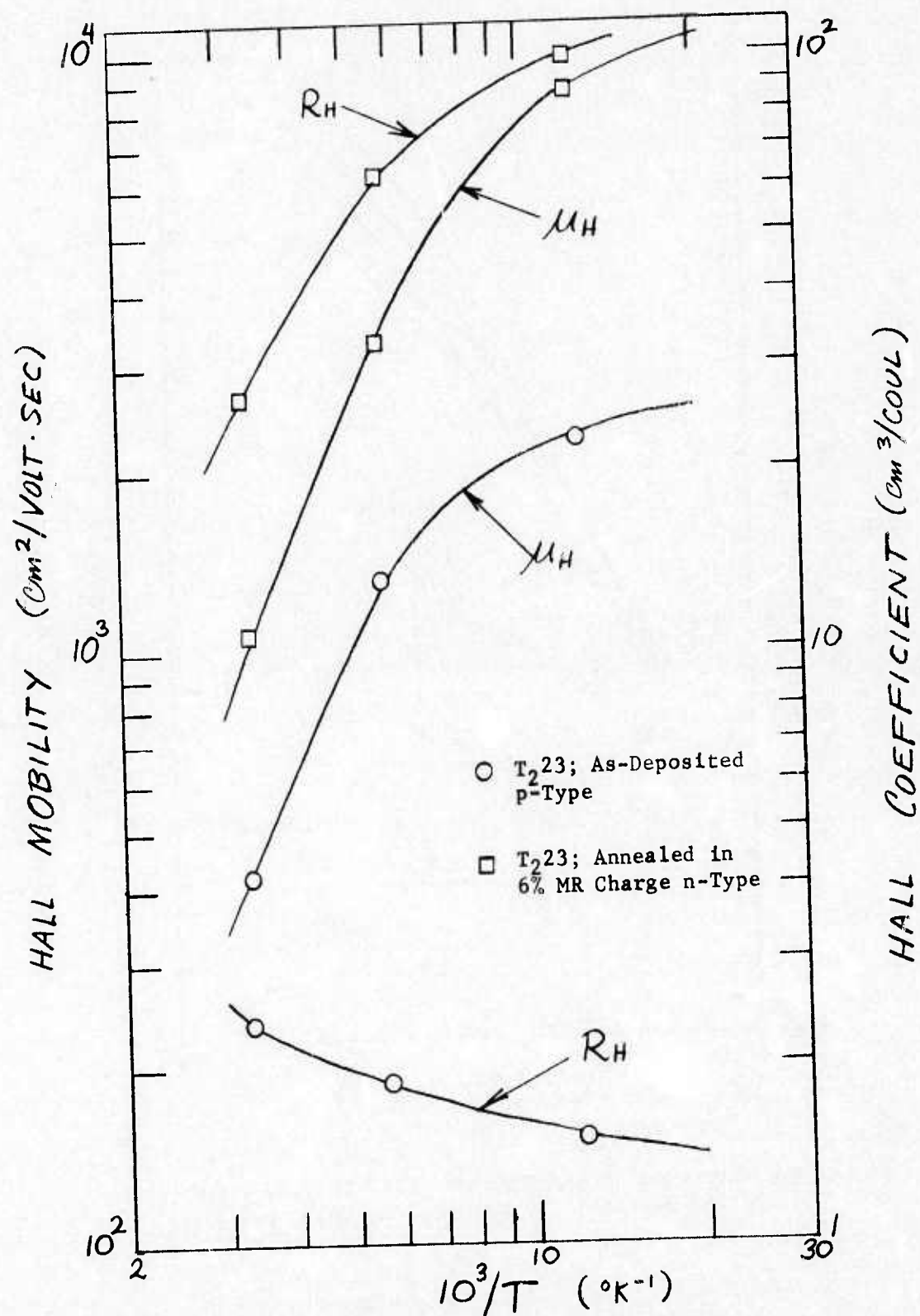
Figure 3-91   Effect of Isothermal Annealing on Electrical
Properties of $Pb_{.80}Sn_{.20}Te$ Film

3-169
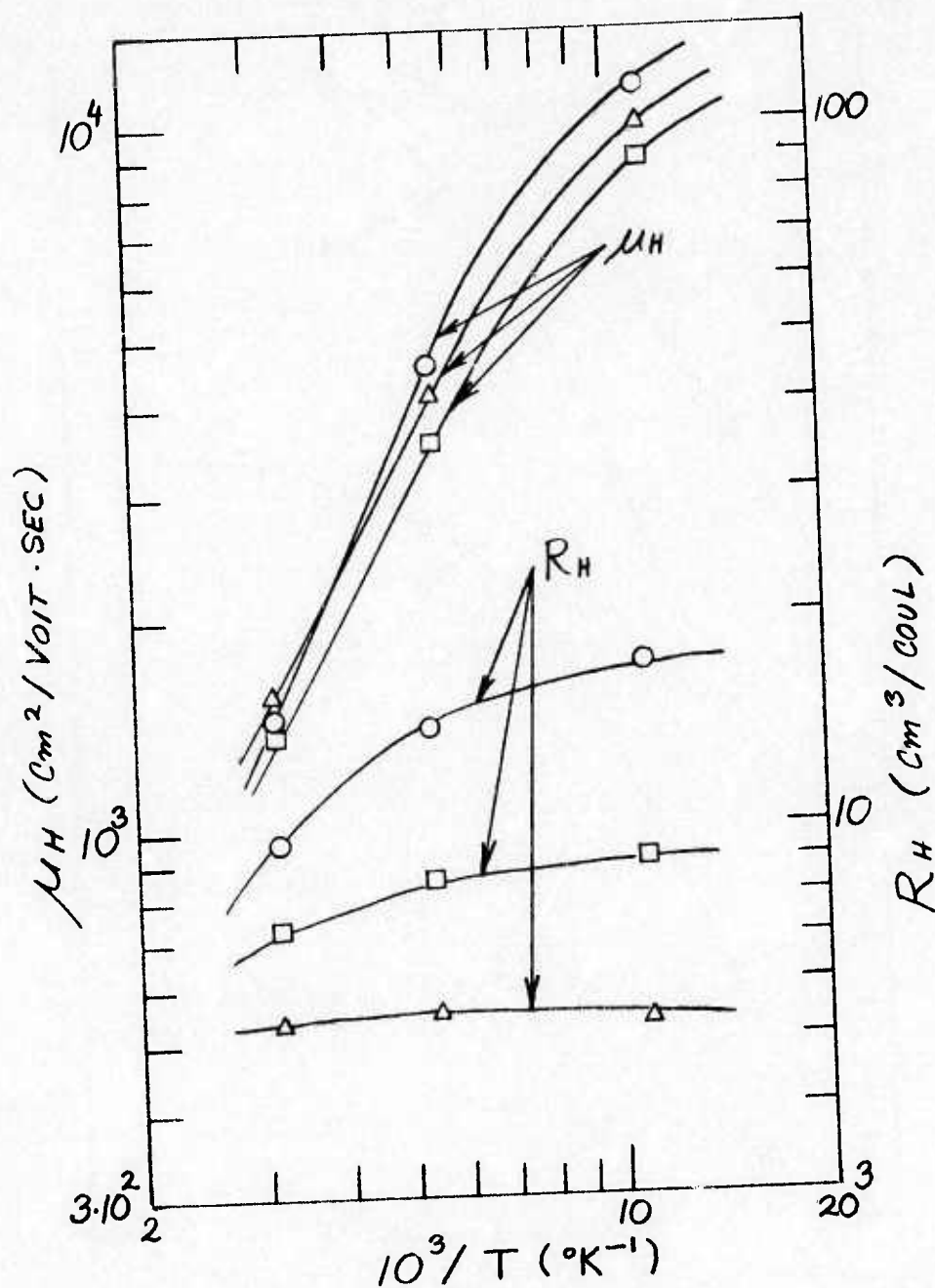
Figure 3-92 Electrical Properties of (111) $Pb_{.84}Sn_{.16}Te$ Films Isothermally Annealed in 10% Metal Rich Charge

○ CaF_2; 600°C; 14 hours n-type
△ BaF_2; 600°C; 19 hours n-type
□ CaF_2; 600°C; 10 hours n-type
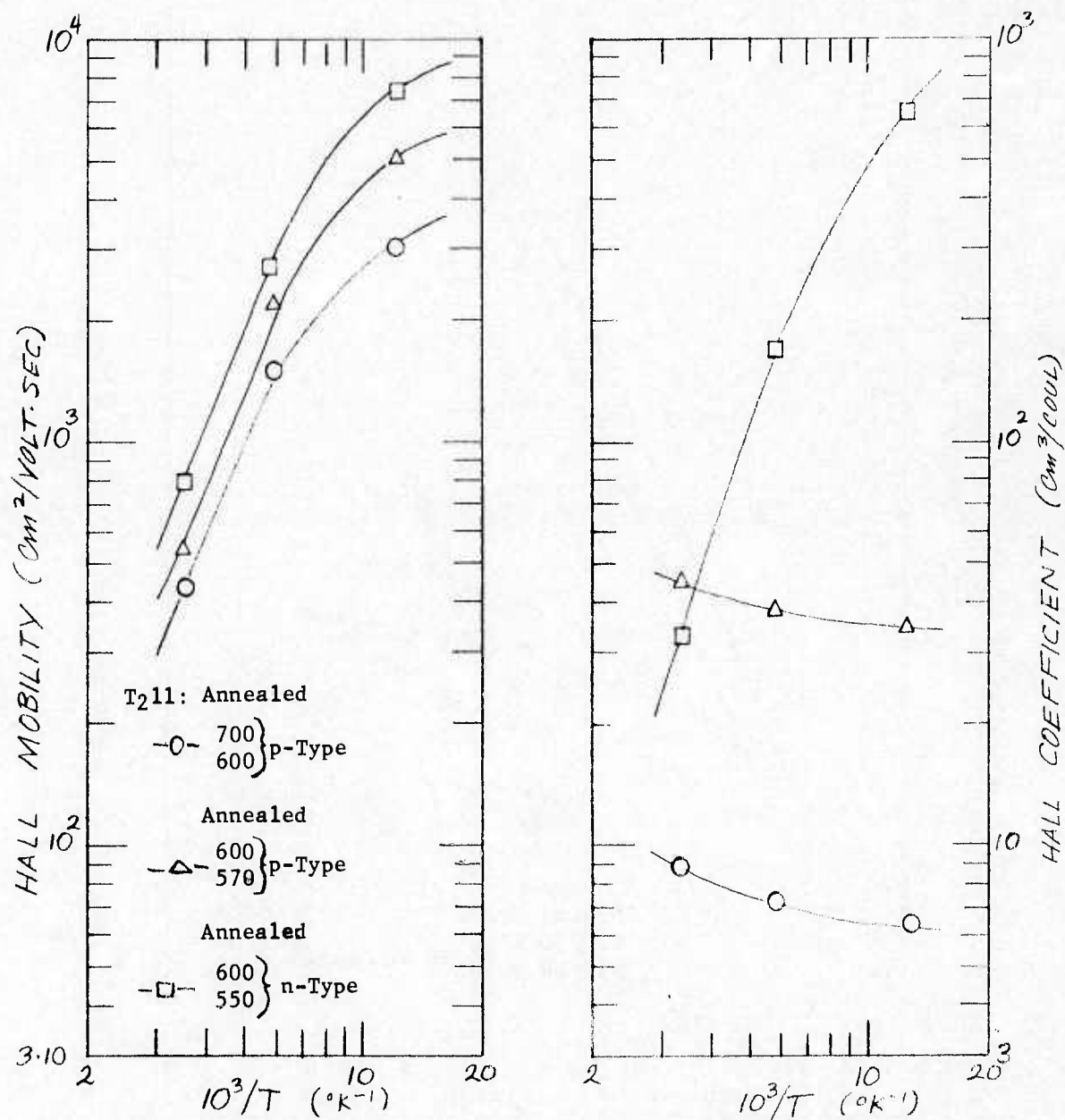
Figure 3-93 Electrical Properties of $Pb_{.81}Sn_{.19}Te$ Film at Various
Annealing Conditions in a 6% Metal Rich Charge
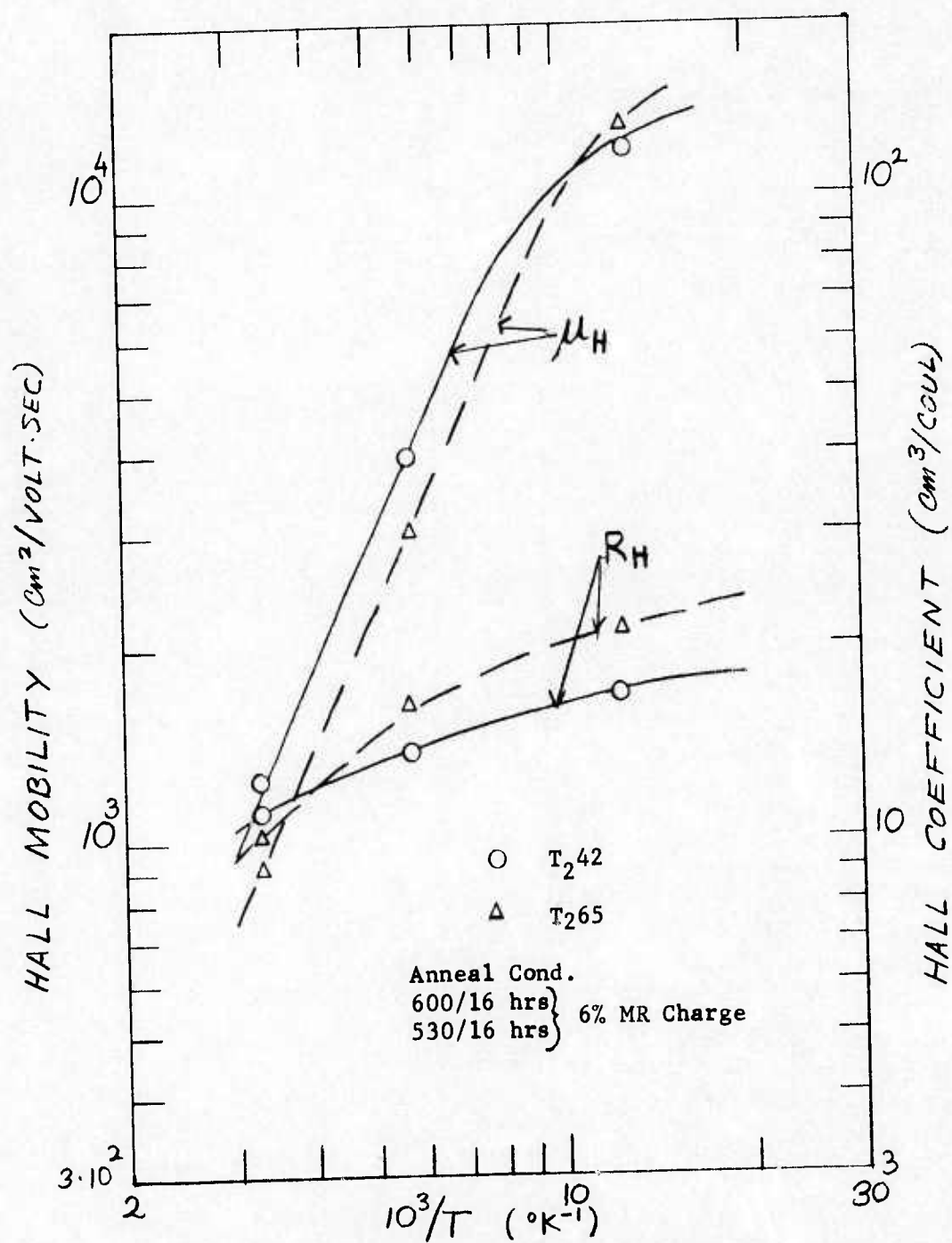
Figure 3-94   Electrical Properties of Two $Pb_{.81}Sn_{.19}Te$
Films Isothermally Annealed Under Nearly
Identical Conditions

3-172
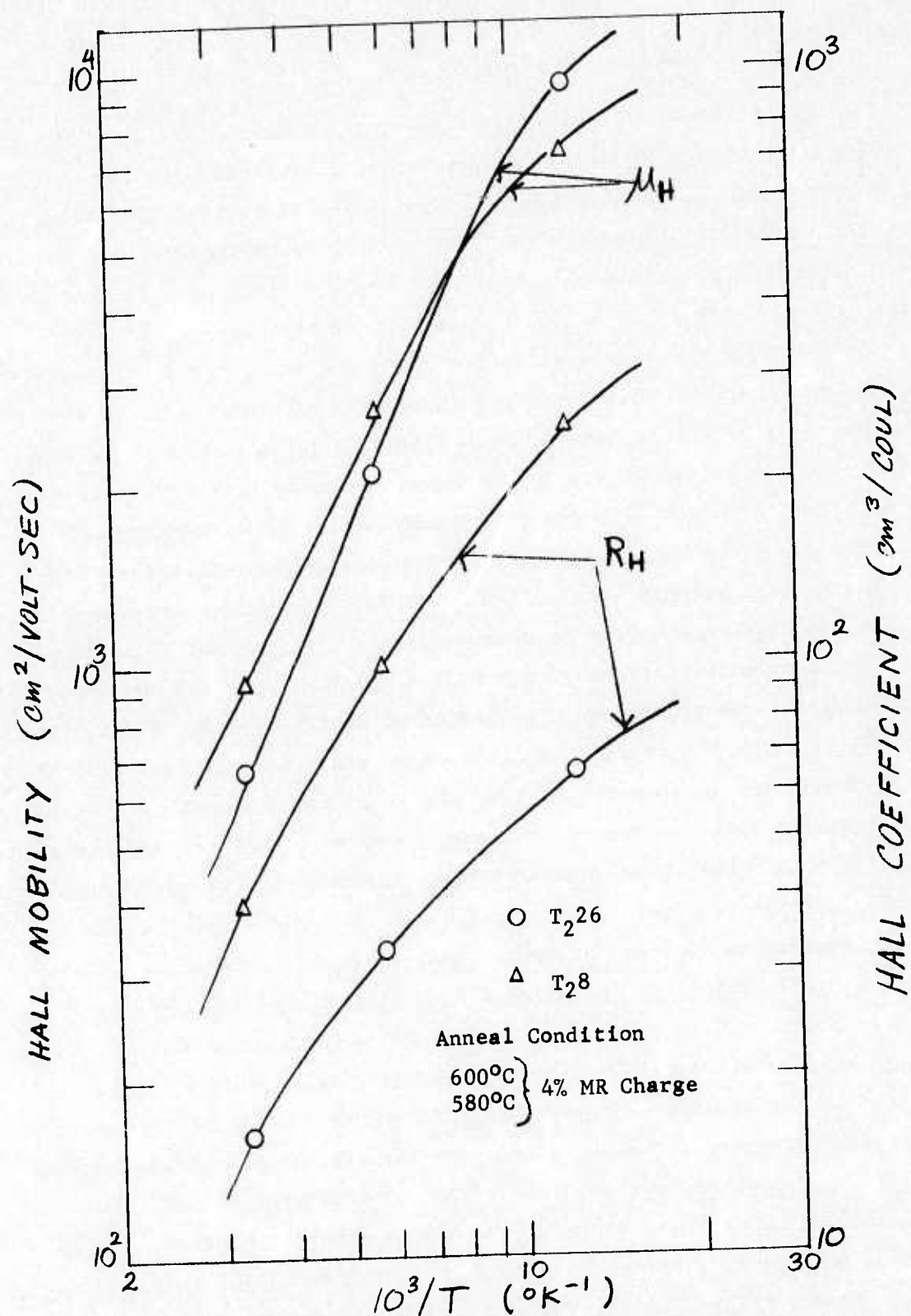
Figure 3-95 Electrical Properties of Two Pb$_{.83}$Sn$_{.17}$Te Films Isothermally Annealed Under Nearly Identical Conditions

3-173

Figures 3-94 and 3-95, aside from giving some typical data on the effects of different annealing temperatures, illustrate one area which is very critical for achieving the lowest possible carrier concentrations. The final annealing temperature in Figure 3-94 is nominally 530°C for both films. If we refer again to Figure 3-80 it is seen that this is more than 20°C below the critical switching temperature for a film composition of $x = 0.19$ and as indicated in the same figure, the carrier concentration should not be too sensitive to small temperature deviation. Repeatability of results should, therefore, be quite good at this temperature. The results in Figure 3-94 are in reasonable agreement with this. By contrast, Figure 3-95 shows the properties and their temperature dependence for two $Pb_{.83}Sn_{.17}Te$ films annealed at nominally identical final annealing temperatures of 580°C. Reference again to Figure 3-80 shows that this temperature is quite near the critical switching temperature for a film composition of $x = 0.17$. The R_H values are obviously quite different for the two films. As indicated in Figure 3-80, this is not surprising since the carrier concentrations are extremely sensitive to small deviations in temperature near the switching temperature. It is thus apparent that in order to achieve, repeatably, carrier concentrations below 10^{16} cm^{-3} the annealing temperature control must be extremely precise and the temperature uniformity over the sample near perfect. In fact, temperature accuracy of better than 0.2°C is required.

3.4.2.2 Effect of Annealing Charge Composition on Film Properties. To this point we have shown that the annealing conditions and procedures for achieving best possible electrical properties require critical control of the annealing temperature, the degree of metal richness of the annealing charge, the annealing times as well as the sample cooling rate. In particular, the critical effect of deviating only slightly from the switching temperature stands out as a severe control problem. Another potential optimization parameter is the annealing charge composition. To investigate, a special set of experiments was carried out to establish the relation between the x-value or composition of the annealing charge and the x-value of the as-deposited film.

3-174
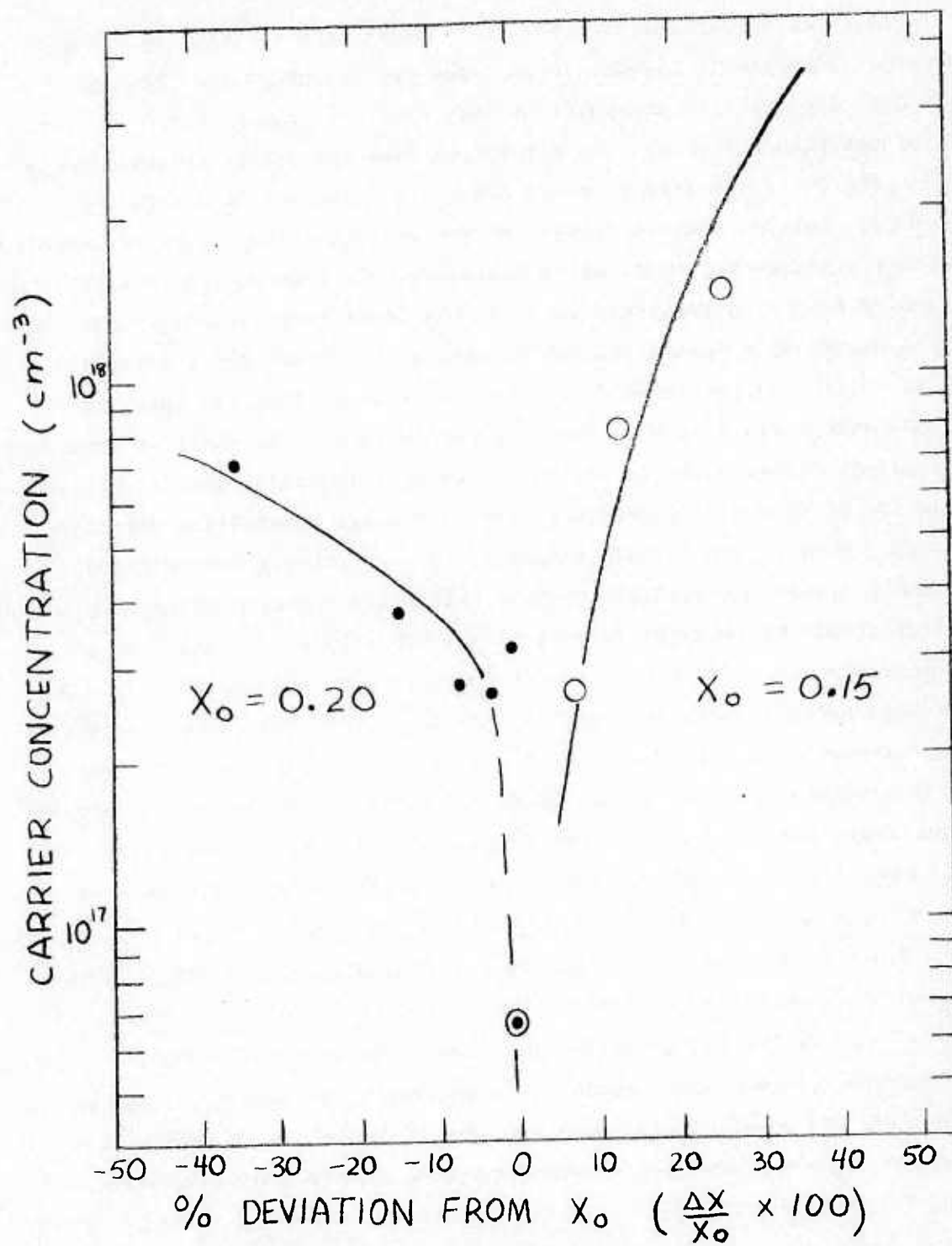
Figure 3-96 Effect of Annealing Charge Composition on Carrier Concentration

Table 22 summarizes the results of these experiments. As noted, two conditions are included. In one case the charge composition is $x_o = 0.15$ and the film compositions vary from $x = 0.16$ to $x = 0.19$; i.e., are always higher than x_o. In the second case the charge composition is $x_o = 0.20$, while the film x-values are $\leq x_o$ and range from $x = 0.13$ to $x = 0.20$. All films are initially p-type and change to n-type on annealing. In these experiments, combination annealing cycles were used; however, the secondary annealing temperatures (i.e. the lower temperatures in the table) were designed to coincide reasonably well with the switching temperature for each film composition. It can thus be assumed that the observed effects are primarily due to the differences in film to charge composition. Figure 3-96 illustrates the results. The post-annealing carrier concentrations are plotted as a function of the percentage composition deviations ($\Delta x /x_o$, where $\Delta x = x$ (film composition) $- x_o$ (charge composition)). Generally speaking the carrier concentrations of annealed films seem to be less sensitive to negative composition deviations ($x < x_o$) than to positive deviations ($x > x_o$), except for very small values ($\Delta x/x_o \leq 5\%$). Most important, though, is that the data point with the lowest concentration corresponds to $\Delta x/x_o \sim 0$ ($n = 6 \times 10^{16}$ cm^{-3}) and that, for best results, composition match must be as carefully controlled as the annealing temperature. As can be seen from Table 22 the annealing conditions for the film with the lowest concentration (film T$_2$23) represent the most carefully controlled annealing cycle in every respect.

3.4.2.3 <u>A Simplified Isothermal Annealing Technique for Sputtered</u> <u>Pb$_{1-x}$Sn$_x$Te Films Utilizing Charges Consisting of Small Traces of Pb$_{1-x}$Sn$_x$</u> <u>Alloys.</u> The isothermal annealing techniques (References 24 and 25) utilized in this work to date have involved the equilibration, under isothermal conditions, of a relatively large Pb$_{1-x}$Sn$_x$-rich Pb$_{1-x}$Sn$_x$Te charge with x-values being the same for as-deposited film samples to be annealed and annealing charges.

A simplified annealing technique, which has been used successfully for bulk $Pb_{1-x}Sn_xTe$ (Reference 26), has been investigated as to its utility to sputtered $Pb_{1-x}Sn_xTe$ films. This technique involves the use of small traces of the metal alloy, $Pb_{1-x}Sn_x$ only, as the annealing charge, without imposing any critical x-value matching requirement between $Pb_{1-x}Sn_x$ and the as-deposited film sample.

In fact, it was found that the only requirement is that the composition of the sample and charge combined ($x_{film} + x_{charge}$) lie between the solidus and liquidus curve at the annealing temperature. The amount of charge required is as shown in Reference 26 given by the following relation:

$$\text{atoms of charge} > \left| p \text{ (sample)} - p \text{ (at the solidus line)} \right| \left| \frac{V}{c} \right|$$

where p is the carrier concentration, V the volume of the sample, and c is the number of carriers per vacancy. As implied by the inequality, it is unnecessary to use the exact amount of charge and, in general, it may be larger than that calculated from the expression above. However, if the amount of charge used is so large as to prevent the charge from reaching the liquidus line before the sample reaches the solidus line, then surface melting of the sample will occur. Thus, to prevent the melting of the sample, there is an upper limit to the amount of pure PbSn or Te charges which should be used. These upper limits are, from Reference 26, defined by:

$$\text{atoms of PbSn charge} \leq \left[\frac{\Delta p \, V}{c} \right] \left[\frac{1-x}{x} \right]$$

$$\text{atoms of Te charge} \leq \left[\frac{\Delta p \, V}{c} \right. \left[\frac{x}{1-x} \right]$$

in which $\Delta p V/c$ is given by the initial inequality relation and x is the composition of the appropriate liquidus at the annealing temperature.

The $Pb_{1-x}Sn_x$ alloy charges were prepared to have a Pb:Sn ratio as close to that of the $Pb_{1-x}Sn_xTe$ sample as possible. However, it is not necessary to match the Pb:Sn ratio in the charge and sample very exactly as long as the charge is kept small with respect to the sample. Thus,

one advantage of this technique is the fact that the charge preparation is simpler than that used for the standard technique which uses $Pb_{1-x}Sn_xTe$ charges. Another advantage is that the charge and the sample can be accommodated in a much smaller quartz ampoule; thus, the whole ampoule will be more nearly in the region of constant temperature in the furnace. Also the smaller size of the quartz ampoule lends itself for achieving higher quenching rates due to the reduced thermal mass.

The results of the isothermal annealing experiments utilizing this simplified technique with PbSn charges are presented in Table 23 and Figures 3-97 through 3-100. Table 23 includes data on the structure, composition and annealing conditions as well as on the unannealed (as-deposited) and annealed electrical properties of films utilized for these experiments. Figure 3-97 plots the $77^\circ K$ carrier concentrations as a function of annealing temperature for $Pb_{.82}Sn_{.18}Te$ films annealed with $Pb_{.82}Sn_{.18}$ metal alloy charges. Reproduced in Figure 3-97 are similar data for $Pb_{.81}Sn_{.19}Te$ films annealed with the standard metal-rich $Pb_{.81}Sn_{.19}Te$ charge. As noted in this figure, the trends resulting from these two techniques are indeed very similar. The apparent switching temperatures for the two film compositions (i.e. $x = 0.18$ and $x = 0.19$) are consistent with those expected from our previous thin film data (see, for example, Figure 3-78) and from previous bulk $Pb_{1-x}Sn_xTe$ work. It appears, therefore, that the simplified annealing techniques utilizing small traces of $Pb_{1-x}Sn_x$ alloy may be quite adequate for annealing sputtered $Pb_{1-x}Sn_xTe$ films. Additional annealing data shown in Figure 3-98 confirm this. Here we plot the $77^\circ K$ carrier concentration for three $Pb_{1-x}Sn_xTe$ films having different x-values annealed with $Pb_{1-x}Sn_x$ alloy charges of corresponding compositions as a function of annealing temperature. The trends are, again, as expected. The switching temperatures are also consistent with those obtained utilizing the standard annealing charges. However, we do note from Figure 3-98 and Table 23 that the lowest carrier concentration obtained, to date, utilizing this annealing technique is just above 1.0×10^{17} (as compared with $< 10^{16}$ cm^{-3}).
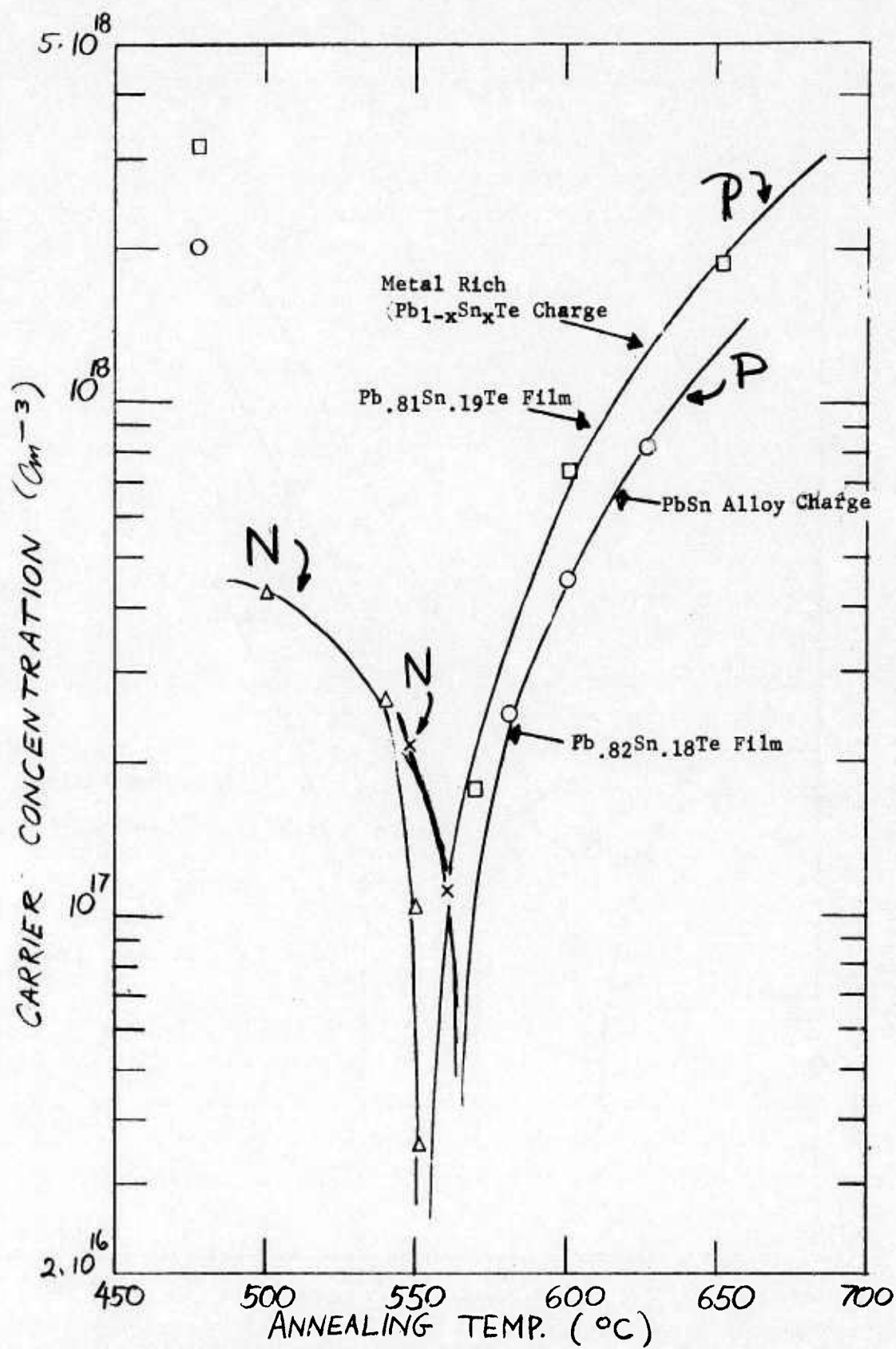
Figure 3-97 Comparison of Isothermally Annealed $Pb_{1-x}Sn_xTe$ Films in Metal Rich $Pb_{1-x}Sn_xTe$ Charges and in Trace $Pb_{1-x}Sn_x$ Alloy Charges

3-179
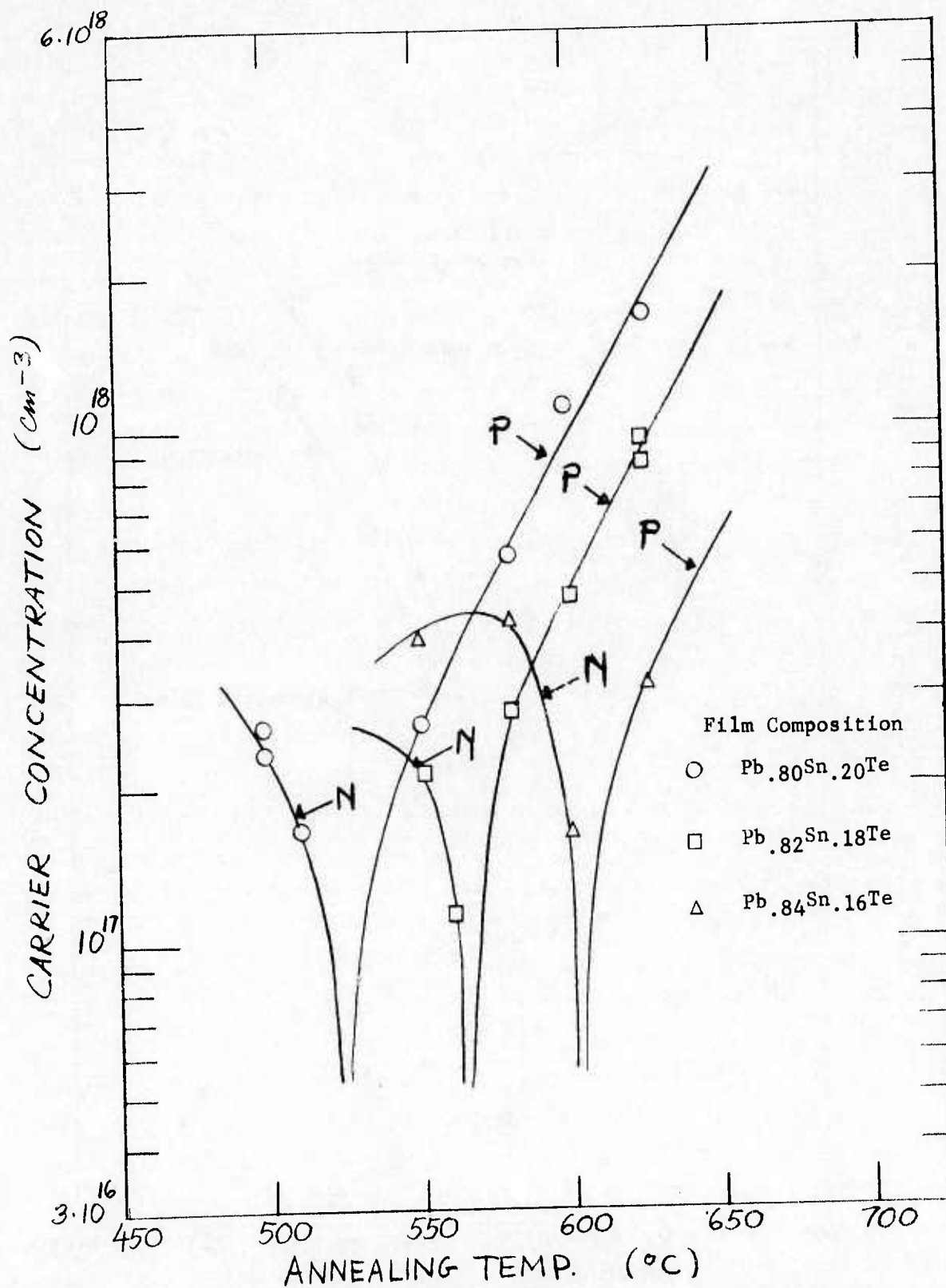
Figure 3-98 Isothermal Annealing Results Using Small Traces
of $Pb_{1-x}Sn_x$ Alloy Charges

3-180
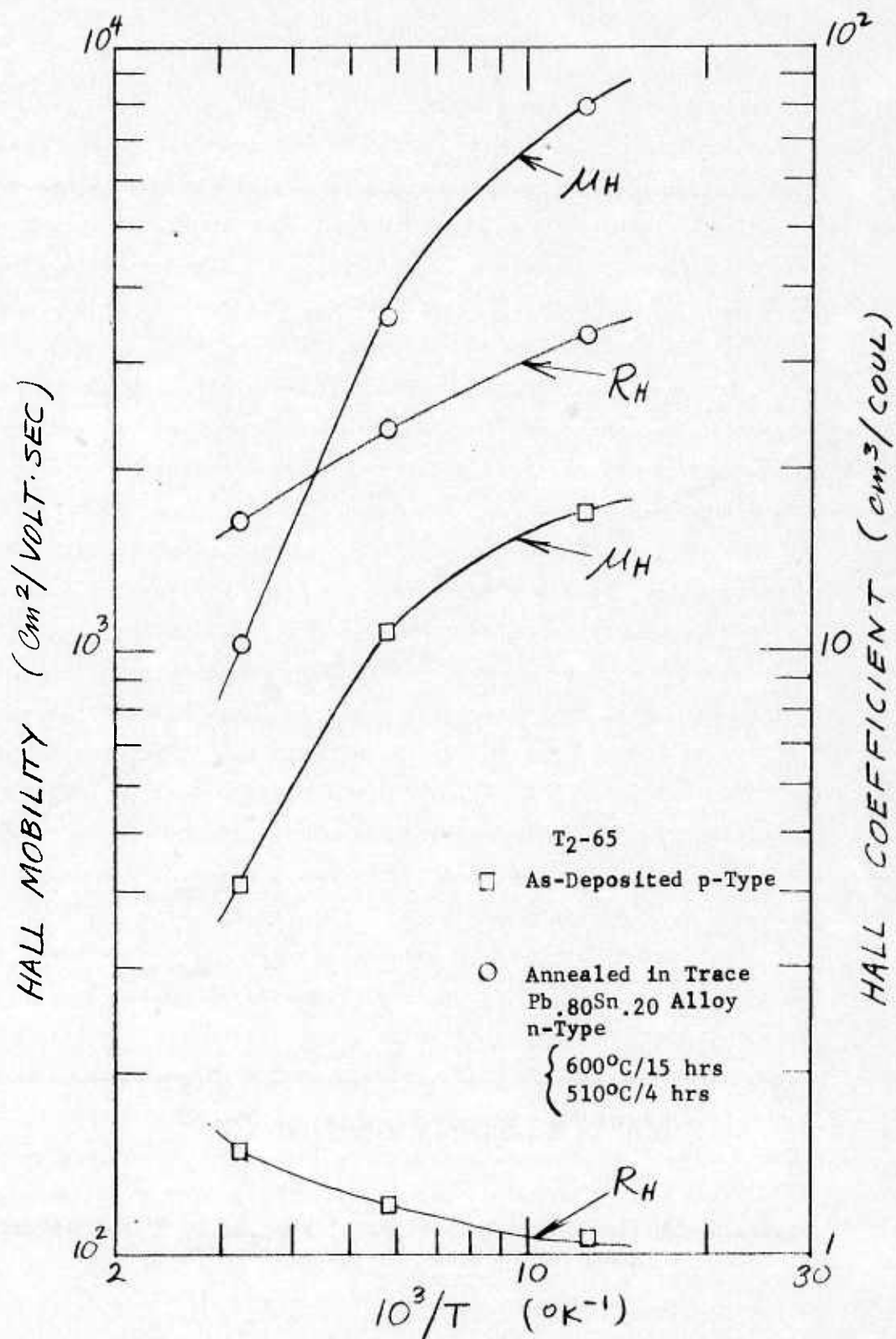
Figure 3-99   Electrical Properties of Single Crystal $Pb_{.80}Sn_{.20}Te$
Film Annealed in Trace $Pb_{.80}Sn_{.20}$ Alloy Charge
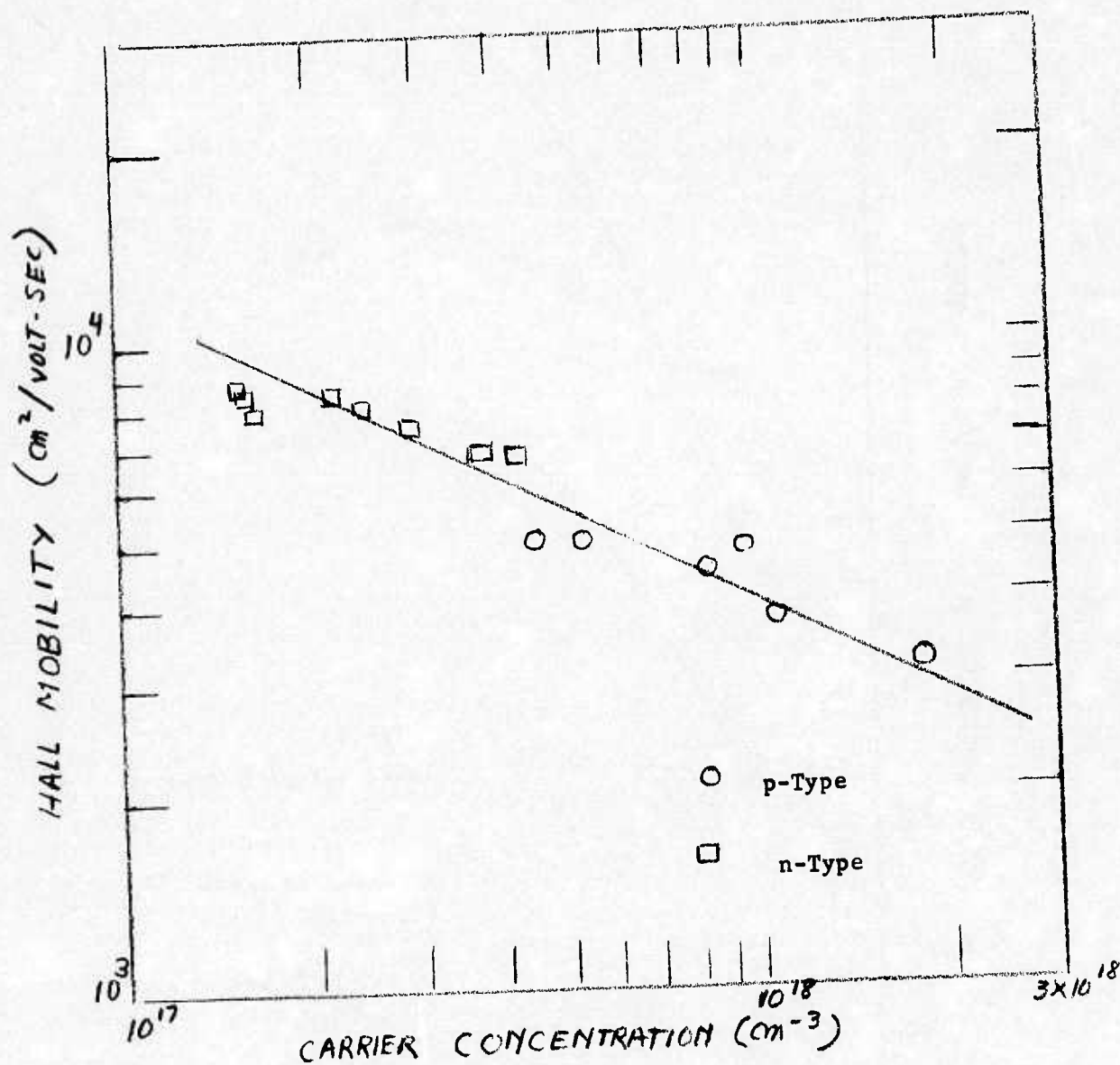
Figure 3-100 Electrical Properties of $Pb_{1-x}Sn_xTe$ Films Isothermally Annealed in Trace $Pb_{1-x}Sn_x$ Alloy Charge

3-182

However, only a limited number of experiments have been performed to date utilizing this technique so that no attempt was made as yet to optimize for the lowest carrier concentration. For example, we see from Table 23 that most annealings were performed for 4 hours only. As we have already shown, the optimum annealing time with the standard annealing charge was found to be 15 or more hours. Furthermore, as also seen from Table 23, most annealings were performed at a single temperature. The annealing cycle [e.g. $700^{\circ}C \rightarrow 600^{\circ}C \rightarrow T_{c}^{\circ}$ (switching)] which was found to be optimum for the standard charge, has not yet been used with the metal alloy charges. Finally, the annealing tubes and quenching procedures were the same as those used with the standard technique. Thus, the possibility of using smaller annealing tubes and correspondingly faster quench rates, which may aid in achieving better results, has not been investigated as yet. It is thus expected that some optimization of annealing time and procedures will significantly lower the achievable carrier concentrations with the metal alloy charges.

As has been the case for all annealings performed to date, the observed reductions in carrier concentration on annealing with the PbSn alloy charge are accompanied by an increase in mobility as shown in Table 23. This is also demonstrated in Figure 3-99 which shows a typical temperature dependence of mobility and Hall coefficient for an as-deposited p-type ($Pb_{.80}Sn_{.20}Te$) film, before and after annealing in a $Pb_{.80}Sn_{.20}$ charge. As noted in Figure 3-99 and Table 23, this film was annealed to a temperature of $510^{\circ}C$ which can be seen from Figure 3-78(b) to be considerably below the switching temperature (which is near $525^{\circ}C$ for $x = 0.20$). This should result in a fairly high, n-type carrier concentration and relatively low mobilities - which is consistent with the results shown in Figure 3-99 and Table 23. Still, as substantial an annealing effect is observed as with the standard annealing procedures.

Figure 3-100 summarizes the carrier concentrations and mobilities measured in films annealed with PbSn alloy charges. The linearity of the relation between these two parameters is preserved and comparison of these results with those shown in Figure 3-84 shows the mobility-carrier

3-183

concentration behavior to be comparable with the trends resulting from annealing with 3% and 4% metal-rich $Pb_{1-x}Sn_xTe$ charges.

From the initial results presented, it can be concluded that the simplified annealing technique yields results which are consistent with those achieved with the standard annealing technique. As we shall show in a later section, utilizing this simplified technique with Te annealing charge yields results which are also consistent with standard annealing techniques using Te-rich $Pb_{1-x}Sn_xTe$ charges. However, further experimentation is required in both cases to achieve better electrical properties, in particular lower carrier concentrations, by annealing, for example, closer to the switching temperatures. The advantages in terms of simplicity certainly warrant further evaluation, if annealing is to be used at all.

3.4.2.4 <u>Isothermal Annealing with Tellurium-Rich Charges</u>. In addition to annealing in metal-rich and stoichiometric $Pb_{1-x}Sn_xTe$ charges, annealings have also been performed in Te-rich $(Pb_{1-x}Sn_x)Te$ charges. Although we know from bulk $Pb_{1-x}Sn_xTe$ that annealing in a Te-rich charge produces p-type film with very high carrier concentrations (10^{19} cm^{-3} range), we have found such annealing to be useful under certain conditions. As we have seen, n-type characteristics can be found in as-deposited films (see for example Figures 3-1 to 3-6). Depending on deposition conditions and film structure, these as-deposited, n-type films may have carrier concentrations ranging from less than 1×10^{17} cm^{-3} to the high 10^{17} or low 10^{18} cm^{-3} range. Te-rich annealing was initiated early in the program and was aimed at improving the films with high n-type carrier concentrations. Now, annealing n-type films (with high carrier concentrations) in a vacuum or with metal-rich charges leads generally to poor electrical properties. However, it has been found in this first effort that very careful annealing in a Te-rich charge at an optimized temperature between 200^oC and 300^oC can change as-deposited n-type films into p-type film without much degradation in the film properties. It has been found also possible to re-anneal these p-type
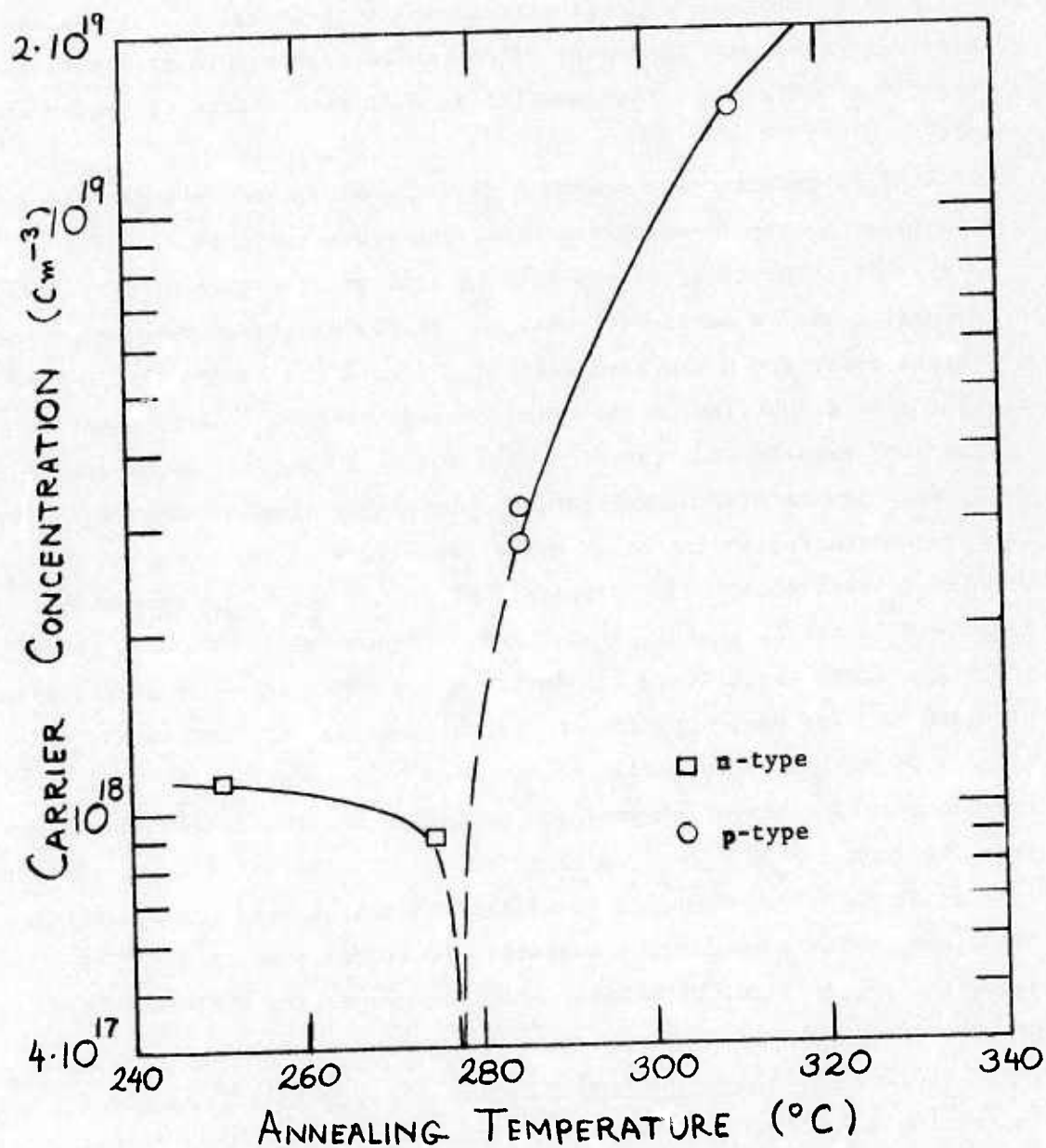
Figure 3-101 Carrier Concentration vs. Annealing Temperature for Isothermal Te-Rich Annealing of $Pb_{.80}Sn_{.20}Te$ Films

films in a metal-rich charge at a carefully established temperature and produce n-type films with carrier concentrations in the low 10^{17} cm^{-3} range and with enhanced mobilities. In fact, all the trends in mobility and carrier concentrations that were shown in the metal-rich annealing results with as-deposited p-type films can be observed in as-deposited n-type films which are first annealed in a Te-rich charge to render them p-type.

Typical results of systematic tellurium-rich PbSnTe annealing experiments of n-type as-deposited films are shown in Table 24 and in Figure 3-101. The behavior observed is analogous to that of p-type film on annealing with a metal-rich charge. As the annealing temperature is increased above 200°C the as-deposited n-type films become less n-type resulting in a lowering of the carrier concentration. At an apparent "crossover" temperature, the film will switch to p-type, still with a relatively low carrier concentration. At higher temperatures, the p-type carrier concentration increases quite rapidly, with the measured hole carrier concentration being proportional to the amount of excess Te dissolved in the $Pb_{.80}Sn_{.20}Te$ lattice. Figure 3-101 indicates that the temperature range (here 275 to 285°C) in which an n- or p-type film with low carrier concentration can be obtained is very narrow and critical. By reasonable control we have been able to establish Te-rich annealing conditions which produced p-type film with carrier concentrations between 1×10^{18} cm^{-3} and 2×10^{18} cm^{-3}. These films, as already discussed, were then annealed in metal-rich charges and the resulting films had, after annealing, comparable electrical properties to as-deposited p-type films of similar starting properties annealed under similar conditions.

3.4.2.5 <u>Isothermal Annealings with Small Traces of Te Charge</u>. In Section 3.4.2.3 we discussed the simplified annealing procedure in which the charge instead of having a metal-rich $Pb_{1-x}Sn_xTe$ composition consists only of small quantities of the metal alloy $Pb_{1-x}Sn_x$. In this section, the effects of using pure Te annealing charges instead of Te-rich $Pb_{1-x}Sn_xTe$ charges, presented in the preceding section, will be discussed.

While the annealings performed in Te-rich $Pb_{1-x}Sn_xTe$ charges were to convert n-type films with high carrier concentration to p-type films for further annealing with the standard metal-rich $Pb_{1-x}Sn_xTe$ charges to produce low carrier concentrations, the annealing experiments with Te charges were more directly aimed at improving the electrical properties of as-deposited, n-type films (i.e., without a second annealing step). The results utilizing this more direct approach are given in Table 27 and are illustrated in Figures 3-102 through 3-104. Figure 3-102 reproduces results shown in Figure 3-101 which utilized a Te-rich $Pb_{1-x}Sn_xTe$ charge along with the results of annealings with Te only. As noted, the two techniques give very similar results. That is, starting with n-type films, with similar as-deposited carrier concentrations, the films become less n-type as the annealing temperature is increased above $200^{o}C$, as evidenced by a lowering in the carrier concentration. At a critical temperature between $270^{o}C$ and $280^{o}C$, the n-type film switches to p-type in both cases. As the annealing temperature is further increased, the p-type carrier concentration increases rapidly. As is evident from Figure 3-102, the temperature range in which switching occurs is very narrow and careful control is required in order to achieve the desired low carrier concentrations.

Of interest is the fact that, without much effort to control the critical temperature, n-type carrier concentrations are reduced to reasonable values by this technique (e.g. 5×10^{17}). Furthermore, along with the lowering of the carrier concentration, a considerable improvement in the mobilities is observed. Figure 3-103 shows the temperature dependence of the Hall mobility and Hall coefficient of a typical n-type film before and after annealing in small traces of Te charge. As noted, there is a particularly significant improvement in the mobility and a fairly significant increase in the Hall coefficient after the Te anneal. As the figure shows, the temperature dependence of mobility of the annealed film shows very little deviation from the $(1/T)^{5/2}$ dependence down to $77^{o}K$. The annealing temperature for this film was $275^{o}C$, so that the film remained n-type. The effects of the Te-annealing procedure are further

3-187
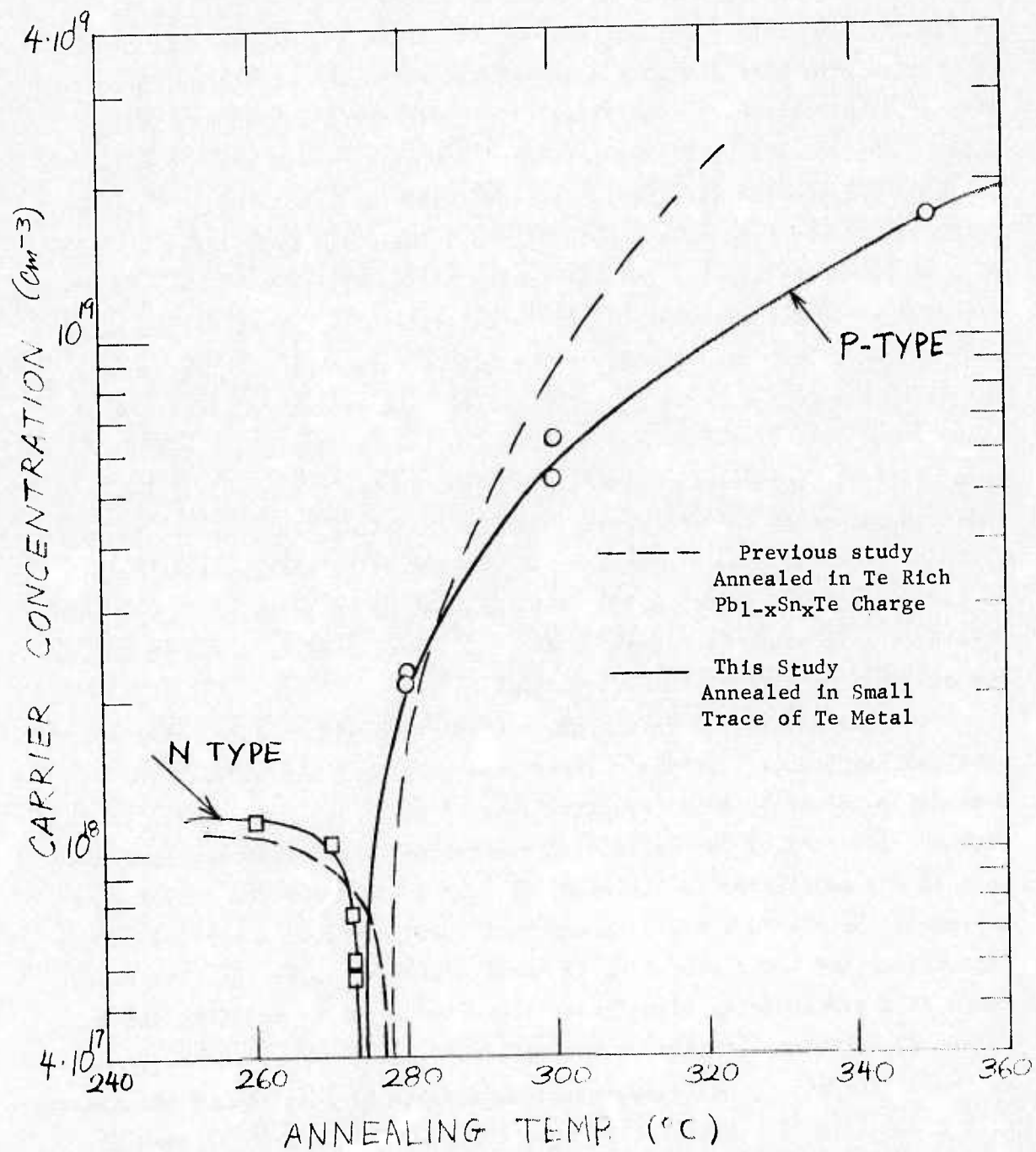
Figure 3-102 Isothermal Tellurium Annealing Results Using Small Traces
of Tellurium as Annealing Charge

3-188
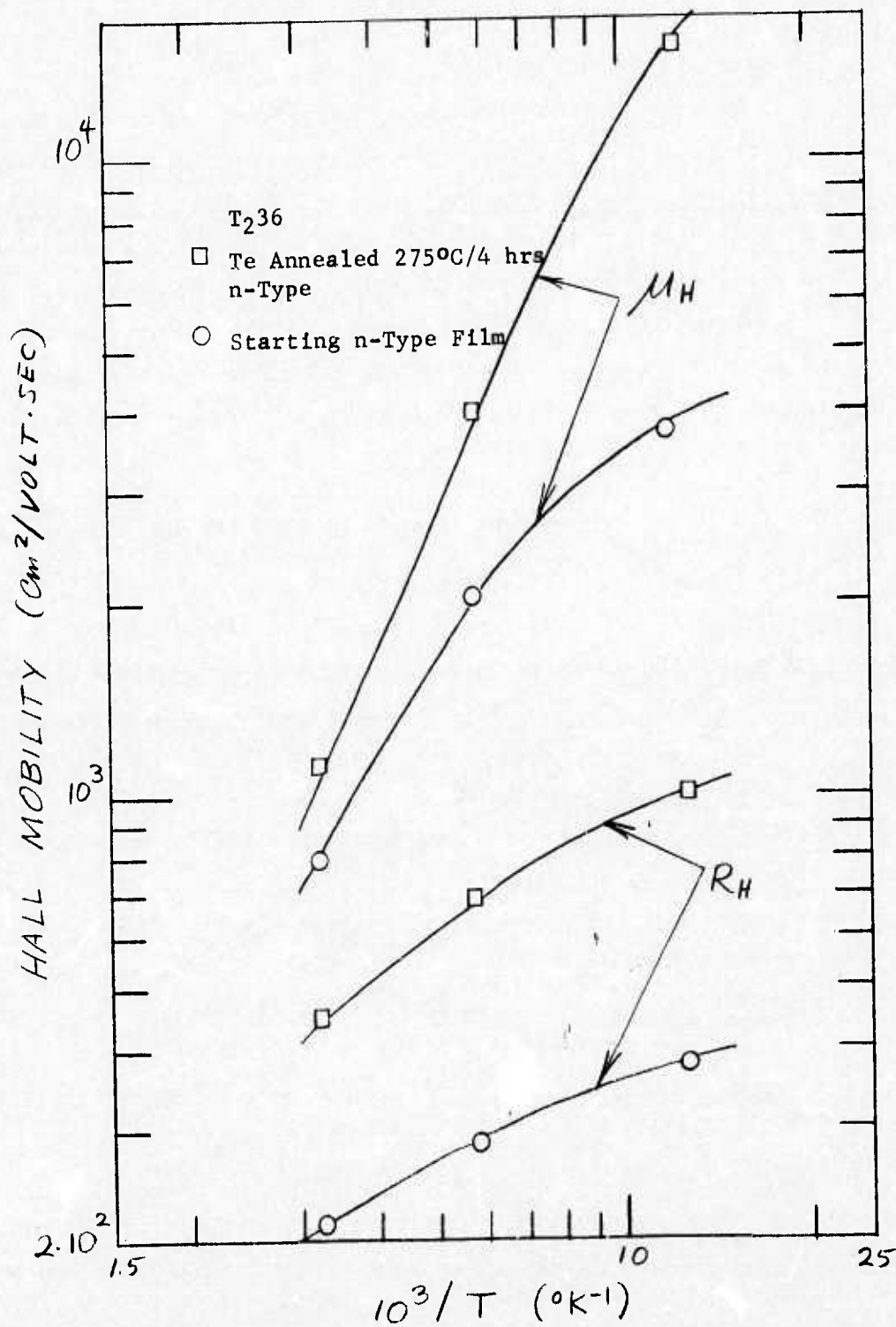
Figure 3-103 Electrical Properties of (111) $Pb_{.79}Sn_{.21}Te$ Film Annealed in Small Trace of Te
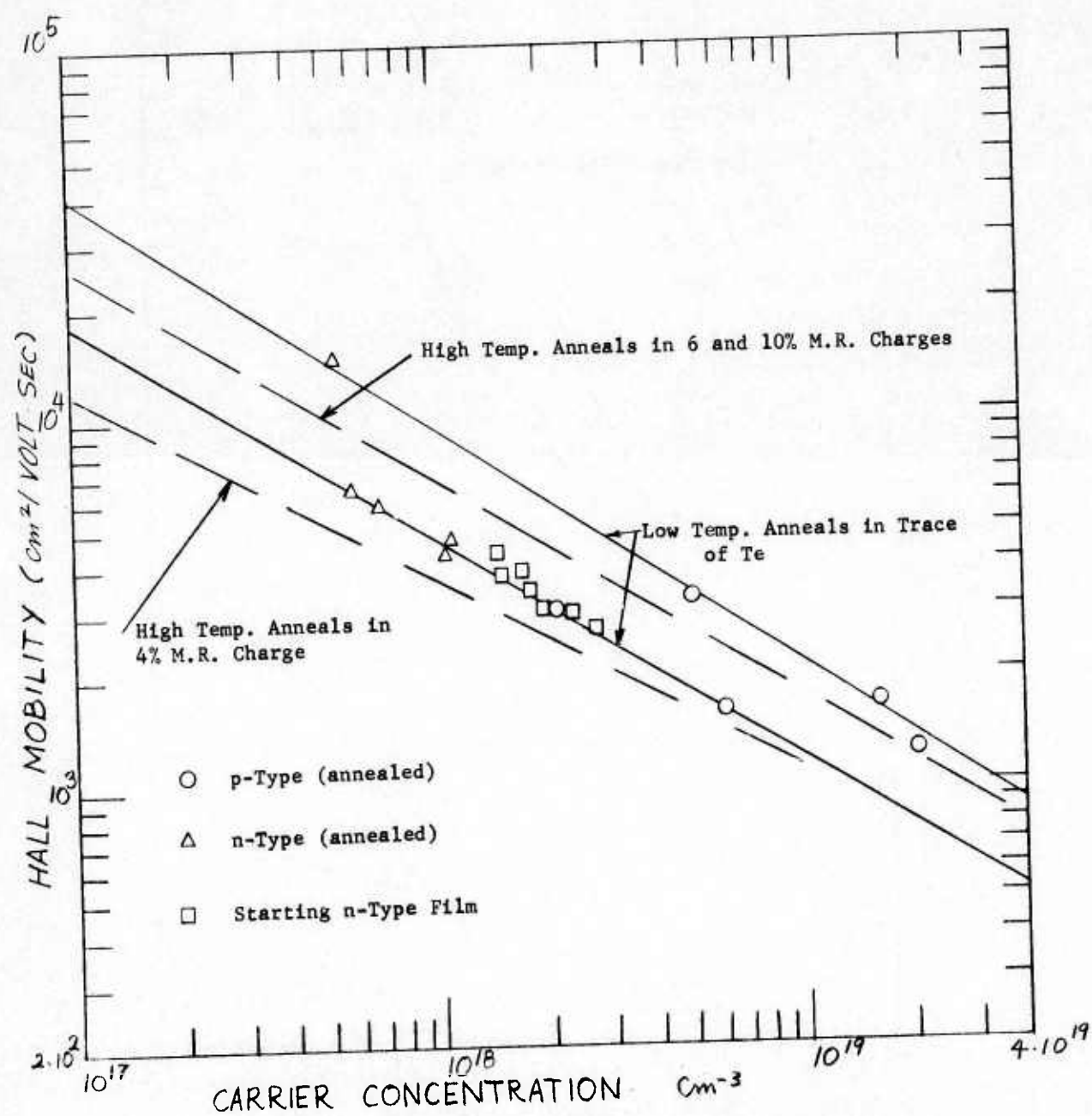
Figure 3-104 Isothermal Annealing Results-Electrical Properties of $Pb_{1-x}Sn_xTe$ Films Annealed in Small Traces of Te

illustrated in Figure 3-104. Here, the relation between carrier concentration and Hall mobility is given for three sets of films: a) Starting n-type films, either annealed or as-deposited, with relatively high carrier concentrations, b) n-type films annealed in Te at a temperature below that at which switching to p-type occurs, and c) initially n-type films which converted into p-type films by annealing in Te at a sufficiently high temperature to induce switching. The trends for annealings performed with 4%, 6% and 10% metal-rich charges, using initially p-type films, are reproduced in this figure for comparison (dotted lines). It is apparent that the simplified Te annealing procedures, carried out at relatively low temperatures, result in trends which are quite compatible with metal-rich annealed films. As noted, the Te data straddle the highly metal rich (6% and 10%) data on both sides of the trend curve and some very respectable film properties are achieved with the Te annealing process from some rather poor starting material.

The results of the Te annealing work demonstrate that such a procedure provides: 1) a possible alternative technique to high temperature annealing in metal-rich $Pb_{1-x}Sn_xTe$ charges for achieving good electrical film properties, and 2) a technique for improving process yields by utilizing as-deposited n-type films with high carrier concentrations and converting them to acceptable materials (which can be further annealed in metal-rich charges to achieve even lower carrier concentration n-type film).

3.4.2.6 <u>Low-Temperature Isothermal Annealing of Sputtered $Pb_{1-x}Sn_xTe$ Films</u>. In this section, another very interesting result is discussed, the definition of an apparent, second crossover temperature in the equilibrium phase diagram of $Pb_{1-x}Sn_xTe$ at a lower temperature than that defined by T_x in Figure 3-78(a). It is also shown that this second crossover (or switching) temperature may be as useful as T_x in terms of a critical annealing temperature for achieving low carrier concentrations.

As has been extensively discussed, most as-deposited or as-grown $Pb_{1-x}Sn_xTe$ material is off-stoichiometry and requires annealing in order to render the material completely stoichiometric. Referring again to the

schematic represented in Figure 3-78(a), to our knowledge no experiments have been performed to determine how closely the metal-saturated solidus, indicated by broken lines, approaches the stoichiometric composition at lower temperatures. In the course of this work, we performed experiments with sputtered $Pb_{1-x}Sn_xTe$ films at temperatures considerably below T_x. The results of some of these annealings are presented in Tables 24 and 25 and in Figures 3-105 through 3-107. The pertinent structures, composition, annealing cycles and conditions, and the electrical properties of both unannealed and annealed films are presented in the tables. The carrier concentrations of the annealed films are plotted in Figures 3-105 and 3-106 as a function of annealing temperature. Figure 3-105 shows only low temperature (<500°C) annealing results. We consider here n-type films (x = 0.19) which had previously been annealed at a temperature near 550°C where they were switched from as-deposited p-type characteristics to n-type. We note that a decreasing annealing temperature results in a decrease of the n-type carrier concentration down to what appears to be a second critical temperature near 375°C, below which the film switches back to p-type. Annealings at still lower temperatures appear to increase the p-type carrier concentration. However, this latter behavior is not as well defined since the annealing procedure was changed for annealings below 350°C. From here, we utilized temperature cycles such as $T_1 = 500°C \rightarrow T_2 = 400°C \rightarrow T_3 = 300°C$. It is also not possible to know exactly at which temperature the films, annealed in this manner, switched. The quenching speed may be such that the actual switching temperature is lower than that shown. Additional systematic annealing experiments below 350°C are required before any conclusions concerning the p-type carrier concentrations below this temperature can be drawn. However, one result appears definite: n-type films do switch back to p-type at some annealing temperature considerably lower than T_x. Figure 3-106 combines the data shown in Figure 3-105 with high temperature annealing results. These two sets of data show a surprising continuity which supports the validity of our conclusions. The critical annealing temperature, T_x 550°C for a composition x = 0.19, has been repeatedly
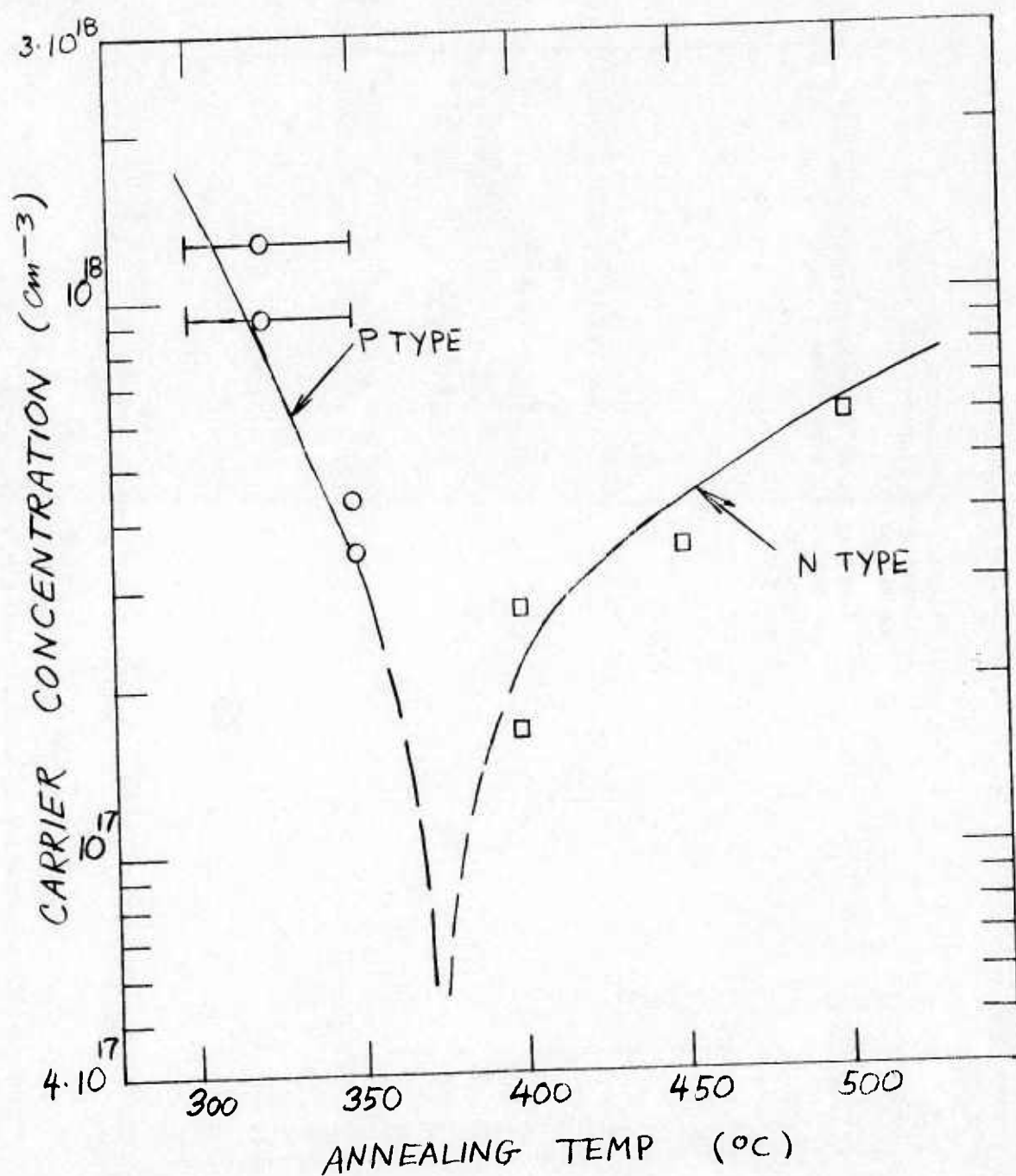
Figure 3-105   Isothermal Low Temperature Annealing Results
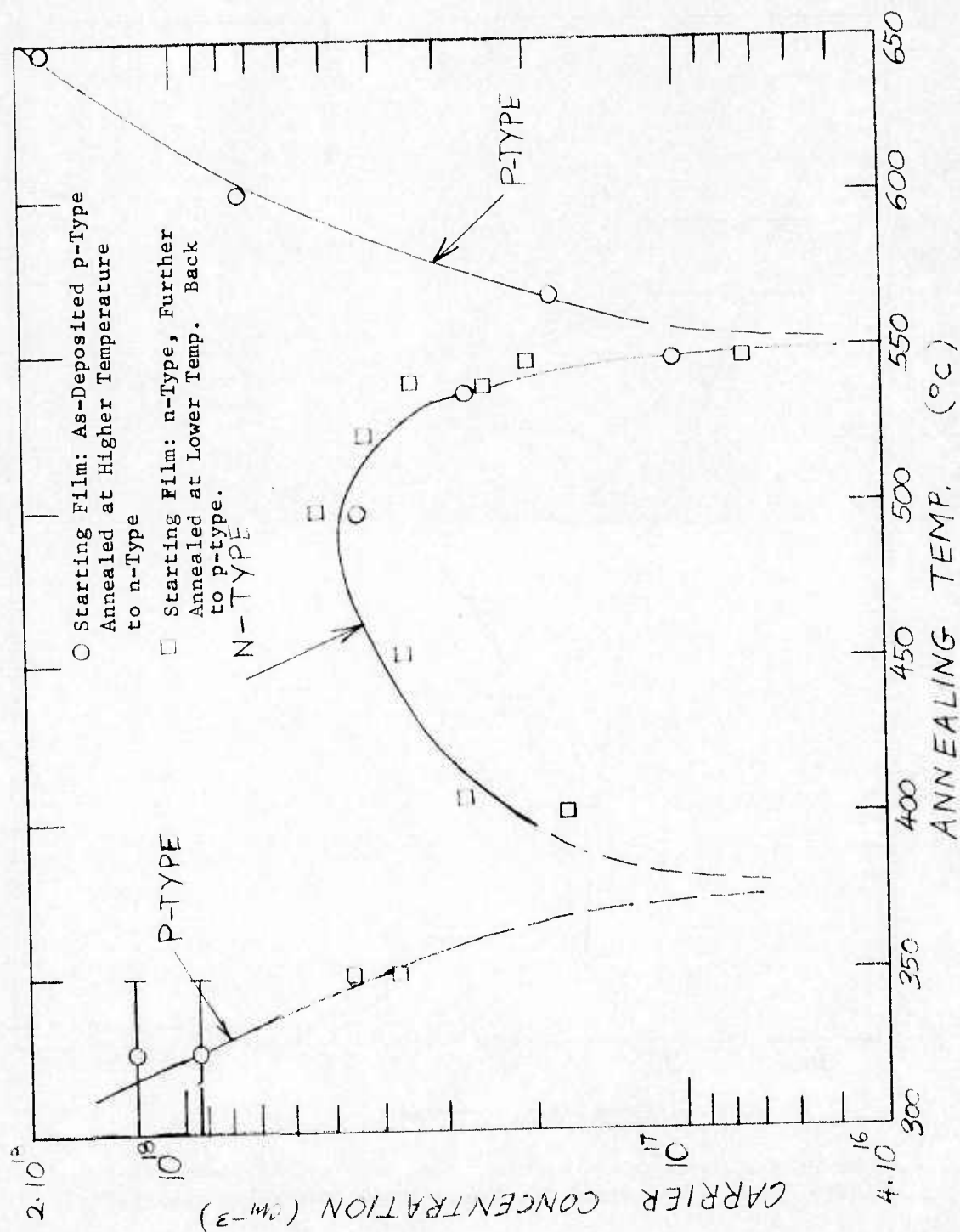
Figure 3-106 Isothermal Low and High Temperature Annealing Results

3-194
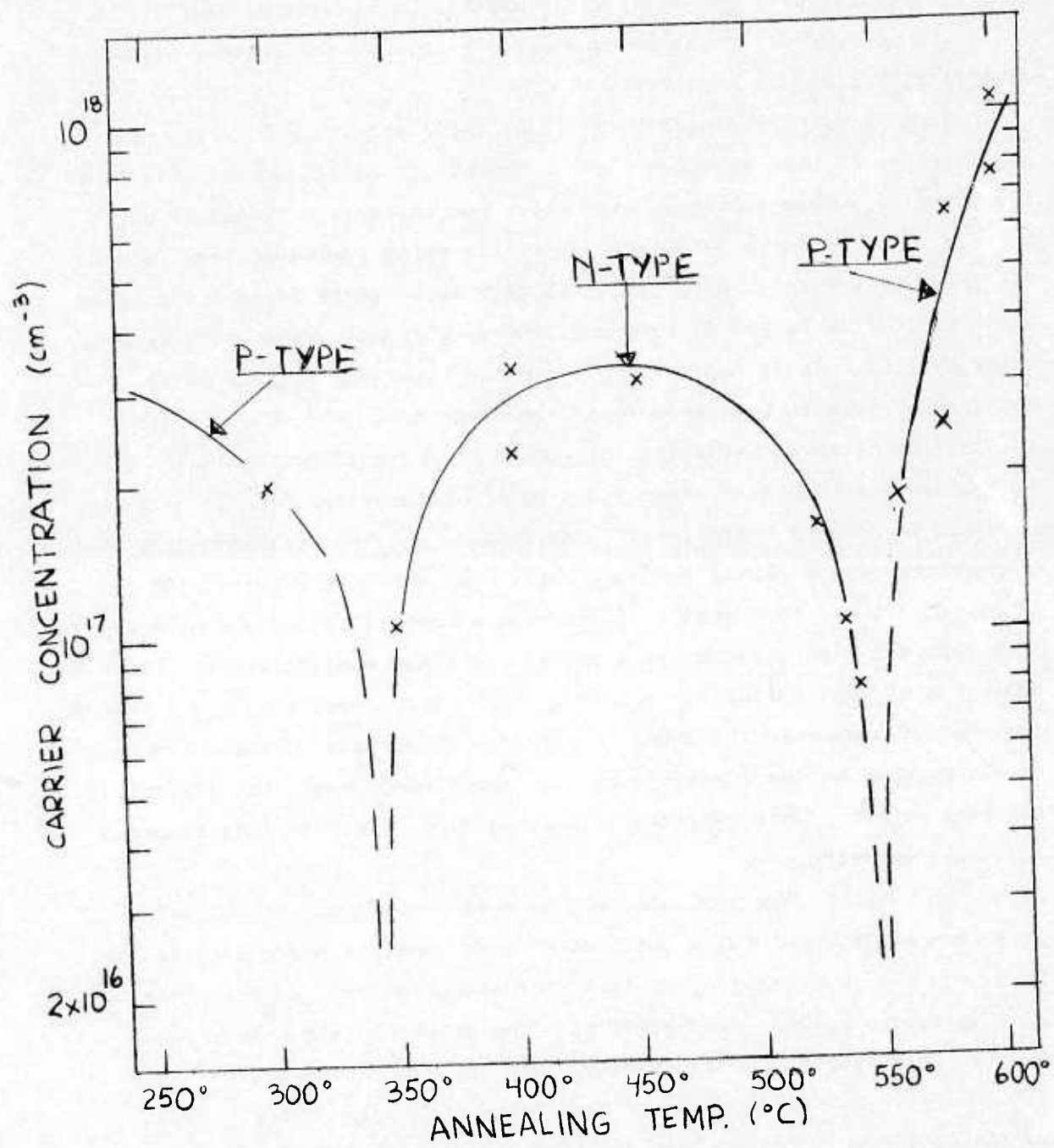
Figure 3-107 Isothermal Annealing Results at High and Low Temperature
for $Pb_{.81}Sn_{.19}Te$ Films Deposited at Zero Bias (Target #9)

verified. This composition seems to be associated with a critical low temperature switching condition which appears to be located near $375^{o}C$. While the latter must still be considered tentative for reasons already discussed, the trends seem real.

This is further apparent in Figure 3-107 and Table 25 which present data similar to that just shown for a second set of films. In this case the annealings were performed with films sputtered from Target #9 while those shown in Figures 3-105 and 3-106 used films sputtered from Target #4. Also, the results with Target #4 were obtained early in the program while those from Target #9 were obtained considerably later to establish repeatability. As is apparent by comparing Figures 3-106 and 3-107, consistency between the earlier and later experiments is definitely obtained in terms of verifying the second low-temperature critical switching temperature at which films switch from n-type back to p-type. However, we note in Figure 3-107 that this second critical annealing temperature occurs closer to $350^{o}C$ while that shown in Figure 3-106 is closer to $375^{o}C$. Both sets of films have a composition of $x = 0.19$ and both show the high temperature critical annealing temperature at $550^{o}C$ which, as already noted, is as expected for this composition. The reason for the difference at the lower temperature is perhaps only the uncertainty induced by the limited number of experiments near the critical low temperature. More experiments are required to define this temperature more accurately.

The results just presented can be used to define, with actual experimental data points, a modified or more complete phase diagram for $Pb_{.81}Sn_{.19}Te$ in general or at least for sputtered $Pb_{1-x}Sn_xTe$. This is done in Figure 3-108. Comparison with the schematic shown in Figure 3-78(a) demonstrates the similarity. However, to our knowledge, no other bulk or thin film data for conditions much below the higher switching temperature, T_x, are available for comparison in the literature. One reason is, of course, that for bulk $Pb_{1-x}Sn_xTe$, the annealing times at these low temperatures would be prohibitively long - approaching months perhaps. While the results given in Figure 3-108 are tentative,
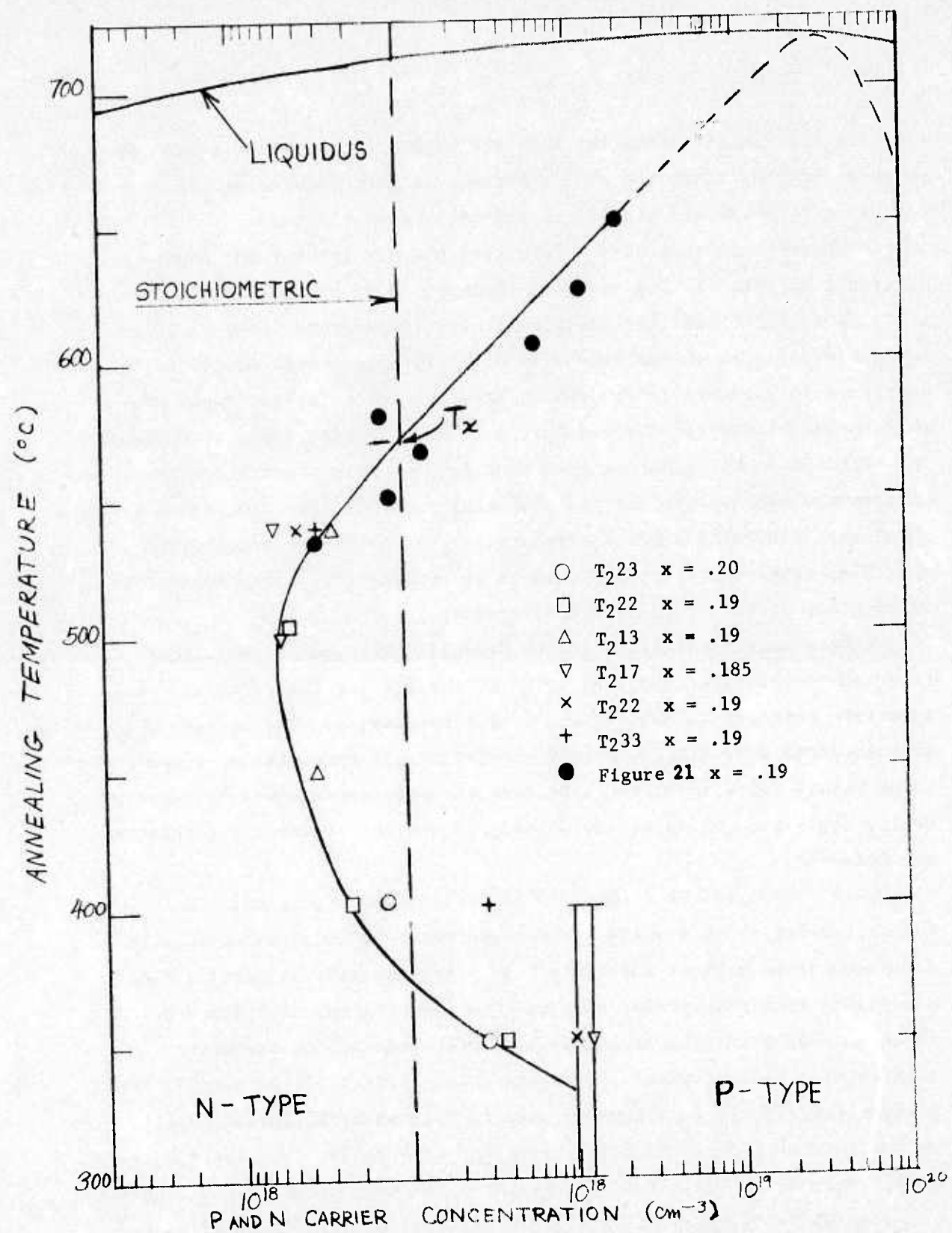
Figure 3-108 Equilibrium Phase Diagram of Single Crystal $Pb_{.81}Sn_{.19}Te$
Single Crystal Films Near the Stoichiometric Composition

the fact that it is consistent with the behavior of various films prepared at various times and with different targets throughout the course of this program should provide considerable credibility.

An analysis of this very interesting observation has not been attempted as yet. A more detailed exploration of the characteristics of films annealed near the lower switching temperature needs to be performed before such an analysis will be fruitful. It is, of course, of considerable interest if as much of an improvement in electrical properties (n, μ) can be achieved at the lower switching temperature as at T_x. Finally, a key question in the utility of this observation is whether photoconductive (or photovoltaic) response is optimized by using the lower critical annealing temperature. If both improvements are feasible, these new findings would be of considerable advantage in the preparation of thin film detector materials.

Perhaps more interesting is the deduction that can be made that this low temperature annealing point is the key for the critical substrate temperature experienced during sputtering. The latter, which we associated with stoichiometric perfection, is in a similar temperature range (above 300°C). It could be that the film experiences "annealing" during deposition which at a critical temperature produces the observed stoichiometry.

3.4.3 ANNEALING OF FILMS DEPOSITED WITH SUBSTRATE BIAS. The annealings for which results were presented above were performed with films deposited without substrate bias. As discussed in Section 3.4.3, annealings were also performed, later in the program, with films which had been deposited with substrate bias. The results of annealing studies with bias sputtered films utilizing Targets #8, #9 and #10 are presented in Tables 28 through 31 and in Figures 3-109 through 3-114. We present the results on films sputtered with Target #9 first since, to date, the most complete set of data has been accumulated for this case.

Figures 3-109 and 3-110 and Table 28 show, as a function of bias voltage, the effects of two sets of annealing conditions on the carrier
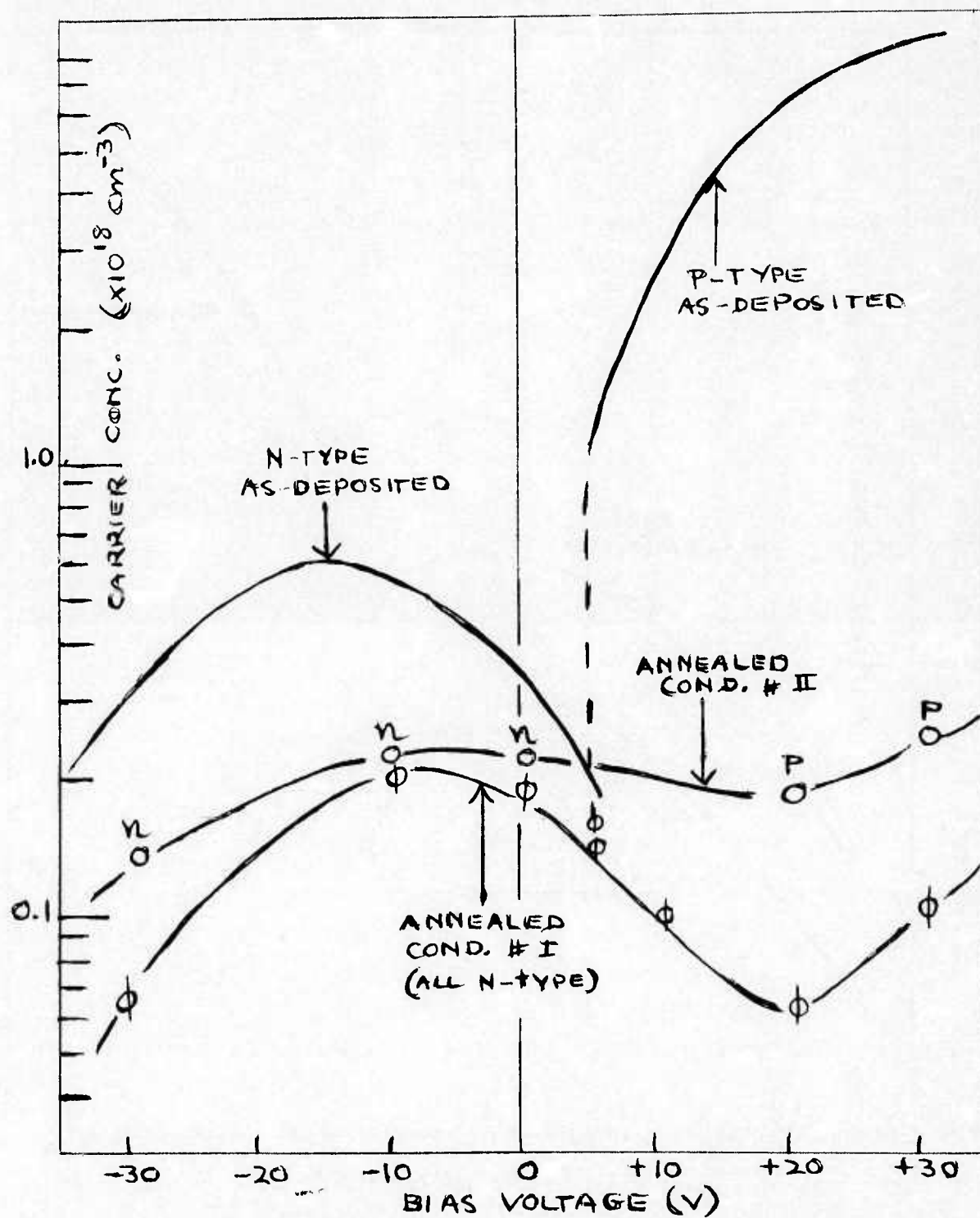
Figure 3-109   Isothermal Annealing Results for $Pb_{.80}Sn_{.20}Te$ Films Deposited
with Substrate Bias - BaF_2 Substrates (Target #9)
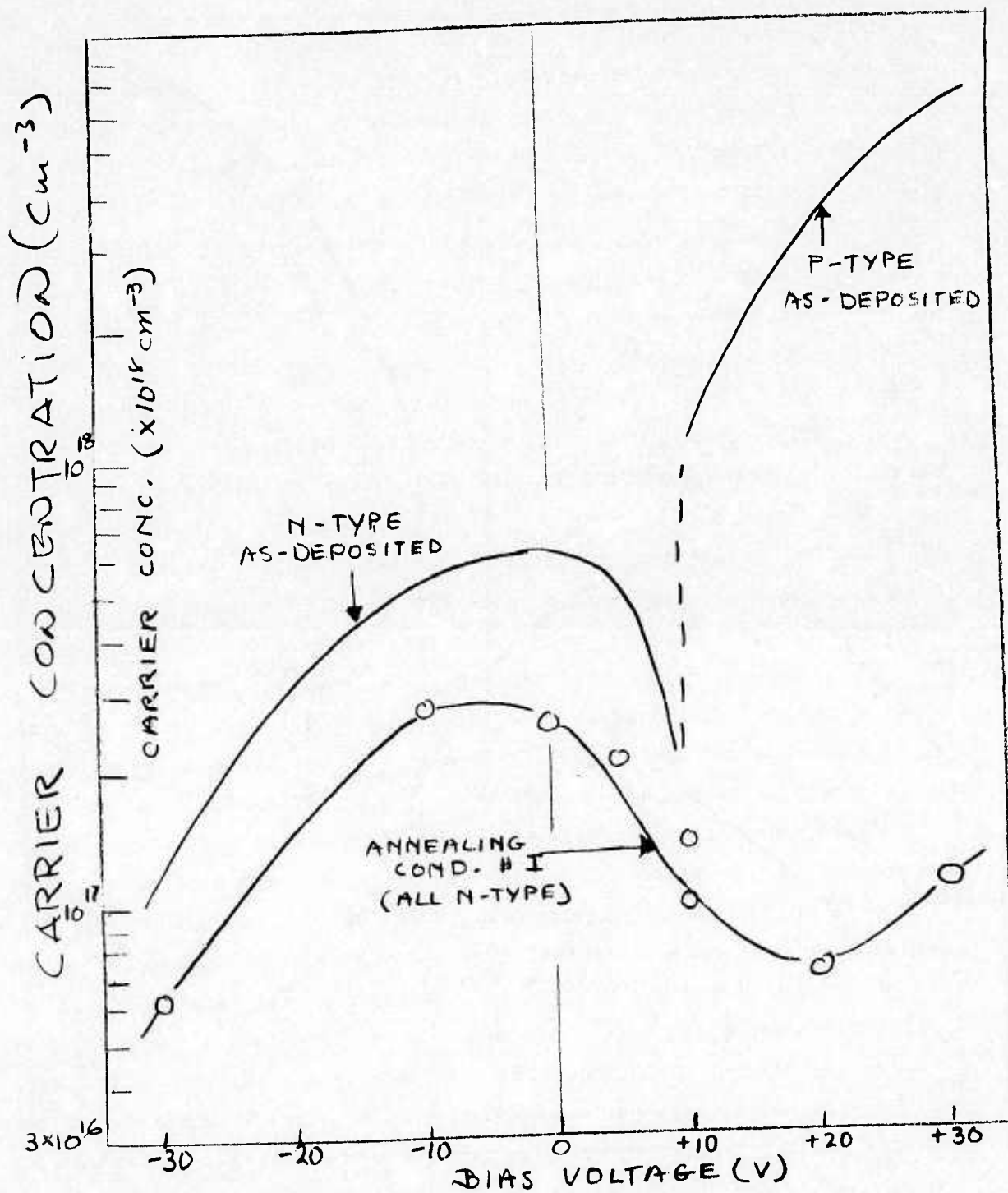
Figure 3-110 Isothermal Annealing Results for Pb.80Sn.20Te Films
Deposited with Substrate Bias - CaF$_2$ Substrate (Target #9)

concentration for films deposited with Target #9. In one figure, the films used were deposited on BaF_2 substrates, in the other figure on CaF_2 substrates. All annealing conditions represented entail initially a 6% metal-rich charge and a 12 Hr anneal at $600^{o}C$. Beyond this, one condition, defined as Condition I, has an additional low temperature anneal of 4 hours at $520^{o}C$, while the other condition, defined as Condition II, experienced an additional anneal of 4 hours at $540^{o}C$. Condition I causes all films to convert to n-type. In contrast, Condition II retains the carrier type (p- or n-type) of the as-deposited films. In both Figures 3-109 and 3-110, data on carrier concentration versus bias voltage for the unannealed films are reproduced (see Figure 3-31) for comparison.

As can be seen in Figure 3-109, both annealing Conditions I and II are exceptionally effective in reducing the carrier concentration, except in films deposited near the critical bias of about +5V which, as was expected, already had a relatively low carrier concentration. The carrier concentrations in films annealed at Condition I appears to show some dependence on the bias voltage and some of the lowest annealed carrier concentrations are achieved in films which were deposited at fairly high positive and negative biases. Indeed, the largest reduction in carrier concentration occurs in films deposited at the higher positive biases. It appears, therefore, that the observed dependence of annealed carrier concentrations on substrate bias is probably related to the as-deposited stoichiometry (i.e., largest reduction on annealing occurs in films with the largest deviation from stoichiometry). Of particular interest, however, is the observation that at certain annealing temperatures, such as given by Condition II in this case, both films deposited with positive or negative bias can be annealed simultaneously, resulting in a lowering of the carrier concentrations in both films and not affecting the p- and n-type film characteristics of either. The significance of this observation relates to the potential of forming p-n junctions in a single deposition by merely varying the bias potential

during the run and then to anneal the resulting p-n junctions in a single annealing run which lowers both the p- and n-type carrier concentrations.

It should be noted that although Figure 3-109 shows that relatively low carrier concentrations (in the 10^{16} cm^{-3} range) have been achieved under the specified annealing conditions, in neither case were these annealing temperatures optimized for the lowest carrier concentrations and further optimization should lead to even lower carrier concentrations. The data shown in Figure 3-110 for CaF_2 substrates reveal no new trends. It is interesting, however, that although the unannealed carrier concentrations are somewhat below those of the films on BaF_2, after annealing under Condition I, the carrier concentrations are almost identical for the two substrate cases over the entire bias voltage range considered.

While Figures 3-109 and 3-110 give the results for two sets of annealing conditions, Figure 3-111 and Table 29 show similar results for $Pb_{.81}Sn_{.19}Te$ films, also sputtered from Target #9, and annealed at several sets of annealing conditions. As noted, 1) the as-deposited p- and n-type films retain their carrier type but with lowered carrier concentration at an annealing temperature of $550^{o}C$, 2) the as-deposited p- and n-type films are found exclusively n-type after annealing below $550^{o}C$ (i.e., at $540^{o}C$ and $525^{o}C$) but with still lower carrier concentrations, and 3) all films are p-type if annealed above $550^{o}C$ (i.e., $580^{o}C$) and have higher carrier concentrations.

In Figure 3-112, we plot, from the available data, the carrier concentration as a function of annealing temperatures for films deposited at three bias conditions. Although the data are somewhat limited, they are adequate to show that a) films deposited with substrate bias exhibit the same behavior on annealing as films deposited at zero bias conditions and b) the bias has no significant effect on the critical annealing temperature.

Two cases illustrating the annealing effects on bias sputtered films from other targets are given in Figures 3-113 and 3-114 and Tables 30 and 31. The observed effects are quite similar to those demonstrated
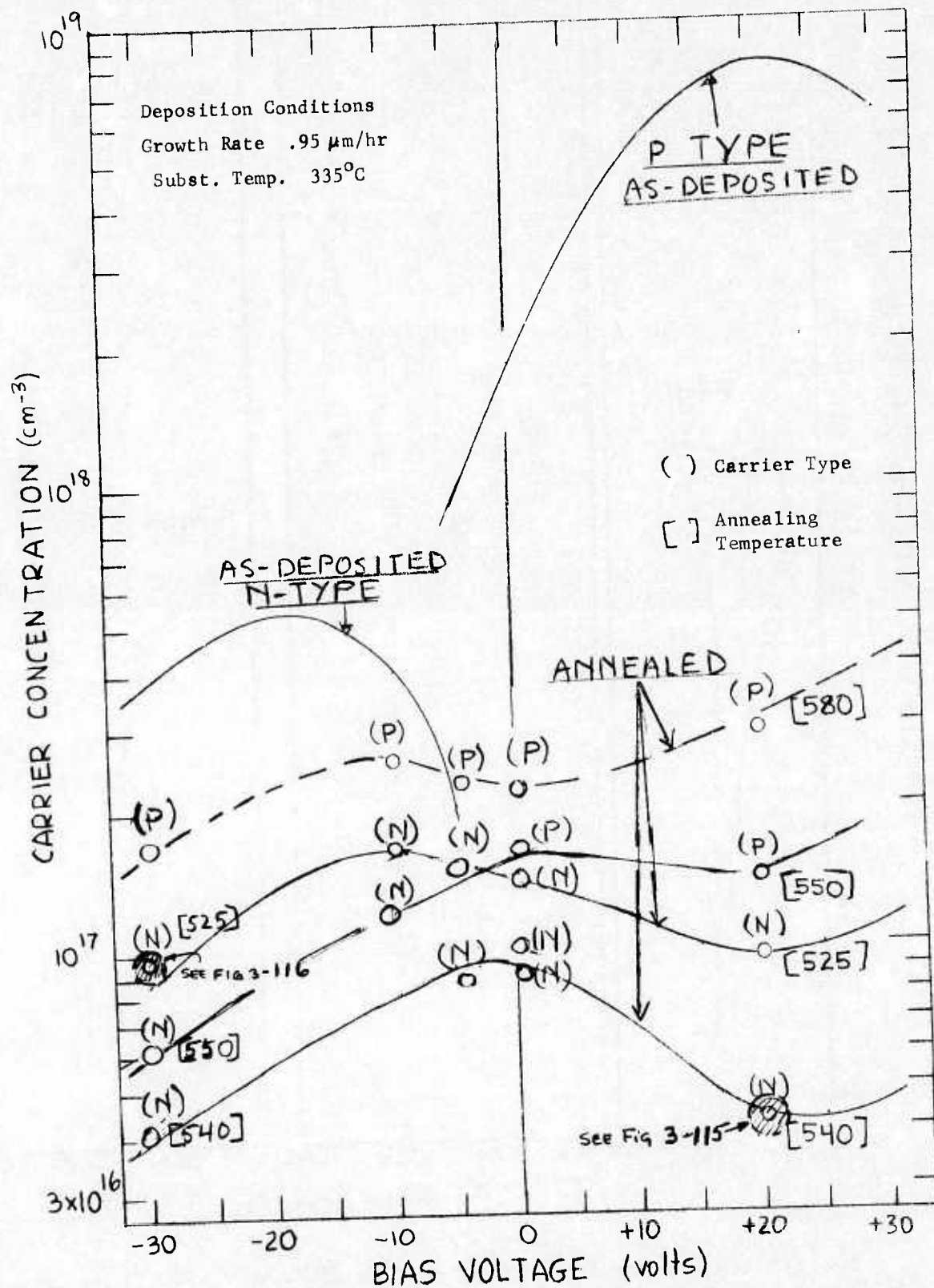
Figure 3-111 Results on Isothermal Annealing at Various Annealing Temperatures-Single Crystal $Pb_{.81}Sn_{.19}Te$ Films - Deposited with Substrate Bias Target #9

3-203
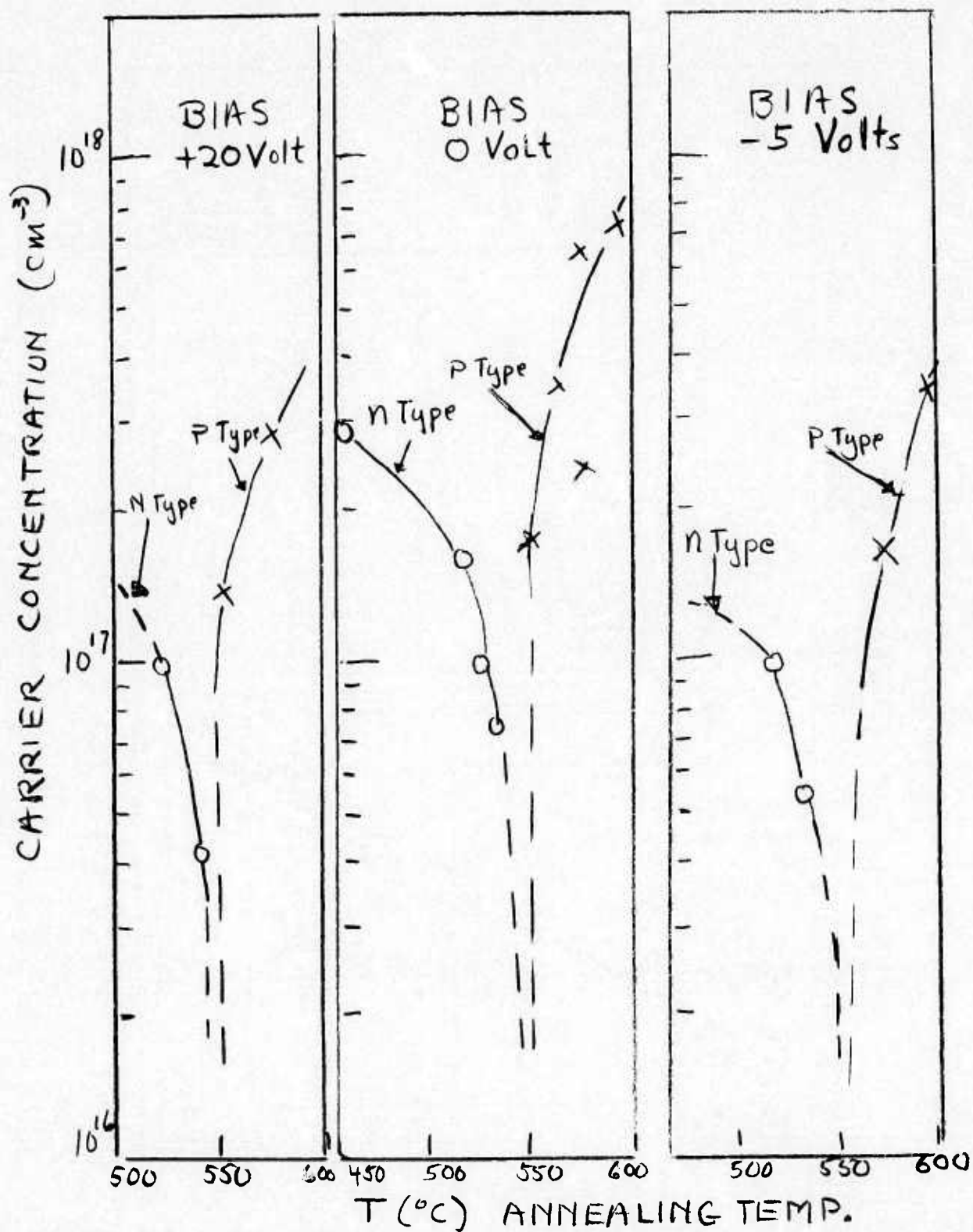
Figure 3-112 Isothermal Annealing Results of Pb.81Sn.19Te Films Deposited with Various Bias Voltages (Target #9; Subst. Temp. 335°C, Growth Rate .95 μm/hr)
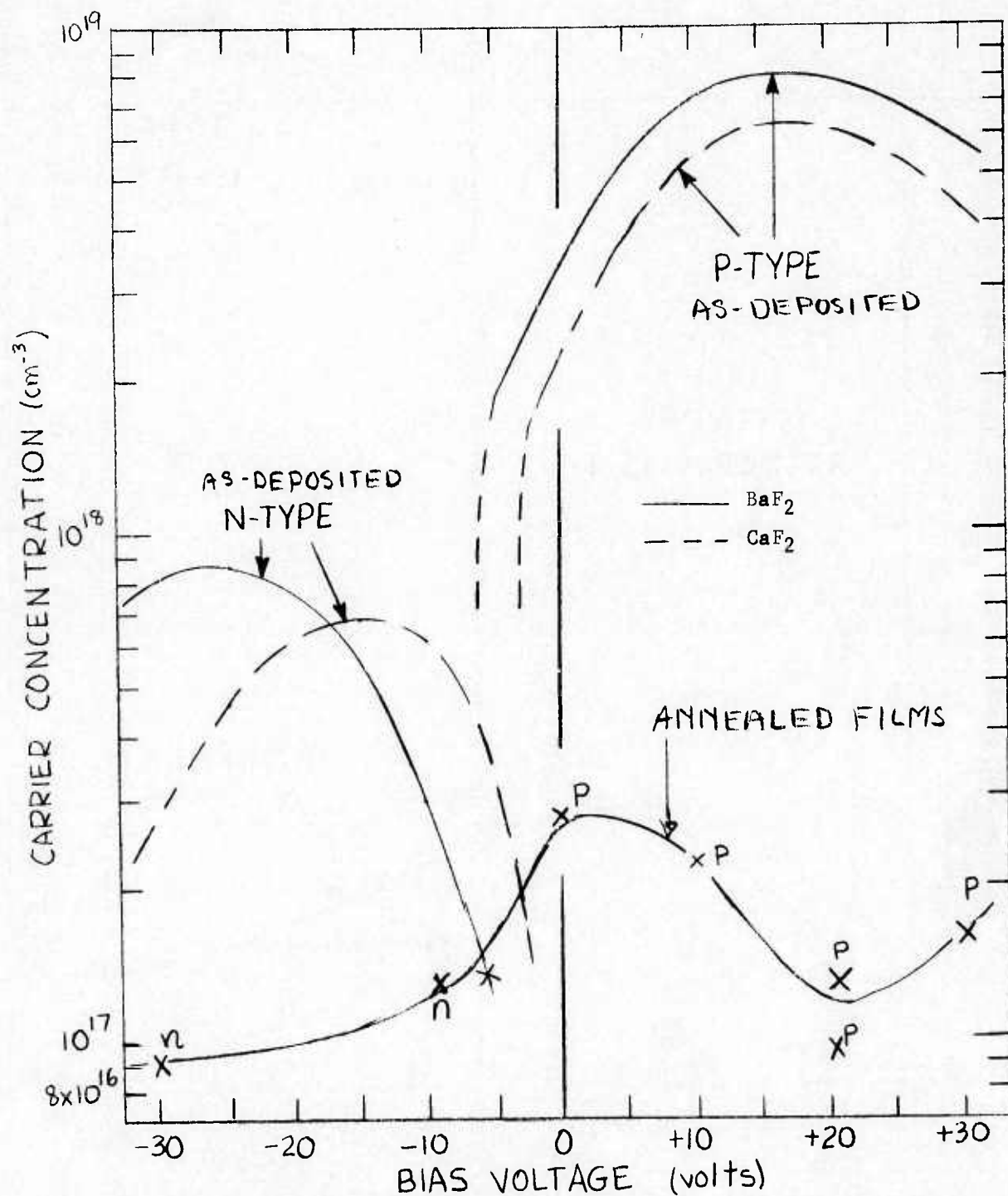
Figure 3-113 Isothermal Annealing Results for Single Crystal $Pb_{.78}Sn_{.22}Te$ Films Deposited with Substrate Bias (Target #8 - Substrate Temp. 355^oC, Growth Rate $0.8 \mu m/hr$)

Annealing Conditions: 600^oC 16 hrs
520^oC 6 hrs   (6% M.R. Charge)
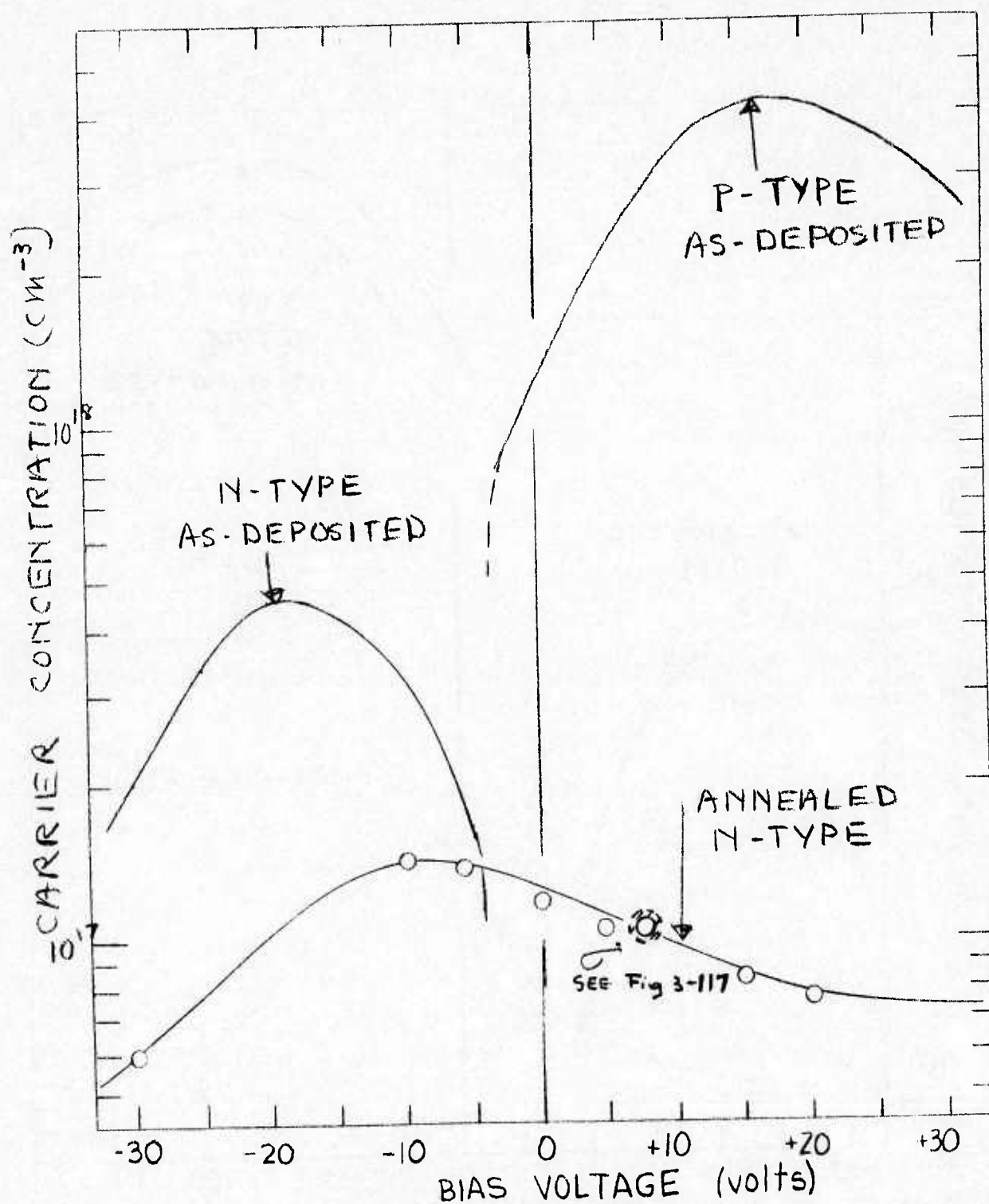
Figure 3-114 Isothermal Annealing Results for Single Crystal Pb.78Sn.22Te Films Deposited with Substrate Bias (Target #10; Substrate Temp. 340°C, Growth Rate 1.05 μm/hr)
Annealing Conditions: 500°C) 6 hrs. (6% M.R. Charge)
                      475°C) 14 hrs.

for films from Target #9 in the previous figures. This provides certainly for some confidence relative to the generality of the annealing trends. In comparing the data for Targets #8 and #10 with Target #9 results, attention must first be given to the film x-values, which are $x = 0.22$ for both the Target #8 case in Figure 3-113 and the Target #10 case in Figure 3-114. Since the Target #9 data, in Figure 3-112, were obtained with films having x-values of $x = 0.19$, the switching temperature should be considerably lower in the examples for Targets #8 and #10. Consequently, the annealing conditions in Figure 3-113, which are similar to the Condition I case ($T_{final} = 520^{\circ}C$) previously discussed, caused no change in the carrier type of the films bias sputtered with Target #8. But we see again a large reduction in both n- and p-type carrier concentration in the films which were sputtered at bias voltages which deviate from the critical bias voltage of -5V, while films sputtered at this critical value show little improvement. In Figure 3-114 the annealing conditions include temperature values considerably lower than in the previous examples ($T_{final} = 475^{\circ}C$) and all bias sputtered films, independent of the initial carrier type, are found to be n-type after annealing.

The next few figures deal with the effects of annealing on the transport properties of bias sputtered films. The pertinent Hall mobility data are presented in Tables 28 through 31. As noted, mobilities exceeding 10^4 cm^2/v-sec at 77°K are consistently measured in the annealed films. The corresponding figures (3-115 through 3-118) show that in all cases, qualitatively similar temperature dependencies of the Hall mobilities (and the Hall coefficients) exist at temperatures from 300°K to 77°K. However, some variations are apparent in the magnitudes of the Hall mobilities (and the Hall coefficients) which can be related to the deposition and annealing conditions. For example, the annealed $Pb_{.81}Sn_{.19}Te$ films shown in Figures 3-115 and 3-116 were deposited with two significantly different bias voltages (+20V and -30V) and annealed with two somewhat different temperature histories (600°C/540°C and 600°C/525°C). Reference to Figure 3-111 shows (shaded circles) that the first set of conditions yields the lower carrier concentration after annealing. Now
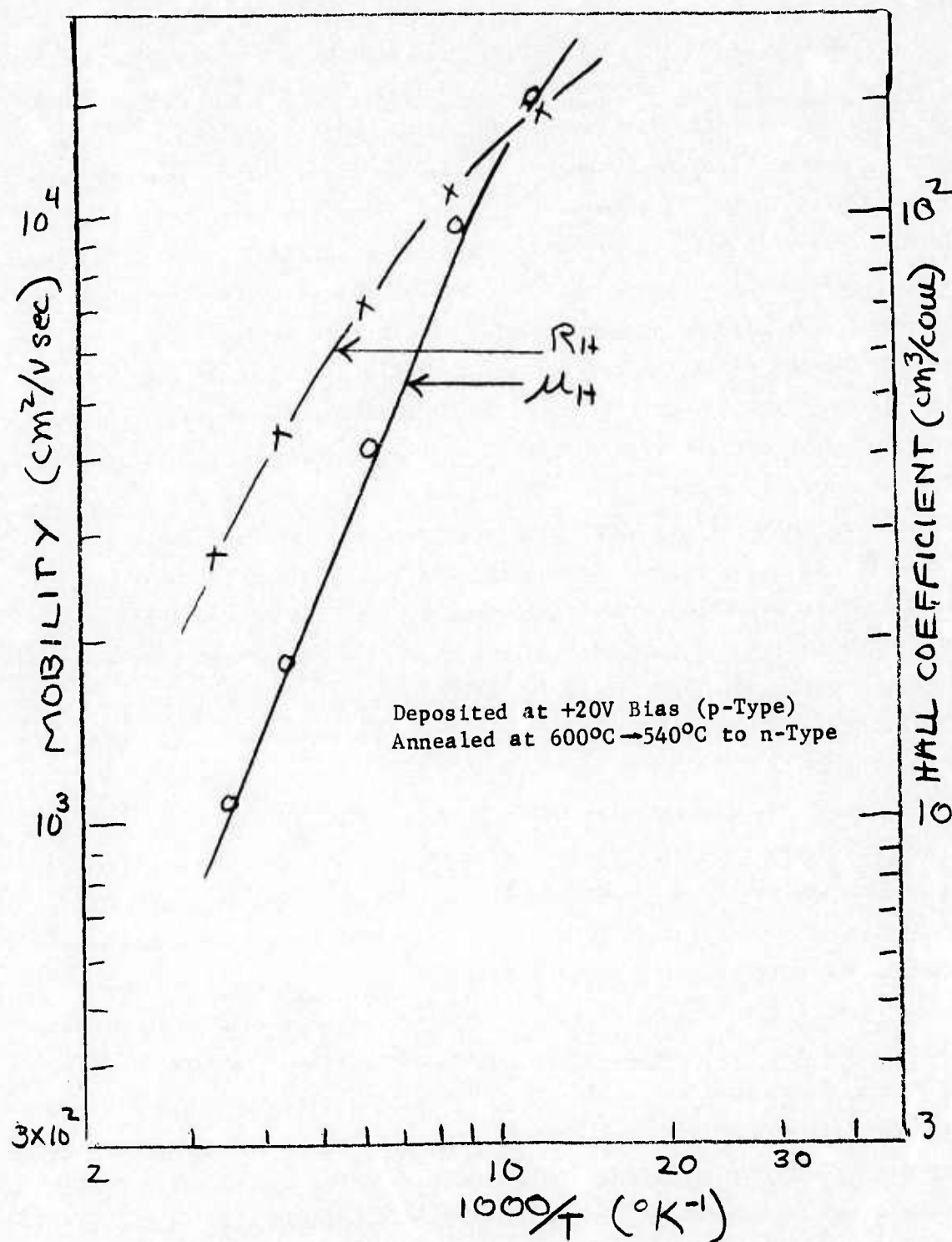
Figure 3-115 Temperature Dependence of Hall Mobility and Hall Coefficient for Isothermally Annealed Pb$_{.81}$Sn$_{.19}$Te Film (Sputtered from Target #9 at +20V Bias)
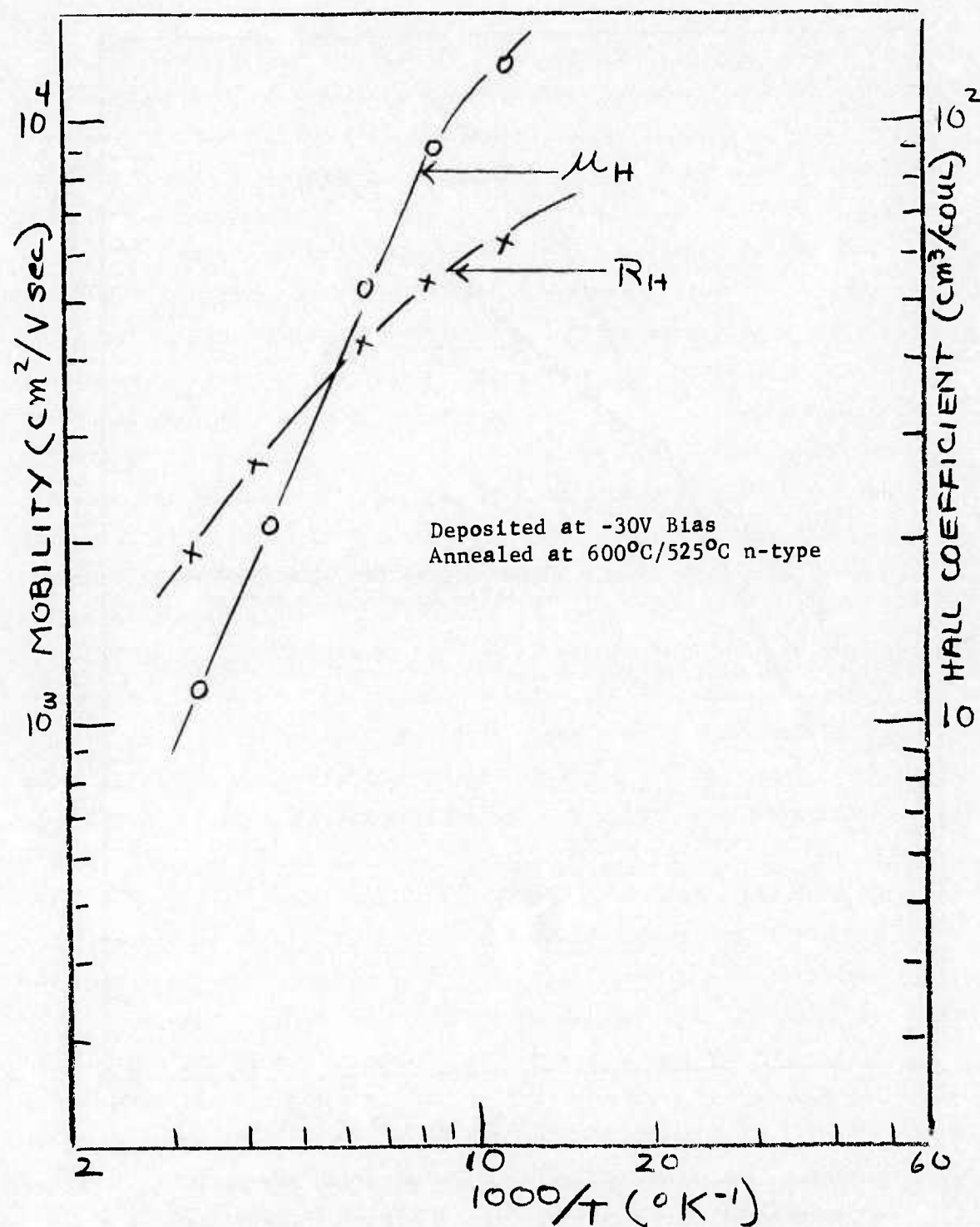
Figure 3-116 Temperature Dependence of Hall Mobility and Hall
Coefficient for Isothermally Annealed $Pb_{.81}Sn_{.19}Te$
Film (Sputtered from Target #9 at -30V Bias)
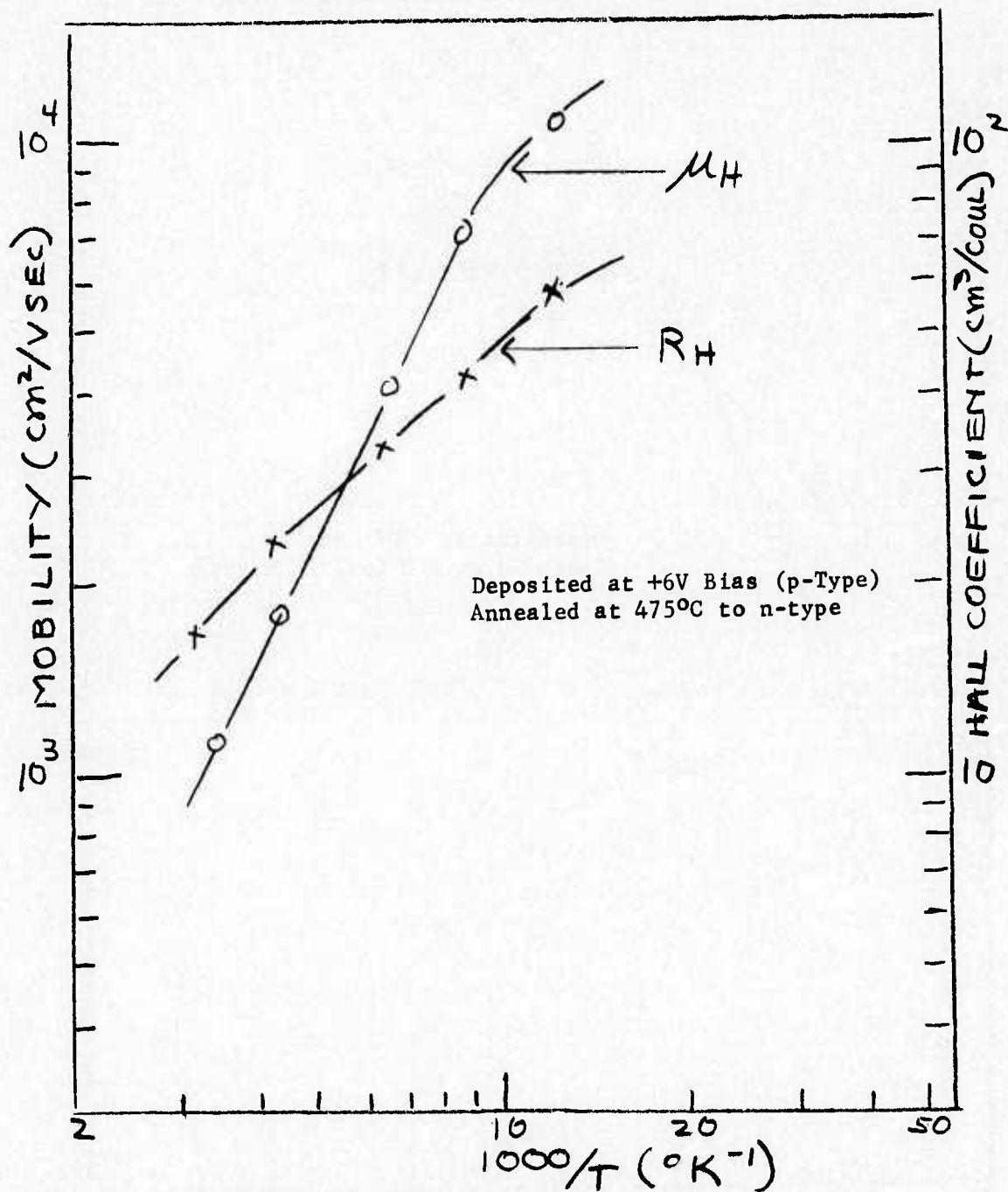
Figure 3-117 Temperature Dependence of Hall Mobility and Hall
Coefficient for Isothermally Annealed $Pb_{.78}Sn_{.22}Te$
Film (Sputtered from Target #10 at +6V Bias)
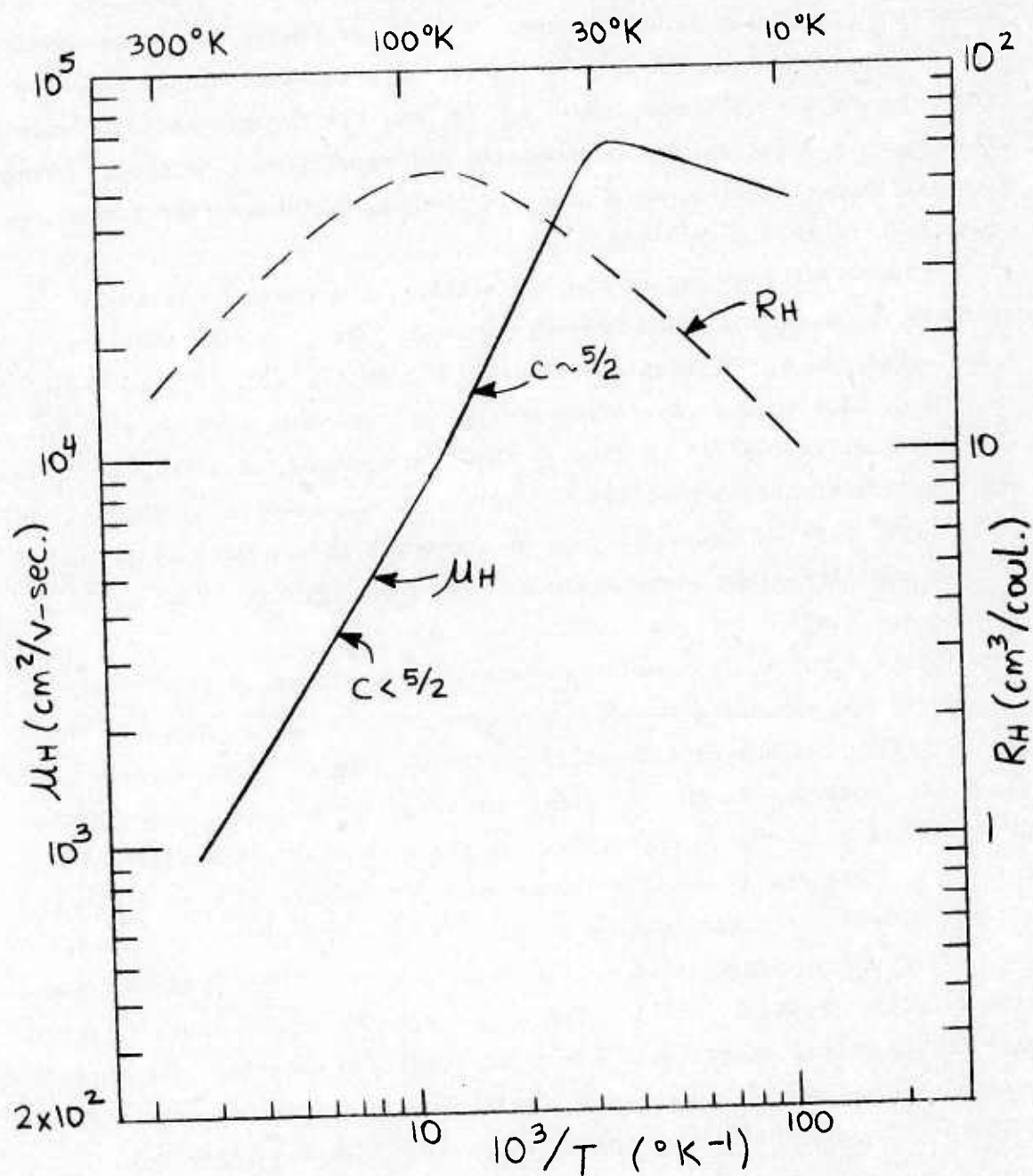
Figure 3-118 Temperature Dependence of Hall Mobility and Hall Coefficient for Annealed Pb.84Sn.16Te Film - Liquid He Measurement Facility

the mobility data indicate that in both cases, the mobilities are similarly high and show excellent adherence to the $T^{-5/2}$ phonon limited behavior down to close to $77^{\circ}K$. However, in Figure 3-116, i.e. for the films with the higher carrier concentration, the temperature dependence starts to deviate from the $T^{-5/2}$ relation at a somewhat higher temperature. The Hall coefficient shown in the same two figures reflects more drastically the difference in annealing and deposition conditions, being directly representative, of course, of the respective carrier concentration depicted in Figure 3-111.

Figure 3-117 shows, as another example, the mobility behavior (and the R_H temperature dependence) for a $Pb_{.78}Sn_{.22}Te$ film sputtered from Target #10 at +6V bias and annealed at $600^{\circ}C/475^{\circ}C$. Figure 3-114 (shaded circle) showed the corresponding carrier concentration at $77^{\circ}K$. Its magnitude is similar to that in the film represented in Figure 3-116 and the carriers are n-type also. Obviously, the results in Figure 3-117 reflect the carrier concentrations with respect to the Hall coefficient and the mobility slope shows again a $T^{-5/2}$ dependence to below $100^{\circ}K$, being quite similar to those in Figure 3-116.

At this point, it seems important to call attention to the fact that while the annealing results show considerable improvements in the Hall mobility and the Hall coefficient of the sample films, equally good films can be obtained, for the same film compositions, without annealing, provided the bias sputtering conditions are carefully controlled and optimized. Figures 3-60 and 3-61, if used for comparison with Figures 3-115 and 3-116, can attest to that.

It could be argued that annealing allows for a less critical deposition condition control. While this may be true to some degree, it would call for an even more critical annealing condition control. It stands to reason that the annealing process itself and its critical control are considerably more time consuming and expensive than the relatively simple application of the purely electrical bias control.

As can be inferred from Figures 3-115 and 3-116, the major scattering mode in films that are well annealed is that due to lattice scattering since the mobilities show a $T^{-5/2}$ dependence on temperatures from $300^{\circ}K$ to close to $77^{\circ}K$. However, in some cases, small deviations from this dependence set in near $77^{\circ}K$. As discussed in connection with the as-deposited and doped $Pb_{1-x}Sn_xTe$ films, to explore the scattering mechanisms responsible for these deviations studies and measurements over a wider temperature range is required.

An example of the temperature dependence of Hall mobility and Hall coefficient from room temperature to close to liquid He temperatures, for an annealed film, is shown in Figure 3-118. We show the results for this particular film since it exhibits a behavior slightly different from that usually observed. That is, this particular film shows a Hall mobility which varies as T^{-c} with a value of c which is slightly less than 5/2 above $77^{\circ}K$. However, between $77^{\circ}K$ and $30^{\circ}K$, c is almost exactly 5/2 a behavior which is typical only for good bulk crystals. Below about $30^{\circ}K$, the Hall mobility appears to "saturate"; in fact c is actually slightly negative.

We have noted this saturation of mobility near $30^{\circ}K$ in most of our "better" annealed films. However, critically controlled deposition conditions seem to yield as-deposited films with the same results, independent of whether the depositions entailed bias sputtering or not, or whether doping took place. A sample comparison can be made between Figure 3-118 for the annealed film and Figure 3-62 for an as-deposited film sputtered at conditions (e.g. substrate bias voltage) which yield close to stoichiometric films. Both films, for example, show the same $T^{-5/2}$ increase in Hall mobility at temperatures between $77^{\circ}K$ and $30^{\circ}K$ (and the as-deposited film has the same dependence to 300°). Below $30^{\circ}K$ the as-deposited film "saturates" also, indicating that the scattering modes operating in both films, below about $30^{\circ}K$, have similar origins. These, as we have previously discussed, may originate from imperfections (due to remaining stoichiometric deviations or impurities).

3-213

3.4.4 ANNEALING OF FILM SPUTTERED IN OXYGEN AND NITROGEN ENVIRON-
MENTS. Some results of isothermal annealing experiments performed on
films which were sputtered in partial oxygen and nitrogen pressures
with and without substrate bias are presented in Table 32. For all
cases, 4% and 6% metal rich charges were utilized. As seen, the results
are limited. However, they seem adequate to illustrate some annealing
effects. We consider, first, the films sputtered with zero substrate
bias. As noted in Table 32, these films, if sputtered in low partial
nitrogen pressures (SN12, SN14), are n-type prior to annealing with
carrier concentrations in the mid 10^{17} cm^{-3} range. On annealing close
to the critical annealing temperature for the identified composition
(x = 0.21) a decrease in carrier concentration with a corresponding
increase in mobility is measured in these films. The films remain
n-type. This is a desired and typical annealing result. If we, on
the other hand, look at the annealing results of films (SN7 and SN6)
which were sputtered with partial oxygen pressures between 2 x 10^{-6}
and 5 x 10^{-6} Torr and were annealed at temperatures above the critical
temperature (i.e. $580^{o}C,>Tc$ for x = .20) the results differ considerably.
The films remained p-type on annealing but the carrier concentration
increased to values in the high 10^{17} cm^{-3} range from values in the mid
10^{16} to mid 10^{17} cm^{-3} range. The increase in p-type carrier concentra-
tion may be due to: 1) the oxygen, which caused compensation or
produced traps, being released on annealing, 2) a stoichiometric ad-
justment toward the Te-rich side. By contrast, annealing slightly
below the critical annealing temperatures (e.g. final anneal of sample
SN7 in Table 32) causes the film to switch to n-type and lower the
carrier concentration which is again typical annealing behavior for a
$Pb_{.80}Sn_{.20}Te$ film. Sample SN8 was sputtered with a rather low partial
pressure of oxygen but under less than optimum conditions. The high
carrier concentration is slightly improved on annealing but remains
higher than usual.

Annealing results for films deposited in pp O_2 and N_2 environments and with substrate bias are also presented in Table 32. As noted, the results are limited to films deposited with a substrate bias of +30V and with relatively low partial pressures of O_2 and N_2. The starting films were, in all cases, p-type with carrier concentrations in the 10^{18} cm^{-3} range. That is all films were deposited under conditions which yielded rather non-stoichiometric compositions. As can be seen for samples, SN16, SN19, SN15, and SN17, for the annealing temperatures used, the film properties realized were very typical of those achieved with undoped $Pb_{1-x}Sn_xTe$ films of the corresponding compositions. Final carrier concentrations ranged from the low 10^{17} cm^{-3} to the low 10^{16} cm^{-3}. Of course, it is possible, perhaps probable, that the doping that had taken place in these latter films was minute due to the low partial pressures of O_2 and N_2 used and the relatively high positive substrate bias applied.

3.5 PROTON BOMBARDMENT OF SPUTTERED PbSnTe FILMS.

The purpose of an, at least, cursory investigation of ion implantation in this program is aimed at exploring its potential in improving electro-optical properties of sputtered PbSnTe films as well as its potential in the preparation of PbSnTe sensor devices. For example, ion implantation may be used to improve the properties of $Pb_{1-x}-Sn_xTe$ films by reducing the effective carrier concentration via impurity compensation or it may be used to introduce trapping centers for the potential enhancement of the photo-electric responsivity of our sputtered films. For device objectives ion implantation has its natural application in the preparation of p-n junctions. The implantation of heavy ions has severe limitations for LWIR sensor materials because of the ion penetration depths of most useful impurities. One approach to solve this problem is to use proton bombardment followed by impurity diffusion as discussed in detail in our proposed program (Reference 27). However, proton bombardment can be used also alone to control material properties for many applications. For example, it

3-215

has already been well demonstrated for bulk and thin film materials that proton bombardment can change p-type $Pb_{1-x}Sn_xTe$ to n-type (References 28 and 29). In certain cases, n-p junctions were achieved and photovoltaic response recorded (Reference 29).

As part of the program of ion implantation or proton-bombardment followed by ion diffusion, we initiated first the experiments on the effect of implanted protons on the properties of sputtered $Pb_{1-x}Sn_xTe$ films. Initial, limited results are presented in Table 33. As noted, the initial experiments were performed with relatively low proton energies (~ 60 - 80 KeV). For these proton energies, proton doses of 9×10^{15} p/cm^2 are required in order to change the carrier type. Proton doses of 1×10^{15} p/cm^2 did not result in change of carrier type regardless of the starting carrier concentration. However, the carrier concentrations showed a small decrease.

For proton doses in the 10^{16} p/cm^2 range larger decreases in carrier concentration resulted along with the change in carrier type. These decreases were greater than an order of magnitude, yielding films with effective carrier concentrations in the low 10^{16} cm^{-3} range.

The mobility in each film was increased after bombardment by factors on the order of four if the films changed carrier type. For films which did not change carrier type, the mobility increase was limited to within a factor of two. Although the results shown are preliminary, they demonstrated the fact that in sputtered $Pb_{1-x}Sn_xTe$ films, the as-deposited properties can be altered by proton bombardment without any degradation. In fact, improvements result in most cases.

3.6 ION BEAM SPUTTERING

3.6.1 INTRODUCTION. The proposed plan for the latest phases of this program, called for emphasis on ion-beam sputtering as the technique for the deposition of $Pb_{1-x}Sn_xTe$ thin films. However, before the ion-beam sputtering system could be used as a major technique, a modification in the ion-gun assembly had to be implemented. Primarily

this entailed an increase in the ion-current and, therefore, the deposition rates of PbSnTe films. Without this modification, un-economically long times were required to deposit sufficiently thick films for most of the proposed applications such as for photovoltaic devices. Perhaps more importantly though, the range of the possible composition control, such as reflected in the phase diagrams for supported discharge sputtering (e.g., see Figure 3-1) would be undesirably limited. Furthermore, the modification was aimed at allowing the study of kinetic energy effects, independent of the ion beam density (or deposition rate) effects. However, it became apparent soon after the start of this phase of the contract that some delay would be experienced in the implementation of these modifications. Severe difficulties were experienced with the newly procured ion-gun assembly - resulting from inferior construction of several parts. This required extended waiting periods for replacement parts from the manufacturer and severe delays in the assembleage.

Despite these difficulties, some initial experiments for defining the range of deposition conditions for which single crystal films can be formed and the measurement of the corresponding electrical and compositional properties have been performed and are discussed below.

3.6.2 INITIAL ION BEAM SPUTTERING EXPERIMENTS. In the experiments carried out it was possible to cover a reasonable set of depositions with ion beam energies ranging from less than 2 kV to 10 kV, with substrate temperatures from RT to near 400°C and with film growth rates from 0.01 to 0.5μm/hr. As was seen later, the growth rates are deceptive in many cases due to post deposition reevaporation.

Thus far it was not yet possible to determine the entire range of conditions for which single crystal films can be formed - on substrates of CaF_2 and BaF_2. One fact has, however, been confirmed; excellent single crystals are produced at far lower substrate temperatures than by the other sputtering techniques. At temperatures as low as 250°C very good (mono-) crystallinity was observed both by electron

microscopy and x-ray analysis. This is at least 50°C below the temperature at which comparable quality film was found by the other sputtering techniques. Typical examples of epitaxial film structure (electron microscopy) film orientation (x-ray diffraction) etc. are shown in Figures 3-119 and 3-120. In Figure 3-119 we show a typical 2θ scan of an ion-beam sputtered $Pb_{.85}Sn_{.15}Te$ film on a (111) CaF_2 substrate. As is apparent from this figure, the film is epitaxially (111) oriented on the (111) substrate (confirmed by the presence of (111), (222), (444) lines for both the substrates and the films). Indeed, to date, all single crystal films, ion-beam sputtered on (111) CaF_2 and (111) BaF_2 substrate, have shown a (111) orientation. These x-ray results are supported by reflection electron diffraction results. To illustrate, typical epitaxial film structures of an ion-beam sputtered $Pb_{.85}Sn_{.15}Te$ film are shown in Figure 3-120. Here we see the $(1\bar{1}0)$ and the $(1\bar{2}1)$ electron diffraction patterns of a cleaved CaF_2 (111) substrate and of the $Pb_{.85}Sn_{.15}Te$ film deposited on the same substrate. As noted, since the <111> direction in the film is normal to the surface and, therefore, parallel to the substrate <111> axis, the $(1\bar{1}0)$ and $(1\bar{2}1)$ patterns are obtained by proper positioning of the sample and rotation about its normal. A rotation angle of 30 degrees separates the $(1\bar{1}0)$ orientation from the $(1\bar{2}1)$ orientation, as expected for the cubic lattice. It is apparent, from this figure that the film patterns indicated a crystal quality which is comparable to that of the substrate.

As was mentioned above good quality single crystal films are sputtered with ion-beam sputtering at temperatures as low as 250°C. These low epitaxial temperatures may be the solution to two problem areas discussed in the following paragraphs - low growth rates and re-evaporation.

The unit contains a substrate holder which can accomodate up to nine substrates. The substrates are arranged in sets of three and each set is exposed simultaneously to the target by means of a shutter

Relative Intensity

30KVP/20 ma

CaF$_2$ K α2 (444)

CaF2 K α1 (444)

CaF2 K β (444)

K α 2 (444)

K α 1 (444)

CaF$_2$ K α2 (333)

CaF$_2$ K α1 (333)

CaF$_2$ K β (333)

150   140   130   120   110 2θ 100   90
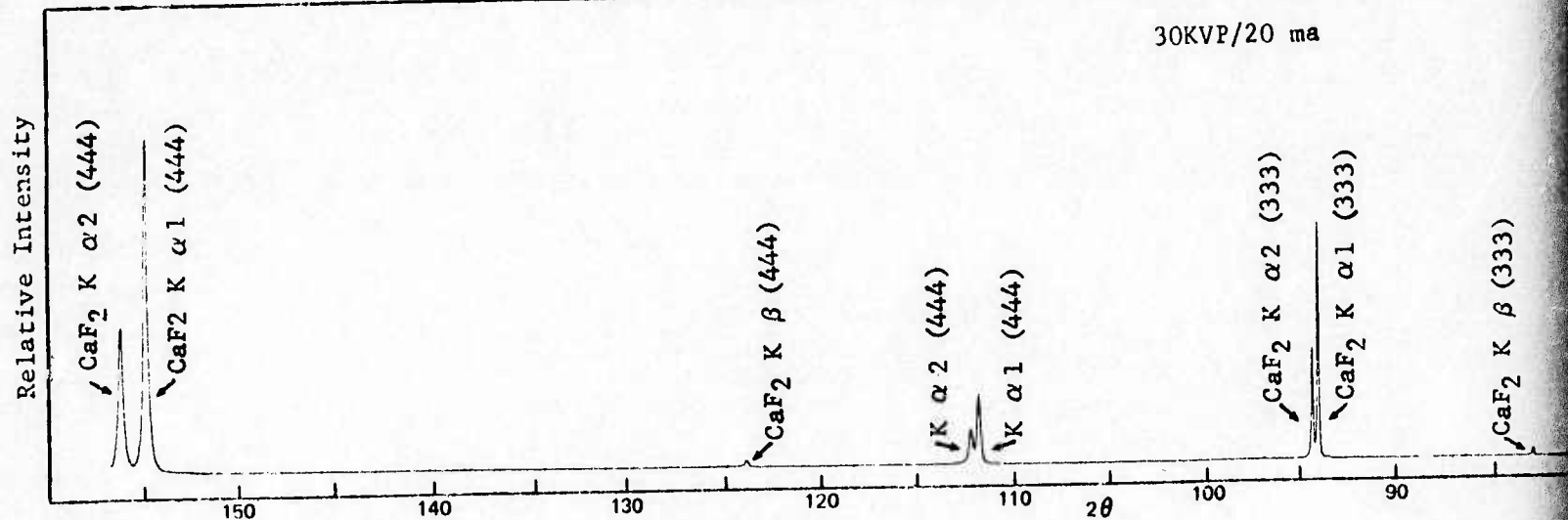
Figure 3-119   Two Theta Scan of Ion Beam Sputte

KVP/20 ma

CaF$_2$ K α2 (333)

CaF$_2$ K α1 (333)

CaF$_2$ K β (333)

K α2 (333)

K α1 (333)

CaF$_2$ K α2 (222)

CaF$_2$ Kα1 (222)

K α (222)

K β (222)

CaF$_2$ K α (111)

CaF$_2$ K β (111)

K α (111)

K β (111)

100   90   80   70   60   50   40   30   20
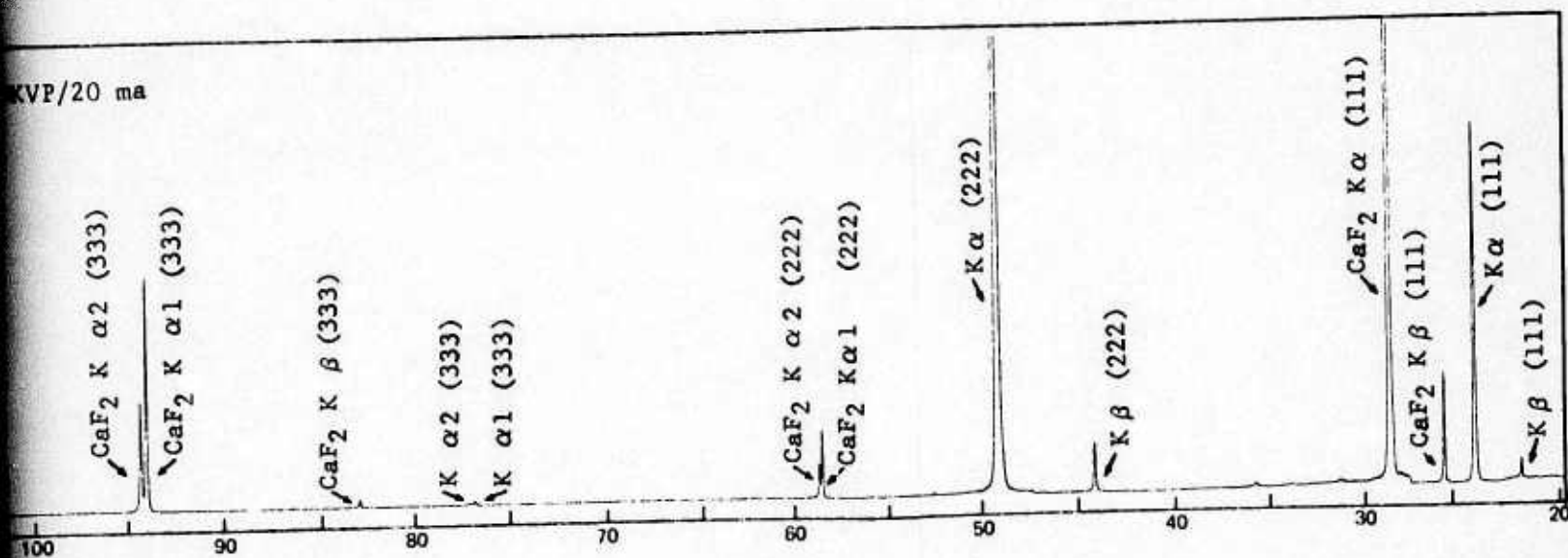
Scan of Ion Beam Sputtered Pb$_{.85}$Sn$_{.15}$Te Film on CaF$_2$ Substrate
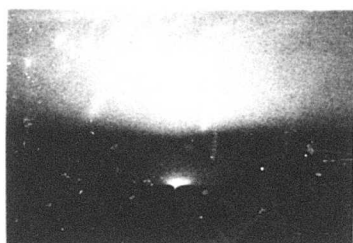
$(1\bar{1}0)$ $(1\bar{2}1)$

CaF_2 (111) Substrate
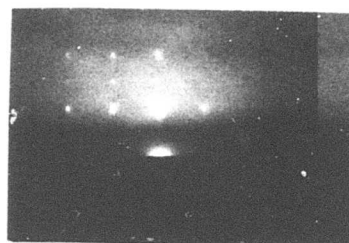
$(1\bar{1}0)$ $(1\bar{2}1)$

(111) $Pb_{.85}Sn_{.15}Te$ Film

Figure 3-120 Reflection Electron Diffraction Patterns for Ion Beam
Sputtered Single Crystal $Pb_{.85}Sn_{.15}Te$ Film on CaF_2 (111) Substrate

aperture. In this fashion, three experiments can be run during any one pump down - each experiment using a different set of deposition conditions. Considering the fact that at least an overnight pumpdown is required to establish the desired background pressure of 1×10^{-8} torr or less; this arrangement represents a considerable time savings. Unfortunately, we have now found that, in the case of $Pb_{1-x}Sn_xTe$, we may not be able to take advantage of this feature. During the time one set of films is being deposited, any of the films previously deposited are subject to re-evaporation. In part this is due to the fact that the substrate heater is common, i.e. all sample, are at the same temperature before, during and after deposition. A new substrate heater arrangement could eliminate this problem. Yet, even in single sets of films, a considerable amount of evaporation takes place after the completion of a deposition, i.e. during the time required to cool the substrate holder system to a reasonable temperature near ambient so that venting of the system can be safely performed. Maintaining a background pressure of high purity argon of about 2×10^{-7} torr can, to a large degree, reduce this re-evaporation.

The re-evaporation is certainly an undesirable phenomenon. It reduces the effective deposition rate to in some cases unusable levels (e.g. < .02 μm/hr in cases where multiple substrate sets were used and to lower than desired levels in all cases). More importantly, it is feared that it is associated with a preferential re-evaporation of the higher vapor pressure film components, in particular tellurium. This seems to be reflected in some rather high n-type carrier concentrations in films in which re-evaporation was not controlled. The difference between the carrier concentrations of films sequentially deposited under identical conditions may be as high as two orders of magnitude depending on effective deposition rates.

Another problem which has not been confirmed but may be real is that high energy argon, ionized or neutral, may be implanted in the film during deposition. It must, of course, be expected that a

certain percentage of the ions in the ion beam is elastically reflected from the target. A portion of these ions, perhaps neutralized on collision with the target, will be incident on the substrate surface. Although the sticking coefficient for physical adsorption should be relatively low, it may be considerably increased by partial imbedding of the relatively high energy argon particles. All this would be maximized with the inherent system geometry where incident beam and substrates are at angles of 45° from the surface of the target. The density of the elastically reflected particles is in this case highest in the direction of the substrate, as would be the energy of particles reaching the substrate. The same arguments hold for any impurity ions or atoms in the argon beam which could be the result of sputtering from orifice walls etc. Since the original design had exactly the apparently most undesirable geometry, experiments have been carried out with considerably different arrangements. In particular it was found that a target whose surface is nearly normal to the incident beam (and the substrate surface) can actually enhance the sputtering rate - while theoretically at least minimizing the incidence of elastically reflected elements of the ion-beam on the substrate. Such an arrangement has the added advantage that target mounting is greatly simplified. Since the beam comes from the top, the target can simply be layed down on a (cooled) supporting surface - without special bonding requirements.

All identified problems appear readily solvable and are actually only significant because the environment is so much improved over that in the other sputtering system. This gives cause for optimism that exceptionally high purity samples - approaching intrinsic carrier concentration - can be produced without the need for post-deposition annealing. For the present, the few experiments run show already the advantage of this technique on film structure. Electrically, unannealed samples range from poor to good. Generally poor were those which were subject to considerable re-evaporation, as discussed. On the other hand, the very few samples which were annealed thus far produced

carrier concentrations as low as the 10^{16} cm^{-3} range - quite compatible with sample prepared by other, far more optimized techniques.

3.7 ELECTRO-OPTICAL MATERIAL ANALYSIS.

3.7.1 INTRODUCTION. As explained in Section 3.1 perhaps the most revealing and relevant test of the quality of the thin films prepared under this program is to evaluate their electro-optical properties since electro-optical device application is the ultimate goal. Therefore, as also discussed in Section 3.1, our approach has been to systematically establish the deposition conditions under which device quality PbSnTe films can be deposited by determining those conditions which yield structurally and compositionally high quality films and to then correlate these preparation conditions with the device related electrical and electro-optical properties. Those properties which are found to be of particular relevance to the functional performance (e.g. photoconductive, photo-voltaic response) are then optimized by suitable selection of the preparation parameters.

The work to be reported in this section includes results on electro-optical measurements on both as-deposited and annealed single crystal films prepared under a variety of conditions - with and without substrate bias. The electro-optical measurements include photoconductive responsivity as a function of wavelength and frequency, noise measurements as a function of current and frequency, as well as lifetime measurements. Where applicable, D* values are indicated. The temperature range of measurement with some samples was to $90^{\circ}K$, others to $77^{\circ}K$ and selected measurements were made to below $30^{\circ}K$. The differences are due to the fact that at the beginning of this program, the dewar utilized for these measurements permitted measurement to $90^{\circ}K$ only. During the course of this program, the new Janis dewar was installed which permits electro-optical measurements down to liquid He temperatures ($4^{\circ}K$ or below). It was then possible to make measurements to $77^{\circ}K$ routinely and to lower temperatures when desired.

As will be seen, a considerable number of our sputtered films have been evaluated electro-optically during the course of this program. The results of these investigations demonstrated, relatively early in the program, that the measured photoconductive responses are fully correlatable with structure, structural quality, and composition. As will also be shown, the cut-off wavelengths obtained agree quite well with the bandgaps predicted from the measured x-values of the films. Also, stoichiometry, electrical properties such as carrier concentration and mobility - in short, all quality or control parameters of interest in this study - are equally correlatable with the electro-optical properties. There is little doubt left that films with the best structural and electrical properties have, in general, the highest responses as well as the lowest noise characteristics. These early results not only proved the value of our approach to assessing film quality, but demonstrated also that good quality films with electro-optical properties comparable with bulk single crystals could be prepared. The fact that it was possible to establish a direct parametric relationship between the PbSnTe film preparation conditions and the electro-optical properties is a very valuable consequence of this work relative to producibility specifications.

With this general progress achieved early in the program, one of the principal objectives of the subsequent investigations was, of course, the improvements of those properties which should lead to improved photo-electric properties of the sputtered PbSnTe films.

One example, the utilization of bias sputtering,(a technique which as we have seen was introduced during the later phases of this work to improve film electrical properties, in particular, carrier concentration and mobility) was ultimately aimed at the improvement of electro-optical properties. Results presented in the following sections will certainly show that bias sputtering is affecting the electro-optical properties as advantageously as the electrical properties.

A second example includes the methods for achieving improved photo-response by investigating means by which trap-enhanced photo-response might be achieved. As may be recalled, the observation in a number of films of some exceptionally high photo-conductive responses which appeared to be due to (uncontrolled) trap enhancement lead us in this direction. The doping of $Pb_{1-x}Sn_xTe$ films during sputtering, by the addition of a partial pressure of oxygen and nitrogen in the sputtering gas was one attempt. We have seen in Section 3.3 a substantial effect of such doping on the electrical properties. As we shall see in the following sections, simultaneous systematic increase in photoconductive responses have been observed also as a function of the partial pressure of the O_2 and N_2 in the sputtering gas.

Although the indication is that the doping of $Pb_{1-x}Sn_xTe$ film by sputtering in partial oxygen and nitrogen pressures is introducing trapping centers, it was too difficult, without more extensive experimentation and analysis to identify these as traps. In fact, there is considerable uncertainty as to what constitutes effective traps in $Pb_{1-x}Sn_xTe$. For this reason as well as others, one of the objectives in this phase of the study was to extend electrical, optical and electro-optical measurements to temperatures of less than 15^oK. It is the only possible means for a meaningful study of trapping behavior as well as of scattering mechanisms and other response limiting properties in small energy gap materials. The results of electrical measurements down to liquid helium temperatures were already presented. Some results of photo-responses in $Pb_{1-x}Sn_xTe$ films measured at these lower temperatures are presented in the following sections.

Finally, as repeatedly stated, photoconductive behavior was primarily evaluated. This in spite of the fact that PbSnTe is generally accepted as being principally useful in the photo-voltaic mode. The reason stated was that photoconductive behavior is more directly relatable to material properties. As this work has shown, photoconductive response is by no means impossible for device

application - based on the enhancement achieved thus far. Therefore, the photoconductive evaluation is relevant to device potential also. However, beyond this, results will also be included on several PbSnTe p-n junction and Schottkybarrier photo-voltaic response characteristics as a function of preparation parameters. The latter are selected data from the General Dynamics IRAD activities referred to above.

3.7.2 ELECTRO-OPTICAL PROPERTIES OF FILMS DEPOSITED WITH ZERO SUBSTRATE BIAS. Based on the manner in which this program proceeded, results are given in sequence for films prepared without substrate bias and with substrate bias. This section reports the electro-optical behavior observed in films deposited without substrate bias. Results on measurements on films deposited with substrate bias are presented in a later section.

3.7.2.1 Photoconductive Response, Noise and Lifetime Measurements. Figures 3-121 and 3-122 show the absolute spectral responsivities and detectivities, at $90^{\circ}K$, for several typical $Pb_{1-x}Sn_xTe$ sputtered films with composition from $x = .14$ to $x = .20$. The photoconductive detector performance data for these films are also presented in Table 34. The as-deposited photoconductive response value of, for example, 2.8v/watt at $90^{\circ}K$, with noise properties that lead to a D* value of 2.4×10^8 cm $Hz^{\frac{1}{2}}/w$ ($300^{\circ}K$, 2π background), is in the range of or better than values for annealed films or bulk single crystal reported by other investigators (References 17 & 30)-if extrapolated to $77^{\circ}K$. These sources quote responsivities from about .2 to 5.4 v/watt and D* values in the range of 1.2 to 2.7×10^8 at $77^{\circ}K$. Extrapolation of our data can be based on later measurements to $77^{\circ}K$ with the new Janis dewar referred to above. These measurements showed that operation at $77^{\circ}K$ should produce an increase in responsivity by at least a factor of 2.2 over values measured at $90^{\circ}K$.

As we have already stated, measurable photo-response could only be found in single crystal films with excellent structures. Correspondingly, it was found that the measured noise was a very critical
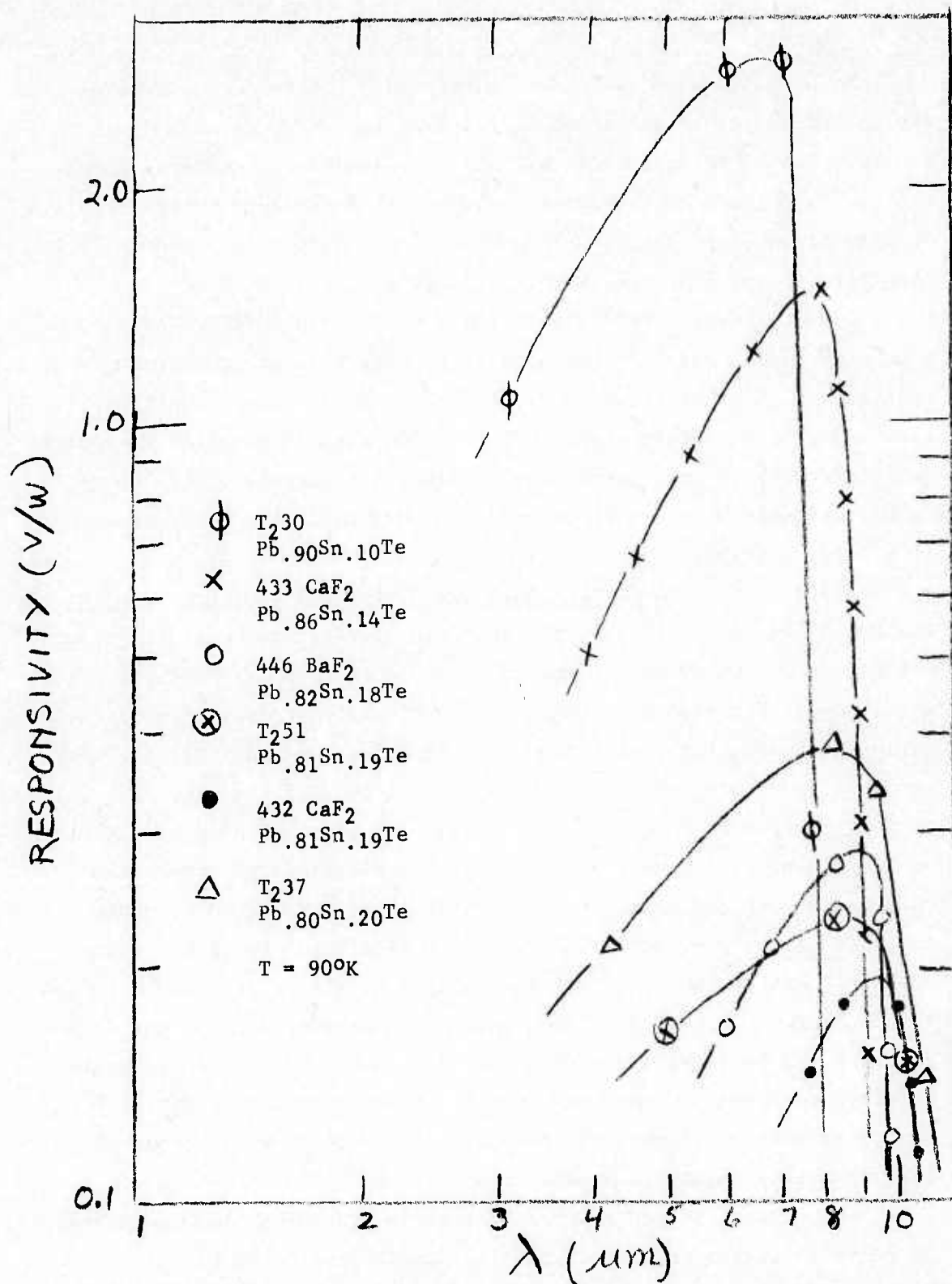
Figure 3-121 Absolute Spectral, Photoconductive Responsivity of
As-Deposited $Pb_{1-x}Sn_xTe$ Films
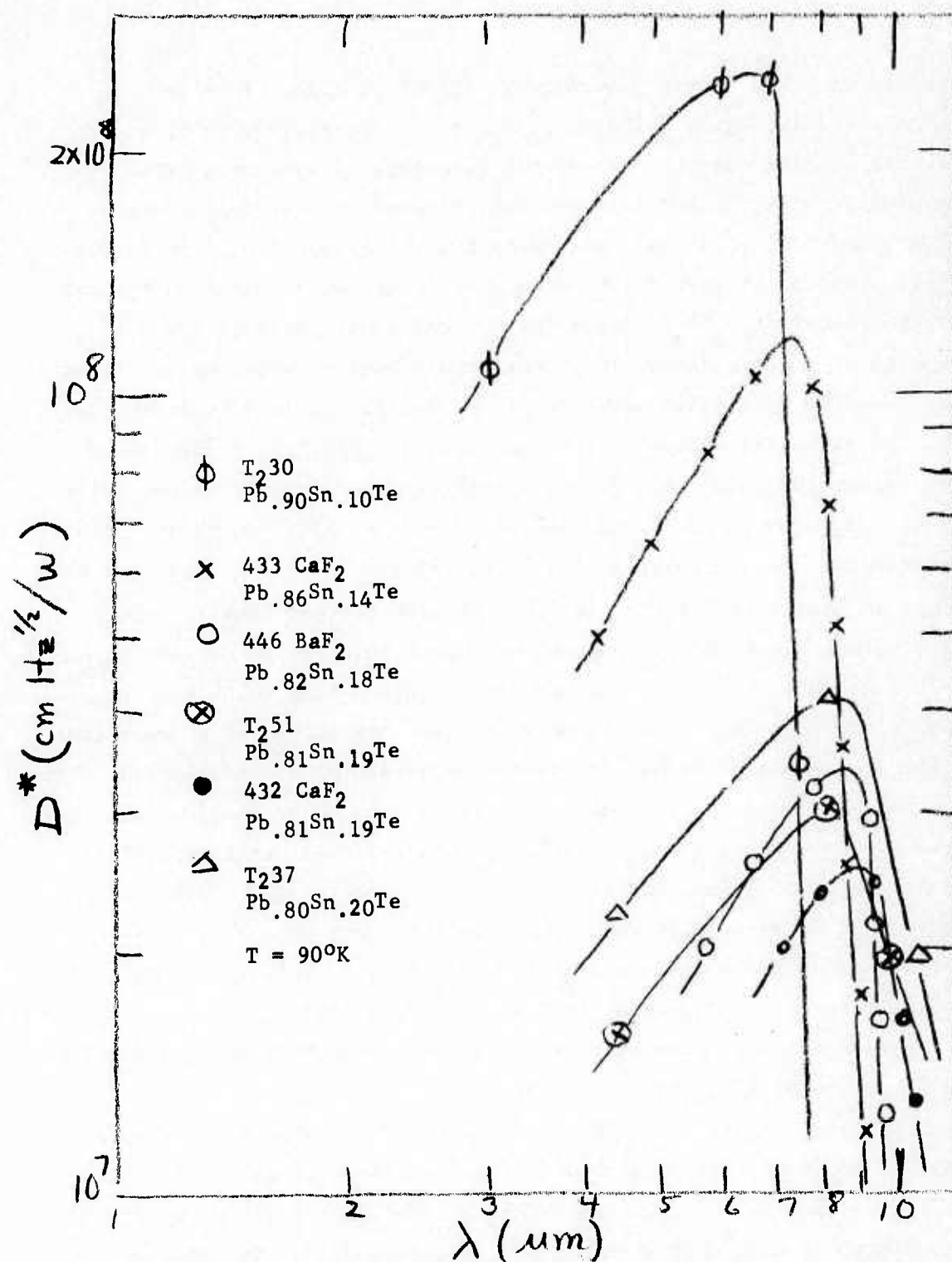
Figure 3-122   Absolute Spectral, Photoconductive Detectivity
of As-Deposited $Pb_{1-x}Sn_xTe$ Films

function of the structural quality of the films also. This is demonstrated in Figure 3-123 which shows noise measurements as a function of bias current for several as-deposited sputtered films. The significantly better noise characteristics in the single crystal films (curves b, c, d) as compared to the polycrystalline film (curve a) are obvious. Figure 3-124 shows the noise measurement on typical single crystal $Pb_{1-x}Sn_xTe$ films (one of which was annealed - $T_2 37$) prepared at a later date. They show significantly better noise values than even the best films shown in Figure 3-123. It is noteworthy that very low noise values can be obtained with <u>as-deposited</u> films. They are, to our knowledge, the lowest values reported to date on any films of $Pb_{1-x}Sn_xTe$, annealed or unannealed (Reference 30). Obviously they approach the Johnson noise at the lower current levels as reflected by values of less than 1×10^{-9} $nv/\sqrt{Hz}$ at such current levels. Still lower values are found at frequencies higher than the 1 KHz used here for the measurements (see, for example, Figure 3-128). It is very encouraging that unannealed films show noise characteristics equivalent to those of annealed films. In fact, comparison of electro-optical properties of annealed and unannealed films has shown that, in general, as long as the carrier concentrations and mobilities are comparable in the two types of films, the electro-optical properties are also comparable. Some results which indicate this, are presented in Table 35 and Figures 3-125 and 3-126. The figures show the normalized spectral response for several typical $Pb_{1-x}Sn_xTe$ films. In these figures, examples of unannealed films are #435 and #442 in Figure 3-126 and #$T_2 32$ and #$T_2 48$ in Figure 3-125.

We note, first, in Figure 3-125 that the annealed films ($T_2 440$, $T_2 30$, $T_2 39$), show responses which are consistent with the electrical properties (see Table 35). For example, films with lower carrier concentrations show correspondingly higher responses. The same appears true for the unannealed films. The response of film $T_2 13$ is an exception. The variations in the magnitude of the relative responses
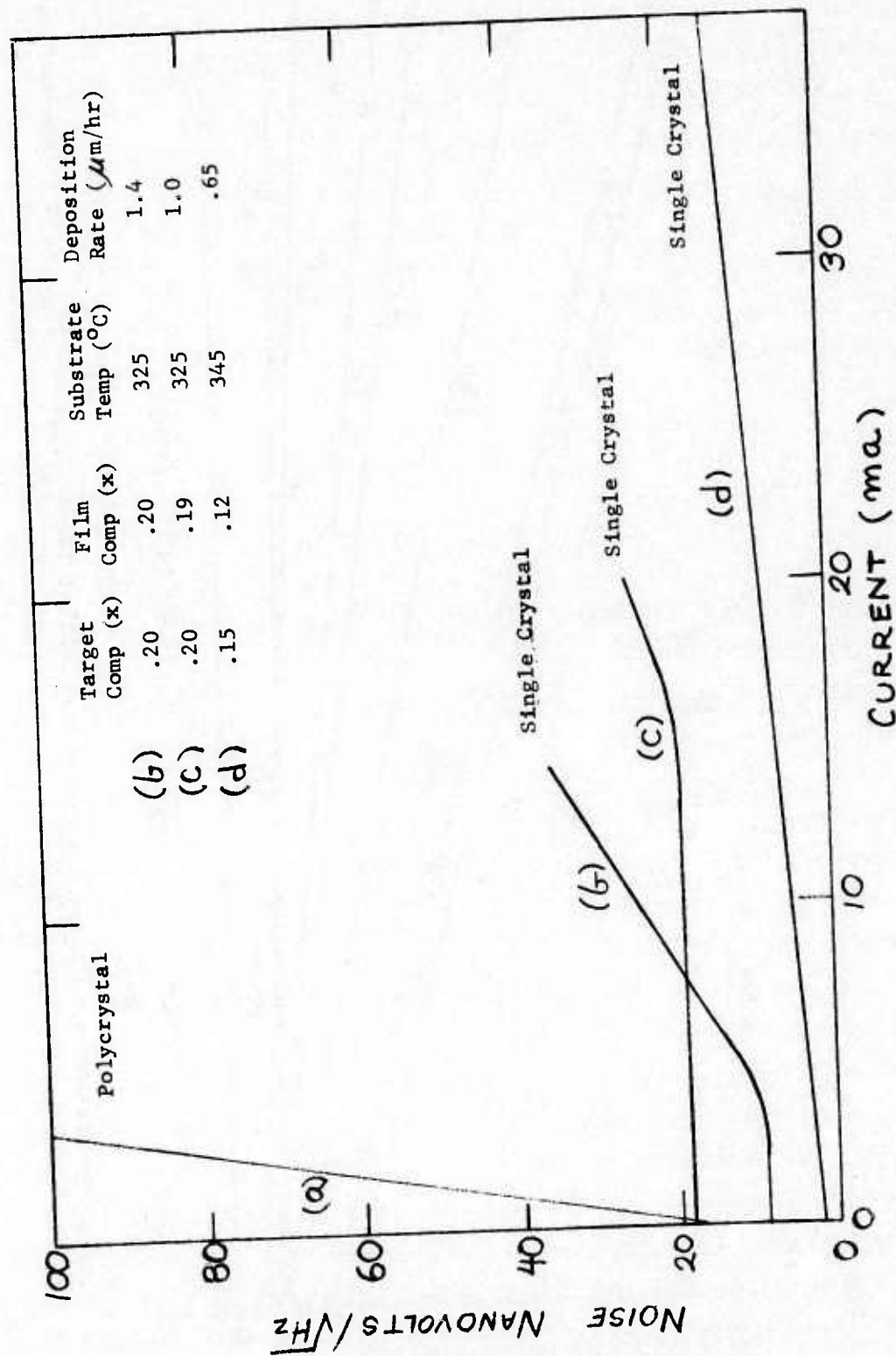
Figure 3-123 Dependence of Noise Voltage on Bias Current for As-Deposited $Pb_{1-x}Sn_xTe$ Films - Early Films
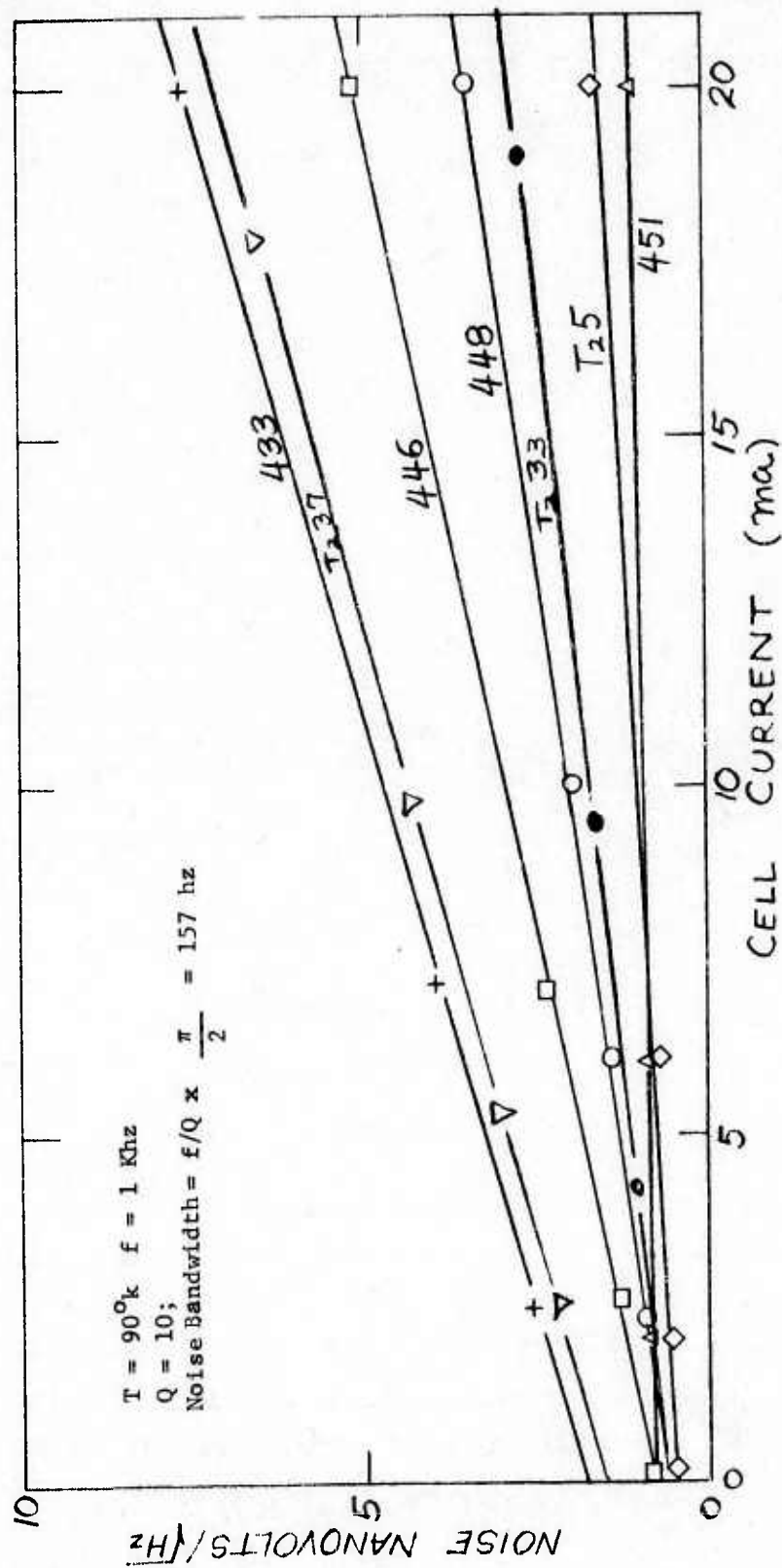
Figure 3-124 Dependence of Noise Voltage on Bias Current for As-Deposited $Pb_{1-x}Sn_xTe$ Films-Improved Films

given in this figure are of course also related to the cut-off wave-length of the individual films (which are correlatable with the film x-values). It is a typical trend in $Pb_{1-x}Sn_xTe$, that larger energy gaps result in higher responsivities under identical operating conditions.

Figure 3-126 shows similar normalized spectral responses for three typical $Pb_{1-x}Sn_xTe$ films again with different carrier concentrations as specified in this figure. It is apparent here also that the film with the lowest carrier concentration shows the highest response. The differences indicated are considerably higher than could exclusively be due to energy gap variations.

We indicated one exception from the typical trend ($T_2 13$ - Figure 3-125). As shown in Table 35, the carrier concentration of this annealed film is 3.5×10^{16} cm^{-3} and should, therefore, exhibit very good response characteristics. Instead, we note in Figure 3-125, the response exhibited by this film is lower than that of the others, all having higher carrier concentrations. The problem, which does not seem to be as critical with higher carrier concentration films, was definitely associated with the lead deposition. The reported concentrations were measured immediately before the lead deposition, while, immediately after the lead deposition, the remeasured electrical properties showed some deterioration. It was found that, in general, films with carrier concentrations in the low 10^{16} cm^{-3} and high $10^{15} cm^{-3}$ range must be very carefully handled (i.e. kept in a oxygen and moisture-free environment before and during measurements). Subsequent measurements of photoconductive responses in carefully handled films have shown values consistent with low carrier concentrations.

We note in Figures 3-125 and 3-126 that higher x-values corresponded, as expected, to longer wavelength cut-offs. The consistency of the x-value effect on cut-off wavelength (or bandgap) is perhaps more clearly shown in Figure 3-127 by the normalized relative spectral response of three $Pb_{1-x}Sn_xTe$ films with different compositions. Other results on the measurements of energy gaps from photoconductive response data are presented in the next section.
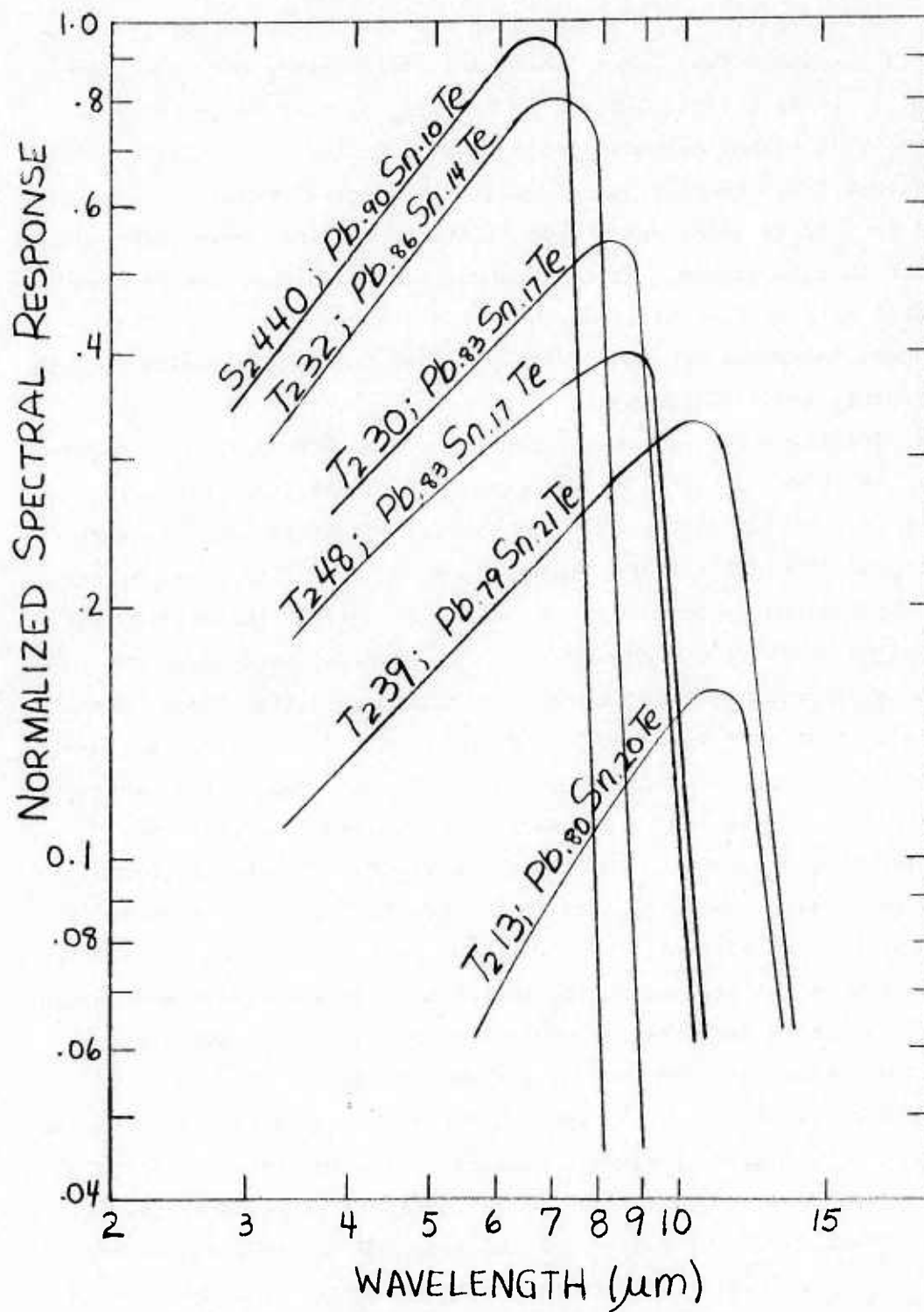
Figure 3-125 Normalized Spectral Response for As-Deposited and Annealed $Pb_{1-x}Sn_xTe$ Films
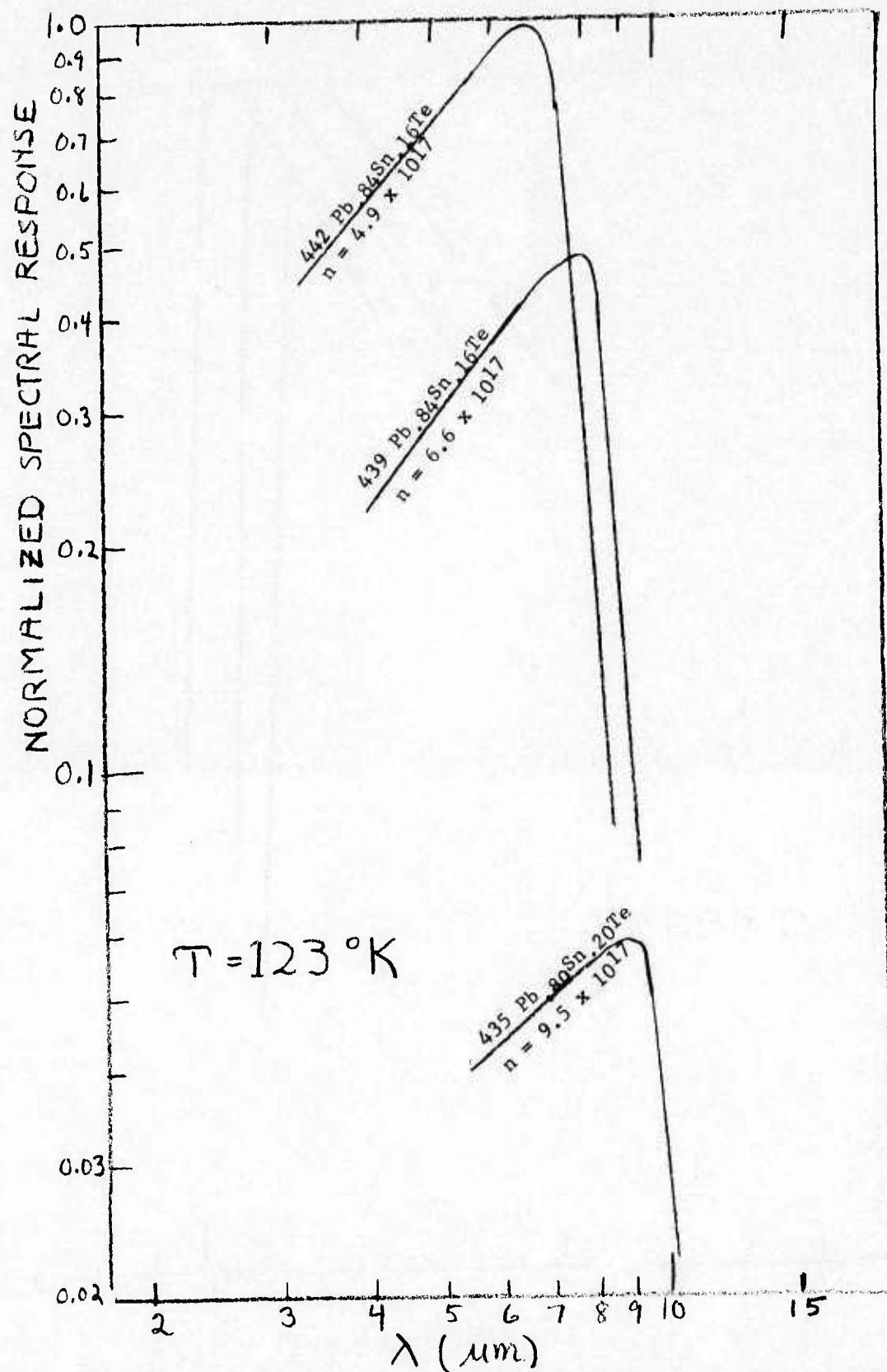
Figure 3-126 Comparison of Spectral Response for As-Deposited $Pb_{1-x}Sn_xTe$ Films with Carrier Concentration
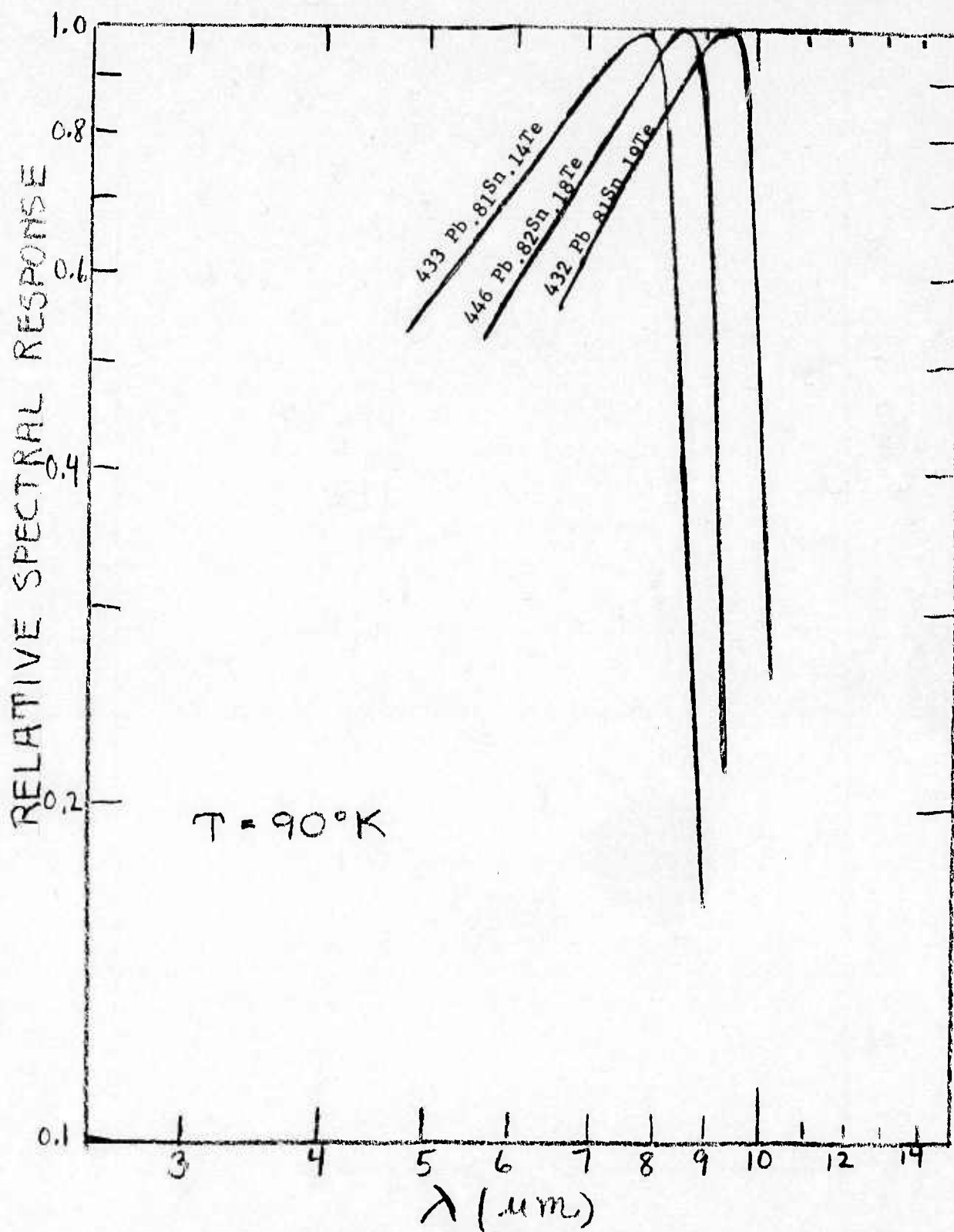
Figure 3-127　The Relative Response vs. Wavelength for $Pb_{1-x}Sn_xTe$
Films of Different Compositions

To further evaluate the sputtered $Pb_{1-x}Sn_xTe$ material quality, noise and response measurements were performed as a function of frequency. Examples are presented in Figure 3-128 which shows the frequency dependence of responsivity and noise for two $Pb_{1-x}Sn_xTe$ films. We note that the noise shows a 1/f dependence up to relatively high frequencies. The response, on the other hand, is independent of the frequencies over the measured range. The latter trend indicates very short lifetimes which is consistent with pure $Pb_{1-x}Sn_xTe$ material. That is, the responses do not reflect trap enhanced characteristics. The observation of decreasing noise along with a constant response with increasing frequency shows that higher detectivity values (i.e., D*) can be expected at higher frequencies than those shown in Figure 3-122, since the noise was measured at 1 KHz for these data.

Additional information concerning the quality of our sputtered $Pb_{1-x}Sn_xTe$ films and concerning the nature and origin of the photoconductive response can be obtained by lifetime measurements as described in Section 2.0. As noted, the measurement setup includes an RCA GaAs laser diode TA7964. The diode is pulsed with a laser diode pulser at a nominal rate of 50 pulses per second. The power output from the diodes is measured using a phototube. The laser current pulse for the measurement was about 46 ma with the peak radiant power output of approximately 5 watts. The rise and fall time of the laser driving pulse is shown in Figure 3-129(a) and can be estimated to be of the order of 70 ns. Utilizing this arrangement, response times from a number of $Pb_{1-x}Sn_xTe$ films were measured. A typical result is shown in Figure 3-129(b) for a $Pb_{.90}Sn_{.10}Te$ film ($T_2$30 - see Figures 3-121 and 3-122 for responsivity and detectivity). From the waveform of the sample signal, the measurable lifetime of this sample is seen to be less than 100 ns or on the order of 70 ns, which is the limit of the response time of the equipment used for this particular measurement. An improved pulsing and sampling setup is being implemented as discussed in Section 2.7.1.3 for the generation of faster pulses (~ 1-5 ns).
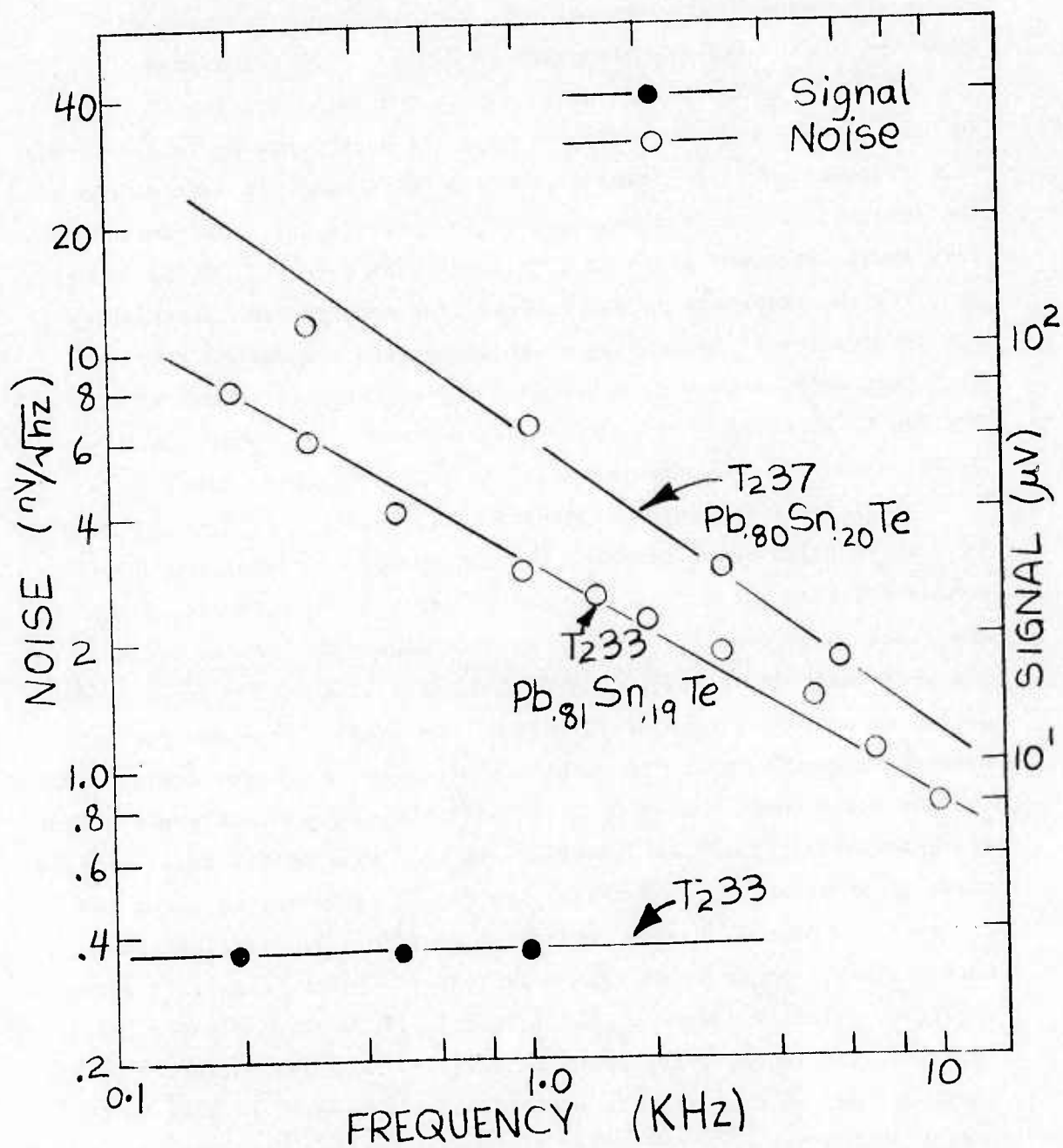
Figure 3-128 Frequency Dependence of Response and Noise in Some Sputtered
Pb$_{1-x}$Sn$_x$Te Films

.5 V/cm
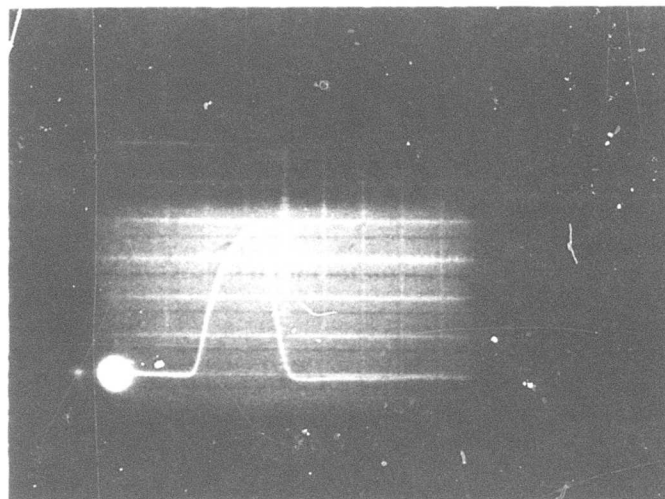
100 n sec/cm

(a) Laser Driving Pulse

5 mv/cm
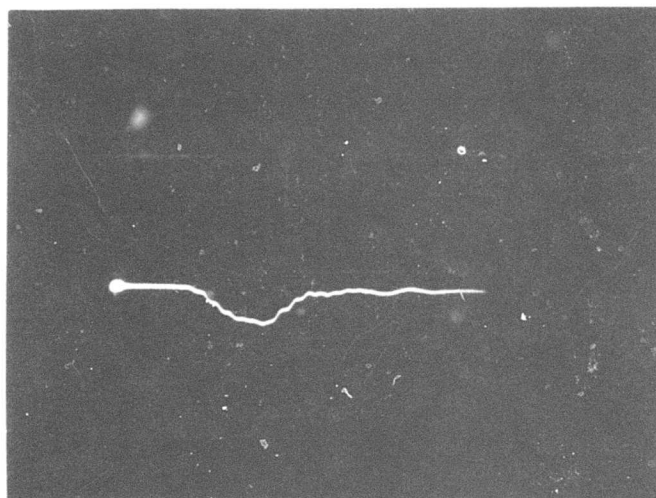
100 n sec/cm

(b) Sample Photoconductive Response - $T_2 30$

Figure 3-129 Lifetime Measurement in Sputtered $Pb_{.90}Sn_{.10}Te$ Film

3-239

Furthermore, a laser diode array to increase the radiant power output will replace the single diode used for these measurements.

The results of the lifetime measurements associated with the photoconductive response in our films, in any case, indicate that all films with better quality have response times below 70 nanoseconds, which values are consistent with that expected for good $Pb_{1-x}Sn_xTe$ material.

3.7.2.2 <u>Energy Gaps from Photoconductive Response</u>. It is apparent from Figures 3-126 and 3-127 that there is consistency between the film composition and wavelength cut-off obtained from the photoconductive response. Optical energy gaps were obtained from such data by defining the energy gap as that photon energy at which the photoconductive response is about one third (1/e) of the peak value (i.e. close to the cut-off wavelength). Results from such measurement, along with the film compositions, are presented in Table 36. In Figure 3-130, the computed energy gaps are plotted against the film composition for four measurement temperatures. Included in this Figure are $77^{\circ}K$ bulk data obtained by other investigators (References 23, 31 and 32) for comparison. These results do show fairly good consistency between energy gaps obtained from photo-response data and film compositions. Interpolation between $300^{\circ}K$ data (see Figure 3-68) and the $77^{\circ}K$ bulk data shown in Figure 3-130, verifies that results shown for $123^{\circ}K$, $100^{\circ}K$, $90^{\circ}K$ and $77^{\circ}K$ have very much the expected values.

3.7.3 ELECTRO-OPTICAL PROPERTIES OF FILMS DEPOSITED BY BIAS SPUTTER-ING. As may be recalled, the bias voltage affected as-deposited carrier type and concentrations in two significant ways: 1) at a critical bias voltage, V_o - the carrier concentration approaches a minimum and the films switch type, 2) at large negative biases ($V \leq -30$ volts) large reductions in carrier concentration are found also. Consistent with this, the electro-optical properties of sputtered $Pb_{1-x}Sn_xTe$ films seem to be affected most significantly by the same two bias conditions.

3-240
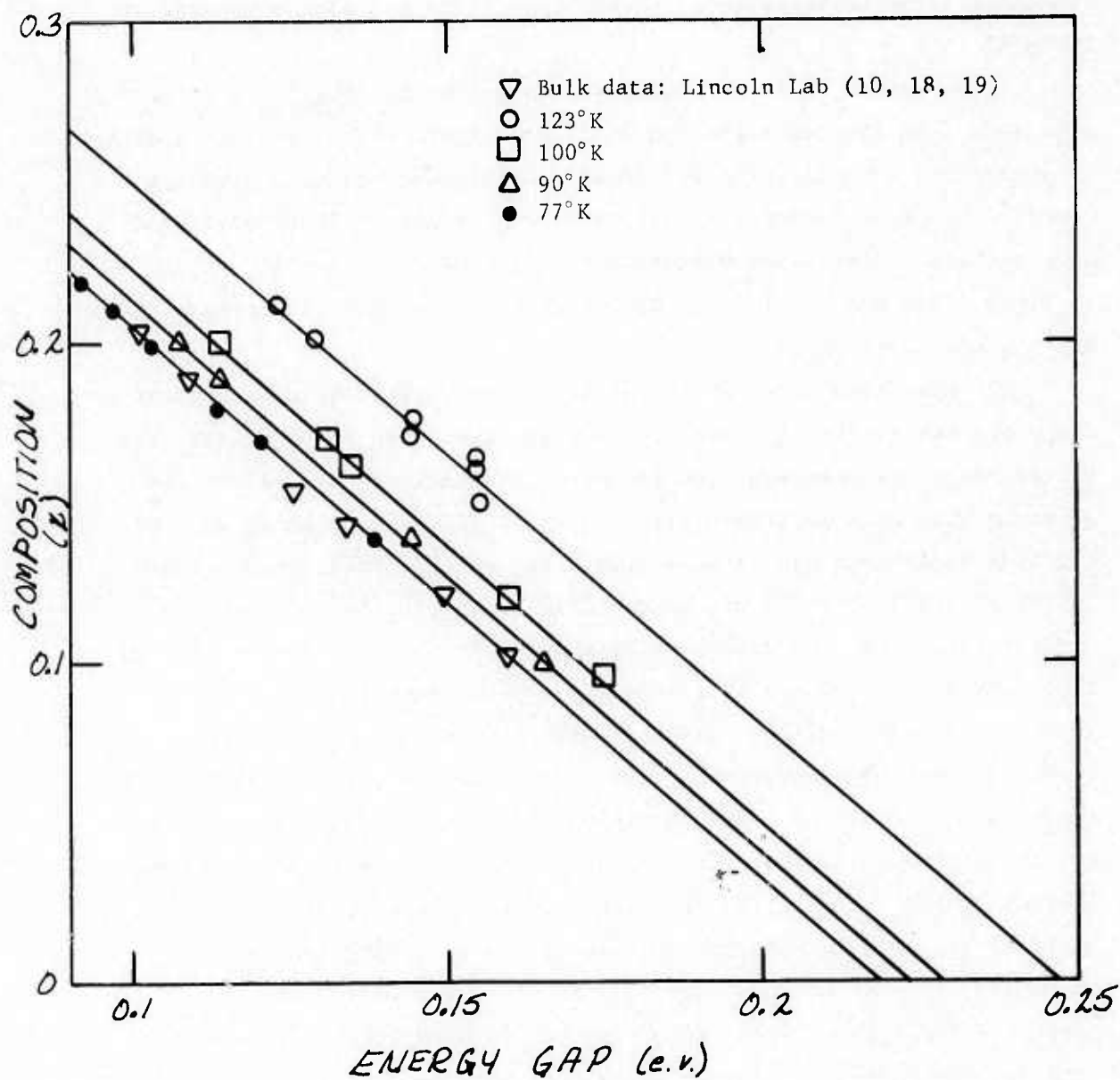
Figure 3 130.   Composition Dependence of Energy Gap of $Pb_{1-x}Sn_xTe$ Thin
Films (from Photoconductive Threshold)

Figures 3-131 and 3-132 which illustrate these findings, show the absolute, 77°K spectral responsivities and detectivities for several as-deposited $Pb_{1-x}Sn_xTe$ films deposited at various bias voltages. The photoconductive performance data for these films are also presented in Table 37.

It may first be noted that the bias sputtered $Pb_{1-x}Sn_xTe$ films represented in Figures 3-131 and 3-132 show again higher photoconductive responses and detectivities for undoped films than has been previously reported by us or by other investigators for films of these particular compositions. That these responses are intrinsic in nature, can be concluded from the consistency of the relation between film compositions and cut-off wavelengths.

The bias conditions which result in the highest photoconductive responses are apparently measured in films deposited at -30V bias, the largest negative bias explored to date. The next highest values are obtained with film sputtered with a bias of -5V. The significance of the bias conditions can be seen more clearly if we refer to the inset in Figure 3-131 which shows, schematically the relation between the carrier concentrations and the bias conditions in films represented in this figure. We compare first the films with composition $x = 0.21$. As noted the -30V and -5V bias conditions are associated with the lowest carrier concentrations. The bias voltage of -5V corresponds, as shown in the schematic, to a condition close to (and on the n-type side of) the critical bias condition V_0 which we have associated with near perfect stoichiometry. The -2V bias condition is also close to the critical bias (but on the p-type side of the switching conditions). Therefore, the latter film does not exhibit the same low carrier concentration seen at -5V. Returning to the photoconductive response data in Figure 3-131, it can be seen that the $x = 0.21$ films sputtered at -5V and -30V show nearly the same responsivities. The latter is slightly higher, corresponding to the somewhat lower carrier concentrations associated with this condition. The -2V bias
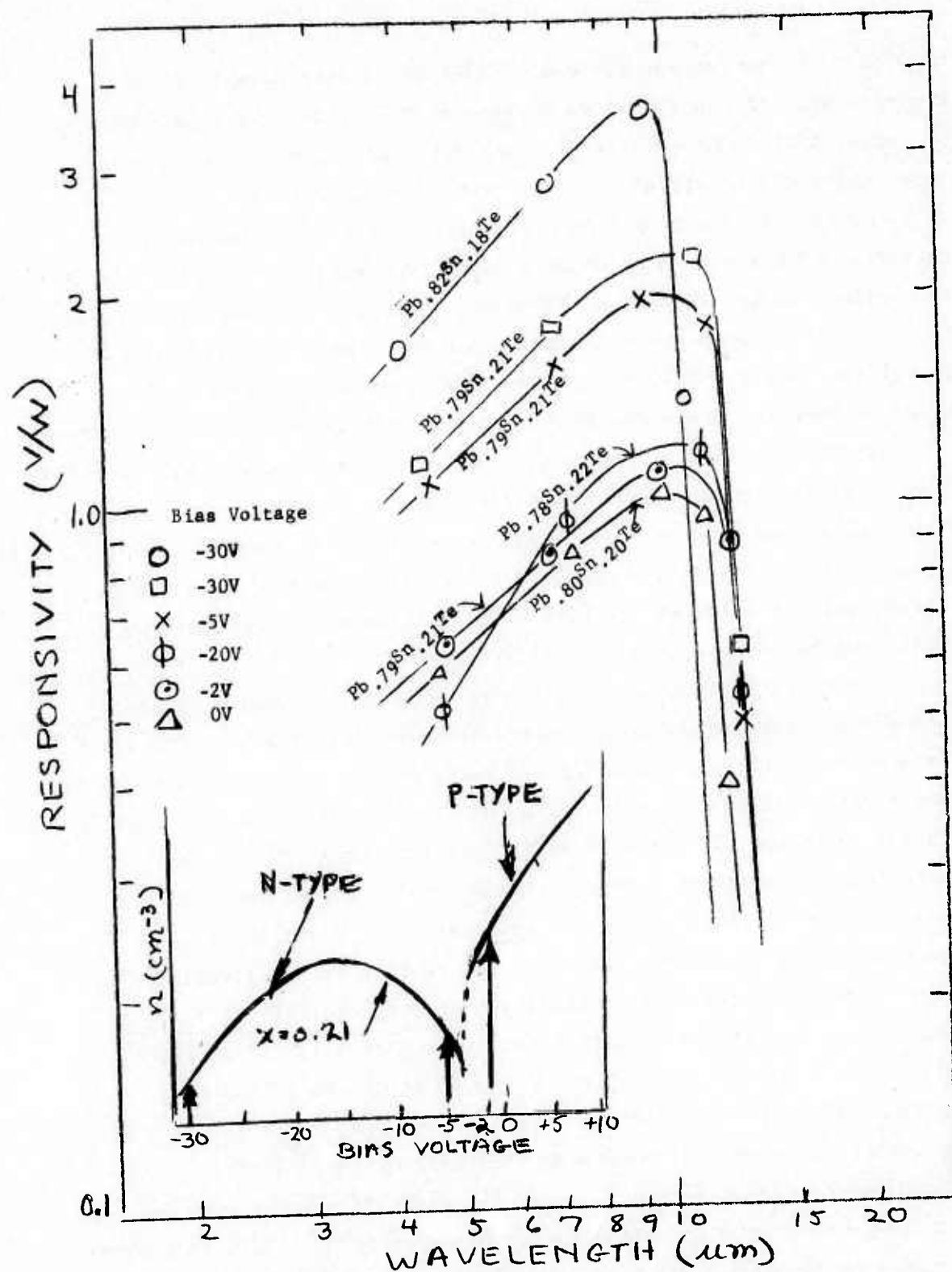
Figure 3-131 Absolute Spectral Photoconductive Responsivity of As-Deposited $Pb_{1-x}Sn_xTe$ Films - Effect of Substrate Bias Voltage

condition by comparison yielded a film with a considerably lower response even though it had an x-value of 0.21 also. It should also be noted, that independent of responsivity differences, the cut-off wavelengths are identical for all three x = 0.21 films.

As to the remaining film responses, the x = .18 composition sputtered with a -30V bias shows a higher response yet than its x = .21 counterpart sputtered with a -30V bias. However, this can be attributed to the typical composition dependence of the photo-electric response in PbSnTe. The x = 0.20 film, which should normally have a higher response than the x = 0.21 films has been sputtered without the benefit of substrate bias and has actually the lowest peak response of all films. The x = 0.22 film which would normally have the lowest response does show better than expected performance since its bias conditions of -20V is apparently sufficiently negative to benefit from the reduction in carrier concentration at the high negative biases. (Note that the inset applies only to x = 0.21 film).

The detectivities shown in Figure 3-132 follow similar trends with a few minor exceptions. Comparing again first the x = 0.21 films, the difference between the effect of the -30V and -5 bias conditions is considerably larger on the D^* value than on the responsivity. This is quite interesting, if verified as typical from other films. By implication, the larger negative bias causes a greater reduction in detector noise. Thus, for device application it might be more advantageous to reduce the carrier concentration by the effects of large negative biases than by the stoichiometry controlling V_o bias condition. The other interesting fact in Figure 3-132 is that the detectivities of the x = 0.20 and x = 0.22 films are in the more typical order with respect to relative magnitudes. This points out also, that in assessing photo-electric property improvements by the various techniques explored in this program it is important to evaluate all film characteristics contributing to the useful quality indicators of infrared sensors. One other observation of interest (and of importance
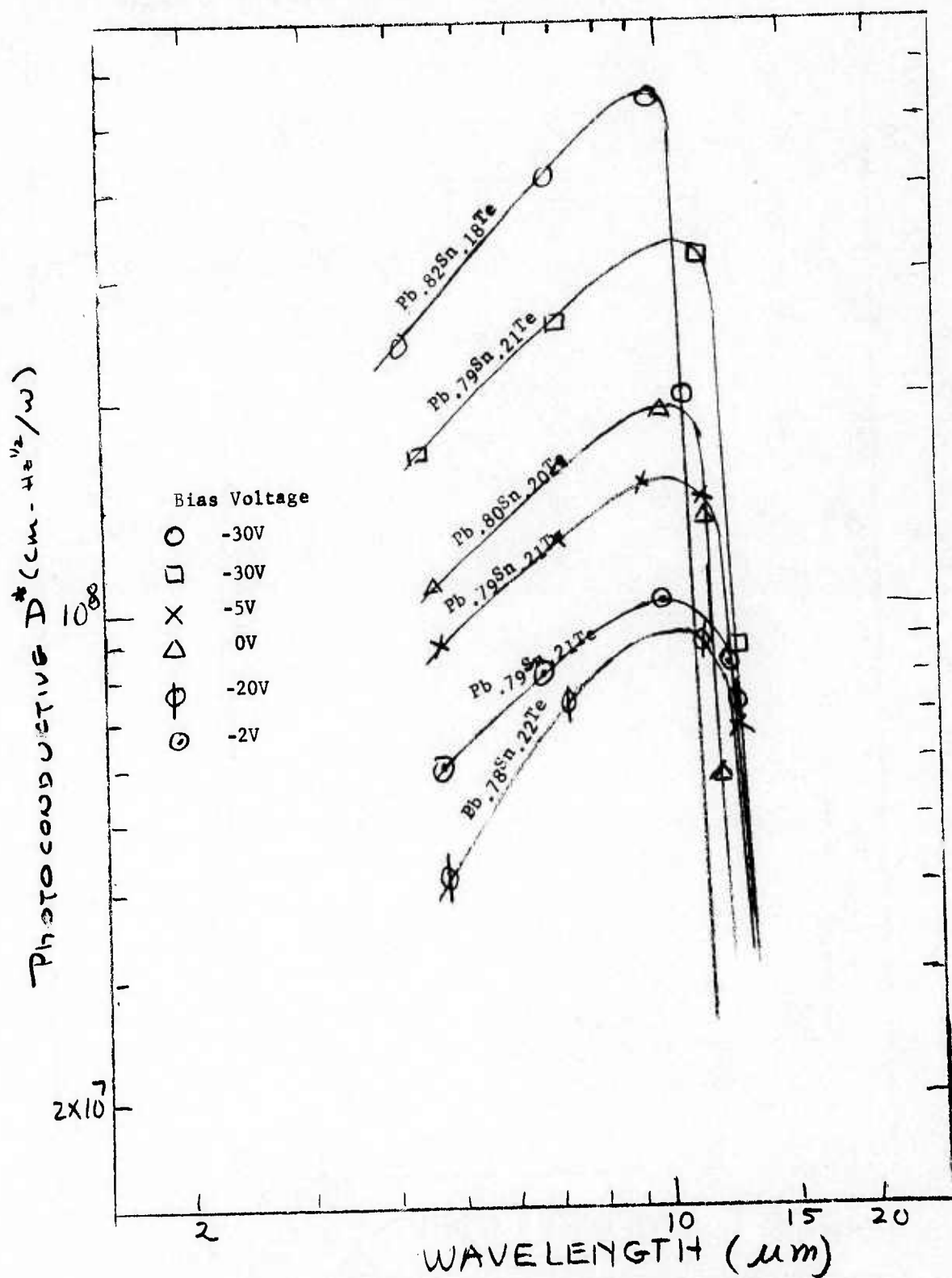
Figure 3-132 Absolute Spectral Photoconductive Detectivity of As-
Deposited $Pb_{1-x}Sn_xTe$ Films - Effect of Substrate
Bias Voltage
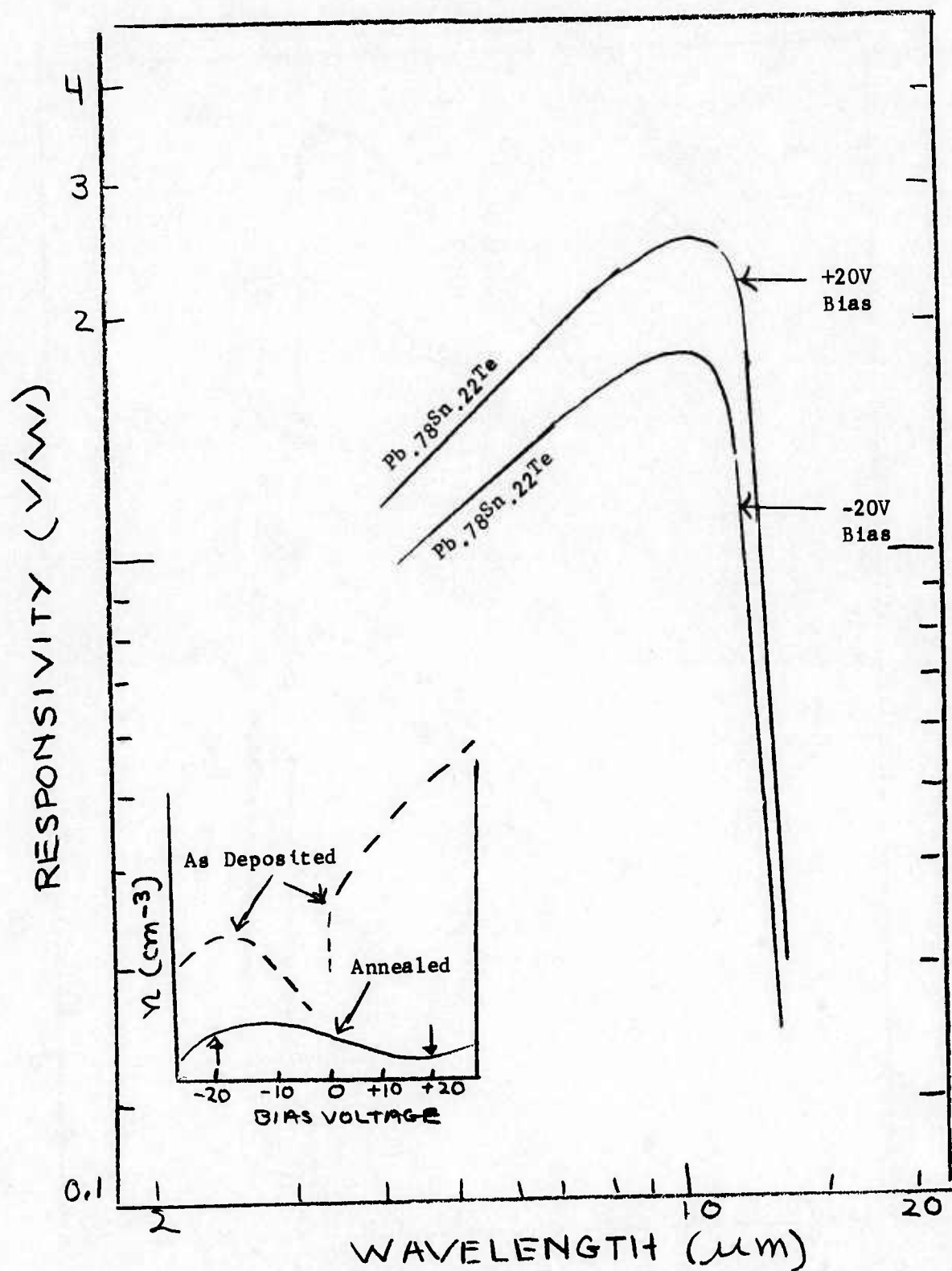
Figure 3-133 Absolute Spectral Photoconductive Responsivity of
Annealed $Pb_{1-x}Sn_xTe$ Films (Deposited with Substrate Bias)
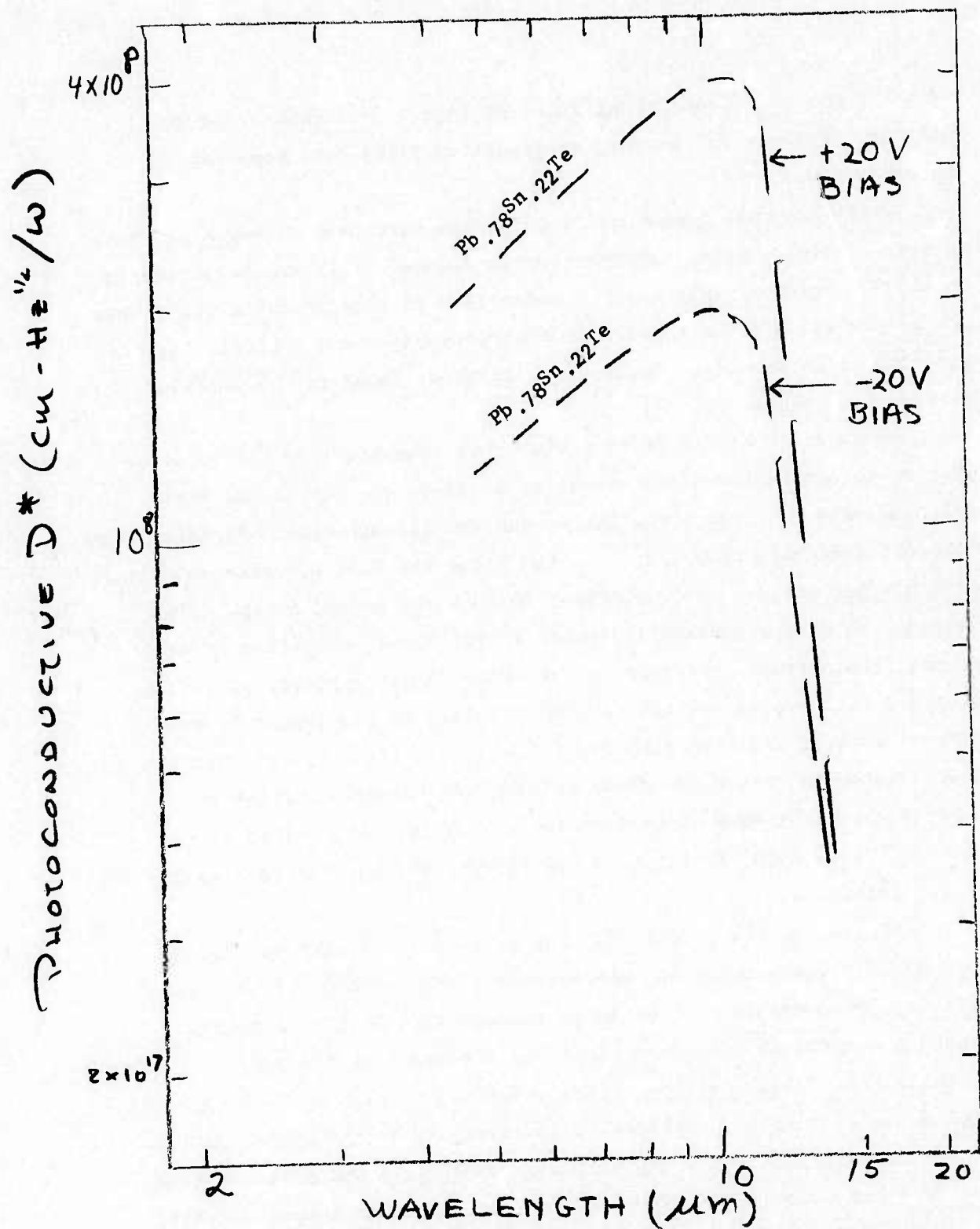
Figure 3-134 Absolute Spectral Photoconductive Detectivity of Annealed $Pb_{1-x}Sn_xTe$ Films (Deposited with Substrate Bias)

for p-n junction formation) is found in Figure 3-131 and 3-132 and
Table 37. Both p- and n-type, as-deposited films show comparable
photo-responses.

Photo-response measurements were also performed on annealed, bias
sputtered films. Examples are shown in Figures 3-133 and 3-134 and in
Table 37. Interestingly enough, comparison of these results with those
for as-deposited films shows that photo-responses and detectivities of
anneaḷed films are of the same order as those found in the better,
as-deposited films.

An inset in Figure 3-133 again shows schematically the relative
carrier concentration of the annealed films at the particular bias
voltages used to prepare the films used for illustration. As noted, the
bias voltages used to prepare the two films resulted in relatively high
as-deposited carrier concentrations in both the p- and n-type film.
However, as also schematically shown in the inset, annealing greatly
reduced the carrier concentration in these films. However, the film
prepared with a bias voltage of +20V resulted in a somewhat lower
carrier concentration on annealing. We see in Figure 3-133 that the
photo-responses of the two films reflect the relative carrier con-
centrations. The same holds true for the detectivity values of the
same two films shown in Figure 3-134 except that the differences are
more significant.

In summary, the photoconductive properties of bias sputtered
$Pb_{1-x}Sn_xTe$ films - while not approaching photo-voltaic values - show
definite improvements over other photoconductive PbSnTe materials.
Properly controlled bias conditions yield responsivities and
detectivities in as-deposited films which are as high as those achieved
with annealed films. Considerable improvements in the optimized bias
control can be expected - which should result in comparable response
improvements. Consistent with this, the noise properties of our as-
deposited and annealed, bias sputtered films, examples of which are given
in Figure 3-135, are also comparable with those of good single crystal
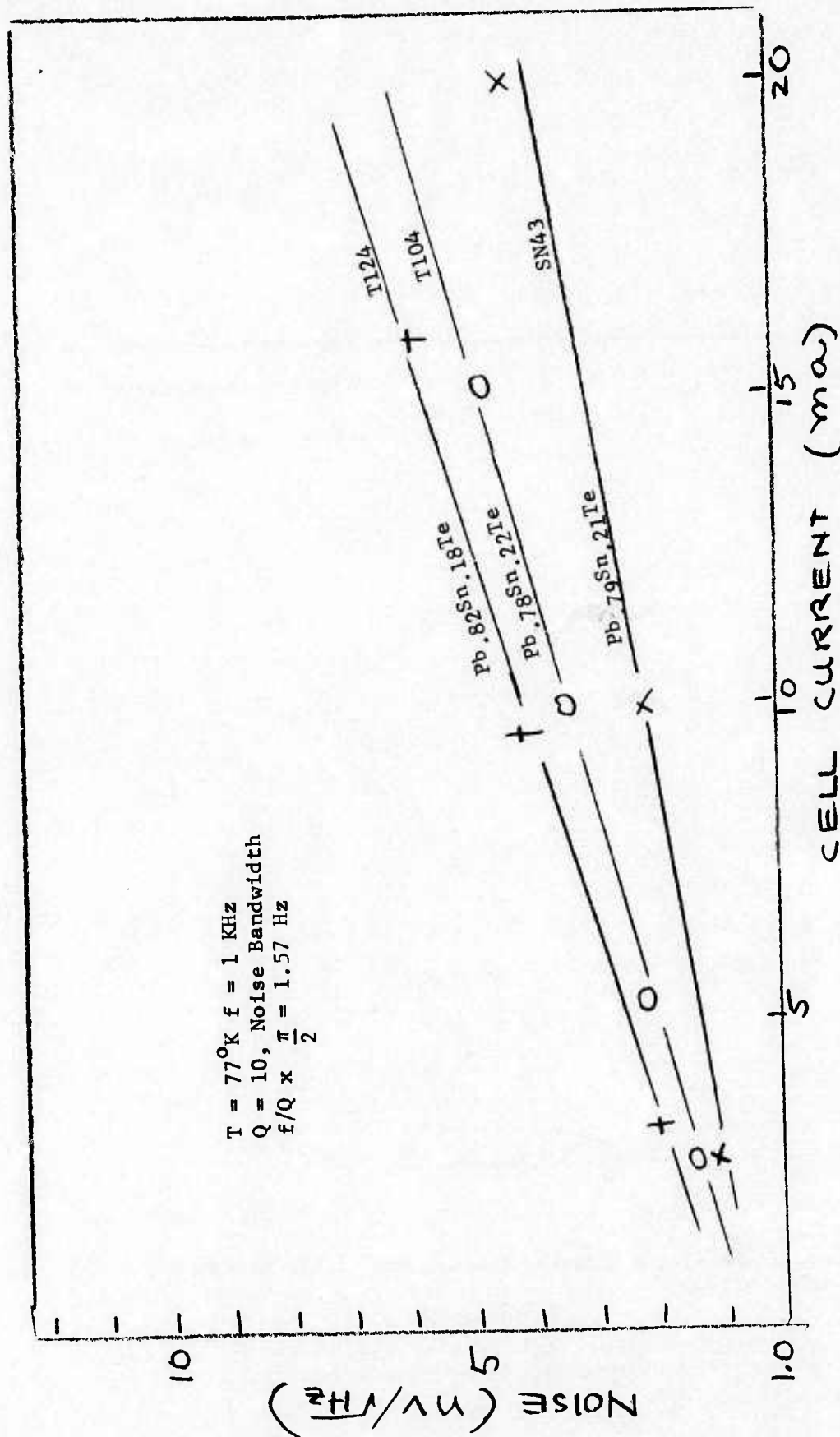
Figure 3-135 Dependence of Noise Voltage on Bias Current for Sputtered $Pb_{1-x}Sn_xTe$ Films
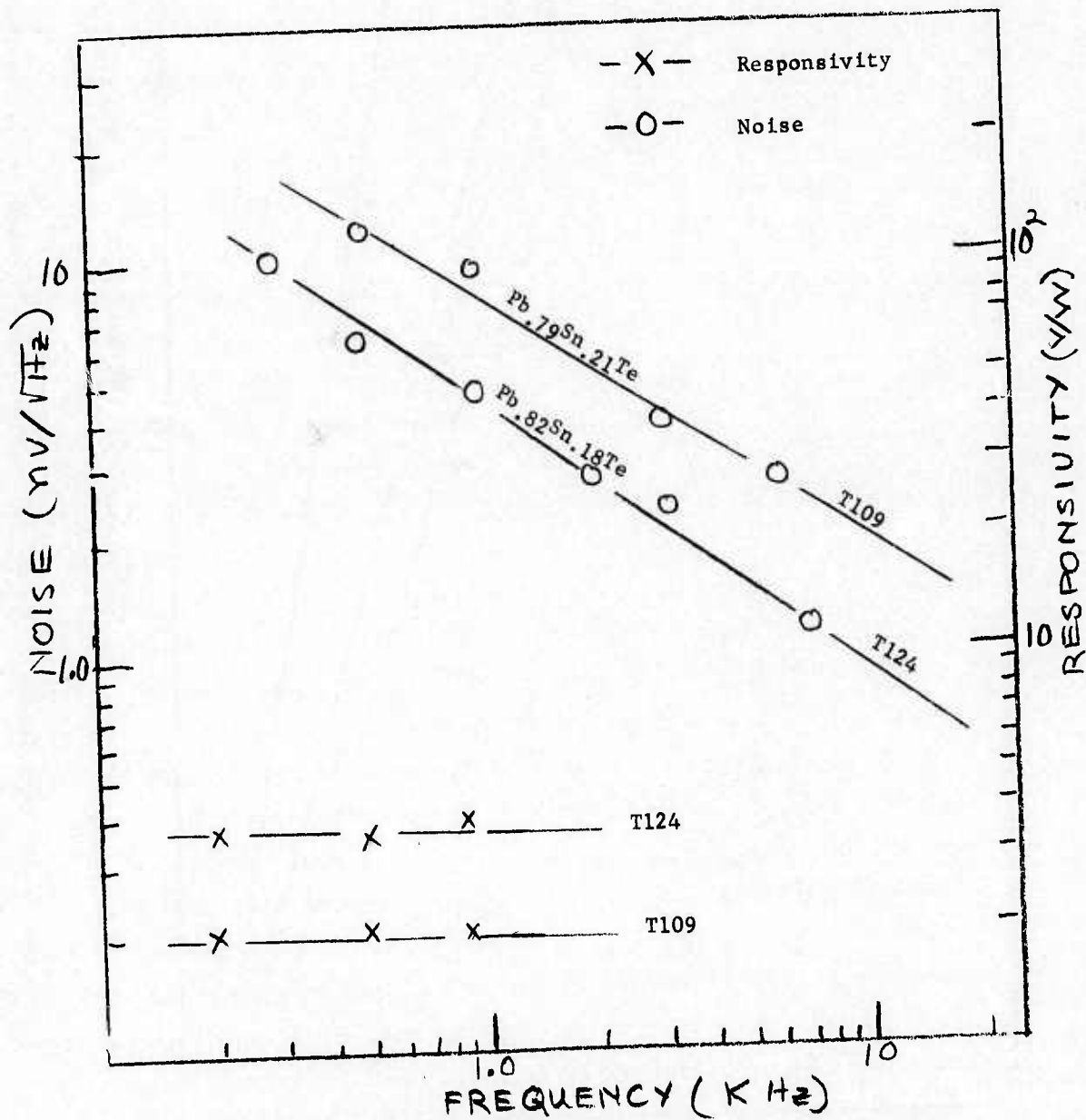
Figure 3-136   Frequency Dependence of Response and Noise in Some
Sputtered $Pb_{1-x}Sn_xTe$ Films

$Pb_{1-x}Sn_xTe$. As is apparent from the latter figure, sputtered $Pb_{1-x}Sn_xTe$ single crystal films (annealed and unannealed) exhibit noise values approaching Johnson noise at the lower current levels and remaining quite low up to rather large current values.

Additional measurements, which have been and are still being carried out to further evaluate the bias sputterd $Pb_{1-x}Sn_xTe$ material quality, involve noise and response measurement as a function of frequency. Two examples in Figure 3-136 show representative data for some of the $Pb_{1-x}Sn_xTe$ films already used for illustration in previous figures. As noted, the noise shows again a 1/f dependence up to relatively high frequencies, while the response is quite independent of frequency over the measured range. As in the case of films sputtered without bias the data implys a short lifetime consistent with that expected in pure $Pb_{1-x}Sn_xTe$ material. The observed decrease in noise with increasing frequency, along with the constant response, promises higher detectivity values than those shown in Figure 3-132 at the higher frequencies. The noise measurements on which the detectivities shown in Figure 3-132 were based, were carried out at 1 kHz. Thus, for the $Pb_{.82}Sn_{.18}Te$ film (T124) shown in Figures 3-131 and 3-132, a detectivity of about $D^* = 2.2 \times 10^9$ cm-Hz$^{\frac{1}{2}}$/w can be calculated from the measured responsivity in Figure 3-131 and noise measured above 5KHz (see Figure 136) - a fairly respectable value for photoconductive PbSnTe with a 300°K, 2π background.

3.7.4 FILMS WITH EXCEPTIONAL PHOTOCONDUCTIVE RESPONSE BEHAVIOR. During the course of this program, a small number of samples have exhibited rather exceptional photoconductive response characteristics. Two types of behavior were observed: 1) some samples showed exceptionally high photoconductive responses, 2) other samples, also with high responses at the expected peak wavelength, showed, in addition, a high short wavelength response peak at about 2.5 μm.

Figure 3-137 and Table 38 present some results on films which exhibit the exceptionally high responses. As noted in Figure 3-137, a responsivity as high as 420 v/w was observed in one sample. This is two
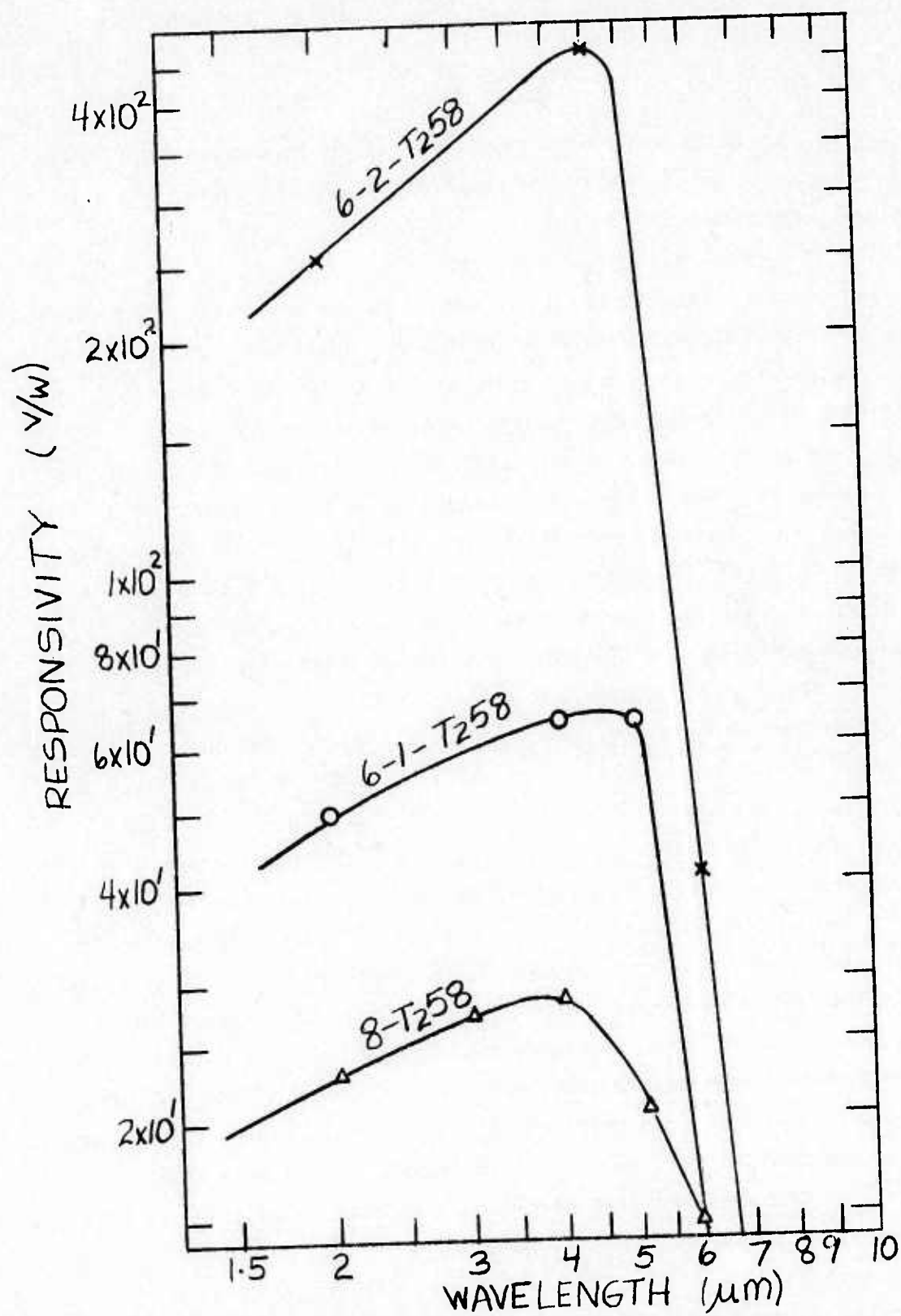
Figure 3-137 Exceptionally High Responsivities in Some As-
Deposited $Pb_{1-x}Sn_xTe$ Films

orders of magnitude higher than in typical $Pb_{1-x}Sn_xTe$ of highest quality. Notable is that the films which exhibit these high responsivities are unannealed and have very low x-values (x = .05 - .12) as determined by x-ray techniques. Furthermore, the energy gaps obtained from the photoconductive response cut-offs in these high responsivity films are consistent with their x-values. Several observations indicate that the enhanced photo-responses in these films are due to some form of carrier compensation. The as-deposited carrier concentrations in these films measured in the 10^{14} cm^{-3} range which indicates heavily compensated films. It is suspected that a higher than usual partial pressure of air was present during the deposition. Subsequent experiments with identical deposition conditions and typically low background pressures gave the expected results. Moreover, the measured compositions and carrier types of these films are, for the deposition conditions used, not those expected from a target of x = 0.20 (Target #7). Finally, the measured responses in these films are in excess of theoretically predicted values for uncompensated $Pb_{1-x}Sn_xTe$. However, since the spectral photoresponses appear to be consistent with the measured film x-values, and since it was not possible to determine (from x-ray) the presence of any secondary phase, it appears that the enhanced response is not due to secondary phases but to carrier compensation. In addition, and most importantly, it will be shown in the next section that controlled background additives yield comparable response enhancement - though not quite as dramatic as yet. This makes the compensation or trap enhancement concept all the more plausible.

The data in Figure 3-137 was obtained reasonably early in this program. Thus of considerable interest is that an even higher response was measured recently in a film which had been prepared during the same set of experiments as that for which data is shown in Figure 3-137, and stored. This (singular) result is shown in Figure 3-138. The corresponding data are listed in Table 38. As can be seen, a response of $> 10^3$ v/w is measured in this $Pb_{.93}Sn_{.07}Te$ film. While we don't

3-253
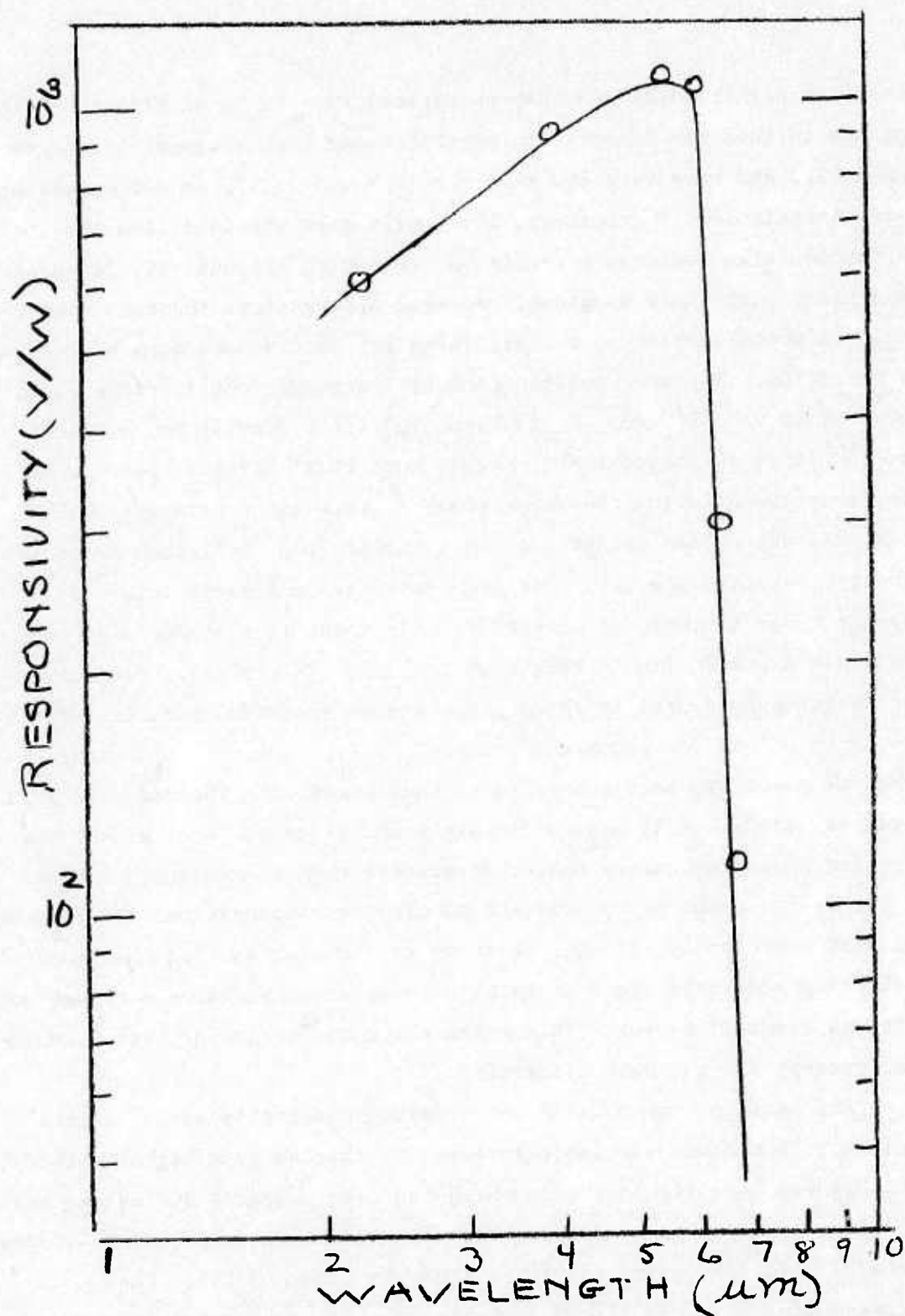
Figure 3-138 Exceptionally High Responsivity in an As-Deposited
$Pb_{.93}Sn_{.07}Te$ Film

3-254
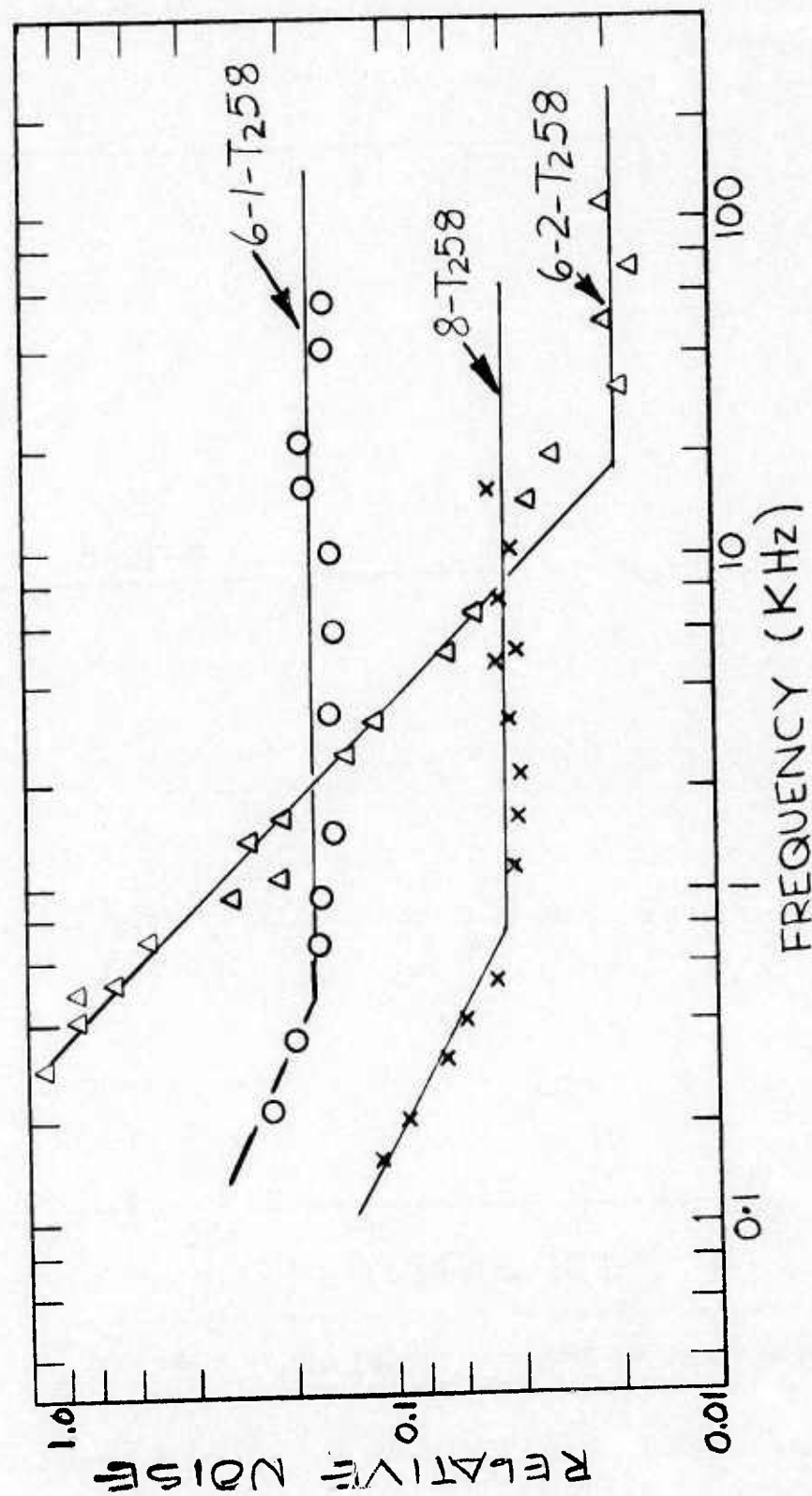
Figure 3-139 Noise vs Frequency for $Pb_{1-x}Sn_xTe$ Films with Exceptionally High Responsivities
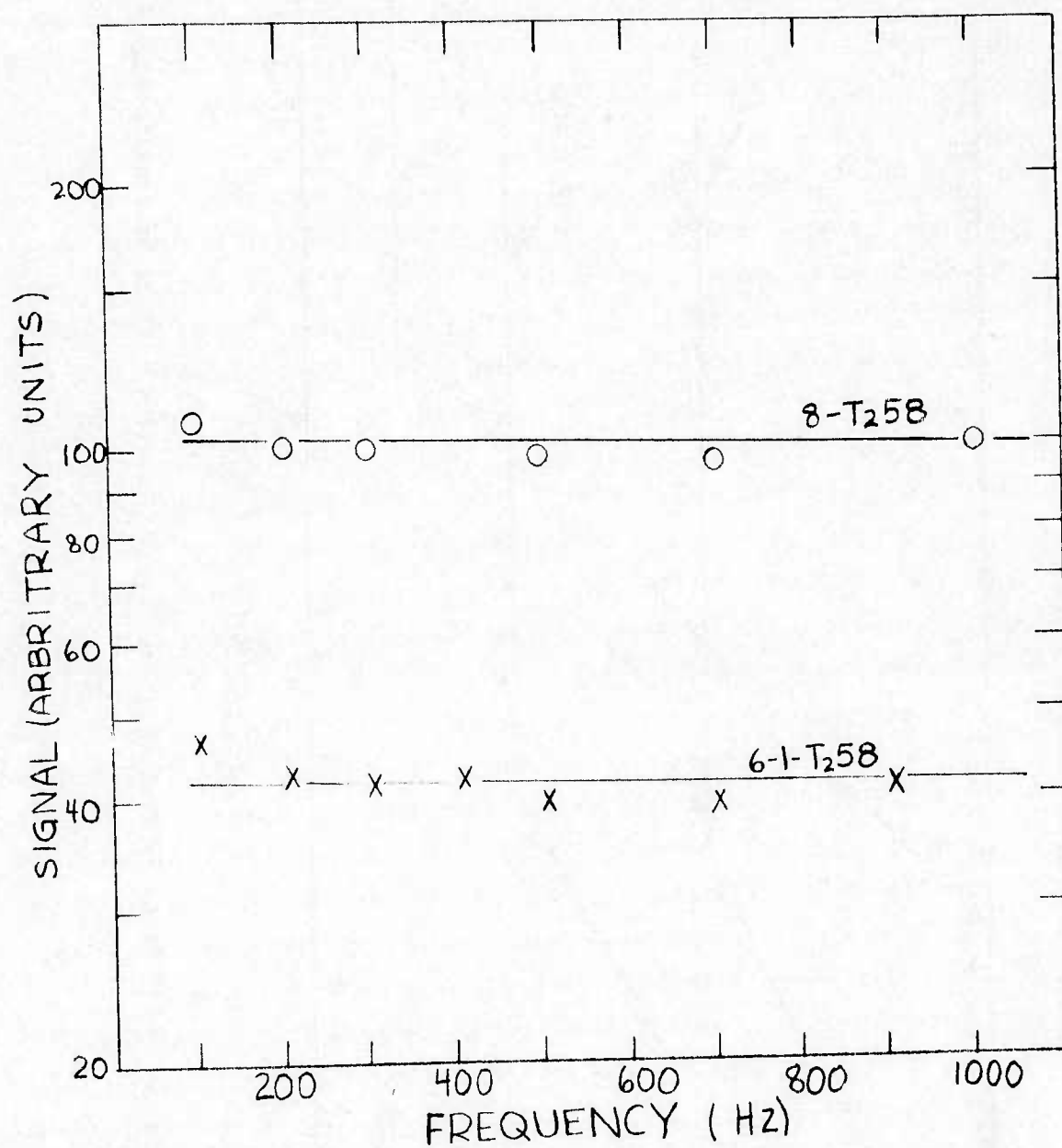
Figure 3-140 Signal vs Frequency for $Pb_{1-x}Sn_xTe$ Films with Exceptionally High Responsivities

consider this result of practical consequence, it is just one added bit of evidence that very high photoconductive responses, in particular, and significant beneficial impurity enhancement, in general, are feasible in sputtered $Pb_{1-x}Sn_xTe$ films.

While in these particular cases the cut-off wavelength is consistent with the film composition, the film composition was not that expected from the target x-value used to sputter the film.

To further explore the origin of these unexpected results, measurements of noise and response were performed as a function of frequency as shown in Figures 3-139 and 3-140, respectively. We note in Figure 3-139, some differences in behavior for three different high response films. In two cases ($6-1-T_258$ and $8-T_258$) the noise remains relatively constant from near 1 KHz to 10^5 Hz and shows $1/f$ behavior below this frequency while in another case ($6-2-T_258$) the noise shows a $1/f^{\alpha}$ dependence up to about 2×10^4 Hertz. By contrast, the photo-response remains constant to frequencies far below 1 KHz. This is shown in Figure 3-140. These results seem to indicate that the response times in these films are, in spite of compensation, still relatively short. As we shall show, films which do exhibit slow response times also show large changes of responsivities with frequency.

The second type of exceptional behavior which was referred to above is represented by a small number of samples which exhibited relatively high responses of up to 10 v/w at the expected peak wavelengths but in addition, a short wavelength response peak at approximately 2.5 μm with response values of some 50% higher than those at the primary peak. Figure 3-141 shows a typical example. Considering earlier, similar observations by other investigations in evaporated PbSnTe (Reference 33) and PbS film (References 34 and 35) it was suspected that a secondary phase and/or trap formation generates the short wavelength response peaks.

For a more careful exploration three approaches were used. First, the spectral response and noise were determined as a function of
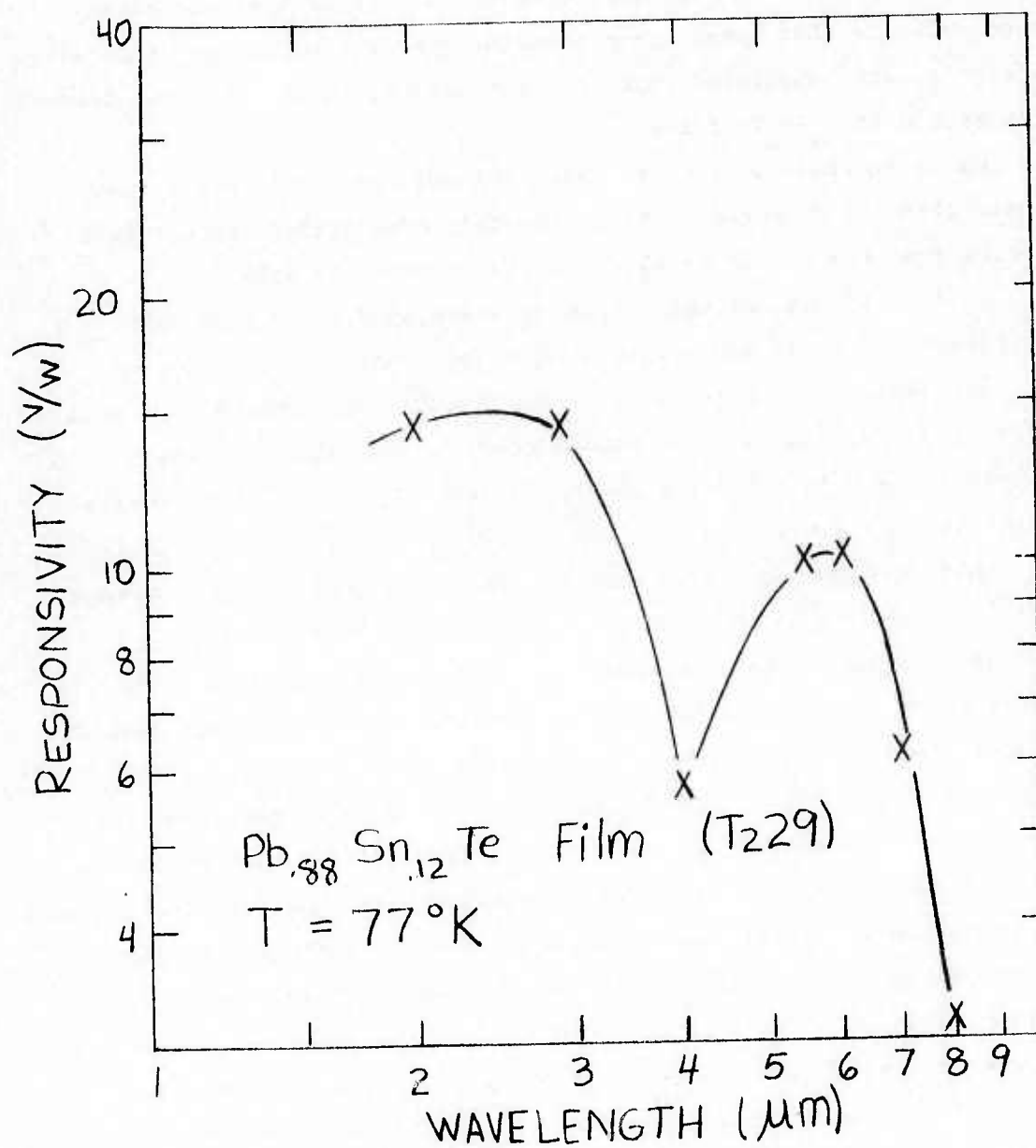
Figure 3-141 Absolute Spectral, Photoconductive Response of As-Deposited Pb$_{.88}$Sn$_{.12}$Te Film
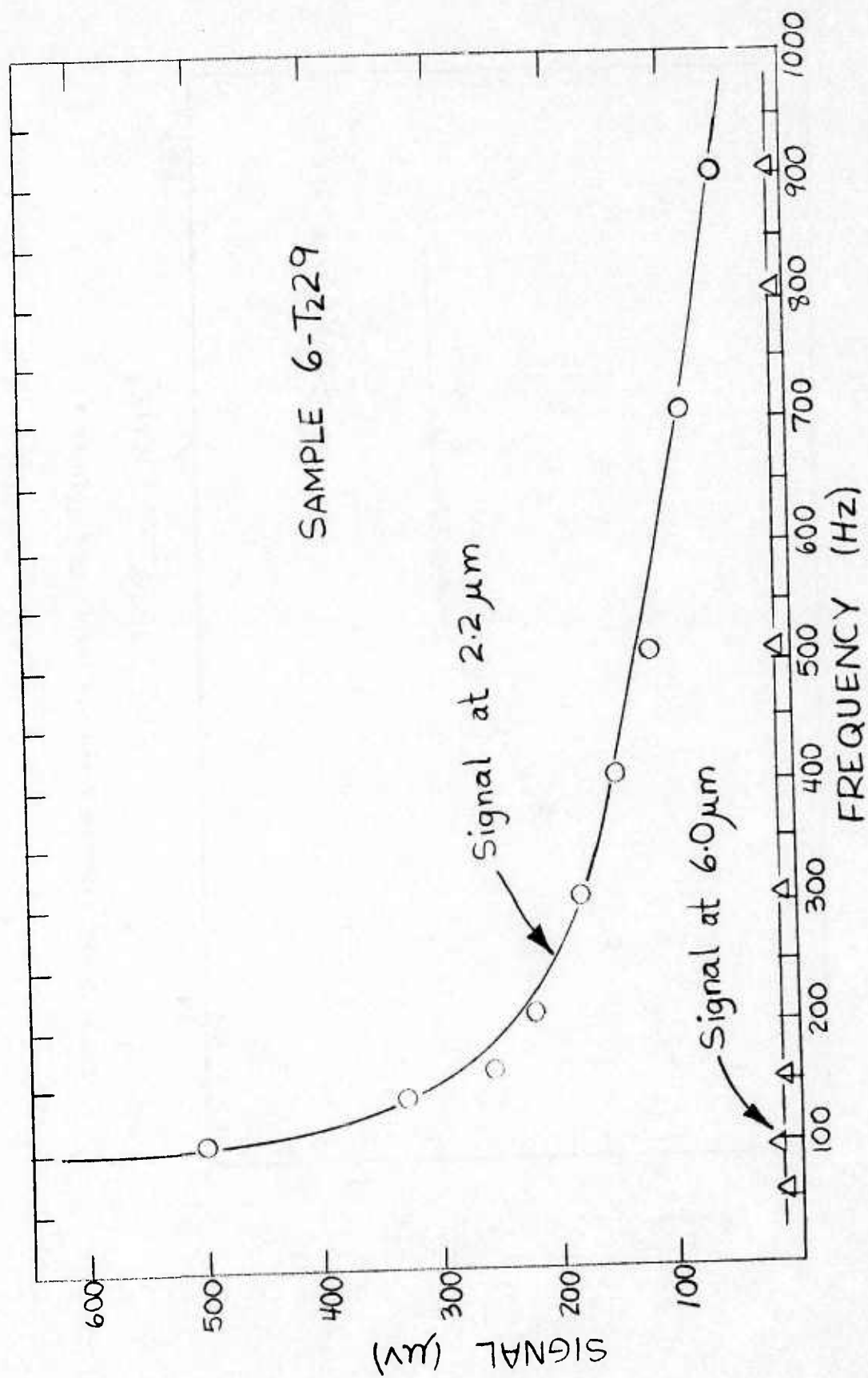
Figure 3-142 Frequency Response for Pb.88Sn.12Te Film at Two Wavelengths
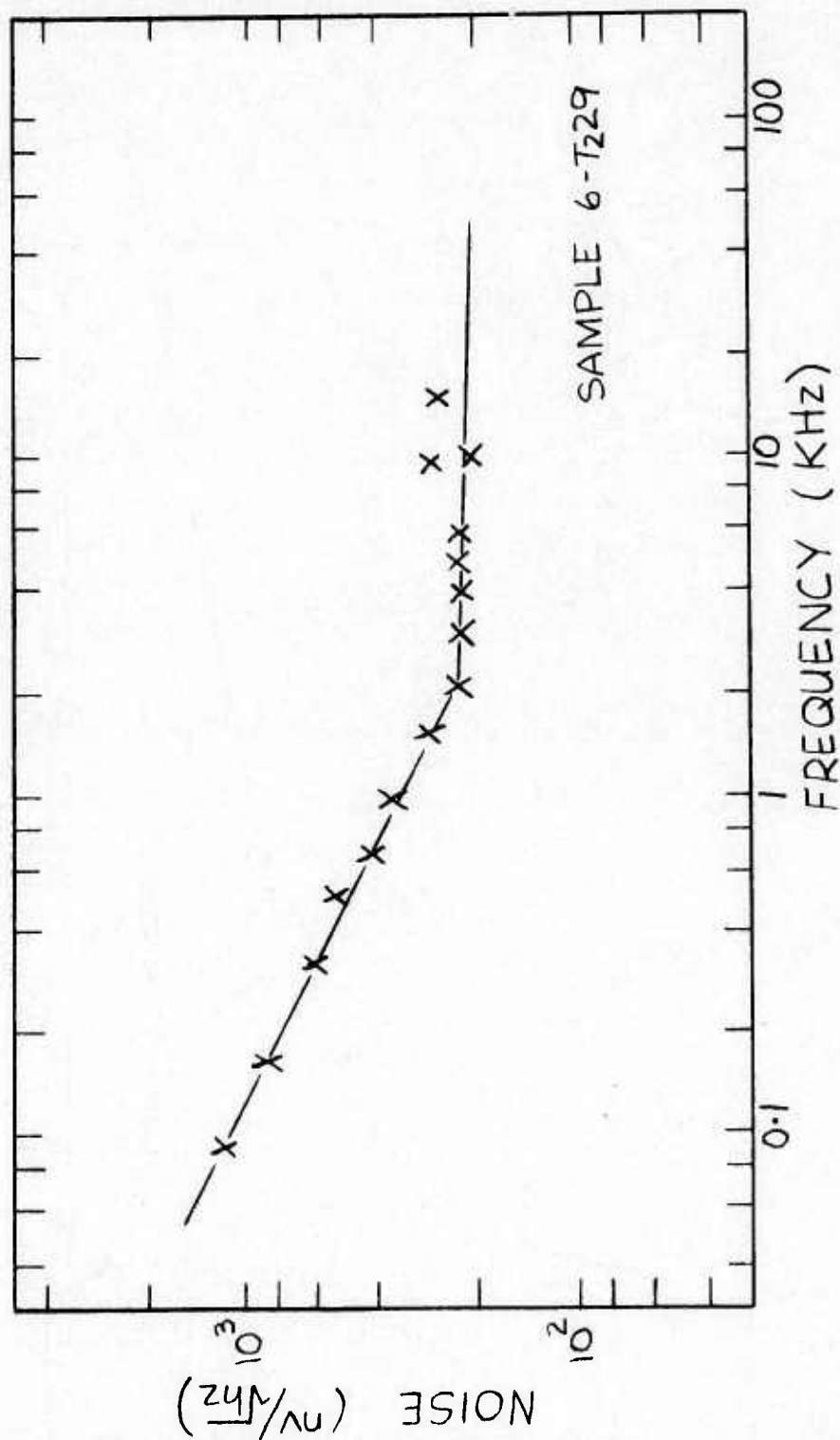
Figure 3-143 Noise vs Frequency for Pb.88Sn.12Te Film

2 mv/cm
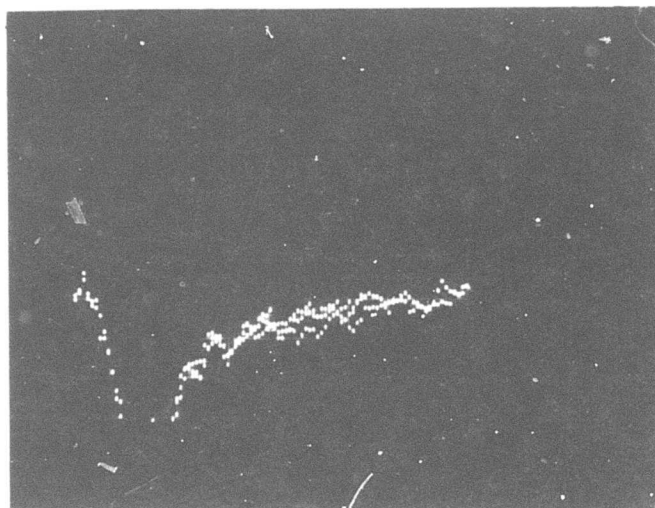
200 ns/cm

Sample Photoconductive Response 6-T_2-29

Figure 3-144 Lifetime Measurement in Sputtered Pb$_{.88}$Sn$_{.12}$Te Film

Trace A 3 μ Filter over Nernst Glower Source. Maximum Gain Available Used
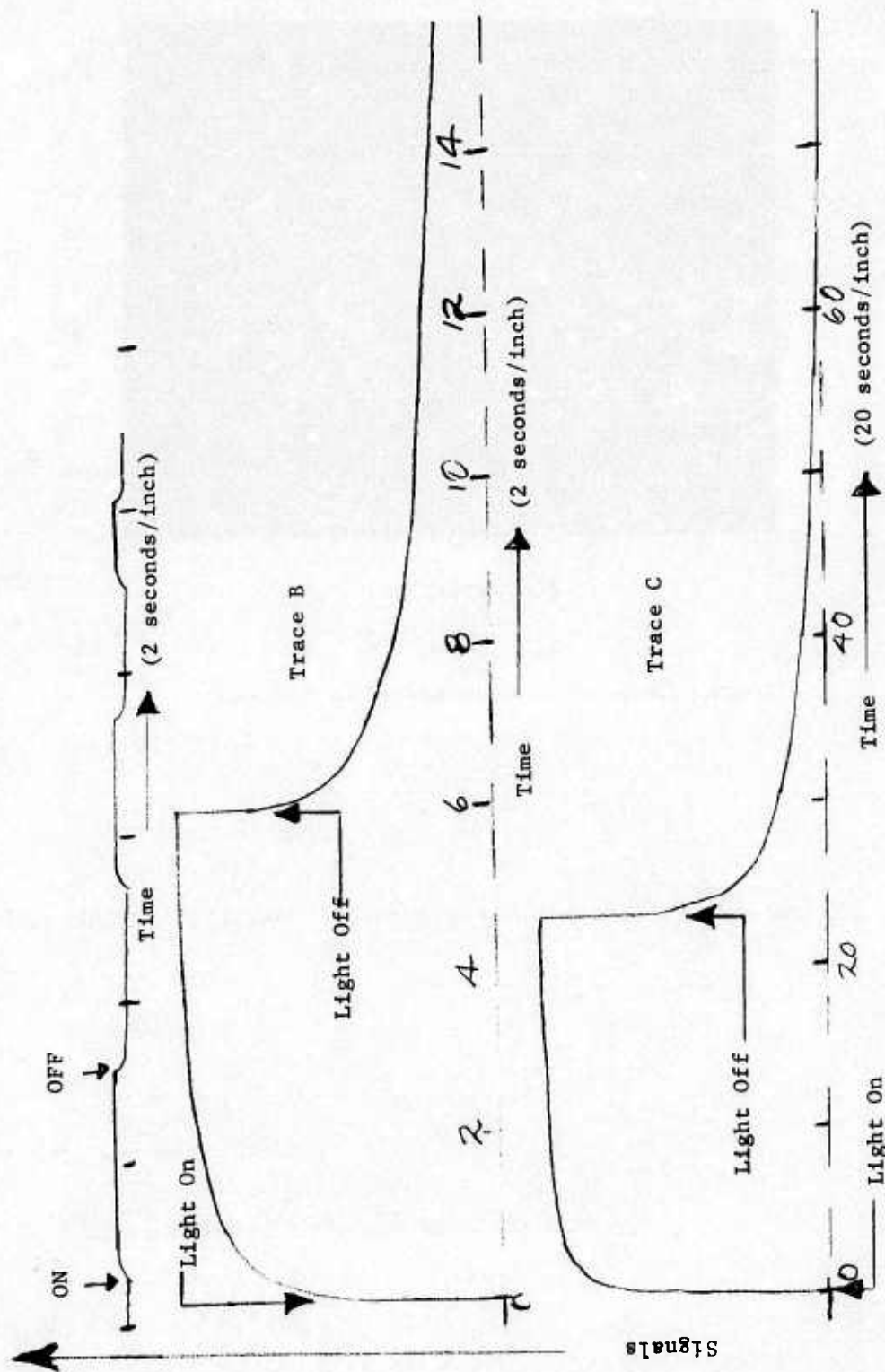
Figure 3-145 "Very Slow" Effects in Rise and Fall of Photocurrent Tracings of Chart Recorder Data of Signal vs Time. For Traces B&C, Total Nernst Glower Radiation was used, at Two Different Time Scales

.2 mv/cm
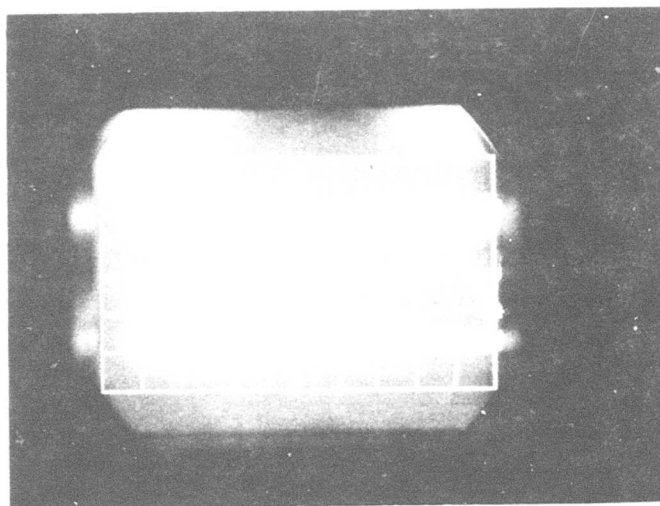
0.1 sec/cm   f_{chopping}   0.8 Hz

.05 mv/cm
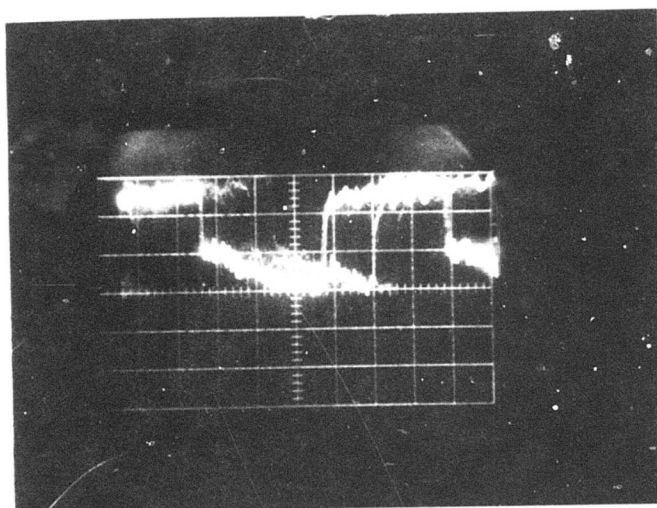
5 ms/cm   f_{chopping}   30 Hz

Figure 3-146 Response Time Measurements in $Pb_{.88}Sn_{.12}Te$ Film

3-263

frequency. Secondly, the response time characteristics of these films were measured with the pulsed GaAs laser source. Finally, the response time characteristics were measured with a chopped blackbody source using alternately: no-filter, a $3\,\mu$m and a $5\,\mu$m cut-on filter. The results of these measurements are shown in Figure 3-142 thru 3-146.

Figure 3-142 shows the response signal as a function of frequency for measurements taken at the two wavelengths (i.e. $2.2\,\mu$m and $6\,\mu$m). It can be seen that the response at the short wavelength peak ($2.2\,\mu$m) shows a decrease of nearly an order of magnitude for a variation of frequency from 100 Hz to 900 Hz, while the longer wavelength peak response, shows practically no change over the same frequency range - clearly indicating different response times for the two peaks. In Figure 3-143, the noise, measured from 100 Hz to 10^4 Hz, shows a 1/f dependence at frequencies below 2 KHz, while above 2 KHz the noise is constant with frequency.

Measurements utilizing the pulsed GaAs laser source resulted in responses which clearly showed a decay time having two components - one near or below 100 nanoseconds and one of approximately 600 nanoseconds. The wave form for the sample signals is shown in Figure 3-144.

Finally, unfiltered blackbody response showed a decay indicative of a response time of several seconds as shown in Figure 3-145, along with an initial, fast decay component. With a $3\,\mu$m cut-on filter, response time components considerably below 1 millisecond as well as exceeding 100 milliseconds were observed. This is more clearly shown in Figures 3-146(a) and 3-146(b). Interestingly enough, the slow response components showed a dependence on the irradiance level-typically increasing with lower source intensity. With a $5\,\mu$m cut-on filter, only the fast response time component was observed.

The results presented are consistent with the conclusion that the response associated with the shorter wavelength peak has a long response time and may be due, in heavily "doped" films, to the presence of secondary phases (e.g. lead oxides), oxygen absorption or other surface

and bulk trap formation; whereas, the response associated with the longer wavelength peak has the fast response time associated with PbSnTe.

3.7.5 ELECTRO-OPTICAL PROPERTIES OF FILMS SPUTTERED IN THE PRESENCE OF PARTIAL PRESSURES OF OXYGEN AND NITROGEN. We have seen in the results presented above the first evidence that oxygen and/or nitrogen added to $Pb_{1-x}Sn_xTe$ in the sputtering background environment may provide some form of compensation or trapping, resulting in enhancement in photoconductive response. Since one objective of this program was to investigate various menas by which such enhanced photo-response in $Pb_{1-x}Sn_xTe$ could be achieved, we explored these effects more systematically. To this end, a series of experiments were performed to define electrical and electro-optical behavior of thin film $Pb_{1-x}Sn_xTe$ as a function of the partial pressure of gaseous species in the sputtering gas. In Section 3.3, we presented results on the electrical, structural and compositional properties of films deposited with controlled additives of O_2 and N_2 in the sputtering gas (see Figures 3-71 and 3-76). The corresponding effects on the electro-optical properties are presented in Figures 3-147 through 3-149 and in Table 39. Figure 3-147 shows the spectral responsivity in some representative films. The overriding observation is the relatively high photoconductive responses compared to the response of all typical films shown earlier which were sputtered without the presence of O_2 and N_2. This response enhancement is obviously a systematic function of the partial pressure of eith O_2 or N_2. However, not to be overlooked should be that there appears to be a shift in the photoconductive cut-off wavelength to shorter wavelengths at the higher partial pressures of the two additives. In the following we will consider each of these observations in somewhat more detail. First, the reader is referred to Figure 3-71 which shows a typical relationship between the partial pressures of O_2 and N_2 and the carrier concentration. On close inspection of Figure 3-147, it becomes then immediately obvious that the responsivity is directly relatable to the carrier concentration resulting from the additives. Oxygen is apparently more effective in small quantities than nitrogen, with a ppO_2 of about
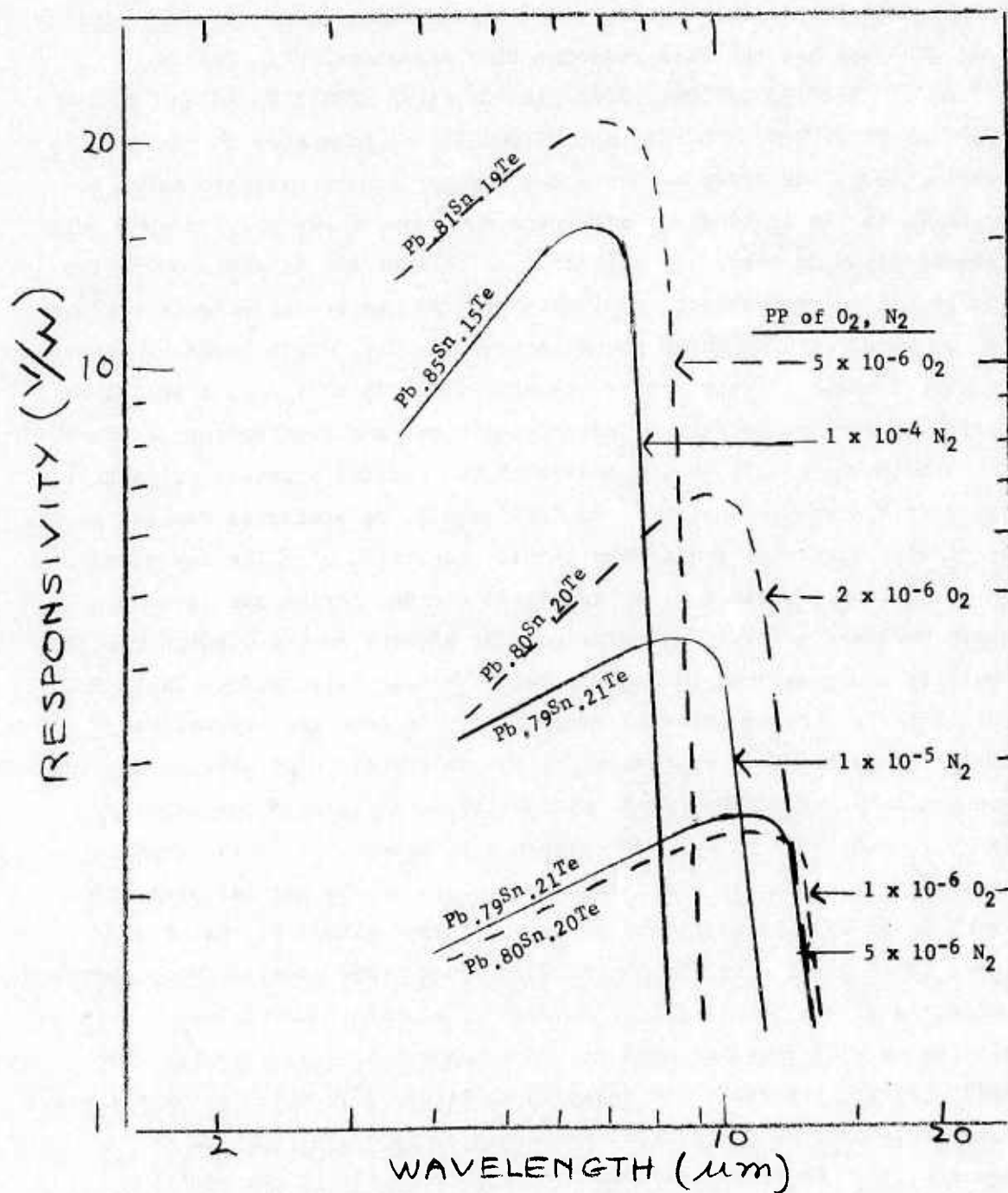
Figure 3-147 Absolute Spectral Photoconductive Responsivity of As-Deposited $Pb_{1-x}Sn_xTe$ Films - Effect of O_2 and N_2 Addition During Sputtering

5×10^{-6} torr yielding a higher response than a ppN_2 of 1×10^{-4} torr - this in an $x = 0.15$ film which should normally have a higher response than the $x = 0.19$ film having the O_2 additive in the background. As can be seen from Figure 3-71, a ppO_2 of 5×10^{-6} torr appears to be a near optimum value relative to reduction (or compensation) of carriers and a ppN_2 of 1×10^{-4} yields about the same carrier concentration.

Directly comparable in Figure 3-147 are films with composition $x = 0.20$ for O_2 effects and $x = 0.21$ for N_2 effects. From the former we note that even films "doped" with the low value of $ppO_2 = 1 \times 10^{-6}$ yield a higher responsivity than "undoped" films. Doubling the ppO_2 increases the responsivity by nearly a factor of three and a slight blue shift is observed in the cut-off wavelength. A corresponding increase in ppN_2 from 5×10^{-6} to 1×10^{-5} torr causes the peak responsivity to almost double and a considerably larger shift in cut-off wavelength occurs than with O_2.

While no directly comparable data are shown in Figure 3-147, the cut-off wavelength of the highest responsivity film ($R \sim 20V/W$, $x = 0.19$) is also considerably shorter than films without O_2 additives (see e.g. $x = 0.18$ films in Figure 3-132). However, it may be recalled that at these pressures there is a small change in the film composition between O_2 doped film and films sputtered without O_2 under the same conditions. Specifically $x = 0.19$ with O_2 and $x = 0.20$ without O_2 which should yield a somewhat larger energy gap in the O_2 doped films. In N_2 doped film, the change is even greater for high ppN_2 values. At 1×10^{-4} torr an x-value of $x = 0.15$ was produced for the same sputtering conditions with corresponding shifts to shorter wavelengths. This feature, i.e., the shift to shorter wavelengths can, of course, be controlled. If a high response is desired at a particular wavelength the depositing conditions and target compositions is adjusted correspondingly, i.e. to values which would yield somewhat higher x-values if the additives were not present.

In summary, there is significant and systematic enhancement in photoconductive response with increasing partial pressures of N_2 and O_2

3-267

in the sputtering gas. The increase can be orders of magnitude. These enhanced responses are possible in both p-type (i.e., O_2 doped) and n-type (N_2 doped) films. Although there is a shift to shorter cut-off wavelengths, this is easily compensated for by deposition control.

In order to obtain more information concerning causes of the enhanced responses intensive studies are required. One approach is the measurement of the frequency response of doped or compensated films. Some early examples are shown in Figures 3-148 and 3-149 for response and noise data respectively. The photo-response in Figure 3-148 shows frequency independence for all films, i.e. over the range measured. This would indicate that the response times for the response enhanced films are still relatively short. Values considerably below a millisecond are certain. This is, of course, highly desirable. However, lifetime measurements below the microsecond range are required to determine whether small effects on response times can be observed which could reveal the mechanisms as trap enhanced, for example. Such experiments are still to be performed. Figure 3-149 shows the noise voltage as a function of frequency for several of the films whose responsivity was shown in Figure 3-147. As can be seen, the noise voltage shows a large 1/f component but only to several kHz - i.e. over a somewhat smaller frequency range than in the "undoped" films. It might be interesting that detectivities calculated from the responsivities and the noise characteristics above 5 kHz yield D* values of 5.5×10^9 cm-Hz$^{\frac{1}{2}}$/w for the highest responsivity films in this set. With corresponding noise values, for the highest responsivity film shown in Figure 3-138, a peak detectivity of 1.7×10^{10} cm-Hz$^{\frac{1}{2}}$/w is calculated, which is approaching Blip conditions. Further optimization should be possible by careful impurity control and application of antireflection coatings. This would make photoconductive $Pb_{1-x}Sn_xTe$ as competitive for practical devices as photo-voltaic $Pb_{1-x}Sn_xTe$.
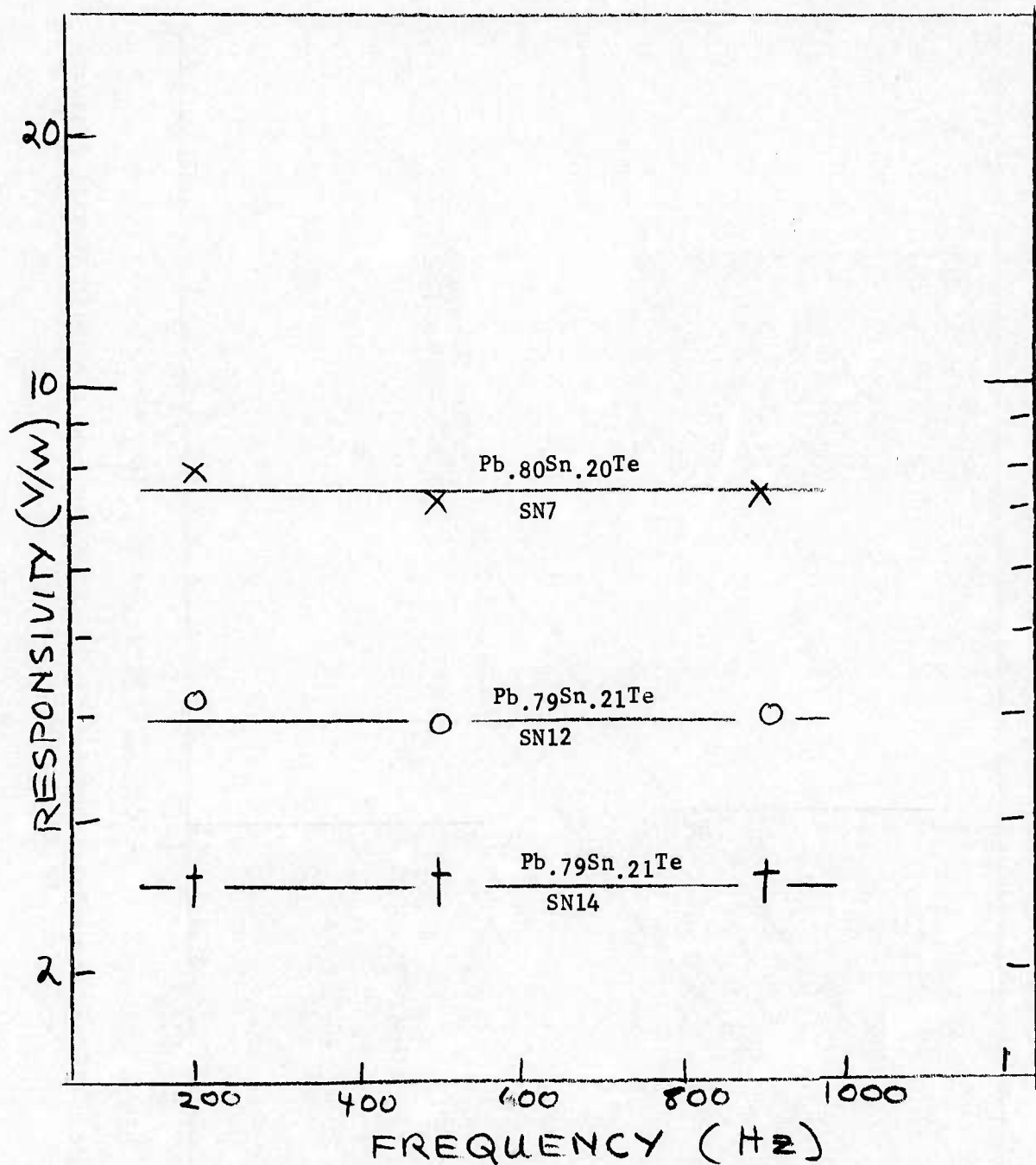
Figure 3-148   Responsivity vs Frequency for $Pb_{1-x}Sn_xTe$ Films Deposited
in Presence of O_2 and N_2 in Sputtering Gas
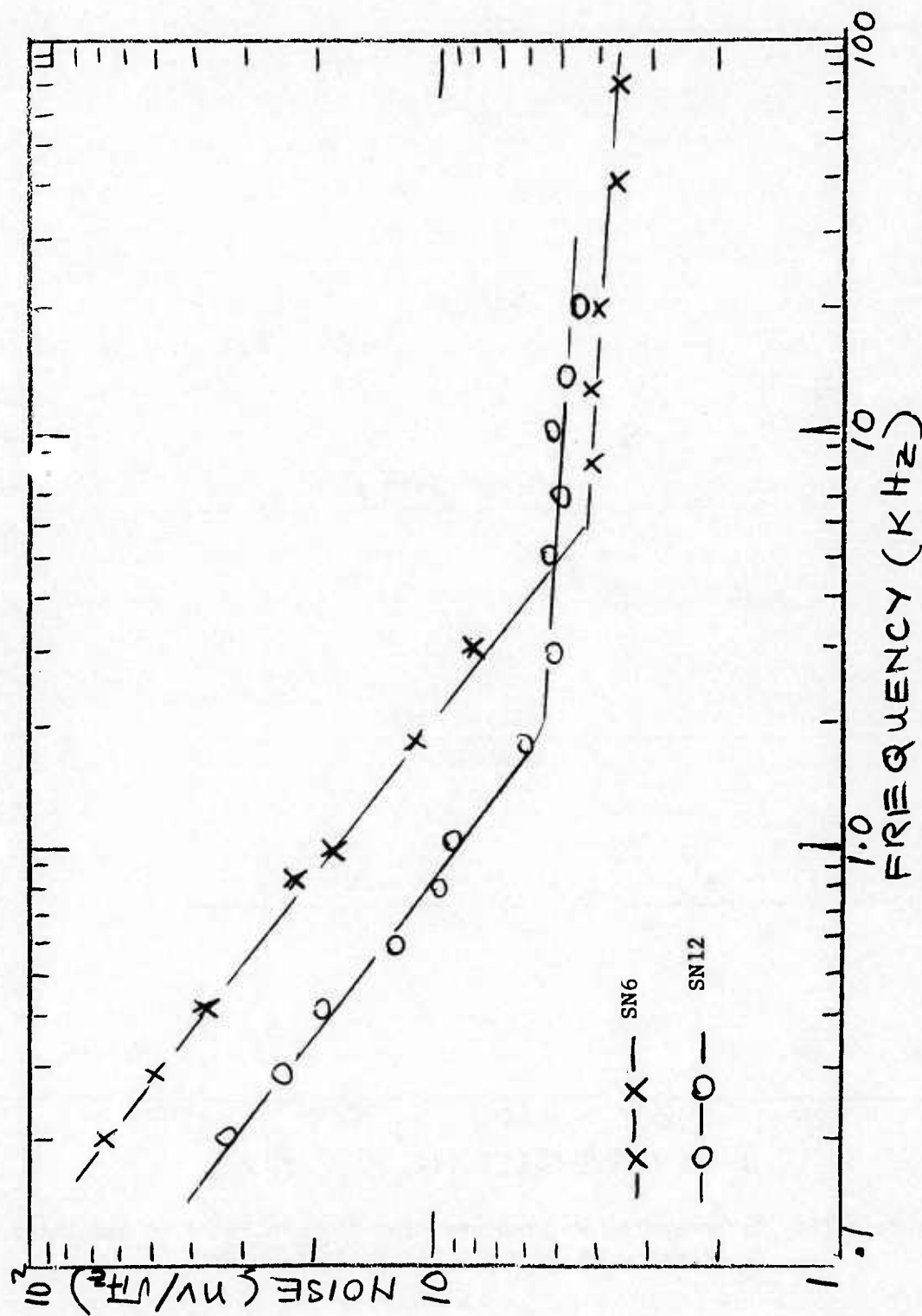
Figure 3-149 Noise vs Frequency for $Pb_{1-x}Sn_xTe$ Films Deposited with Partial Pressure of O_2 and N_2 in Sputtering Gas

3.7.6 LOW TEMPERATURE PHOTOCONDUCTIVE RESPONSE AND DETECTIVITY OF
SPUTTERED $Pb_{1-x}Sn_xTe$. The electro-optical properties presented in the
preceding sections were measured at $77^{\circ}K$. The importance of lower
temperature measurements has been pointed out before. In particular,
it provides for the identification of noise and response limiting
mechanisms, and permits an analysis of detector performance over a
wide range of temperature. Results of such low temperature measure-
ments are still limited. A few representative photoconductive response
and detectivity data for $Pb_{1-x}Sn_xTe$ sputtered films are shown in
Figures 3-150 through 3-153. The first example, a $Pb_{.84}Sn_{.16}Te$ film,
is certainly not one of our better samples. However, Figure 3-150
and 3-151 demonstrate that even relatively low quality sputtered
$Pb_{1-x}Sn_xTe$ films show a substantial enhancement of both the response
and the detectivity if operated at the low temperatures. As expected,
the photo-response experiences a shift to longer wavelength at the lower
temperature. However, while the cut-off wavelength at $77^{\circ}K$ is consistent
with the film composition, the shift is larger than expected as the
operating temperature is decreased to $30^{\circ}K$. But, the enhancement of
photoconductive response is also greater than one might expect for this
temperature decrease. As the results show a detectivity with a D* in
the high 10^9 cm $Hz^{\frac{1}{2}}/w$ is measured at $30^{\circ}K$.

Corresponding response and detectivity measurements in one of
our better films show corresponding improvements. Data for one such
film are illustrated in Figures 3-152 and 3-153. As noted a detectivity,
D*, slightly above 1×10^{10} cm $Hz^{\frac{1}{2}}/w$ is measured in this case at the
lower temperature.

As implied, the number of samples measured over the larger
temperature range is still limited. Of course, the long time required
for actual measurements is a factor. As discussed in connection with
the low temperature electrical properties, measurement of more samples
over the wider temperature range are required for any thorough analysis
of the results.
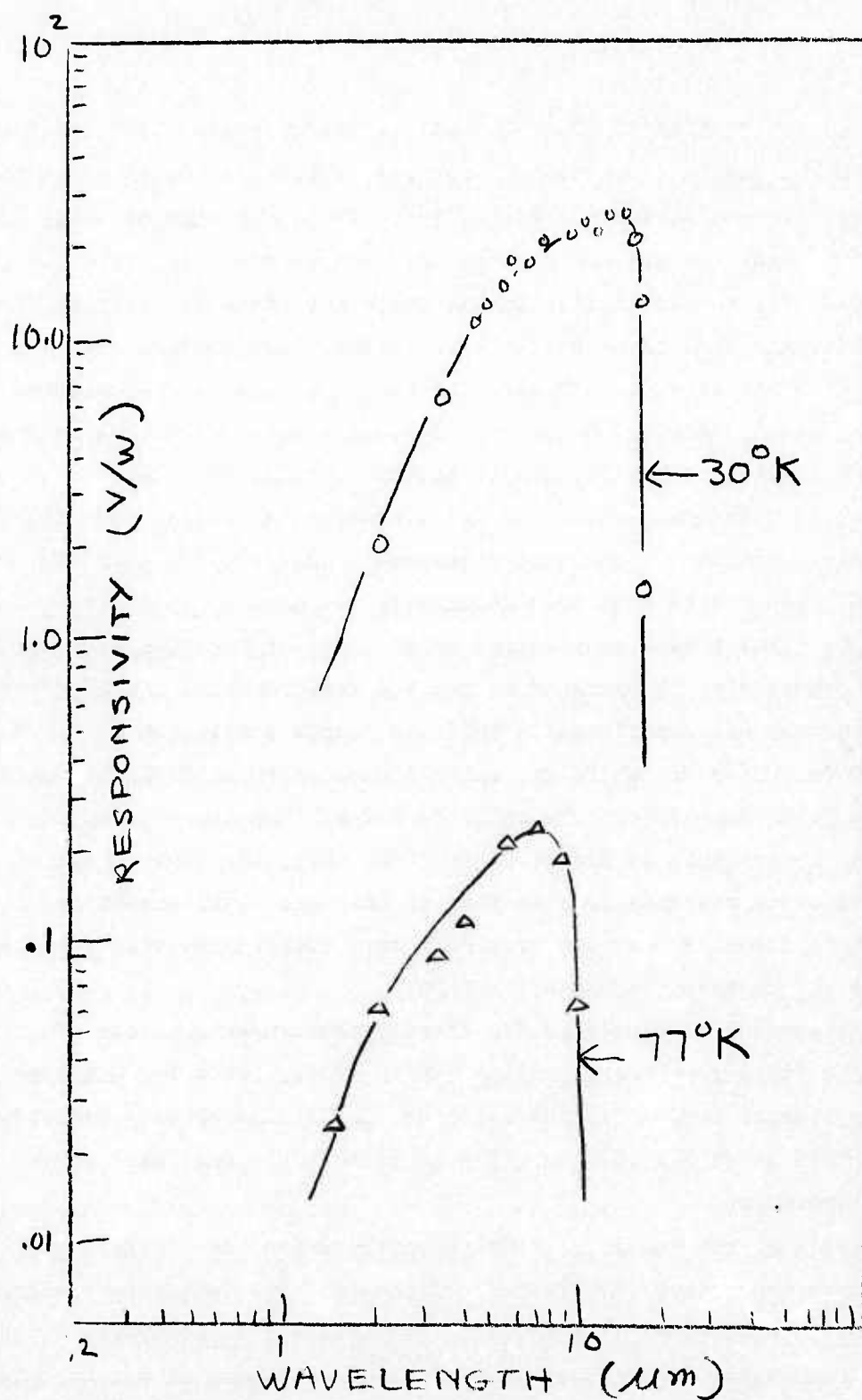
Figure 3-150 Spectral Photoconductive Responsivity of Sputtered
Pb$_{.84}$Sn$_{.16}$Te Film vs Operating Temperature - Liquid
He Measurement Facility

3-272
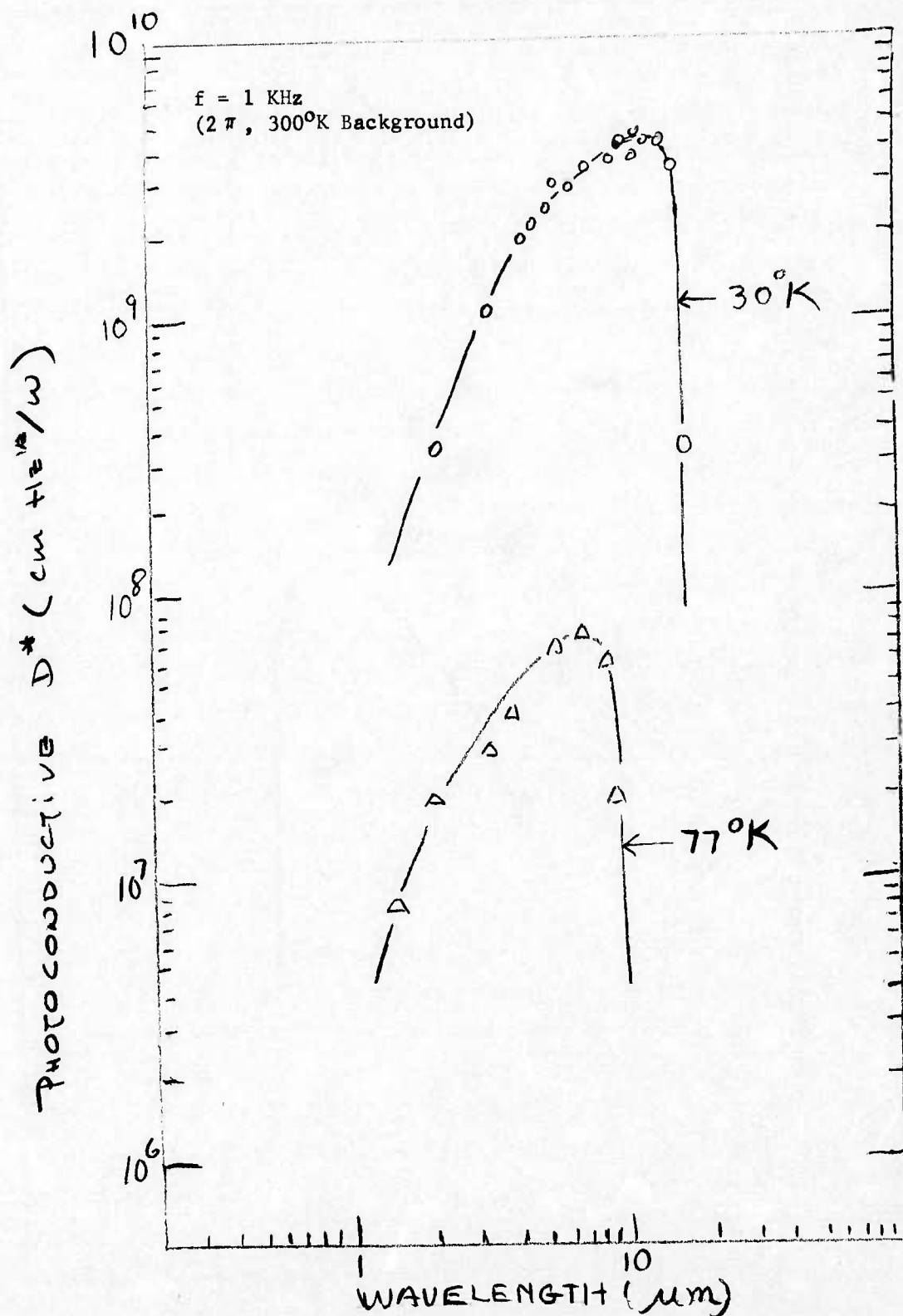
Figure 3-151 Spectral Photoconductive Detectivity of Sputtered
Pb$_{.84}$Sn$_{.16}$Te Film vs Operating Temperature - Liquid
He Measurement Facility
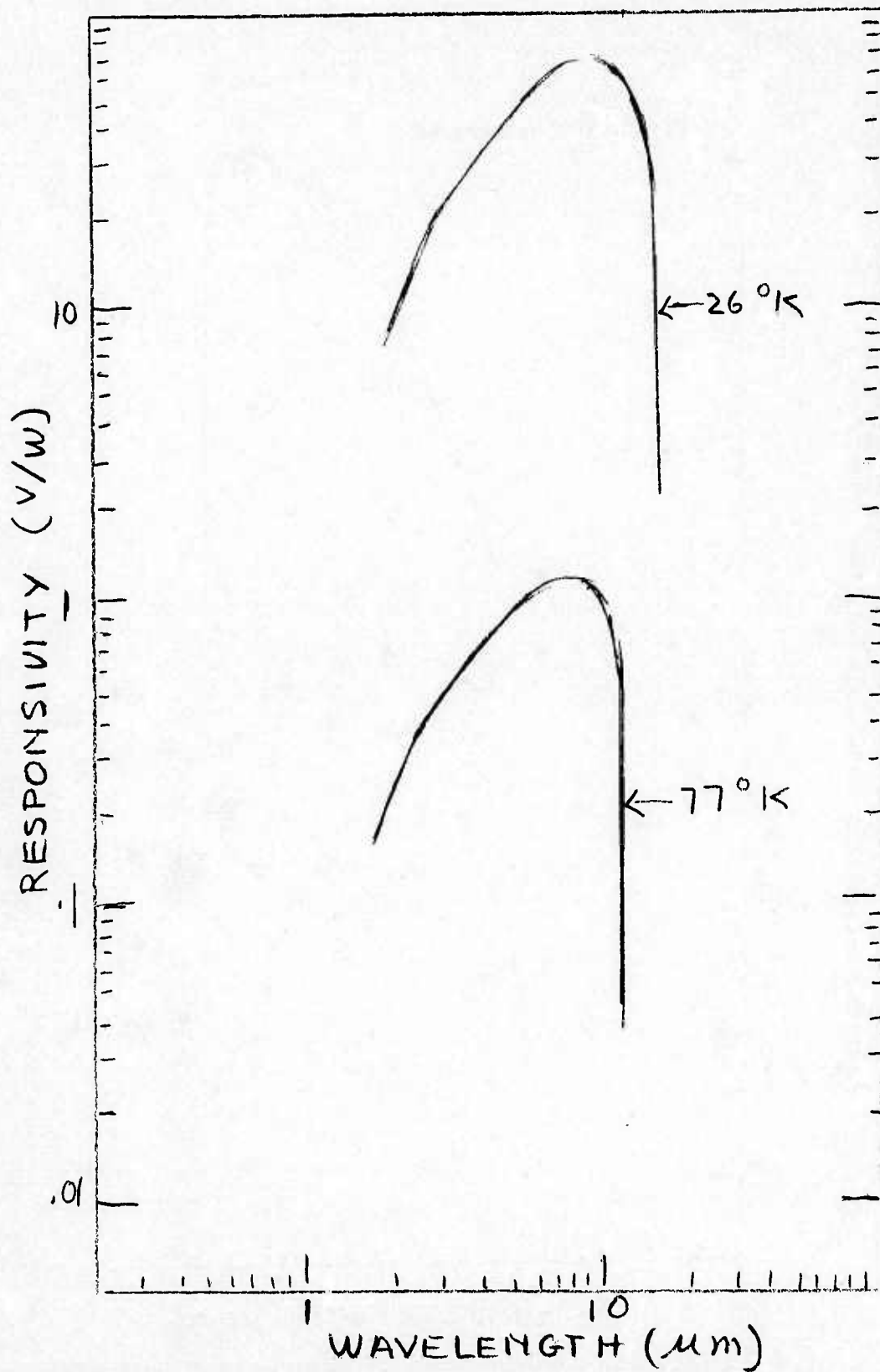
Figure 3-152 Spectral Photoconductive Responsivity of Sputtered
Pb$_{.80}$Sn$_{.20}$Te Film vs. Operating Temperature
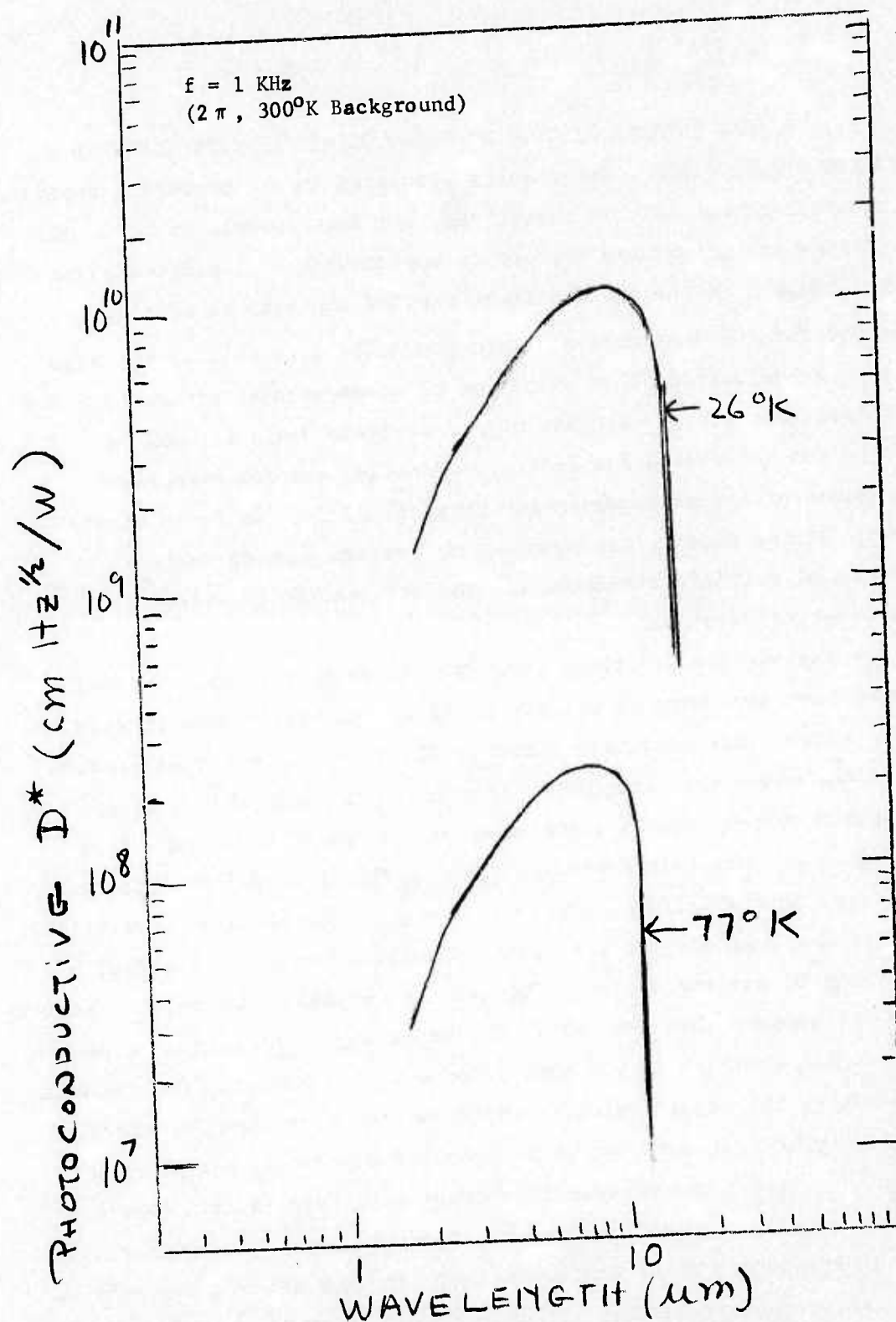
Figure 3-153 Spectral Photoconductive Detectivity of Sputtered
Pb.80Sn.20Te Film vs. Operating Temperature

3.7.7 SOME INITIAL RESULTS ON PHOTOVOLTAIC EFFECTS OBSERVED IN
SPUTTERED PbSnTe FILMS. The results presented in the preceding sections
are significant not only in themselves, but more importantly, in their
utilization and uniqueness for device application. Of particular importance
in this respect is the obvious simplicity of the bias sputtering
technique for the preparation of p-n photodiodes as well as the high
quality, as-deposited films which can be prepared with either type and
any composition for other types of photovoltaic devices (such as
Schottky and heterojunction diodes). Finally, the demonstrated
enhancement of the photoconductive response of $Pb_{1-x}Sn_xTe$ by simple
"doping" during deposition, promises to provide photoconductive
detectors of sufficient sensivity for utilization in military
electro-optical systems.

To explore the practical potential of these findings, initial
attempts have been made to prepare various feasibility demonstration
devices under other funding - entirely based on the material studies
carried out under this program. For example, an initial number of
bias sputtered p-n layered structures were prepared which exhibited
encouraging photovoltaic responses characteristic of p-n photodiodes.
Since these initial efforts were only aimed at establishing feasibility,
no particular emphasis was placed on optimizing device configuration,
passivation or antireflection. Instead, the emphasis was on such aspects
as to what happens when two PbSnTe layers of different carrier type are
deposited sequentially in the same pumpdown. For example, the question
as to whether the layers maintain their carrier type when deposited
sequentially as distinctly as when deposited separately was checked
thoroughly. By the use of special shutter positions, single layers
of p- and n-type $Pb_{1-x}Sn_xTe$ were deposited along with the samples
having p- and n-type diode configuration. In this manner, the various
electrical, compositional and structural properties of the individual
p- and n-type layers could be compared with those of the diode configuration.

Table 40 lists some of the experiments performed toward the preparation of p-n photodiodes. Also included are selected data on the properties of individual layers. As noted, Target #13 was used for some of these experiments. This was the latest sputtering target prepared and had a larger diameter than earlier versions in order to deposit uniform layers over larger areas than was required for the earlier experiments. This was aimed at future work on array deposition, but it was also valuable for the preparation of the relatively large, single diode structures used in the feasibility studies. Figure 3-154 shows some of these configurations used. Their main advantage is simplicity, requiring only simple shuttering and mechanical masking. As noted, platinum was used for the ohmic contact to the p-type $Pb_{1-x}Sn_xTe$ layers while indium was used for the ohmic contact to the n-type layer. In some cases the platinum was deposited on the BaF_2 (or CaF_2) substrate before the deposition of the diode, while in others it was deposited on top of the p-type $Pb_{1-x}Sn_xTe$ layer. In the former case, the platinum was deposited to form a single crystal film. To achieve this, a separate, small investigation was pursued to establish deposition conditions under which single crystal platinum film could be sputtered onto single crystal $BaF_2(111)$ and $CaF_2(111)$ substrates. It was then attempted to produce epitaxial $Pb_{1-x}Sn_xTe$ on single crystal platinum film. The result was that essentially the same conditions under which epitaxy of $Pb_{1-x}Sn_xTe$ occurs on $BaF_2(111)$ can be used to produce epitaxy of PbSnTe on single crystal platinum. Thus it became possible to utilize the two illustrated techniques for making platinum contacts to the p-type layer, i.e. above and below this layer. Both the Pt and In ohmic contacts were carefully checked for ohmic characteristics. As shown in Figure 3-154, both types of contacts were deposited in such a way that they were partially located on the $Pb_{1-x}Sn_xTe$ film and partially on the uncoated substrate for lead attachment. Leads were attached with In solder at a location sufficiently far away from the PbSnTe film area to avoid alloying or other problems.
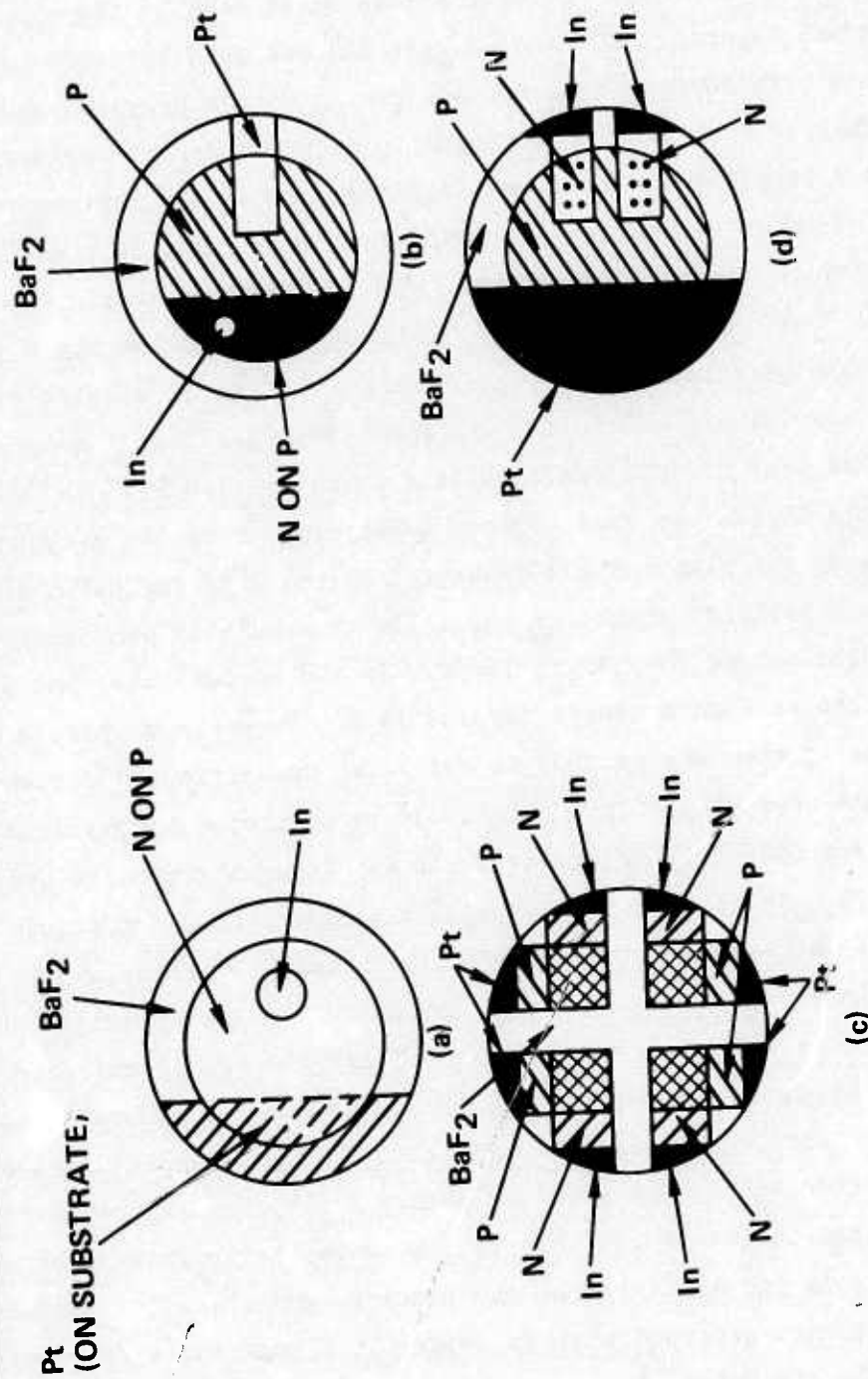
FIGURE 3-154 CONFIGURATIONS FOR BIAS SPUTTERED DIODES

F123582 7104

3-278

Figures 3-155 and 3-156 give a few examples of typical, relative spectral photovoltaic responsivities measured in such p-n diode structures. All were deposited by bias sputtering. Exact active area definition was not feasible with these initial samples. However, the main features of the observed spectral responsivities, in particular cut-off wavelength, etc. are consistent with that which is expected for $Pb_{1-x}Sn_xTe$ films of the composition noted and the measurement temperature of $90^{o}K$. The undulations in the response curves can be attributed to optical interference due to the fact that the optical thickness of the films are on the order of magnitude of the response wavelengths. A convincing number of samples of this type have been measured to date which exhibit the characteristic photovoltaic response of $Pb_{1-x}Sn_xTe$. Careful analyses were performed to insure that, in all cases, the measured responses are indeed those resulting from the p-n junction and not from contact rectification, Dember effects or other phenomena.

Absolute values of responsivities in our most recent samples are becoming quite respectable but surface passivation and antireflection must yet be completed before truly high performance diodes are possible.

While the preparation of photovoltaic p-n junction devices was only recently initiated, photovoltaic diodes of the Schottky-barrier type were briefly explored at an earlier date. As in the case of the p-n junction devices, the work with Schottky-barriers was limited to a feasibility study only. That is, no extensive device optimization has been performed. Again, these efforts led to encouraging results. A number of films were successfully converted into photovoltaic diodes, with typical Schottky-barrier behavior. Pb, Al, and In were utilized for the non-ohmic or barrier contact. These contacts were deposited in strips of approximately 2 mm by 10 mm. Part of each strip was located on p-type $Pb_{1-x}Sn_xTe$ film to form the active area, the remainder extended onto the substrate for lead attachment. The ohmic contact for p-type $Pb_{1-x}Sn_xTe$ was platinum. Again the Pt contacts were
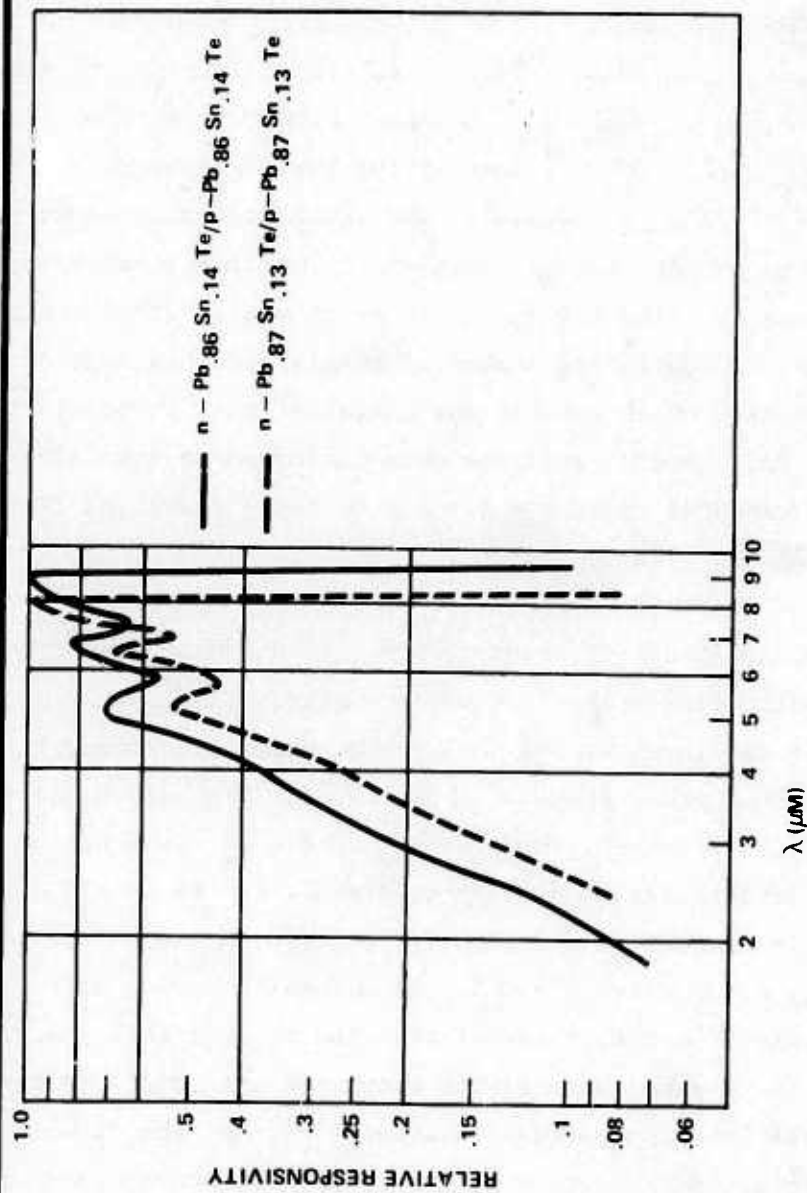
FIGURE 3-155 PHOTOVOLTAIC RESPONSE OF BIAS SPUTTERED PbSnTe DIODES

F123557 7104
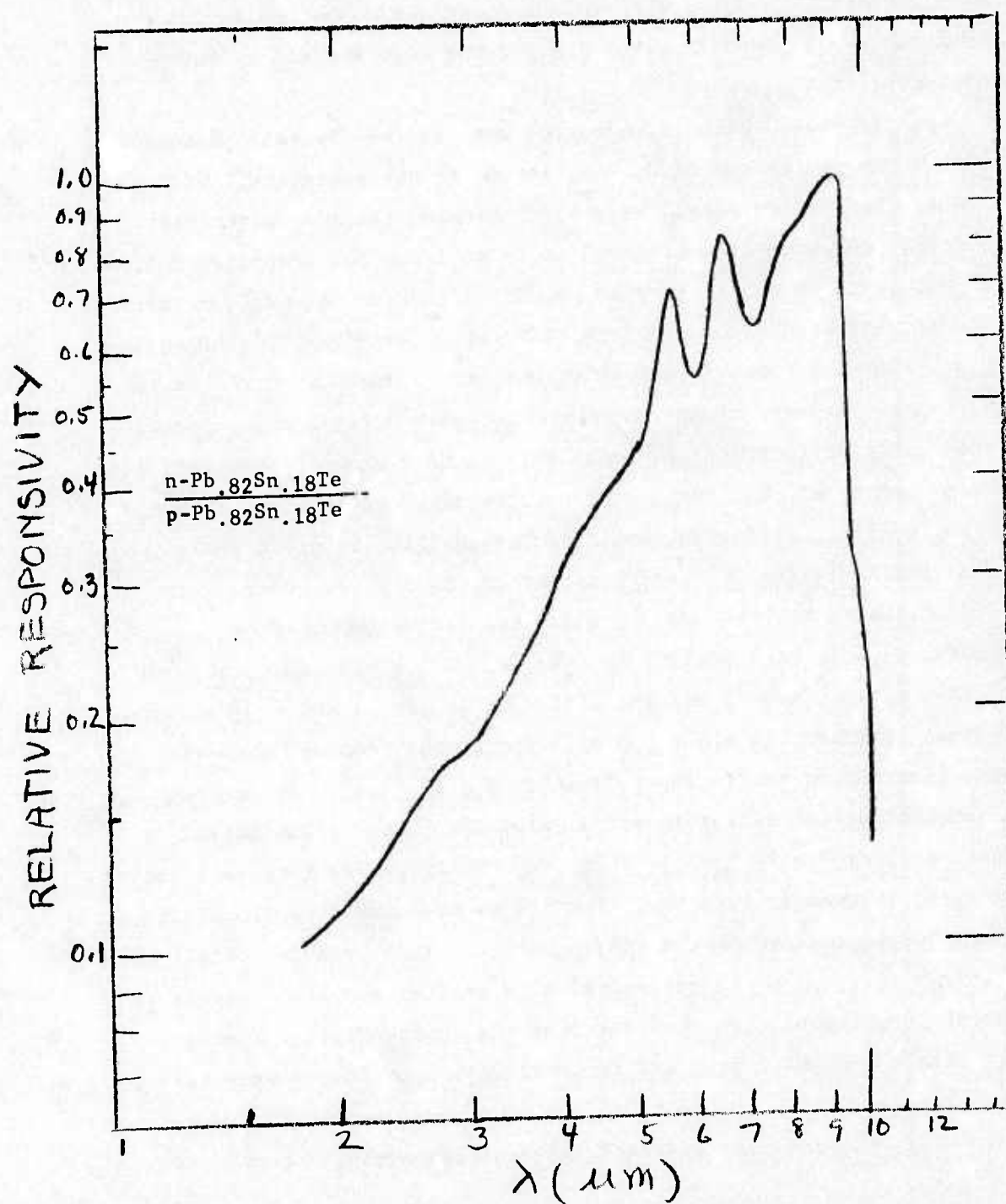
Figure 3-156 Photovoltaic Response of Bias Sputtered $Pb_{.82}Sn_{.18}Te$ Diode

carefully checked to insure ohmic behavior. In all Schottky-barrier
samples prepared, to date, the ohmic contact was deposited on top of
the p-type $Pb_{1-x}Sn_xTe$ film also, i.e. on the same surface as the
barrier metal.

Both front and back illumination was used to generate photovoltaic
signals. For the latter case, BaF_2 served as the substrate. With
indium as the barrier metal, very thin infrared transparent barriers
were deposited which were measured to be at least 80% transparent from
8-14 μm. With Pb and Al barrier metals, no effort was made, to date,
to deposit infrared transparent thicknesses. Therefore, the effective
"active" area for front illumination was rather limited in the latter
case, consisting only of the peripheral region defined approximately
by the diffusion length of the optically excited minority carriers and
the edge length of that portion of the "barrier" strip located on the
$Pb_{1-x}Sn_xTe$ film. Diffusion length in PbSnTe films is quite small.
This diffusion length, L, can be estimated, to a first order, from
classical theory by $L = \sqrt{D \cdot \tau}$, where the diffusion constant
$D = \mu (kT/e)$. In high quality $Pb_{1-x}Sn_xTe$, with a time constant, τ, on
the order of 10^{-8} sec, a maximum diffusion length is about 10 microns.
A typical periphery is about 0.8 cm. Hence, the "active" area for
front illumination has an upper limit of 8×10^{-3} cm^2. By contrast
the somewhat better definable active area for "back" illumination is
on the order of 7×10^{-2} cm^2. Thus, the effective front to back active
area ratio is greater than ten. The active area for back illumination
is, of course, defined by the entire barrier metal area in contact with
the PbSnTe film (plus the peripheral area defined above). This is in
reasonable agreement with the fact that the photovoltaic responses,
where observed by both back and front illumination in the same cells,
showed response ratios of up to 25:1. Of course, reflection loss
differences between front and back illumination contribute to this
ratio also.

Figure 3-157 gives an example of the response measured by both front and back illumination in a Schottky-barrier diode. The measurement temperature was at or above $90^{\circ}K$ and the barrier metal was Pb. In this case and in other samples similarly measured, no efforts were made to account for or minimize reflection losses nor was any attempt made to minimize substrate losses or $Pb_{1-x}Sn_{x}Te$ absorption losses in films of thicknesses exceeding the absorption length at the measurement wavelengths. All of these factors can considerably degrade the response under back illumination. The uncertainty in the front illumination cases, relative to the actual active area size, is likely to yield far better than reported responses since the estimate of the active area, if anything, was conservative. Figure 3-158 shows the relative spectral responsivities of some front illuminated Schottky-barrier diodes with transparent In barrier metal. Again, exact absorption and/or reflection losses are not known or accounted for. However, the spectral responsivity curves show trends consistent with the film compositions (i.e. cut-off wavelengths) for $90^{\circ}K$ measurement temperature. A number of more recent samples are now being evaluated which better define active area geometry and other improvements.

Although the work was not extensive as yet, the absolute photovoltaic cell responsivities, as achieved during the course of this work, improved in orders of magnitude, ranging from initial low values of 10^{-1} v/watt to more recent (but not final) values exceeding 10 v/watt at $77^{\circ}K$. Considering the relatively simple, unoptimized configuration utilized to date, considerable improvements can confidently be expected, as passivation, antireflection and optimized thicknesses are introduced.
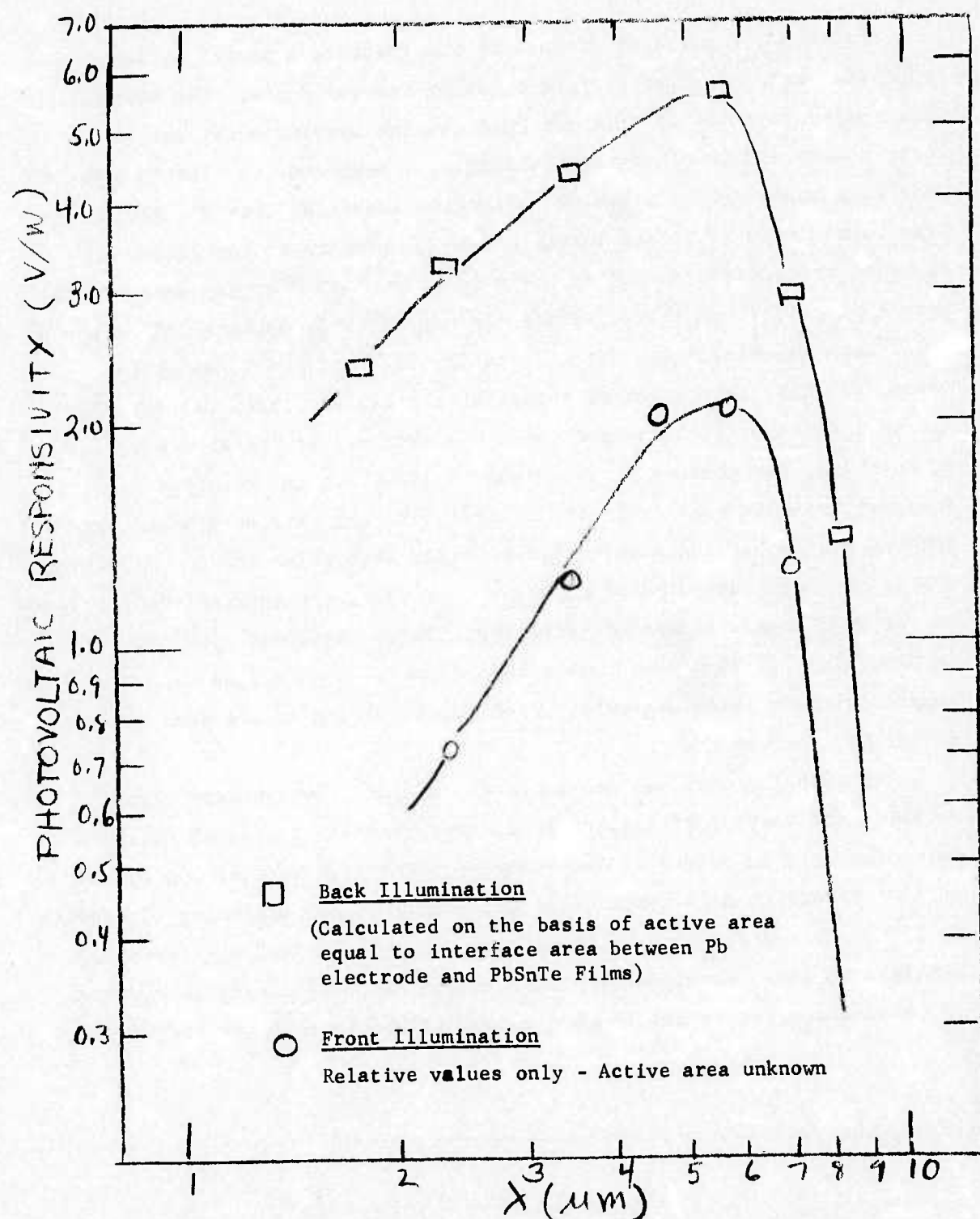
Figure 3-157   Photovoltaic Responsivity in As-Deposited Sputtered
PbSnTe Films

3-284
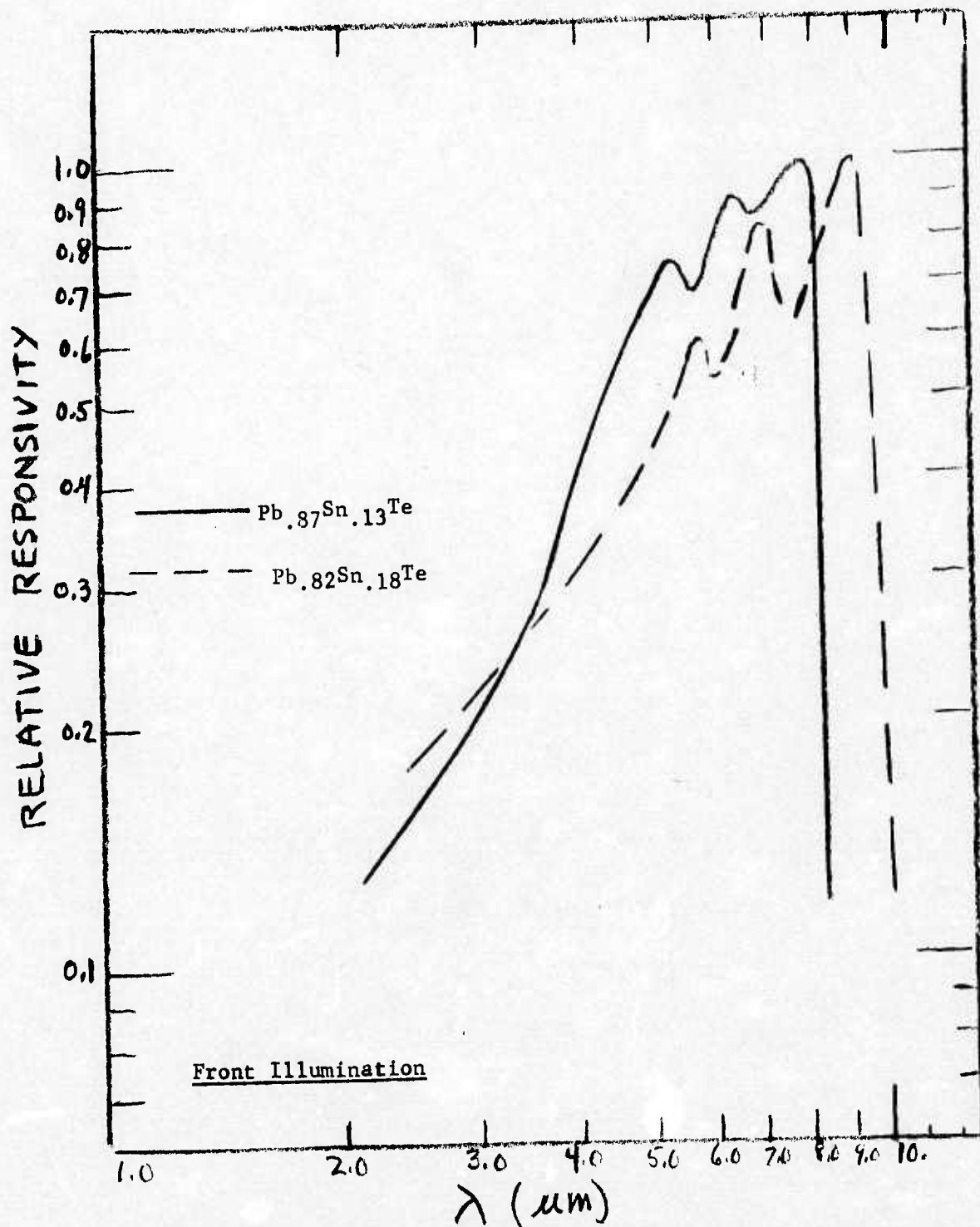
Figure 3-158   Photovoltaic Response in Transparent Schottky Barrier
Detectors on As-Deposited Sputtered Single Crystal
Thin Films of $Pb_{1-x}Sn_xTe$

Section 4
REFERENCES

1. Krikorian, E., Crisp, M. J., "$Pb_{1-x}Sn_xTe$ Variable Band Gap Alloy System Study", Interim Reports No. 1, 2 and 3, AFML - Contract No. F33615-72-C-1042.

2. Corsi, C., Alfieri, I., and Petrocco, G., APL 24, 10, May 1974, p. 484.

3. Holloway, H., and Logethetis, F. M., JAP 42, 11, October 1974, p. 4522.

4. Tao, T. F., Kasai, F. I, and Butler, J. F., J. Vac. Sci. Tech. 6, 917, (1969).

5. Farinre, T. O. and Zemel, J. H., J. Vac. Sci Tech. 7, 121 (1970).

6. Hohnke, D. K., Kaiser, S. W., JAP 45, 2, February 1974, p. 892.

7. Jacobus, G. F., Pohlman, J. L. W., Proc. of IRIS Specialty Group on IR Detectors, March 1973, p. 357.

8. Longo, J. T., Fertner, E. R., Joseph, A. S., APL 19, 6, Sept. 1971, p. 202.

9. Baldini, G., and Rigaldi, L., Opt. Soc. Am., 60, 495 (1970).

10. Van der Pauw, L. J., Philips Research Reports 13, pl (1958).

11. Butler, J. F., Harman, T. C., J. Electrochem. Soc. 116, 260 (1969).

12. Melngailis, I., and Harman, T. C., "Single Crystal Lead-Tin Chalcogenides" in Semiconductors and Semimetals, Vol. 5, ed. R. K. Willardson and A. C. Beer, Academic Press, New York, 1970.

13. Nill, K. et al., Applied Physics Letters 16, 1970, p. 375.

14. Krikorian, E., Sneed, R. J., JAP 37, 3665 (1966); AFAL-TR-66-89; AFAL-TR-69-300.

15. Calawa, A. R., et al., Trans. Metal Soc., AIME, 242, p. 375 (1968).

16. Zemel, J. M., Jensen, J. D., and Schoolar, R. B., Phys. Rev. 140, p. 330 (1965).

17. Tao, T. F., Wang, C. C., AFML-TR-71-238, p. 115.

18. Hall, J. F., J. Opt. Soc. $\underline{46}$, p. 193 (1956).

19. Walton, A. K., Moss, T. S., Proc. of Physical Soc. $\underline{81}$, pt. 3, No. 521, p. 509, March 1963.

20. Schoolar, R. B., Dixon, J. R., J. Opt. Soc. of Am. $\underline{58}$, p. 119, Jan. 1968.

21. Bylander, E. G., Material Sci. Engr. $\underline{1}$ 190 (1966).

22. Nikolic, P. M., Brit. J. Appl. Phys. $\underline{16}$, 1075 (1965).

23. Melngailis, I., Harman, T. C., Chapt. 4 in "Semiconductors and Semimetals", Vol. 5 Edited by R. K. Williardson and A. Beer, Academic Press (1970).

24. Bubrick, R. F. and Allgaier, R. S., J. Chem. Phys. $\underline{32}$, 1826, (1960).

25. Calawa, A. R., Harman, T. C., Finn, M nd Youtz, P. Trans. AIME 242, 374 (1968).

26. Dionne, G. and Woolley, J. C., J. Electro Chem. Soc. Solid State Science p. 748, June 1972.

27. CPC 3355, Technical Proposal for $Pb_{1-x}Sn_xTe$ Variable Bandgap Alloy System Study - Contract F-33615-72-C-1042.

28. Tao, T. F., Wang, C. C., Sunier, S. W. APL $\underline{20}$, p 235 (1972).

29. Donelly, J. P., Harman, T. C. Foyt, A. F., Solid State Research Report, Lincoln Lab, 1971.

30. Logethetis, E. M., and Holloway, H., J. Appl. Physics $\underline{43}$, No. 1, Jan. 1972.

31. Melngailis, I. J. Ie. Phys. 29, p. 4 (1968).

32. Melngailis, I., Harman, T. C., Appl. Phys Lett. $\underline{13}$, 18 (1968).

33. Riedle, H. R. and Schoolar, R. B., PbSnTe Epitaxial Films, Final Report, March 1971, AD 722786 - prepared for U.S. Army Electronics Command, Night Vision Laboratory, Ft. Belvoir, Va.

34. Schoolar, R. B., Appl. Phys. Lett. $\underline{16}$, 446 (1970).

35. Bykova, T. T., Soviet Phys. Solid State $\underline{8}$, 759 (1969).

APPENDIX

This Appendix contains a comprehensive, tabulated data
base for the results discussed and plotted in Section 3.0.

Table 1   CHARACTERISTICS OF TARGETS INVESTIGATED TO DATE

Target No.	Starting Material	Preparation Technique	Target Composition
1	Pb, Sn, Te	Standard*	0.32
2	Pb, Sn, Te	Standard	0.20
3	PbTe, SnTe	Standard	0.15
4	Pb, Sn, Te	Standard	0.25
5	Pb, Sn, Te	Standard	.020 (10% Metal-Rich)
6	Pb, Sn, Te	Standard	0.23
7	Pb, Sn, Te	Standard	0.20
8	Pb, Sn, Te	Standard	0.25
9	Pb, Sn, Te	Standard	.020 (1% Te Rich)
10	Pb, Sn, Te	Modified**	0.23
11	Pb, Sn, Te	Modified	0.23
12	Pb, Sn, Te	Modified	0.23
13	Pb, Sn, Te	Modified	0.23

*   Standard refers to initial technique described in Section 2.2.1

** Modified refers to improvements in preparation and handling described in Sections 2.2.1 and 2.2.3

Table 2   CORRELATION OF $Pb_{1-x}Sn_xTe$ TARGET COMPOSITION WITH ACHIEVABLE, SINGLE CRYSTAL FILM COMPOSITION

Target Composition		Deposition Conditions		Film Composition Range		
Target No.	x-value of Target	Substrate Temp. Range (°C)	Growth Rate Range (μm/hr)	x-value of p-type Films	x-value of n-type Films	x-values on p-n Transition Curve
4	.25	275 - 350	.1 - 1.2	.16 - .24	-	-
8	.25	275 - 350	.5 - 1.5	.16 - .25	.25 - .27	.25 - .26
		275 - 350	.5 - 1.7	.16 - .27	.25 - .27	
2	.20	275 - 350	.1 - 1.5	.15 - .19	.19 - .20	.19 - .20
		250 - 350	.1 - 2.5	.15 - .23	.17 - .275	
9	.20 (Te-Rich)	275 - 350	.5 - 1.5	.15 - .20	.20 - .21	.20 - .21
		275 - 350	.5 - 2.0	.15 - .23	.20 - .23	
3	.15	275 - 350	.1 - 1.5	.03 - .16	.16 - .19	.15 - .16
		250 - 350	.1 - .21	.03 - .18	.16 - .25	

Table 3   DEPOSITION CONDITIONS, STRUCTURE COMPOSITION AND ELECTRICAL PROPERTIES OF AS-DEPOSITED SPUTTERED $Pb_{1-x}Sn_xTe$ FILMS - TARGET #2

Sample	Substrate	Rate μm/hr	Temp. °C	Thick. (μm)	Struct	Composition (x)	Carrier Type	Carrier Concentration n(1/cm³) 300°K	88°K	Hall Mobility μ(cm²/V sec) 300°K	88°K
400	CaF_2(111)	.80	300	.8	SC		P				
		.33	300	.3	SC		P				
		1.0	300	.99	SC	.18	P				
401	CaF_2(111)	.90	325	.90	SC	.18	P				
		1.06	325	1.06	SC	.19	N	2.2×10^{17}	1.6×10^{17}	900	7120
402	CaF_2(111)	.90	300	.90	SC	.18					
		1.65	300	1.65	SC	.21	P				
		2.25	300	2.25	SC		N				
		2.04	300	2.04	SC	.23					
		2.7	300	2.7	PC						
403	CaF_2(111)	1.35	325	1.35	SC		N		0.6		5500
		2.20	325	2.20	SC	.25	N				
	CaF_2(100)	1.50	325	1.50	SC	.21	N		0.8		4750
		2.30	325	2.30	SC	.275	N	9×10^{17}		750	
407	CaF_2(111)	.85	335	.75	SC		P		0.80		4500
		1.0	335	1.5	SC		N		0.25		6080
	CaF_2(100)	1.0	360	1.0	Fiber	.21	N				
		2.47	360	2.47	Fiber	.21	N				
408	CaF_2(111)	1.43	375	1.43	Fiber		N				
		2.28	375	2.28	Fiber	.275	N				
	CaF_2(100)	2.59	375	2.59	Fiber		N				

* All films on CaF_2(111) have and BaF_2(111) have (111) orientation
All films on CaF_2(100) have (100) orientation

A-3

Table 3 (Cont'd)   DEPOSITION CONDITIONS, STRUCTURE COMPOSITION AND ELECTRICAL PROPERTIES OF
AS-DEPOSITED SPUTTERED $Pb_{1-x}Sn_xTe$ FILMS - TARGET #2

Sample	Substrate	Rate μm/hr	Temp. °C	Thick. (μm)	Struct	Composition (x)	Carrier Type	Carrier Concentration n (1/cm³) 300°K	88°K	Hall Mobility μ(cm²/V sec) 300°K	88°K
409	CaF₂(111)	.625	375	.625	Fiber	.19	N				
		2.05	375	2.05	Fiber	.275	N				
411	CaF₂(111)	1.47	345	1.47	SC	.22	N	1x10¹⁸		976	
		1.81	345	1.81	SC	.23	N				
	CaF₂(100)	1.30	345	1.30	SC	.21	N				
412	BaF₂(111)	1.85	340	1.85	SC	.23	N				
414	CaF₂(111)	1.96	250	1.96	PC		N				
		2.19	250	2.2	PC		N				
415	CaF₂(111)	1.80	250	1.80	PC	.13	N	1.6x10¹⁸		631	
		2.17	250	2.17	PC		N	1.6x10¹⁸		578	
416	CaF₂(111)	.85	220	.85	PC		P	4x10¹⁸		200	
		.50	220	.50	P+SC						
		1.01	310	1.01	SC	.18	P	3.3x10¹⁸	3.4x10¹⁸	390	1900
		.44	225	.44	SC		P				
	CaF₂(100)	1.01	310	1.01	SC	.18	P	2.77x10¹⁸	2.30x10¹⁸	320	1500
418	CaF₂(111)	1.35	305	1.55	SC		P	4x10¹⁸		320	
		.30	305	.35	SC	.13	P				
419	CaF₂(111)	.89	250	.89	SC		P	4x10¹⁸		283	
	CaF₂(100)	1.29	250	1.29	P+SC		N				
		1.15	250	1.15	P+SC		N				
	BaF₂(111)	2.07	250	2.07	PC		N				
		.74	250	.74	SC		P	2.6x10¹⁸		300	

Table 3 (Cont'd)   DEPOSITION CONDITIONS, STRUCTURE COMPOSITION AND ELECTRICAL PROPERTIES OF AS-DEPOSITED SPUTTERED $Pb_{1-x}Sn_xTe$ FILMS - TARGET #2

Sample	Substrate	Rate μm/hr	Temp. θc	Thick. (μm)	Struct *	Composition (x) and Carrier Type		Carrier Concentration n (1/cm³)		Hall Mobility μ(cm²/V sec)	
								300°K	88°K	300°K	88°K
420	CaF$_2$(111)	.65	270	.7	SC	.15	P	4.8×10^{18}		300	
	CaF$_2$(100)	1.53	270	1.89	SC	.19	P	5×10^{18}		290	
	BaF$_2$(111)	1.20	270	1.59	SC		P				
	BaF$_2$(111)	1.70	270	1.90	PC		P	4×10^{18}		237	
421	CaF$_2$(111)	.34	305	.34	SC	.15	P				
		2.37	305	2.37	SC		N				
		1.83	305	1.83	SC	.23	P				
	BaF$_2$(111)	.59	305	.59	SC		P				
		1.85	305	1.85	SC	.23	P	3.0×10^{18}	2.5×10^{18}	320	1900
423	CaF$_2$(111)	1.75	310	1.8	SC	.22	N	1.4×10^{18}	1.3×10^{18}	850	2500
		2.0		1.8	SC	.23	P				
	CaF$_2$(100)	1.15		1.2	SC		P				
	BaF$_2$(111)	.75		1.4	SC		P				
		1.50		1.3	SC	.21	N	8×10^{17}	6.2×10^{17}	1098	4800
424	BaF$_2$(111)	1.25	320	3.4	SC	.17	N	1.9×10^{17}		1305	
	BaF$_2$(111)	.7	320	3.1	SC	.17	P				
425	CaF$_2$(111)	.7	320	3.2	SC	.17	P	1.4×10^{18}		500	

Table 4   DEPOSITION CONDITIONS, STRUCTURE, COMPOSITION, ELECTRICAL PROPERTIES OF AS-DEPCSITED SPUTTERED $Pb_{1-x}Sn_xTe$ FILMS – TARGET #3

Sample	Substrate	Rate μm/hr	Temp. °C	Thick (μm)	Struct	Composition (x)	Carrier Type	Carrier Concentration n (1/cm³) 300°K	88°K	Hall Mobility μ(cm²/V sec) 300°K	88°K
427	CaF_2(111)	.34	300	1.1	SC	.03	P				
	CaF_2(100)	.28	300	.9	SC	.03	P				
	BaF_2(111)	.30	300	.93	SC	.03	P				
		.39	300	1.23	SC	.03	P				
428	CaF_2(111)	.39	340	1.21	SC	.09	P				
		.50	340	1.62	SC		P				
	CaF_2(100)	.52	340	1.55	SC	.09	P				
	BaF_2(111)	.58	340	1.79	SC	.09	P		0.8		3000
429	CaF_2(111)	.96	325	3.06	SC		N				
	CaF_2(1-11)	1.06	325	3.21	SC		N				
	CaF_2(100)	.85	325	2.70	SC	.16	P				
		.58	325	1.83	SC	.09	P		1.0		2200
	BaF_2(111)	.58	325	1.8	SC	.09	P	6×10^{17}		580	
		.76	325	2.40	SC	.09	P	1.92×10^{18}	6×10^{17}	700	3600
430	CaF_2(111)	.55	345	1.18	SC	.13	P	8×10^{17}		1150	
		.65	345	1.40	SC		N			1145	
		.80	345	1.48	SC		N	5.0×10^{17}			
	CaF_2(100)	.50	345	1.13	SC	.12	P				
		.50	345	1.13	SC	.13	P	8×10^{17}	8.9×10^{17}	645	
	BaF_2(111)	.65	345	1.26	SC	.13	N		2×10^{17}	1450	2095

A-6

Table 4 (Cont'd) DEPOSITION CONDITIONS, STRUCTURE, COMPOSITION, ELECTRICAL PROPERTIES OF AS-DEPOSITED SPUTTERED $Pb_{1-x}Sn_xTe$ FILMS - TARGET #3

Sample	Substrate	Rate μm/hr	Temp °C	Thick (μm)	Struct	Composition (x)	Carrier Type	Carrier Concentration n (1/cm³) 300°K	88°K	Hall Mobility μ(cm²/V sec) 300°K	88°K
432	CaF$_2$(111)	.89	330	3.3	SC		N	1.9×10^{17}		1005	
		.75	330	2.8	SC	.165	P				
	CaF$_2$(100)	.89	330	3.1	SC	.19	N				
		1.20	330	3.4	SC		N		2×10^{17}		4000
	BaF$_2$(111)	.75	330	3.3	SC	.165	P				
		1.0	330	3.3	SC	.17	N		3.5×10^{17}		6050
433	CaF$_2$(111)	.86	335	3.3	SC	.15	N	5×10^{17}	4×10^{17}	903	4000
		.77	335	3.0	SC		N		3.5×10^{17}		4300
	CaF$_2$(100)	.97	335	3.8	SC		N				2035
		.60	335	2.2	SC	.12	P	1.5×10^{18}	2.0×10^{18}	411	4255
	BaF$_2$(111)	.84		3.3	SC		N	2×10^{17}	1.5	1156	3100
434	CaF$_2$(111)	.7	335	5.0	SC	.13	N	1.8×10^{17}	1.9×10^{17}	950	
	CaF$_2$(100)	.7	335	5.1	SC		N				
	BaF$_2$(111)	.7	335	5.3	SC		N	1.8×10^{17}		1120	
435	CaF$_2$(111)	1.35	352	1.8	SC	.20	N		1.5×10^{18}		1800
		1.75	352	2.0	SC	.23	N				
	CaF$_2$(100)	1.25	352	1.3	SC	.20	N		9.5×10^{17}		5000
	BaF$_2$(111)	1.34	352	2.0	SC	.20	N				
436	CaF$_2$(111)	.40	330	1.4	SC	.13	P	1.0×10^{18}		540	
		.60	330	1.8	SC		P		1.5×10^{18}		2020
		1.11	330	3.3	SC	.18	N				

Table 4 (Cont'd)   DEPOSITION CONDITIONS, STRUCTURE, COMPOSITION, ELECTRICAL PROPERTIES OF AS-DEPOSITED SPUTTERED $Pb_{1-x}Sn_xTe$ FILMS - TARGET #3

Sample	Substrate	Rate μm/hr	Temp °C	Thick (μM)	Struct	Composition (x)	Carrier Type	Carrier Concentration n (1/cm³) 300°K	88°K	Hall Mobility μ (cm²/V sec) 300°K	88°K
437	CaF_2(111)	1.37	340	1.6	SC		N	8.5×10^{17}		900	
		1.64	340	1.87	SC	.21	N		1.2×10^{18}		2400
		1.96	340	2.2	SC	.22	N				
	BaF_2(111)	1.99	340	2.5	SC		N				
		1.07	340	1.2	SC		N		6×10^{17}		5200
		1.44	340	1.6	SC	.20	N				
440	CaF_2(111)	.85	354	3.08	SC	.18	N				
	CaF_2(100)	.89	354	3.21	SC		N				
	BaF_2(111)	.84	354	3.05	SC		N				
441	CaF_2(111)	.80	326	1.5	SC	.16	N	4×10^{17}	2.5×10^{17}	950	3455
									2×10^{17}		4100
	CaF_2(100)	.80	326	1.5	SC	.16	N	4×10^{17}	3.8×10^{17}	1355	4941
	BaF_2(111)	.80	326	1.43	SC	.16	N				
442	CaF_2(111)	.90	311	1.58	SC	.16	P	2×10^{18}	1.8×10^{18}	450	1848
	CaF_2(100)	.90	311	1.65	SC		P	9×10^{17}	9.7×10^{17}	500	2192
	BaF_2(111)	.90	311	1.83	SC		P	1.6×10^{17}	1.55×10^{17}	1050	4696
443	CaF_2(111)	.75	335	1.63	SC	.16	N				
	CaF_2(100)	.75	335	1.44	SC		N	2.4×10^{17}	2.96×10^{17}	1450	5569
	BaF_2(111)	.75	335	1.55	SC		N				
444	CaF_2(111)	.30	325	1.25	SC		P	1.8×10^{18}	2.0×10^{18}	550	1907
	CaF_2(100)	.30	325	1.22	SC		P	1.1×10^{18}	1.23×10^{18}	650	1954
	BaF_2(111)	.30	325	1.21	SC		P				

Table 4 (Cont'd)   DEPOSITION CONDITIONS, STRUCTURE, COMPOSITION, ELECTRICAL PROPERTIES OF AS-DEPOSITED SPUTTERED $Pb_{1-x}Sn_xTe$ FILMS - TARGET #3

Sample	Substrate	Rate μm/hr	Temp °C	Thick (μm)	Struct*	Composition (x) and Carrier Type		Carrier Concentration n (1/cm³) 300°K	88°K	Hall Mobility μ(cm²/V sec) 300°K	88°K
445	CaF_2(111)	.75	285	1.58	SC	.09					
	CaF_2(100)	.75	285	1.53	SC						
	BaF_2(111)	.75	285	1.44	SC						
446	CaF_2(111)	1.02	325	1.58	SC	.18	N	5×10^{17}	4.2×10^{17}	825	2957
	CaF_2(100)	1.53	325	1.59	SC		N				
	BaF_2(111)	1.07	325	1.67	SC		N	4×10^{17}	3.9×10^{17}	1350	5684
447	CaF_2(111)	1.1	345	1.72	SC	.19	N		7×10^{17}		3200
	CaF_2(100)	1.13	345	1.89	SC		N				
	BaF_2(111)	1.06	345	1.70	SC		N				
448	CaF_2(111)	1.12	303	2.08	SC	.175	N	1×10^{18}	9×10^{17}	800	2897
	BaF_2(111)	1.13	303	2.1	SC		N	1.1×10^{18}	1×10^{18}	1150	5690
	BaF_2(111)	.96	303	1.78	SC		N				
450	BaF_2(111)	1.10	307	1.17	SC	.17	N	7×10^{17}	6.4×10^{17}	1250	5936
451	BaF_2(111)	.70	345	1.02	SC	.16	N	6×10^{17}	4.8×10^{17}	1500	5590
	BaF_2(111)	.55	345	.97	SC		P		8×10^{17}		4095
	CaF_2(111)	.55	345	.94	SC		P		0.9×10^{17}		3362
T_25	CaF_2(111)	.90	327	1.8	SC	.16	N	7.5×10^{17}	6.5×10^{17}	1000	5440
	CaF_2(111)	.90	327	1.5	SC	.16			1.09×10^{18}		3022

Table 5 DEPOSITION CONDITIONS, STRUCTURE, COMPOSITION, ELECTRICAL PROPERTIES OF AS-DEPOSITED SPUTTERED $Pb_{1-x}Sn_xTe$ FILMS - TARGET #4

Sample	Substrate	Rate μm/hr	Temp °C	Thick (μm)	Struct *	Composition (x) and Carrier Type		Carrier Concentration N (1/cm³) 300°K	88°K	Hall Mobility μ(cm²/V sec) 300°K	88°K
T22	CaF₂(111)	.503	322	.88	SC	.19	P	3.8×10^{18}	4.5×10^{18}	320	840
T23	CaF₂(111)	.77	350	2.01	SC	.22	P	3.6×10^{18}	4.1×10^{18}	490	1800
		.54	350	2.34	SC	.20	P	2.3×10^{18}	3.1×10^{18}	540	2300
		.830	350	2.09	SC	.22	P	4.3×10^{18}	4.4×10^{18}	570	1650
438	BaF₂(111)	.558	350	2.02	SC	.21	P	2.6×10^{18}	3.0×10^{18}	550	2200
T24	CaF₂(111)	.567	345	1.20	SC	.20	P	3.4×10^{18}	5.7×10^{18}	650	2146
	CaF₂(111)	.43	345	1.31	SC	.20	P	3.8×10^{18}	5×10^{18}	520	2100
	BaF₂(111)	.53	345	1.17	SC	.20	P	3.2×10^{18}	5×10^{18}	580	2120
	CaF₂(111)	.45	345	1.20	SC	.20	P		9.6×10^{18}		1390
	CaF₂(111)	.52	345	1.35	SC	.20	P		8.0×10^{18}		1660
T26	CaF₂(111)	.8	325	1.06	SC	.21	P		1×10^{19}		1419

Table 5 (Cont'd)   DEPOSITION CONDITIONS, STRUCTURE, COMPOSITION AND ELECTRICAL PROPERTIES OF
AS-DEPOSITED SPUTTERED $Pb_{1-x}Sn_xTe$ FILMS – TARGET #4

Sample	Substrate	Rate μm/hr	Temp. °C	Thick. (μm)	Struct	Composition (x)	Hall Mobility $\mu(cm^2/v\ sec)$ 77°K	Carrier Concentration $n \times 10^{18}$ (cm^{-3}) and Carrier Type 77°K
T_27	$BaF_2(111)$	.5	350	1.34	SC	.195	2506	4.20 (P)
T_210	$CaF_2(111)$	.6	334	1.48	SC	.20	2052	7.6 (P)
	$BaF_2(111)$	.45	335	1.13	SG	.185	2246	3.9 (P)
	$BaF_2(111)$	.6	334	1.48	SC	.20	2228	4.9 (P)
	$CaF_2(111)$	.45	335	1.15	SG	.185	2350	3.6 (P)
T_211	$CaF_2(111)$	.5	340	1.74	SC	.19	2268	5.5 (P)
	$BaF_2(111)$	.47	340	1.39	SC	.19	2323	4.0 (P)
T_213	$CaF_2(111)$	.45	345	1.28	SC	.19	1987	5.5 (P)
T_214	$CaF_2(111)$	.45	345	1.74	SC	.19	2300	5.5 (P)
T_215	$CaF_2(111)$	.55	350	1.71	SC	.20	2399	4.87 (P)
	$CaF_2(111)$	.38	350	1.24	SC	.185	2052	5.6 (P)
T_216	$CaF_2(111)$	.34	345	1.27	SC	.18		
T_217	$CaF_2(111)$	.40	350	1.30	SC	.185	2520	4.3 (P)
T_219	$CaF_2(111)$	.31	345	.923	SC	.17	2332	3.6 (P)
	$CaF_2(111)$	.32	345	1.54	SC	.17	2252	3.5 (P)
	$BaF_2(111)$	.32	345	.965	SC	.17	2516	3.4 (P)
T_220	$BaF_2(111)$	.39	345	1.86	SC	.185	2842	3.4 (P)
	$BaF_2(111)$	.38	345	1.80	SC	.185	3542	2.4 (P)
T_221	$BaF_2(111)$	.4	350	1.58	SC	.185	2893	2.6 (P)
	$CaF_2(111)$	.4	350	1.37	SC		2438	4.3 (P)
T_221	$CaF_2(111)$	.27	350	1.25	SC	.17	2656	3.54 (P)

Table 5 (Cont'd)   DEPOSITION CONDITIONS, STRUCTURE, COMPOSITION AND ELECTRICAL PROPERTIES OF AS-DEPOSITED SPUTTERED $Pb_{1-x}Sn_xTe$ FILMS - TARGET #4

Sample	Substrate	Rate μm/hr	Temp. °C	Thick. (μm)	Struct	Composition (x)	Hall Mobility μ(cm²/v sec) 77°K	Carrier Concentration n x 10^18 (cm^-3) and Carrier Type 77°K
$T_2$22	CaF_2(111)	.44	350	1.59	SC	.19	2355	5.24 (P)
	BaF_2(111)	.44	350	1.54	SC	.19	2810	4.5 (P)
$T_2$23	CaF_2(111)	.90	345	1.76	SC	.24	2292	3.66 (P)
	CaF_2(111)	.60	345	1.22	SC	.20	1761	7.65 (P)
$T_2$24	CaF_2(111)	.80	325	1.66	SC	.21	1539	9.0 (P)
$T_2$24	CaF_2(111)	1.0	325	2.04	SC	.24	1493	6.0 (P)
$T_2$25	CaF_2(111)	.8	300	1.54	SC	.20	1599	6.3 (P)
$T_2$25	BaF_2(111)	.7	300	1.64	SC	.19	2598	2.5 (P)
$T_2$26	CaF_2(111)	.42	300	.928	SC	.16	1607	**5.4 (P)**
	BaF_2(111)	.58	300	1.17	SC	.18	1768	4.5 (P)
$T_2$26	CaF_2(111)	.5	300	1.05	SC	.17	1939	3.69 (P)
$T_2$27	CaF_2(111)	.41	320	1.20	SC	.17	2830	2.1 (P)
	CaF_2(111)	.4	320	1.20	**SC**	.17	1921	4.2 (P)
	BaF_2(111)	.40	320	1.12	SC	.17		
$T_2$28	CaF_2(111)	.80	345	1.52	SC	.22	2080	**2.7 (P)**
$T_2$28	CaF_2(111)	.68	345	1.55	SC	.21	2838	2.72 (P)
$T_2$33	CaF_2(111)	.4	350	1.12	SC	.185	2432	4.27 (P)
	CaF_2(111)	.44	350	.835	SC	.19	2284	3.3 (P)
$T_2$33	CaF_2(111)	.45	345	.84	SC	.19	2645	2.78 (P)
$T_2$33	CaF_2(111)	.45	345	1.12	SC	.19	2252	4.6 (P)
$T_2$33	BaF_2(111)	.52	350	1.04	SC	.195		

Table 5 (Cont'd)   DEPOSITION CONDITIONS, STRUCTURE, COMPOSITION AND ELECTRICAL PROPERTIES OF AS-DEPOSITED SPUTTERED $Pb_{1-x}Sn_x$ Te FILMS - TARGET #4

Sample	Substrate	Rate μm/hr	Temp. °C	Thick. (μm)	Struct	Composition (x)	Hall Mobility μ(cm²/v sec) 77°K	Carrier Concentration n x 10^{18} (cm^{-3}) and Carrier Type 77°K
$T_2$34	CaF$_2$(111)	.4	325	.80	SC	.17	1960	4.20(P)
$T_2$35	CaF$_2$(111)	.84	325	2.52	SC	.21	1719	8.30 (P)
$T_2$36	CaF$_2$(111)	.75	340	3.32	SC	.21	5480	0.79 (P)
$T_2$37	CaF$_2$(111)	.90	325	1.90	SC	.22	1600	8.00(P)
$T_2$38	CaF$_2$(111)	.70	350	1.40	SC	.21		
$T_2$39	CaF$_2$(111)	.55	350	1.1	SC	.20	2346	5.06 (P)
$T_2$40	CaF$_2$(111)	.5	350	.856	SC	.195		
$T_2$41	CaF$_2$(111)	.5	350	1.2	SC	.195	1448	6.64 (P)
$T_2$41	CaF$_2$(111)	.5	350	1.88	SC	.195	2345	0.95 (P)
$T_2$42	BaF$_2$(111)	.48	345	1.43	SC	.19	2669	2.52 (P)

Table 6   DEPOSITION CONDITIONS, STRUCTURE, COMPOSITION AND ELECTRICAL PROPERTIES OF AS-DEPOSITED
SPUTTERED $Pb_{1-x}Sn_xTe$ FILMS - TARGET #7

Sample	Substrate	Rate μm/hr	Temp. °C	Thick. (μm)	Struct	Composition (x)	Hall Mobility $\mu(cm^2/v\ sec)$ 77°K	Carrier Concentration $nx10^{18}$ (cm^{-3}) and Carrier Type 77°K
T_243	CaF$_2$(111)	1.0	330	1.99	SC	.19	6222	0.217 (N)
T_244	BaF$_2$(111)	.8	345	1.65	SC	.19	2823	2.51 (P)
T_244	BaF$_2$(111)	.9	340	1.87	SC	.19	4803	0.82 (N)
T_245	CaF$_2$(111)	.7	344	1.4	SC	.18	3625	2.36 (P)
T_245	BaF$_2$(111)	.8	340	1.9	SC	.19	2356	3.23 (P)
T_246	BaF$_2$(111)	1.1	340	2.4	SC	.20	4604	0.91 (N)
T_248	CaF$_2$(111)	.95	335	1.98	SC	.19	6187	0.295 (N)
T_249	BaF$_2$(111)	.54	300	1.18	SC	.17	1770	4.50(P)
T_257	CaF$_2$(111)	1.3	325	3.35	SC	.20	6235	0.60(N)
T_257	BaF$_2$(111)	1.0	325	2.92	SC	.19	4645	0.794 (P)
T_257	BaF$_2$(111)	1.1	325	2.09	SC	.19	7082	0.162 (N)
T_259	CaF$_2$(111)	.82	325	1.68	SC	.18	4911	1.00(P)
T_256	CaF$_2$(111)	.9	335	1.87	SC	.19	4207	0.787 (P)
D4	CaF$_2$(111)	1.0	335	2.05	SC	--	5365	0.277 (N)
D5	CaF$_2$(111)	1.5	350	3.75	SC	--	4487	1.05 (N)
T_360	BaF$_2$(111)	.55	325	1.38	SC	--	2602	3.12 (P)
T_259	CaF$_2$(111)	.7	325	1.89	SC	.175	2990	2.10(P)

Table 7 DEPOSITION CONDITIONS, COMPOSITION AND ELECTRICAL PROPERTIES OF AS-DEPOSITED SPUTTERED SINGLE CRYSTAL $Pb_{1-x}Sn_xTe$ FILMS - TARGET #8

Sample No.	Substrate	Substrate Temp. °C	Deposition Rate μm/Hr.	Composition (x)	Carrier Type	Carrier Concentration $x10^{18}cm^{-3}$	Mobility cm^2/Vsec
61	CaF₂	325	1.7	.27	P	3.09	2818
	BaF₂	325	1.7	.27	P	2.55	3150
62	CaF₂	335	1.17	.25	P	6.	2300
	BaF₂	335	1.42	.26	P	.8	5300
	BaF₂	335	1.43	--	N	.32	7441
	BaF₂	335	1.29	.255	P	1.2	4450
63	CaF₂	350	1.05	.25	N	.26	8478
	CaF₂	350	.93	--	P		
	BaF₂	350	.95	.24	P	6.	2025
64	CaF₂	325	.94	.22	P	8.	1950
	BaF₂	325	.95	.22	P	7.5	2150
65	CaF₂	330	.88	.22	P	7	1950
	BaF₂	330	.87	--	P		
66	CaF₂	330	1.7	--	N	.67	6761
	BaF₂	330	1.65	.27	N	--	
67	CaF₂	330	.91	.22	P	7	2022
	BaF₂	330	.99	.23	P	8	1998
69	CaF₂	330	1.4	.26	P	2	3320
	BaF₂	330	1.35	--	P	--	
70	CaF₂	320	.62	.19	P	4	2900
71	CaF₂	322	1.08	.23	P	9	1750
	BaF₂	322	1.13	.24	P	11	1650

A-15

Table 7 (Cont'd) DEPOSITION CONDITIONS, COMPOSITION AND ELECTRICAL PROPERTIES OF AS-DEPOSITED SPUTTERED SINGLE CRYSTAL $Pb_{1-x}Sn_xTe$ FILMS - TARGET #8

Sample No.	Substrate	Substrate Temp. °C	Deposition Rate μm/Hr.	Composition (x)	Carrier Type	Carrier Concentration x10^{18} cm^{-3}	Mobility cm^2/Vsec
72	CaF$_2$	310	1.06	.22	P	10	1800
	CaF$_2$	310	1.20	--	P	--	
73	CaF$_2$	328	.70	.20	P	5	2110
	CaF$_2$	328	.8	--	P	6	2250
74	CaF$_2$	335	.77	.21	P	5	2500
	BaF$_2$	335	.84	--	P	6	2325
75	CaF$_2$	350	1.32	--	N	.81	6960
	BaF$_2$	350	1.30	.26	N	4	2846
76	CaF$_2$	330	.65	.20	P	5	2492
	BaF$_2$	330	.67	.20	P	4.5	2425
77	CaF$_2$	345	.68	.21	P		
	BaF$_2$	345	.67	.21	P		
78	CaF$_2$	345	.98	.24	P	7	2300
	BaF$_2$	345	.93	--	P		
79	CaF$_2$	345	.5	.19	P	3	3600
	BaF$_2$	345	.52	.19	P		
80	CaF$_2$	355	.80	.22	P	2.5	3135
	BaF$_2$	355	.78	.22	P	3.5	2950
81	CaF$_2$	335	.89	.22	P	6.5	2050
	BaF$_2$	335	.85	--	P	--	--
82	CaF$_2$	350	.56	.20	P	3	2950
	BaF$_2$	350	.58	.20	P		
83	CaF$_2$	345	1.2	.255	N	.30	7250
	BaF$_2$	345	1.15	--	P	.70	5450

Table 8 DEPOSITION CONDITIONS, COMPOSITION AND ELECTRICAL PROPERTIES OF AS-DEPOSITED SPUTTERED SINGLE CRYSTAL $Pb_{1-x}Sn_xTe$ FILMS - TARGET #9

Sample No.	Substrate	Substrate Temp. °C	Deposition Rate μm/Hr.	Composition (x)	Carrier Type	Carrier Concentration $\times 10^{18}$ cm^{-3}	Mobility cm^2/Vsec
$T_2$84	CaF_2(111)	345	.95	.20	N	.6	5050
	BaF_2	345	.85	.19	P	1.04	3950
$T_2$85	CaF_2	335	.6	--	P	1.18	3700
	CaF_2	335	.72	.18	P	1.40	3500
	CaF_2	335	.8	--	P	--	
	CaF_2	335	.92	.19	P	0.8	4600
	BaF_2	335	.8	--	P	1.0	4100
	BaF_2	335	.85	.19	P	0.8	4500
$T_2$86	CaF_2	325	.87	--	P	--	
	CaF_2	325	.89	.185	P	2.5	2925
	CaF_2	325	1.2	--	P	0.9	4250
	CaF_2	325	1.70	.22	N	0.9	5420
$T_2$86	BaF_2	325	.81	.18	P	3.0	2850
	BaF_2	325	.70	--	P	3.5	2725
$T_2$87	CaF_2	325	1.45	.21	N	0.5	5850
	BaF_2	330	1.2	--	N	0.28	6920
	BaF_2	330	1.4	.21	N	0.42	6050
$T_2$88	CaF_2	330	.92	.19	P	1.24	3950
	CaF_2	330	1.04	--	P	0.87	4125
	CaF_2	330	1.25	--	N	0.301	6750
	BaF_2	330	1.0	--	P	--	
	BaF_2	330	0.7	--	P	1.7	3420

Table 8 (Cont'd)   DEPOSITION CONDITIONS, COMPOSITION AND ELECTRICAL PROPERTIES OF AS-DEPOSITED SPUTTERED SINGLE CRYSTAL $Pb_{1-x}Sn_xTe$ FILMS - TARGET #9

Sample No.	Substrate	Substrate Temp. °C	Deposition Rate μm/Hr.	Composition (x)	Carrier Type	Carrier Concentration x10^{18} cm^{-3}	Mobility cm^2/Vsec
$T_2$91	CaF$_2$	335	0.97	--	P	0.7	4125
	CaF$_2$	335	1.12	.20	N	0.21	7600
	CaF$_2$	335	1.3	--	N	0.38	5980
	CaF$_2$	335	1.6	--	N	0.70	5125
$T_2$92	CaF$_2$	332	.33	--	P	2.1	3225
	CaF$_2$	332	.38	--	P	2.0	3500
	CaF$_2$	332	.5	.15	P	2.0	3625
$T_2$93	CaF$_2$	332	1.6	.22	N	.80	5400
	CaF$_2$	332	2.0	.25	N	1.46	5135
	CaF$_2$	320	1.35	.20	P	--	
	CaF$_2$	320	1.7	--	N	.5	6020
	BaF$_2$	315	2.0	.23	P	1.26	3800
	BaF$_2$	315	1.80	.22	P	--	

Table 9   EFFECT OF SUBSTRATE BIAS VOLTAGE ON PROPERTIES OF AS-DEPOSITED SINGLE CRYSTAL PbSnTe FILMS - TARGET #10

Sample No.	Substrate Temp. °C	Bias Voltage (volts)	BaF$_2$ Substrates				CaF$_2$ Substrates			
			Growth Rate μm/hr	Comp. (x)	Carrier Concentration n × 10^{18} cm^{-3}	Mobility cm^2/v-sec	Growth Rate μm/hr	Comp. (x)	Carrier Concentration n × 10^{18} cm^{-3}	Mobility cm^2/v-sec
SN53	340	+30	1.09	22	3.0 P	4900	1.1	22	2.1 P	6220
SN50	340	+20	1.1	22	4.1 P		1.15	22.5	3.1 P	4600
SN51	340	+20	1.08		4.2 P	3925	1.05		3.4 P	5150
SN41	340	+20	1.05	-	4.0 P	4316	1.10	-	2.8 P	
SN25	340	+15	1.05	22.0	4.1 P	4860	1.07	22	2.7 P	5512
SN40	340	+10	1.05	-	3.5 P	5320	1.06	-	2.3 P	6500
SN31	340	+6	1.03	21.5	2.5 P		1.10	22	1.7 P	
SN24	340	+5	1.07		2.1 P	4973			1.3 P	
SN26	340	+5		21.5	2.5 P		1.05	21.5	1.5 P	6900
SN32	340	+3	1.05	22	1.8 P	6600	1.07	22	1.2 P	
SN34	340	+2	1.06	22	1.6 P	4600	1.07	22	1.1 P	
SN28	340	0	1.05		1.3 P		1.03		.8 P	8000
SN44	340	0	1.0	21.5	1.1 P		1.05	21.5	.85 P	7840
SN35	340	-2	1.03		1.0 P	8250			.65 P / .16 N	12,500
SN29	340	-5	1.0	.22	.8 P / .15 N	13,540	1.0	21.5	.28 N	10,500

Table 9 (Cont'd)   EFFECT OF SUBSTRATE BIAS VOLTAGE ON PROPERTIES OF AS-DEPOSITED PbSnTe FILMS - TARGET #10

Sample No.	Substrate Temp. °C	Bias Voltage (volts)	BaF$_2$ Substrate				CaF$_2$ Substrate			
			Growth Rate μm/hr	Comp. (x)	Carrier Concentration n x 10^{18} cm^{-3}	Mobility cm^2/v-sec	Growth Rate μm/hr	Comp. (x)	Carrier Concentration n x 10^{18} cm^{-3}	Mobility cm^2/v-sec
SN37	340	-6	1.04	-	.21 N		1.0	-	.30 N	
SN38	340	-6			.18 N				.32 N	
SN39	340	-6			.20 N	14,328			.33 N	12,460
SN30	340	-10	1.0	-	.30 N	12,500	1.01	22	.38 N	9,800
SN42	340	-20	1.05	22	.43 N	8,900	1.05	21.5	.35 N	11,500
SN43	340	-30	1.05	21.5	.18 N		.99	21.5	.11 N	
SN58	340	+20	1.20	.235	.3 P	4,900	1.20	.23	2.2 P	5,450
SN33	342	+3	1.15	.23	.8 P } .13 N	7,925 14,500	1.15	.23		
SN36	340	-3	1.22	-	.35 N	12,500	1.22	.23	.42 N	11,800
SN54	341	-10	1.23	.23	.48 N	9,950	1.23	-	.38 N	9,860
SN55	340	-20	1.20	-	.28 N	12,438	1.20	-		
SN52	342	-30	1.19	.235	.11 N	13,250	1.19	.235	.1 N	12,520
SN45	325	+20	1.06	.21	4.2 P	4,400	1.06	-	4.5 P	5,150
SN46	323	+5	1.07	.21	4.5 P	3,950	1.07	.21	3.3 P	4,916
SN56	324	-10	1.05	-	1.2 P } .14 N	7,650 14,250	1.05	-		
SN57	325	-30	1.04	.21	.3 N	11,500	1.04	.21		

Table 10   EFFECT OF SUBSTRATE BIAS VOLTAGE ON PROPERTIES OF AS-DEPOSITED
SINGLE CRYSTAL PbSnTe FILMS - TARGET #11

Sample No.	Substrate Temp. °C	Bias Voltage (volts)	Growth Rate m/hr	Comp. (x)	Carrier Concentration n x 10^{18} cm^{-3}	Mobility x 10^3 cm^2/v-sec
61	342	0	1.02	.22	1.1 (p)	9
62	340	+10	1.03	--	2.3 (p)	6.5
63	338	-10	1.05	.22	.23 (n)	15
64	343	+5	1.01	--	1.8 (p)	7
65	345	+20	--	.22	2.8 (p)	6
66	340	-5	1.04	--	.095 (n) } .5 (p)	17
67	341	-20	1.05	.215	.30 (n)	13
68	339	+30	--	.22	2.0 (p)	7
69	342	-15	1.03	--	.28 (n)	--
T130	340	-30	1.05	.22	.15 (n)	--
90	342	-2	--	--	.8 (p)	9.5

A-21

Table 10 (Cont'd) EFFECT OF SUBSTRATE BIAS VOLTAGE ON PROPERTIES OF AS-DEPOSITED SINGLE CRYSTAL PbSnTe FILMS - TARGET #11

Sample No.	Substrate Temp. °C	Bias Voltage (volts)	Growth Rate m/hr	Composition (x)	Carrier Concentration n x 10^{18} cm^{-3}	Mobility x 10^3 cm^2/v-sec
70	344	+30	1.25	.23	2.8 (p)	5.5
71	345	-20	1.22		.18 (n)	12.5
72	343	-5	1.26	.235	.31 (n)	8.8
73	346	+10	1.28	.24	1.0 (p)	
74	345	-10	1.23	--	(n)	6.5
75	343	+20	1.25	.23	2.3 (p)	9.5
76	346	+10	1.24	--	.85 (p) / .13 (n)	16
77	344	-10	1.25	.24	.26 (n)	5.3
78	343	+20	1.25	--	2.6 (p)	13
79	345	+5	1.22	.23	.26 (n)	
80	345	-30	1.26	.24	.11 (n)	12
81	344	0		.235	.34 (n)	
134	330	+10	1.02	.21	3.2 (p)	5.8
129	330	-5	1.05	.215	1.5 (p)	7.6
126	332	-10	1.06	.21	.18 (n)	13
128	330	-20	1.04	--	-- (n)	
143	325	-5	--	.20	1.9 (p)	
145	325	-10	1.06	.21	.75 (p)	
144	325	-15	1.05	.20	.20 (n)	7

Table 11   EFFECT OF SUBSTRATE BIAS VOLTAGE ON PROPERTIES OF AS-DEPOSITED SINGLE
CRYSTAL PbSnTe FILMS - TARGET #12

Sample No.	Substrate Temp °C	Growth Rate μ m/hr	Bias Voltage (volts)	Comp. (x)	Carrier Concentration n x 10^{18} cm^{-3}		Mobility x 10^3 cm^2/v-sec	
					BaF$_2$ Substrate	CaF$_2$ Substrate	BaF$_2$ Substrate	CaF$_2$ Substrate
S 87	341	1.04	+20	.22	1.7 (p)	1.5 (p)	7	7.5
T 133	340	1.03	+10	--	1.5 (p)	1.2 (p)	7.8	8.0
S 83	342	1.05	0	.22	.78 (p)	.5 (p)	9.8	--
S 85	340	1.01	-2	--	.5 (p)	.1 (n)	11	16
S 89	342	1.04	-5	.215	.085 (n)	--	18	--
S 86	340	1.03	-10	.22	.17 (n)	.2 (n)	--	13
S 91	341	1.05	-20	--	.19 (n)	.15 (n)	14	15
T 141	340	1.04	-30	.22	.12 (n)	.1 (n)	--	--
S 88	342	1.05	+5	--	1.2 (p)	--	8.0	--
T 135	325	1.05	-5	.21	1.0 (p)	--	8.5	--
T 131	325	1.04	-10	--	.5 (p)	--	--	--
T 139	325	1.05	-15	.21	.14 (n)	--	--	--
T 136	330	1.21	0	.225	.7 (p)	--	10	--
T 132	330	1.20	+5	.23	1.1 (p)	--	8.5	--
T 138	330	1.22	-5	--	.12 (n)	--	--	--
T 137	330	1.20	-10	.225	.2 (n)	--	15	--
T 149	340	1.21	+10	--	1.4 (p)	.9 (p)	7.8	8.5
T 147	340	1.22	+5	.23	.90 (p)	--	8.5	--
T 142	340	1.20	+2	.235	.1 (n)	.15 (n)	--	--
T 148	340	1.21	-5	--	.22 (n)	.2 (n)	14	12
T 146	340	1.20	-15	.23	.16 (n)	.13 (n)	--	--

Table 12   EFFECT OF SUBSTRATE BIAS VOLTAGE ON PROPERTIES OF AS-DEPOSITED SINGLE CRYSTAL $Pb_{1-x}Sn_xTe$ FILMS - TARGET #8

Sample No.	Substrate Temp. °C	Growth Rate μm/hr	Bias Voltage (volts)	BaF₂ Substrate Comp. (x)	Carrier Concentration n x 10¹⁸ cm⁻³	Mobility cm²/v-sec	CaF₂ Substrate Comp. (x)	Carrier Concentratin n x 10¹⁸ cm⁻³	Mobility cm²/v-sec
T_2104a	355	.8	+30	.22	6 P	2800	.22	4.5 P	3300
T_2104b	355	.82	+20	.215	7.8 P	2500	.22	6.2 P	2750
T_2104c	355	.79	+10	.22	7.4 P	2650	.22	5.4 P	3400
T_280	353	.84	0	.22	3.5 P	2950	.225	2.5 P	3125
SN27	353	.82	-3	--	2.4 P	4430	--	.16 N	11500
T_2109	355	.8	-5	.215	1.9 P	4850	.22	.25 N	10500
SN22	355	.82	-6	--	1.6 P / .14 N	5150 / 10800	--	.43 N	9800
T_2102	355	.8	-10	.22	.32 N	9750	.215	.6 N	9250
T_296	353	.79	-30	.225	.8 N	8600	.22	.25 N	12300
T_295	355	.81	-20	.22	.84 N	8050	.22	.47 N	8800
SN23	340	.83	-15	.21	.2 N	9920	.215	.4 N	7850
SN21	342	.81	-10	--	2.8 P	3850	--	2 P / .16 N	4425 / 10250
SN20	340	.80	-5	.21	4.5 P	3025	.21	3 P	3900
T_2100	365	1.18	+30	--	7 P	2450	.255	5.5 P	2780
T_2107	365	1.21	+40	--	6 P	2625	.26	4.5 P	3125
T_2103	365	1.2	+10	--	2 P	4225	.26	1.3 P / .2 N	5480 / 7890

Table 13   EFFECT OF SUBSTRATE BIAS VOLTAGE ON PROPERTIES OF AS-DEPOSITED SINGLE CRYSTAL $Pb_{1-x}Sn_xTe$ FILMS - TARGET #9

Sample No.	Substrate Temp. °C	Growth Rate μm/hr	Bias Voltage (volts)	BaF2 Substrate Comp. (x)	Carrier Concentration n x 10^{18} cm^{-3}	Mobility cm^2/v-sec	CaF2 Substrate Comp. (x)	Carrier Concentration n x 10^{18} cm^{-3}	Mobility cm^2/v-sec
T99	345	.95	+30	.20	8 P	2600	-	5.5 P	2920
T116	345	.95	+20	.20	5.8 P	2700	.20	3.5 P	3600
T112	345	.95	+15	-	4.5 P	3430	.20	2.2 P	4129
T111	345	.95	+10	.20	2.5 P	4090	-	1 P / .22 N	4605 / 7100
T110	345	.95	+5	-	1.2 P / .20 N	5050 / 8800	-	.45 N	6219
T84	345	.95	0	.20	.40 N	7150	.20	.6 N	6950
T113	345	.95	-10	-	.52 N	7100	.20	.5 N	7420
T98	345	.95	-30	.20	.3 N	7620	-	.13 N	9810
T94	336	.93	+20	.19	8 P	2600	-	6.4 P	2750
T85	335	.95	0	.19	1.2 P	4010	.19	.9 P	4250
T114	335	.95	-5	.195	.85 P / .16 N	5300 / 9850	-	.3 N	7650
T115	335	.95	-10	.19	.37 N	7200	.195	.5 N	6550
T101	337	.94	-30	-	.4 N	6950	-	.28 N	7720

Table 13 (Cont'd)   EFFECT OF SUBSTRATE BIAS VOLTAGE ON PROPERTIES OF AS-DEPOSITED SINGLE CRYSTAL $Pb_{1-x}Sn_xTe$ FILMS - TARGET #9

Sample No.	Substrate Temp. °C	Growth Rate μm/hr	Bias Voltage (volts)	BaF$_2$ Substrate Comp. (x)	Carrier Concentration n x 10^{18} cm^{-3}	Mobility cm^2/v-sec	CaF$_2$ Substrate Comp. (x)	Carrier Concentration n x 10^{18} cm^{-3}	Mobility cm^2/v-sec
T106	345	1.05	+30	.21	5.5 P	2950	.21	3.6 P	3613
S60	344	1.04	+15	-	1.2 P } .2 N	5150 } 8250	-	.5 N	6625
S59	345	1.05	+10	.20	.48 N	6925	-	.7 N	6218
S48	343	1.06	0	.205	.7 N	5025	.21	.7 N	4950
T123	346	1.06	-10	-	.58 N	6850	.205	.38 N	7520
S49	345	1.05	-30	.205	.20 N	6410	-	.11 N	11420
T108	335	1.95	+40	.255	4.74 P	3650	-	3 P	3800
T105	335	1.95	+30	-	1.4 P } .3 P	4800 } 8013	-	.5 N	7200
T93	335	1.95	0	.25	.8 N	4630	.25	.7 N	4720
S47	350	.95	+10	.20	.9 P } .2 N	5150 } 8812	.20	.3 N	8400

A-26

Table 14   EFFECT OF SUBSTRATE BIAS VOLTAGE ON PROPERTIES OF AS-DEPOSITED SINGLE CRYSTAL
PbSnTe FILMS - TARGET #2

Sample No.	Substrate Temp. °C	Growth Rate μm/hr	Bias Voltage (volts)	BaF$_2$ Substrate			CaF$_2$ Substrate		
				Comp. (x)	Carrier Concentration n x 10^{18} cm^{-3}	Mobility cm^2/v-sec	Comp. (x)	Carrier Concentration n x 10^{18} cm^{-3}	Mobility cm^2/v-sec
T$_2$116	335	.95	+30	.19	7 P	3065	.19	6 P	3173
T$_2$118	335	.95	+10	-	2.75 P	4663	-	1.8 P	5422
T$_2$121	335	.95	+5	.195	1.3 P / .14 N	5803 / 11848	.193	.31 N	7908
T$_2$117	335	.95	0	.19	.3 N	7561	-	.42 N	6931
T$_2$120	335	.95	-5	-	.5 N	7801	.19	.55 N	6796
T$_2$119	335	.95	-10	-	.6 N	7025	.195	.51 N	7871
T$_2$122	335	.95	-30	.19	.30 N	8534	-	.18 N	9646

Table 15   OPTICAL ENERGY GAP OF $Pb_{1-x}Sn_xTe$ FILMS DETERMINED FROM ABSORPTION EDGE

Experiment No.	X-Ray Data Lattice Parameter	(X)	Optical Data Absorption Edge 300°K (e.v.)	(λ)
401	1.608	.21		
402	1.609	.18		
408	1.606	.275		
411	1.6073	.23	.189	6.6
412	1.6060	.275	.191	6.5
415	1.6103	.13	.25	5.0
418	1.609	.18	.22	5.6
421	1.6067	.23	.189	6.6
423	1.6073	.23	.197	6.3
424	1.6090	.17	.229	5.4
425	1.6106	.15	.234	5.3
428	1.6111	.09	.265	4.7
429	1.6111	.09	.265	4.7
430	1.6108	.12	.240	5.20
431	1.6108	.12	.25	5
432	1.6083	.20	.225	5.5
433	611	.14	.234	5.30
435	1.6083	.20	.212	5.85
436	1.6088	.19	.215	5.75
437	1.6088	.19	.207	6
T_2^2	1.6077	.22	.202	6.15
T_2^3	1.6073	.23	.202	6.15
439	116095	.16	.215	5.75

Table 16   CONTROLLED INTRODUCTION OF IMPURITIES INTO PbSbTe FILMS - "DOPING" WITH GASEOUS ADDITIVES DURING DEPOSITION

Expt. No.	Deposition Conditions Substrate Temp. °C	Deposition Rate m/hr	ppO_2 (Torr)	ppN_2 (Torr)	Film Structure	Film Composition (x)	Bias Voltage (v)	Carrier Type	Carrier Concentration (cm^{-3})	Hall Mobility $cm^2/vsec$
SN13	331	.70	--	1×10^{-4}	SC + PC	.15	0	N	$2\text{-}4 \times 10^{16}$	3989
SN12	330	.73	--	1×10^{-5}	SC	.21	0	N	4×10^{17}	6600
SN14	345	.78	--	5×10^{-6}	SC	.21	0	N	$7\text{-}8 \times 10^{17}$	6100
SN11	345	.73	--	--	SC	.22	0	P	3×10^{18}	3150
SN10	330	.80	5×10^{7}		SC	.21	0	P	2×10^{18}	3278
SN8	330	.78	1×10^{-6}		SC	.21	0	P	$1\text{-}2 \times 10^{18}$	3550
SN7	329	.82	2×10^{-6}		SC	.205	0	P	4×10^{17}	5550
SN6	330	.73	5×10^{-6}		SC	.19	0	P	4×10^{16}	5720
SN5	330	.85	1×10^{-5}		SC + PC	.13	0	P	$2\text{-}3 \times 10^{18}$	1850
SN16	330	.82		5×10^{-6}	SC	.21	+30	N } / P }	1.4×10^{17} / 9×10^{17}	8500 / 5394
SN19	329	.79		3×10^{-6}	SC		+30	N } / P }	5×10^{17} / $1\text{-}2 \times 10^{18}$	7120 / 4382
SN15	331	.81	1×10^{-6}		SC	.21	+30	P	3×10^{18}	3653
SN17	330	.785	2×10^{-6}		SC	.20	+30	P	$.8\text{-}1 \times 10^{18}$	4661

Table 17   ISOTHERMAL ANNEALING RESULTS - 3% METAL RICH CHARGE

Sample	Substrate	Struct	Thickness (μm)	Composition (x)	Annealing Conditions	Unannealed		Annealed	
						Carrier Conc. n (cm^{-3}) 88°K	Hall Mobility μ (cm^2/V sec) 88°K	Carrier Conc. n (cm^{-3}) 88°K	Hall Mobility μ (cm^2/V sec) 88°K
439	CaF$_2$(111)	SC	2.22	.16	600°C/2 hrs	6x10^{18}(P)	1400	4x10^{17}(N)	6380
432	CaF$_2$(111)	SC	3.2	.16	600°C/2 hrs	6x10^{18}(P)	1400	2.5x10^{17}(N)	6700
439	BaF$_2$(111)	SC	2.34	.16	580°C/4 hrs	7x10^{18}(P)	1600	6x10^{17}(N)	6800
439	BaF$_2$(111)	SC	2.11	.16	560°C/4 hrs	7.8x10^{18}(P)	1300	6x10^{17}(N)	6167
439	BaF$_2$(111)	SC	2.11	.16	540°C/4 hrs			7x10^{17}(N)	6416
439	CaF$_2$(111)	SC	2.11	.16	450°C/4 hrs			9.5x10^{17}(N)	5178
T$_2$3	CaF$_2$(111)	SC	2.09	.20	600°C/2 hrs	5.8x10^{18}(P)	1700	1.3x10^{18}(P)	3500
			2.09		560°C/4 hrs	4.1x.1^{18}(P)	1800	8x10^{17}(P)	4500
			2.09		550°C/4 hrs	5.8x10^{18}(P)	1700	3.6x10^{17}(P)	5800
T$_2$3	CaF$_2$(111)	SC	2.09	.20	540°C/4 hrs	7.2x10^{18}(P)	1600	1x10^{17}(N)	5095
T$_2$4	CaF$_2$(111)	SC	1.35	.20	500°C/4 hrs	8x10^{18}(P)	1660	4.4x10^{17}(N)	5376
T$_2$3	CaF$_2$(111)	SC	2.18	.20	450°C/4 hrs	2.8x10^{18}(P)		5.7x10^{17}(N)	6056
	CaF$_2$(111)	SC	1.92	.20	400°C/15 hrs	4.8x10^{18}(P)	1800	5.6x10^{17}(N)	5000
438	CaF$_2$(111)	SC	2.22	.21	600°C/2 hrs	4x10^{18}(P)	2200	1.44x10^{18}(P)	4280
			2.46	.21	580°C/2 hrs			9.5x10^{17}(P)	5800
			2.38	.21	560°C/4 hrs			7.5x10^{17}(P)	5861
			1.97	.21	400°C/19 hrs			6.9x10^{17}(N)	5142
421	CaF$_2$(111)	SC	1.83	.23	600°C/2 hrs	1.5x10^{18}(P)	1900	2.9x10^{18}(P)	2400
					550°C/21 hrs			2x10^{18}(P)	2700
423	CaF$_2$(111)	SC	1.8	.23	450°C/90 hrs	1.3x10^{18}(P)	2000	9x10^{16}(N)	5000
435	BaF$_2$(111)	SC	5.0	.23	400°C/18 hrs			3.5x10^{17}(N)	6000

Table 18 ISOTHERMAL ANNEALING EXPERIMENTS - 4% METAL RICH CHARGE

Sample	Subst-rate	Film Struct.	Film Composition (x)	Annealing Cond.			Unannealed		Annealed	
				Temp °C	Time (hr)	Quench	Mobility μ(cm²/v sec)	Carrier Conc. $nx10^{18}$ (cm⁻³)	Mobility μ(cm²/v sec)	Carrier Conc. $nx10^{18}$ (cm⁻³)
$T_2 20$	CaF₂ (111)	SC	.19	700 650	1/2 4	H₂O + LN₂	1427	7.0 (P)	3734	2.5 (P)
$T_2 19$	CaF₂ (111)	SC	.19	600 580	16 4	H₂O + LN₂	1387	11.0 (P)	7224	.86 (P)
				600 550	16 4	H₂O + LN₂	1637	9.3 (P)	9627	.11 (N)
$T_2 13$	CaF₂ (111)	SC	.19	650	4	H₂O + LN₂	1281	10.0 (P)	3500	2.5 (P)
				600 570	16 4	H₂O + LN₂			5749	.74 (P)
				500	16	H₂O + LN₂			7062	.38 (N)
				525	16	H₂O + LN₂			6100	.40 (N)
$T_2 10$	CaF₂ (111)	SC	.185	600 510	16 4	H₂O + LN₂	2350	3.6 (P)	8250	.26 (N)

Table 18 (Cont'd)   ISOTHERMAL ANNEALING EXPERIMENTS - 4% METAL RICH CHARGE

Sample	Substrate	Film Struct.	Film Composition (x)	Annealing Cond. Temp °C	Time (hr)	Quench	Unannealed Mobility μ(cm^2/v sec)	Unannealed Carrier Conc. $n\times10^{18}$ (cm^{-3})	Annealed Mobility μ(cm^2/v sec)	Annealed Carrier Conc. $n\times10^{18}$ (cm^{-3})
T$_2$38	CaF$_2$ (111)	SC	.21	600 580	16 4	H$_2$O + LN$_2$	1345	8.36 (P)	3200	2.34 (P)
				600 510	16 4	H$_2$O + LN$_2$			6900	0.15 (P)
				500	16	H$_2$O + LN$_2$			8200	0.10 (N)
T$_2$24	CaF$_2$ (111)	SC	.21	600 550	4 16	H$_2$O + LN$_2$	1503	7.36 (P)	6898	1.02 (P)
T$_2$42	CaF$_2$	SC	.21	600 480	24 4	H$_2$O + LN$_2$	1670	6.18 (P)	7559	.25 (N)
T$_2$27	CaF$_2$ (111)	SC	.17	600	5	H$_2$O + LN$_2$	2830	2.1 (P)	6900	0.115 (P)
T$_2$19	CaF$_2$ (111)	SC	.17	600 700 600 570	17 1/2 4 15	H$_2$O + LN$_2$	2334	3.6 (P)	9211	0.255 (N)
T$_2$33	CaF$_2$ (111)	SC	.19	600 540	18 4	H$_2$O + LN$_2$	2432	4.27 (P)	8808	0.26 (N)
T$_2$23	CaF$_2$ (111)	SC	.22	500	5	H$_2$O + LN$_2$			6662	0.23 (P)

Table 18 (Cont'd)   ISOTHERMAL ANNEALING EXPERIMENTS - 4% METAL RICH CHARGE

Sample	Substrate	Film Struct.	Film Composition (x)	Annealing Cond. Temp °C	Annealing Cond. Time (hr)	Quench	Unannealed Mobility $\mu(cm^2/v\ sec)$	Unannealed Carrier Conc. $nx10^{18}$ (cm^{-3})	Annealed Mobility $\mu(cm^2/v\ sec)$	Annealed Carrier Conc. $nx10^{18}$ (cm^{-3})
$T_2 10$	CaF_2 (100)	SC	.19	600 540	16 4	$H_2O +$ LN_2	1400	7.4 (P)	9445	0.18 (N)
$T_2 26$	CaF_2 (111)	SC	.17	600 580	16 4	$H_2O +$ LN_2	1768	4.5 (P)	9458	0.09 (N)
$T_2 33-1$	BaF_2 (111)	SC	.19	600 540	16 4	H_2O	2252	4.6 (P)	6913	0.33 (N)
$T_2 33-2$	CaF_2 (111)	SC	.19	600 540	16 4	$H_2O +$ LN_2	2284	3.3 (P)	7819	0.26 (N)
$T_2 33-3$	BaF_2 (111)	SC	.19	600 540	16 4	H_2O	1578	7.97 (P)	7499	0.26 (N)
$T_2 42$	BaF_2 (111)	SC	.18	600 540	16 4	H_2O	2432	3.76 (P)	6475	0.32 (N)
$T_2 8$	CaF_2 (111)	SC	.17	600 580	16 4	$H_2O +$ LN_2	6640	3.3 (N)	7096	.023 (N)
$T_2 21$	CaF_2 (111)	SC	.19	600 540	16 4	$H_2O +$ LN_2	2072	6.6 (P)	8068	.199 (N)

Table 19   ISOTHERMAL ANNEALING EXPERIMENTS - 6% METAL RICH CHARGE

Sample	Subst-rate	Film Struct.	Film Composition (x)	Annealing Cond.			Unannealed		Annealed	
				Temp °C	Time (hr)	Quench	Mobility $\mu(cm^2/v\ sec)$	Carrier Conc. $nx10^{18}$ (cm^{-3})	Mobility $\mu(cm^2/v\ sec)$	Carrier Conc. $nx10^{18}$ (cm^{-3})
$T_2 65$	BaF_2 (111)	SC	.19	700 600 540	1/2 16 4	H_2O	1997	3.2 (P)	10,892	0.633 (N)
$T_2 65$	CaF_2 (111)	SC	.19	700 600 - 540	1/2 16 4	H_2O + LN_2	1943	3.71 (P)	10,756	0.28 (N)
$T_2 21$	CaF_2 (111)	SC	.17	650	5	H_2O + LN_2	2565	3.54 (P)	8864	0.82 (P)
$T_2 13$	CaF_2 (111)	SC	.19	600 500	18 4	H_2O + LN_2	1480	8.5 (P)	9409	0.4 (N)
$T_2 23$	CaF_2 (111)	SC	.20	600 700 600 525	18 1/2 4 5	H_2O + LN_2	2292	3.66 (P)	8610	0.065 (N)
$T_2 42$	BaF_2 (111)	SC	.19	600 530	16 4	H_2O	2669	2.52 (P)	10,992	0.37 (N)
$T_2 19$	CaF_2 (111)	SC	.16	600 580	16 4	H_2O + LN_2	1252	6.3 (P)	9860	0.38 (N)
$T_2 21$	BaF_2 (111)	SC	.185	600 540	16 4	H_2O	1890	8.27 (P)	9896	0.36 (N)

Table 19 (Cont'd)   ISOTHERMAL ANNEALING EXPERIMENTS - 6% METAL RICH CHARGE

Sample	Subst-rate	Film Struct.	Film Composition (x)	Annealing Cond. Temp °C	Time (hr)	Quench	Unannealed Mobility μ(cm²/v sec)	Carrier Conc. $n \times 10^{18}$ (cm⁻³)	Annealed Mobility μ(cm²/v sec)	Carrier Conc. $n \times 10^{18}$ (cm⁻³)
$T_2$33	CaF_2 (11$\bar{1}$)	SC	.19	600/500	16/4	H_2O + LN_2	2645	2.78 (P)	9305	.38 (N)
$T_2$15	CaF_2 (11$\bar{1}$)	SC	.185	600/510	15/2	H_2O	2052	5.6 (P)	9892	.34 (N)
$T_2$13	CaF_2 (11$\bar{1}$)	SC	.19	700	1/2	H_2O	1323	6.7 (P)	3000	3.0 (P)
				600/510	18/4	H_2O + LN_2			9705	.38 (N)
$T_2$11	CaF_2 (11$\bar{1}$)	SC	.19	700/600	1/2 15	H_2O	1486	6.6 (P)	4684	.9 (P)
				600/570	16/4	H_2O + LN_2			7927	.17 (P)
				600/550	16/4	LN_2			6325	.0096 (N)
$T_2$14	CaF_2 (11$\bar{1}$)	SC	.19	600	15	H_2O	1326	7.8 (P)	3400	.66 (P)
$T_2$13	CaF_2	SC	.185	700	1/2	H_2O	1300	7.0 (P)	3500	2.8 (P)
				600/500	16/4	H_2O + LN_2			12,000	0.035 (N)

Table 19 (Cont'd)   ISOTHERMAL ANNEALING EXPERIMENTS – 6% METAL RICH CHARGE

Sample	Subst-rate	Film Struct.	Film Composition (x)	Annealing Cond. Temp °C	Time (hr)	Quench	Unannealed Mobility μ(cm²/v sec)	Unannealed Carrier Conc nx10^{18} (cm^{-3})	Annealed Mobility μ(cm²/v sec)	Annealed Carrier Conc nx10^{18} (cm^{-3})
T$_2$40	BaF$_2$ (11$\bar{1}$)	SC	.185	600 / 580	2 / 8	LN$_2$ / LN$_2$	2246 / 2246	3.9 (P) / 3.9 (P)	3550 / 5236	.99 (P) / .4 (P)
T$_2$42	BaF$_2$ (11$\bar{1}$)	SC	.19	600} / 540}	16 / 4	H$_2$O + / LN$_2$	2319	4.99 (P)	11,670	.278 (N)

Table 20 ISOTHERMAL ANNEALING RESULTS IN 6% METAL RICH CHARGES - FILM PREPARED FROM TARGET #8 (WITHOUT BIAS)

Sample	Substrate	Film Struct.	Film Comp.	Annealing Condition Temp °C	Time (hrs)	Unannealed Mobility cm^2/v-sec	Carrier Concentration $\times 10^{18}(cm^{-3})$	Annealed Mobility cm^2/v-sec	Carrier Concentration $\times 10^{18}(cm^{-3})$
$T_2 73$	CaF_2 (111)	SC	.20	625	6	2425	5 (P)	5350	2.1 (P)
$T_2 76$	CaF_2 (111)	SC	.20	625	6	2846	4 (P)	5303	1.90 (P)
				600	16			7680	1.0 (P)
				580	6				
	BaF_2 (111)	SC	.20	600	16	2492	5 (P)	11,538	.3 (P)
				540	6				
				600	16			9863	.04 (N)
				525	6				
$T_2 82$	BaF_2 (111)	SC	.20	600	16	2950	3 (P)	12,341	.2 (N)
				500	6				
				450	6			9932	.25 (N)
$T_2 78$	CaF_2 (111)	SC	.24	700	1/2	2500	7 (P)	3303	5 (P)
				600	16				
				500	6				

Table 21   ISOTHERMAL ANNEALING RESULTS - 10% METAL-RICH CHARGES

Entry	Sample	Subst rate	Struct	Thickness	Composition (x)	Annealing Conditions	Unannealed Carrier Conc. n (cm^{-3}) 88°K	Unannealed Hall Mobility (cm^2/V sec) 88°K	Annealed Carrier Conc. n (cm^{-3}) 88°K	Annealed Hall Mobility (cm^2/V sec) 88°K
1	451	BaF$_2$(111)[1]	SC	.94	.16	600°C/19 hrs	2.9x10^{18}(P)	1478	1x10^{18}(N)	9806
2	T$_2$4	BaF$_2$(111)[1]	SC	1.20	.22	600°C/2 hrs	8.6x10^{18}(P)	2310	8.6x10^{17}(N)	8782
3	T$_2$4	BaF$_2$(111)[1]	SC	1.17	.20	600°C/4 hrs	5.1x10^{18}(P)	2100	1.16x10^{18}(N)	8174
4	T$_2$4	CaF$_2$(111)[2]	SC	1.31	.20	600°C/2 hrs	5.0x10^{18}(P)	2100	1.47x10^{18}(N)	6870
5	T$_2$4	CaF$_2$(111)[2]	SC	1.2	.20	600°C/15 hrs	9.6x10^{18}(P)	1390	3.6x10^{17}(N)	9850
6	451	CaF$_2$(111)[2]	SC	1.0	.16	600°C/14 hrs	3.9x10^{18}(P)	1362	3.7x10^{17}(N)	11971
						+ 600°C/17 hrs			1x10^{17}(N)	5012
7	T$_2$6	CaF$_2$(111)[2]	SC	1.19	.20	600°C/17 hrs	7.4x10^{18}(P)	1390	2.8x10^{17}(N)	5258
8	T$_2$4	CaF$_2$(111)[2]	SC	1.31	.20	600°C/14 hrs	5.7x10^{18}(P)	2146	1.1x10^{17}(N)	6905
9	442	CaF$_2$(111)[2]	SC	3.26	.18	700°C/2 hrs	1.8x10^{18}(P)	1848	6x10^{17}(N)	8205
10	451	CaF$_2$(111)[2]	SC	1.01	.20	600°C/10hrs	3.8x10^{18}(P)	1500	7x10^{17}(N)	9000
11	T$_2$11	BaF$_2$(111)[2]	SC	1.5	.19	600/16 hrs	13.3 (P)	1349	1.2 (N)	6831
12	T$_2$22	BaF$_2$(111)[2]	SC	2.1	.19	600/16 hrs	4.54 (P)	2810	1.43 (N)	5587
13	T$_2$41	CaF$_2$(111)[3]	SC	1.9	.195	600/16 hrs 580/4 hrs	6.64 (P)	1448	0.664	7889

(1) Air Quench

(2) Water Quench

(3) Water/Liq. N$_2$ Quench

Table 22 ISOTHERMAL ANNEALING EXPERIMENTS—EFFECT OF ANNEALING CHARGE COMPOSITION ON CARRIER CONCENTRATION

Sample	Substrate	Film Struct.	Film Composition (x)	Anneal Charge	Annealing Cond. Temp °C	Time (hr)	Quench	Unannealed μ(cm²/v sec)	$n \times 10^{18}$ (cm⁻³)	Annealed μ(cm²/v sec)	$n \times 10^{18}$ (cm⁻³)
$T_2$30	CaF_2 (111)	SC	.16	6% Metal Rich Pb.85-Sn.15Te	600⎫580⎭	16 4	H_2O + LN_2	1499	2.41(P)	9830	0.26(N)
$T_2$27	CaF_2 (111)	SC	.17	6% Metal Rich Pb.85-Sn.15Te	600⎫575⎭	16 4	H_2O + LN_2	1921	4.5(P)	7710	0.80(N)
$T_2$20	BaF_2 (111)	SC	.19	6% Metal Rich Pb.85-Sn.15Te	600⎫540⎭	16 4	H_2O	2841	3.4(P)	5860	1.4(N)
D_3	CaF_2 (111)	SC	.13	6% Metal Rich Pb.80-Sn.20Te	650	4	H_2O + LN_2	1197	0.4(P)	7064	.7(N)
$T_2$19	CaF_2 (111)	SC	.17	6% Metal Rich Pb.80-Sn.20Te	600⎫575⎭	16 4	H_2O + LN_2	2516	5.4(P)	9232	0.379(N)
$T_2$21	BaF_2 (111)	SC	.185	6% Metal Rich Pb.80-Sn.20Te	600⎫540⎭	16 4	H_2O	1890	8.27(P)	8696	0.262(N)

Table 22 (Cont'd) ISOTHERMAL ANNEALING EXPERIMENTS—EFFECT OF ANNEALING CHARGE COMPOSITION ON CARRIER CONCENTRATION

Sample	Substrate	Film Struct.	Film Composition (x)	Anneal Charge	Annealing Cond.			Unannealed		Annealed	
					Temp °C	Time (hr)	Quench	μ (cm^2/v sec)	nx10^{18} (cm^{-3})	μ (cm^2/v sec)	nx10^{18} (cm^{-3})
T$_2$41	CaF$_2$ (111)	SC	.195	6% Metal Rich Pb.80-Sn.20Te	600 } 525	16 4	H$_2$O + LN$_2$	2345	0.95(P)	8723	.258(N)
T$_2$42	CaF$_2$ (111)	SC	.20	6% Metal Rich Pb.80-Sn.20Te	600 } 525	16 4	H$_2$O + LN$_2$	1870	6.18(P)	9559	.350(N)
T$_2$23	CaF$_2$ (111)	SC	.20	6% Metal Rich Pb.80-Sn.20Te	600 700 } 600 540	18 1/2 4 5	H$_2$O + LN$_2$	2292	3.66(P)	8610	.065(N)

A-40

Table 23   ISOTHERMAL ANNEALING RESULTS—Pb$_{1-x}$Sn$_x$ ALLOY CHARGES

Sample	Subst.	Struct	Comp. (x)	Anneal Condition	Thick μm	Unannealed Mobility μ(cm²/v sec)	Unannealed Carrier Conc. nx10^{18}(cm^{-3})	Annealed Mobility μ(cm²/v sec)	Annealed Carrier Conc. nx10^{18}(cm^{-3})
T₂27	BaF₂ (111)	SC	.16	625°C/4 hours Pb.85Sn.15 Alloy		2736	3.0 (P)	5680	.314 (P)
D-2	BaF₂ (111)	SC	.16	600/4 hours Pb.85Sn.5 Alloy		2723	2.39 (P)	8437	0.16 (N)
				580/4 hours Pb.85Sn.15 Alloy				6769	0.430 (N)
				550/4 hours Pb.85Sn.15 Alloy				5862	0.38 (N)
T₂62	BaF₂ (111)	SC	.18	625/4 hours Pb.80Sn.20 Alloy		1755	5.74 (P)	4872	.95 (P)
T₂10	BaF₂ (111)	SC	.18	600/4 hours Pb.80Sn.20 Alloy		2228	5.1 (P)	5191	0.45 (P)
T₂61	CaF₂ (111)	SC	.18	625/4 hours 580/4 hours Pb.80Sn.20 Alloy		2518	3.09 (P)	4376 5328	.820 (P) .280 (P)
T₂61	CaF₂ (111)	SC	.18	600/16 hours 560/4 hours Pb.80Sn.20 Alloy		2197	3.50 (P)	8078	0.155 (N)
T₂61	BaF₂ (111)	SC	.18	550/4 hours Pb.80Sn.20 Alloy		1880	4.7 (P)	8241	0.22 (N)
T₂61	CaF₂ (111)	SC	.20	625/4 hours Pb.80Sn.20 Alloy		1742	4.35 (P)	3114	1.77 (P)
T₂42	CaF₂ (111)	SC	.20	600/4 hours Pb.80Sr.20 Alloy		1554	5.74 (P)	4593	1.01 (P)
T₂64	CaF₂ (111)	SC	.20	600/16 hours 580/4 hours Pb.80Sn.20 Alloy		1687	7.7 (P)	4842	0.53 (P)

Table 23 (Cont'd)   ISOTHERMAL ANNEALING RESULTS—$Pb_{1-x}Sn_x$ ALLOY CHARGES

Sample	Subst.	Struct	Comp (x)	Anneal Condition	Thick μm	Unannealed		Annealed	
						Mobility $\mu(cm^2/v\ sec)$	Carrier Conc. $nx10^{18}(cm^{-3})$	Mobility $\mu(cm^2/v\ sec)$	Carrier Conc. $nx10^{18}(cm^{-3})$
$T_2$23	CaF$_2$ (111)	SC	.20	600/16 hours 550/4 hours Pb.80Sn.20 Alloy		1596	5.8 (P)	5416	0.287 (P)
				500/4 hours Pb.80Sn.20 Alloy				7392	0.27 (N)
$T_2$64	BaF$_2$ (111)	SC	.20	500/4 hours Pb.80Sn.20 Alloy		2583	3.70 (P)	7894	0.24 (N)
$T_2$65	CaF$_2$ (111)	SC	.20	600/16 hours 510/4 hours Pb.80Sn.20 Alloy		1692	5.97 (P)	7824	0.17 (N)

Table 24   ISOTHERMAL LOW TEMPERATURE ANNEALING RESULTS ON FILMS PREPARED FROM TARGET #4

Sample	Subst-rate	Film Struct.	Film Composition (x)	Anneal Charge	Annealing Cond. Temp °C	Time (hr)	Quench	Unannealed μ(cm^2/v sec)	Unannealed $n \times 10^{18}$ (cm^{-3})	Annealed μ(cm^2/v sec)	Annealed $n \times 10^{18}$ (cm^{-3})
$T_2 17$	CaF$_2$ (111)	SC	.185	6% Metal Rich	600 / 540	16 / 4	H$_2$O + LN$_2$	1711	6.93 (P)	7647	0.35 (N)
					500	16	H$_2$O + LN$_2$			7737	0.5 (N)
					500 / 400 / 300	4 / 6 / 16	H$_2$O + LN$_2$			5104	1.36 (P)
$T_2 22$	CaF$_2$ (111)	SC	.19	4% Metal Rich	600 / 700 / 600 / 525	16 / 1/2 / 4 / 4	H$_2$O + LN$_2$	1511	4.98 (P)	7000	0.4 (N)
					500 / 400 / 300	4 / 6 / 16	H$_2$O + LN$_2$			5172	.98 (P)
$T_2 23$	BaF$_2$ (111)	SC	.19	4% Metal Rich	600 / 540	16 / 4	H$_2$O	1598	7.97 (P)	7499	0.26 (N)
				Pb .80 Sn .20 Alloy	400	6	H$_2$O			6148	0.32 (P)

Table 24 (Cont'd) ISOTHERMAL LOW TEMPERATURE ANNEALING RESULTS ON FILMS PREPARED FROM TARGET #4

Sample	Substrate	Film Struct.	Film Composition (x)	Anneal Charge	Temp °C	Annealing Cond. Time (hr)	Quench	Unannealed μ(cm²/v sec)	Unannealed $n \times 10^{18}$ (cm⁻³)	Annealed μ(cm²/v sec)	Annealed $n \times 10^{18}$ (cm⁻³)
$T_2$22	BaF_2 (111)	SC	.19	4% Metal Rich	600 540	16 4	H_2O	2584	4.39 (P)	5970	0.35 (N)
				Pb.80-Sn.20 Alloy	500	6	H_2O			5120	0.53 (N)
				Pb.80-Sn.20 Alloy	400	16	H_2O			6230	.278 (N)
				Pb.80-Sn.20 Alloy	350	16	H_2O			5460	0.42 (P)
$T_2$13	CaF_2 (111)	SC	.19	6% Metal Rich	600 540	16 4	H_2O + LN_2	6723	.27 (N)	8684	.20 (N)
					450	16	H_2O + LN_2			8677	0.347 (N)
$T_2$26	CaF_2 (111)	SC	.17	4% Metal Rich	600 580	16 4	H_2O + LN_2	1374	7.10 (P)	9458	.093 (N)
				Pb.80-Sn.20 Alloy	350	16	H_2O + LN_2			4900	0.60 (P)

Table 24 (Cont'd)   ISOTHERMAL LOW TEMPERATURE ANNEALING RESULTS ON FILMS PREPARED FROM TARGET #4

Sample	Substrate	Film Struct.	Film Composition (x)	Anneal Charge	Annealing Cond. Temp °C	Time (hr)	Quench	Unannealed $\mu(cm^2/v\ sec)$	Unannealed $nx10^{18}$ (cm^{-3})	Annealed $\mu(cm^2/v\ sec)$	Annealed $nx10^{18}$ (cm^{-3})
$T_2$23	CaF₂ (111)	SC	.20	6% Metal Rich	600 700 600 540	16 1/2 4 15	H₂O + LN₂	2292	3.66 (P)	8610	0.065 (N)
				Pb .80- Sn .20 Alloy	400	16	H₂O + LN₂			7940	.164 (N)
				Pb .80- Sn .20 Alloy	350	16	H₂O + LN₂			2535	0.35 (P)

A-45

Table 25   ISOTHERMAL ANNEALING RESULTS ON FILMS PREPARED FROM TARGET #9

Sample	Substrate	Film Struct.	Film Comp.	Annealing Condition Temp °C	Time (hrs)	Unannealed Mobility cm²/v-sec	Unannealed Carrier Concentration x10¹⁸(cm⁻³)	Annealed Mobility cm²/v-sec	Annealed Carrier Concentration x10¹⁸(cm⁻³)
$T_2$84	BaF$_2$	SC	.19	600	16	3950	1.04 (P)	7213	1 (P)
				700⎫600⎬580⎭	1/2 16 6			8500	.656 (P)
$T_2$84	CaF$_2$	SC	.19	600⎫525⎭	16 6	3604	1.2 (P)	12,143 9893	.16 (N) .075 (N)
				600⎫540⎭	16 6			11250 12682	.31 (N) .23 (N)
				450 400	16 16			7923	.75 (P)
$T_2$85	CaF$_2$	SC	.19	600⎫700⎬600⎭580	16 1/2 16 6	4600	0.8 (P)	9615	.283 (P)
$T_2$84	CaF$_2$	SC	.19	350 300	16 16	2950	1.2 (P)	11,913 9363	.11 (N) .21 (P)
$T_2$85	CaF$_2$	SC	.19	600⎫560⎭	16 6	4250	1.0 (P)	9528	.18 (P)
				600⎫535⎭	16 6			14860	.098 (N)
$T_2$85	BaF$_2$	SC	.19	400	16	4500	.8 (P)	9518	.339 (N)
$T_2$79	CaF$_2$	SC	.19	600 580	16 6	3600	3 (P)	5983	1.5 (P)
	CaF$_2$	SC	.19	700 600 525	1/2 16 6	3725	2.89 (P)	10,138	.35 (N)

A-46

Table 25 (Cont'd)   ISOTHERMAL ANNEALING RESULTS ON FILMS PREPARED FROM TARGET #9

Sample	Substrate	Film Struct	Film Comp.	Annealing Condition Temp °C	Time (hrs)	Unannealed Mobility cm^2/v-sec	Unannealed Carrier Concentration x10^{18}(cm^{-3})	Annealed Mobility cm^2/v-sec	Annealed Carrier Concentration x10^{18}(cm^{-3})
T$_2$86	CaF$_2$	SC	.185	700 600 580	1/2 16 6	2925	2.5 (P)	8988	.59 (P)
				600 525	16 6			11,123	.213 (N)
T$_2$88	CaF$_2$	SC	.19	600 525	16 6	3950	1.24 (P)	10496	.15 (N)

Table 26 ISOTHERMAL ANNEALING RESULTS - Te RICH CHARGE

Sample	Substrate	Struct.	Comp. (x)	Annealing Conditions	Thickness (μm)	Carrier Conc. (cm^{-3}) and Carrier Type Unannealed	Annealed
424	BaF_2	SC	.17	250°C/2 hrs	3.4	1.15×10^{18}(N)	1.1×10^{18}(N)
433	BaF_2	SC	.15	275°C/4 hrs	3.2	1.5×10^{18}(N)	9×10^{17}(N)
433	BaF_2	SC	.15	285°C/4 hrs	3.2	1.5×10^{18}(N)	2.8×10^{18}(P)
434	BaF_2	SC	.15	285°C/4 hrs	3.8	1.15×10^{18}(N)	3.3×10^{18}(P)
423	BaF_2	SC	.21	310°C/4 hrs	1.3	1.2×10^{18}(N)	1.6×10^{19}(P)
438	CaF_2(111)	SC	.20	500°C/4 hrs	2.02	1.5×10^{18}(N)	3.2×10^{19}(P)

Table 27   ISOTHERMAL ANNEALING RESULTS - Te CHARGE

Sample	Substrate	Struct.	Composition (x)	Annealing Conditions	Thick (μm)	Unannealed Mobility μ(cm²/v sec)	Unannealed Carrier Conc. $n \times 10^{18}$ (cm^{-3})	Annealed Mobility μ(cm²/v sec)	Annealed Carrier Conc. $n \times 10^{18}$ (cm^{-3})
$T_2$66	CaF$_2$	SC	.22	260/4 hrs	2.33	2999	2.06 (N)	4842	1.15 (N)
$T_2$65	CaF$_2$	SC	.22	270/4 hrs	1.53	4342	2.12 (N)	4324	1.1 (N)
$T_2$34	CaF$_2$	SC	.17	275/4 hrs	1.88	3490	1.9 (N)	5667	0.77 (N)
$T_2$23	CaF$_2$	SC	.21	275/4 hrs	2.49	3992	1.83 (N)	6323	.609 (N)
$T_2$36	CaF$_2$	SC	.21	275/4 hrs	4.53	3770	1.60 (N)	14,771	.593 (N)
				520/4 hrs				1188	20.7 (P)
$T_2$60	BaF$_2$	SC	.175	280/4 hrs	1.96	3249	1.83 (N)	2428	2.07 (P)
$T_2$61	BaF$_2$	SC	.21	280/4 hrs	1.81	4286	1.53 (N)	2950	2.2 (P)
$T_2$60	BaF$_2$	SC	.175	300/4 hrs	2.27	2968	2.3 (N)	3020	5.46 (P)
$T_2$57	CaF$_2$	SC	.20	300/4 hrs	3.60	2558	2.97 (N)	1519	6.2 (P)
$T_2$47	BaF$_2$	SC	.21	350/4 hrs	2.03	3328	1.95 (N)	1654	17.4 (P)

Table 28   ISOTHERMAL ANNEALING RESULTS ON $Pb_{.80}Sn_{.20}Te$ FILM PREPARED WITH SUBSTRATE BIAS - TARGET #9

Sample No.	Subst. Temp. °C	Growth Rate μm/hr	Bias Voltage (volts)	Annealed at: Cond. I 600/12 hr 520/4 hr 6% MR Charge Carrier Concentration $n \times 10^{18}$ cm^{-3} CaF$_2$ Substrate	Annealed at: Cond. I 600/12 hr 520/4 hr 6% MR Charge Carrier Concentration $n \times 10^{18}$ cm^{-3} BaF$_2$ Substrate	Annealed at: Cond II. 600/12 hr 540/4 hr 6T MR Charbe Carrier Concentration $n \times 10^{18}$ cm^{-3} BaF$_2$ Substrate
T99	345	.95	+30	.11 (N)	.10 (N)	.25 (P)
T116	345	.95	+20	.07 (N)	.06 (N)	.18 (P)
T111	345	.95	+10	.1 (N) .19 (N) }	.1 (N)	
T110	345	.95	+5	.21 (N)	.19 (N) .20 (N) }	
T84	345	.95	0	.25 (N)	.20 (N)	.25 (N)
T113	345	.95	-10	.28 (N)	.24 (N)	.21 (N)
T98	345	.95	-30	.07 (N)	.065 (N)	.08 (N)

Table 29   ISOTHERMAL ANNEALING RESULTS—FILMS PREPARED FROM TARGET #9 (WITH BIAS)

Sample	Substrate	Film Comp (x)	Bias Voltage (v)	Annealing Condition Temp. °C	Time (hrs)	Unannealed Mobility cm²/v-sec	Unannealed Carrier Concentration nx10^{18}(cm^{-3})	Annealed Mobility cm²/v-sec	Annealed Carrier Concentration nx10^{18}(cm^{-3})
94	BaF$_2$	.19	+20	600 / 580	16 / 6	2600	8 (P)	9813	.28 (P)
94	CaF$_2$	.19	+20	600 / 550	16 / 6	222	7.09 (P)	9673	.14 (P)
94	BaF$_2$	.19	+20	600 / 540	16 / 6	2185	5.78 (P)	13,143	.042 (N)
94	BaF$_2$	.19	+20	600 / 525	16 / 6	1586	9.48 (P)	12,683	.162 (N)
85	CaF$_2$	.19	0	700 / 600 / 580	1/2 / 16 / 6	4600	0.8 (P)	9873	.223 (P)
				600 / 540	16 / 6				.075 (N)
85	CaF$_2$	.19	0	600 / 535	16 / 6	4250	1.0 (P)	14,623	.098 (N)
85	BaF$_2$	.19	0	600 / 525	16 / 6	3950	1.04 (P)	9981	.16 (N)
114	BaF$_2$	.195	-5	600 / 580	16 / 6	5300	.85 (P)	9505	.21 (P)
114	BaF$_2$	.195	-5	600 / 540	16 / 6			12,040	.06 (N)
114	BaF$_2$	.19	-5	600 / 525	16 / 6	4950	1.0 (P)	11,152	.11 (N)

Table 29 (Cont'd)   ISOTHERMAL ANNEALING RESULTS--FILMS PREPARED FROM TARGET #9 (WITH BIAS)

Sample	Substrate	Film Comp (x)	Bias Voltage (V)	Annealing Condition Temp. °C	Time (hrs)	Unannealed Mobility cm²/v-sec	Carrier Concentration nx10^{18}(cm^{-3})	Annealed Mobility cm²/v-sec	Carrier Concentration nx10^{18}(cm^{-3})
115	CaF$_2$	.195	-10	600 / 580	16 / 6	5145	0.57 (N)	8916	.25 (P)
115	BaF$_2$	.19	-10	600 / 525	16 / 6	7395	0.342 (N)	10,680	.17 (N)
101	BaF$_2$	.19	-30	600 / 580	16 / 6	6950	.4 (N)	9513	.162 (P)
101	BaF$_2$	.19	-30	700 / 600 / 550	1/2 / 16 / 6	5782	.450 (N)	12,938	.068 (N)
				540	16			9542	.041 (N)
101	BaF$_2$	.19	-30	600 / 525	16 / 6	6651	.611 (N)	15,543	.10 (N)
106	BaF$_2$	.21	+30	600 / 580	16 / 6	2950	5.5 (P)	8802	.425 (P)
105	CaF$_2$	.25	+30	600 / 500	16 / 6	7200	.5 (N)	9801	.12 (N)
108	BaF$_2$	.255	+40	600 / 500	16 / 6	3780	4.74 (P)	10,442	.154 (N)

Table 30   ISOTHERMAL ANNEALING RESULTS—FILMS PREPARED FROM TARGET #10 (WITH BIAS)

Sample	Substrate	Film Comp (x)	Bias Voltage (v)	Annealing Condition Temp. °C	Time (hrs)	Unannealed Mobility cm²/v-sec	Unannealed Carrier Concentration $nx10^{18}$ (cm⁻³)	Annealed Mobility cm²/v-sec	Annealed Carrier Concentration $nx10^{18}$ (cm⁻³)
SN58	CaF₂	.23	+20	400	13	7850	.9 (P)	9953	.093 (N)
SN33	BaF₂	.23	+3	400	24	9550	.41 (N)	14,221	.14 (N)
SN33	BaF₂	.23	+3	475	13	10,650	.13 (N)	7980	0.21 (P)
SN54	CaF₂		-10	400	13			9260	0.113 (N)
SN52	CaF₂	.235	-30	400	13			12162	.084 (N)
SN51	CaF₂	.22	+20	450	16	4355	2.7 (P)	12,242	.15 (N)
SN41	BaF₂		+20	600/520	16/6	4068	3.9 (P)	10426	.26 (P)
	BaF₂		+20	475	13	3894	3.8 (P)	14063	.075 (N)
SN25	BaF₂	.22	+15	475	14	4797	3.91 (P)	12208	0.098 (N)
SN31	BaF₂		+6	520 } 475	6 14	5506	2.5 (P)	9340 11204	0.279 (P) 0.105 (N)
SN31	CaF₂		+6	450	13	6862	1.85 (P)	11,569	0.22 (N)
SN26		.22	+5	500 } 475	6 14	5480	2.6 (P)	10447	.116 (N)
SN44	BaF₂		0	475	14			9213	.135 (N)
SN39	CaF₂		-6	475	14			11443	.15 (N)
SN30	BaF₂	.22	-10	475	14	9582	.327 (N)	9932	0.140 (N)
SN43	CaF₂	.215	-30	500 } 475	6 14	9040	.158 (N)	9872	.062 (N)

A-53

Table 31   ISOTHERMAL ANNEALING RESULTS—FILMS PREPARED FROM TARGET #8 (WITH BIAS)

Sample	Substrate	Film Comp (x)	Bias Voltage (v)	Annealing Condition Temp. °C	Time (hrs)	Unannealed Mobility cm^2/v-sec	Unannealed Carrier Concentration $n \times 10^{18}$(cm^{-3})	Annealed Mobility cm^2/v-sec	Annealed Carrier Concentration $n \times 10^{18}$(cm^{-3})
T104a	BaF$_2$	.22	+30	600 / 520	16 / 6	2614	6 (P)	12793	.158 (P)
T104b	BaF$_2$	.215	+20	600 / 520	16 / 6	2404	7.8 (P)	11776	.091 (P)
T104b	BaF$_2$	.22	+20	600 / 520	16 / 6	2579	6.9 (P)	9783	0.129 (P)
T104c	CaF$_2$	.22	+10	600 / 520	16 / 6	3400	5.4 (P)	8698	0.237 (P)
T80	CaF$_2$	.225	0	600 / 520	16 / 6	3125	2.5 (P)	9958	0.275 (P)
T109	CaF$_2$	.22	-5	600 / 520	16 / 6	10538	.35 (N)	11007	0.115 (N)
T102	CaF$_2$	.215	-10	600 / 520	16 / 6	8755	.78 (N)	11427	0.135 (N)
T96	BaF$_2$	.22	-30	600 / 520	16 / 6	8600	.8 (N)	12195	.094 (N)
T96	CaF$_2$	.22	-30	600 / 580	16 / 6	9825	.25 (N)	9540	.210 (P)
T107	BaF$_2$	.25	+40	500 / 400	16 / 4	2575	5.19 (P)	11886	0.172 (N)
T103	BaF$_2$	.25	+10	500 / 400	16 / 6	4309	2.1 (P)	11609	.215 (N)
	BaF$_2$			300	24			9639	.0651 (P)

Table 32   ISOTHERMAL ANNEALING RESULTS—FILMS PREPARED WITH O_2 and N_2 ADDITIVES (WITH AND WITHOUT BIAS)

Sample	pp. O_2 (Torr)	pp. N_2 (Torr)	Film Comp. (x)	Bias (volts)	Annealing Condition Temp. °C	Time (hrs)	Unannealed Carrier Concentration 10^{18} cm⁻³	Mobility cm²/v-sec	Annealed Carrier Concentration 10^{18} cm⁻³	Mobility cm²/v-sec
SN12		1×10^{-5}	.21	0	500	16	.4 (N)	6837	.104 (M)	9653
SN14		5×10^{-6}	.21	0	500	16	.7 - .8 (N)	7300	.122 (N)	11402
SN8	1×10^{-6}		.21	0	540	12	2 (P)	3200	1 (P)	5320
SN7	2×10^{-6}		.20	0	600 / 580	16 / 8	.4 (P)	6500	.8 (P)	7800
					500	16			.16 (N)	9032
SN6	5×10^{-6}		.19	0	600 / 580	16 / 8	.04 (P)	3800	0.9 (P)	7760
SN16		5×10^{-6}	.21	+30	500	16	.9 (P) .14 (N)	6894 9402	.12 (N)	12622
SN19		3×10^{-6}		+30	600 / 500	16 / 8	1.6 (P)	3638	0.027 (N)	10936
SN15	1×10^{-6}		.21	+30	600 / 540	16 / 8	3 (P)	3653	.27 (P)	8843
SN17	2×10^{-6}		.20	+30	500	16	1 (P)	4900	.13 (N)	9913

Table 33   RESULTS ON PROTON BOMBARDMENT OF $Pb_{1-x}Sn_xTe$ FILMS

Sample	Thickness (μm)	Film Comp. (x)	Proton Energy (KeV)	Proton Dose (p cm^{-2})	Carrier Concentration at 77°K (cm^{-3})
$T_2$110	1.98	.20	80	Before	3×10^{17} (P)
				1×10^{15}	2.6×10^{17} (P)
$T_2$93	2.09	.20	80	Before	5×10^{17} (P)
				1×10^{15}	3×10^{17} (P)
$T_2$100	1.68	.22	60	Before	1×10^{18} (P)
				1×10^{15}	1×10^{18} (P)
$T_2$77	1.37	.21	68	Before	7.3×10^{17} (P)
				1×10^{16}	3×10^{17} (N)
$T_2$80	1.13	.22	76	Before	8×10^{17} (P)
				1×10^{16}	1×10^{17} (N)
SN15	1.31	.21	80	Before	2.8×10^{17} (P)
				9×10^{15}	1.2×10^{17} (N)
SN21	1.82	.21	80	Before	2.4×10^{17} (P)
				9×10^{15}	9×10^{16} (N)
SN22	1.07	.21	80	Before	6.5×10^{17} (P)
				9×10^{15}	3.1×10^{16} (N)

Table 34   PHOTOCONDUCTIVE DETECTOR PERFORMANCE OF SOME AS-DEPOSITED $Pb_{1-x}Sn_xTe$ FILMS - MEASURED AT $\approx 90°K$ (2π, $300°K$ Background)

Sample & Substrate	Comp. (x) and Carrier Type	Struct.	Thickness (μm)	Noise $nv/\sqrt{Hz}$	Cell Resistance Ω	Bias Current (ma)	R_{max} (V/W)	D^*_{max} ($cm\ Hz^{\frac{1}{2}}/w$)
433 CaF$_2$(100)	.14 (N)	SC	3.0	6.4	90	20	1.5	1.2×10^8
446 BaF$_2$(111)	.18 (N)	SC	1.33	5	23	20	.29	3.3×10^7
432 CaF$_2$(111)	.19 (N)	SC	2.6	5	60	20	.20	2.6×10^7
T$_2$30	.10 (N)	SC	1.28	8	300	20	2.8	2.4×10^8
T$_2$37	.20 (N)	SC	1.50	6.4	300	18	.42	4.6×10^7
T$_2$51	.19 (N)	SC	1.12	6.7	170	17	.25	3×10^7

* Measurement Frequency - 1 KHz

A-57

Table 35   PROPERTIES OF $Pb_{1-x}Sn_xTe$ FILMS USED FOR ELECTRO-OPTICAL MEASUREMENTS

Sample	Subst.	Comp. (x)	Carrier Type	Thickness (μm)	Carrier Concentration $n \times 10^{18}$ (cm^{-3})	Hall Mobility $\mu(cm^2/v\ sec)$
T_230	BaF_2	.1	N	1.28	.39	5471
T_237 *	CaF_2	.20	N	1.50	.49	5236
T_251 *	CaF_2	.19	N	1.12	.25	7610
S_2440*	CaF_2	.10	N	3.09	.27	7936
T_232	CaF_2	.14	N	2.01	.25	6452
T_230 *	CaF_2	.17	N	2.08	.36	9380
T_248	CaF_2	.17	N	1.98	.395	6187
T_239 *	CaF_2	.21	N	1.53	.70	7568
T_213 *	CaF_2	.20	N	1.28	.035	11,650

* Annealed

Table 35 (Cont'd) PROPERTIES OF $Pb_{1-x}Sn_xTe$ FILMS USED FOR ELECTRO-OPTICAL MEASUREMENTS

Sample	Substrate	Comp. (x) and Carrier Type	Thickness (μm)	Carrier Conc. - N ($1/cm^3$) 88°K	Hall Mobility μ(cm^2/V sec) 88°K
432	CaF_2(111)	.19 (N)	2.6	2×10^{17}	4000
442	BaF_2(111)	.16 (N)	1.29	4.9×10^{17}	5800
439*	BaF_2(111)	.16 (N)	2.2	6.6×10^{17}	6800
435	BaF_2(111)	.20 (N)	1.85	9.5×10^{17}	5000
433	CaF_2(100)	.14 (N)	3.0	4×10^{17}	4000
446	BaF_2(111)	.18 (N)	1.33	3.9×10^{17}	5684

* Annealed Film

Table 36 OPTICAL ENERGY GAP DETERMINED FROM PHOTOCONDUCTIVE THRESHOLD

Sample	Substrate	Comp. (x) and Type	Thickness (μm)	Energy Gap from Photo Response (e.v.)			
				123°K	100°K	90°	77°K
424	BaF$_2$(111)	.17 (N)	3.4	.145			
425	BaF$_2$(111)	.15 (P)	1.4	.155			
432	CaF$_2$(111)	.19 (N)	2.6			.115	
433	CaF$_2$(100)	.14 (N)	3.0			.145	
435	BaF$_2$(111)	.20 (N)	1.85		.115		
442	BaF$_2$(111)	.165 (N)	1.29	.155			
443	CaF$_2$(111)	.16 (N)	1.56	.155			
445	CaF$_2$(111)	.095	1.6		.175		
448	BaF$_2$(111)	.175 (N)	2.07	.146			
T$_{23}$	CaF$_2$(111)	.20 (P)	2.3	.13			
438	CaF$_2$(111)	.21 (P)	2.2	.125			
439	BaF$_2$(111)	.16 (N)	2.2	.155			
451	BaF$_2$(111)	.16 (N)	.973		.135		
449	BaF$_2$(111)	.17	1.03		.131		
441	BaF$_2$(111)	.16 (N)	1.50	.155			
430	BaF$_2$(111)	.12 (N)	1.1		.16		

Table 36 (Cont'd)   OPTICAL ENERGY GAP DETERMINED FROM PHOTOCONDUCTIVE THRESHOLD

Sample	Substrate	Comp. (x) and Type	Thickness (μm)	Energy Gap from Photo Response (e.v.)			
				123°K	100°K	90°K	77°K
$T_2$30	BaF_2	.10 (N)	1.28			.165	
$T_2$37	BaF_2	.20 (N)	1.50			.107	
$T_2$51	BaF_2	.19 (N)	1.12			.114	
S440	BaF_2	.10 (N)	3.09			.165	
$T_2$32	BaF_2	.14 (N)	2.01				.139
$T_2$30	CaF_2	.17 (N)	2.08				.12
$T_2$48	CaF_2	.17 (N)	1.98				.12
$T_2$13	CaF_2	.20 (N)	1.28				.102
$T_2$39	CaF_2	.21 (N)	1.53				.096
$T_1$24	BaF_2	.18 (N)	2.44				.113
SN 43	BaF_2	.21 (N)	1.50				.096
T109	BaF_2	.21 (N)	1.89				.096
T95	BaF_2	.22 (N)	1.90				.092
SN 35	BaF_2	.21 (P)	1.81				.096
T91	BaF_2	.20 (N)	2.0				.099
T104	BaF_2	.22 (N)	2.68				.092

Table 37 PHOTOCONDUCTIVE DETECTOR PERFORMANCE OF SOME $Pb_{1-x}Sn_xTe$ FILMS (DETECTOR TEMPERATURE, ~77°K, BACKGROUND 2π, 300°K)

Sample	Composition (x)	Carrier Type	Substrate Bias (V)	Structure	Thickness	Noise* ($nV/\sqrt{Hz}$)	Cell Resistance (Ω)	Bias Current (mA)	R Max (V/W)	D* ($cm\text{-}Hz^{1/2}/W$)
T124	0.18	n	-30	SC	2.44	4.8	380	15	3.6	5.4×10^8
SN 43	0.21	n	-30	SC	1.50	4.4	340	20	2.2	3.2×10^8
T109	0.21	n	-5	SC	1.89	10	300	18	2.0	1.5×10^8
T95	0.22	n	-20	SC	1.90	10	220	22	1.2	9.6×10^7
SN 35	0.21	p	-2	SC	1.81	9	280	15	1.10	1×10^8
T91	0.20	n	0	SC	2.0	5	240	14.5	1.05	1.89×10^8
ANNEALED										
T104	0.22	n	+20	SC	2.68	6	280	16	2.6	4×10^8
T95	0.22	n	-20	SC	1.90	8	250	18	1.9	2×10^8

* Measured at Frequency of 1 kHz.

Table 38 EXCEPTIONALLY HIGH RESPONSIVITIES IN SOME AS-DEPOSITED $Pb_{1-x}Sn_xTe$ FILMS

Sample	Composition (x)	Carrier Type	Cell Resistance	Bias Current	R_{max}^{*} (v/w)
6-2-$T_2$58	.05	(N)	1.6 MΩ	8 μa	420
6-1-$T_2$58	.05	(N)	.9 MΩ	22 μan	65
8-$T_2$58	.07	(P)	300 KΩ	60 μm	25
6D$_3$	.12	(P)	950 Ω	11 ma	3.9
$T_2$58	.07	-	400 KΩ	.3 ma	1055

* Measurement Frequency - 1 KHz

A-63

Table 39 PHOTOCONDUCTIVE RESPONSES IN SOME $Pb_{1-x}Sn_xTe$ FILMS PREPARED WITH O_2 and N_2 ADDITIVES

Sample	Composition (x)	PP O_2 (Torr)	PP N_2 (Torr)	Carrier Type	Cell Resistance	Bias Current	R_{max} (V/W)
SN6	.19	5×10^{-6}		P	52 KΩ	.06 ma	20
SN7	.20	2×10^{-6}		P	610 Ω	5.7 ma	7.2
SN8	.20	1×10^{-6}		P	350 Ω	10 ma	2.2
SN13	.15		1×10^{-4}	N	32 KΩ	.17 ma	15
SN12	.21		1×10^{-5}	N	510 Ω	8 ma	4
SN14	.21		5×10^{-6}	N	400 Ω	9 ma	2.5

Table 40   EXPERIMENTS AND DATA ON PbSnTe FILMS FOR PREPARATION OF p-n PHOTODIODES

Single Layers

Sample No.	Substrate Temp. °C	Growth Rate μm/hr	Bias Voltage (volts)	Film Comp. (x)	Carrier Concentration n x 10^{18} (cm^{-3})	Target No.
S108	346	1.2	+20	.23	1.2 (p)	13
S107	344	1.2	+10	.23	.85 (p)	13
111	344	1.2	+5	--	.12 (n)	13
109	343	1.2	0	.23	.22 (n)	13
113	344	1.2	-2	--	.21 (n)	13
112	344	1.21	-5	.225	.2 (n)	13
110	342	1.2	-20	--	.13 (n)	13
106	348	1.22	-30	.23	.09 (n)	13
151	335	.53	-10	.18	.65 (p)	13
152	335	.52	-20	.18	.13 (n)	13
153	335	.50	-30	.18	.10 (n)	13
T 92	332	.51	-30	.14	.11 (n)	2
93	331	.50	-15	--	.13 (n)	2
94	332	.48	-10	.14	.75 (p)	2
95	330	.5	-5	.14	1.0 (p)	2
96	330	--	+5	--	2.0 (p)	2

Table 40 (Cont'd)   EXPERIMENTS AND DATA ON PbSnTe FILMS FOR PREPARATION OF p-n PHOTODIODES

Double P/N Layer in Diode Configuration

Sample No.	Substrate Temp oC	Growth Rate μm/hr	Bias Voltage	Film Carrier Type	Target No.
104	331	.5	-10/-30	P/N	2
105	330	.5	+5/-30	P/N	2
T 149	335	.5	-10/-20	P/N	13
T 150	335	.5	+20/-30	P/N	13
T 151	335	.5	-10/-30	P/N	13
T 97	335	.95	+20/-30	P/N	9
T 101	335	.95	+20/-30	P/N	9
T 99	335	.95	+10/-30	P/N	9
T 100	330	.50	+5/-30	P/N	9
T 98	330	.50	-10/-20	P/N	9
T 102	330	.51	+10/-30	P/N	9

A-66